

**College of Engineering
University of South Florida**



**Feasibility of Fiberglass Pretensioned
Piles in a Marine Environment**

Rajan Sen
Mohsen Issa
Daniel Mariscal

August 1992

Report No. CEM/ST/92/1

College of Engineering
University of South Florida
4202 Fowler Avenue
Tampa, Florida 33620-5350

Department of Civil Engineering and Mechanics
The University of South Florida

Feasibility of Fiberglass Pretensioned
Piles in a Marine Environment

Rajan Sen
Mohsen Issa
Daniel Mariscal

August 1992

Report No. CEM/ST/92/1

A Report on a Research Project Sponsored by the Florida
Department of Transportation in cooperation with the U.S.
Department of Transportation
Contract C-3321

Tampa, Florida

Technical Report Documentation Page

1. Report No. 0510528	2. Government Accession No.	3. Recipient's Catalog No. 2104-144-LO	
4. Title and Subtitle Feasibility of Fiberglass Pretensioned Piles in a Marine Environment		5. Report Date August, 1992	
		6. Performing Organization Code CEM/FDOT/144-LO	
7. Author's Rajan Sen, Mohsen Issa (UIC) and Daniel Mariscal		8. Performing Organization Report No. CEM/ST/92/1	
9. Performing Organization Name and Address Department of Civil Engineering and Mechanics University of South Florida, Tampa, FL 33620 Creep Study (under sub-contract) University of Illinois at Chicago Chicago, IL 60680		10. Work Unit No. (TRAIS)	
		11. Contract or Grant No. C-3321	
		13. Type of Report and Period Covered Final Report November 1989 - December 1991	
12. Sponsoring Agency Name and Address Florida Department of Transportation Structural Research Center 2007 East Dirac Drive Tallahassee, FL 32310 Attention: Dr. Mohsen Shahawy		14. Sponsoring Agency Code	
15. Supplementary Notes Prepared in cooperation with the Federal Highway Administration			
16. Abstract The primary aim of the study was to investigate the feasibility of using fiberglass pretensioned piles to replace steel in a marine environment. As a consequence experimental investigations were carried out to determine the short term, long term and impact response of specimens pretensioned using S-2 glass/epoxy composites. For comparability, identical steel specimens were also tested. The short term tests investigated transfer length, losses, static response of under-reinforced beams and the elastic and ultimate behavior of axially and eccentrically loaded columns. The long term tests examined fatigue and creep in concrete and in identically stressed fiberglass prestressed columns. In addition, a major investigation was carried out to determine the durability of pre-cracked and uncracked fiberglass pretensioned beams exposed to wet/dry cycles in 15% salt solution. The impact study investigated stresses in full sized fiberglass pretensioned piles under the application of a 3 kip drop hammer to drive it through medium to dense sands. The study indicated that the response of identical fiberglass and steel pretensioned specimens is, in general, comparable and may be predicted with reasonable accuracy using non-linear finite element analyses incorporating appropriate material properties. However, the long term durability study indicated that the fiberglass strands suffered degradation under wet/dry cycles. Pre-cracked specimens deteriorated between 3-9 months of exposure and the uncracked specimens between 12-18 months. Scanning electron micrographs showed degradation of the glass fibers in the alkaline concrete environment. Recommendations for overcoming this problem are addressed in the report.			
17. Key Words Pretensioning, fiberglass, beams, columns, piles, fatigue, creep, durability	18. Distribution Statement No restrictions. This document is available to the public through the National Technical Information Service, Springfield, VA 22161		
19. Security Classif.(of this report) Unclassified	20. Security Classif. (of this page) Unclassified	21. No. of Pages 318	22. Price

DISCLAIMER

The opinions, findings and conclusions expressed in this publication are those of the authors and not necessarily those of the State of Florida Department of Transportation or the US Department of Transportation.

CONVERSION FACTORS, US CUSTOMARY TO METRIC UNITS

<i>Multiply</i>	<i>by</i>	<i>to obtain</i>
inch	25.4	mm
foot	0.3048	meter
square inches	645	square mm
cubic yard	0.765	cubic meter
pound (lb)	4.448	newtons
kip (1000 lb)	4.448	kilo newton (kN)
newton	0.2248	pound
kip/ft	14.59	kN/meter
pound/in ²	0.0069	MPa
kip/in ²	6.895	MPa
MPa	0.145	ksi
ft-kip	1.356	kN-m
in-kip	0.113	kN-m
kN-m	0.7375	ft-kip

PREFACE

The investigation reported was funded by a contract awarded to the University of South Florida, Tampa by the Florida Department of Transportation in cooperation with the US Department of Transportation. Dr. Mohsen Shahawy, Chief Structural Analyst, Florida Department of Transportation was the Project Manager. It is a pleasure to acknowledge his overall contribution to the project. Additional financial support was provided by the College of Engineering, University of South Florida with matching support from the Division of Sponsored Research (DSR). We are indebted to Dr. Mel Anderson, Associate Dean, Dr. Tom Wade, Associate Dean of Research, (both from the College of Engineering) and Mr. Frank Lucarelli, former Director, DSR for this support. Dr. Wayne Echelberger Jr., Chairman, Department of Civil Engineering and Mechanics, provided critical financial support for students last summer. We are very grateful for this assistance and also for his interest in the project.

The Principal Investigator for the project was Dr. Rajan Sen, University of South Florida and the Co-Principal Investigator was Dr. Mohsen Issa, University of Illinois at Chicago (UIC). Dr. Srinivasa Iyer, School of Mines and Technology, Rapid City, SD was a consultant for the project. He played an invaluable role in the initial start up phase and in the pretensioning of the fiberglass specimens. All fiberglass strands were pretensioned using a proprietary system he developed and he also fabricated the fiberglass spirals used. Tests to determine the tensile strength of the fiberglass strands were conducted at Rapid City, SD. We wish to record our sincerest appreciation for his contribution to this study.

The support and encouragement of many researchers from within the United States and abroad is gratefully acknowledged. We wish to thank Mr. Arie Gerritse of the Hollandsche Beton Groep, The Netherlands, Mr. Mark Greenwood, of Owens Corning, Ohio, Mr. Paul Ulbrich, of Shell, Mr Bob Landgren of Wiss Janney, Chicago, Dr. Neal Burke of W R Grace, Boston, Dr. John Lybas, of the University of Florida, Gainesville, Mr. Peter Head of Maunsell Structural Plastics, UK, Dr. Reinhard Wolff and Dr. Hans-Joachim Miessler, both of Strabag Bau-Ag, Germany, Dr. Charles Dolan, University of Wyoming, Dr. Noel Nathan, formerly Professor at the University of British Columbia, Vancouver, Canada, Dr. Jean-Louis Briad (of Texas A & M), Mr. Dirk Pletcher of Polygon, Indiana and Mr. Richard Dauksys of BASF Structural Materials. The project benefited greatly from the cooperation shown by our colleagues in the Florida Department of Transportation. We wish to thank Dr. Joe Caliendo, Dr. Chin Kuo, Dr. Brent Hamil, Mr. Paul Passe, Mr. Bipin Pancholy, Dr. Moussa Issa, Mr. Rod Powers and Mr. Rick Kessler. The technical assistance and cooperation of FDOT's technical staff Frank Cobb, Randy Bradley, Tony Johnston, Ron Caldi and Gregory Martin at the Structures Research Center, Tallahassee is gratefully acknowledged.



Several faculty and staff at the University of South Florida assisted in the study. In particular, we wish to thank Dr. Alberto Sagues, Dr. John Ratliff, Dr. Robert Carnahan, Mr. Gray Mullins, Mr. Robert Tufts, Mr. Kevin Dempsey, Dr. Eleanor Snow (Geology), Mr. Bruce Antolik (Geology), Ms. Alicia Sue Slater, Ms. Alicia GarciaRubio and Mr. Brian Burgess. As always, the Engineering Shop's unceasing efforts in fabricating items needed for testing, often at very short notice, enabled us to meet our deadlines. We are indebted to Mr. Ray Cornett, Mr. Bob Smith, Mr. Jerry Miller and Mr. Bryan O'Steen for their cooperation and assistance.

The support from local industry is gratefully acknowledged. We wish to thank Mr. Jack Roebuck, retired Vice President, Florida Mining and Materials, Mr. Ed Dunstan and Mr. Dan Green (both of Florida Mining and Materials), Mr. Michael Huff and Mr. Robert Lutz (both of Southern Prestressed), Mr. John Robertson of Hardaway and Mr. Sameer Moussly, of PSI for their contribution. The fabrication of the pile specimens was carried out at Henderson Prestress, Tarpon Springs, FL. We are very grateful to Mr. Dirk Henderson for allowing us access to the prestressing facilities for almost one week and also for technical assistance in the testing of the transfer block and splicing chucks that were used. We also wish to thank his crew for their assistance in the fabrication of the specimens. Mr. Mohamad Hussein, Partner, GRL & Associates, Orlando was the consultant for the pile driving study. We wish to record our sincerest appreciation for his contribution. The piles were driven by Gulf Coast Marine Construction, Inc. of St. Petersburg, FL. Mr. Jack Harrington, Vice President, Brown Testing Laboratory, Tampa, FL was instrumental in securing the Tierra Verde site of a proposed condominium where the piles were driven. We are especially grateful to Mr. Bill Moore for allowing us permission to drive the piles and for his hospitality. We are also indebted to Mr. Alfred Spillett for his contribution.

This project could not have been completed without the enthusiastic and often times voluntary support of numerous undergraduate and graduate students at the University of South Florida. Mr. Steve Tozier, an undergraduate student played a key role during the first seven months of the project. This was taken over by Mr. Ken Spillett and Mr. Daniel Mariscal without whose indefatigable efforts this project would not have been completed. The contribution of the following students and former students (not in any order) is gratefully acknowledged: Ms. Patricia Wadsack, Ms. Lily Sun, Ms. Barbara Washington, Ms. Helvethia Perez-Duran, Ms. Yufeng Wang, Mr. Ali Sadaat, Mr. Larry Jones, Mr. Ed Doyle, Mr. Eric Scott, Mr. Mike Mulchard, Mr. Mark Grant, Mr. Henry Jean, Mr. Tom Washington, Mr. Robert Reis, Mr. Keith Tozier, Mr. Brian Jory (of Dames and Moore, Tampa), Mr. Robin DeRose (of Testing Lab, Tampa), Mr. David Hodge (of DRC & Associates, Tampa), Mr. Tony Russo and Mr. Ronald Chin (both of Florida Department of Transportation). Mr. Ahmad Hammad (of UIC) provided technical assistance in the fabrication of the beam and pile specimens. Mr. Narayan Iyer (University of Minnesota) assisted in the fabrication of the durability specimens and Mr. Paul Digirolano (Penn State) assisted in the static testing of beams.

EXECUTIVE SUMMARY

The feasibility of replacing steel by S-2 glass/epoxy strands in pretensioning applications for piles driven in a marine environment was examined. S-2 glass is a trademark product of Owens-Corning and is a three component magnesia-aluminasilicate glass. Shell Epon 9310 resin was used as the polymer matrix. The fiberglass strands comprised seven 0.125 in. diameter rods held together mechanically by plastic ties. A total of 63 identical steel and fiberglass pretensioned beams, columns and pile specimens were fabricated and tested. The smaller specimens were fabricated at the University of South Florida, Tampa and the larger pile and column specimens at Henderson Prestress, Tarpon Springs, one of Florida's largest producers of commercial piling.

The investigation examined the short term and the long term response. The short term response included determination of transfer length, losses and the elastic and ultimate response of beams and columns. Additionally, driving stresses in full scale piles were investigated. The long term response included cyclic fatigue tests, long term creep and shrinkage and durability studies. Excepting for the fatigue study, the response of identical fiberglass and steel pretensioned specimens under the same prestressing force was investigated.

Measurements of transfer length were made for seven fiberglass pretensioned specimens. Two of the specimens were eccentrically pretensioned while the remaining five were concentrically pretensioned. The specimens were all 6 in. wide by 4 in. deep and 8 ft 6 in. long. The prestressing force was provided by two 3/8 in. strands. The results indicated that the transfer length of fiberglass specimens was about 27 times the strand diameter or 10 in. This is 23 % smaller than the transfer length for 3/8 in. steel strands stressed to the same level.

In the static beam tests, under reinforced fiberglass pretensioned beams with cross-sections of 6 in. x 8 in., 6 in. x 10 in., 6 in. x 12 in. and a span of 8 ft were tested under two point loading. The results showed that the elastic response of the fiberglass pretensioned beams was identical to that of its steel pretensioned counterpart. However, the post-elastic response of the fiberglass pretensioned beams was more flexible. All failures were tension failures with secondary crushing of concrete in the compression zone. The failure modes were ductile and in every test the ultimate deflection of the fiberglass beams was larger than the comparable steel specimen. The spacing of crack widths was a little greater in the fiberglass pretensioned beams. The results of the tests showed good agreement with predictions from non-linear finite element analysis.

In the column tests, four fiberglass pretensioned columns 8 in. x 8 in. x 8 ft were tested under axial and eccentric loads. The columns were pretensioned using eight 3/8 in. strands and the effective prestress in the fiberglass columns was estimated to be 1,160 psi. Two of the columns tested were all fiberglass columns that were provided with fiberglass spiral ties. The other two were provided with spiral steel ties. All columns

failed at the ends but the results indicated that the comparative response of the fiberglass and steel pretensioned columns was very similar. However, the fiberglass ties ruptured in one of the tests indicating that its ductility did not match that of the steel ties.

Four fiberglass pretensioned piles 10 in. x 10 in. x 25 ft were pretensioned using eight 3/8 strands in a commercial prestressing facility. Two of the piles were all fiberglass and two others were provided with steel ties. The effective prestress in the fiberglass piles was estimated to be about 740 psi. The piles were driven using a 3 kip drop hammer and a 8 ft drop through medium to dense sands in Tierra Verde, FL within 100 yards of Tampa Bay. Pile driving stresses were monitored using a Pile Driving Analyzer. The results indicated that the driving stresses in the piles were comparable to those in prototype piles. No signs of distress were observed under normal driving. Subsequently, the drop height was increased to 15 ft and some damage was recorded. As for the column study, some of the fiberglass ties ruptured during this operation indicating that its ductility was smaller than that of the steel ties which did not suffer similar damage.

In the fatigue study, two fiberglass pretensioned beams 6 in. x 10 in. and 6 in. x 12 in. with a span of 8 ft were subjected to 2 million cycles at 3 Hz. The applied load varied between 40% and 60% of the measured ultimate static capacity. The minimum stress in the fiberglass strands was 42% of the ultimate tensile strength. The maximum stress varied from 47-56% of this value. One of the beams subjected to a stress range of 7.3 of the ultimate failed while the other subjected to a lower 4 % range survived. The results of these tests compare favorably with those recorded in similarly stressed steel beams reported in the literature. The surviving beam was statically tested to failure and only showed a slightly smaller ultimate capacity.

Material and structural creep studies were carried out simultaneously. The material creep study was conducted at the University of South Florida whereas the structural creep study was carried out at the University of Illinois at Chicago. In both studies, the specimens were subjected to loads corresponding to 20 % and 30 % of the ultimate concrete strength. The material creep study showed that the creep variation was consistent with the average value proposed by ACI. The structural creep investigated 6 in. x 4 in. x 8.5 ft concentrically pretensioned columns. The same tests were repeated in an environmental chamber where the temperature and humidity was varied to simulate Florida conditions. These results showed that prestress losses in the steel specimens were between 16-34% greater than that in the comparable fiberglass specimens. Additionally, losses in average field conditions were comparable to those measured in the laboratory.

In the durability study, eight fiberglass pretensioned beams 6 in. wide x 4 in. deep x 8 ft 6 in. long, eccentrically pretensioned with two 3/8 in S-2 glass/epoxy strands were exposed to wet/dry cycles in 15 % salt solution for 20 months to simulate conditions experienced by piles. Ready mixed concrete with a water cement ratio of 0.41 was used and the minimum cover was an inch. Four of the specimens were pre-cracked at the top and bottom prior to the commencement of the test. Four unexposed control specimens

were used to assess changes in ultimate strength due to exposure. The ultimate capacity of the specimens was measured at 3 monthly intervals excepting for the first and last tests that were conducted after 1.5 months and 20 months respectively. The tests indicated a complete loss of effectiveness of the fiberglass strands after an average of 6 months for the pre-cracked specimens and 15 months for the uncracked specimens. Subsequent, examination under scanning electron microscope indicated degradation of the glass in the wet and splash zones but none in the dry concrete. It is believed that this is due to diffusion of hydroxyl ions through the epoxy resin. No comparable loss was detected in identical steel specimens that were also tested.

Overall, the study indicated that fiberglass had the properties required for prestressing and displayed adequate ductility and resistance to impact forces. The response of fiberglass pretensioned specimens is very similar to that of steel pretensioned ones and differences were attributable to differences in material properties. However, the durability of fiberglass in concrete was found to be unsatisfactory. The Shell Epon 9310 resin used was unable to protect the S-2 glass fibers from dissolution in an alkaline environment. If a suitable resin system can be invented, fiberglass can be used to replace steel in pretensioning applications in a marine environment.

TABLE OF CONTENTS

PREFACE	iii
EXECUTIVE SUMMARY	v
LIST OF TABLES	xv
LIST OF FIGURES	xvii
LIST OF PLATES	xxi
LIST OF SYMBOLS AND ABBREVIATIONS	xxiv
1. INTRODUCTION	1-1
1.1 Introduction	1-1
1.2 New Prestressing Materials	1-1
1.3 Materials Used for Study - S-2 Glass/epoxy	1-5
1.4 Previous Studies	1-6
1.5 Objectives and Scope of Study	1-6
1.6 Organization of Report	1-9
2. PROPERTIES OF S-2 GLASS®	2-1
2.1 Introduction	2-1
2.2 Fiberglass	2-1
2.2.1 S-2 Glass®	2-1
2.3 Resin Matrix	2-3
2.4 Pultrusion Process	2-5
2.4.1 Fiberglass Spirals	2-5
2.5 S-2 Glass® Rods	2-5
2.6 S-2 Glass® Strands	2-9
2.7 Anchorage Mechanism for FRP	2-12
3. LONG-TERM RESPONSE OF FRP	3-1
3.1 Introduction	3-1
3.2 New Non-Metallic Prestressing Materials	3-1
3.2.1 Polystal®	3-1
3.2.2 Arapree®	3-2
3.2.3 Carbon Fiber Composite Cable	3-2
3.3 Long-Term Engineering Properties	3-3
3.3.1 Stress-Rupture	3-3
3.3.2 Relaxation	3-3
3.3.3 Fatigue	3-5
3.4 Environmental Effects	3-6

3.4.1	Effect of Alkaline Environment	3-6
3.4.2	Effect of Moisture	3-6
3.4.3	Effect of Salt	3-7
3.5	Comparison of New Prestressing Materials	3-8
4.	FABRICATION OF SPECIMENS	4-1
4.1	Introduction	4-1
4.2	Concrete	4-2
4.3	Prestressing Steel	4-3
4.4	Reinforcing Steel	4-6
4.5	Fabrication at USF	4-6
4.5.1	Prestressing Bed	4-6
4.5.2	Pre-tensioning Procedure	4-9
4.6	Fabrication of Durability and Creep Specimens	4-11
4.7	Fabrication of Beam Specimens	4-15
4.8	Fabrication at Henderson Prestress	4-18
5.	SHORT TERM LOSSES	5-1
5.1	Introduction	5-1
5.2	Strain Gages	5-1
5.3	Correlation with Load Cell Results	5-2
5.4	Short Term Prestress Losses	5-2
5.5	Effective Prestress in Piles and Columns	5-6
6.	TRANSFER LENGTH	6-1
6.1	Introduction	6-1
6.2	Previous Studies	6-1
6.3	Experimental Program	6-2
6.3.1	Instrumentation	6-2
6.3.2	Test Set Up and Release	6-4
6.4	Test Results and Discussion	6-4
6.4.1	Theoretical Transfer Strains	6-6
6.4.2	Experimental Transfer Length	6-6
6.4.3	Long Term Transfer Length	6-8
6.4.4	Prediction of Fiberglass Transfer Length	6-8
7.	BEAM STUDY	7-1
7.1	Introduction	7-1
7.2	Instrumentation	7-2
7.2.1	Strain Gages	7-2
7.2.2	Deflection	7-2
7.2.3	Neutral Axis	7-3
7.2.4	Slip	7-3
7.2.5	Crack Width	7-3
7.2.6	Data Recording	7-3

7.2.7	Static Test	7-3
7.2.8	Test Procedure	7-5
7.3	Static Response	7-5
7.3.1	Load-deflection	7-5
7.3.2	Concrete Strains	7-9
7.3.3	Prestressing Strand Strain	7-9
7.3.4	Neutral Axis	7-9
7.3.5	Crack Pattern	7-9
7.3.6	Slip	7-17
7.3.7	Failure Mode	7-18
7.4	Finite Element Analysis	7-18
8.	COLUMN STUDY	8-1
8.1	Introduction	8-1
8.2	Experimental Program	8-1
8.3	Test Set Up and Instrumentation	8-1
8.3.1	Test Procedure	8-4
8.4	Test Results	8-4
8.4.1	Failure Load and Failure Mode	8-4
8.4.1.1	Axial Loads	8-5
8.4.1.2	Eccentric Load	8-9
8.4.2	Comparison of Response of Fiberglass and Steel Columns	8-9
8.5	Finite Element Analysis	8-12
9.	PILE STUDY	9-1
9.1	Introduction	9-1
9.2	Scope of Study	9-1
9.3	Wave Equation Analysis	9-5
9.3.1	One Dimensional Wave Equation	9-6
9.3.1.1	Finite Difference Solution	9-8
9.3.2	Finite Element Solution	9-9
9.4	Pre-driving Analysis	9-10
9.4.1	Test Site	9-10
9.4.2	GRLWEAP Analysis	9-11
9.4.3.1	GRLWEAP Input	9-13
10.	PILE DRIVING	10-1
10.1	Introduction	10-1
10.2	Pile Driving Analyzer	10-1
10.3	Test Procedure and Instrumentation	10-2
10.4	Test Results	10-4
10.4.1	Driving Stresses	10-6
10.4.2	Hammer and Driving System	10-13
10.4.3	Bearing Capacity	10-13
10.5	Assessment of Fiberglass Piles	10-15

11.	FATIGUE RESPONSE	11-1
11.1	Introduction	11-1
11.2	Literature Review	11-3
11.2.1	Steel Strands	11-4
11.2.2	Fiberglass Strands	11-4
11.3	Scope of Study	11-5
11.4	Test Parameters	11-6
11.5	Experimental Study	11-6
11.5.1	Test Set Up	11-6
11.5.5.1	Test Procedure	11-7
11.5.2	Fatigue Response of Fiberglass Pretensioned Beams	11-8
11.5.2.1	Fatigue Life	11-8
11.5.2.2	Deflection	11-8
11.5.2.3	Crack Width	11-10
11.5.2.4	Strains	11-10
11.5.2.5	Ultimate Capacity After Cyclic Load	11-16
11.6	Comparison with Harajli & Namaan	11-16
12.	CREEP IN CONCRETE	12-1
12.1	Introduction	12-1
12.2	Test Setup	12-2
12.3	Results	12-3
13.	LONG TERM CREEP LOSSES	13-1
13.1	Introduction	13-1
13.2	Experimental Program	13-1
13.3	Experimental Results	13-3
13.3.1	Laboratory Environment (Group I)	13-3
13.3.2	Environmental Chamber (Group II)	13-5
13.4	Analysis and Results	13-5
13.4.1	Laboratory Environment (Group I)	13-5
13.4.2	Environmental Chamber (Group II)	13-6
13.5	Analytical Prediction	13-7
14.	DURABILITY STUDY	14-1
14.1	Introduction	14-1
14.2	Basis of Experimental Program	14-1
14.3	Tidal Simulation	14-2
15.	DETERMINATION OF SEQUENCE OF TESTING	15-1
15.1	Introduction	15-1
15.2	Half-Cell Potentials Measurements	15-1
15.2.1	Discussion of Results	15-2
15.3	A.C. Impedance Measurements	15-5
15.3.1	Discussion of Results	15-5

15.4	Resistivity Measurements	15-8
15.4.1	Discussion of Results	15-10
15.5	Selection of Sequence for Testing	15-10
15.5.1	Sequence for Steel Pre-tensioned Specimens	15-10
15.5.2	Sequence for Fiberglass Pre-tensioned Specimens	15-11
16. ULTIMATE CAPACITY TESTS		16-1
16.1	Introduction	16-1
16.2	Experimental Program	16-1
16.2.1	Test Set Up	16-1
16.2.2	Instrumentation	16-3
16.2.4	Test Procedure	16-3
16.3	Test Results	16-4
16.3.1	Steel Pre-tensioned Beams	16-4
16.3.2	Fiberglass Pre-tensioned Beams	16-9
16.3.2.1	Corrosion Failure Mode	16-19
16.4	Effect of Salt Water on Concrete	16-22
16.5	Effect of Salt Water on Bond	16-22
16.5.1	Test Results	16-24
16.5.2	Discussion of Results	16-24
16.6	Implication of Results	16-26
17. POST-ULTIMATE TEST EXAMINATION		17-1
17.1	Introduction	17-1
17.2	Visual Inspection	17-1
17.2.1	Test Procedure for Carbonation	17-2
17.2.2	Visual Inspection and Carbonation Results	17-2
17.2.2.1	Inspection of ST-E3	17-2
17.2.2.2	Inspection of FG-E3	17-2
17.2.2.3	Inspection of ST-M3	17-4
17.2.2.4	Inspection of ST-M2	17-4
17.3	Chloride Content	17-6
17.3.1	Test Results and Discussion	17-6
18. SCANNING ELECTRON MICROSCOPY EXAMINATION		18-1
18.1	Introduction	18-1
18.2	Scope of Investigation	18-1
18.3	Results and Discussion of SEM Examination	18-3
18.3.1	Permanently Dry Location	18-3
18.3.2	Splash Zone	18-3
18.3.3	Permanently Wet Location	18-7
18.3.4	Discussion of Results	18-7

19.	CONCLUSIONS	19-1
19.1	Introduction	19-1
19.2	Short Term Response	19-1
19.2.1	Transfer Length	19-1
19.2.2	Beam Study	19-2
19.2.3	Column Study	19-2
19.2.4	Pile Study	19-3
19.3	Long Term Response	19-4
19.3.1	Fatigue Response	19-4
19.3.2	Material Creep in Concrete	19-5
19.3.3	Long Term Creep Losses	19-5
19.3.4	Durability Study	19-5
20.	RECOMMENDATIONS	20-1
20.1	Introduction	20-1
20.2	Enhancing Alkali Resistance	20-1
20.3	Prestressing Requirements	20-2
21.	REFERENCES	21-1

LIST OF TABLES

1.1	Properties of High-Strength Fibers	1-3
1.2	Relative Cost of Non-Metallic Prestressing Materials	1-3
1.3	Test Program for Short Term Studies	1-7
1.4	Test Program for Long Term Studies	1-8
2.1	Approximate Chemical Composition of S-2 and E Glass Fibers	2-2
2.2	Typical Properties for S-2 and E Glass Fibers	2-2
2.3	Typical Properties for the Un-reinforced Epon® Resin 9310 System	2-4
2.4	Typical Properties for S-2 Glass/Epoxy Composites	2-8
2.5	Mechanical Properties of S-2 Glass Strands	2-11
3.1	Properties of Different Prestressing Materials	3-9
4.1	Summary of Specimens Cast	4-1
4.2	Concrete Mix Design for Specimens Cast at USF	4-2
4.3	Concrete Mix Design for Specimens Cast at Henderson Prestress	4-3
4.4	Steel Strand Properties for Pours 1 and 2 (December 1989)	4-4
4.5	Steel Strand Properties for March 1990 (Pour 3) and June 1990 (Pour 4)	4-4
4.6	Steel Strand Properties for Flexure and Fatigue Study (Pour 5)	4-5
4.7	Steel Strand Properties for Column and Pile Study (Pour 6)	4-5
5.1	Comparison of Load Cell Readings & Strain Gage Readings at Jacking	5-3
5.2	Comparison of Load Cell Reading & Strain Gage Reading before Release	5-4
5.3	Summary of Prestressing Operation	5-5
5.4	Tensioning Stress Summary for Steel Beams	5-6
5.5	Tensioning Stress Summary for Fiberglass Beams	5-7
5.6	Prestress Loss Summary	5-8
5.7	Embedded Concrete Gage Data at Release	5-9
5.8	Surface Concrete Gage Data at Release	5-9
6.1	Prestressing Force Summary (March 1990)	6-4
6.2	Theoretical Transfer Strains (Fiberglass)	6-7
6.3	Theoretical Transfer Strains (Steel)	6-7
6.4	Experimental Transfer Length	6-7
7.1	Beam Details for Static Test	7-1
7.2	Summary of Static Load Test Results	7-13
7.3	Summary of Slip and Failure Mode in Beams	7-17
8.1	Summary of Column Test Details	8-2
8.2	Summary of Ultimate Capacity and Failure Mode	8-5
9.1	Typical Effective Prestress in Piles Used by FDOT	9-4
9.2	Details of Piles Tested	9-5
9.3	Results of Static Bearing Capacity Calculations	9-16
9.4	Summary of Typical Input Data for GRLWEAP Analysis	9-17
9.5	Drivability Study	9-18
10.1	Summary of Pile Driving Stresses	10-6
10.2	PDA Result Summary for 15 ft Drop	10-8
10.3	Comparison of Static Bearing Capacity	10-14

LIST OF TABLES (Contd.)

10.4	PDA Result Summary : New Edison Bridge	10-16
11.1	Proposed S-N Equations for Prestressing Steel Strands	11-5
11.2	Fatigue Test Parameters	11-7
11.3	Comparison of Fatigue Results with Harajli & Namaan	11-22
13.1	Average Prestress Forces Before Loading (Group I)	13-2
13.2	Average Prestress Forces Before Loading (Group II)	13-2
13.3	Stress/Strength Ratios (Group I)	13-3
13.4	Stress/Strength Ratios (Group II)	13-4
14.1	Details of Experimental and Control Beams	14-4
14.2	Chemical Composition of Water Softening Pellets	14-4
14.3	Applied Load for Pre-cracked Specimens	14-7
15.1	Different Half-Cell Potential Thresholds for Corrosion	15-2
15.2	Different Concrete Resistivity Thresholds for Corrosion	15-10
15.3	Half-Cell Potentials (mV) for Un-cracked Specimens	15-11
15.4	Half-Cell Potentials (mV) for Pre-cracked Specimens	15-12
15.5	Nyquist's Plot Diameters (ohms) for Un-Cracked Specimens	15-12
15.6	Nyquist's Plot Diameters (ohms) for Pre-Cracked Specimens	15-12
15.7	Sequence of Steel Pre-Tensioned Beams Tested	15-13
15.8	Sequence of Fiberglass Pre-tensioned Beams Tested	15-14
16.1	Details of Steel Beams Tested	16-5
16.2	Ultimate Results for Steel Beams	16-6
16.3	Ultimate Results for Pre-cracked Steel Beams (in salt water)	16-6
16.4	Ultimate Results for Control Steel Beams	16-6
16.5	Details of Fiberglass Beams	16-10
16.6	Ultimate Results for Un-cracked Fiberglass Beams (in salt water)	16-12
16.7	Ultimate Results for Pre-cracked Fiberglass Beams (in salt water)	16-12
16.8	Ultimate Results for Control Fiberglass Beams	16-12
16.9	Corrosion Failure Mode for Fiberglass Pre-tensioned Beams	16-20
16.10	Summary of Corrosion Mode Failed Beams	16-21
16.11	Pull-Out Test Results (cast 12/28/89)	16-25
16.12	Durability Study (cast 03/13/90)	16-26

LIST OF FIGURES

1.1	Stress-Strain Relation For GFR Rods and its Components	1-4
2.1	Typical Stress-Strain Plot for Shell Epon Resin System	2-3
2.2	Stress-Strain Relation for S-2 Glass/Epon Resin Rods	2-9
2.3	Typical Stress-Strain Plot for S-2 Glass Strands	2-11
2.4	Stress-Strain Relation for S-2 Glass/Epon Resin Strands and Rods	2-12
3.1	Stress-Rupture for Polystal and Arapree	3-4
3.2	Relaxation of Different Prestressing Materials	3-4
3.3	Fatigue of Performance of Different Prestressing Materials	3-5
3.4	Schematized Long-Term Behavior in Alkaline Environment	3-7
3.5	Typical Stress-Strain Relations for Different Prestressing Materials	3-8
5.1	Strand Numbering and Fiberglass Strand Lengths	5-2
6.1	Strain Variation along Length for FG-M1	6-10
6.2	Strain Variation along Length for FG-M3	6-10
6.3	Strain Variation along Length for FG-W4	6-11
6.4	Strain Variation along Length for FG-M4	6-11
6.5	Strain Variation along Length for FG-E4	6-12
6.6	Strain Variation along Length for FG-E5	6-12
6.7	Strain Variation along Length for FG-M7	6-13
6.8	Strain Variation along Length for ST-W5	6-13
6.9	Strain Variation along Length for ST-M5	6-14
6.10	Strain Variation along Length for ST-M6	6-14
6.11	Strain Variation along length for ST-E6	6-15
6.12	Strain Variation along length for ST-M7	6-15
6.13	Transfer Length vs Time for Fiberglass and Steel Columns	6-16
6.14	Stress-Strain Curve for Concrete Tested at Release	6-16
7.1	Beam Details	7-2
7.2	Comparative Load Deflection Plot for 6 in. x 12 in. Beams	7-6
7.3	Comparative Load Deflection Plot for 6 in. x 10 in. Beams	7-6
7.4	Comparative Load Deflection Plot for 6 in. x 8 in. Beams (FG-M8)	7-7
7.5	Comparative Load Deflection Plot for 6 in. x 8 in. Beams (FG-M9)	7-7
7.6	Comparative Concrete Strain in 6 in. x 12 in. Beams	7-10
7.7	Comparative Strand Strain in 6 in. x 12 in. Beams	7-10
7.8	Comparative Concrete Strain in 6 in. x 10 in. Beams	7-11
7.9	Comparative Strand Strain in 6 in. x 10 in. Beams	7-11
7.10	Comparative Concrete Strain in 6 in. x 8 in. Beams	7-12
7.11	Comparative Strand Strain in 6 in. x 8 in. Beams	7-12
7.12	Comparative Crack Patterns in 6 in. x 12 in. Beams	7-14
7.13	Comparative Crack Patterns in 6 in. x 10 in. Beams	7-15
7.14	Comparative Crack Patterns in 6 in. x 8 in. Beams	7-16
7.15	Finite Element Mesh for Beam Study	7-18
7.16	Finite Element Load Deflection Correlation for Steel Beam	7-20
7.17	Finite Element Load Deflection Correlation for Fiberglass Beam	7-20
7.18	Finite Element Concrete Strain Correlation for Steel Beam	7-21

LIST OF FIGURES (Contd.)

7.19	Finite Element Concrete Strain Correlation for Fiberglass Beam	7-21
7.20	Finite Element Strand Strain Correlation for Steel Beam	7-22
7.21	Finite Element Strand Strain Correlation for Fiberglass Beam	7.22
8.1	Cross-Section and Lateral Reinforcement of Column Specimens	8-2
8.2	Column Test Set Up	8-3
8.3	Load-Strain Response for Column ST-C2	8-7
8.4	Load-Strain Response for Column FG-C2	8-7
8.5	Load-Strain Response for Column FG-C1	8-8
8.6	Load-Strain Response for Column FG-FG-C1	8-8
8.7	Load-Strain Response for Column ST-C1	8-10
8.8	Load-Strain Response for Column FG-FG-C2	8-10
8.9	Load-Deflection Response for Eccentrically Loaded Columns	8-11
8.10	Load-Strain Response for Axially Loaded Columns	8-11
8.11	Comparison of Load-Strain Variation in Eccentrically Loaded Columns	8-12
8.12	Finite Element Mesh	8-12
8.13	Test and Theoretical Load-Strain Response for Column ST-C2	8-13
8.14	Test and Theoretical Load-Strain Response for Column FG-C2	8-13
8.15	Test and Theoretical Load-Strain Response for Column FG-C1	8-14
8.16	Test and Theoretical Load-Strain Response for Column FG-FG-C1	8-14
8.17	Test and Theoretical Load-Strain Response for Column ST-C1	8-15
8.18	Test and Theoretical Load-Strain Response for Column FG-FG-C2	8-15
8.19	Test and Theoretical Load-Deflection Response for Eccentrically Loaded Columns	8-16
9.1	Pile Cross-Section and Tie Details	9-3
9.2	Boundary Conditions	9-7
9.3	Finite Difference Discretization	9-8
9.4	Soil Idealization	9-9
9.5	Blow Count for Test Site	9-12
10.1	Blow Count Variation with Depth (Site 1)	10-7
10.2	Blow Count Variation with Depth (Site 2)	10-7
10.3	Pile Driving Stresses (Site 1)	10-9
10.4	Pile Driving Stresses (Site 2)	10-10
11.1	Typical S-N Curve	11-1
11.2	Stress Moment Diagram	11-2
11.3	Fatigue Failure Envelope for Prestressing Steel	11-3
11.4	Load-Deflection Curves for Beam FG-W9	11-11
11.5	Load Deflection Curves for Beam FG-E9	11-11
11.6	Deflection vs Number of Cycles at $0.6P_u$ and $0.4P_u$	11-12
11.7	Crack Width vs Number of Cycles at $0.6P_u$ and $0.4P_u$	11-13
11.8	Concrete Strain vs Number of Cycles at $0.6P_u$ and $0.4P_u$	11-14
11.9	Prestressing Strand Strain vs Number of Cycles at $0.6P_u$ and $0.4P_u$	11-15
11.10	Comparison of Load Deflection for Beams FG-E9 and FG-E8	11-16
11.11	Comparison of Strains in Beams FG-E9 and FG-E8	11-18

LIST OF FIGURES (Contd.)

11.12	Crack Pattern for Beam FG-W9 and FG-E9	11-19
11.13	Maximum Fatigue Deflection Comparison with Namaan	11-20
11.14	Maximum Crack Width Comparison with Namaan	11-20
11.15	Comparison of Fatigue Life	11-21
12.1	Comparison of Creep Coefficient for Rig 1 (0.2f'c) with ACI	12-4
12.2	Comparison of Creep Coefficient for Rig 2 (0.3f'c) with ACI	12-4
13.1	Test Set Up Details (Plan View)	13-10
13.2	Typical Strain History of Shrinkage Specimen	13-11
13.3	Typical Strain History of Creep Specimen	13-11
13.4	Strain History for Fiberglass Column at Stress level 0.3f'c	13-12
13.5	Strain History for Steel Column at Stress Level of 0.3f'c	13-12
13.6	Strain History for Fiberglass Columns at Different Stress Levels	13-13
13.7	Strain History for Steel Columns at Different Stress Levels	13-13
13.8	Strain History for Fiberglass and Steel Columns at Midheight	13-14
13.9	Prestress Losses for Fiberglass and Steel Columns at Midheight	13-14
13.10	Prestress Losses for Fiberglass Columns at Different Stress Levels	13-15
13.11	Prestress Losses for Steel Columns at Different Stress Levels	13-15
13.12	Prestress Losses vs Stress/Strength Ratios	13-16
13.13	Effective Prestress for Stress Level of 0.3f'c	13-16
13.14	Measured and Predicted Strain History for Fiberglass Column	13-17
13.15	Measured and Predicted Effective Prestress for Fiberglass Columns	13-17
13.16	Strain History for Fiberglass Columns at Different Stress Levels	13-18
13.17	Strain History for Steel Columns at Different Stress Levels	13-18
13.18	Prestress Losses for Fiberglass Columns at Different Stress Levels	13-19
13.19	Prestress Losses for Steel Columns at Different Stress Levels	13-19
13.20	Effective Prestress for Fiberglass Columns at Different Stress Levels	13-20
13.21	Effective Prestress for Steel Columns at Different Stress Levels	13-20
13.22	Strain History for Fiberglass and Steel Columns at Midheight	13-21
13.23	Prestress Losses for Fiberglass and Steel Columns at Midheight	13-21
13.24	Effective Prestress for Fiberglass and Steel columns at Midheight	13-22
14.1	Beam Details	14-2
14.2	Beam Position in Tank	14-9
15.1	Half-Cell Potentials for Un-cracked Beam	15-3
15.2	Half-Cell Potentials for Pre-cracked Beam	15-3
15.3	Half-Cell Potentials for Un-cracked Control Beam	15-4
15.4	Half-Cell Potentials for Pre-cracked Control Beam	15-4
15.5	EIS Measurements for ST-M3	15-6
15.6	EIS Measurements for ST-E2	15-7
15.7	Concrete Resistivity for Pre-cracked Steel Beam in Tank № 1	15-9
15.8	Concrete Resistivity for Un-cracked Fiberglass Beam in Tank № 1	15-9
16.1	Load-Deflection for Un-cracked Steel Beams	16-7
16.2	Load-Deflection for Pre-cracked Steel Beams	16-7
16.3	Load-Deflection for Control Steel Beams	16-8

LIST OF FIGURES (Contd.)

16.4	Load-Deflection for Steel Beams — Shear Failure	16-8
16.5	Load Variation Relative to Time for Steel Beams	16-9
16.6	Load-Deflection for Un-cracked Fiberglass Beams	16-16
16.7	Load-Deflection for Pre-cracked Fiberglass Beams	16-16
16.8	Load-Deflection for Fiberglass Control Beams	16-17
16.9	Load-Deflection for Fiberglass Beams — Corrosion Failure	16-17
16.10	Load Variation Relative to Time for Fiberglass Beams	16-18
16.11	Variation of Concrete Strength with Time	16-22
16.12	Variation of Bond Stress with Time of Exposure	16-25
17.1	Typical Chloride Content for Un-cracked Beams — 1.0 in. Cover	17-8
17.2	Typical Chloride Content for Un-cracked Beams — 2.5 in. Cover	17-8
17.3	Typical Chloride Content for Pre-cracked Beams — 1.0 in. Cover	17-9
17.4	Typical Chloride Content for Pre-cracked Beams — 2.5 in. Cover	17-9
17.5	Typical Chloride Content for Control Beams — 1.0 in. Cover	17-10
17.6	Typical Chloride Content for Control Beams — 2.5 in. Cover	17-10

LIST OF PLATES

1.1	(top) John's Pass Bridge, Madeira Beach, FL (btm) Close up of Pile Corrosion in Splash Zone	1-2
2.1	(top) Overview of Pultrusion Process (btm) Glass Rovings Pulled through Epoxy Bath	2-6
2.2	(top) S-2 glass/epoxy Strand Instrumented for Tension Test (btm) Fabrication of Fiberglass Spiral for Columns	2-7
2.3	Set Up for Tension Test	2-10
4.1	(top) Fabrication of Stirrups for Beams (btm) Fabrication of Spiral Ties for Piles and Columns	4-7
4.2	(top) Pretensioning Bed (btm) Header Plate at Ends	4-8
4.3	(top) End Form for Specimens (btm) Concreting of Specimens	4-12
4.4	(top) Curing of Specimens (btm) Release of Prestressing Force	4-13
4.5	(top) Failure of Fiberglass Strand (03/13/90) (btm) Reinforcement Cage for Beams	4-15
4.6	(top) Installation of Forms (btm) Adjustment of End Eccentricity	4-16
4.7	(top) Reinforcement of FG-W8 and FG-W9 (btm) Release of Prestress Force	4-17
4.8	(top) Transfer Block Bolted to Header Plate at Dead End (btm) Fiberglass/steel Transfer Blocks in Bed	4-19
4.9	(top) Load Cells at Jacking End (btm) Prestressing Jack Used	4-21
4.10	(top) Instrumented Fiberglass Pile with Steel Ties (btm) Instrumented all Fiberglass Pile before Concreting	4-22
4.11	(top) Instrumented Fiberglass Column with Steel Ties (btm) Instrumented all Fiberglass Column before Concreting	4-23
4.12	(top) Instrumented Steel Pile Prior to Pour (btm) Instrumented Steel Column Prior to Pour	4-24
4.13	(top) Concreting of Specimens (btm) Curing of Specimens	4-25
4.14	(top) Release of Prestress Force in Steel Specimen (btm) Removal of Fiberglass Pile Specimen from Bed	4-26
6.1	(top) Transfer Length Study (12/22/89) (btm) Transfer Length Study (03/13/90)	6-3
7.1	(top) Set Up of LVDTs (btm) Measurement of Crack Width in Fatigue Test	7-4
7.2	(top) Deflection in Beam FG-E8 at 90% of its Failure Load (btm) Deflected Form of FG-M8 at Failure	7-8
8.1	End Failure in Column	8-6

LIST OF PLATES (Contd.)

9.1 (top)	Aerial View of Tierra Verde	9-2
(btm)	Hidden Lagoon site	
9.2	Drop Hammer used for Test Piles	9-14
9.3	Pile Driving Rig and Set Up	9-15
10.1	Test Pile Layout	10-3
10.2 (top)	Strain Transducer, upper; Accelerometer, lower	10-5
(btm)	PDA Set Up for Testing	
10.3	View of Piles after Driving at Site 1	10-11
10.4 (top)	Pile Damage after 15 ft Drop Test at Site 2	10-12
(btm)	Rupture of Fiberglass Ties in FG-FG-P1	
11.1 (top)	View of Beam FG-W9 after Fatigue Failure	11-9
(btm)	Close up of Large Crack at Mid-Span	
11.2 (top)	View of FG-E9 after 1.75 million Cycles	11-17
(btm)	Ultimate Deflected Shape of FG-E9 after Static Test	
12.1	Set Up and Instrumentation for Creep Study	12-2
13.1	Three Sets of Compression Members in Laboratory Environment	13-8
13.2	Three Sets of Compression Members in Environmental Chamber	13-9
14.1 (top)	Placing Salt in Mixing Container	14-5
(btm)	15% Salt Solution in Test Tank	
14.2 (top)	High Tide - Tank № 1	14-6
(btm)	Low Tide - Tank № 2	
14.3 (top)	Application of Epoxy Coating at Ends	14-8
(btm)	Marking Locations for Half-Cell Readings	
16.1 (top)	Typical Set Up for Steel Pretensioned Beam	16-2
(btm)	Typical Set Up for Fiberglass Pretensioned Beam	
16.2 (top)	Compression Failure Mode in Steel Beam	16-13
(btm)	Compression Failure Mode in Fiberglass Beam	
16.3 (top)	Shear Failure Mode in Fiberglass Beam	16-14
(btm)	Corrosion Failure Mode in Fiberglass Beam	
16.4 (top)	Corrosion Failure in Pre-cracked Fiberglass beam	16-15
(btm)	Close Up of Failure	
16.5 (top)	Corrosion Failure in Wet Half after 9 Months	16-19
(btm)	Corrosion Failure in Wet Half after 18 Months	
16.6 (top)	Fabrication of Pull Out Specimens	16-23
(btm)	Set Up for Pull Out Test	
17.1 (top)	Sawing Beam	17-3
(btm)	Fiberglass Beam after 12 months in Tank	
17.2 (top)	Carbonation Tests on ST-M2	17-5
(btm)	Metal Loss in Steel Strand in ST-M3	
17.3 (top)	Filtration of Digested Sample	17-7
(btm)	Potentiometric Titration of Sample	
18.1 (top)	Permanently Wet Sample in Concrete for 18 Months	18-2
(btm)	Unexposed Fiberglass Sample Used as Control	

LIST OF PLATES (Contd.)

18.2	(top) Unexposed Control Specimen at $\times 4,500$	18-4
	(btm) Always Dry Specimen at $\times 4,000$	
18.3	(top) Splash Zone Specimen away from Concrete Interface	18-5
	(btm) Splash Zone Specimen near Concrete Interface	
18.4	(top) Submerged Specimen away from Concrete Interface	18-6
	(btm) Submerged Specimen near Concrete Interface	

LIST OF SYMBOLS AND ABBREVIATIONS

AR	= Alkali Resistant
A _s	= Area of prestressing strand
b	= Width of beam
B	= Corrosion constant for iron
d	= Distance from extreme compressive fiber to centroid of prestressing force
Defl	= Deflection
e	= eccentricity
E _c	= Modulus of elasticity of composite
E _f	= Modulus of elasticity of fiber
E _i	= Initial modulus of elasticity of concrete
E _L	= Longitudinal Modulus
E _m	= Modulus of elasticity of matrix
E _s	= Secant modulus of elasticity of concrete Young's modulus of prestressing strands
E _T	= Transverse Modulus
f' _c	= Compressive strength of concrete
FG	= Fiberglass pre-tensioned specimen
F _I ^{su}	= Inter-laminar Shear
F _L ^{cu}	= Longitudinal Compression
F _L ^{su}	= In-Plane Shear
F _L ^{tu}	= Longitudinal Tension
F _T ^{cu}	= Transverse Compression

LIST OF SYMBOLS AND ABBREVIATIONS (Contd.)

F_T^u	=	Transverse Tension
FRP	=	Fiber Reinforced Plastic
f_{pe}	=	Effective stress
f_{pu}	=	Ultimate strength of prestressing steel
G_{LT}	=	Axial Shear Modulus
gr/cc		Grams per cubic centimeter
GRP	=	Glass Reinforced Plastic
hr	=	hour
I_{corr}	=	Corrosion current
in.	=	inches
ksi	=	kilo-pounds per square inch
lbs	=	pounds
M_{cr}	=	Cracking moment
mth	=	Months
M_u	=	Ultimate moment
P_c	=	Load carried by the composite
P_{cr}	=	Cracking load
P_f	=	Load carried by the fiber
P_e	=	Effective prestress force
phr	=	Parts per hundred
P_i	=	Initial prestressing force

LIST OF SYMBOLS AND ABBREVIATIONS (Contd.)

ppm	=	Parts per million
psi	=	pounds per square inch
P _u	=	Ultimate load
R _p	=	Polarization resistance
ST	=	Steel pre-tensioned specimen
v _f	=	Fiber content in volume
β ₁	=	Factor for concrete strength
ε _L ^{cu}	=	Longitudinal Compression
ε _T ^{cu}	=	Transverse Compression
ε _L ^{tu}	=	Longitudinal Tension
ε _T ^{tu}	=	Transverse Tension
ν _{LT}	=	Poisson's Ratio
γ _T ^u	=	In-Plane Shear
σ _c	=	Tensile strength of composite
σ _f	=	Tensile strength of fiber
σ _m	=	Tensile strength of matrix
σ _(t)	=	Tensile strength at time t
σ _u	=	Ultimate tensile strength of composite
ω _p	=	Reinforcing index for prestressed beams
°F	=	Degrees Fahrenheit
°C	=	Degrees Centigrade

1. INTRODUCTION

1.1 Introduction

Florida's long coastline and sub-tropical climate makes reinforcing and prestressing steel vulnerable to corrosion. Over the last seventy five years measures adopted to control it, such as increasing the cover, reducing the permeability, using epoxy coating, have not always proven effective. Indeed, a recent random survey of fifteen Florida bridges, Powers 1988 [1.1] indicated that on an average, visible corrosion was evident, within 11.5 years of construction.

Corrosion is particularly prevalent in elements such as prestressed concrete piles that are exposed to the 'splash zone', i.e. within 2-6 ft of the water line (see Plate 1.1). The combination of deposition of salt on the pile surface and alternate dry/wet cycles due to tidal changes provide ideal conditions for corrosion in steel. Its inevitability is even factored in current Florida Department of Transportation Structures Design Guidelines [1.2]. This requires prestressed piles located in saltwater or brackish water exceeding a 0.2 % chloride content to be at least 24" x 24", *regardless of loading*. The rationale is that in time spalling of the concrete cover will reduce the cross-section so that if a 24 in. square pile were used originally, a central core of 18 in. square would remain. While this may be a structurally safe solution, cosmetic repairs may still be needed to allay public concerns for safety. Consequently, the continuing use of prestressed (steel) piles is very costly to the State both in initial costs (because of over design) and in subsequent maintenance costs.

A possible solution for Florida's corrosion problem is the use of new prestressing materials'. Such materials must not only match steel's high strength, stiffness and ductility but also its low cost, ready supply and ease in construction. More importantly, it must provide high resistance to corrosion.

1.2 New Prestressing Materials

Over the past decades, advances in composite materials has led to the development of several high strength, lightweight *fiber reinforced plastics, FRP*. Of the commercially available fibers three, *glass*, *aramid* and *carbon* fibers, have the necessary combination of strength and stiffness suitable for prestressing (see Table 1.1). Resins or polymers form the continuous matrix to which these fibers are bonded. The most commonly used resins are *polyesters*, *vinylesters* and *epoxies*, Rostasy, 1988 [1.3]. Although, these composites are more expensive than prestressing steel (see Table 1.2), *life cycle costs may be significantly lower*, Gerritse and Schurhoff, 1986 [1.4], Dolan, 1990 [1.5].

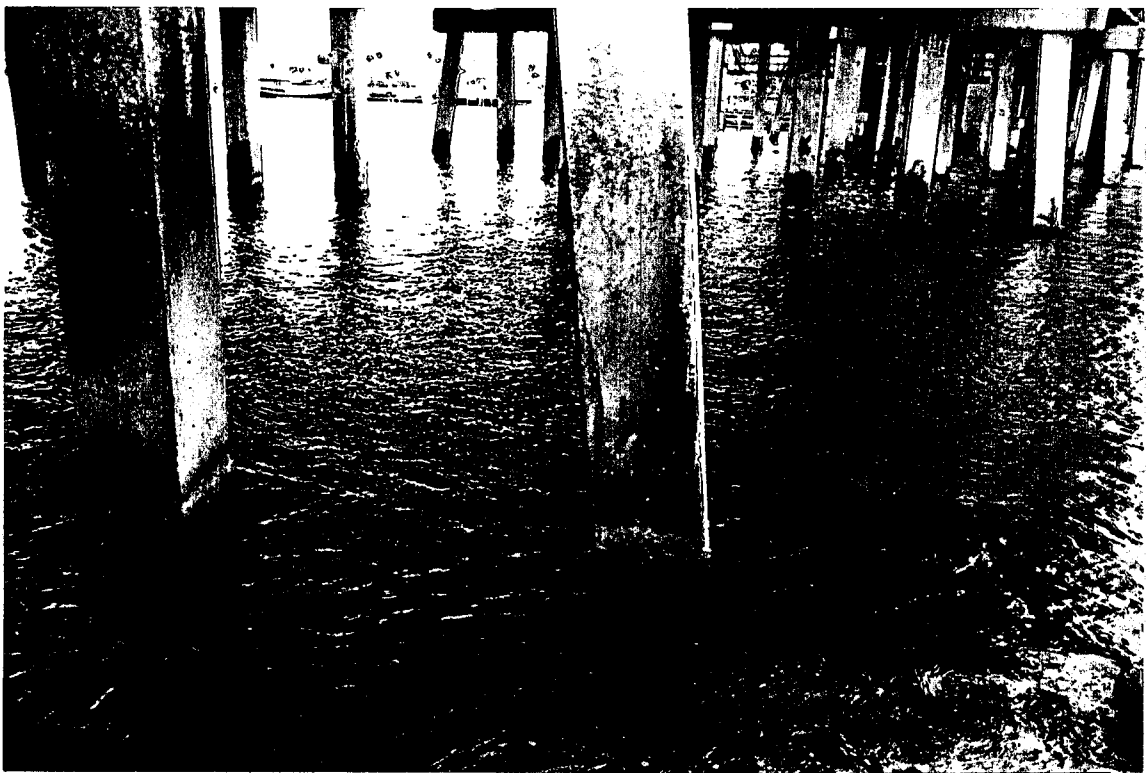


Plate 1.1 (top) John's Pass Bridge, Madeira Beach, FL
(btm) Close up of pile corrosion in splash zone

Table 1.1 Properties of High-Strength Fibers [1.7]

Type of Fiber	Brand Name	Tensile Strength (ksi)	Modulus of Elasticity ($\times 10^6$ psi)	Producers (examples)
Glass	E Glass	334	10.7	<i>Bayer AG</i>
	E Glass ¹	525	10.3	<i>Owens-Corning</i>
	S Glass	566	12.6	<i>Owens-Corning</i>
	S-2 Glass ¹	550	10.5	<i>Owens-Corning</i>
Aramid	Twaron HM	406	18.1	<i>Aramid Maatschappij</i>
	Kevlar 49	384	18.6	<i>Du Pont</i>
Carbon	Carbon HP; HS	464	33.4	<i>Hysol Grafil</i>
	Carbolon	435	33.4	<i>Enka/Nippon Carbon Co.</i>
	Torayca T300	464	33.4	<i>Toray Industries</i>
	Besfight HTA ²	526	34.0	<i>Toho Rayon Co.</i>

¹ From reference [1.8]

² From reference [1.9]

Table 1.2 Relative Cost of Non-Metallic Prestressing Materials [1.10]

Fiber Reinforcement	Glass	Carbon	Aramid	High-Tensile Steel Wire
Fiber Fraction, % wt	80	72	67	---
Materials Cost Ratio* on a Weight Basis	6	16-20	10-15	1
Materials Cost Ratio* on a Strength Basis	3	4-5	2-3	1
Materials Cost Ratio* on a Stiffness Basis	7	5-6	5-8	1

* Materials cost ratio here is the 1987 cost relative to steel wire for use in cables or ropes. Cost ratios for other applications will be different.

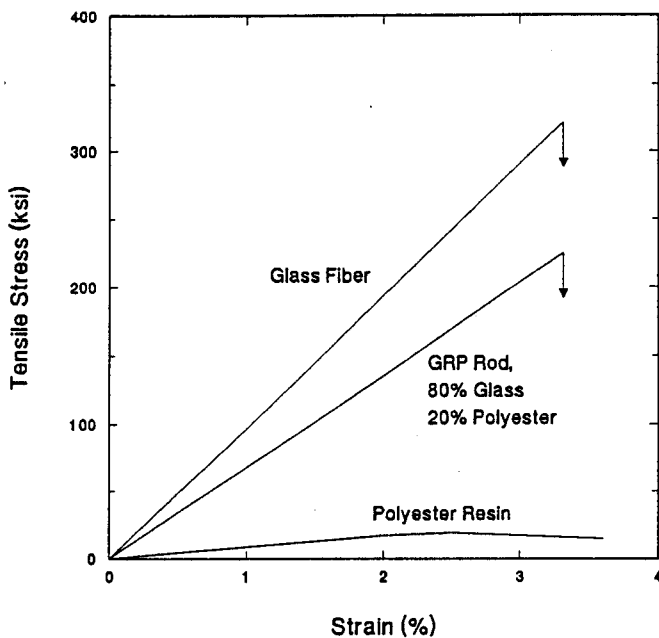


Figure 1.1 Stress-Strain Relation for GFR Rods and its Components [1.11]

The high strength fibers make up between 60 to 70% of the reinforced plastic cross-section. Since they are much stiffer than the polymer matrix (see Figure 1.1), they carry most of the load, Mallick, 1988 [1.6]. However, stresses are generally calculated on the basis of the gross cross sectional area so that the actual fiber stresses are as much as 40%-70% higher [1.5].

The polymer matrix serves several critical functions beyond simply holding the reinforcement in place. It acts as a physical barrier against environmental effects, e.g. temperature, humidity, ultraviolet light and also protects the fiber surface from corrosion or abrasion. Moreover, it distributes the longitudinal load taken by the reinforcement. It is evident that by changing the type and content of the resin, FRPs can be designed to fulfil exact service needs. The resin industry's considerable experience in defence and aerospace applications provides the necessary background to achieve such an objective. Glass fiber reinforced composites have been in use since the 1920s and indeed fiberglass was the first alternative material used for prestressing concrete, Rubinsky & Rubinsky, 1951 [1.12]. Subsequent developments have taken place mostly in Germany where E Glass fibers in polyester resin (trademark Polystal® by Bayer AG, Germany) have been used to prestress major structures. Several bridges have been built and others are planned or are under construction, Miessler & Preis [1.13]. The first posttensioned application of fiberglass in the US was in a section of the slab in a bridge deck in the South Dakota Cement Plant, Iyer 1992 [1.14].

Aramid fiber reinforced composites are much stiffer and stronger than glass. Prestressing applications using aramid fibers (trademark Kevlar* by Du Pont, USA) in thermoplastic sheath tendons (trademark Parafil® G by Imperial Chemical Industries, Great Britain) were reported in 1985, Burgoyne & Chambers, 1985 [1.15]. In the United States, the first prestressing applications using Kevlar (aramid) fibers were conducted by Dolan, 1989 [1.16]. The major development of this fiber, however, was carried out in Europe, Gerritse & Werner, 1991 [1.17] where aramid fibers (trademark Twaron® by Aramide Maatschappij v.o.f, The Netherlands) in epoxy resin (trademark Arapree® by AKZO, Germany and Hollandsche Beton Groep nv, The Netherlands) were recently used in the construction of a noise barrier along a busy freeway near Rotterdam.

Carbon fibers were first produced by Shindo, Japan, in 1964, Chawla, 1987 [1.18]. Carbon Fiber Composite Cables (carbon fibers in epoxy resin) were developed by Tokyo Rope Mfg. and Toho Rayon, Japan, and used in a pre-tensioned application for the construction of a pilot bridge in Japan, Tokyo Rope, 1989 [1.10].

Several important differences between fiber reinforced plastics and metals should be recognized

1. They are anisotropic, i.e. elastic, physical and mechanical properties are direction dependent. Strengths are maximum in the direction of the fibers (longitudinal) and minimum in the orthogonal (transverse) direction.
2. Their long-term tensile strength under sustained loading is considerably lower than the short-term value.
3. They are brittle materials having a low ultimate strain and a linear strain-stress curve with no yielding.
4. They may be more vulnerable in an alkaline environment rather than an acid environment where steel corrodes.
5. Their modulus of elasticity is lower than that of steel.
6. Their properties may vary depending on the fiber content but more importantly on the degree of fiber alignment achieved during production.

These differences have profound implications on their use as prestressing materials and have to be integrated in design, fabrication and construction procedures.

1.3 Material used for study - S-2 Glass/epoxy

As already noted, fiberglass is not only the cheapest alternate prestressing material (see Table 1.2) but also the one most used to date in both model and full scale construction.

In view of this, fiberglass was selected for this study. S-2 glass fibers were used because of its toughness and superior resistance to fatigue and impact. An epoxy resin was used since the amine cured resins are among the best systems for resisting the effects of an alkaline and saline environment. A complete description of material properties is presented in Chapter 2.

Although fiberglass has been extensively used in Germany, its applications have been limited to *post-tensioned* construction that is relatively rare in the United States. If new materials are to be serious challengers for replacing steel, then the feasibility of pretensioned applications must be demonstrated. Consequently, this study only considered pretensioned application of fiberglass.

1.4 Previous studies

Although great strides have been made in the post-tensioned application of fiberglass in the past decade, e.g. Miesseler and Preis [1.13] comparatively little progress has been made in pretensioned applications. Unfortunately, many important design parameters in post-tensioned and pretensioned construction are *mutually exclusive*. For example, transfer length is important in pretensioned construction but is irrelevant in post-tensioned construction where prestress loads are directly transferred by permanent anchors. Similarly, durability of fiberglass in an alkaline concrete environment is a major concern for pretensioning but is inconsequential in post-tensioned construction since strands are protected from the concrete. In any event, since the resin system used plays such a critical role in the performance of the fiberglass composite, long term properties relating to corrosion resistance, creep rupture or fatigue resistance from the German studies (using E-glass and a polyester resin) will be different for the S-2 glass/epoxy composite used in this study.

Only a few studies relating to the pretensioned fiberglass beams have been reported in the literature. The overwhelming technical problems associated with gripping and tensioning fiberglass restricted the scope of earlier studies. Even where specimens were successfully pretensioned, premature failures were often recorded, e.g. Somes, 1963; US Corp of Engineers, 1967 [1.19, 1.20] which used E-glass. More recently, results for S-2 glass/polyester composites were reported by Iyer & Kumeraswamy, 1988 [1.21]. Preliminary findings from a follow-up study using S-2 glass/vinylester composites are reported in Iyer, Khubchandani and Feng, 1991 [1.22].

1.5 Objectives and Scope of Study

The aim of this study was to investigate pretensioning applications of S-2 glass/epoxy composites. Piles were selected as the primary structural member since they are relatively simple to prestress and offered the prospect of immediate application in view of corrosion problems experienced in Florida. To facilitate such an application,

fiberglass piles were cast at a commercial prestressing yard using plant and equipment normally used for fabricating steel pretensioned piles.

Since the properties of the fiberglass composites are dependent on the properties of the fiber and resin system used, complete reliance cannot be placed on results obtained by other researchers using different resin systems. In view of this, several studies were initiated to examine the short term and the long term response of pretensioned elements using S-2 glass/epoxy composites.

The short term study included tests for the determination of transfer length, static flexure, axial compression and impact resistance of fiberglass pretensioned piles. The long term study examined cyclic fatigue resistance, creep and durability of fiberglass pretensioned specimens in simulated tidal conditions. Details of these studies are summarized in Tables 1.3 and 1.4.

Table 1.3 Test Program for Short-Term Studies

Study	Number	Type	Size (in × in × ft)	Remarks
<i>Transfer Length</i>	7	FG		
<i>Flexure</i>	7	ST	6 × 4 × 8.5	Specimens from durability and structural creep study.
	4	FG	6 × 8 × 8.5	
<i>Compression</i>	3	ST	6 × 10 × 8.5	Under-reinforced specimens, tested under 2 point loading.
			6 × 12 × 8.5	
				Two all fiberglass columns; four axial and two eccentric tests with $e/h = 0.25$.
<i>Pile Driving</i>	4	FG		Two all FG specimens, driven by 3 kip drop hammer in dense sand.
	2	ST	10 × 10 × 25	

In all the studies (excepting fatigue where comparisons would be somewhat meaningless because minimum stress in steel and fiberglass differed), the response of the fiberglass specimens was evaluated by comparison with an identical steel pretensioned specimen that had been cast *simultaneously*. The steel specimens were designed to current specifications. Fiberglass strands were then provided in the comparable section to ensure that the prestressing force was identical. In essence, the service response of the fiberglass specimens was designed to be the same as that of its steel counterpart. The study took slightly over two years to complete. In the first year, basic tests were conducted relating to transfer length and flexural response of beams. Additionally, all specimens required for long term durability and creep studies were cast. In the second year, columns and piles were fabricated and tested and the long term studies concluded.

Table 1.4 Test Program for Long-Term Studies

Study	Number	Type	Size (in × in × ft)	Remarks
<i>Cyclic Fatigue</i>	2	FG	6 × 10 × 8.5 6 × 12 × 8.5	Two million cycles at 3 Hz followed by static test.
<i>Concrete Creep</i>	2	---	6 × 12 cyl.	Axial compression at 0.2 f'c and 0.3 f'c for 19 months.
<i>Structural Creep¹</i>	6	FG	6 × 4 × 8.5	Axial compression at 0.2 f'c and 0.3 f'c in air and controlled environment for 15 months.
<i>Durability</i>	12	FG ST	6 × 4 × 8.5	Sixteen specimens, half pre-cracked, exposed to wet/dry cycles in 15% salt water for 20 months.
<i>Bond Strength</i>	9	FG ST	3 × 3 × 1	Eight unstressed specimens exposed to wet/dry cycles in 15% salt water for 17 months.

¹ At UIC

1.6 Organization of Report

This report is organized into *four* segments covering *materials and fabrication* (Chapters 2 and 3), *short term tests* (Chapters 5-10), *long term tests* (Chapters 11-18) and *conclusions and recommendations* (Chapters 19-20).

The material properties of the S-2 glass/epoxy composites used in this study are presented in Chapter 2. A brief summary of the long term response of FRPs is contained in Chapter 3 for completeness. The fabrication of *all* the pretensioned specimens is described in Chapter 4 to avoid repetition.

The analysis of short term losses in beams and columns is discussed in Chapter 5. The results from the transfer length study is presented in Chapter 6. The static response of beams and columns are described in Chapters 7 and 8 respectively. Background information related to the pile study is contained in Chapter 9. The actual results from the pile testing are summarized in Chapter 10.

The results of the long term fatigue tests are described in Chapter 11. Material creep in concrete is discussed in Chapter 12. The long term creep study conducted at the University of Illinois at Chicago is presented in Chapter 13. The major thrust of the long term study, the durability of fiberglass pretensioned specimens is covered in Chapters 14-18. The conclusions from each of the studies together are summarized in Chapter 19. Its overall implications and recommendations for future work are contained in the last chapter.

2. PROPERTIES OF S-2 GLASS®

2.1 Introduction

This chapter provides essential data on S-2 Glass®/epoxy composites used in this project. The properties of fibers and the epoxy resin used are presented in Sections 2.2 and 2.3, respectively. The pultrusion process used for manufacturing the S-2 Glass rods and the fiberglass ties is described in Section 2.4. The results of tension tests for pultruded rods and strands reported by Iyer, 1991 [2.1] are summarized in Section 2.5 and 2.6 respectively. Finally, a brief discussion on anchorage systems is included in Section 2.7 for completeness.

2.2 Fibers

Glass fibers are silica based (50-65 % SiO₂) filaments 5-25 microns (1 micron = 0.00004 in.) in diameter. They are designated as "E, C or S" glass depending on their composition and properties. E (electrical) glass, the most popular, is a good electrical insulator besides having good strength and reasonable Young's modulus. C (corrosion) glass has a better resistance to chemical corrosion. S (strength) glass provides superior strength, modulus and heat resistance.

In filament form, fiberglass has a high tensile strength and a low modulus of elasticity compared to steel making it very attractive for prestressing purposes. A tensile strength of 700 ksi and a Young's modulus of 12.4x10⁶ psi were recorded in laboratory tests, Nawy & Neuwerth, 1977 [2.2].

Glass fibers have properties that make it useful in many applications. Some of these are inherent to glass such as hardness, strength, transparency, resistance to attack, stability, and inertness. It is incombustible, inorganic, non-absorbent and chemically stable. Its fiber form provides characteristics such as flexibility, processing capability and low weight. Compared to high strength steel, it has a high strength-to-weight ratio and is 33.5 as strong on a pound-per-pound basis, Owens-Corning, 1985 [2.3].

2.2.1 S-2 Glass®

S-2 Glass® is a trademark product of Owens-Corning Fiberglass Corporation, Toledo, Ohio, and is a lower cost version of the military grade S glass fiber. It is a low alkali, magnesia alumina-silicate. The chemical composition of E Glass and S-2 Glass are summarized in Table 2.1.

Table 2.1 Approximate Chemical Composition of S-2 and E Glass Fibers [2.4]

Component (Wt%)	S-2 Glass	E Glass
SiO ₂	65	55
CaO	--	19
Al ₂ O ₃	25	14
B ₂ O ₃	--	6
MgO	10	0.5
Na ₂ O, K ₂ O	--	1.2
Other'	*	4.3

' Other includes Fe₂O₃, Zr₂O₃, TiO₂, ZnO**Table 2.2** Typical Properties for S-2 and E Glass Fibers [2.5]

Property	ASTM Standard	E Glass	S-2 Glass
Density , gr/cc	C693	2.58-2.61	2.47-2.50
MOH Hardness		6.5	6.5
Tensile Strength , ksi at			
72°F (Single Filament)	D2101	500-550	665-700
700°F		380	545
1000°F		250	350
Tensile Strength , ksi at	D2343		
72°F (Impregnated Strand)		270-390	530-620
Tensile Modulus , x 10 ⁶ psi at			
72°F	D2343	10-10.5	12.5-13
1000°F		11.8	12.9
Failure Strain , %	D2343	4.5-4.9	5.4-5.8
Toughness , ksi	D2343	9-10	12-13
Creep , % of Initial Strain at 50% of Strength, 10,000 Hours	D2990	10-20	5-15
Moisture Regain , %	D1990	0	0

According to its manufacturer, S-2 Glass is said to be a glass fiber with better properties in comparison to those of conventional glass (E glass), aramid and carbon fibers. Also, it offers better weight and cost performance with a combination of six enhanced properties: strength, impact resistance, stiffness, temperature resistance, fatigue resistance and radar transparency, Owens-Corning, 1990 [2.5].

S-2 Glass is currently used in a wide range of applications from firemen's air bottles, helicopter blades, wind surfers and running shoes to catalytic filters, aircraft flooring, shipboard armor and Space Shuttle booster rockets. It is said to outperform other materials for its high strength, toughness and low weight; and for having a better modulus of resilience, Owens-Corning, 1990 [2.5]. A comparison of the properties of E Glass and S-2 Glass fibers is presented in Table 2.2.

2.3 Resin Matrix

Epon® Resin 9310 (trademark by Shell Chemical Company, Houston, Texas) was used in the production of the S-2 Glass rods utilized in this study. This epoxy system uses Epon Curing Agents 9360 and Epon Curing Agents Accelerator 537, also produced by Shell [2.6].

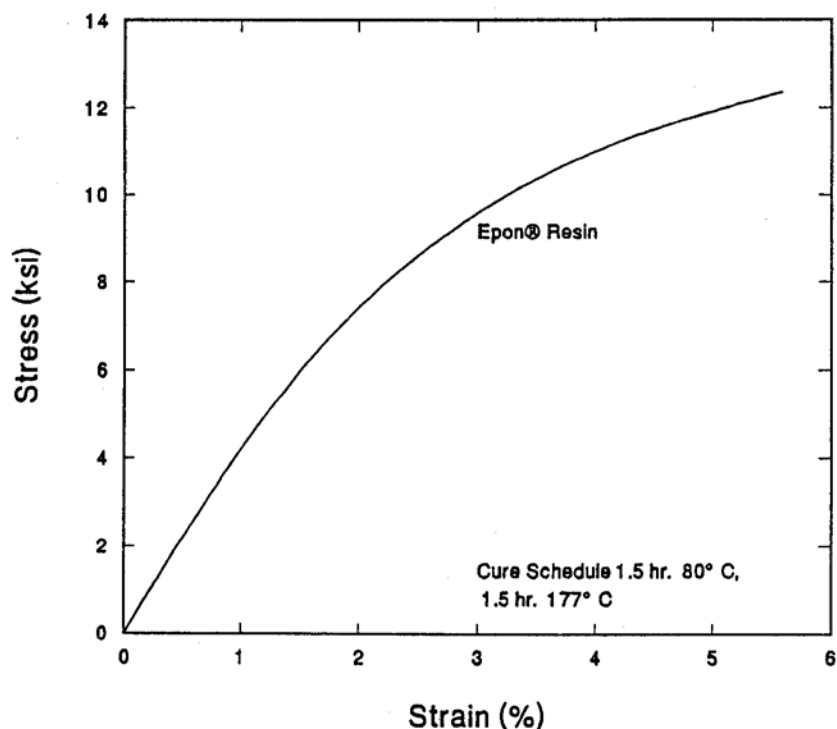


Figure 2.1 Typical Stress-Strain Plot for Shell Epon Resin System

Epon resin is a low viscosity, quick curing resin system based on a bisphenol A epoxy resin, modified with reactive monomer. The Epon Curing Agent is a mixed aromatic amine system, also modified with a reactive monomer. In pultrusion, this system is said to proceed at high line speeds with low back loads and good surface quality. Additionally, it is stable in many corrosive environments, has excellent fatigue resistance and retains its properties up to 150°C.

Table 2.3 shows typical properties of the un-reinforced resin for the recommended mix ratio and two curing schedules. A generic plot of the stress-strain curve for Epon resin is shown in Figure 2.1.

Table 2.3 Typical Properties for the Un-reinforced Epon® Resin 9310 System [2.6]

Property	System A ¹	System B ²
Density, gr/cc	1.18	1.20
Moisture Absorption³, % wt, 14 days	1.5	--
Tensile Strength, ksi at		
73°F	11	11
300°F	--	3.8
Tensile Modulus, ksi at		
73°F	450	453
300°F	--	205
Failure Strain, % at		
73°F	4	4.0
300°F	--	5.2
Flexural Strength, ksi at		
73°F, dry	16	--
200°F, dry	11	--
200°F, wet	10	--
250°F, dry	9	--
Flexural Modulus, ksi at		
73°F, dry	457	--
200°F, dry	322	--
200°F, wet	320	--
250°F, dry	273	--

¹ Cure schedule: 1.5 hours at 175°F, 1 hour at 350°F.

² Cure schedule: 1 hour at 175°F, 1 hour at 250°F, 1 hour at 300°F, 2 hours at 350°F.

³ Sample immersed in 200°F water.

2.4 Pultrusion Process

The fiberglass rods used were made by a process called pultrusion that has been used since 1948 for making profile shapes [2.7]. In this process, fiberglass bundles are pulled continuously through a thermosetting resin bath, then shaped into a circular cross-section through a shaping die and cured to hardness. The process is continuous and is activated primarily through the application of heat that initiates a chemical reaction in the resin compound as it passes through the die. Since curing must take place during passage through the die, lengths of three feet or more are not uncommon. The pultrusion process ensures that all fibers are oriented in the same direction so that a high strength fiberglass composite is produced.

The first set of 0.113 in. diameter S-2 Glass rods used in the December 1989 pour were pultruded by Owens Corning. Subsequently, Polygon (Walkerton, Indiana) made the pultruded rods with the same fiber volume but increased the diameter of the rods to 0.125 in. to provide a smooth finish, Iyer 1991 [2.1]. A fiber content of 78% by weight (65 % by volume) was used in the pultrusion process. The effective area of the pultruded rod, based on the effective diameter of 0.113 in. is 0.01003 in².

Plate 2.1 shows part of the pultrusion process for S-2 Glass rods used in the pile and column study (Courtesy, Polygon, IN).

2.4.1 Fiberglass spirals

Fiberglass spirals were used in the fabrication of two of the column and pile specimens. E Glass fibers (see Table 2.2) were used since it could provide the required force with Shell Epon 815 resin (modulus of 450,000 psi and ultimate tensile strength of 10,500 psi) and catalyst U, for room temperature cure. The fiber content was 70 % by volume. The internal dimensions of the spirals were 5.5 in. x 5.5 in. and the cross-sectional area was determined on the basis of force equivalency, i. e. the force in the steel and spiral tie were identical although two different cross-sectional areas of 0.0227 in² and 0.0303 in² were used to determine their relative performance. The pitch for the spirals was the same that of the steel ties (see Figure 9.1). It was made in Rapid City, SD by Dr. Iyer by winding the wet fiberglass yarn around a wooden mold covered by a polyethylene sheet. For the 25 ft piles, the spirals were made in two sections as shown in Plate 2.2 (Courtesy, Iyer, 1991).

2.5 S-2 Glass Rods

Since the properties of the fiberglass rods depend on the degree of alignment of the fibers and the effectiveness of the curing process, there is considerable scatter in the measured mechanical properties. Table 2.4 summarizes typical property variations of S-2 Glass rods impregnated with various epoxy systems.

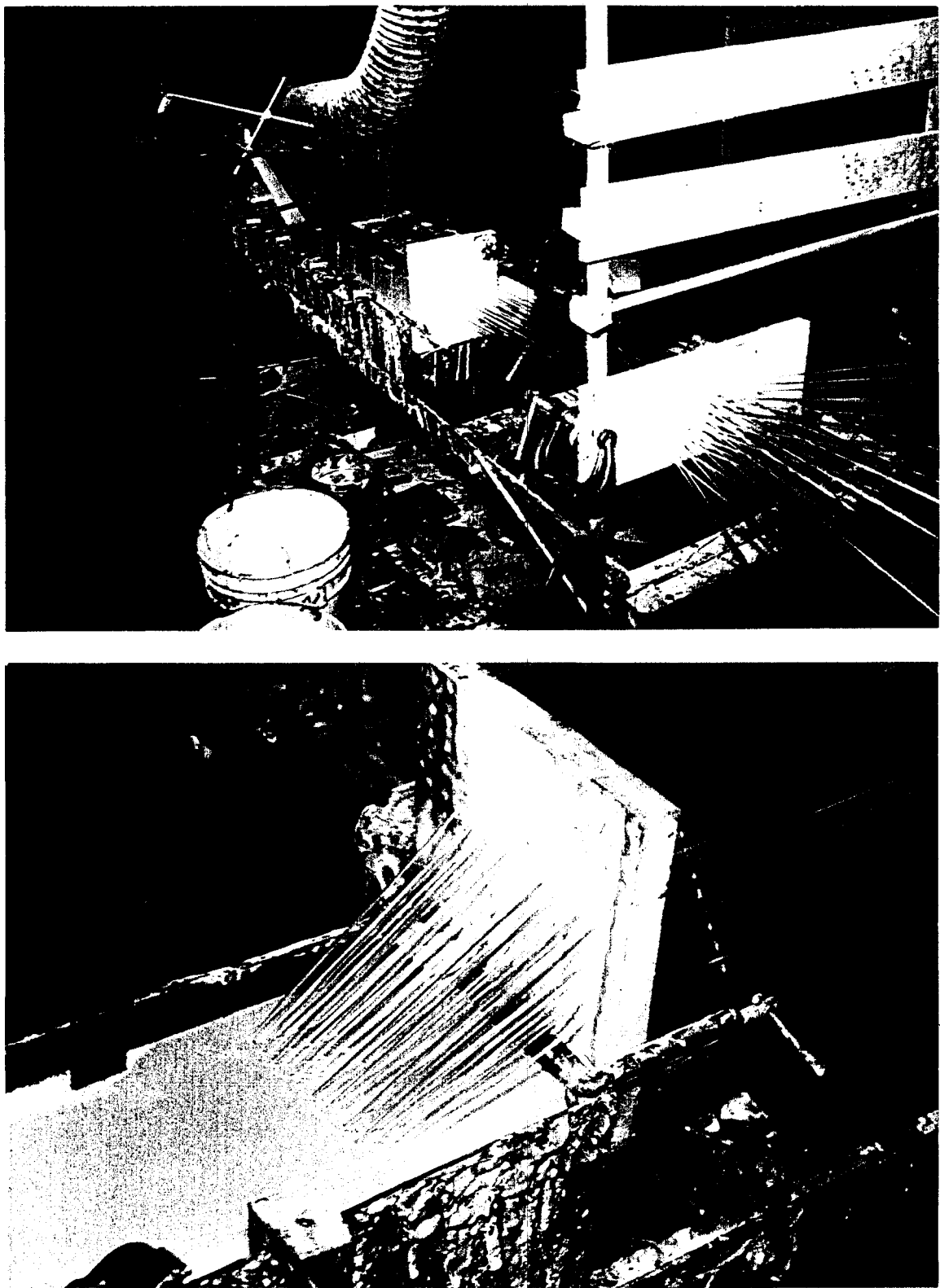


Plate 2.1. (top) Overview of pultrusion process
(btm) Glass rovings pulled through a resin bath
(Courtesy, Polygon Company)

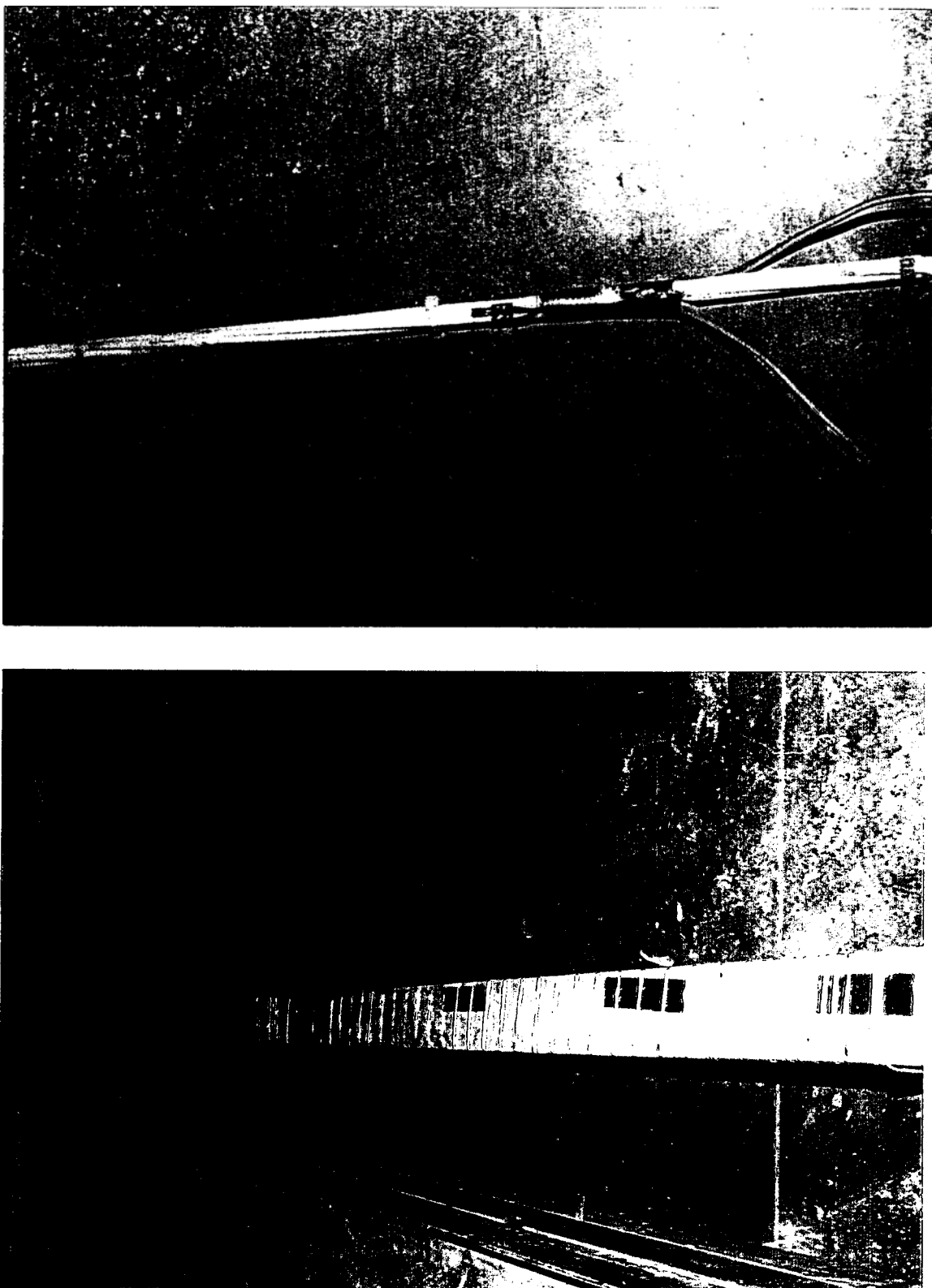


Plate 2.2 (top) S-2 glass/epoxy strand instrumented for tension test
(btm) Fabrication of fiberglass spiral for columns (Courtesy Dr. Iyer)

The S-2 Glass rods pultruded by Owens Corning are estimated to have approximately 69,000 glass fibers. The short-term ultimate strength reported by Owens-Corning for such a rod (83% fiber content by weight) indicated a tensile strength of 313 ksi, an ultimate strain of 3.7%, and an initial modulus of elasticity of 9.56×10^6 psi, as shown in Figure 2.2, Greenwood, 1990 [2.8]. Inspection of this figure shows that the response is linear up to a strain of 2.5%, and non-linear beyond. This indicates, of course, that the load was not equally shared by the fibers.

Table 2.4 Typical Properties for S-2 Glass/Epoxy Composites [2.5]

Property	ASTM Standard	75°F, Dry*
Elastic Modulus, $\times 10^6$ psi		
Longitudinal Modulus, E_L	D3039	7.7-8.5
Transverse Modulus, E_T	D3039	2.3-2.9
Axial Shear Modulus, G_{LT}	D3518	0.9-1.3
Poisson's Ratio, ν_{LT}	D3039	0.26-0.28
Strength Properties, ksi		
Longitudinal Tension, F_L^u	D3039	230-290
Longitudinal Compression, F_L^{cu}	D3410	100-180
Transverse Tension, F_T^u	D3039	6-12
Transverse Compression, F_T^{cu}	D3410	16-29
In-Plane Shear, F_L^{su}	D3518	9-24
Inter-laminar Shear, F_I^{su}	D2344	8-15
Longitudinal Flexure	D790	180-250
Longitudinal Bearing	D953	68-80
Ultimate Strains, %		
Longitudinal Tension, ϵ_L^u	D3039	2.7-3.5
Longitudinal Compression, ϵ_L^{cu}	D3419	1.1-1.8
Transverse Tension, ϵ_T^u	D3039	0.25-0.50
Transverse Compression, ϵ_T^{cu}	D3410	1.1-2.0
In-Plane Shear, γ_T^u	D3518	1.6-2.5
Physical Properties		
Fiber Volume, %	D2734	57-63
Density, gr/cc	D792	1.97-2.02

Typical allowable property range with different epoxy resin

Ultimate tensile strengths for the S-2 Glass/Epon resin rods pultruded by Owens-Corning and Polygon (65% fiber volume) tested by Iyer, 1991 varied from 259-339 ksi. The effective diameter of these rods was 0.113 in. (0.125 in. nominal diameter) giving a cross sectional area of 0.01003 in², Iyer, 1991 [2.1].

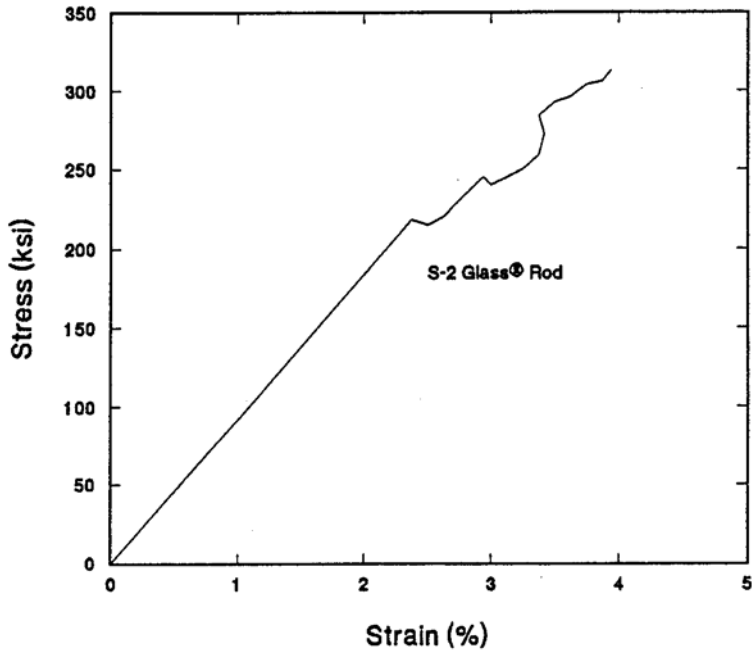


Figure 2.2 Stress-Strain Relation for S-2 Glass/Epon Resin Rods [2.8]

2.6 S-2 Glass Strands

The S-2 Glass strands used in this study consist of seven 0.113 in. diameter pultruded rods that were given one twist per foot and held in place mechanically using plastic ties (see Plate 2.2). The effective cross sectional area of the strands is 0.0702 in² although the nominal area for the rods pultruded by Polygon (see Section 2.4) was somewhat larger (0.0859 in), Iyer, 1991 [2.1].

As noted earlier, the properties of S-2 Glass rods are highly dependent on the degree of alignment of the fibers. Iyer [2.1] tested numerous samples and found that the effective modulus of the samples varied between $6.62-11.38 \times 10^6$ psi and its ultimate stress from 252-320 ksi. A typical set up for the tension test is shown in Plate 2.3 (Courtesy, Iyer, 1991).

A summary of the mechanical properties of the fiberglass strands is presented in Table 2.5. Inspection of this table shows that the properties of the rods pultruded by Polygon are about 10% higher than those pultruded by Owens Corning (#3N3). The maximum strain reported in this table is the last recorded value and is lower than the 3.7% value from tests conducted by Owens Corning (see Figure 2.2). A plot of the stress-strain curve is shown in Figure 2.3.

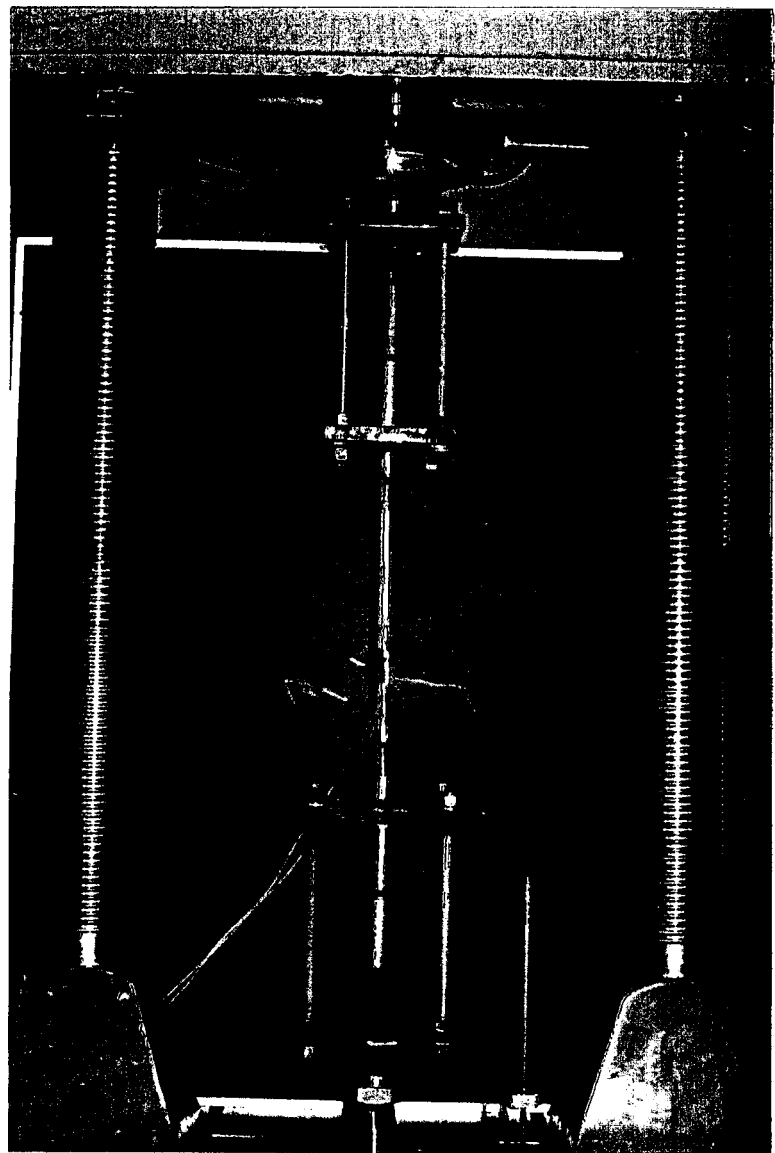


Plate 2.3 Set up for tension test (Courtesy, Dr. Iyer)

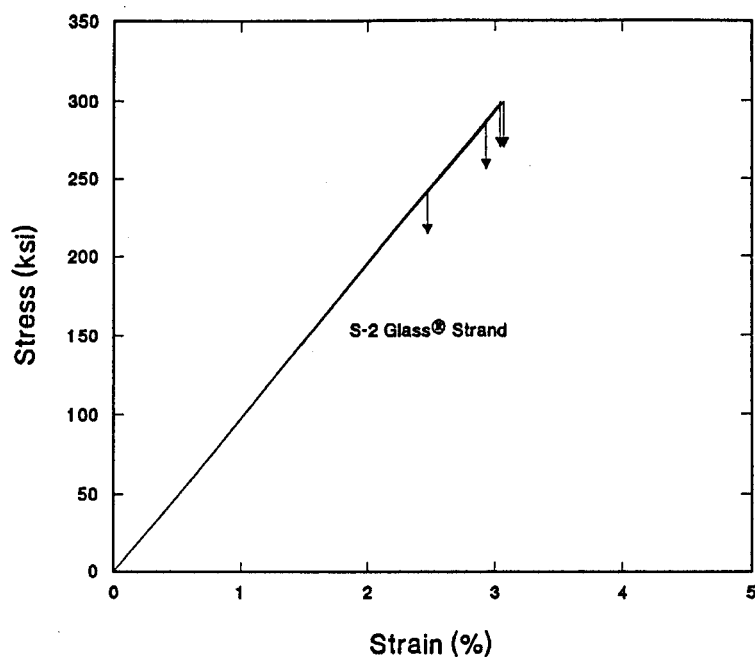


Figure 2.3 Typical Stress-Strain Plot for S-2 Glass Strands

Table 2.5 Mechanical Properties of S-2 Glass Strands [2.1]

Strand	Modulus of Elasticity ($\times 10^6$ psi)	Tensile Strength (ksi)	Last Strain Reading (%)	Study
#3N3	9.04	273.5	2.98	Durability
#E1	10.60	(142.5) ¹	(1.34)	Creep
#E2	10.17	(228.9) ²	(1.99)	Beam
#1	10.35	292.7	2.85	
#2	10.68	261.8	2.43	
#3	10.16	299.2	3.07	Column & Pile
#4	9.4	299.2	3.04	

¹ at 10,000 lbs

² after cyclic test

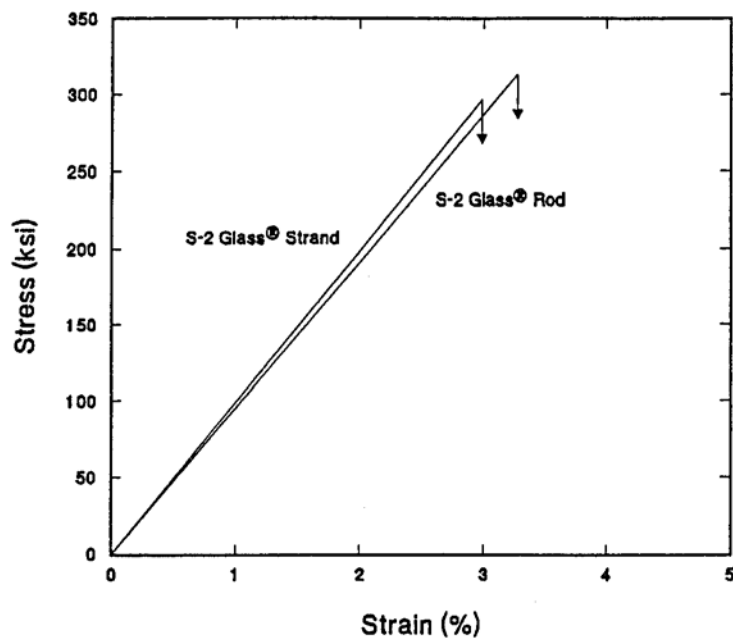


Figure 2.4 Stress-Strain Relation for S-2 Glass/Epon Resin Strands and Rods

Comparison on average strain-stress relation for S-2 Glass strands and rods are shown in Figure 2.4. Inspection of this figure indicates that although the ultimate strength of rods is somewhat higher than that of strands, the stiffness is almost identical.

2.7 Anchorage Mechanism for FRP

Due to FRPs low transverse compressive strength (see Table 2.4), conventional anchorage systems (chucks) cannot be used. Moreover, the smoothness and hardness of the glass surface causes slippage and the hardened points of serrated surface metal grips have a tendency to break the surface fibers of the fiberglass rods. Consequently, an effective anchorage system must rely on friction-compression or shear bond to transfer loads to the strand during jacking, Babaei & Gloyd, 1989 [2.9].

In friction-compression anchorages, the prestressing force is transmitted to the strands by shear-friction forces generated by transverse compressive forces applied by a clamping device, Rostdsy, 1988 [2.10]. In shear bond anchorages the ends of the strands are suitably reinforced using concrete or resin mortars cast in cylindrical or conical shapes. In this case, the prestressing force is transferred to the tendons by shear bond stresses which depend upon the embedded length and the prestressing force itself [2.9].

In this study both ends of the strands were strengthened by a proprietary method developed by Dr. Iyer in 1987 and subsequently refined to increase the holding capacity of chucks to more than the ultimate strength of the strands [2.11].

3. LONG-TERM PROPERTIES OF FRPs

3.1 Introduction

From a prestressing application point of view, long-term properties of particular interest are stress-rupture, relaxation and fatigue. In addition, durability in aggressive environments is also of concern.

In order to have the right perspective, long-term properties of S-2 Glass/epoxy composites should not be assessed in isolation but by comparison with other non-metallic prestressing materials. Consequently, a brief review of Polystal, Arapree and Carbon Fiber Composite Cables (CFCC) is presented in section 3.2. The long-term engineering properties related to stress rupture, relaxation and fatigue are discussed in section 3.3. The effect of alkaline environment, moisture and salt is considered in 3.4. A comparative assessment of the properties of these prestressing materials is presented in section 3.5.

3.2 New Non-Metallic Prestressing Materials

3.2.1 Polystal

Polystal® (trademark by Bayer AG, Germany) is an E Glass fiber composite which uses an unsaturated polyester resin matrix. It is manufactured by a patented process different from conventional pultrusion and uses 80% glass fiber by weight (68% by volume). It has a maximum short-term strength of 242 ksi, a modulus of elasticity of 7.4×10^6 psi and an ultimate strain of 3.3%. Its Poisson's ratio is 0.28. The unsaturated polyester resin used has a tensile strength of 11 ksi, a modulus of elasticity of 44 ksi and an ultimate strain of 4 %. A complete description is given by Miesseler & Preis [3.1].

Polystal has been used exclusively in post-tensioning applications. The round bars are given a protective polyamide coating against alkaline environment and also to withstand high prestressing frictional forces. Its first application was in the construction of the *Lunen'sche Gasse* pedestrian bridge in the city of Dusseldorf, Germany. This 30 ton capacity 23 ft bridge was built as a pilot structure. The first traffic bridge was also constructed in Dusseldorf in 1986. The two span, 49 ft wide *Ulenbergstrasse* bridge had spans of 70 and 84 ft. Other structures completed using Polystal include the externally prestressed two span *Marienfelde* pedestrian bridge built in Berlin in 1988 (with spans of 91 and 72 ft), and the *Schiessbergstrasse* bridge in Leverkusen that was scheduled for construction in 1990.

3.2.2 Arapree

Arapree® (trademark by AKZO, Germany and HBG, The Netherlands) is a composite prestressing material made of Twaron® HM (trademark by Aramide Maatschappij, The Netherlands) aramid fibers and epoxy, with a 50% fiber content by volume. It has a short-term tensile strength (related to the net fiber cross-section) of 435 ksi, a modulus of elasticity of 18.5×10^6 psi and an ultimate strain of 2.3 %. Its Poisson's ratio is 0.38, Gerritse & Werner, 1991 [3.2].

Arapree is available as rectangular bars or circular rods in several sizes. The first practical application of Arapree has been in the construction of a noise barrier along a busy highway near Rotterdam. It has also been used in prestressing masonry walls and hollow-core floor slabs.

3.2.3 Carbon Fiber Composite Cable (CFCC)

CFCCs were developed by a joint effort from Tokyo Rope Mfg. Co., Ltd. and Toho Rayon Inc., Japan. Its uses PAN carbon fibers and epoxy based resin systems mixed at an approximate 60/40% ratio by volume. The carbon fibers have a tensile strength of 526 ksi, a modulus of elasticity of 34×10^6 psi and an ultimate strain of 1.5%. The three grades of resin systems used in their manufacture have tensile strengths that range from 9.9 to 12.8 ksi, modulus of elasticity ranging from 0.5 to 0.6×10^6 psi, and ultimate strains between 1.7 to 4.2%, Tokyo Rope, 1989 [3.3].

In the manufacture of CFCCs, more than 12,000 filaments as thin as 7 microns in diameter (1 micron = 0.0004 in.), are grouped together with resin to form strands that are later twined into cables. Commercially available sizes range from 3.0 mm singlerods to 40.0 mm 37-rod cables.

Compared to other non-metallic composites, CFCCs exhibit higher tensile strengths of over 300 ksi, higher modulus of elasticity of over 21×10^6 , but a failure strain of only 1.6%. This low ultimate strain limits its use in prestressing since much of the strain capacity is utilized in tensioning, leaving insufficient strain capacity for developing flexural strains with an appropriate safety factor, Dolan, 1990 [3.4].

The *Shinmiyabushi* bridge, the world's first carbon fiber prestressed structure, was built in Japan in mid 1988. The 26 ft span bridge is supported by sixteen pre-cast girders pretensioned with eight cables per girder. The fabrication of the girders was identical to that used for steel. According to data gaged from an additional probe beam placed adjacent to the main girders, no reduction of the tendon strain was recorded over a period of two years, BASF [3.5]. More recently, carbon fiber composites have been used in the posttensioned construction of a four span bridge in the chemical plant of BASF in Ludwigshafen, Germany. The capacity of the steel prestressed bridge has been increased by the provision of four carbon fiber tendons [3.6].

3.3 Long-Term Engineering Properties

3.3.1 -Stress-Rupture

A characteristic of FRPs is their tendency to lose strength under sustained loading. This phenomenon is referred to as stress-rupture. For example, the failure load for Kevlar 49/epoxy strands after 100 years is estimated to be only 50-60% of the nominal breaking load, Burgoyne & Chambers, 1985 [3.7]. It is evident, therefore, that stress-rupture characteristics dictate jacking stresses that can assure safety of a structure.

A major study, Glaser et al., 1983 [3.8] on the stress-rupture characteristics for S-Glass® (trademark by Owens-Corning) fiber reinforced epoxy (Dow DER 332, Union Carbide ERL 4206) was conducted over a ten-year period at the Lawrence Livermore National Laboratory, California, from 1969 to 1980. In this study, seven stress levels ranging from 84 % to 33 % of the 575 ksi failure strength were investigated. Each test used a minimum of forty six specimens, but usually over one hundred specimens. The results indicated that at the highest stress level of 84%, all specimens failed in less than two days. At a 50% stress level, over 90% of the specimens survived the ten year test period. Of the remainder, 5 % failed after three years and only 2 % failed within the first year. At a 40% stress level, only 2 % failed while no failures were recorded for a 35% stress level.

Figures 3.1 shows the stress-rupture curves for Polystal and Arapree. It may be seen that the projected reduction for Polystal is 70% over 100 years, whereas Arapree has a 65% and almost 50% reduction for exposure to air and an alkaline environment, respectively, Rostasy, 1988 [3.9]. Based on un-published stress-rupture characteristics of S-2 Glass/epoxy composites in aggressive environments, the jacking stresses in this study were limited to 45-50% of the short-term ultimate strength.

3.3.2 Relaxation

Relaxation refers to stress loss with time under sustained loading. Unlike steel, where relaxation losses are related to the stress level, limited studies indicate that for some FRPs, e.g. Arapree, it is independent of the stress level [3.2].

Projected relaxation losses for S-2 Glass, Polystal, Arapree and CFCC are shown in Figure 3.2. For comparison, steel losses of 2.3% are also shown in the same figure. It should be noted that this value corresponds to a stress level of 72% whereas for the FRPs the sustained stress is only 50% of the ultimate short-term strength.

The Arapree values (18%) shown in Figure 3.2 relate to those reported by Rostasy, 1988 [3.9]. However, much lower values ranging from 7-9% have been reported by Gerritse, 1991 [3.2].

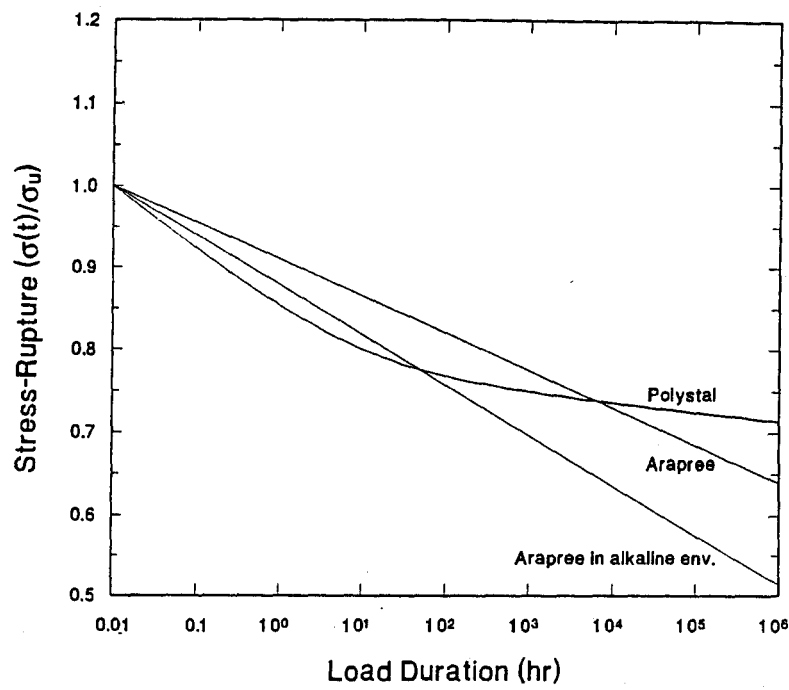


Figure 3.1. Stress-Rupture for Polystal and Arapree [3.8]

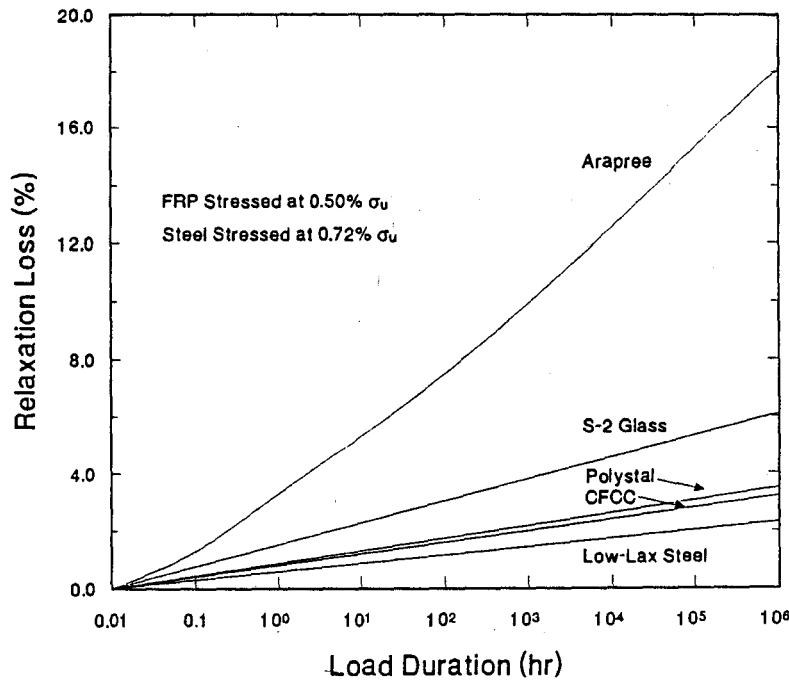


Figure 3.2 Relaxation of Different Prestressing Materials [3.1,3.2,3.3]

The relaxation loss value (6.2%) for S-2 Glass/epoxy shown in the same figure is based on projections from test results over 200 hours, at a stress level of 45 % of the short-term strength. This value is somewhat higher than the projected 3.2% and 3.5% values reported for Polystal [3.1] and CFCC [3.3], respectively.

3.3.3 Fatigue

Fatigue refers to as "the process of progressive permanent internal structural change in a material subjected to repetitive stresses", ACI 215 Committee, 1974 [3.10]. Compared to prestressing steel, tests indicate that with the exception of glass, aramid and carbon composites display superior fatigue characteristics, Gerritse & Werner, 1991, Tokyo Rope, 1989, Walton & Yeung, 1986 [3.2,3.3,3.12].

On the basis of CEB-FIP definition of fatigue life, after 2 million cycles Polystal has a 10% probability of failure for a stress range of 8 ksi for a maximum stress of 44% of the short-term strength [3.1]. This is much lower than the $0.1f_{p,0}$ range for steel proposed by ACI 215 Committee [3.11]. S-2 Glass is reported to have superior fatigue characteristics to E Glass, Owens-Corning, 1990 [3.13]. A relative plot of the fatigue characteristics of S-2 Glass, E Glass, Kevlar 49 and carbon fibers composites is shown in Figure 3.3.

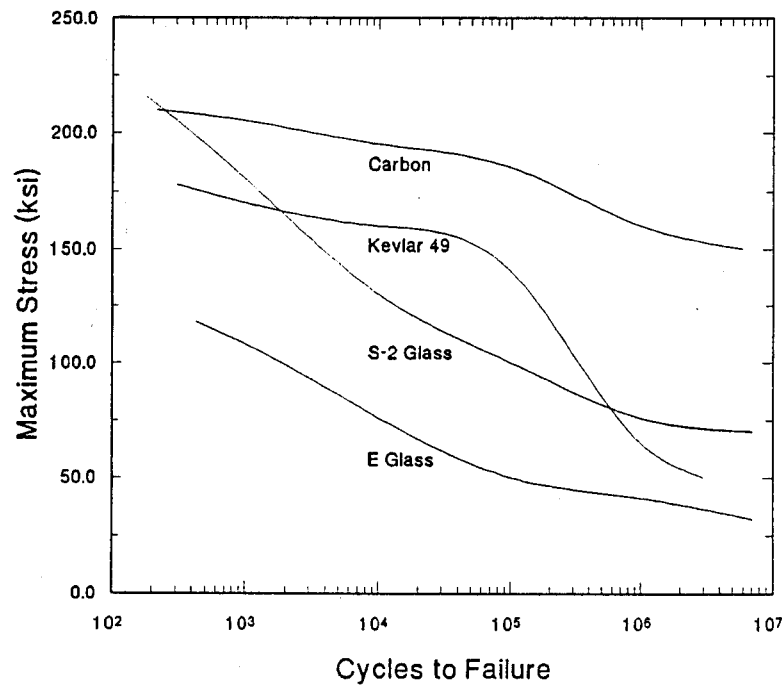


Figure 3.3. Fatigue Performance of Different Prestressing Materials [3.12]

3.4 Environmental Effects

3.4.1 Effect of Alkaline Environment

Portland cement is highly alkaline with a pH of about 13. Whereas glass itself has low resistance to this environment, Bentur & Mindess, 1990 [3.14], fiberglass laminates using thermoset resins have been successfully used in storage tanks for sodium and calcium hydroxide for over 30 years, Greenwood, 1991 [3.15]. It should be noted, however, that in such applications the strain in the fiberglass is relatively small (less than 0.20% under operating conditions). In prestressing applications, strains are in excess of 1.5 % and the thermosetting resins may no longer assure permanent protection of the fibers [3.1]. Consequently, this effect is investigated in this project.

As noted earlier, silica (SiO_2) is the primary component of glass fibers (see Table 2.1). When exposed to an alkaline environment, the high concentration of OR ions induces the breakdown of the Si-O-Si bond of the glass structure. As a result, there is rapid loss of strength, weight and reduction in fiber diameter. In addition, there is damage to the glass surface and the resulting corrosion products may either dissolve or accumulate on its surface [3.14].

In accelerated (at elevated temperatures in the range of 40-80°C) corrosion tests, E glass fibers showed a dramatic 85% decrease in their short-term strength after only 41 days exposure to a portland cement extract solution having a pH of 13.4 [3.13]. In unpublished tests, S-2 Glass fibers in epoxy have also exhibited some loss in strength though not as large as those for E glass.

Some vulnerability is also displayed by aramid fibers in an alkaline environment. However, strength retention of the Arapree composite is much superior in comparison to glass (see Figure 3.4), Gerritse, 1988 [3.16]. Carbon Fiber Composite Cables show very little degradation [3.3].

3.4.2 Effect of Moisture

Although moisture effects on FRPs used for prestressing applications has not been specifically investigated, numerous studies have been conducted on FRPs laminates used in other applications, Hahn, 1987, Springer, 1982, Ishai & Arnon, 1978, DeIasi & Whiteside, 1978, Kasturiarachchi & Pritchard, 1983 [3.17,3.18,3.19,3.20,3.21]. These indicate that moisture can reduce the strength and stiffness of FRPs. Such changes may be either temporary and reversible (disappears on drying), or permanent and irreversible [3.19].

Degradation of GRPs occur mainly in the fiber/matrix interface. The loss in strength is apparently caused by partial hydrolysis of the fiber/matrix interfacial bond as a result of water wicking along the fiber/matrix interface, Lou & Murtha, 1987 [3.22].

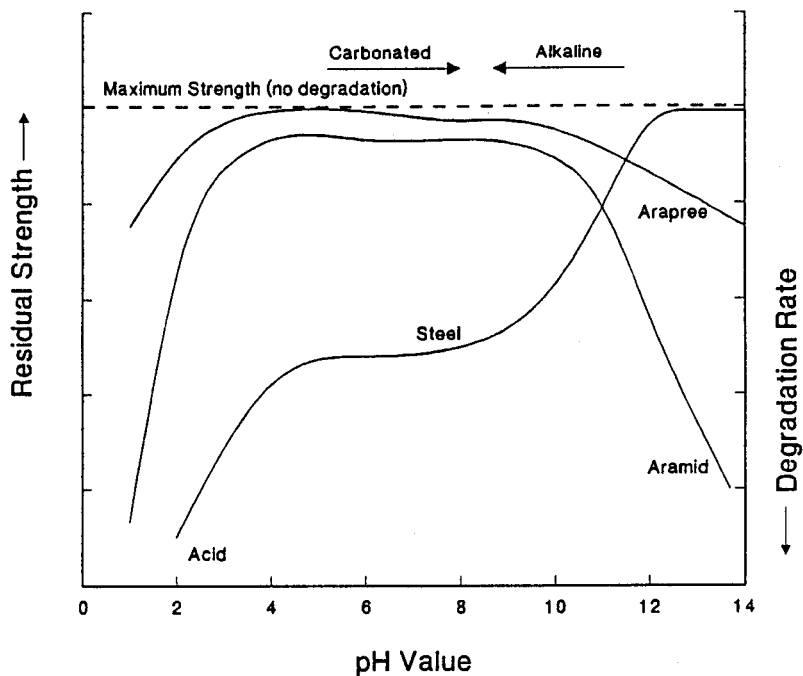


Figure 3.4. Schematized Long-Term Behavior in Alkaline Environment [3.15]

Additionally, moisture may reduce the interfacial bond by breaking chemical bonds, as in glass/epoxy composites, Ashbee & Wyatt, 1969 [3.23], and by altering the surface free energy, as in graphite/epoxy composites, Kaelble et al., 1975 [3.24]. The absorbed moisture not only plasticizes the matrix resin but can also change the state of stress, in favor of cracking through swelling [3.17].

3.4.3 Effect of Salt

Glass fiber reinforced plastics have been used for over 45 years in marine applications. Fiberglass boats are the standard of the industry with roughly 95% of all boats constructed of fiberglass. Durability and performance of fiberglass in saltwater has thus been proven with time [3.15].

Tests on E glass fiber reinforced plastics, reported by the US Naval Applied Science Laboratory, indicate that extended exposure to seawater results in some degree of degradation in properties. However, strength properties stabilize after an initial decrease of 10-15%, Fried, 1968 [3.25]. In another study, glass cloth laminates retained 95% of the original strength and stiffness after a five-year immersion period in seawater, Fried & Graner, 1966 [3.26].

More recently, Polystal was successfully used in prestressed beams that provided a cover over a brine pit [3.1]. The previous reinforced concrete beam and slab system had to be replaced because the steel had entirely rusted. Limited results on carbon fiber composites (CFCCs) exposed to seawater also showed no apparent loss in strength [3.3].

3.5 Comparison of New Prestressing Materials

Typical strain-stress relations for S-2 Glass, Polystal, Arapree, CFCCs, and prestressing steel are shown in Figure 3.5. A comparison of their principal properties is summarized in Table 3.1. It may be seen that S-2 Glass has a 24 % higher tensile strength, a 14 % higher modulus of elasticity and greater ultimate strain than Polystal. Compared to steel, S-2 Glass has an 11 % higher ultimate tensile capacity, about a third of its elastic modulus at almost a quarter of its weight. In prestressing applications, the lower modulus is a definite advantage as prestress losses will be smaller.

Among all non-metallic materials, Arapree is the lightest. CFCCs have the highest modulus of elasticity but is the most brittle. S-2 Glass and Polystal have the highest ductility and are also the least expensive (see Table 1.2). In terms of durability, CFCCs outperform all other materials including steel. Glass fibers and to a much less extent aramid fibers, are vulnerable to alkali attack although tests indicate that the epoxy resin provides adequate protection for the Arapree composite.

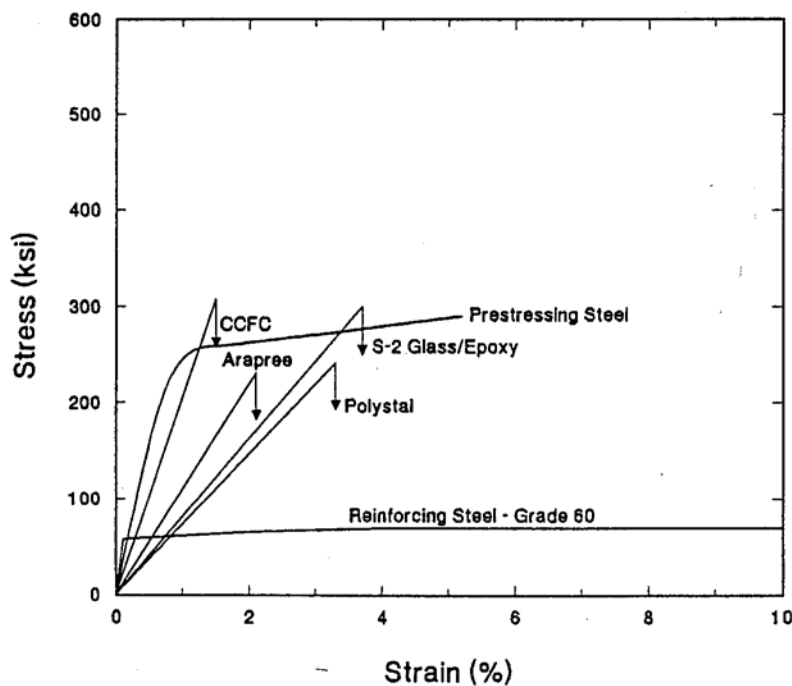


Figure 3.5 Comparative Stress-Strain Curves for FRPs and Steel

Table 3.1 Properties of Different Prestressing Materials

Property	Prestressing Steel Grade 270	S-2 Glass	Polystal	Arapree	CFCC
Fiber Volume Fraction, v_f	--	65	68	50	60
Density, gr/cc	7.86 (1.00)	2.0 (0.25)	2.3 (0.27)	1.25 (0.16)	1.5 (0.19)
Tensile Strength, ksi	270 (1.00)	300 (1.11)	242 (0.90)	200 (0.74)	307 (1.14)
Ultimate Strain, %	5.2 (1.00)	3.7 (0.71)	3.3 (0.63)	2.3 (0.44)	1.5 (0.29)
Modulus of Elasticity, $\times 10^6$ psi	29.00 (1.00)	8.46 (0.29)	7.40 (0.26)	18.50 (0.64)	20 (0.69)
Relaxation, %	2.3 (1.00)	6.2 (2.70)	3.2 (1.39)	8 (3.48)	3.5 (1.52)
Stress-rupture, %	100	--	70	65	--
Fatigue	3	4	5	2	1

4. FABRICATION OF SPECIMENS

4.1 Introduction

The specimens used in this study were cast in six separate pours over a sixteen-month period, from December 1989 to March 1991 as summarized in Table 4.1. The first five pours involved smaller specimens that could be pre-tensioned at the University of South Florida's Structures Research Laboratory. The last pour involved larger specimens and was cast at Henderson Prestress, Tarpon Springs, FL, one of Florida's largest producers of commercial piling.

The properties of the concrete and steel used in the fabrication are provided in Sections 4.2-4.4. Properties of the fiberglass ties and S-2 glass strands used are summarized in Sections 2.4.1 and 2.6 respectively. Since laboratory fabricating procedures differed from those at Henderson Prestress, they are described separately. Laboratory fabrication is presented in Sections 4.5-4.7. Fabrication at the commercial prestressing facility is

Table 4.1 Summary of Specimens Cast

N ²	Study	Cast Date	<u>N² of Specimens</u>		Cross-Section (in x in)	e (in)
			ST	FG		
Pre-tensioned Specimens Cast at USF						
1		12/22/89	Six	Six		1
2	<i>Durabilit</i>	12/28/89	Six	Three	6 x 4	1
4		06/06/90	--	Three		1
3	<i>Creep</i>	03/13/90	Six	Three	6 x 4	0
4		06/06/90	Three	Three		0
	<i>Flexure & Fatigue</i>	06/14/90	Three	Six	6 x 8	2
					6 x 10	3
					6 x 12	4
Pre-tensioned Specimens Cast at Henderson Prestress						
6	Column	03/15/91	Two	Four	8 x 8	0
6	<i>Pile</i>	03/15/91	Two	Four	10 x 10	0

4.2 Concrete

Two different normal weight concrete design mixes were used in the study. For the specimens cast at the University of South Florida's Structures Research Laboratory, an FDOT approved mix design (see Table 4.2) for high early strength cement (Type III) was used. Its minimum design strength was 5,500 psi. It was batched at Southern Prestressed, Inc. Tampa's batching plant and delivered to the Structures Laboratory.

Table 4.2 Concrete mix design for specimens cast at USF

Item	Weight/cy
Cement, lbs	658
Aggregates, lbs	1800
Sand, lbs	1132
Water, lbs	269
Air Entrainment Admixture (MBUR), oz.	2.0
Water Reducing Agent (WRDA 79), oz.	50
Water/Cement ratio, lbs/lbs	0.41
Slump ¹ , in.	
Concrete Cast 12/22/89 - Temperature 54°F	4.5
Concrete Cast 12/28/89 - Temperature 80°F	2.5
Concrete Cast 03/13/90 - Temperature 80°F	3.0
Concrete Cast 06/06/90 - Temperature 99°F	1.8
Concrete Cast 06/14/90 - Temperature 90°F	3.5
Compressive strength ² @ 72 hr. (12/22/89), psi	5,020
Compressive strength ² @ 32 hr. (12/28/89), psi	4,560
Compressive strength ² @ 72 hr. (03/13/90), psi	5,820
Compressive strength ² @ 34 hr. (06/06/90), psi	4,730
Compressive strength ² @ 34 hr. (06/14/90), psi	4,895

¹Target slump range 1.5" - 3.5"

²Expected strength 5,500 psi @ 28 days

The water/cement ratio of the mix was 0.41 and compressive strengths at release ranged from 4,560-5,020 psi. The strength achieved at the time of testing averaged over 6,500 psi. Details of concrete strength at the time of testing is provided in the appropriate chapters presenting test results (Chapters 7,11,13 and 16).

The specimens cast at Henderson Prestress used normal cement (Type I) in a mix design with a minimum design strength of 5,000 psi (see Table 4.3). The concrete was batched and supplied by Tarmac Florida, Inc. of Tarpon Springs.

Table 4.3. Concrete mix design for specimens cast at Henderson Prestress

Item	Weight/cy
Florida Portland Cement Co. Type I, lbs	700
Cement Sand Company Fla. FDOT, lbs	1263
Fla. Rock Industries, Inc. #57 stone, lbs	1815
Water, lb	267
Air entrainment, %	1.0
Daracem 100, W.R. Grace & Co. ASTM C-494, oz.	70
Water/Cement ratio, lbs/lbs	0.38
Slump` , in.	7.00
Concrete unit weight, pcf	147.4
Compressive strength ¹ @ after 96 hours, psi	6,080
Compressive strength ¹ @ pile testing, psi	7,790
Compressive strength ¹ @ column testing, psi	7,705

¹Target Slump range 6.0" - 8.0"

¹Expected strength 3,500 psi @ 18 hr. of curing

It is evident that a very rich mix was used to ensure that a minimum 3,500 psi strength was reached after 18 hours of open air curing. The actual strengths achieved were substantially higher.

4.3 Prestressing Steel

All prestressing steel used in the study were seven-wire strands manufactured by Florida Wire and Cable Company, Jacksonville, Florida. The properties presented in Tables 4.44.7 are those provided by the manufacturer. Excepting for the beam study, low relaxation Grade 270 steel was used throughout.

For the durability specimens cast in December, low relaxation $\frac{1}{2}$ in. diameter Grade 270 strands were used (see Table 4.4). For the creep specimens cast in March and June,

Table 4.4 Steel Strand Properties for Pours 1 and 2 (December 1989)

Property	Seven-Wire Strand
Ultimate Breaking Strength, lb.	43,400
Ultimate Breaking Stress, $f_{p..}$, ksi	283.7
Load at 1 % extension, lb.	40,200
Elongation at 30,975 lb., in/in.	0.007
Ultimate elongation in 24 in., in/in.	5.21
Modulus of elasticity, psi	28.6×10^6
Cross sectional area, in'	0.153

Table 4.5 Steel Strand Properties for March 1990 (Pour 3) and June 1990 (Pour 4)

Property	Seven-Wire Strand
Ultimate Breaking Strength, lb.	45,000
Ultimate Breaking Stress, $f_{p..}$, ksi	269.5
Load at 1 % extension, lb.	40,500
Elongation at 33,750 lb., in/in.	0.00704
Ultimate elongation in 24 in., in/in.	5.21
Modulus of elasticity, psi	28.7×10^6
Cross sectional area, in'	0.167

Table 4.6 Steel Strand Properties for Flexure and Fatigue Study (Pour 5)

Property	Seven-Wire Strand
Ultimate Breaking Strength, lb.	21,900
Ultimate Breaking Stress, $f_{p,\text{,,}}$, ksi	273.3
Load at 1 % extension, lb.	20,300
Elongation at 14,000 lb., in/in.	0.00606
Ultimate elongation in 24 in., in/in.	5.21
Modulus of elasticity, psi	28.9×10^6
Cross sectional area, in'	0.080

Table 4.7 Steel Strand Properties for Column and Pile Study (Pour 6)

Property	Seven-Wire Strand
Ultimate Breaking Strength, lb.	24,600
Ultimate Breaking Stress, $f_{p,\text{,,}}$, ksi	289.4
Load at 1 % extension, lb.	21,900
Elongation at 17,250 lb., in/in.	0.00710
Ultimate elongation in 24 in., in/in.	5.21
Modulus of elasticity, psi	28.6×10^6
Cross sectional area, in ²	0.085

special low relaxation $\frac{1}{z}$ in. diameter Grade 270 strands were used (see Table 4.5). For the beam specimens, normal relaxation $\frac{3}{a}$ in. diameter Grade 250 strands were used (see Table 4:6). For the column and pile study, low relaxation $\frac{3}{a}$ in. diameter Grade 270 prestressing strands were used (see Table 4.7).

4.4 Reinforcing Steel

Reinforcing steel was used for stirrups for the beam study and as spiral ties for columns and piles. Both were custom made as shown in Plate 4.1. Additionally longitudinal top steel was provided for the beam specimens.

Stirrups were made from plain 7/32 in. diameter bars manufactured by Ivy Steel Products, Jacksonville, FL with a yield stress from 57 ksi to 62 ksi. Plain # 2 bars were used as top steel for the 6 in. x 8 in. and 6 in. x 10 in. beams. They were also manufactured by Ivy Steel and ultimate tensile strength was 77 ksi. For the 6 in. x 12 in. beams, deformed # 3 bars were used. These were manufactured by Florida Steel and its yield stress varied between 65 ksi to 72 ksi.

Spiral ties were made from #5 gage wire steel $0.207'' \pm 0.003''$ in diameter, manufactured by Ivy Steel Products, Jacksonville, Florida. Its yield strength was 70 ksi and its ultimate strength, 80 ksi.

4.5 Fabrication at USF

The specimens cast at USF's Structures Research Laboratory related to those used for the durability study, structural creep study, beam flexure and cyclic fatigue studies (see Table 4.1). All the specimens were cast in the same prestressing bed which was adapted to accommodate different sizes and eccentricities of the specimens. To avoid repetition, a description of the pretensioning bed and the basis for nomenclature of the specimens is presented in Section 4.5.1. The tensioning procedure is described in Section 4.5.2. Since the overall dimensions of the specimens used for the durability specimens were identical, their fabrication was very similar. This is presented in Section 4.6. The fabrication of the beam specimens is described in Section 4.7.

4.5.1 Prestressing Bed

Plate 4.2 shows the general arrangement of the 30 ft x 6 ft prestressing bed used in this study. The self straining bed comprised of two thirty feet W14 x 68 sections in the longitudinal direction and a pair of ten feet W14 x 26 sections stacked edgewise on its flange to form each abutment. A one inch square steel bars was sandwiched between

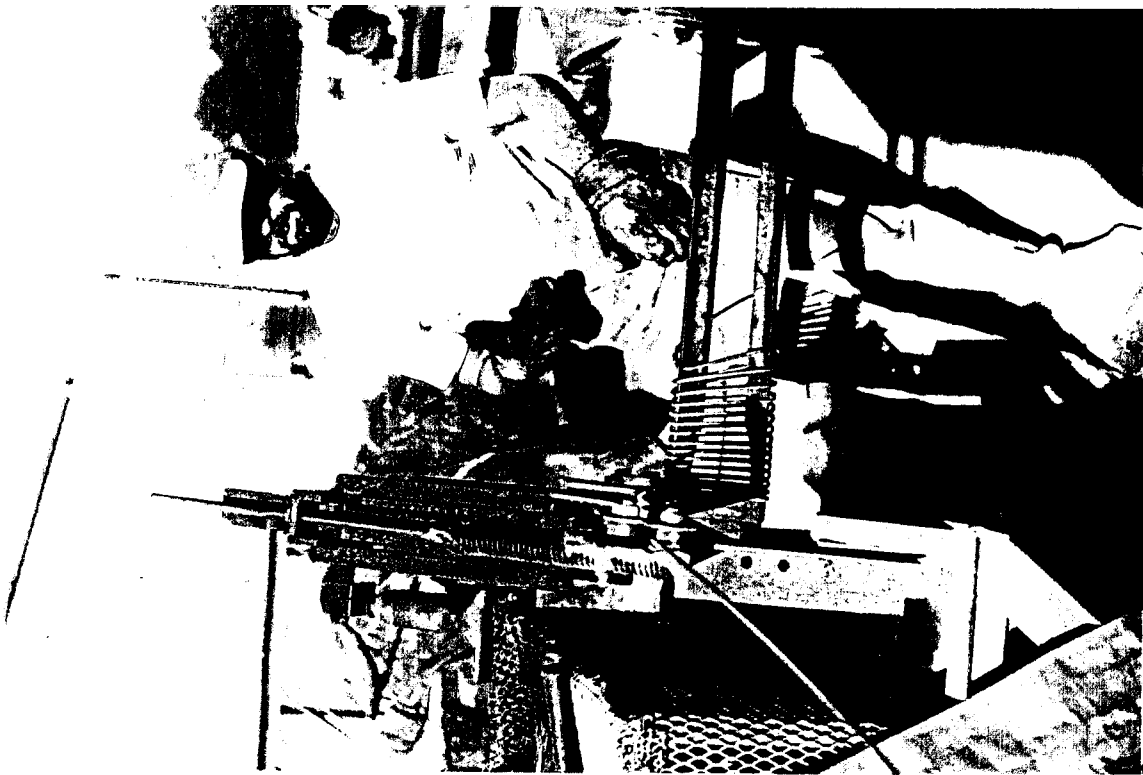


Plate 4.1 (top) Fabrication of stirrups for beams
 (btm) Fabrication of spiral ties for piles and columns

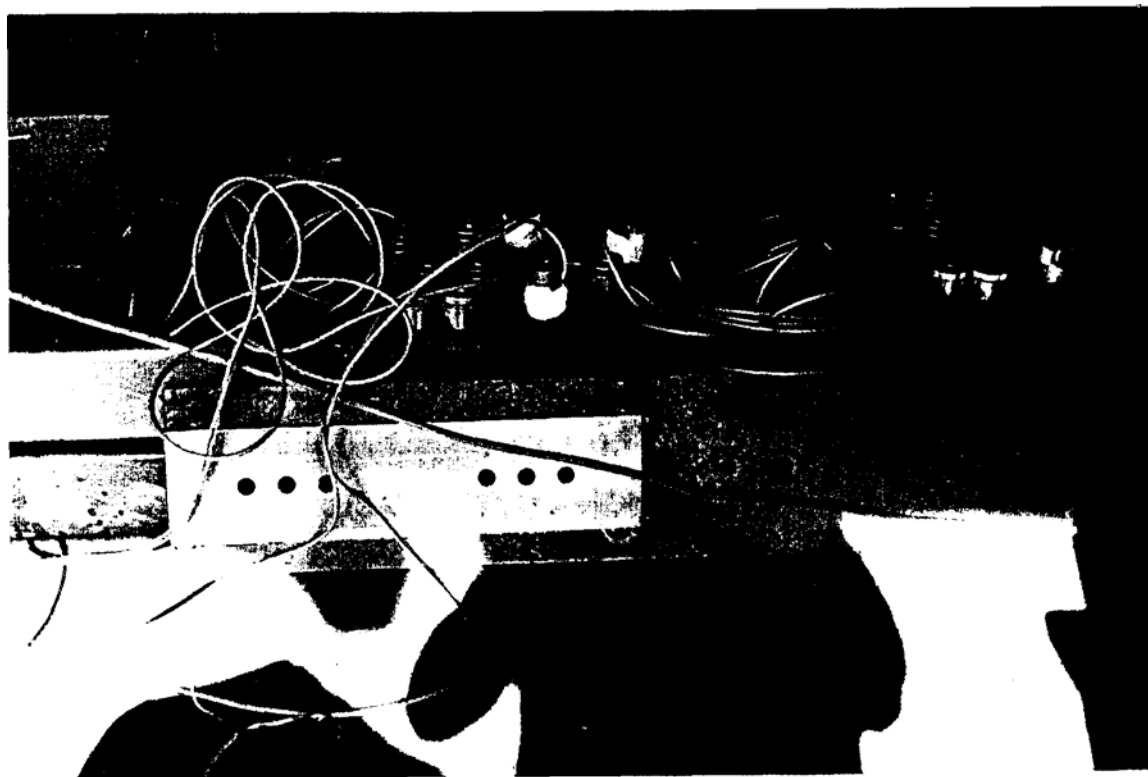


Plate 4.2 (top) Pretensioning bed

(btm) Header plate at ends

the two sections to provide spacing for threading the prestressing strands. Pre-drilled 4 ft x 10 in. x 0.5 in. steel header plates were clamped to the abutments at each end. The spacing of holes in these plates corresponded to the location of the prestressing strands in the specimens.

To allow comparability, fiberglass and steel pretensioned specimens were cast simultaneously in adjacent lines (see Plate 4.2). Excepting for the June pours when there was only one steel prestressing line, two steel and two fiberglass lines were used. Holes drilled in the header plate matched the requirements for the specimens. For example, for the durability and creep study, six holes were drilled corresponding to two steel lines (each containing a single strand) and two fiberglass lines (each containing a pair of strands). For the beam specimens, eight holes were drilled to accomodate the eight strands that were needed (2 steel and 6 fiberglass) as shown in Plate 4.2. Along each line, three 8 ft 6 in. specimens were cast.

A 28 ft x 4 ft plywood platform reinforced with 2 x 4s was constructed and rested on the structural floor. The eccentricity of the specimens could be varied by raising the height of the wooden platform (as was done for casting the durability specimens that had an eccentricity of 1 in. (see Table 4.1). Alternatively, it could also be varied by increasing the specimen depth (as was done for fabricating the specimens for the flexure study).

Since the prestressing bed was oriented in the east-west directions, all specimens were identified by their location in the bed and the prestressing material. A prefix of 'FG' or 'ST' is used to distinguish between fiberglass and steel specimens and the letters W, M, E (for West, Middle and East) followed by a number identified its location in the bed, as shown in Figure 4.1. The number 'n' was sequentially increased. A total of 51 specimens, 27 fiberglass and 24 identical steel specimens were cast. The fiberglass specimens were numbered from FG-W 1 to FG-W9, FG-M1 to FG-M9 and FG-E1 to FG-E9. The corresponding steel specimens were numbered from ST-W1 to ST-W8, ST-M1 to ST-M8 and ST-E1 to ST-E8.

4.5.2 Pre-tensioning Procedure

Each strand was individually tensioned by a 20 ton capacity, 10 in. stroke special PSI PT twin cylinder stressing jack driven by a high pressure electric motor hydraulic pump. The steel strands were always prestressed first followed by the fiberglass strands. Two kip increments were used for pretensioning the steel strands and one kip increment for the fiberglass strands. The prestressing load was monitored by load cells that were provided at the jacking end.

All the specimens used in the creep and durability study were jacked from one end. For the beam specimens, there was insufficient room for all the fiberglass strands to be jacked from the same end and alternate strands were jacked from alternate ends.

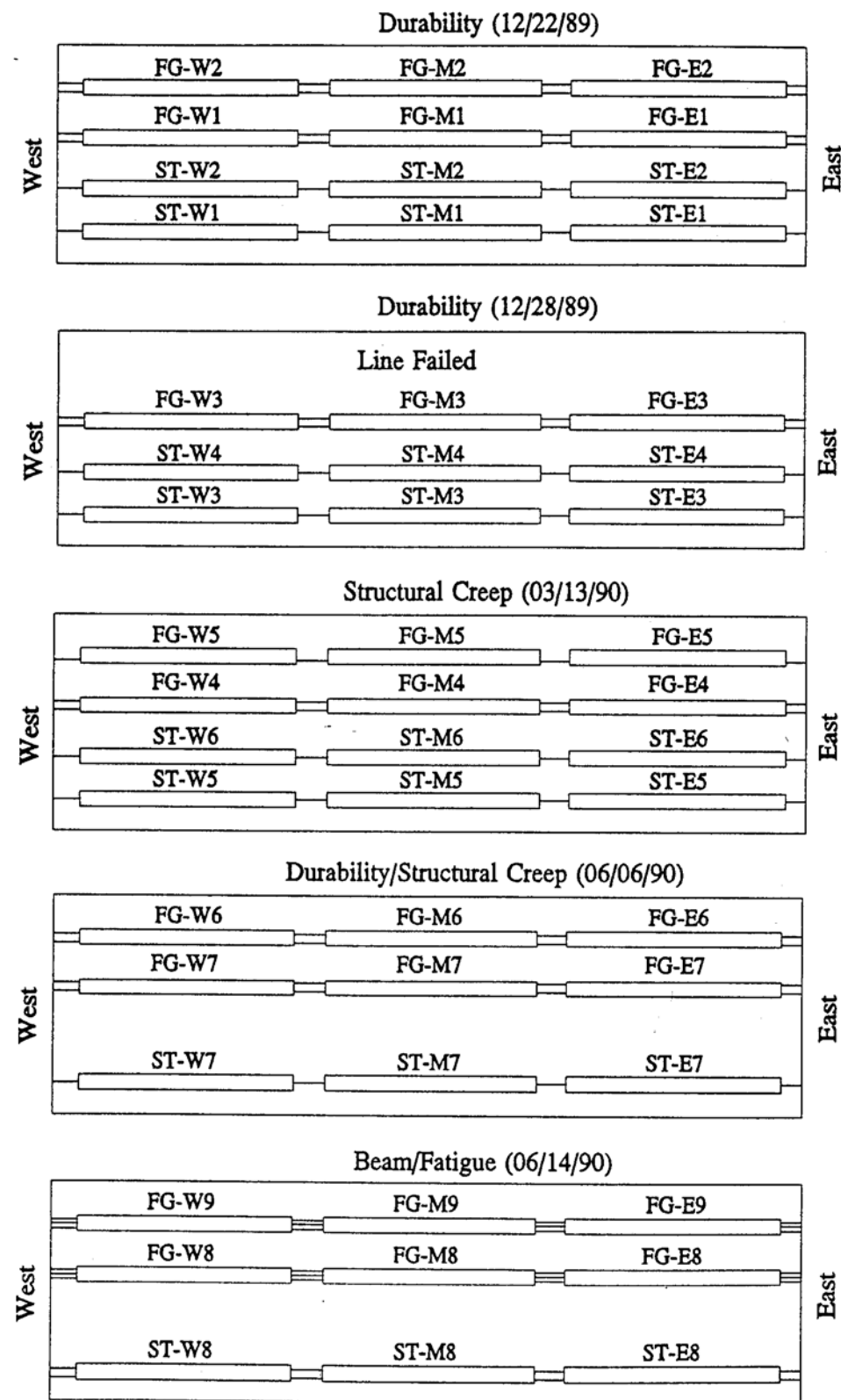


Figure 4.1 Summary of Specimens Cast at USF

4.6 Fabrication of Durability and Creep Specimens

The specimens used for the creep and durability study had identical overall dimensions of 6 in. x 4 in. x 8.5 ft. The only difference was in their eccentricity. The durability specimens had an eccentricity of 1 in. whereas the creep specimens were pretensioned concentrically. A total of 36 specimens were required, twenty four for the durability study and twelve for the creep study. In each case, half the specimens were steel pretensioned and were used as controls to evaluate the performance of fiberglass.

All specimens were fabricated similarly. Eight, 28 ft long steel angles, 4 in. x 3 in. x 0.25 in. were nailed to the wooden platform six inches apart to form the sides of the specimens. The ends of the specimens were made using plywood sections with holes at appropriate spacings to accommodate the prestressing strands (see Plate 4.3). The prestressing bed and the sides and ends of the form were sprayed with a fine coat of oil. Six strands, two steel and four fiberglass, were then threaded through openings in the header plate, 5 in. x 1 in. load cells and clamped at their ends. The 3/8 in. fiberglass strands comprised seven rods held together by plastic ties (see Table 2.5). The ends were strengthened by a proprietary process as stated in Section 2.7. Half in. steel strands were used for the steel specimens (see Tables 4.4 and 4.5).

The target jacking forces for the fiberglass cables was 10 kips. Since the fiberglass specimens were provided with two strands, i.e. the total jacking force was 20 kips, the half in. steel strand was only jacked to 20 kips. For the first two pours in December 1989, load cells were used for monitoring the force in the fiberglass strands. The jacking force in the steel strands was monitored using the pressure gage in the prestressing jack that had been previously calibrated. Details of the jacking force and the initial force after release are summarized in the chapters discussing results (see Chapters 6, 13 and 16).

Concrete was poured approximately two to three hours following completion of the prestressing operation (see Plate 4.3). A laboratory size needle vibrator was used for internal vibration. The concrete surface was levelled, trowel finished, covered by wet burlap and plastic sheets. To accelerate the curing process, electric blankets were placed over plastic sheets and covered by thermal blankets as shown in Plate 4.4.

The concrete strength was checked by testing cylinders and when it exceeded 4,000 psi the prestress force was released. Details of the concrete strength at the time of release for the various pours are summarized in Table 4.2. This was accomplished by carefully cutting the strands with an electric grinder as shown in Plate 4.4.

The specimens for the durability study were cast in two separate pours on December 22 and December 28, 1989. The creep specimens were cast on March 13, 1990. It should be noted that prior to this study, only a limited number of specimens had been successfully pretensioned. Not surprisingly, there were problems with the initial two pours in 12/89 and 03/90 when fiberglass cables failed (see Plate 4.5).

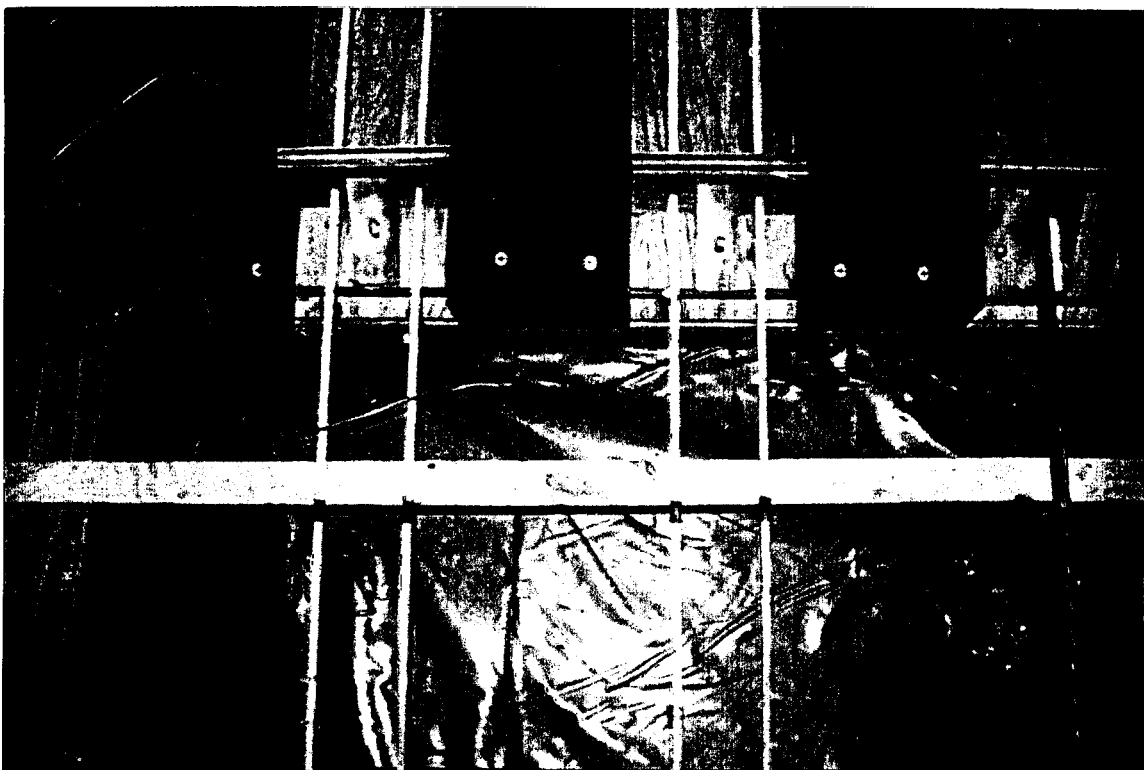


Plate 4.3 (top) End form for specimens
(btm) Concreting of specimens

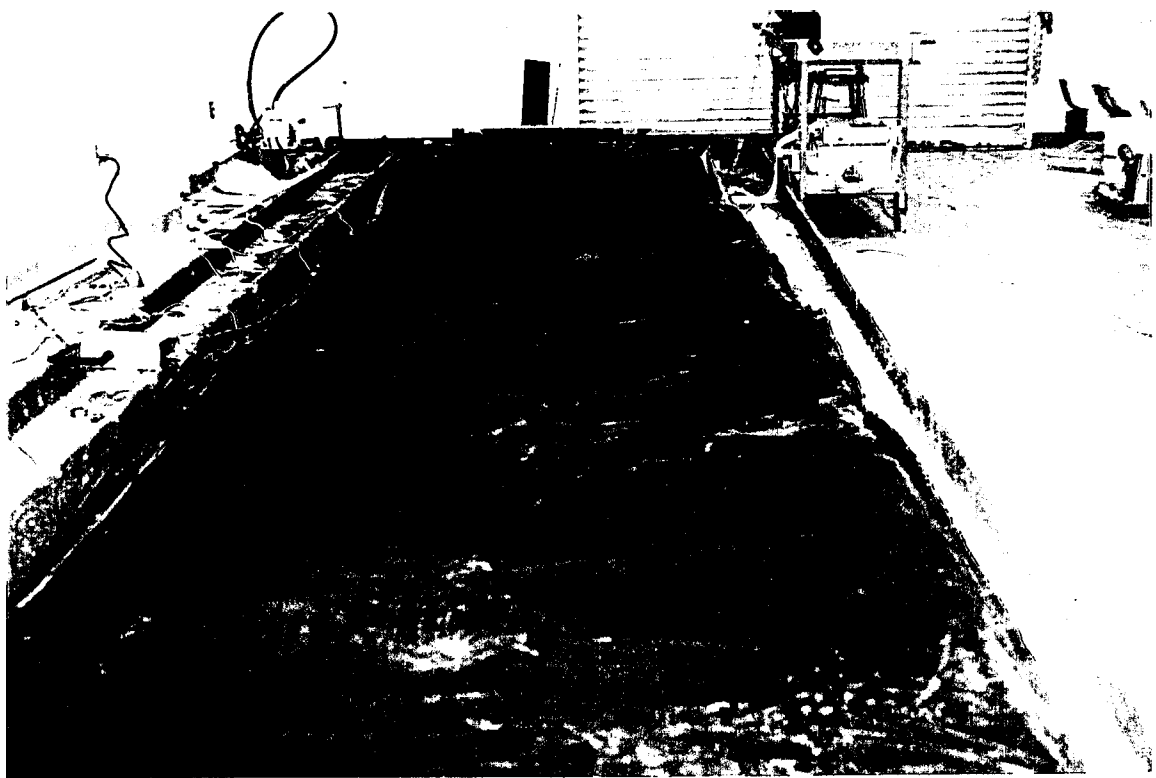


Plate 4.4 (top) Curing of specimens
(btm) Release of prestressing force

4.7 Fabrication of Beam Specimens

A total of nine beam specimens were cast, six fiberglass and three identical steel. Three different sizes, 6 in. x 8 in., 6 in. x 10 in. and 6 in. x 12 in. were fabricated. All beams were provided with steel stirrups and longitudinal top bars as shown in Figure 7.1. The prestressing strand was located 2 in. from the bottom in all the beams. This meant that the differing eccentricities needed for the study could be cast along the same prestressing line by appropriately altering the depth.

For the beam specimens, the spacing of holes in the header plates used for the fabrication of the creep and durability specimens had to be altered. Each header plate now had eight holes drilled at locations corresponding to the eight strands (six for the fiberglass and two for the steel) used in the prestressing operation. The section of the header plate for fiberglass strands was reinforced by a 1" thick plate that was tack welded to it as shown in Plate 4.2. This was to provide additional rigidity since the strands in this region were spaced 2" apart.

As before, the prestressing bed was first sprayed with a fine coating of oil. Prefabricated reinforcement cages were then placed in position in the bed and the prestressing strands were then threaded through the openings and clamped at the dead end. At the live end, 5" long x 1" diameter load cells were used to monitor the prestressing force. A small initial tension of about 500 lbs was applied to remove the slack in the strands. Strain gages were subsequently attached to each strand at the approximate midspan location (after tensioning) of the respective beams.

Following the installation of the strain gages, the strands were stressed to the targeted force of 16 kips for the steel strands and 10 kips for the fiberglass strands. A higher force was used for the steel strands to offset higher anticipated losses. The steel strands were attached to the reinforcement cage using metal ties whereas plastic ties were used to attach the fiberglass strands. This operation took over 6 hours. Wooden forms were now built around each beam and the eccentricity at each end adjusted using wooden blocks (see Plates 4.5-4.7).

Concrete was poured approximately twenty four hours following the completion of the prestressing operation. As before, a laboratory size needle vibrator was used for internal vibration and particular care was taken to ensure that there was no damage to the strain gage installation. The concrete surface was levelled, trowel finished, covered by wet burlap and plastic sheets. To accelerate the curing process, electric blankets were placed over the plastic sheet and covered by thermal blankets as before. After 24 hours, the concrete strength was found to be 4,895 psi and the prestress force was released. The release was accomplished by carefully cutting the stands with a hacksaw as shown in Plate 4.7. At the time of the static tests (see Chapter 7) it had increased to 6,840 psi and after the fatigue test it was 7,120 psi.

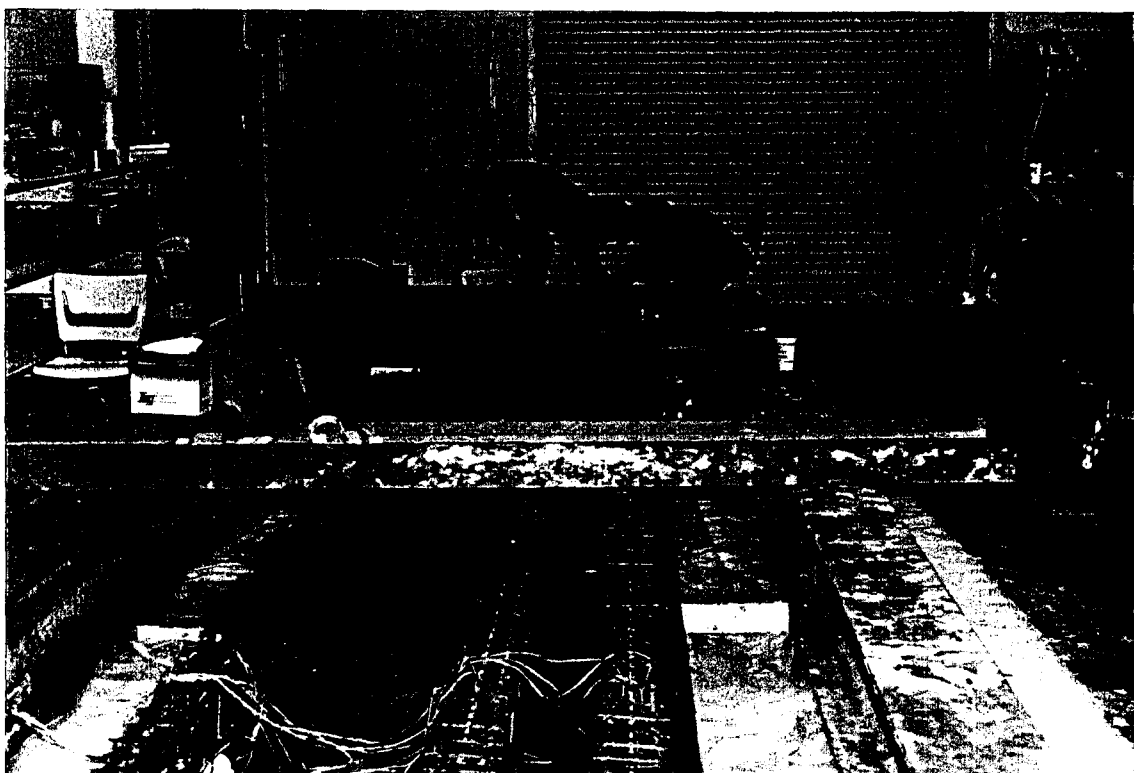


Plate 4.5 (top) Failure of fiberglass strand (03/13/90)
(btm) Reinforcement cage for beams

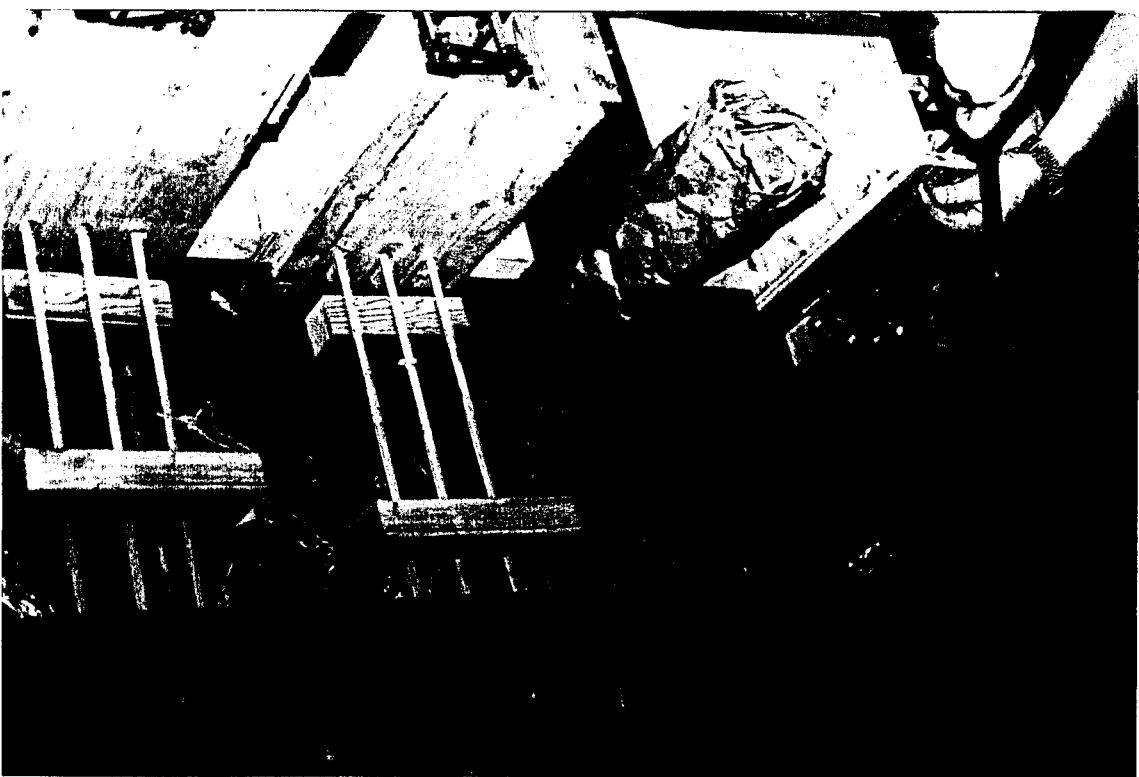
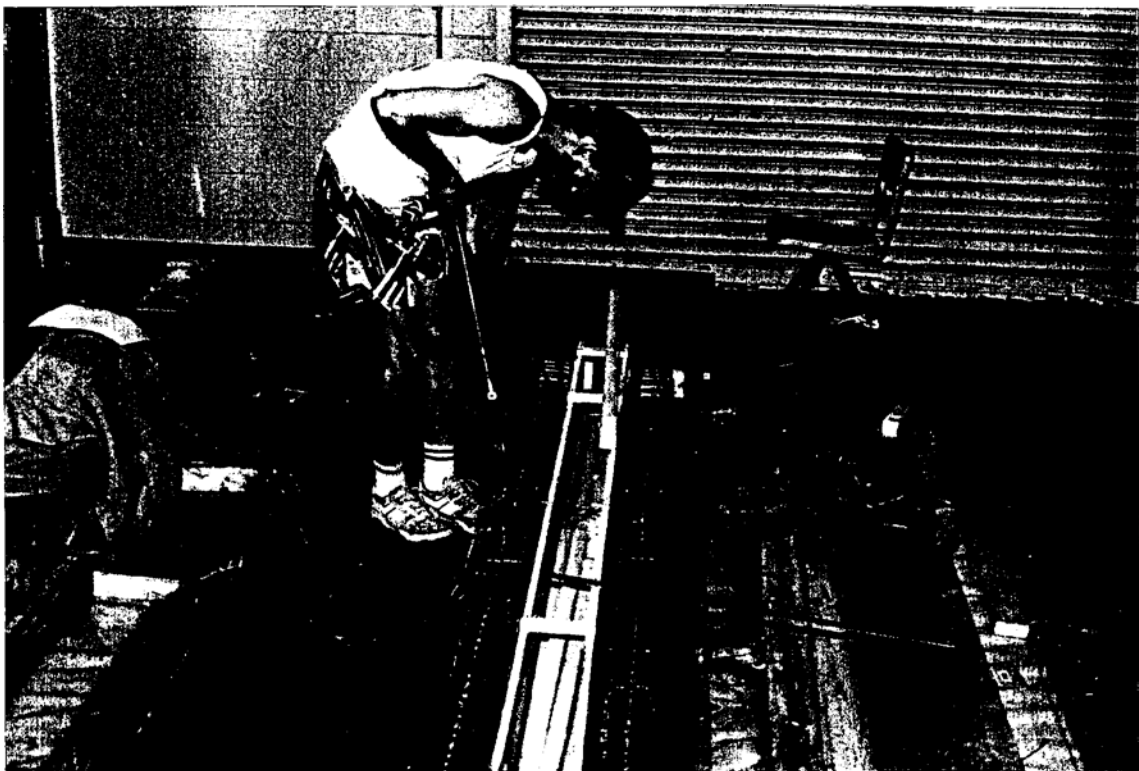


Plate 4.6 (top) Installation of forms
(btm) Adjustment of end eccentricity

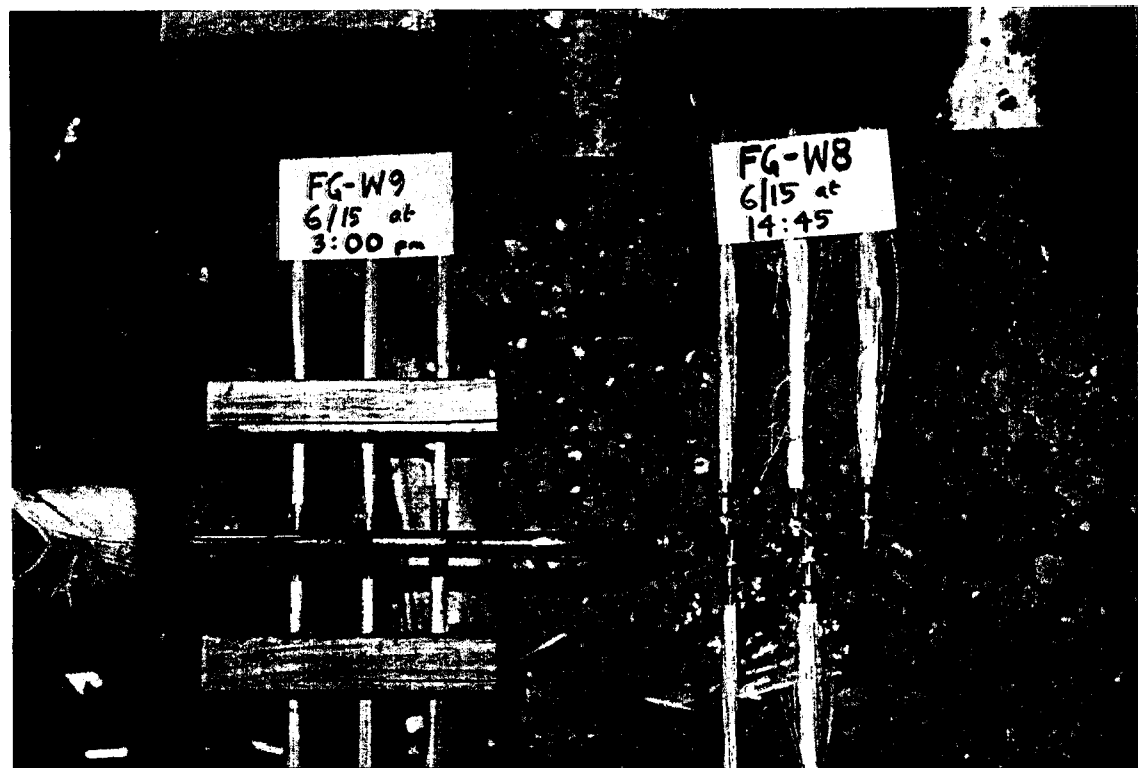
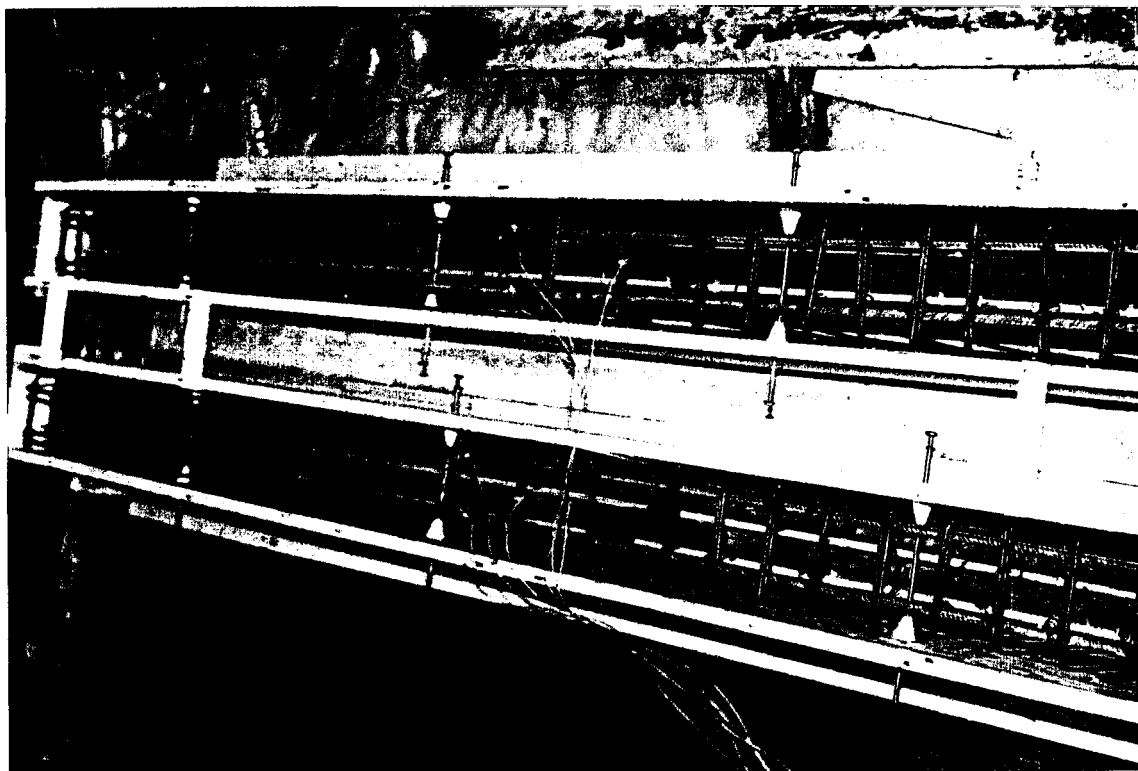


Plate 4.7 (top) Reinforcement for FG-W8 and FG-W9
(btm) Release of prestress force

4.8 Fabrication at Henderson Prestress

Six 25 ft long piles and six 9 ft long columns totaling 204 ft were cast at Henderson Prestress, Tarpon Springs, FL in a 400 ft long prestressing bed used for producing commercial piling. Eight of the twelve specimens cast were fiberglass and four were steel. The fiberglass pre-tensioned specimens totaled 136 ft - 4 piles @ 25 ft and 4 columns Qa 9 ft- and the length of steel elements measured 68 ft -2 piles Q 25 ft and 2 columns @a 9 ft. Each specimen was pre-tensioned by eight 3/8 in. steel or fiberglass strands spaced 2 in. on centers as shown in Figure 8.1 and Figure 9.1. As the cross-section of the columns was only 8 in x 8 in., 8 ft long plywood forms were installed within the prestressing bed and centered between specimen "spacers" that were 9 ft apart, i.e. a 10 in. x 10 in. section extended six inches at each end.

Because the total length of the prestressing bed was 400 ft and the length of the fiberglass specimens totaled 136 ft, each fiberglass strand had to be attached to a steel strand to make up the length of the bed. Although transfer (splicing) chucks are commercially available, they could not be used since it did not provide sufficient length to prevent slippage of the fiberglass strands. A simple scheme was developed to solve this problem. A transfer block shown in Plate 4.8 was provided at the *dead* (non-pulling) end. It consisted of two 2 in. thick plates with eight $\frac{3}{8}$ in. diameter holes matching those in the header plate. These plates were spaced 2 ft apart by four $\frac{3}{8}$ in. x 2 in. x 2 in. welded angles. A set of eight high tension bolts were used to attach one end of the transfer block to the header of the prestressing bed. The other end was used to chuck the fiberglass strands.

The transfer block only solved part of the problem. The more difficult part, that of pulling the strands was exacerbated by the very tight tolerance, since the center to center spacing of the strands was only 2 inches. In the absence of individual transfer chucks, the only possible solution was the use of individual transfer blocks, also shown in Plate 4.8. Eight such blocks were designed, fabricated and tested prior to the pour. Each consisting of two 3 in. x 2 in. x $\frac{3}{8}$ in. plates with centric holes of $\frac{1}{2}$ in. and $\frac{3}{8}$ in. attached to two 2 in. x $\frac{3}{8}$ in. x 18 in. flat bars. The fiberglass and steel strands were chucked at either end of this block as shown in Plate 4.8. Since the spacing between strands was 2 in., the individual transfer blocks had to be staggered within the transfer zone of the bed. Consequently, different sized fiberglass strands were used as shown in Figure 5.1. The difference in length between adjacent strands was 3 ft - its anticipated extension when it was tensioned to the 11 kip jacking force. To limit the tendency of the twisted strands to rotate during jacking, wooden guides were inserted between the individual transfer blocks.

The prestressing bed was initially sprayed with a fine coating of form oil to ease removal of the concrete specimens. Eight sets of steel spiral ties and four sets of fiberglass spiral ties, corresponding to the twelve elements being cast, were positioned inside the bed. Eight fiberglass cables were then carefully threaded individually through the header plate at the *dead end*, through the spiral ties and spacers and chucked to one end of the eight

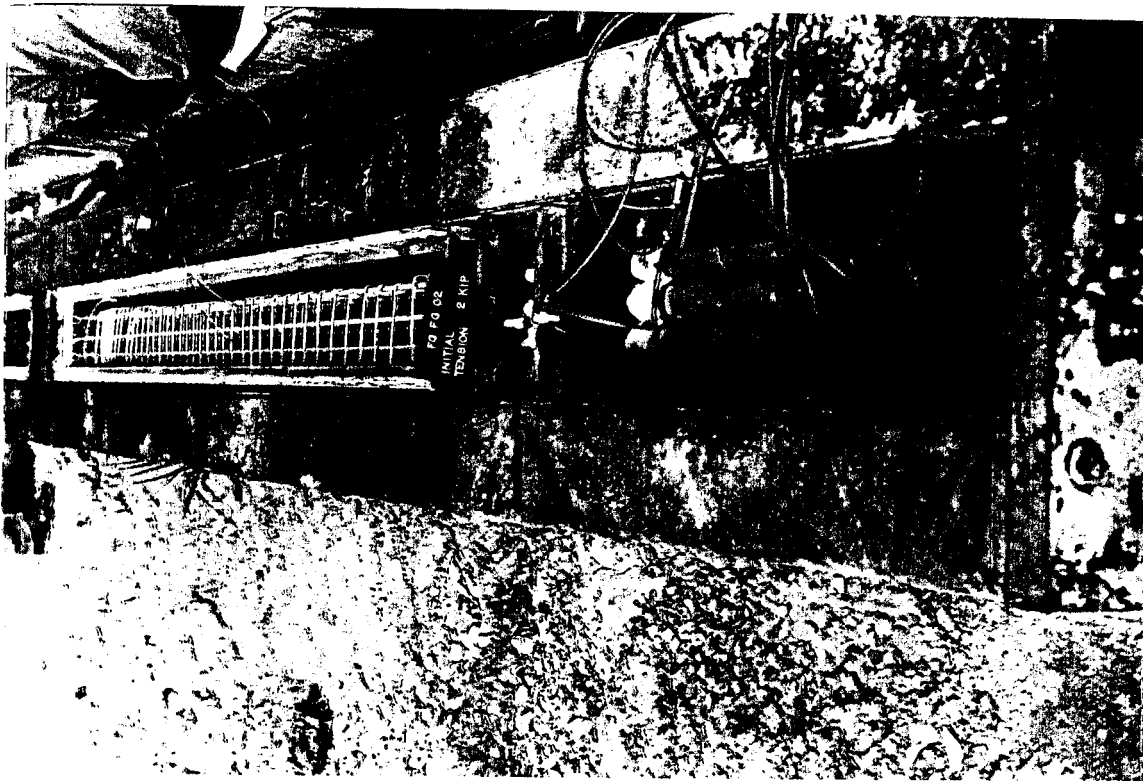


Plate 4.8 (top) Transfer block bolted to header plate at dead end
(btm) Fiberglass/steel transfer blocks in bed

individual transfer blocks as shown in Plates 4.8. Eight steel cables were similarly threaded through the header plate at the live (pulling) end, run through the spiral ties and spacers, and chucked to the other end of the individual transfer blocks. During this maneuver, the leading end of the strands had to be followed carefully to avoid getting tangled. Also, particular care had to be taken in order not to damage the somewhat more delicate fiberglass strands.

Load cells made of hollow steel cylinders 5 in. long by 1 in. diameter were attached to the live and dead ends (see Plate 4.9 and 4.8). An initial tension of about 2 kips (see Table 5.3) was applied to remove the slack in the strands and facilitate their instrumentation. A 30 ton capacity, 48 in. stroke, center hole hydraulic jack manufactured by Hercules and powered by an electric motor was used to tension the strands (see Plate 4.9). Strain gages were then attached to each strand at predetermined locations.

Following instrumentation of strands, they were individually tensioned to the full jacking load using two kip increments. The target jacking force for each strand was 11 kips - 156.7 ksi or 53 % of the ultimate strength of fiberglass and 129.4 or 45 % of the ultimate strength of steel. This provided a total jacking force of 88 kips per specimen and an estimated effective prestress in the 700-800 psi range for the 100 in² pile cross-section. During this operation, the rotation of transfer blocks was carefully monitored. No slippage was observed and the entire jacking operation was completed in about 2 hours. After tensioning was completed, the spacing of the spiral ties was adjusted and each tie was attached to the prestressing strands. For the steel strands, steel wire ties were used, whereas for fiberglass, plastic ties were used (see Plates 4.10-4.12). This procedure took almost six hours since great care was taken not to damage the strain gages that were attached to the surface of the strands. For the pile specimens, all wires coming out from the strain gages were carefully tied together and taken out as a bundle near the "top" of the pile.

Concrete was poured and vibrated approximately twenty one hours following the completion of the prestressing operation. A 2 hp needle vibrator with a 1³/a in. diameter head was used to vibrate the concrete every 12 in. This operation was carried out by a crew from Henderson Prestress in the manner used for commercial production. The concrete surface was levelled, trowel finished and covered by plastic sheets to retain moisture as shown in Plate 4.13. Eighteen 6 in. x 12 in. concrete cylinders were cast simultaneously. Humid and rainy weather following the pour assisted in the curing process of the concrete.

After four days, the concrete strength was 6,080 psi and the prestressing force was released. The release was accomplished by carefully cutting the steel-strands using an oxy-acetylene torch. Since the fiberglass strands could not be cut using the same equipment, a hacksaw was used instead. The specimens were removed from the bed using a forklift as shown in Plate 4.14.

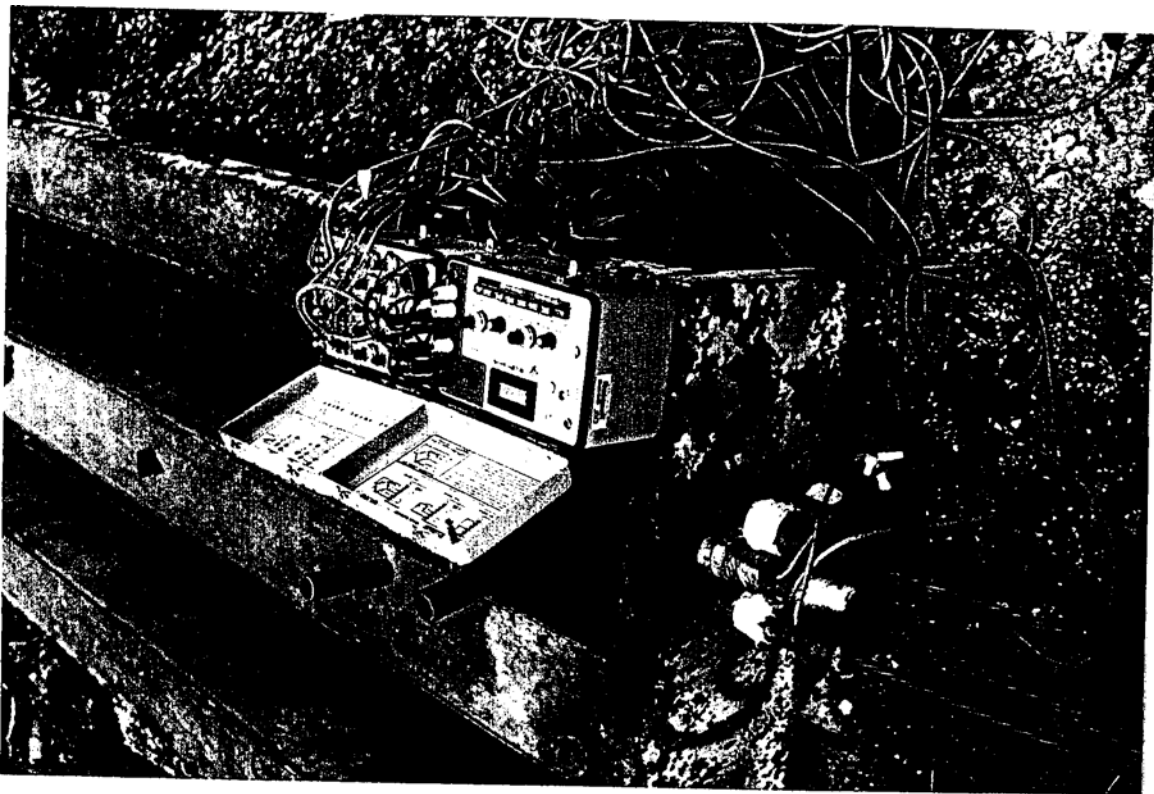


Plate 4.9 (top) Load cells at jacking end
 (btm) Prestressing jack used

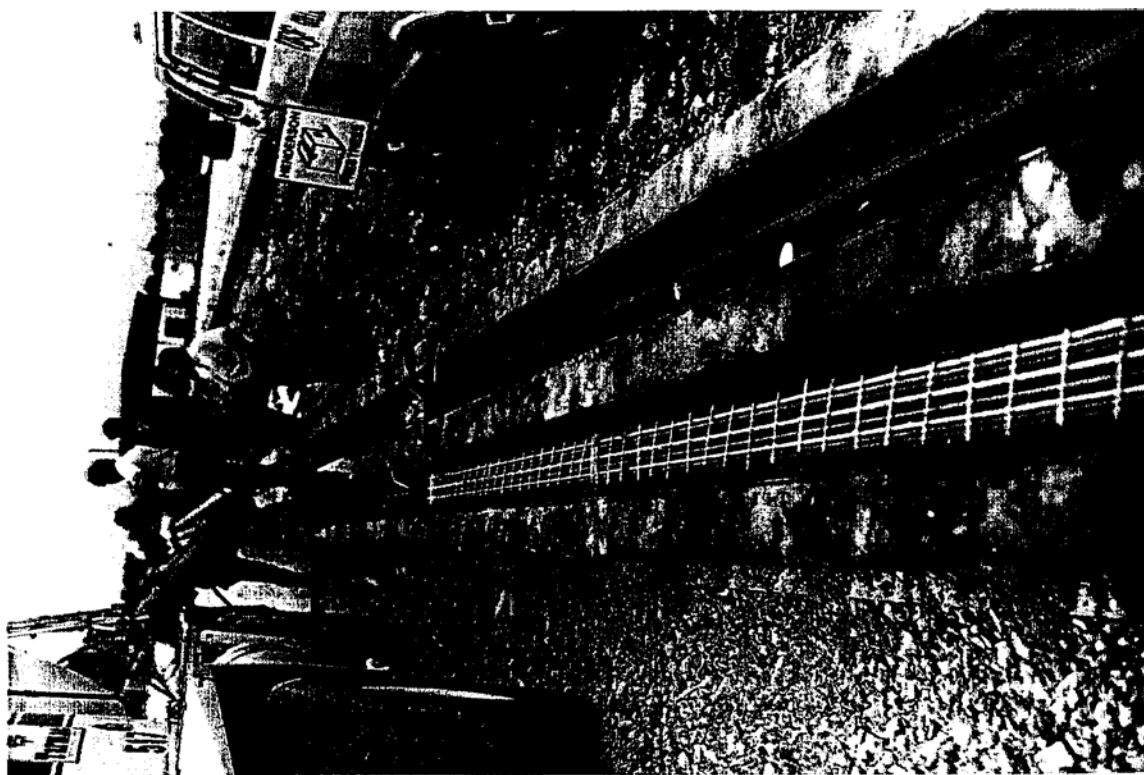
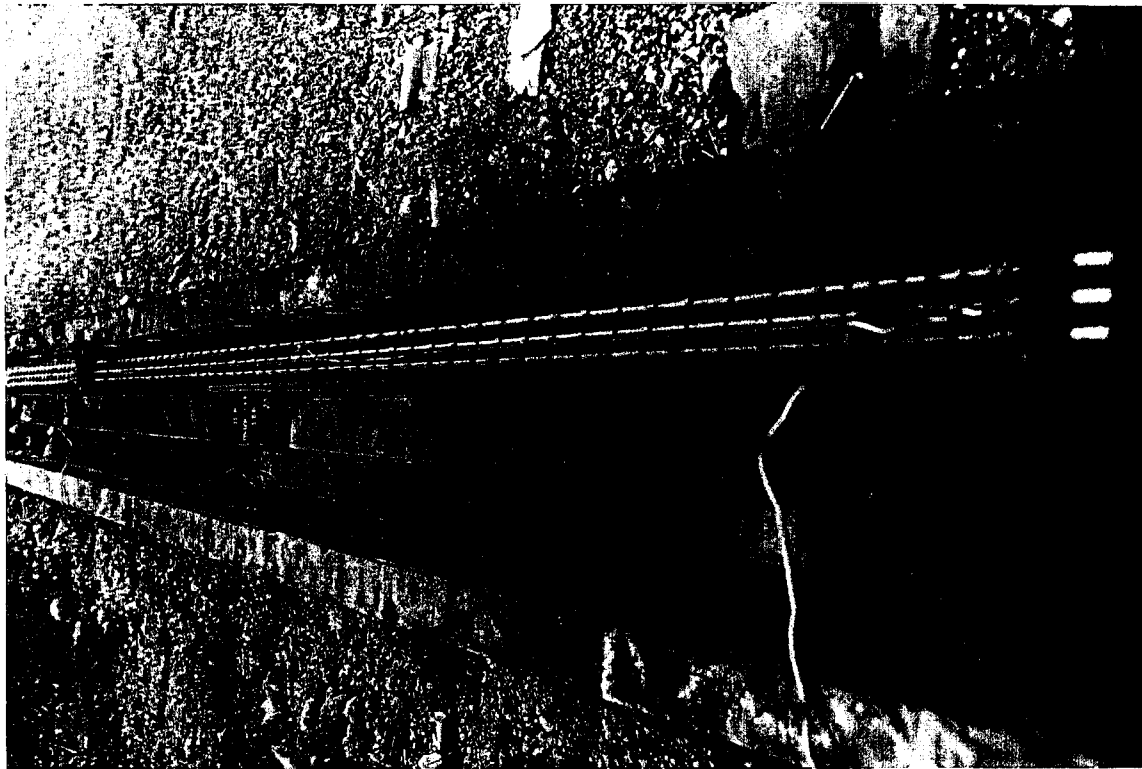


Plate 4.10 (top) Instrumented fiberglass pile with steel ties
(btm) Instrumented all fiberglass pile before concreting

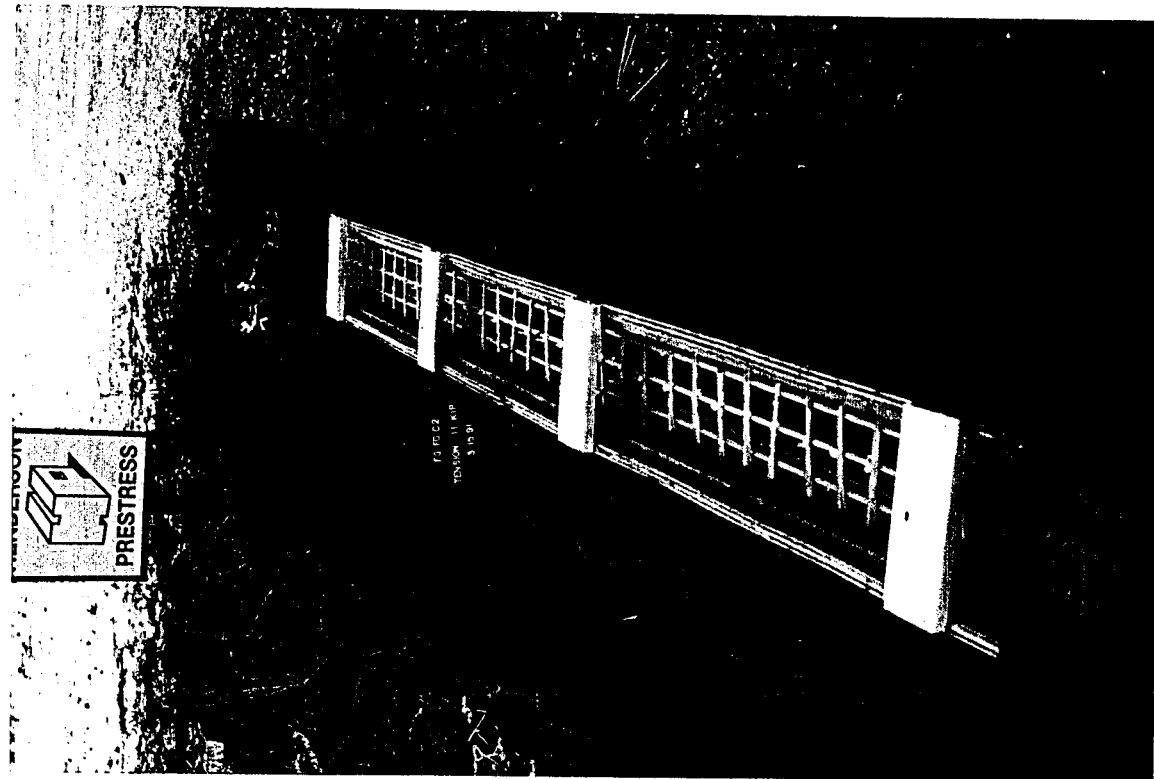
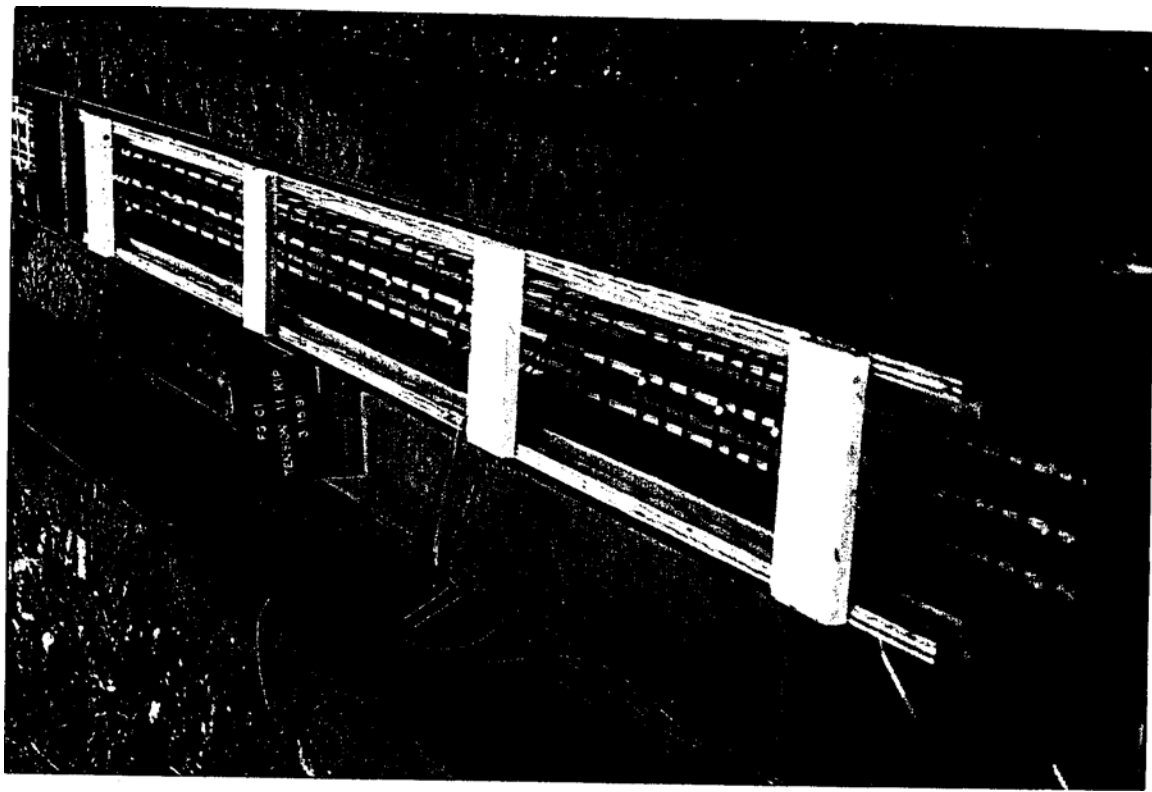


Plate 4.11 (top) Instrumented fiberglass column with steel ties
(btm) Instrumented all fiberglass column before concreting

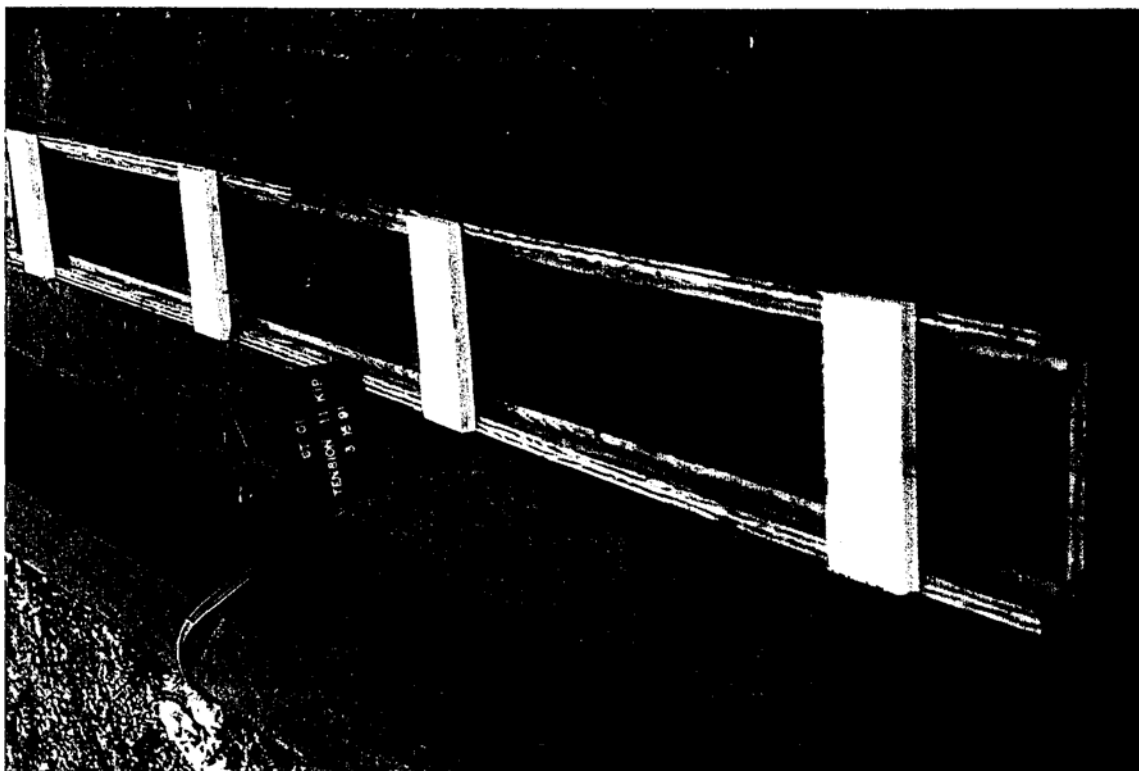


Plate 4.12

(top) Instrumented steel pile prior to pour
(btm) Instrumented steel column prior to pour

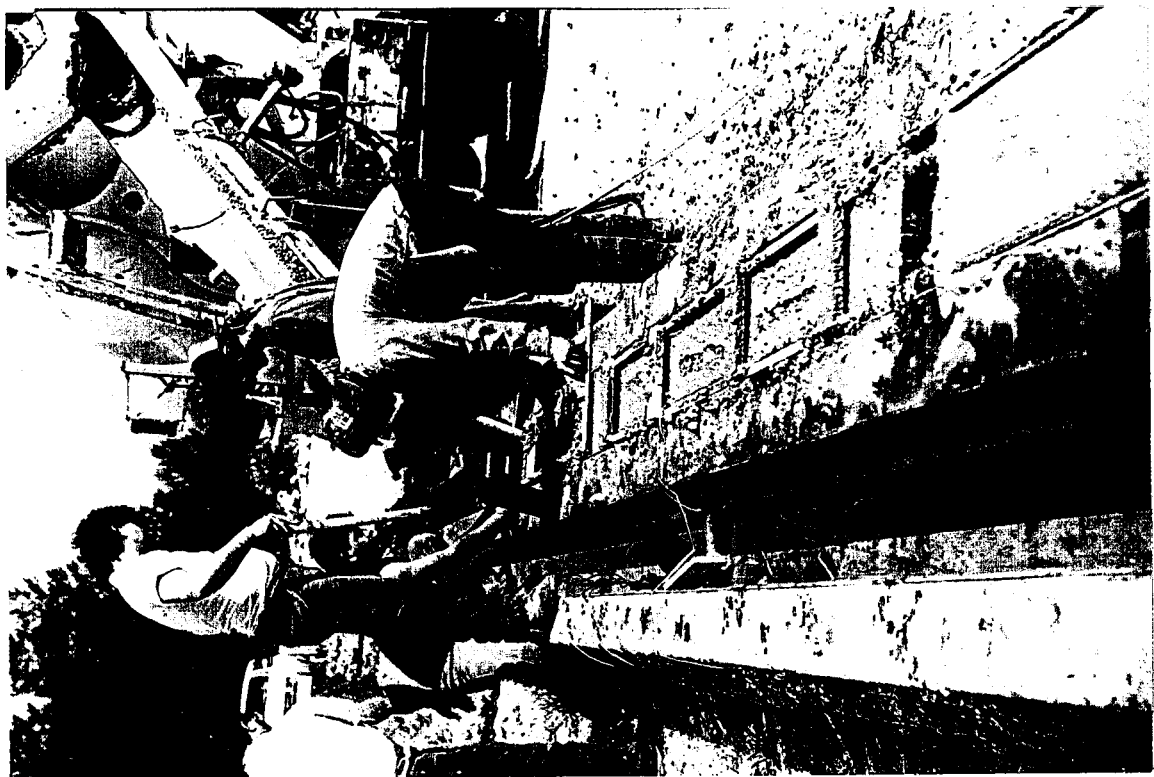


Plate 4.13 (top) Concreting of specimens
 (btm) Curing of specimens

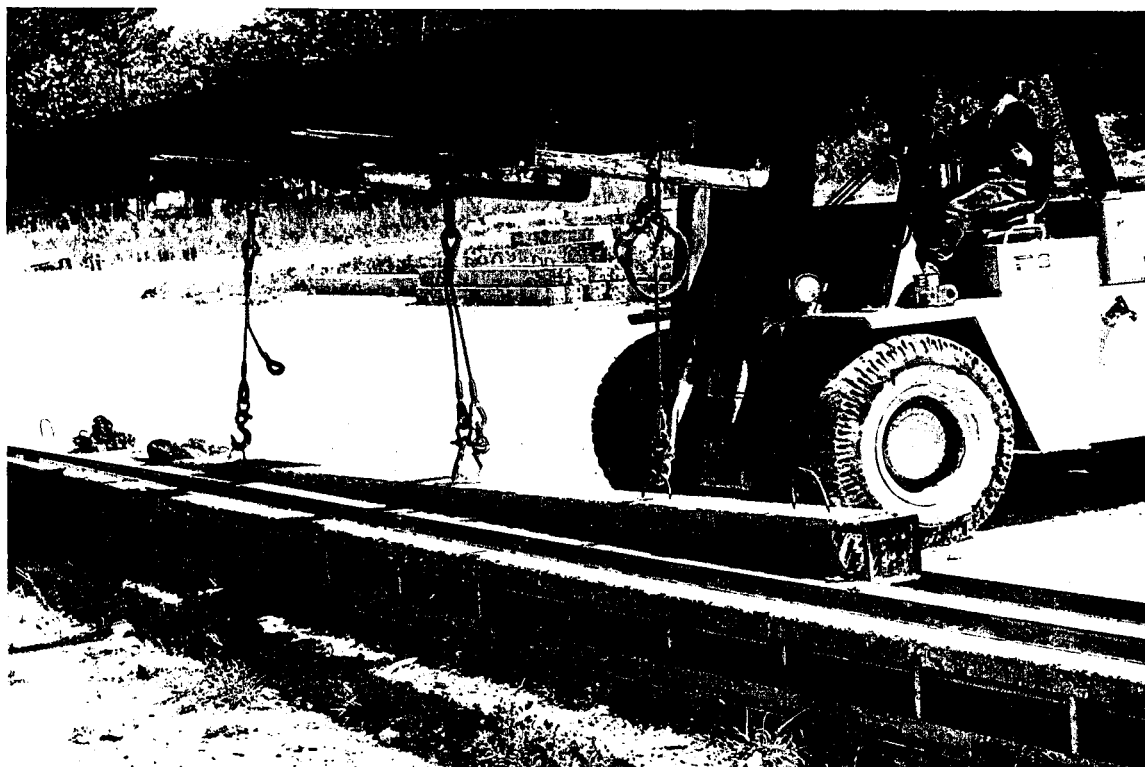
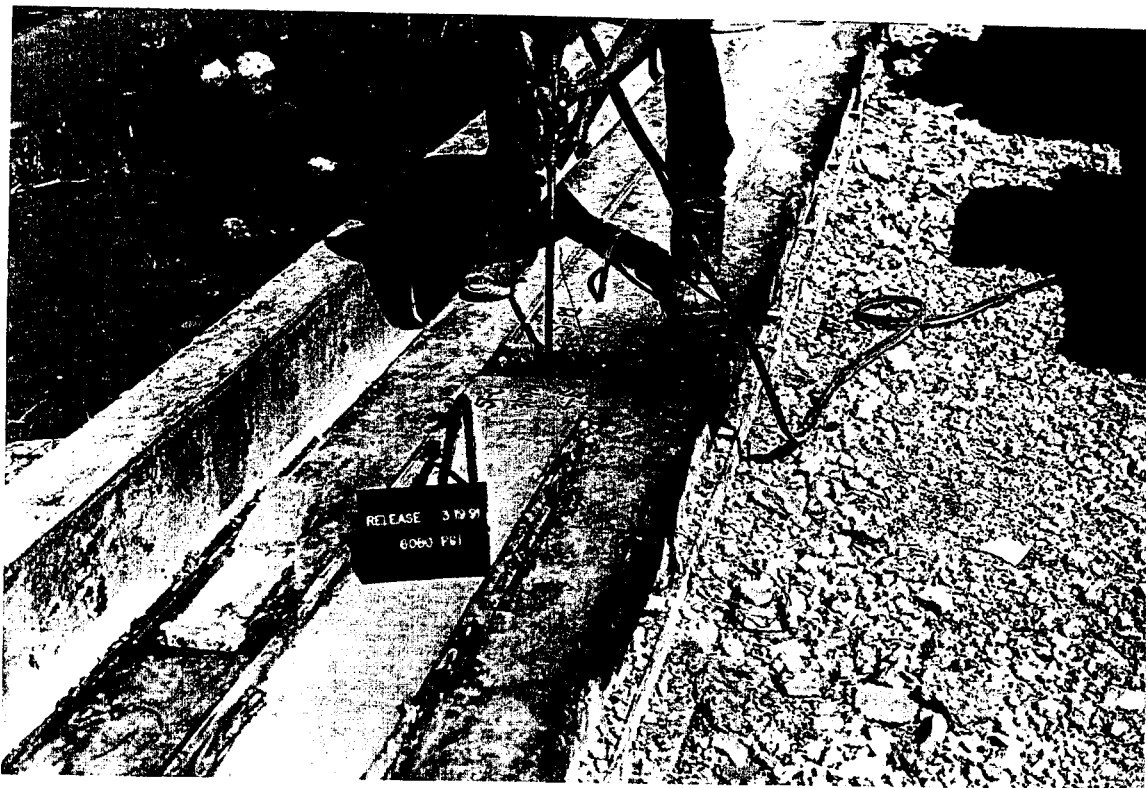


Plate 4.14 (top) Release of prestress force in steel specimen
 (btm) Removal of fiberglass pile specimen from bed

5. SHORT TERM LOSSES

5.1 Introduction

During the fabrication of the beam, column and pile specimens described in the previous chapter, strain gages were installed in the fiberglass and the steel strands. While these gages were primarily intended to provide information on the structural response during testing, they also provided data on short term losses. This chapter provides an analysis of the strain gage data and compares the relative short term losses in identical fiberglass and steel pretensioned specimens.

For completeness, a brief description of the strain gages used and their installation appears in Section 5.2. Since the strain gages were attached to a single rod (wire) of the seven rod (wire) strand, the procedure used for calculating stresses is first assessed by comparison with simultaneous load cell results in Section 5.3. The analysis of strain gage results to determine short term losses in beams is subsequently described in Section 5.4. The interpretation of test results to estimate the effective prestress in piles and columns is discussed in Section 5.5.

5.2 Strain gages

Electrical strain gages were attached to the fiberglass and steel strands following initial tensioning to remove slack. For the 30 ft pretressing bed at the University of South Florida, an initial force of about 500 lbs was needed. A much larger force of about 2 kips was required for the 400 ft long bed at Henderson Prestress.

Model FLE-05-1L strain gages (Gage Factor 2.16) supplied by Texas Measurements were used. For the steel strands, the surface was sanded and treated with CSM-1 degreaser, conditioned with M-Prep A and neutralized with Neutralizer 5 (all supplied by Micro-Measurements, NC). For the fiberglass strands, the surface was lightly sanded and cleaned with Neutralizer 5. The gages were attached to the surface of the strands using M-Bond 200 following directions given in Instruction Bulletin B-127-11. The gages were given a protective coat of MCOAT D and waterproofed using linerless rubber splicing tape.

The gages were positioned on the strands taking into consideration its expected elongation. For the beam study, a total of 24 gages were attached at mid-span so that each strand in each beam was instrumented. Only one gage did not work. For the column and pile study, 60 gages were attached to the strands at locations 1 ft from top and bottom and at mid-span. Unfortunately, due to malfunctioning of the SYSTEM 4000

Data Aquisition System only 40 out of the 100 strain gage channels worked. These related only to the fiberglass strands. The load cells monitoring forces at the dead end were also lost but those hooked to the live end to switch and balance units provided information on the jacking and initial prestressing forces. Of the gages, that were hooked to SYSTEM 4000 about 60% worked.

5.3 Correlation with load cell results

In the beam study, load cell data was recorded from the jacking prior to release of the prestressing force. Tables 5.1-5.2 compare their values with the corresponding strain gage results. Since the strains due to initial tensioning were not recorded they have been added on. Inspection of Tables 5.1 and 5.2 show very good agreement between the strain gage data and load cell readings when average values are used in conjunction with reported values of the modulus (see Table 2.5).

The same approach was also used to compare results from the column and piling study. In this case, eight strands were pulled (see Figure 5.1). Inspection of Table 5.3 shows good agreement with strain gage results being within 4 % of the load cell readings.

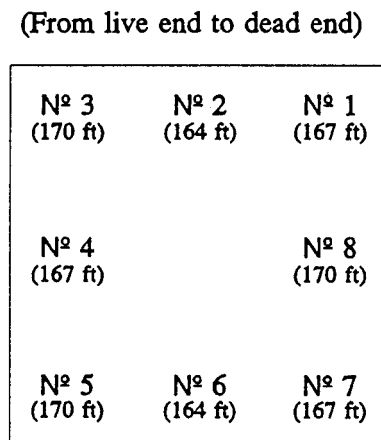


Figure 5.1 Strand Numbering and Fiberglass Strand Lengths

5.4 Short term prestress losses

Stresses in steel and fiberglass strands in the pretensioned beams calculated from strain data are summarized in Tables 5.4-5.6. The stresses at jacking, release and transfer

Table 5.1 Comparison of Load cell Reading & Strain Gage Reading at Jacking

Type of Strand	Line	Load Cell (lb)	Strain Gage Reading (10^6)				Jacking Force ¹ (lb)	Error ²
			Gage 1	Gage 2	Gage 3	Avg.		
Steel	1	15,945	6,890	6,750	7,150	6,930	16,022	-0.0%
	2	15,963	6,913	6,604	6,512	6,676	15,435	3.3%
	3	10,018	14,617	14,530	NG	14,574	10,343	-3.2%
	4	10,000	13,426	13,549	13,307	13,427	9,529	4.7%
Fiberglass	5	10,036	13,815	13,202	13,619	13,545	9,613	4.2%
	6	9,931	14,685	14,098	14,237	14,340	10,177	-2.5%
	7	10,138	15,000	14,715	14,563	14,759	10,475	-3.3%
	8	10,023	14,802	14,692	14,122	14,539	10,318	-2.9%

¹ Jacking force = Avg. strain x Area of strand x Modulus of elasticity
 = Avg. strain x 0.08 x 28.9×10^6 (for steel)
 = Avg. strain x $0.0702 \times 10.11 \times 10^6$ (for fiberglass)

² Error = (Load cell - Jacking force)/Load cell

Table 5.2 Comparison of Load cell Reading & Strain Gage Reading at Release

Type of Strand	Line	Load Cell			Strain Gage Reading (10 ³)			Pre. Force ¹ (lb)	Error ²
		(lb)	Gage 1	Gage 2	Gage 3	Avg.			
Steel	1	13,794	6,061	5,923	6,323	6,102	14,109	-2.3	
	2	13,986	6,138	5,840	5,760	5,913	13,670	2.3%	
	3	9,061	13,488	13,392	NG	13,440	9,539	-5.3%	
	4	9,265	12,586	12,699	12,471	12,585	8,932	3.6%	
	5	9,088	12,704	12,102	12,514	12,440	8,829	2.8%	
Fiberglass	6	9,562	14,098	13,489	13,667	13,751	9,760	-2.1%	
	7	9,401	13,991	13,722	13,572	13,762	9,767	-3.9%	
	8	9,368	13,856	13,775	13,214	13,615	9,663	-3.1%	

^{1,2} Calculated as indicated in Table 5.1

were obtained from strain readings. The effective prestress was calculated on the basis of observed creep and shrinkage. A similar approach was used by Harajli & Namaan, 1984 [5.1] who used a time step analysis in lieu of test data.

Table 5.3 Summary of Prestressing Operation

Cable Number	Tension in Strand (kips)	Initial Tension (kips)	Initial Force (kips)		Average Initial Force ¹ (kips)	Error (%)
			Strand Gage	Load Cell		
Nº 3	8.83	1.78	10.6	11.4	11.0	-3.64
Nº 5	7.36	2.73	10.1	10.3	10.2	-0.98
Nº 8	8.53	1.83	10.4	10.5	10.5	0.00
Nº 4	8.44	2.04	10.5	10.6	10.6	0.00
Nº 7	7.88	1.92	9.8	9.9	9.9	0.00
Nº 1	8.21	2.11	10.3	10.4	10.4	0.00
Nº 6	NG	2.00	10.3 ¹	10.5	10.4	-0.96
Nº 2	8.66	1.77	10.4	10.9	10.7	-1.87
		Total	82.4	84.5	83.5	-1.20

¹ Averaged from all strand gage readings

Although strain gage data was recorded between the time of release and the time of testing of the beams, it showed inexplicable increases. Harajli & Namaan's use of analysis to determine effective prestress rather than the use of strain gage readings suggests that they may have experienced similar problems. This could be the result of local interaction between the gages and protective coating used. For fiberglass strands this increase could be due to shear lag effects in which strains are transferred from the interior of the fiber to the outside where gages are attached. This was also experienced by Somes, 1963 [5.2]. This phenomenon needs further investigation.

A summary of the prestressing losses is presented in Table 5.6. It may be seen that the losses in the fiberglass strands of about 25 ksi are almost half those for the steel pretensioned beams. The lump sum loss for steel is 5 ksi higher than the 45 ksi value in the AASHTO [5.3] specifications for 5,000 psi concrete. In addition, the losses are also expressed as percentages of the jacking stress. These are 17.3 % and 25.4 % for fiberglass and steel respectively.

Table 5.4 Tensioning Stress Summary for Steel Beams

Beam	Line	f_{pj} (ksi)	f_{pi} (ksi)	$f_{tran.}$ (ksi)	f_{pe}^1 (ksi)	$f_{pj} - f_{pe}$ (ksi)
ST-W8	1	199.3	172.4	154.9	148.4	50.9
	2	199.5	174.8	157.5	151.0	48.5
	Avg. (% f_{pj})	199.4	173.6 (12.9%)	156.2 (21.7%)	149.7 (24.9%)	49.7
ST-E8	1	199.3	172.4	154.1	147.2	52.1
	2	199.5	174.8	156.5	149.6	49.9
	Avg. (% f_{pj})	199.4	173.6 (12.9%)	155.3 (22.1%)	148.4 (25.6%)	51.0
ST-M8	1	199.3	172.4	152.9	145.7	53.6
	2	199.5	172.8	157.5	150.3	49.2
	Avg. (% f_{pj})	199.4	173.6 (12.9%)	155.2 (22.2%)	148.0 (25.8%)	51.4

¹ f_{pe} is the effective prestress at time of testing.

5.5 Effective Prestress in Piles and Columns

In addition to strand gages, columns and piles were provided with embedded gages and surface gages. The embedded gages were placed inside the spiral cage and secured with plastic electrical ties before concreting. They were 60 mm long, model PML-60-2LT (Gage Factor 2.12). 60 mm long model PL-60-1L (Gage Factor 2.11) were also attached to the concrete surface. Both gages were supplied by Texas Measurements. All readings were manually recorded using a switch and balance unit in conjunction with a strain indicator box during release.

Table 5.5 Tensioning Stress Summary for Fiberglass Beams

Beam	Line	f_{pj} (ksi)	f_{pi} (ksi)	$f_{tran.}$ (ksi)	f_{pe} (ksi)	$f_{pj} - f_{pe}$ (ksi)
FG-W8	3	142.7	129.1	118.9	116.7	26.0
	4	142.5	132.0	104.9 ¹	102.7 ¹	39.8 ¹
	5	143.0	129.5	117.6	115.4	27.6
	Avg. (% f_{pj})	142.7	130.2 (8.8%)	118.3 (17.1%)	116.1 (18.7%)	26.8
FG-W9	6	141.5	136.2	126.2	123.8	17.7
	7	144.4	133.9	126.1	123.7	20.7
	8	142.8	133.4	119.5	117.1	25.7
	Avg. (% f_{pj})	142.9	134.5 (5.9%)	123.9 (13.3%)	121.5 (15.0%)	21.4
FG-E8	3	142.7	129.1	NG	NG	NG
	4	142.5	132.0	106.5 ¹	104.2 ¹	38.3 ¹
	5	143.0	129.5	116.6	114.3	28.7
	Avg. (% f_{pj})	142.7	130.2 (8.8%)	116.6 (18.3%)	114.3 (20.1%)	28.7
FG-E9	6	141.5	136.2	125.7	123.2	18.3
	7	144.4	133.9	125.7	123.2	21.2
	8	142.8	133.4	119.4	116.9	25.9
	Avg. (% f_{pj})	142.9	134.5 (5.9%)	123.6 (13.5%)	121.1 (15.3%)	21.8
FG-M8	3	142.7	129.1	118.2	115.8	26.9
	4	142.5	132.0	104.8 ¹	102.4 ¹	40.1 ¹
	5	143.0	129.5	116.5	114.1	28.9
	Avg. (% f_{pj})	142.7	130.2 (8.8%)	117.4 (17.8%)	115.0 (19.4%)	27.9
FG-M9	6	141.5	136.2	125.3	122.6	18.9
	7	144.4	133.9	125.6	122.9	21.6
	8	142.8	133.4	119.3	116.6	26.2
	Avg. (% f_{pj})	142.9	134.5 (5.9%)	123.4 (13.6%)	120.7 (15.5%)	22.2

¹ One of the rods in this strand broke during concreting.

Table 5.6 Prestress Loss Summary

Type of Strand	Beam	$f_{pj} - f_{pe}$ (ksi)	Avg. Lump Sum Loss (ksi)	Avg. % f_{pj}
Steel	ST-W8	49.7	50.7	25.4
	ST-E8	51.0		
	ST-M8	51.4		
Fiberglass	FG-W8	26.8	24.8	17.3
	FG-W9	21.4		
	FG-E8	28.7		
	FG-E9	21.8		
	FG-M8	27.9		
	FG-M9	22.2		

Table 5.7 presents results from embedded gages placed at mid-length of the column and pile specimens following transfer. The stress was calculated using the ACI modulus of elasticity for a compressive strength of 6,080 psi at transfer. The effective prestressing force was calculated by multiplying the stress by the area of concrete, 100 in² for piles and 64 in² for columns.

Inspection of Table 5.7 shows that only three of the readings (68.0, 76.0 and 81.8 kips) are in the range of the applied force of 83.5 kips (see Table 5.3). Interestingly, the force obtained from ST-C2 is 10.5% lower than that in FG-P2. The high value of 81.8 kips in FG-FG-P1 indicates the influence of bending strains.

Results from surface gage readings at two locations in four pile specimens are summarized in Table 5.8. The same unfavorable variability found in the embedded readings may also be detected in these gage readings. The stress in the concrete and the effective prestressing force was calculated using the same procedure outlined earlier.

As for the results obtained from embedded gages, the force in the steel pile ST-P2 is lower than that in the fiberglass piles FG-FG-P1 and FG-FG-P2. It is evident from the scatter of results presented in Tables 5.7 and 5.8 only an estimate can be made of the prestress at transfer. A reasonable value for the fiberglass specimens appears to be the average of 76.0 kips (Table 5.7) and 72.4 kips (Table 5.8) for a stress of 742 psi in the piles or 1,160 psi in the columns. The corresponding values for the steel specimens, based on the average of 68.0 kips (Table 5.7) and 64.9 kips (Table 5.8) are 665 psi and 1,038 psi respectively. Since very small losses (1-3%) were recorded for beams between transfer and testing (see Tables 5.4 and 5.5) these stresses are also reasonable estimates of the effective prestress.

Table 5.7 Embedded Concrete Gage Data at Release

Specimen	Measured Strain ($\mu\epsilon$)	Concrete Stress (psi)	Effective Force (kips)
ST-P1	245	1,089	108.9
ST-P2	NG	--	--
FG-P1	NG	--	--
FG-P2	171	760	76.0
FG-FG-P1	184	818	81.8
FG-FG-P2	NG	--	--
ST-C2 ¹	239	1,062	68.0

¹ Column specimen

Table 5.8 Surface Concrete Gage Data at Release

Specimen	Location from Top (in)	Measured Strain ($\mu\epsilon$)	Concrete Stress (psi)	Effective Force (kips)
ST-P2	26	146	649	64.9
	150	139	618	61.8
FG-P1	27	77	342	34.2
	150	129	573	57.3
FG-FG-P1	28	147	653	65.3
	150	163	724	72.4
FG-FG-P2	23	74	329	32.9
	150	153	680	68.0

6.3 Experimental Program

A total of fourteen specimens, seven fiberglass and seven identical steel pretensioned specimens from four separate pours were instrumented to determine transfer length. In addition, changes in transfer length over 20 months for two of these specimens was also investigated at the University of Illinois at Chicago.

Since identical steel and fiberglass pretensioned specimens were investigated under identical conditions, many of the non-quantifiable construction-related factors affecting transfer length mentioned by Zia & Mostafa, 1977 [6.4], such as consolidation and consistency of concrete, are factored out from our investigation. This allows direct comparison of average bond stresses in fiberglass and steel and the suitability of using transfer length equations proposed for steel for fiberglass may also be evaluated.

The specimens tested were the 6 in. x 4 in. x 8 ft 6 in. specimens for the durability and creep study. Details of fabrication of these specimens and relevant material properties are described in Chapter 4. The specimens used for the transfer length study (see Figure 4.1) were FG-M1, ST-M2 (cast December 22, 1989); FG-M3 and ST-M4 (cast December 28, 1989); FG-W4, FG-M4, FG-E4, FG-E5, ST-W5, ST-M5, ST-E6 (cast on March 13, 1990 and FG-M7 and ST-M7 (cast on June 6, 1990). Since the pretensioning force for the steel specimens cast in December was not monitored by load cells, the results for these two beams are not included here.

The specimens cast in December and the specimen FG-E5 cast were *eccentrically* pretensioned. The remaining specimens were pretensioned concentrically. All specimens were cast using type III cement (see Table 4.2) for details. Details of the compressive strength at transfer is also summarized in this table. Properties of the fiberglass strands used are summarized in Table 2.5. Half inch diameter, 270 ksi low relaxation 7 wire strands were used in the steel pretensioned specimens cast in December. Special half inch low relaxation steel strands were used in the March and June pour. Its elastic properties are summarized in Tables 4.4 and 4.5.

6.3.1 Instrumentation

To determine the transfer length, strain gages were attached to the top surface of the specimens. Since little was known about the transfer length of fiberglass beams at the time specimens were cast in December, strain gages were attached over the entire beam (see Plate 6.1). Both electrical strain gages and mechanical gages were used with the electrical strain gages attached to the sides of the beam at the level of the strands since the pretressing force was eccentrically applied.

The major transfer length study was carried out in March 1990 when eight beams were instrumented. In this case, strain gages were attached at one end (see Plate 6.1). The first gage was placed 3 in. from the end and subsequent gages were placed 4 in. apart

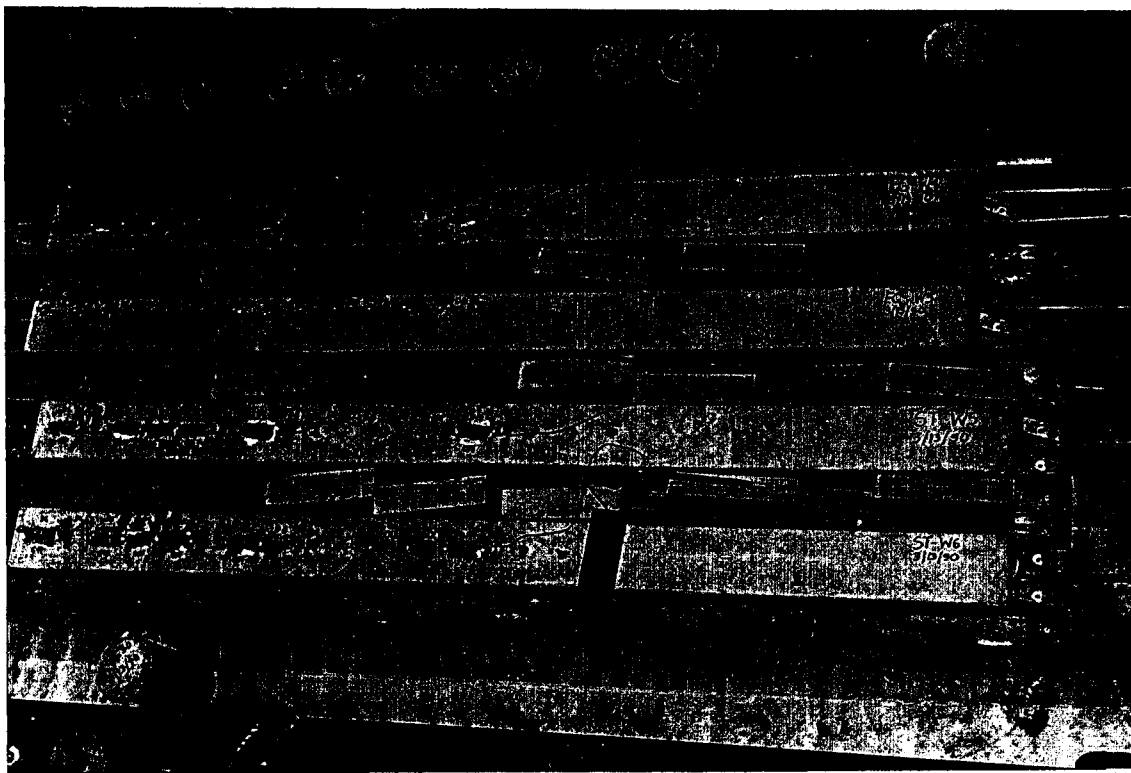
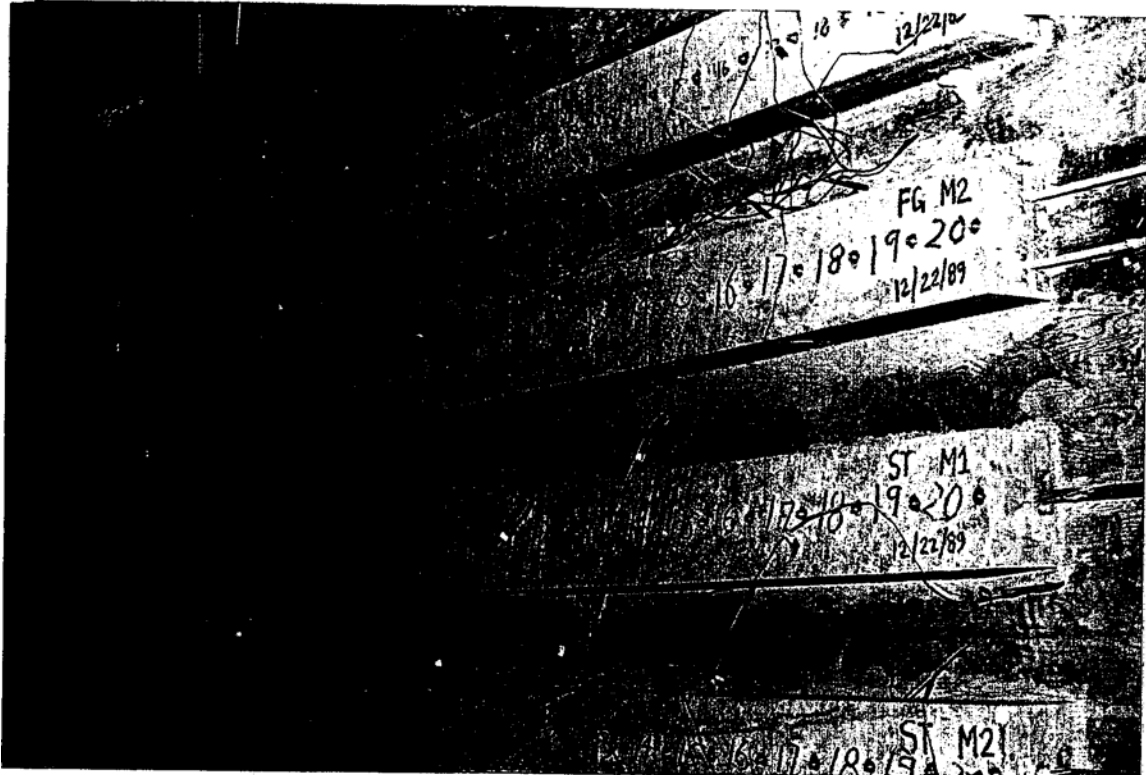


Plate 6.1 (top) Transfer length study (12/22/89)
(btm) Transfer length study (03/13/90)

at 7 in., 11 in., 15 in., 19 in., 23 in. and sometimes 27 in. Additional gages were also placed at 31 in. with the last gage at mid-span, 51 in., from the end.

For the specimens cast in December and March, all gages were hooked to Micro-Measurement's System 4000 data acquisition system that automatically records all readings. For the June pour, when only two specimens were instrumented, a strain indicator box was used in conjunction with a switch and balance unit to record the strains.

Table 6.1 summarizes essential information regarding the jacking force and the force prior to release in each of the specimens tested in March. The prestressing force prior to release in the fiberglass specimens prior to release in December was somewhat lower. It was 16.3 kips for FG-M1 and 16.5 kips for FG-M3.

Table 6.1Prestressing force summary (March1990)

Specimen Type	No. of strands	Diameter Of strand (in.)	Jacking Force in each strand (kips)	Force in each strand before release (kips)
Fiberglass	2	3/8	9.13	8.92
Steel	1	1/2	18.70	18.30

6.3.2 Test Set up and Release

All strain readings were initialized prior to release of the prestressing force which was achieved alternately by cutting both steel and fiberglass strands at the live and dead ends using an electric grinder (see Plate 4.4). The prestressing force for the specimens in the middle of the bed was then released by alternately cutting the strands at its ends. Following release of the prestressing force all strain readings were immediately taken. Details of times for the release of the prestressing force are summarized in Table 4.2.

6.4 Test results and discussion

The variation in strain with distance for the seven fiberglass beams tested are shown in Figures 6.1-6.7. The corresponding plots for the steel pretensioned members appear in Figs. 6.8-6.12. The points on each of these graphs represent strain gage locations along the length.

Figures 6.1-6.2 relate to the first series of tests in which the specimens were eccentrically pretensioned. The results for this case show that the transfer length at the two ends

pretensioned. The results for this case show that the transfer length at the two ends differ as has also been observed in studies for steel pretensioned members. The variation in transfer length is from 6.9 in. to 18.3 in. as indicated in the figures. Since eccentric prestressing introduces bending that complicates matters, the discussion presented in the sequel concentrates on the specimens cast in March and June where the loading was concentrically applied (excepting for specimen FG-E5).

Inspection of Figures 6.3-6.12 indicates that the variation in strain does not follow the classic pattern of a trapezium (when both ends are instrumented) or a ramp function, i.e. a linear increase followed by a plateau indicating that the force is transferred and then remains unchanged. Thus, the definition of transfer length is not obvious. Consequently, possible causes for the discrepancies are first addressed so that the correct transfer strain can be identified by comparison with predictions for the theoretical strain.

Examination of Figures 6.3-6.12 indicates that with the exception of FG-M4 and FG-M7 (Figures 6.4 and 6.7), the strains do not remain constant. For three of the beams, FGW4 (Figure 6.3), ST-W5 (Figure 6.8) and ST-E5 (Figure 6.10) the strains are lower at mid-span. For the remaining five beams FG-E4, FG-E5, ST-M5, ST-E6 and STM7 (Figure 6.5, 6.6, 6.9, 6.11 and 6.12 respectively) mid-span strains are higher.

Since the beams were concentrically pretensioned (with the exception of FG-E5 which was eccentrically loaded), only axial stresses were introduced. Consequently, strains changes beyond the transfer length can only be due to changes in the eccentricity of the cable. In our case, this change in eccentricity was the result of the slope of the structural floor on which the prestressed specimens were cast (Plate 4.2). A clear indication of this is evident from the similarity in the response of specimens FG-M4 and FG-M7 that were cast at the same location in the bed (see Figure 4.1) in separate pours (March 13 and June 6). Clearly, in determining the transfer length, such variations need to be disregarded.

While the trends in strain variation at mid-span were similar for the steel and fiberglass pretensioned specimens, there are important differences near the ends of the beams. For example, steel pretensioned elements do not display any localized peaks. In contrast, with the exception of FG-E5 (for which the applied prestress force was eccentric and consequently bending strains came into play) all other fiberglass pretensioned display "humps". The location of these peaks is variable, but it is generally in the 10-15 in. range.

Since the fiberglass and steel pretensioned beams were cast and instrumented identically, differences in the strain variation are likely to be the result of differences in the surface conditions of the two materials. Whereas special 1/2 in. steel strands were used, the fiberglass strands were made from seven rods that were tied together every 12 in. using plastic ties (see Plate 2.2). The ties held the rods together but during handling they moved along the beam. Because of the plastic ties, the surface of the fiberglass strands could be likened to that of a deformed bar excepting that the deformations occurred

approximately every 10-15 in. At the plastic ties, high radial bond stresses developed. The magnitude of these stresses varied with the orientation of the knotted part of the tie. If it were closer to the top surface (where measurements were made) stresses and strains over that area would show peaks. At other orientations stresses would be high but sharp peaks would not be defined. A re-examination of Figures 6.3-6.7 clearly indicates this behavior with the exception of FG-E5 (Figure 6.6) that was eccentrically loaded.

For the reasons stated above localized peaks and gradual increases or decreases in the concrete strain variation should be disregarded in the determination of transfer length. To find a measure of the strain that should be taken into consideration, it is instructive to first examine the theoretical strains that correspond to the transfer length. This will additionally allow the accuracy of the experimental results to be evaluated.

6.4.1 Theoretical Transfer Strains

The theoretical transfer strain, ϵ is given by Eq. 6.1 as:

$$\epsilon = P_i /EA \quad (6.1)$$

In Eq. 6.1, P_i is the initial prestressing force, E the elastic modulus for concrete and A the cross sectional area of the concrete. The initial prestressing force is commonly taken 90% of the jacking force for steel strands, e.g. Nilson, 1987 [6.5]. Since the elastic modulus for fiberglass is about a third that of steel, losses are lower and an estimate of 5 % is reasonable (see Table 5.2). These percentage reductions are used to estimate the initial pretension in Eq. 6.1.

Since the elastic modulus for concrete is variable, it is established from three methods - ACI method, Nilson 1981 [6.6] and from actual stress-strain variation for concrete shown in Figure 6.14. The secant modulus at $0.45f_{ci}$ is approximately 3.9 million psi for this case as shown. Using the factors of 0.9 and 0.95 on the jacking forces listed in Table 6.1 and appropriate modulus values the calculated theoretical transfer strains are summarized in Tables 6.2 and 6.3 for fiberglass and steel.

Inspection of Tables 6.2 and 6.3 indicate that the theoretical transfer length for both the fiberglass and steel pretensioned members is broadly comparable and are approximately 165 micro in./in. using ACI equations, 175 micro in/in using Nilson's equations, 185 micro in/in using the experimentally obtained value.

6.4.2 Experimental Transfer Length

The strains used to experimentally obtain the transfer length are clearly marked in Figures 6.3-6.12. The experimentally determined transfer length values for each specimen are summarized in Table 6.4 for both the steel and fiberglass specimens. This

Table 6.2 Theoretical Transfer Strains (Fiberglass)

Member	P _j kips	P _i kips	f' _c ksi	E _{ACI} ksi	E _{NIL} ksi	ε _{ACI}	ε _{NIL}
FG-W4	18.3	17.4	5.82	4348	4052	167	179
FG-M4	18.3	17.4	5.82	4348	4052	167	179
FG-E4	18.3	17.4	5.82	4348	4052	167	179
FG-E5	9.2	8.7	5.82	4348	4052	146	156
FG-M7	16.81	16.0	4.73	3920	3751	170	178

Table 6.3 Theoretical Transfer Strains (Steel)

Member	P _j kips	P _i kips	f' _c ksi	E _{ACI} ksi	E _{NIL} ksi	ε _{ACI}	ε _{NIL}
ST-M5	18.66	16.8	5.82	4348	4052	167	179
ST-W5	18.66	16.8	5.82	4348	4052	167	179
ST-E5	18.66	16.8	5.82	4348	4052	167	179
ST-E6	18.77	17.83	5.82	4348	4052	171	183
ST-M7	18.03	16.23	4.73	3920	3751	173	180

Table 6.4 Experimental Transfer Length

Beam	Transfer length	Beam	Transfer Length
FG-W4	11"	ST-W5	17.5"
FG-M4	10"	ST-M5	19"
FG-E4	11"	ST-M6	19"
FG-E5	10"	ST-E6	19"
FG-M7	10"	ST-M7	19"

indicates that the transfer length for fiberglass is about 10 in. For the steel it is about 18.5 in. The variation between the experimental strain and the theoretical strain is generally within 5-10% confirming the accuracy of the measurements.

The transfer length, L_T , for steel pretensioned members can be determined from Eq. 4 specified in the ACI Code as:

$$L_T = f_{se} \cdot d_b / 3 \quad (6.2)$$

In Eq. 6.2, d_b is the diameter of the strand. For the special 1/2 in. strand, the transfer length from Eq. 6.2 works out as 18.3 in. for an effective stress of 109.6 ksi (see Table 6.1). This length is slightly larger than the measured value of 18.5 in. Since the fiberglass strands are only 3/8 in. in diameter compared to the 1/2 in. strand, direct comparisons on transfer length cannot be made. However, since the results of the study show good agreement for steel, it is instructive to compare the transfer length for a 3/8 in. Grade 270 steel strand, stressed to the same level. Substituting, an effective prestress force of $16.8/2 = 8.4$ kips, the calculated transfer length is 12.35 in. This suggests that the bond characteristic of the fiberglass strands used are superior to that of steel. This can be attributed to fiberglass; lower modulus and it could also be due to better chemical bond between fiberglass and concrete.

The test results indicate that the transfer length for fiberglass strands is smaller than that for similarly stressed steel strands. Since the ACI equation for transfer length (Eq. 6.2) is based on a large volume of experimental data, it would be convenient to use this expression to obtain the transfer length for fiberglass pretensioned elements. This will require the use of an appropriate reduction factor that incorporates all material and texture related parameters affecting transfer length.

6.4.3 Long term transfer length

A limited study was also conducted to investigate the long term change in transfer length for the identical fiberglass and steel pretensioned specimens. Plots showing the relative increase in transfer length normalized with respect to the initial length are shown in Fig. 6.13. This increase is possibly due to deterioration in long term bond and has been noted by previous researchers, e.g. Karr and el, 1963 [6.7]. It may be seen that the increase in transfer length of about 40% is about double that for steel (20%).

6.4.4 Prediction of fiberglass transfer length

Since the mechanics of force transfer for steel and fiberglass is similar, a suitable reduction factor may be based on theoretical studies conducted for steel pretensioned specimens. Hoyer, 1939 [6.8] proposed Eq. 6.3 as an expression for transfer length for steel pretensioned elements based on the assumption of lateral expansion.

$$L_T = \frac{d}{2\mu} (1+m_c) \left(\frac{n}{m_s} - \frac{f_i}{E_s} \right) \left(\frac{f_e}{2f_i - f_e} \right) \quad (6.3)$$

where:

m_c, m_s = Poisson's ratio for concrete and steel, respectively

f_i, f_e = initial and effective prestress in steel, respectively

d = diameter of wire

n = modular ratio

μ = coefficient of friction between concrete and steel.

Inspection of Eq. 6.3 shows that it incorporates all material properties (Poisson's ratio, modulus), surface texture (friction coefficient) and the prestressing stress (initial and effective). By substituting appropriate values of the parameters for steel and fiberglass in Eq. 6.3, the theoretical relationship between the transfer length for fiberglass and steel can be established. By comparing this with experimental values, a suitable reduction factor can then be established. For the special case where fiberglass and steel have the same initial stresses, diameter and concrete properties, the relationship between the transfer length for fiberglass and steel is given by Eq. 6.4 as:

$$\frac{(L_T)_{FG}}{(L_T)_{ST}} = K = k_1 k_2 k_3 \quad (6.4)$$

where:

$$k_1 = \mu_{st}/\mu_{fg}, \quad k_2 = E_{fg}/E_{st}, \quad k_3 = m_{st}/m_{fg}$$

Eq. 6.4 was obtained by neglecting the term f_i/E_s , with respect to n/m_s and also assuming that the difference between fiberglass and steel tendons in the term $(f_i/(2f_i - Q))$ was negligible.

Eq. 6.4 indicates that the reduction factor is the product of three sub-factors k_1, k_2 and k_3 that relate the relative surface texture, elastic moduli and Poisson's ratio for the two materials. Of these, k_2 (0.31) and k_3 (1.43) are known, their product being 0.44. Thus, the reduction factor K (Eq. 6.5) is given by:

$$K = 0.44 \text{ (A., l gfs)} \quad (6.5)$$

To match experimental and test results from our study requires $k = 0.72$ (10 in. FG vs. $0.75 \times 18.5 = 13.875$ in. for ST). This indicates that $k_1 = 1.6$ or the bond between fiberglass and concrete is 60 % superior to that of steel. It should be emphasized that Eq. 6.5 is a preliminary relationship that needs to be refined as more experimental results become available. Nevertheless, it indicates that if the relative coefficient of friction between fiberglass/concrete and steel/concrete are known, the transfer length for fiberglass pretensioned elements may be estimated.

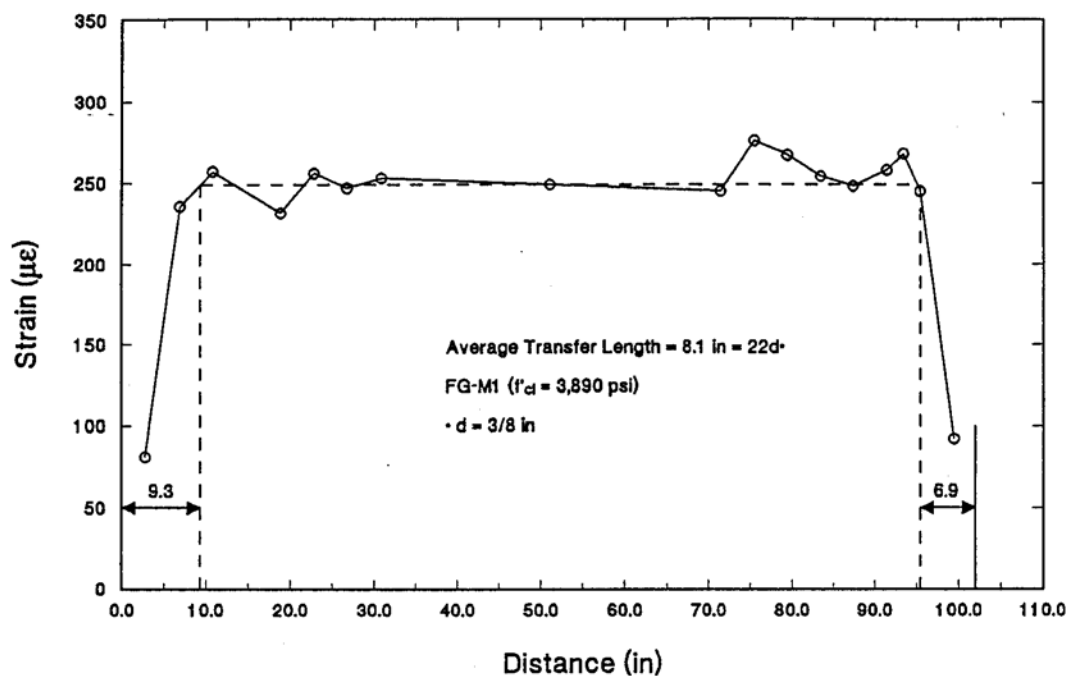


Figure 6.1 Strain variation along length for FG-M1

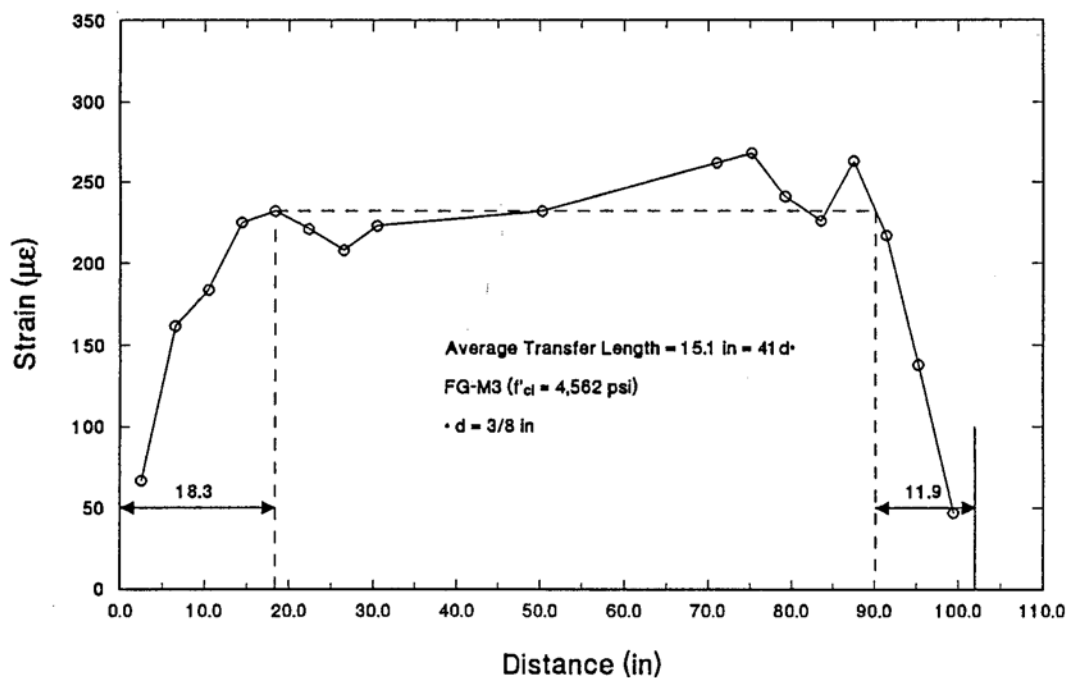


Figure 6.2 Strain variation along length for FG-M3

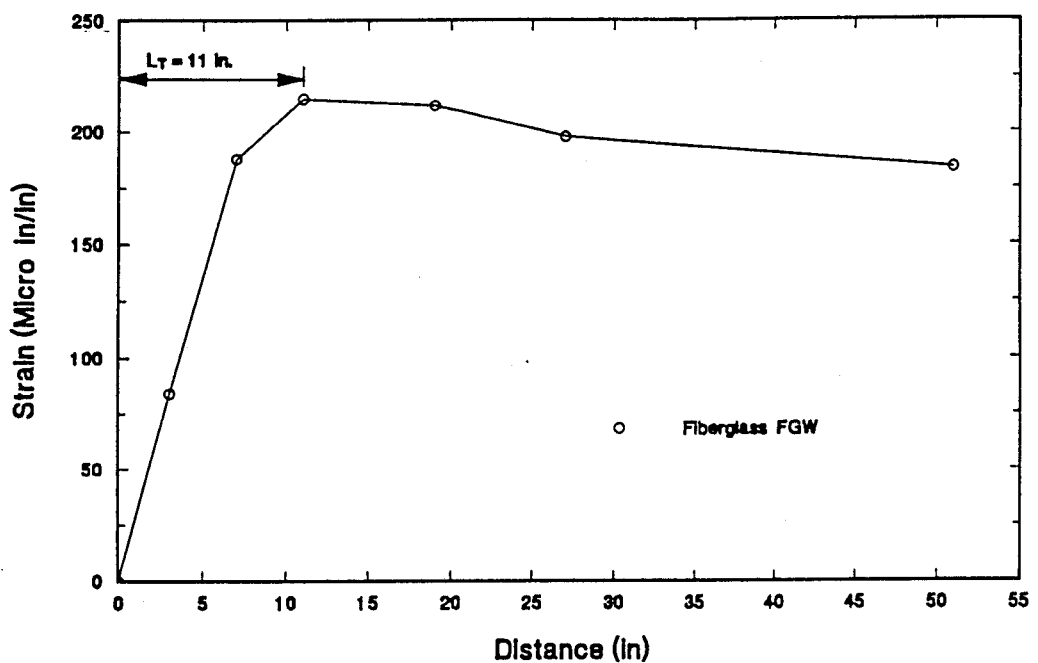


Figure 6.3 Strain Variation along Length for Beam FG-W4

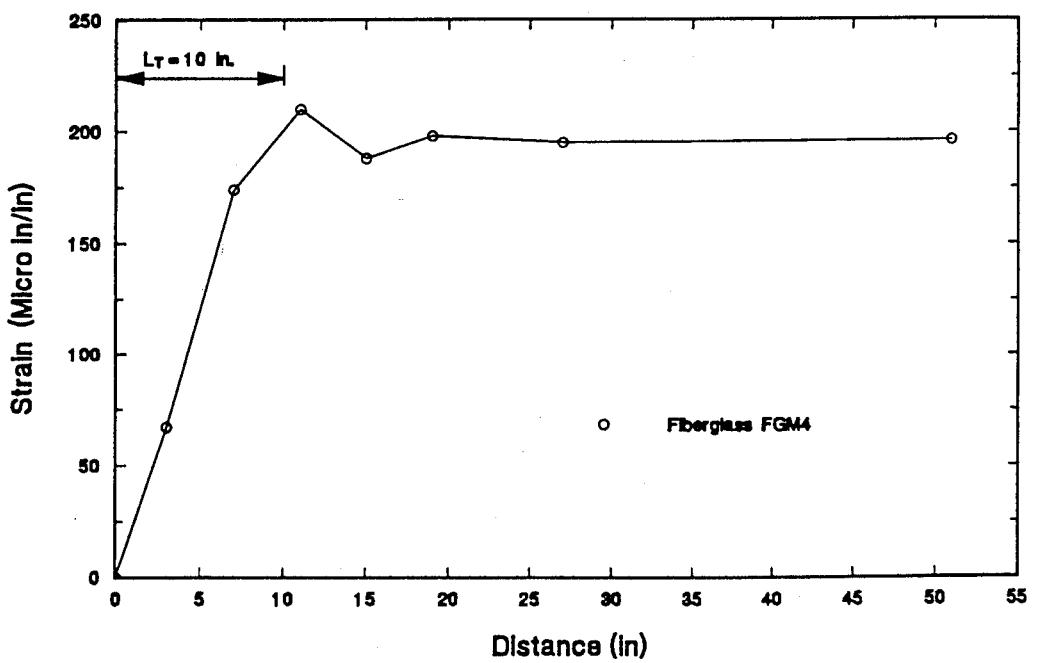


Figure 6.4 Strain Variation along Length for Beam FG-M4

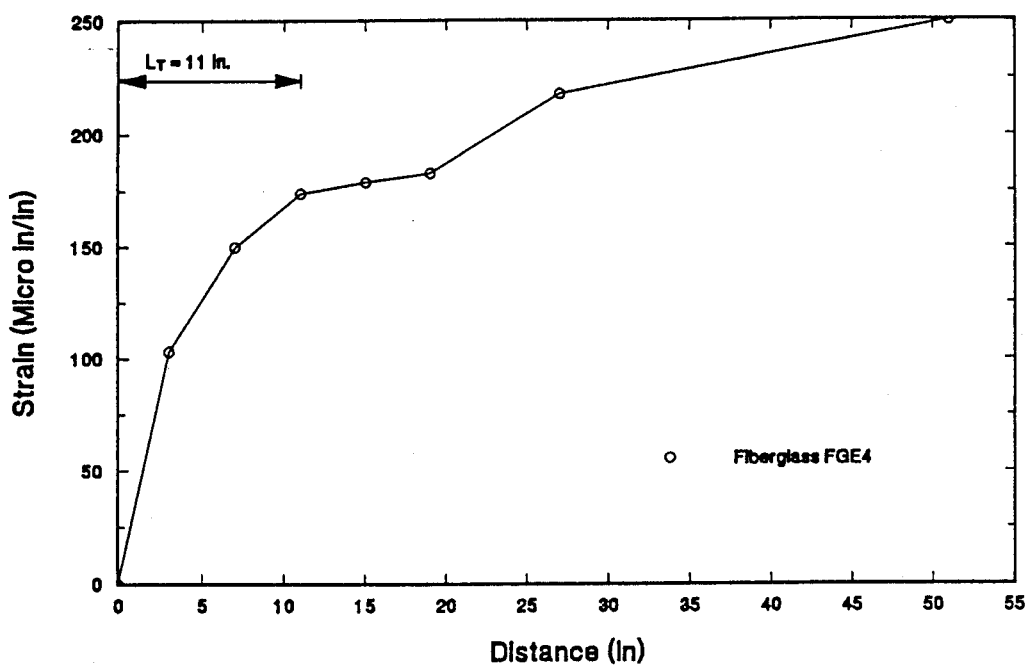


Figure 6.5 Strain Variation along Length for Beam FG-E4

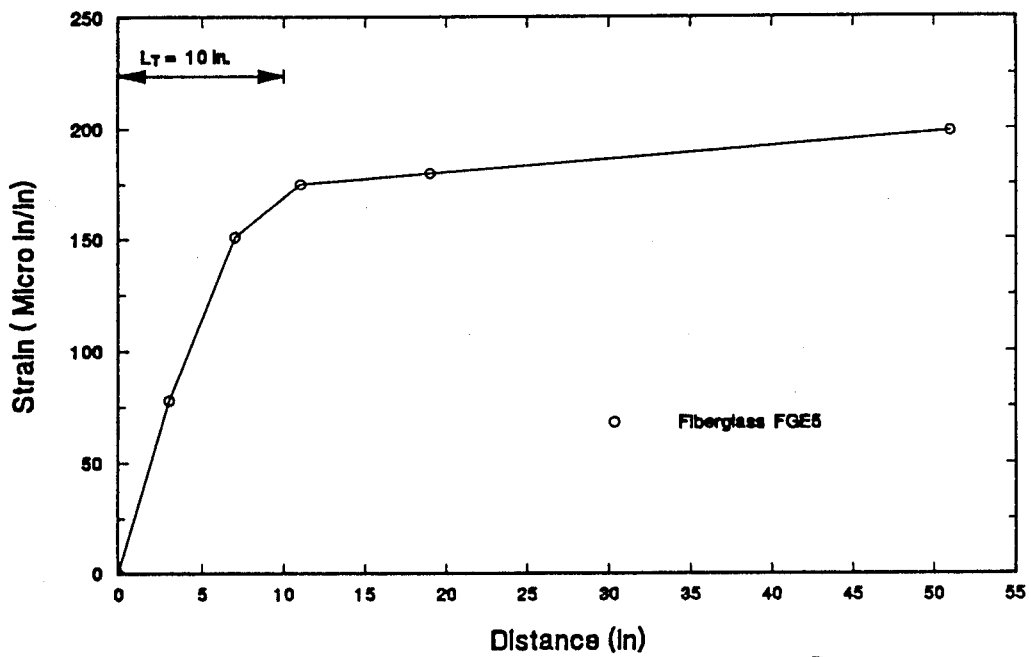


Figure 6.6 Strain Variation along Length for Beam FG-E5

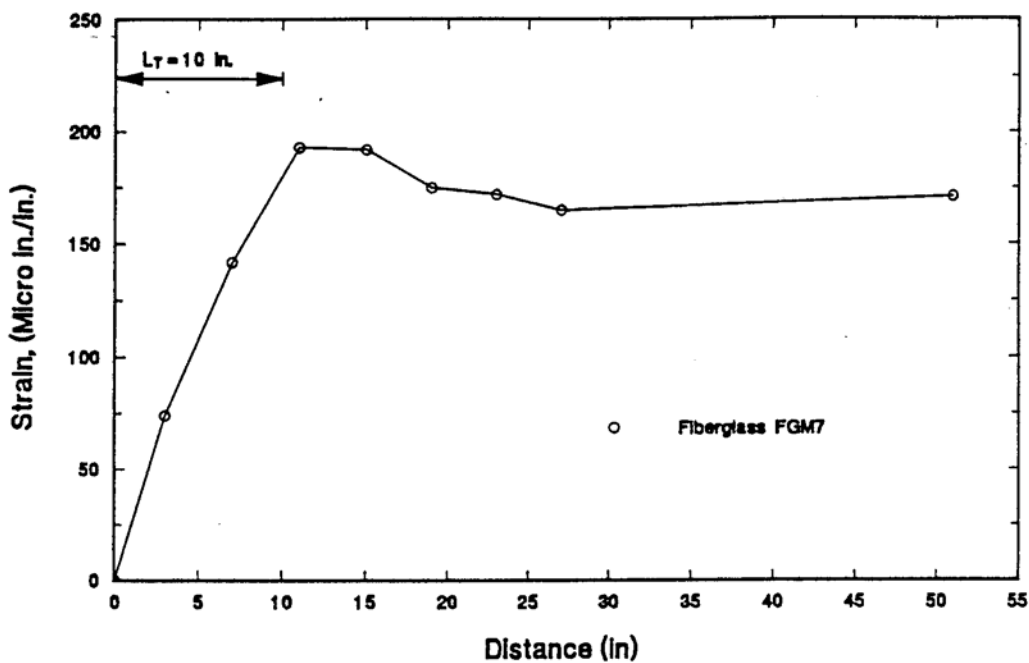


Figure 6.7 Strain Variation along Length for Beam FG-M7

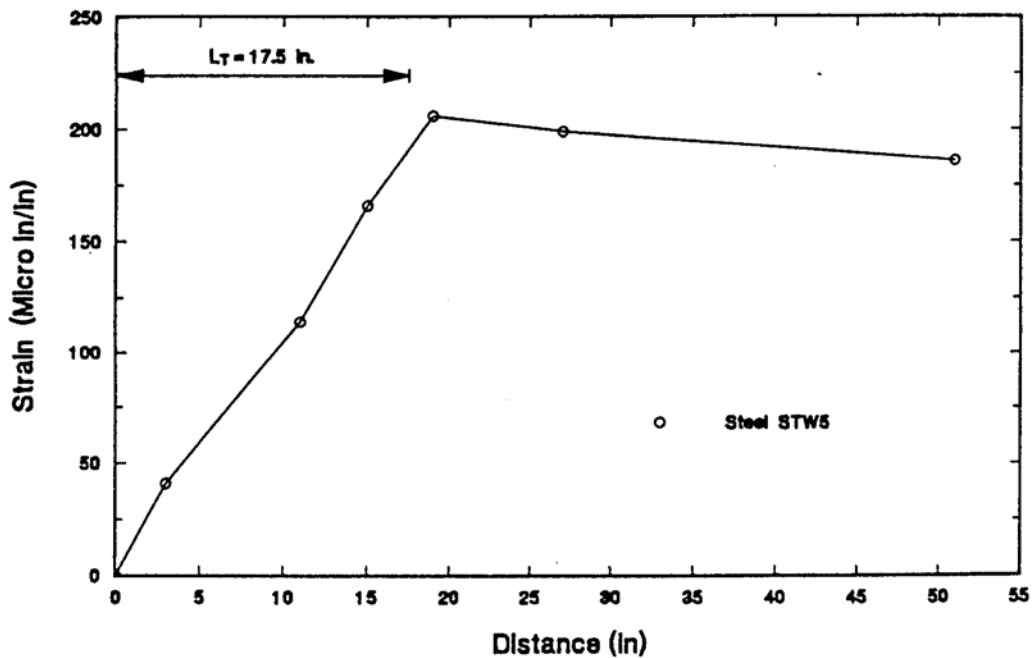


Figure 6.8 Strain Variation along Length for Beam ST-W5

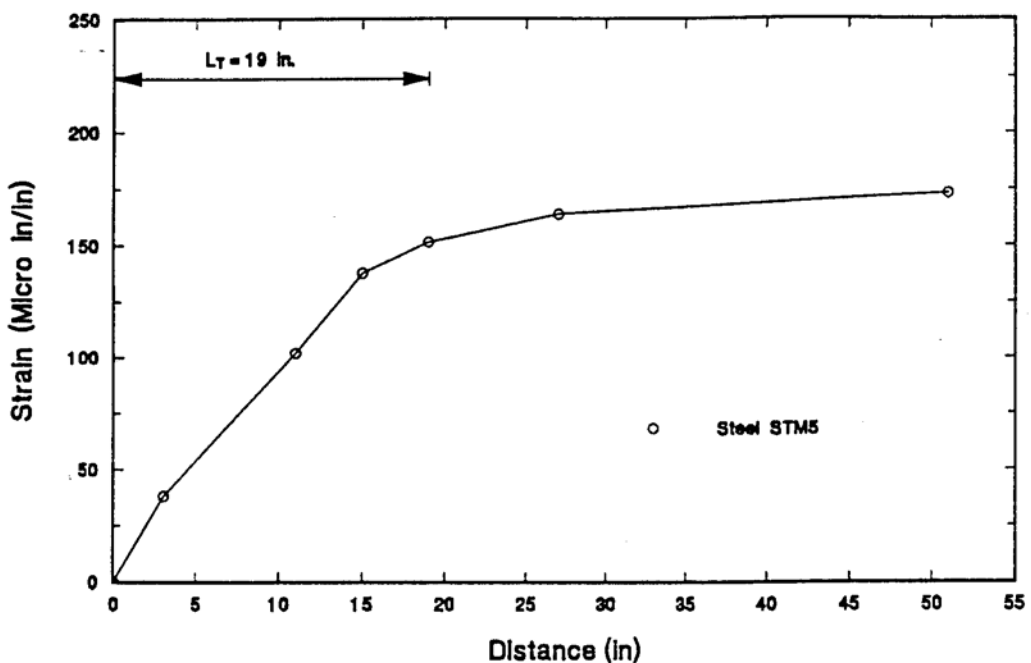


Figure 6.9 Strain Variation along Length for Beam ST-M5

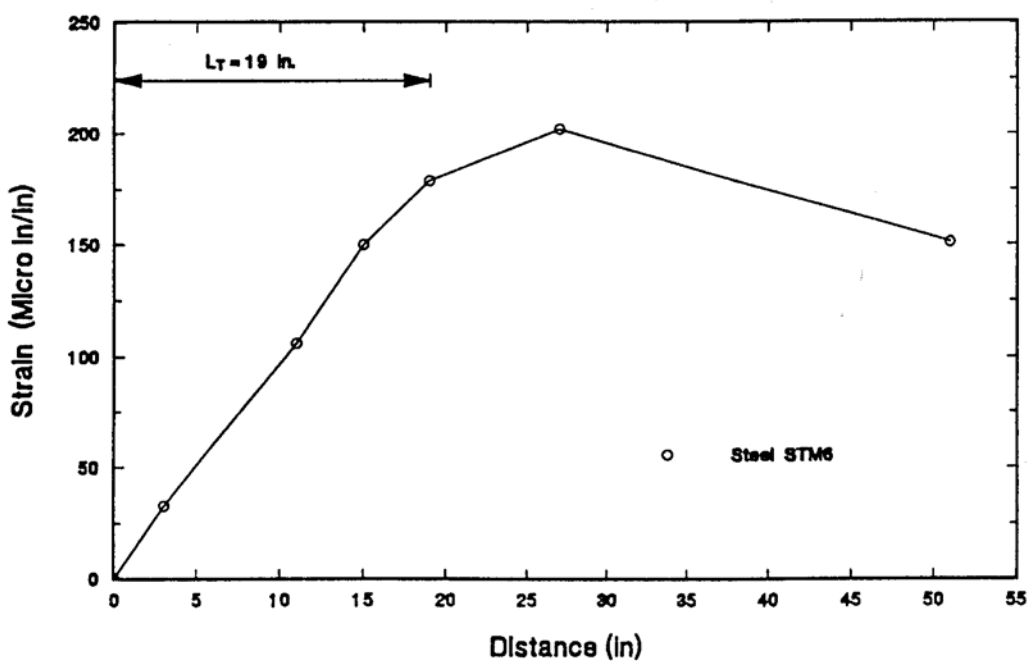


Figure 6.10 Strain Variation along Length for Beam ST-M6

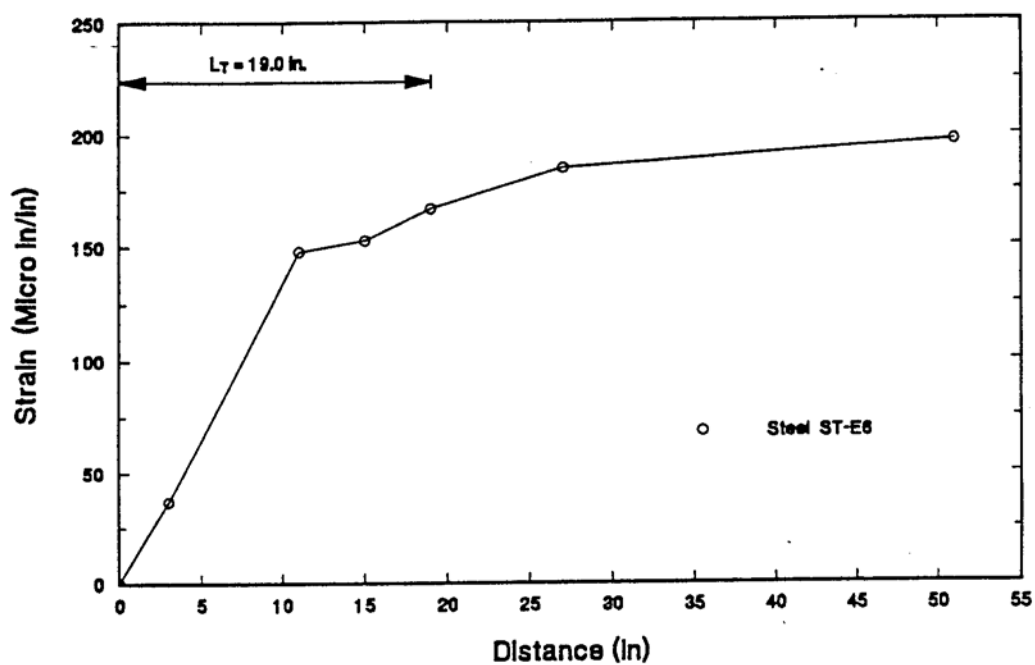


Figure 6.11 Strain Variation along Length for Beam ST-E6

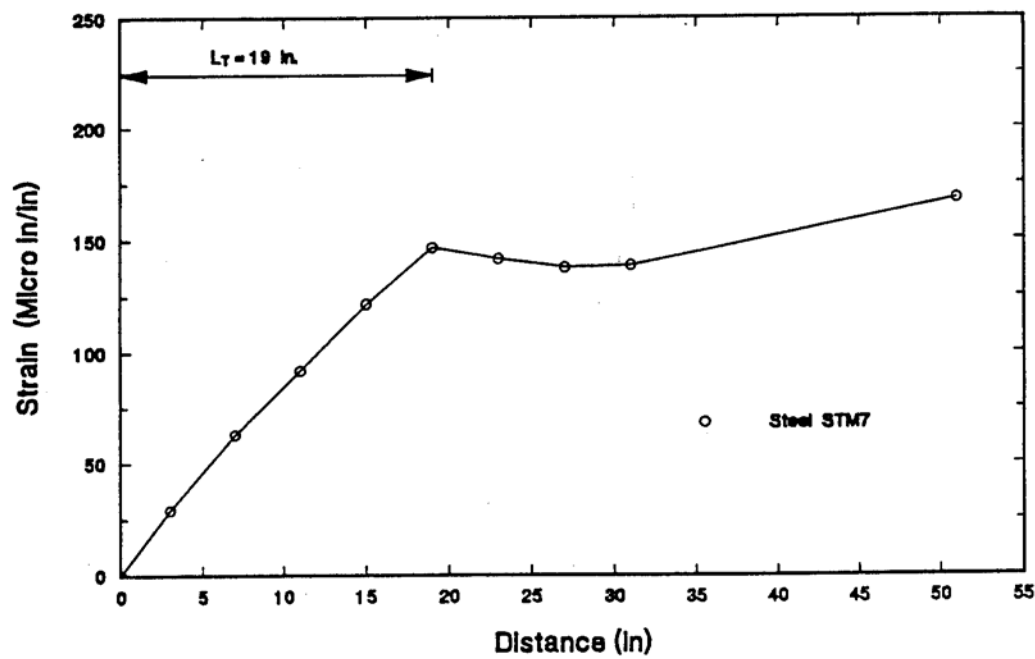


Figure 6.12 Strain Variation along Length for Beam ST-M7

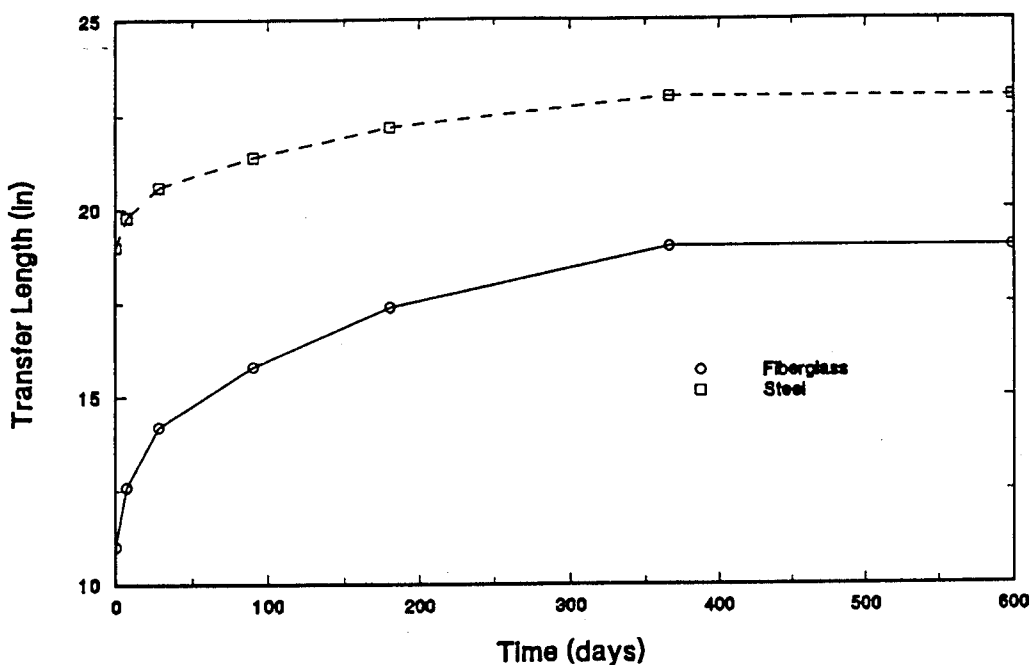


Figure 6.13 Transfer Length Vs. Time for Fiberglass and Steel Columns

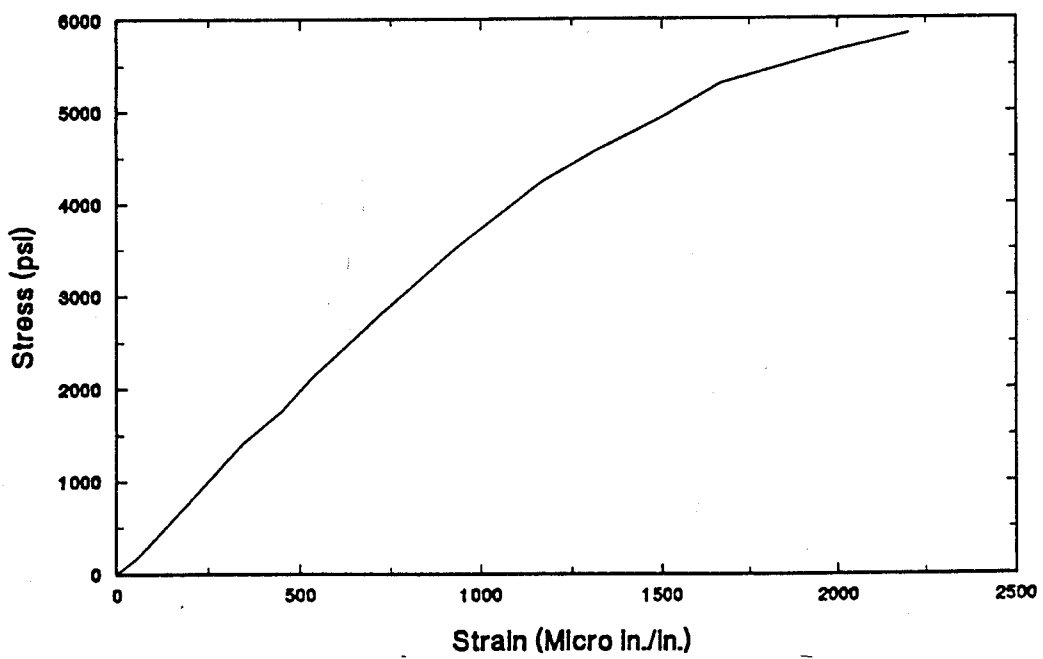


Figure 6.14 Stress-Strain Curve for concrete tested at release

6. STATIC RESPONSE

7.1 Introduction

Seven beams, four fiberglass and three steel pretensioned beams (see Table 7.1 and Figure 7.1), were statically loaded to failure. The steel beams were all under-reinforced and the fiberglass beams were designed to provide the same pretensioning force. The results of these tests are presented in the form of comparative plots showing the response of identical fiberglass and steel pretensioned beams. These show variation in deflection, concrete and prestress strain with load. Additional information relating to slip, crack pattern, cracking load, ultimate load and mode of failure is also provided. The instrumentation and test procedure are summarized in Section 7.2. The results from the study are presented in Section 7.3. Comparisons with non-linear finite element analysis are presented in Section 7.4.

Table 7.1 Beam Details for Static Test

Beam	Cross-Section (in × in)	Type	Nº of Strands	Jacking Force (kips)	e (in)	Reinforcing Index
ST-M8		Steel	2	32	2	0.18
FG-M8	6 × 8	Fiberglass	3	30	2	--
FG-M9		Fiberglass	3	30	2	--
ST-E8		Steel	2	32	3	0.14
FG-E8	6 × 10	Fiberglass	3	30	3	--
ST-W8		Steel	2	32	4	0.11
FG-W8	6 × 12	Fiberglass	3	30	4	--

Notes:

- 1 Strand area for steel is 0.080 in² (Grade 250)
- 2 Strand area for fiberglass is 0.0702 in²

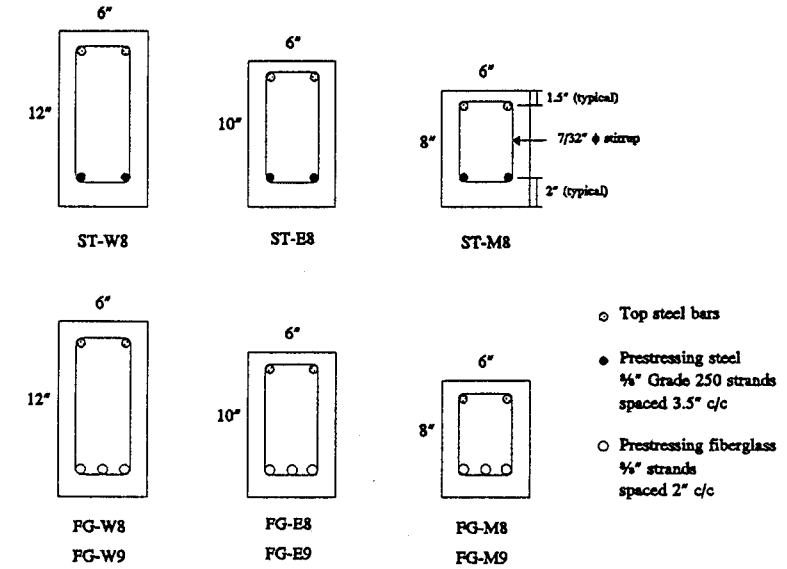


Figure 7.1 Beam Details

7.2 Instrumentation

7.2.1 Strain gages

Strain gages were attached to each of the steel and fiberglass strands in the beams at the mid-span location. Following hardening of the concrete, two gages were attached to the top surface of the beams at midspan for monitoring compressive strains. For the prestressing strands, 5 mm long gages were used (FLE-05-1L; G.F. 2.16). For the concrete surface 60 mm long gages (PL-60-1L; G.F. 2.10) used. Both gages were obtained from Texas Measurements.

7.2.2 Deflection

Deflection of the beam specimens during the test was measured at midspan using two Linear Voltage Differential Transformers (LVDT) placed symmetrically on either side of the beam. The 2 CDP-50 LVDT's were supplied Texas Measurements and had a 2 in. stroke. Both LVDT's were supported by two magnetic bases attached to a plate on the testing bed (see Plate 7.1). Two digital dial gages were used to measure the deflection of the testing bed at each end to detect differential deflection.

7.2.3 Neutral axis

Demountable gages were attached to each beam spaced 10 in. apart, at depths ranging from 1.5-2 in. depending on the beam size. The distance between these points were measured during each increment of loading using a multi-position strain gage supplied by Soiltest. The location of the neutral axis was determined from these measurements.

7.2.4 Slip

Slip of prestressed strand due to possible bond failure was measured during the tests. Two digital dial gages were kept in a horizontal direction with the sensing bar resting directly on one of the prestressing strands.

7.2.5 Crack Width

Crack width was monitored at the location of a crack at midspan using two displacement transducers (PI-5-150) supplied by Texas Measurements in the fatigue tests that are described in Chapter 11. A maximum crack width of 5 mm could be recorded by these gages (See Plate 7.1).

7.2.6. Data recording

All strain data was recorded using a P-3500 Strain Indicator box in conjunction with SB10 Switch and Balance Units, both supplied by the Measurements Group.

7.2.7 Static Test

The beams were supported to allow rotational movement at each end and translation movement at one end. The rollers were securely fastened to a steel box frame that was mounted on the MTS testing machine by plates and threaded rods. The distance between the rollers was adjusted to the 8' span and centered relative to the loading ram by a graduated tape fixed on a square tube section 6 in. x 6 in. x $\frac{3}{8}$ in. This was bolted to a swivel head assembly that was directly screwed to the load cell.

The load was transmitted to the beam (f_c was 6,840 psi at testing) by the hollow square tube section as shown in Plate 7.2. Lead plates were placed directly under the loading pads to allow uniform distribution of the loading. The applied loading comprised two point loads spaced two feet apart, thus creating a constant moment region 2 ft long. The loads were applied using a 200 kip capacity MTS closed loop electro-hydraulic system under load control mode.

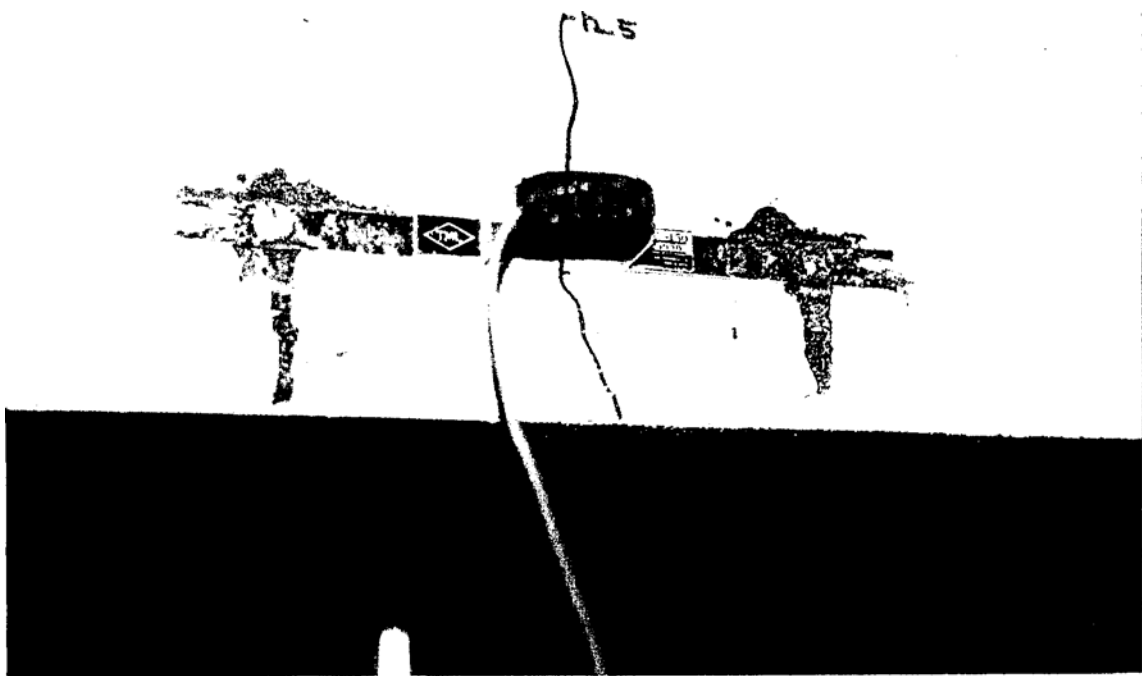
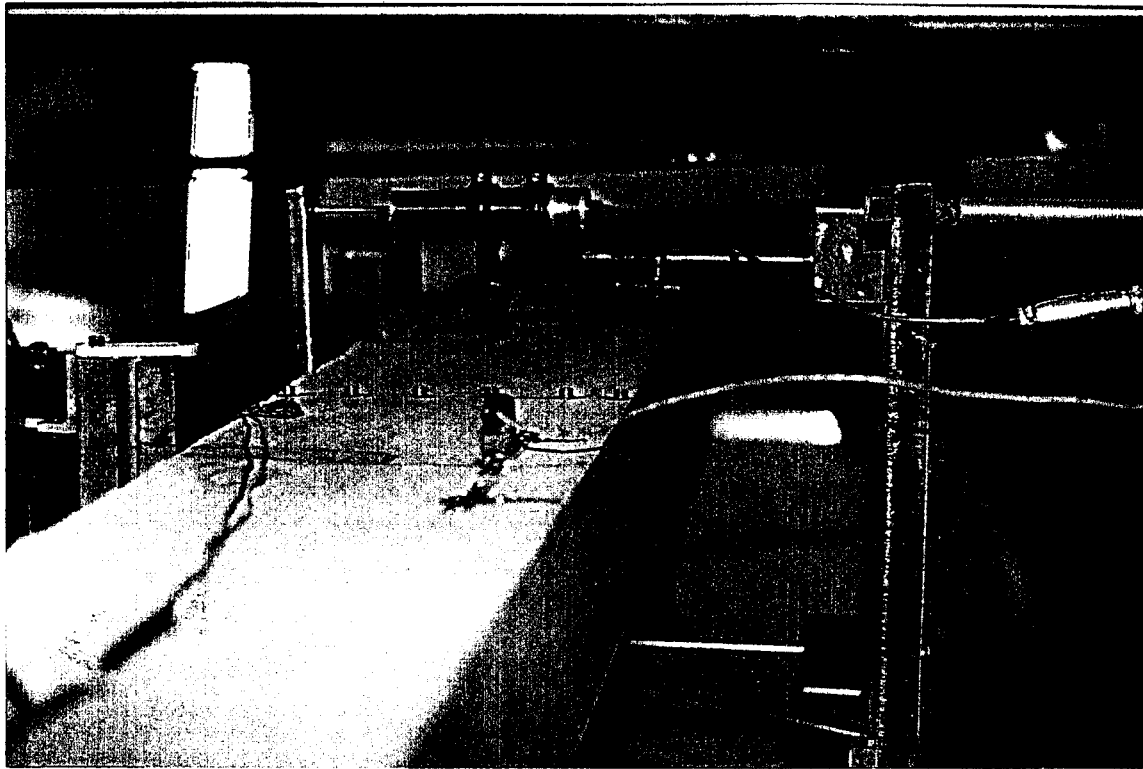


Plate 7.1 (top) Set up of LVDTs
(btm) Measurement of crack width in fatigue test

7.2.8 Test Procedure

Prior to the actual test, the beams were loaded initially to a small fraction (about 5 %) of the ultimate load then unloaded so as to stabilize the beam and also to prevent any possible twisting. The strain gages and LVDT's connected to the switch and balance units were then zeroed. The static load was applied with a 1 kip or 2 kips increment (depending on the beam size). This increment was reduced near the cracking load and when failure loads were approached. For each load increment, all data (deflection, concrete strain, prestressing strand strain, neutral axis, slip) were recorded on forms that had been prepared in advance. This indicated the predicted cracking load and also the calculated failure load.

7.3 Static Response

7.3.1 Load-deflection

Comparative load deflection plots for the three different beam sizes 6 in. x 12 in., 6 x 10 in. and 6 x 8 in. tested appear in Figures 7.2-7.4. Since two 6 in. x 8 in. fiberglass beams were tested, the plot for the second beam is in Figure 7.5.

Inspection of Figures 7.2-7.5 shows that the response of the fiberglass and steel pretensioned beams is initially linear and subsequently non-linear. The linear part corresponds to the uncracked section where the response for both beams is very similar. Any departures are due to differences in the effective prestressing force (see Table 5.2). Where the force is almost the same, as for the 6 in. x 12 in. beams, the corresponding response is near identical (see Figure 7.2).

The post-cracking response of the steel and fiberglass pretensioned beams differ. The load deflection curves then follow the respective stress strain curves for fiberglass and steel (see Figure 3.5) since the beams were all under reinforced. The fiberglass pretensioned beams deflect considerably more than the steel pretensioned beams because of fiberglass' lower modulus; it has to extend approximately three times that of the steel strand to support the same load (see Table 3.1). Thus, even though fiberglass is brittle compared to steel, the response of fiberglass pretensioned beams is ductile and failure is accompanied by large deflections and substantial cracking as shown in Plate 7.2.

A complete summary of pertinent test results such as the cracking load, ultimate load and ultimate deflection values is presented in Tables 7.2. The ratio of the ultimate to the cracking load averaged 1.67 for the steel pretensioned beams but was 2.02 for the fiberglass beams. Similarly, the ratio of the ultimate to the cracking deflection was 10.7 for the steel beams but was 13.1 for the fiberglass beams.

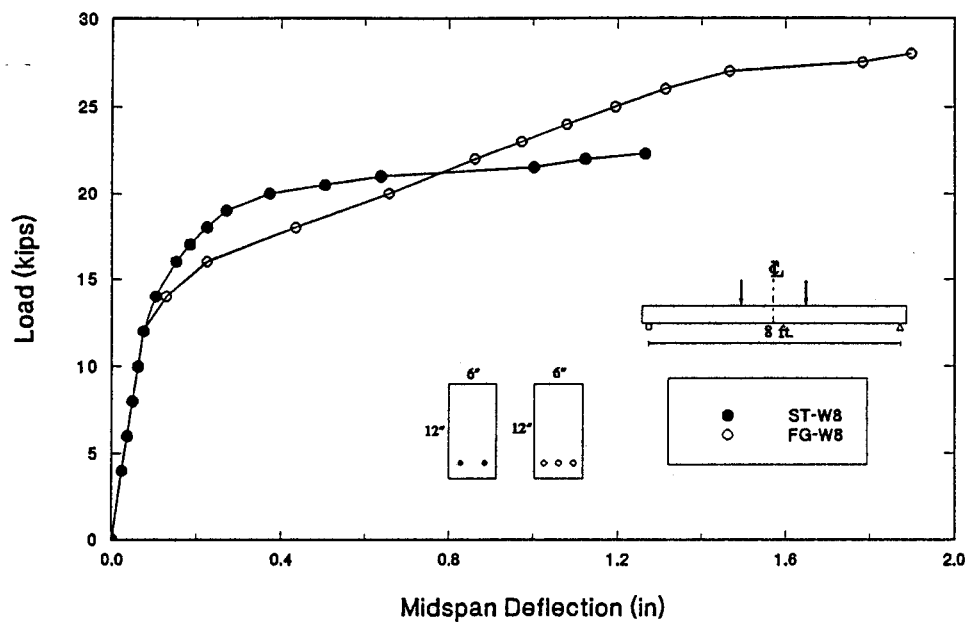


Figure 7.2 Comparative load deflection plot for 6 in. x 12 in. beams

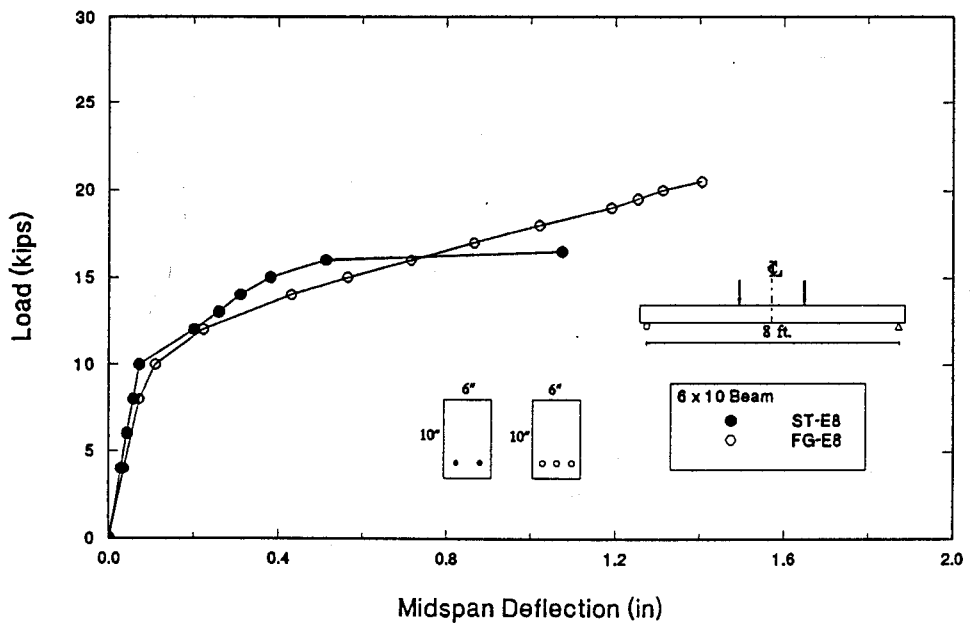


Figure 7.3 Comparative load deflection plot for 6 in. x 10 in. beams

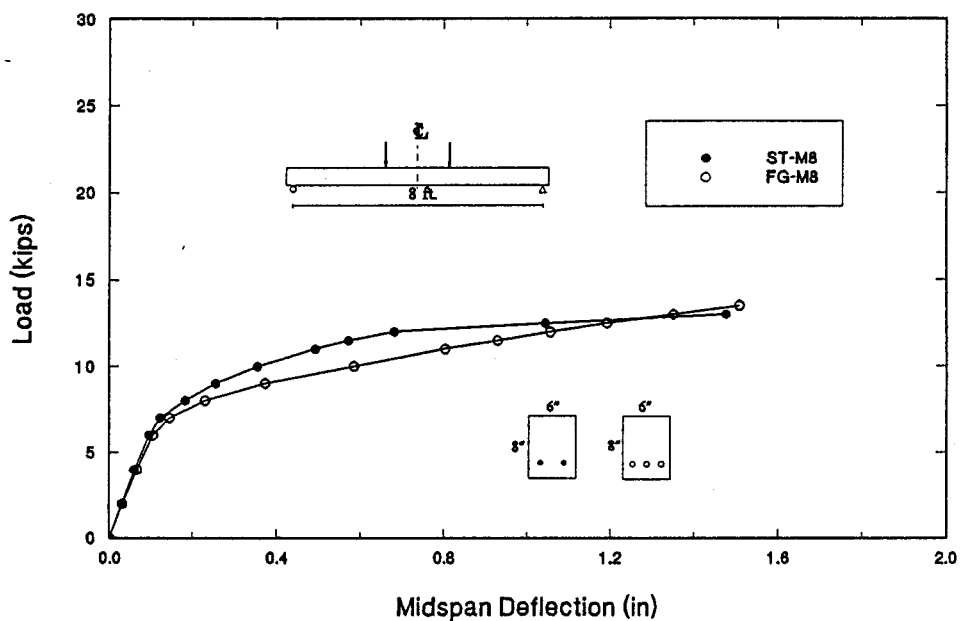


Figure 7.4 Comparative load deflection plot for 6 in. x 8 in. beams (FG-M8)

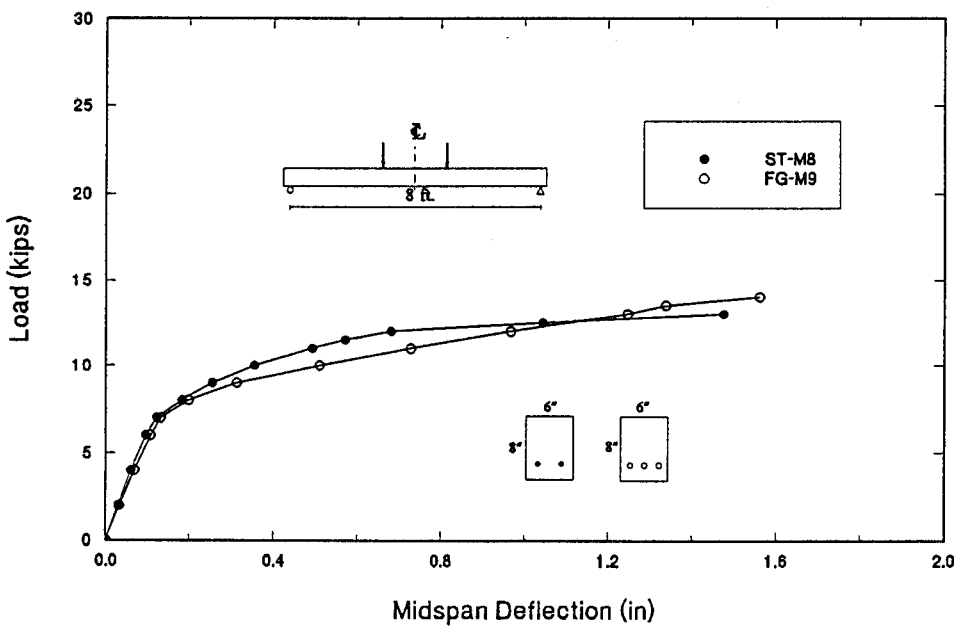


Figure 7.5 Comparative load deflection plot for 6 in. x 8 in. beams (FG-M9)

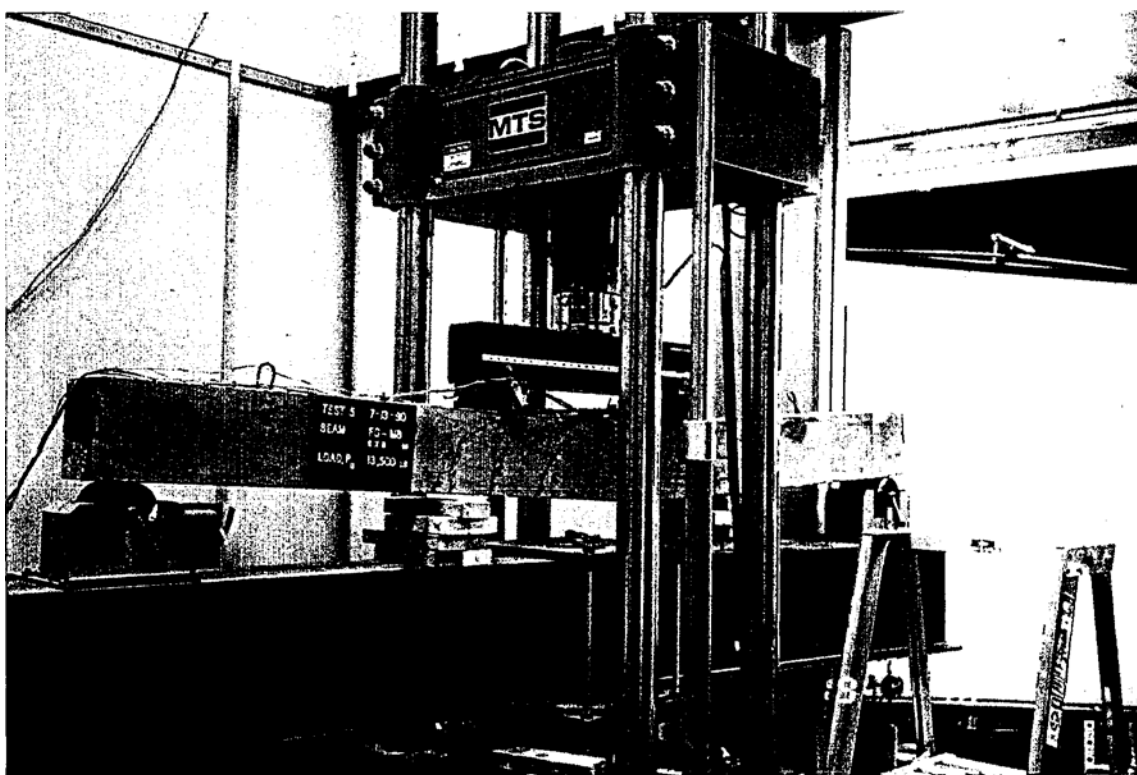


Plate 7.2 (top) Deflection in beam FG-E8 at 90% of its failure load
(btm) Deflected form of FG-M8 at failure

7.3.2 Concrete Strains

The variation of concrete strain with load for the three beam sizes tested are plotted in Figures 7.6-7.11. These show the change in strain as a result of the applied loading. As for the load deflection response, concrete strains vary linearly until cracking. Following cracking, the strain variation with load is also similar to the load-deflection curve. Failure of the beams was in all cases initiated by crushing of concrete. The magnitudes of the last recorded strains before the strain gages were damaged are summarized in Table 7.2.

7.3.3 Prestressing Strand Strain

The variation of the prestressing strand strain with load is also shown in Figures 7.6-7.11. The pattern of these plots mirrors the load and concrete strain variation curves. Large increases in strain were recorded for the last increment of loading and indeed beam ST-E8 failed because the strands broke.

Since several gages were damaged near failure, the failure strain is the last recorded reading and is summarized in Table 7.2. It may be seen that the strains in the fiberglass strands are larger than those in the comparable steel strands. The failure strain in the fiberglass beams ranged from 2.1 % to 2.8 %.

7.3.4 Neutral axis

The location of the neutral axis was determined from readings of the mechanical gages at mid-span. With increasing load, the compression strain in the top fiber of the beam increased and the neutral axis moved up. After cracking, the stiffness of all beams reduced and the neutral axis moved up rapidly. At failure it was about V-2" from the top of the beam. Both steel and fiberglass pretensioned beams behaved similarly. The location of the neutral axis measured from the bottom of the beam is summarized in Table 7.2.

7.3.5 Crack Pattern

The cracking pattern over the constant moment region in identical fiberglass and steel pretensioned beams are shown in Figures 7.12-7.14. The upward propagation of the cracks with increase in load may be seen. Although the crack pattern in the fiberglass and steel pretensioned beams is similar, the average crack spacings are somewhat greater for the fiberglass pretensioned beams (see Table 7.3).

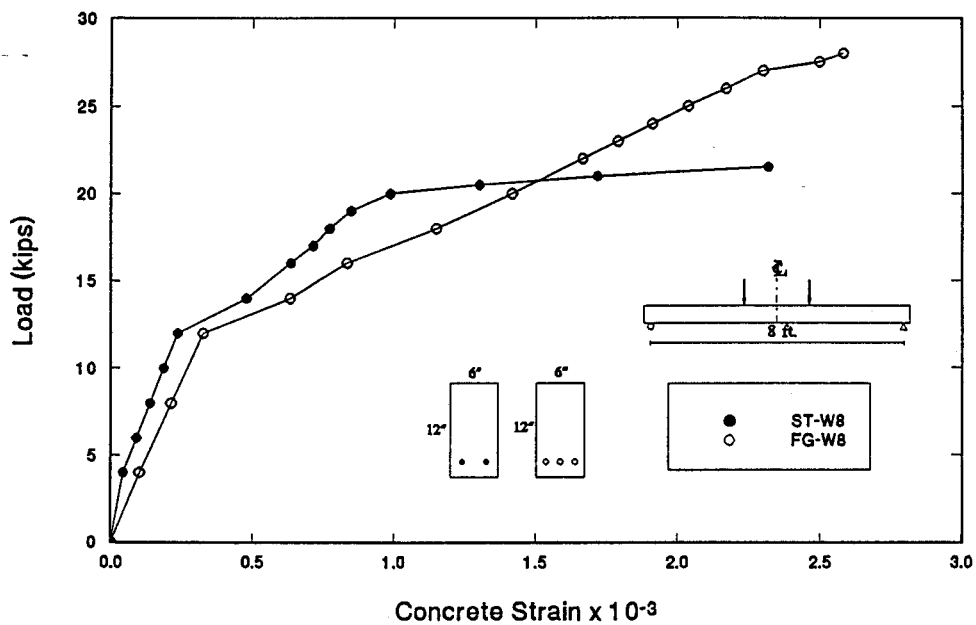


Figure 7.6 Comparative concrete strain in 6 in. x 12 in. beams

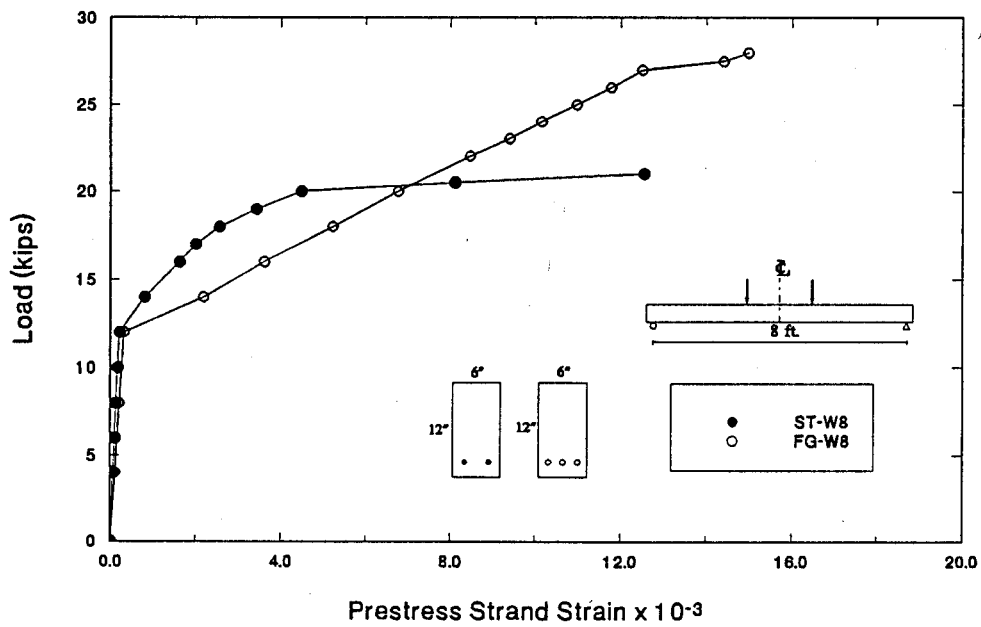


Figure 7.7 Comparative strand strain in 6 in. x 12 in. beams

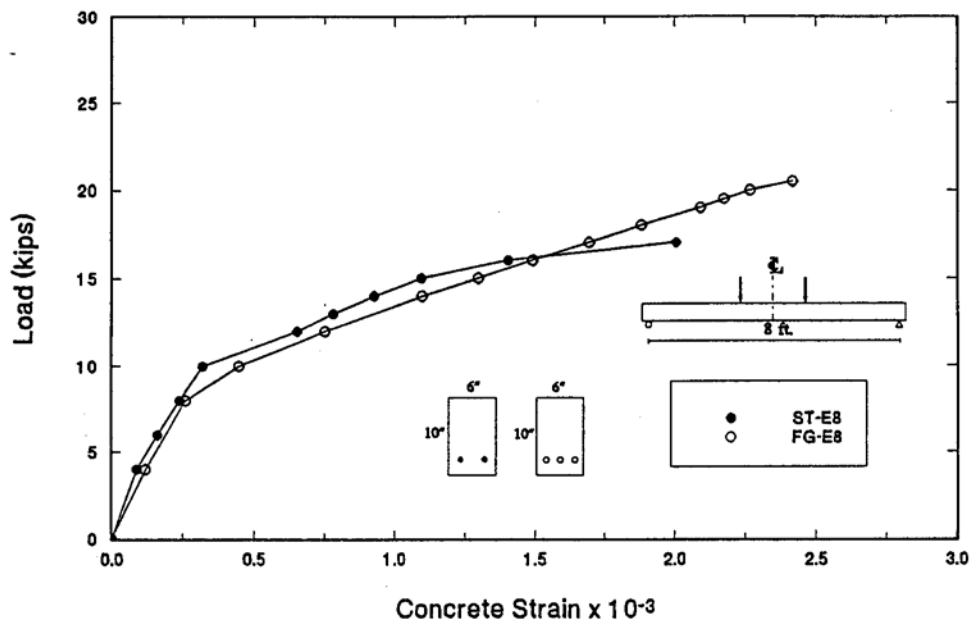


Figure 7.8 Comparative concrete strain in 6 in. x 10 in. beams

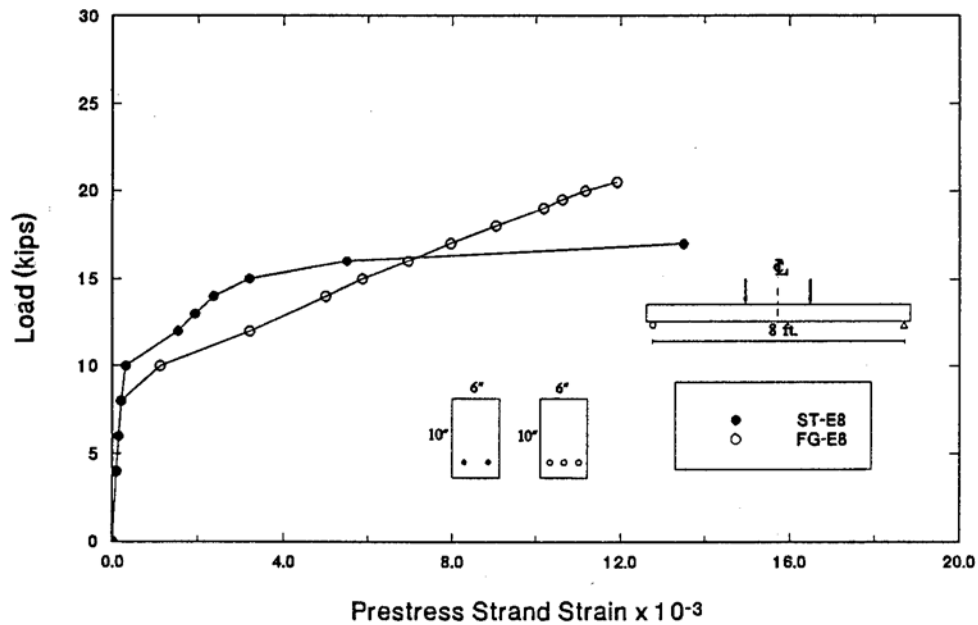


Figure 7.9 Comparative strand strain in 6 in. x 10 in. beams

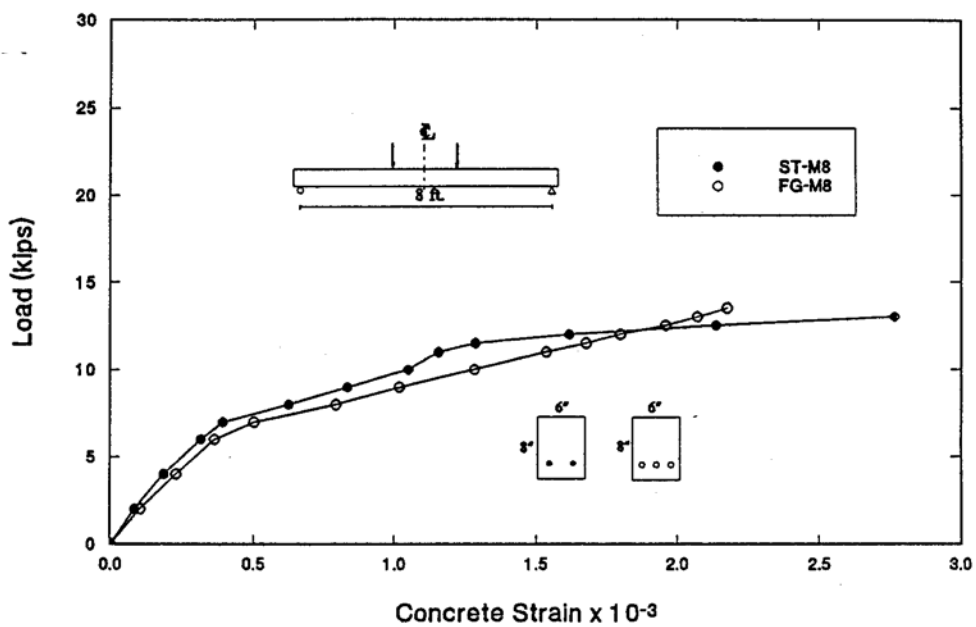


Figure 7.10 Comparative concrete strain in 6 in. x 8 in. beams

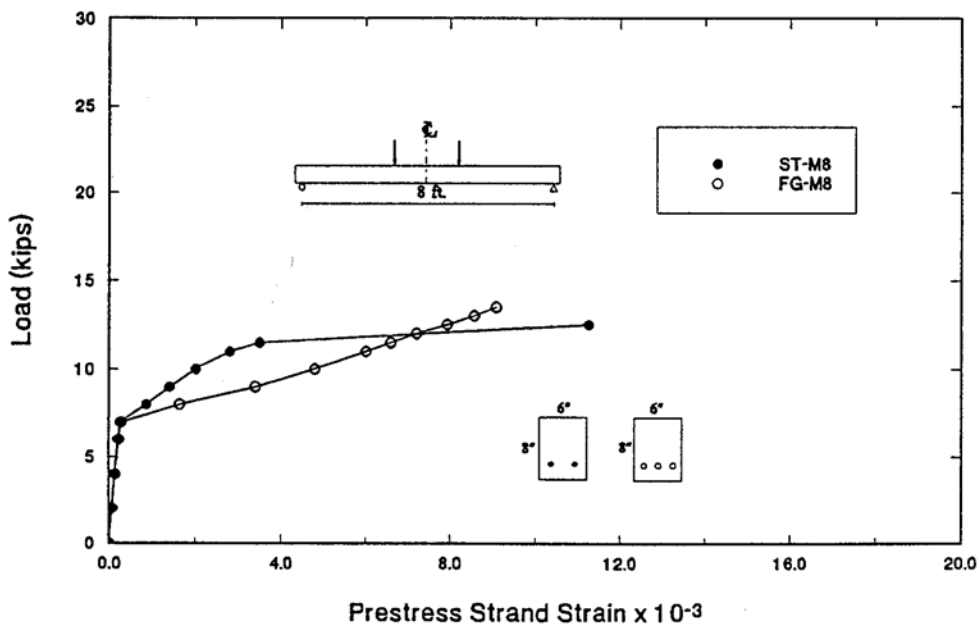


Figure 7.11 Comparative strand strain in 6 in. x 8 in. beams

Table 7.2 Summary of Static Load Test Results

Beam	Cross-Section (in)	Reinf. Index (W)	P_{cr} (kips)	P_u (kips)	P_u / P_{cr}	Δ_u (in)	Δ_{cr} (in)	Δ / Δ_{cr}	ϵ_u ($\mu\epsilon$)	ϵ_{pr} ($\mu\epsilon$)	Neutral Axis (in.)
ST-W8	6 x 12	0.11	13.5	22.3	1.65	1.26	0.10	13.03	2,400	19,284	11.0
ST-E8	6 x 10	0.14	11.0	18.0	1.64	1.21	0.14	8.77	1,946	20,306	9.0
ST-M8	6 x 8	0.18	7.5	13.0	1.73	1.48	0.14	10.39	2,725	17,766	7.0
FG-W8	6 x 12	--	12.6	28.0	2.22	1.90	0.09	21.09	2,517	27,788	11.0
FG-E8	6 x 10	--	10.0	20.5	2.05	1.40	0.11	12.54	2,357	24,264	8.0
FG=M8	6 x 8	--	7.0	13.5	1.93	1.51	0.14	10.55	2,134	21,252	7.0
FG-M9	6 x 8	--	7.5	14.0	1.87	1.56	0.19	8.09	2,277	21,636	7.0

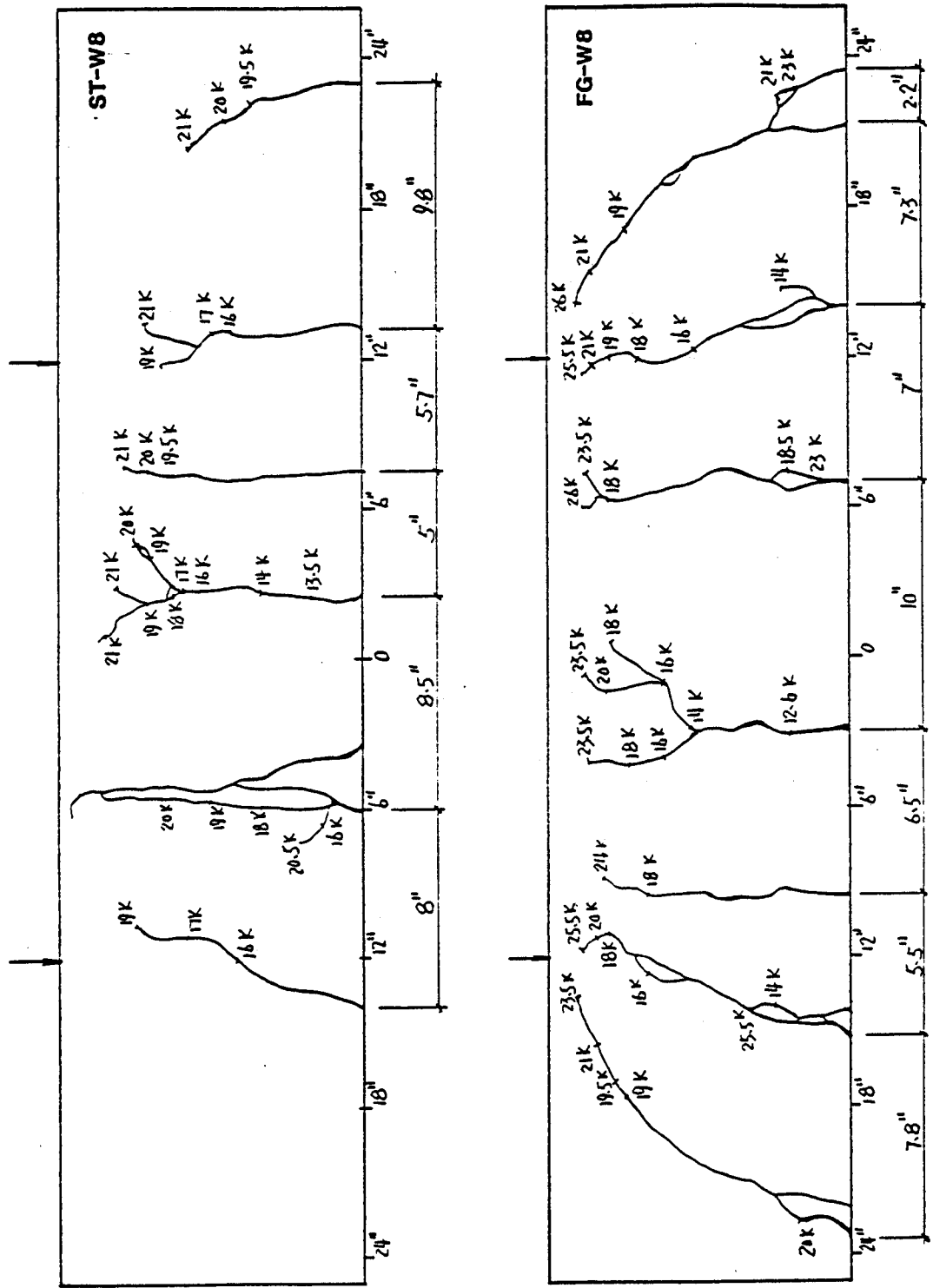


Figure 7.12 Comparative crack patterns in 6 in. \times 12 in. beams

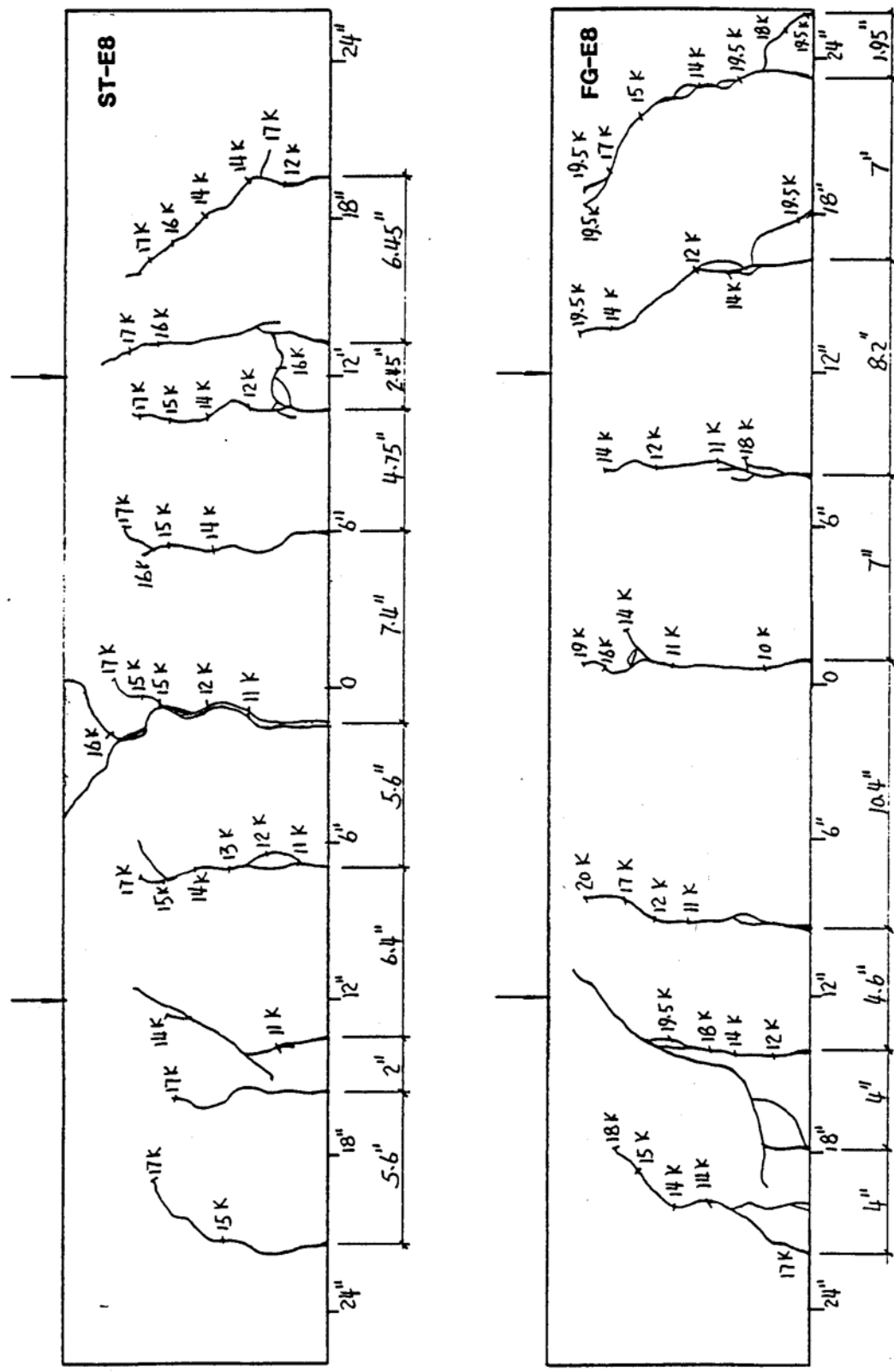


Figure 7.13 Comparative crack patterns in 6 in. x 10 in. beams

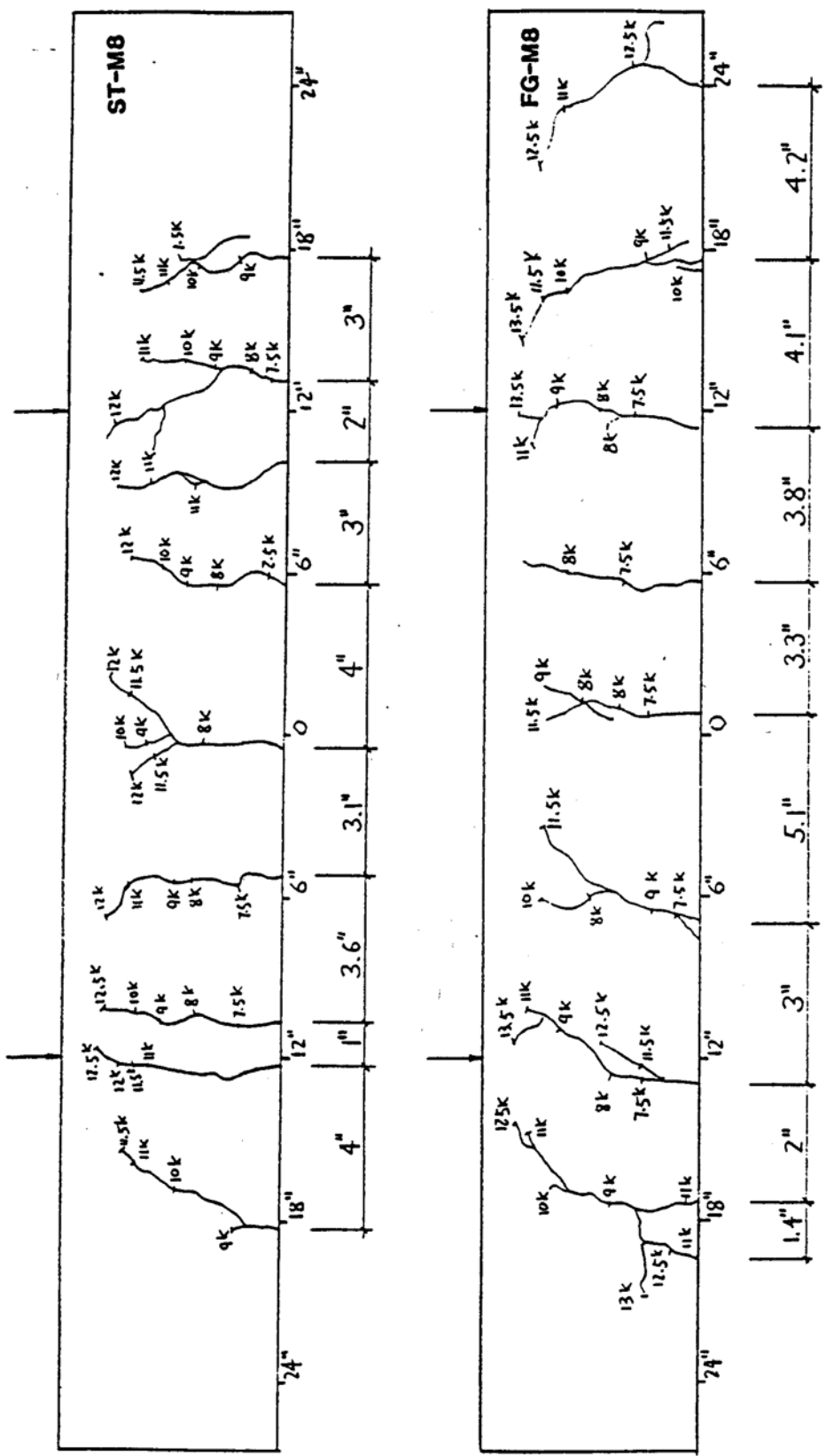


Figure 7.14 Comparative crack patterns in 6 in. \times 8 in. beams

7.3.6 Slip

No slip was recorded in any of the steel pretensioned beams indicating that available development length of 39 in. was adequate. Excepting for the smallest sized beam, several rods of the fiberglass strands, held together by plastic ties, slipped with the application of the last increment of loading. Details of the slip recorded in the beams tested are summarized in Table 7.3. The maximum slip measured was 2" in the 6 in. x 12 in. beam FG-W8.

Table 7.3 Summary of slip and failure mode in beams

Beam	Cross-Section (in)	Reinf. Index (ω)	Slippage (in)	Avg. Crack Spacing Over Constant Zone	Failure Mode
ST-W8	6 × 12	0.11	No slip	6.8"	<i>Tension failure</i> (Secondary crushing of concrete)
ST-E8	6 × 10	0.14	No slip	5.3"	<i>Tension failure</i> (strand ruptured)
ST-M8	6 × 8	0.18	No slip	2.8"	<i>Tension failure</i> (Secondary crushing of concrete)
FG-W8	6 × 12	--	-- 1.50 1.25 ²	2.00 ¹ -- --	7.3" <i>Tension failure</i> (Secondary crushing of concrete)
FG-E8	6 × 10	--	0.63 --	0.75 0.25 ²	1.50 ¹ -- -- 7.6" <i>Tension failure</i> (concrete initiated by slip of strand)
FG-M8	6 × 8	--	No slip	3.8"	<i>Tension failure</i> (Secondary crushing of concrete)
FG-M9	6 × 8	--	No slip	5.7"	<i>As above</i>

^{1,2} Slippage values correspond to the three fiberglass strands in beam (see Figure 7.1).

7.3.7 Failure mode

The steel pretensioned beams were all highly under reinforced (see Table 7.1) and as expected displayed a classic tension failure. Following yielding of the steel (corresponding to a strain of 1%), increases in load could only be accommodated by increases in the lever arm, i. e. by the upward movement of the neutral axis. Failure was eventually initiated by crushing of concrete (secondary compression).

The failure mode of the fiberglass pretensioned beams was almost identical to that of the steel pretensioned beam excepting that it was accompanied by slip of some of the strands (see Table 7.3 for details). This was eventually responsible for a secondary compression failure. Comparable pretensioned steel beam (ST-E8) and fiberglass beam (FG-E8) after failure are shown in Plates 7.2.

7.4 Finite Element Analysis

The non-linear finite element analysis program, PCFRAME, was used to analyze the test beams. This program was originally developed at UC, Berkeley in 1977 [7.1] and can be used to determine the service and ultimate load response of any reinforced or prestressed concrete frame. Since material properties can be input, it may also be used for analyzing fiberglass pretensioned beams.

The results presented in this section were obtained using the mesh shown in Figure 7.15. In view of symmetry, only half the beam was discretized into seventeen members and eighteen nodes. The cross-section was sub-divided into 1 in. thick layers. Separate layers were specified for the both the prestressing and the compression steel.

PCFRAME was run on a IBM Compatible XT with a Math Co-Processor. The analysis of a typical beam having 18 nodes and 15 load steps took approximately 30 minutes. On a 386/20 with a Math Co-Processor, it took about ten minutes.

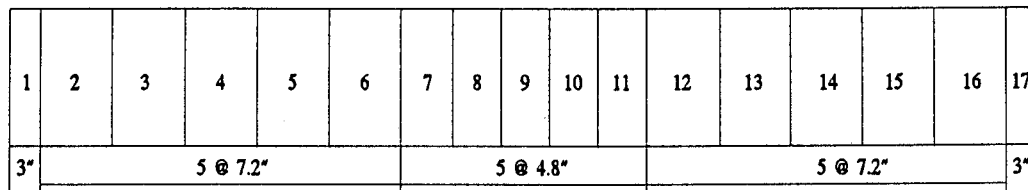


Figure 7.15 Finite element mesh for beam study

Complete input details and results from the non-linear analysis are summarized in Sun, 1991 [7.2]. Only typical results taken from this thesis are presented here. This includes comparisons of deflections, concrete strains and prestressing strand strains for the 6 in x 12 in. beam shown in Figures 7.16-21.

Inspection of Figures 7.16-7.21 indicates that the overall agreement between experiment and analysis is generally quite close. The only exception, is in the prediction of fiberglass strand strains shown in Figure 7.21. This is probably because the linear stress strain relation for fiberglass (see Figure 2.3) assumed in the analysis may not be correct at higher strains. It should be noted that the stress strain relations shown in Figure 2.3 are only valid if all fibers are uniformly stressed. In bending, this is not the case since fibers further from the neutral axis are more heavily stressed. Because the resin matrix provides a medium for re-distribution of loads between fibers, the resulting stress strain relations are non-linear such as those shown in Figure 2.2 obtained from tests conducted by Owens-Corning. Nevertheless, the preliminary results obtained using a linear stressstrain curve are quite satisfactory and suggest that analyses used to determine the response of steel prestressed beams may be readily adapted to analyze fiberglass prestressed beams.

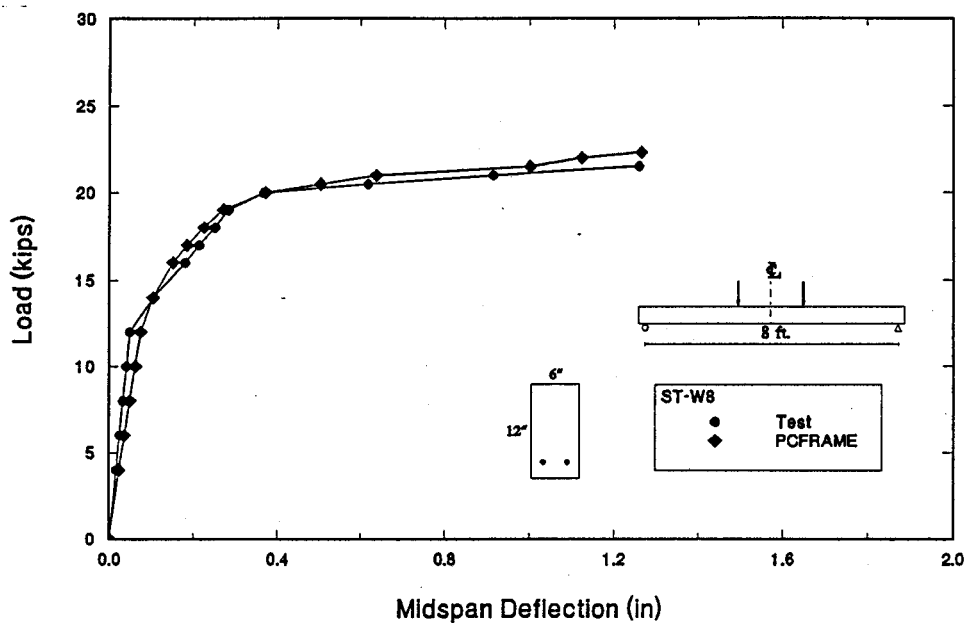


Figure 7.16 Finite element load deflection correlation for steel beam

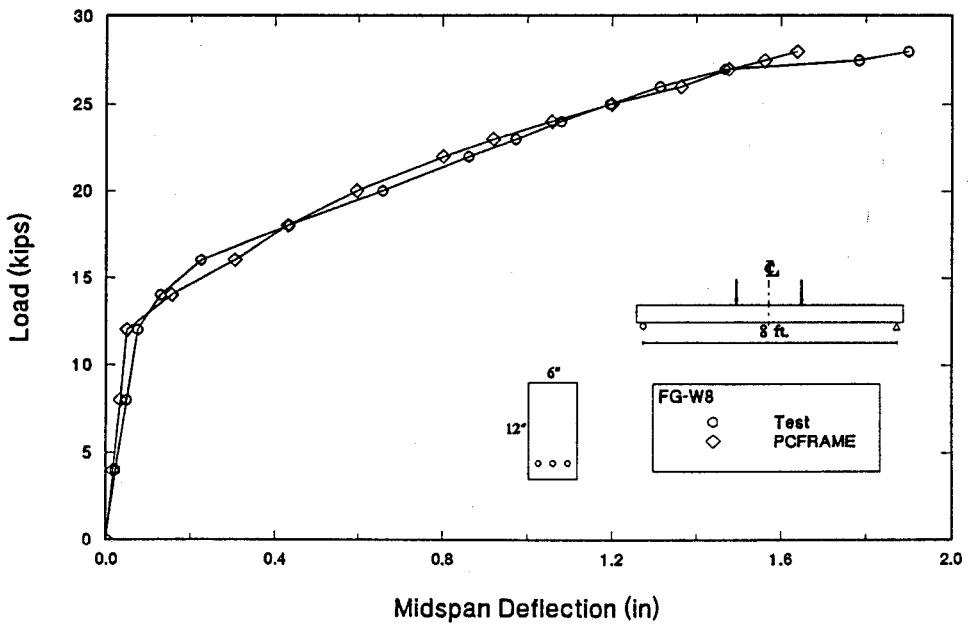


Figure 7.17 Finite element load deflection correlation for fiberglass beam

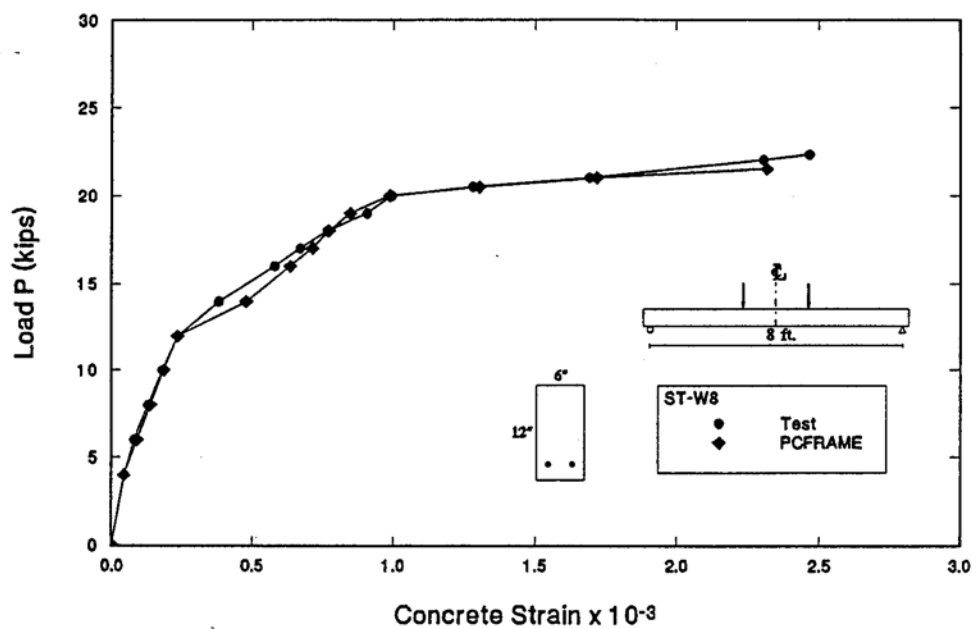


Figure 7.18 Finite element concrete strain correlation for steel beam

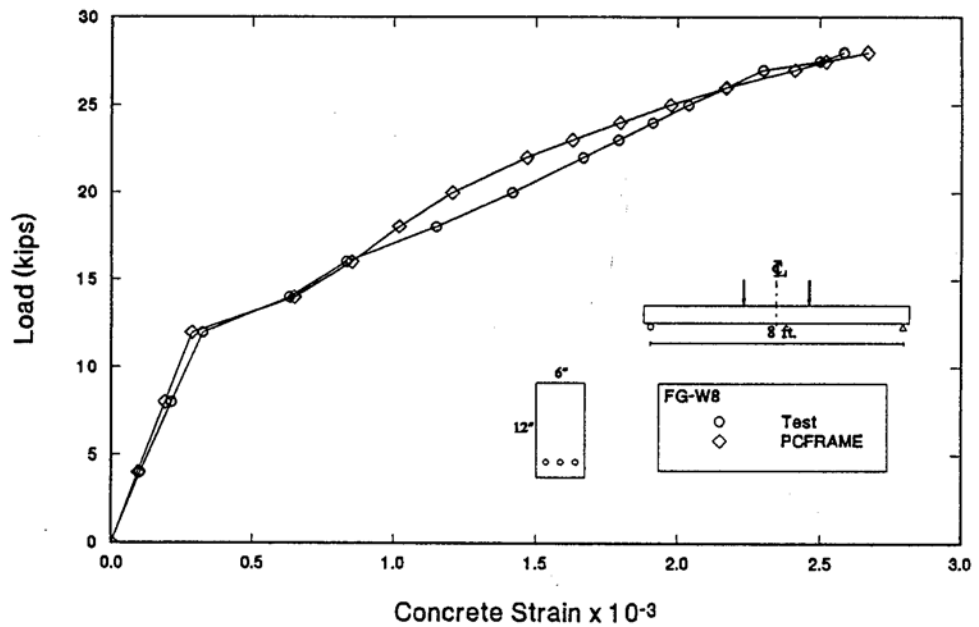


Figure 7.19 Finite element concrete strain correlation for fiberglass beam

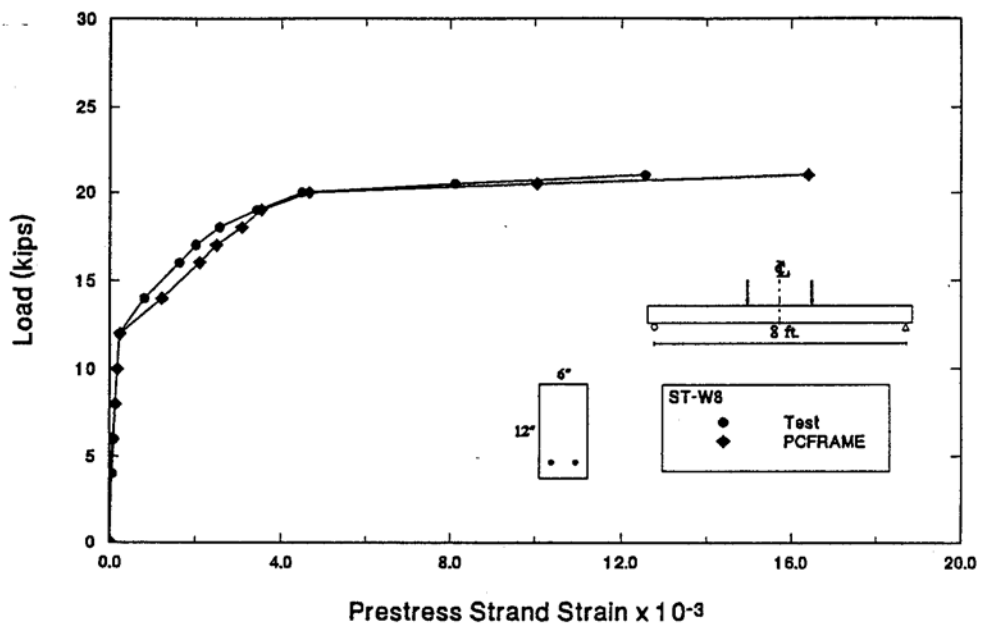


Figure 7.20 Finite element strand strain correlation for steel beam

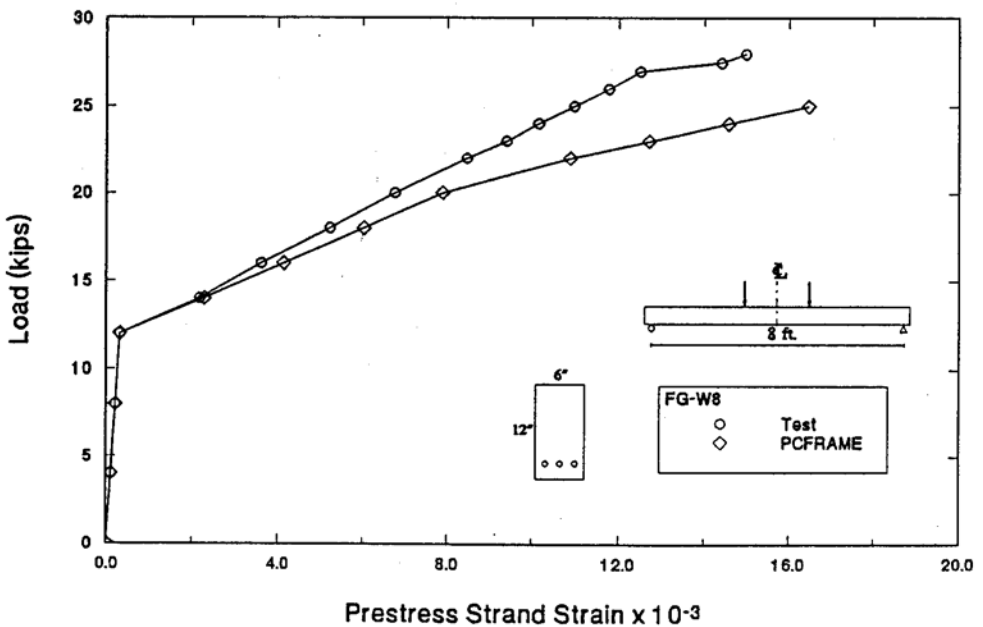


Figure 7.21 Finite element strand strain correlation for fiberglass beam

8. COLUMN STUDY

8.1 Introduction

Six columns - four fiberglass and two identical steel pretensioned columns were loaded to failure. Four of the columns (three fiberglass and one steel) were axially loaded whereas the remaining two columns (one fiberglass, one steel) were eccentrically loaded. The test program is summarized in Section 8.2. The set up, instrumentation and procedure for testing is described in Section 8.3. The results from the study appear in Section 8.4 and comparisons with predictions from non-linear finite element analysis are presented in Section 8.5.

8.2 Experimental Program

The scope of the column study was dictated by test facilities at the Structural Research Center of the Florida Department of Transportation in Tallahassee, Florida where the tests were conducted and also by fabrication considerations. Based on these limitations, an 8 in. x 8 in. x 8 ft column size was selected. To preclude premature failure at the ends, six inch lengths at each end were made 10 in. x 10 in, making the overall length of the columns 9 ft (see Figure 8.1).

A total of six such columns were fabricated and tested, two steel pre-tensioned columns (ST-C1 and ST-C2) and four fiberglass pre-tensioned ones. Of the four fiberglass pre-tensioned columns, two were reinforced with spiral steel ties (FG-C 1 and FG-C2) and two were all fiberglass columns with spiral fiberglass ties (FG-FG-C 1 and FG-FG-C2). Four of the six columns were tested under axial loading. The remaining two were tested under eccentricity, e/h of 0.25. Details of tests are summarized in Table 8.1.

8.3 Test Set Up and Instrumentation

The columns were positioned vertically under a segment of the reaction frame. The ends of the columns were placed inside 10 x in. 10 in. x 6 in. hollow boxes made of $\frac{1}{2}$ in. steel plates as shown in Figure 8.2. The outer side of the top cover plate was machined to accommodate a 1 in. diameter steel roller. A 2 in. thick steel plate with a similar groove provided the pinned support. Four of these boxes were fabricated for the axial

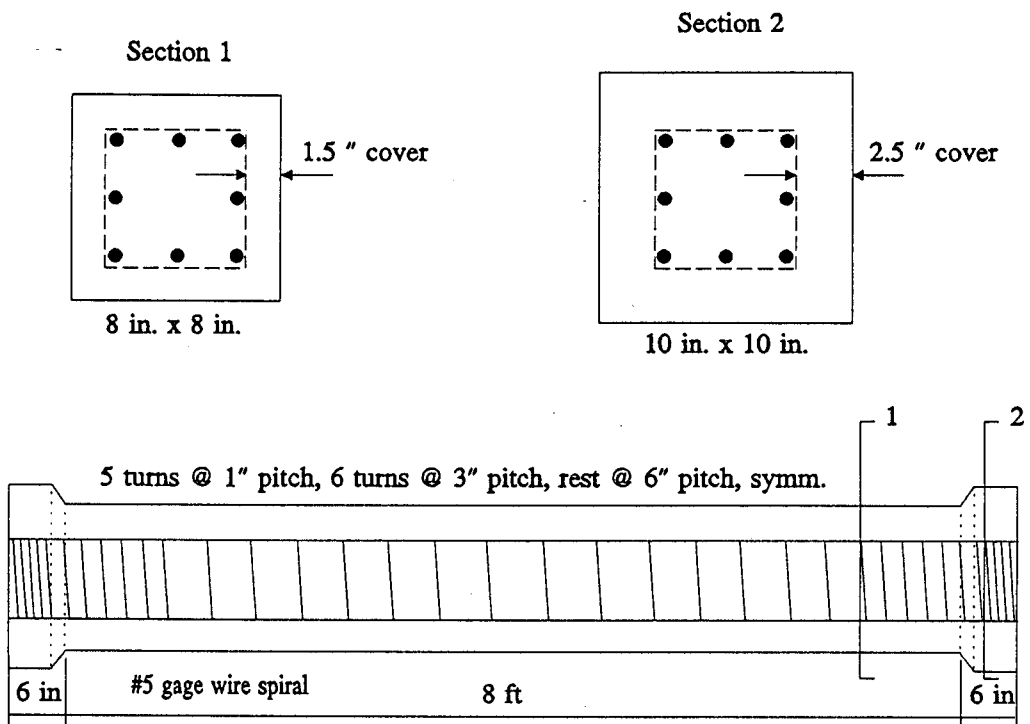


Figure 8.1 Cross-Section and Lateral Reinforcement of Column Specimens

Table 8.1 Summary of Column Test Details

Column	L/r	Eccen. (in)	Remarks
ST-C1	40	2	Steel strand
ST-C2	40	0	Steel spiral
FG-C1	40	0	Fiberglass strand
FG-C2	40	0	Steel spiral
FG-FG-C1	40	0	Fiberglass strand Fiberglass spiral
FG-FG-C2	40	2	

and eccentric load tests, two each for the top and bottom. Proper alignment was assured using levels. At the top, the supports were secured directly to the ram of the hydraulic jack which was connected to the loading frame with C-clamps. The columns were hoisted from their stationary position, moved to the test site and centered below the jack using a fork lift. A $\frac{3}{8}$ in. thick Capralon bearing pad, produced by JVI Inc., Skokie, Illinois, was placed inside the hollow boxes prior to their use to provide a uniform load distribution. Before actual testing commenced, the columns were secured by ropes and a metal screen placed in front for safety.

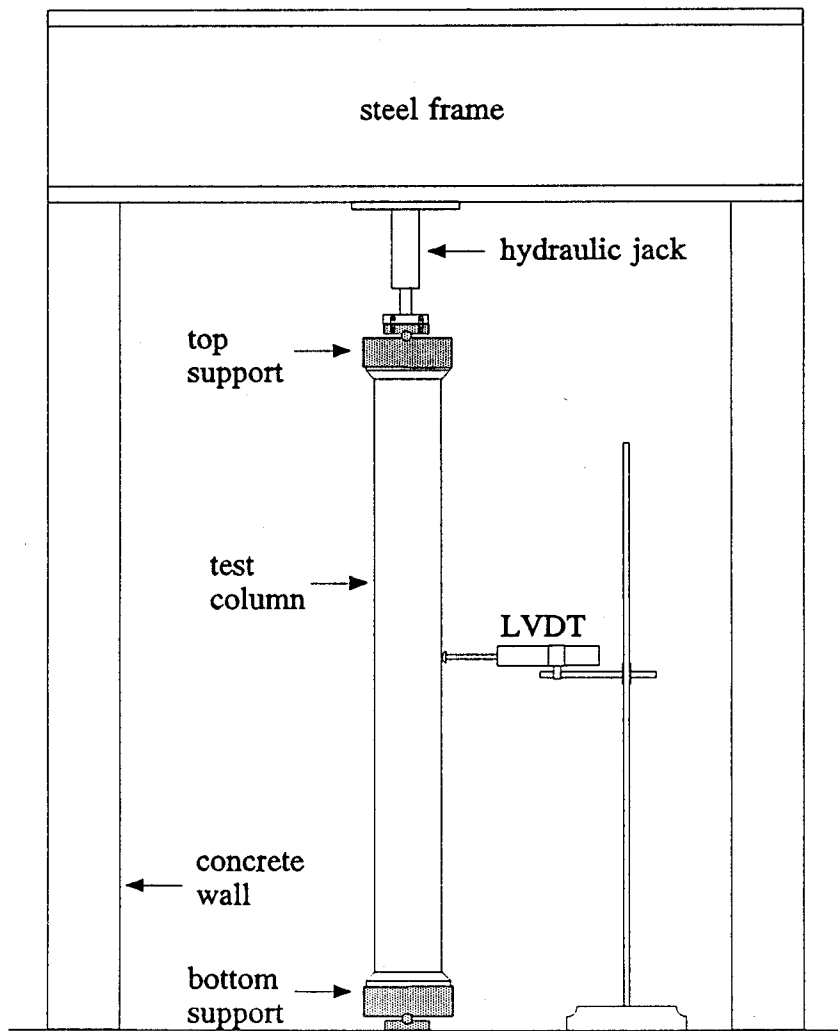


Figure 8.2 Column Test Set Up

Four strain gages were attached in each column to measure concrete strains. A pair of gages were attached on opposite faces at midspan and at the third point. Their averaged values are used in all plots that are presented. Lateral deflection was measured at midspan by a linear voltage differential transformer (LVDT). A model CDP-100 LVDT with a maximum stroke of 4 in. was used. It was placed in a horizontal position at midheight as shown in Figure 8.2.

8.3.1 Test Procedure

A small load was initially applied to the column for set up and subsequently released. All strain gage and LVDT channels hooked to the System 4000 Data Acquisition System were initialized. The load was applied using an Enerpac jack model RR-2006 with a 6 in. stroke and a 200 ton capacity. Readings of the applied load were taken using a Heise gage with a 10 ksi capacity (442 kips).

For the concentrically loaded columns, an increment of 500 psi (22.1 kips) was used up to 5000 psi (221.0 kips) and a 200 psi (8.8 kips) increment thereafter. For the eccentrically loaded columns, the increments were about 100 psi (4.4 kips). For each increment all measurements, barring loading data (there was insufficient clearance for a load cell), were automatically recorded by the System 4000.

8.4 Test Results

8.4.1 Failure Load and Failure Mode

Ultimate capacities and failure modes recorded in the tests are summarized in Table 8.2. They are listed in the order in which the testing was carried out. Axial results are presented in the top part of the table and eccentric load results in the bottom part.

Inspection of this table indicates that there is considerable scatter in the results. For the axially loaded columns, the failure load ranged from 232 kips to 323 kips. The higher load, averaging 318 kips, corresponded to the fiberglass columns including the all fiberglass column, FG-FG-C 1. The lower load averaging 237 kips corresponded to the columns tested first. Interestingly, the capacities of these columns, i.e. ST-C2 and FGC2, were quite similar.

In this instance, the lower failure loads for columns ST-C2 and FG-C2 suggested that they were subjected to some degree of eccentricity. This hypothesis is subsequently borne out in the analysis of concrete strains and deflections reported in the next section.

Only two columns were tested under eccentric loading. Results for these tests show even greater variability than the axial case. The failure load of 49 kips for the all fiberglass

Table 8.2 Summary of Ultimate Capacity and Failure Mode

Column	e (in)	Ultimate Load (kips)	Failure Mode
ST-C2	0.0	243	End failure at top due to vertical cracking and spalling. No failure of exposed steel ties. No damage at bottom.
FG-C2	0.0	232	End failure at bottom due to vertical cracking and extensive spalling. No damage at top.
FG-C1	0.0	323	End failure at top due to vertical cracking and some spalling. No damage in exposed steel ties nor at top.
FG-FG-C1	0.0	314	End failure at bottom due to separation and fracture of fiberglass ties limited to enlarged base. No damage at top.
FG-FG-C2	2.0	49	End failure at bottom due to horizontal cracking. Exposed end reveals honeycombing of concrete. No damage at top.
ST-C1	2.0	116	End failure at bottom. Limited spalling of cover. No damage at top.

column FG-FG-C2 tested first was less than half the 116 kip load in the comparable steel specimen. An examination of the failed fiberglass column revealed the presence of honeycombing that weakened the enlarged end section of the column.

The failure mode of the columns (see Table 8.2) was not due to crushing of concrete or instability but to cracking at the ends (see Plate 8.1). Even though the enlarged ends were surrounded by $\frac{1}{2}$ in. thick steel plates to prevent such failures, it is evident that this did not provide the required confinement. It should be noted, however, that end failures in columns are relatively common and have been reported for tests on steel prestressed columns, e.g. Yuan, 1989 [8.1].

8.4.2 Strains and Deflections

8.4.2.1 Axial Loads

Figures 8.3-8.6 show the variation in the average concrete and prestressing strand strain with load. These relate to the midspan location and were averaged from all the gages that worked. For the concrete strain, the variation is linear up to about 225 kips and non-linear beyond. Thus, it is non-linear for columns FG-C1 (Figure 8.5) and FG-FGC 1 (Figure 8.6) where the failure loads greatly exceeded 225 kips. The strain in the prestressing strand varied linearly. However, the strain in the concrete and the strands differed indicating the presence of bending. The variation did not follow a set pattern.

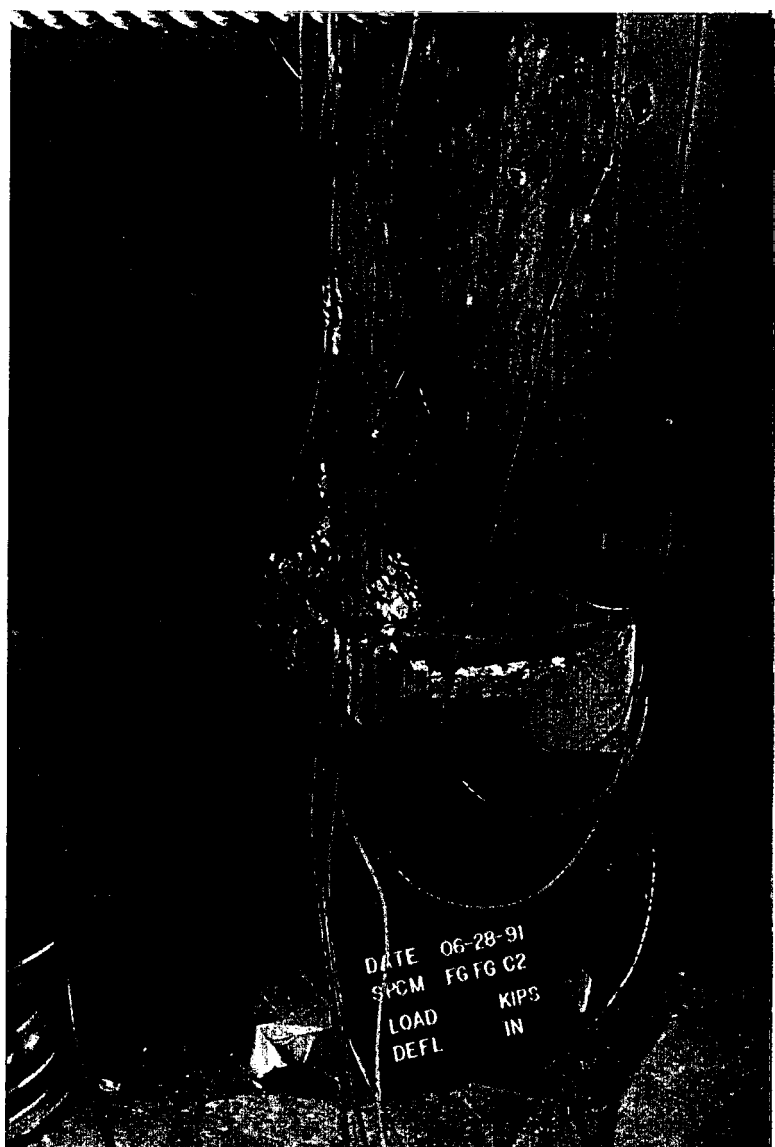


Plate 8.1 End Failure in

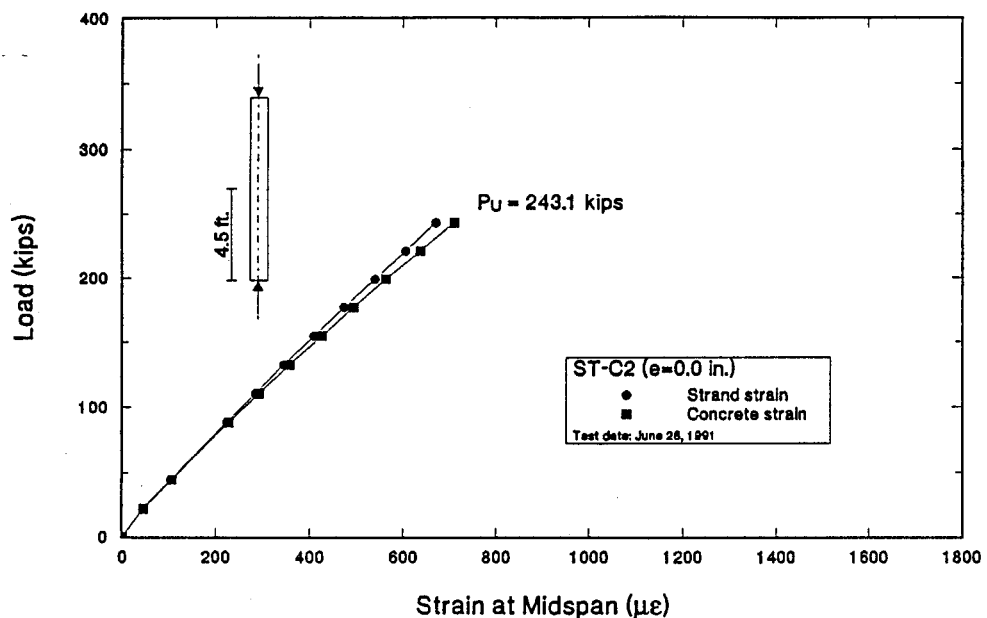


Figure 8.3 Load-Strain Response for Column ST-C2

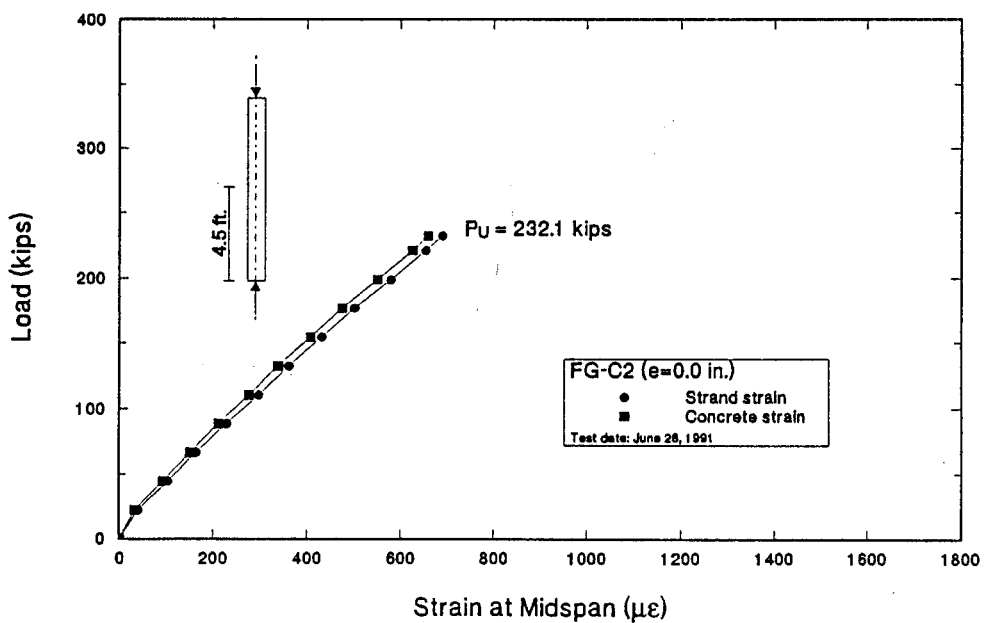


Figure 8.4 Load-Strain Response for Column FG-C2

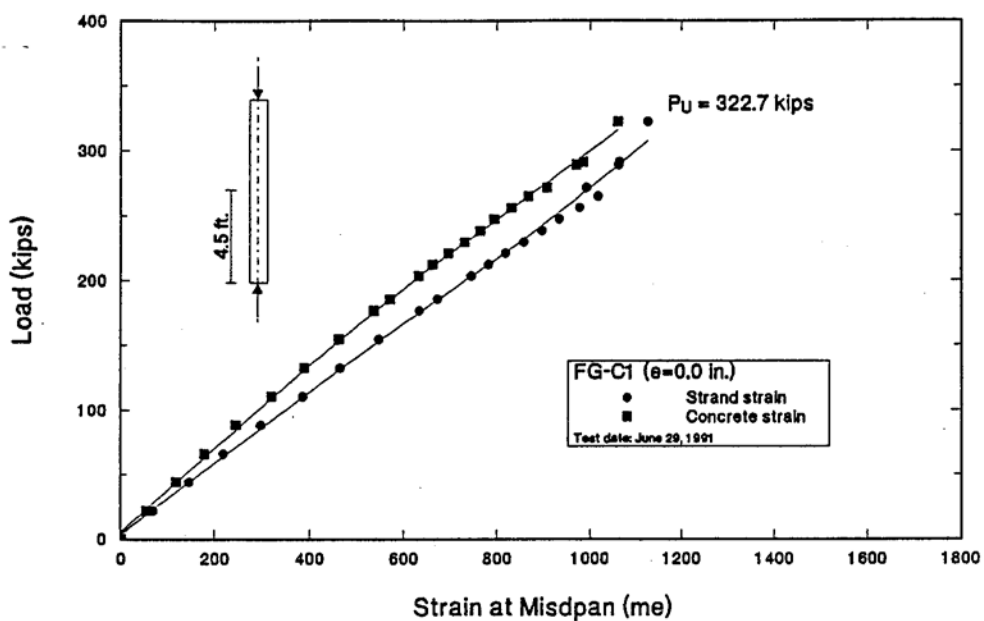


Figure 8.5 Load-Strain Response for Column FG-C1

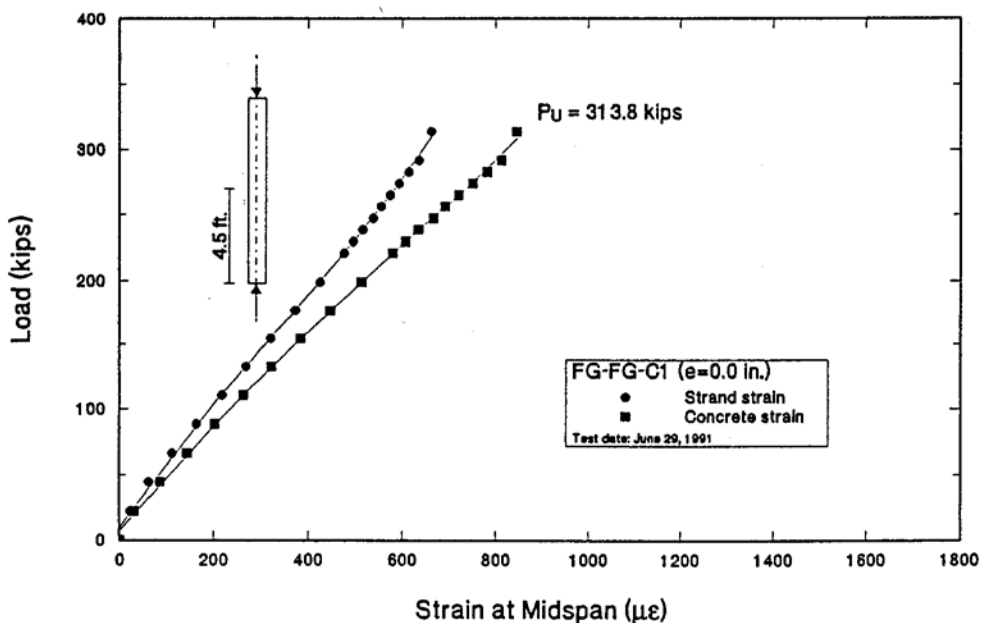


Figure 8.6 Load-Strain Response for Column FG-FG-C1

In some cases it is lower than concrete (Figures 8.4 and 8.5) and in others it is greater (Figures 8.3 and 8.6). This indicates that the instrumented strands were not always on the same side of the axis of bending.

Lateral deflections were negligible for columns FG-C2, FG-C1 and FG-FG-C1 (0.031, 0.002 and 0.056 in. respectively). However, for column ST-C2 a higher value of 0.15 in. was recorded.

8.4.2.2 Eccentric Load

Under eccentric loading, the columns were subjected to bending. Consequently, opposite faces were in tension and compression. Since failure was initiated at relatively low loads at the ends (see Table 8.2), rather than by instability or crushing, a linear response may be anticipated.

Figures 8.7-8.8 plot the variation of the concrete and strand strains with load in the steel (ST-C1) and fiberglass (FG-FG-C2) pretensioned columns. The response of the steel pretensioned column was non-linear at failure whereas the fiberglass column displayed a linear variation since it failed at a very low load.

Figure 8.9 shows the lateral deflection variation with load for the two columns. The maximum recorded deflection was 0.299 in. for ST-C1 and 0.082 in. for FG-FG-C2. The non-linearity in the response of the columns is evident from this figure.

8.4.3 Comparison of Response of Fiberglass and Steel Columns

Since the effective prestress in the fiberglass columns was greater (see Section 5.5), they could be expected to have a lower failure load for the axial case and a higher load under eccentric loading. The test results were exactly opposite. This discrepancy may be attributed to the fabrication of the specimens. The spacers used in Henderson Prestress were damaged and as a result provided an uneven finish. Although the ends of the columns were ground prior to testing, greater irregularities were noticed in the steel specimens. As a result, they were subjected to greater eccentricity.

Comparative plots showing all results for the fiberglass and steel columns are shown in Figures 8.10 and 8.11. Inspection of these figures indicate that the column response, regardless of the prestressing material, is quite similar. This implies that the stiffness of the two types of columns is also similar.

Since only two columns were tested under eccentric loading, there is unsufficient data available to make a valid comparison. However, both columns failed due to inadequate restraint of the hollow steel boxes and also due to lack of pre-compression at the ends since the transfer length exceeded the enlarged section, Aroni 1968 [8.2].

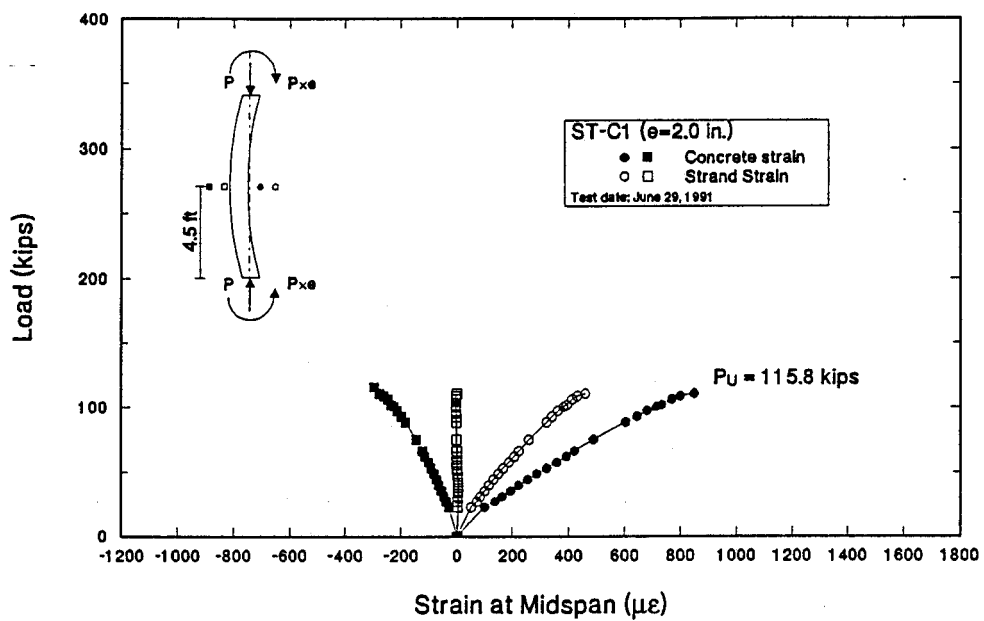


Figure 8.7 Load-Strain Response for Column ST-C1

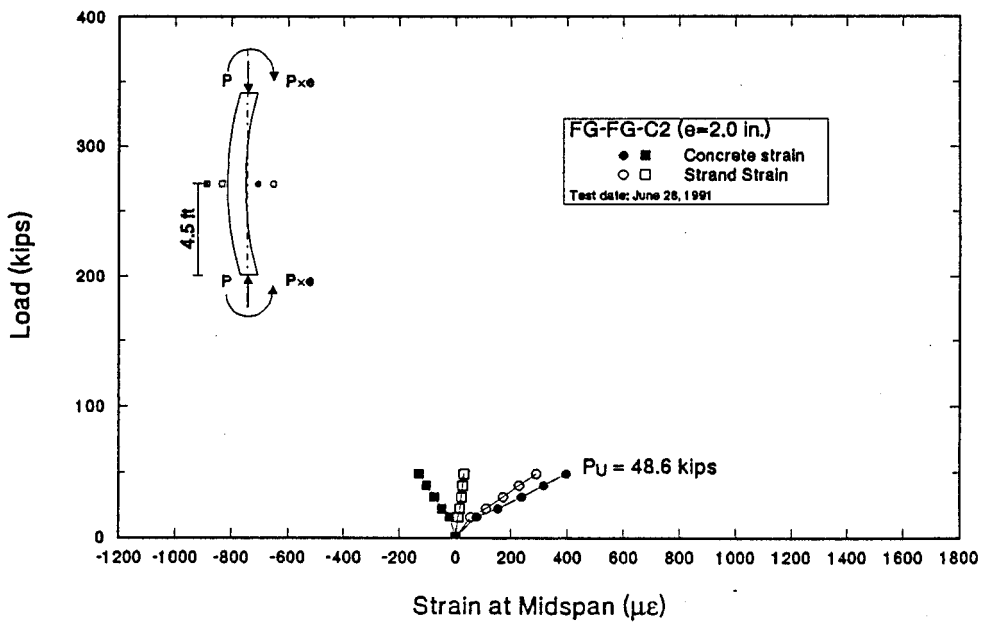


Figure 8.8 Load-Strain Response for Column FG-FG-C2

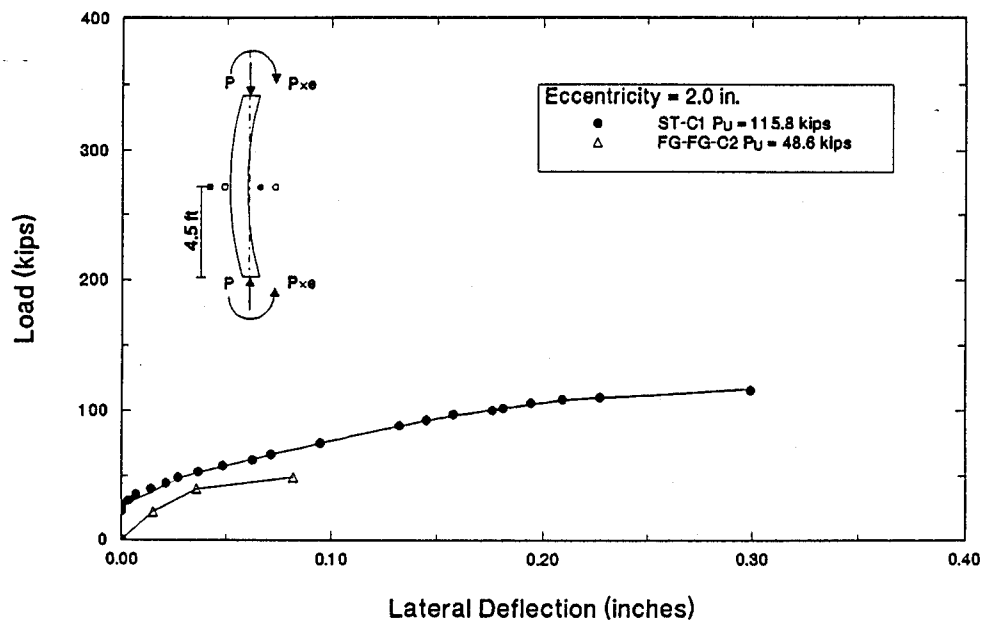


Figure 8.9 Comparison of Load-Deflection Response for Eccentrically Loaded Columns

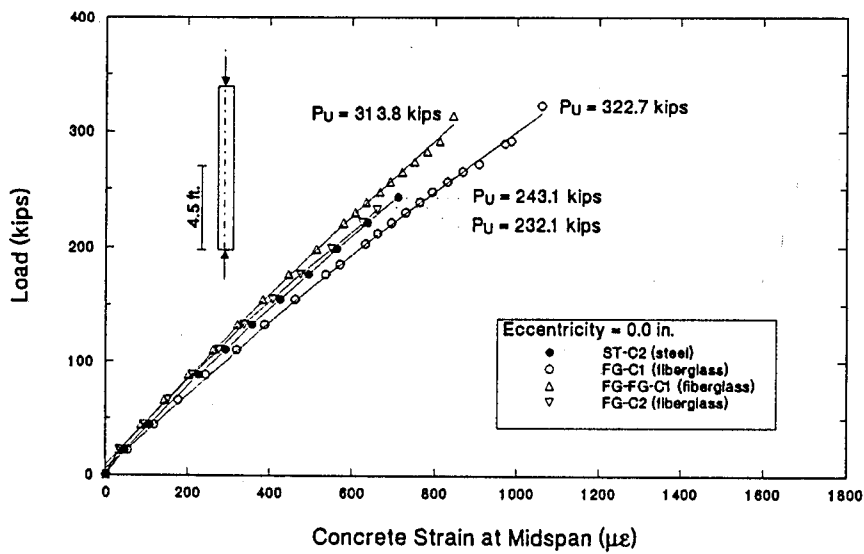


Figure 8.10 Comparison of Load-Strain Response in Axially Loaded Columns

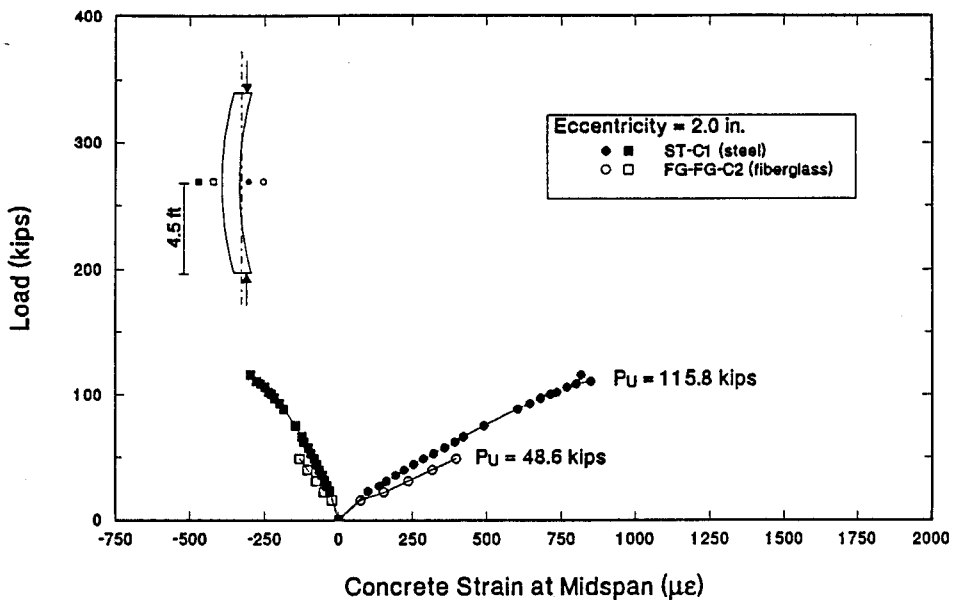


Figure 8.11 Comparison of Load-Strain Variation in Eccentrically Loaded Columns

8.5 Finite Element Analysis

The non-linear finite element program PCFRAME [8.3] was used to predict the response of the fiberglass and steel pretensioned columns. As for the beams, the input data was adjusted to analyze fiberglass columns by specifying the appropriate stress-strain relations and by modifying the relaxation parameter. In view of symmetry, only half the column was discretized (see Figure 8.12). The input parameters for concrete were adjusted so that the experimental and theoretical stress strain curves matched, Mariscal, 1991 [8.4].

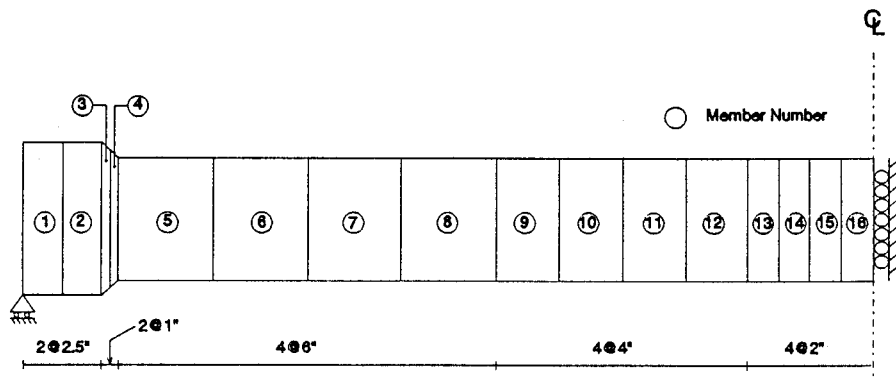


Figure 8.12 Finite Element Mesh

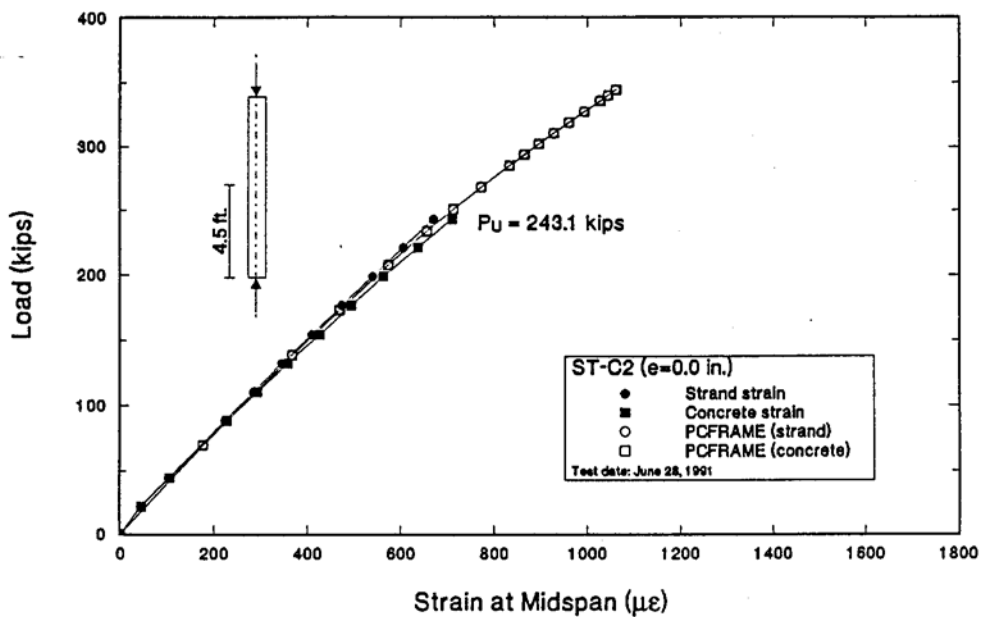


Figure 8.13 Test and Theoretical Load-Strain Response for Column ST-C2

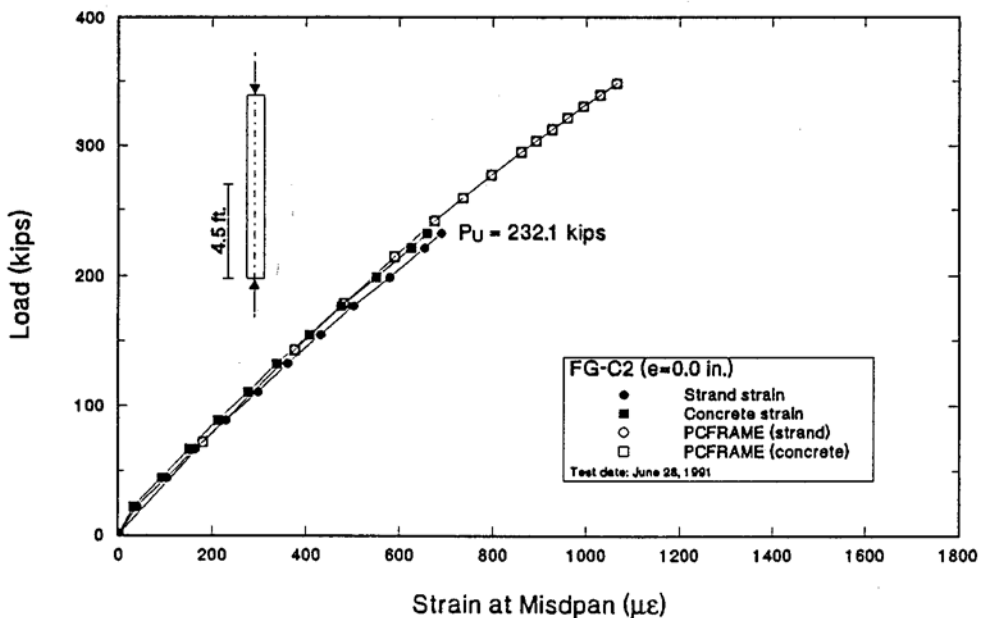


Figure 8.14 Test and Theoretical Load-Strain Response for Column FG-C2

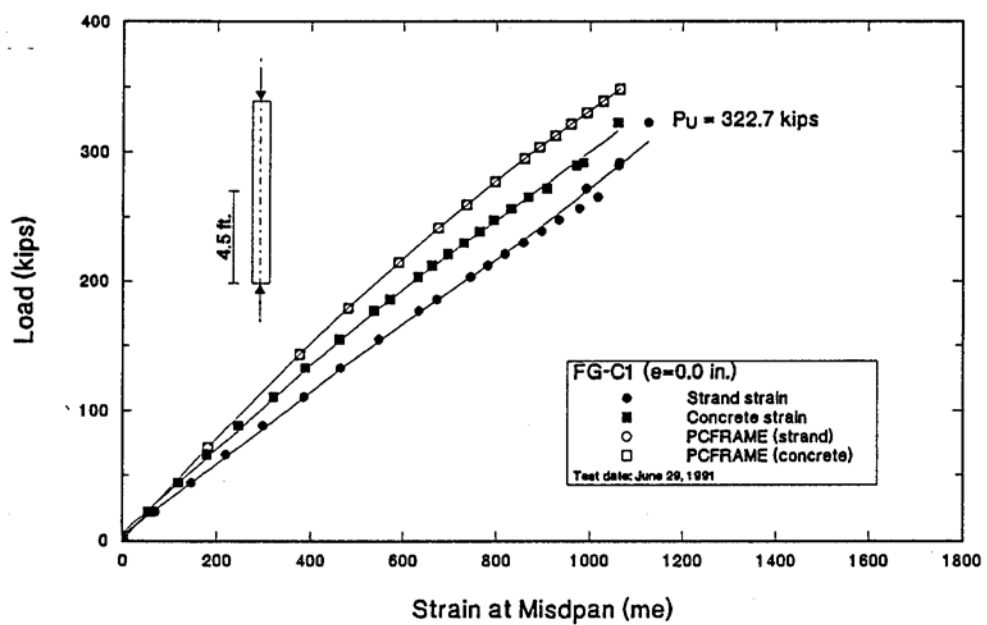


Figure 8.15 Test and Theoretical Load-Strain Response for Column FG-C1

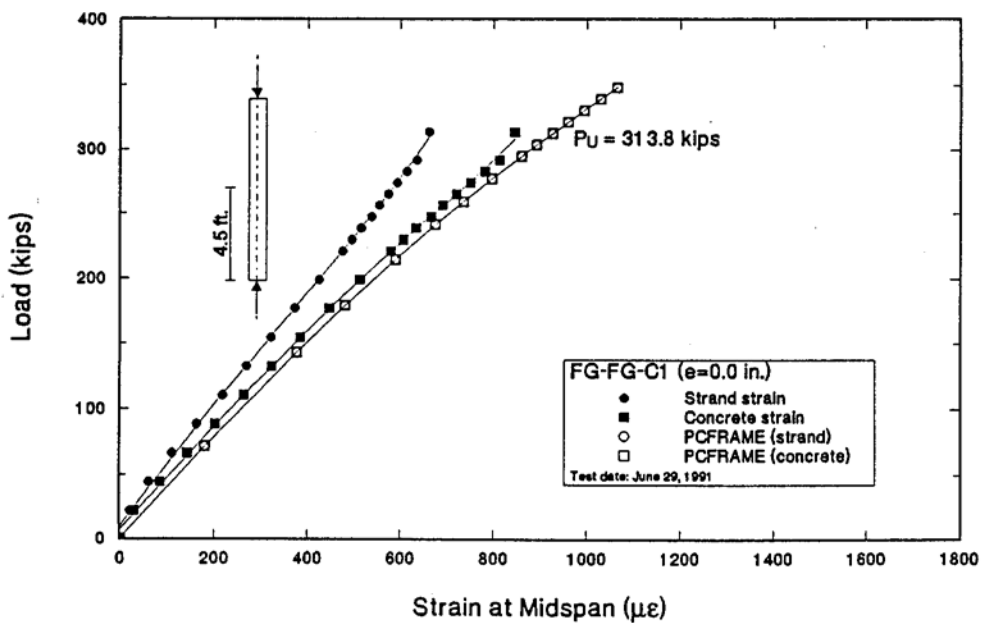


Figure 8.16 Test and Theoretical Load-Strain Response for Column FG-FG-C1

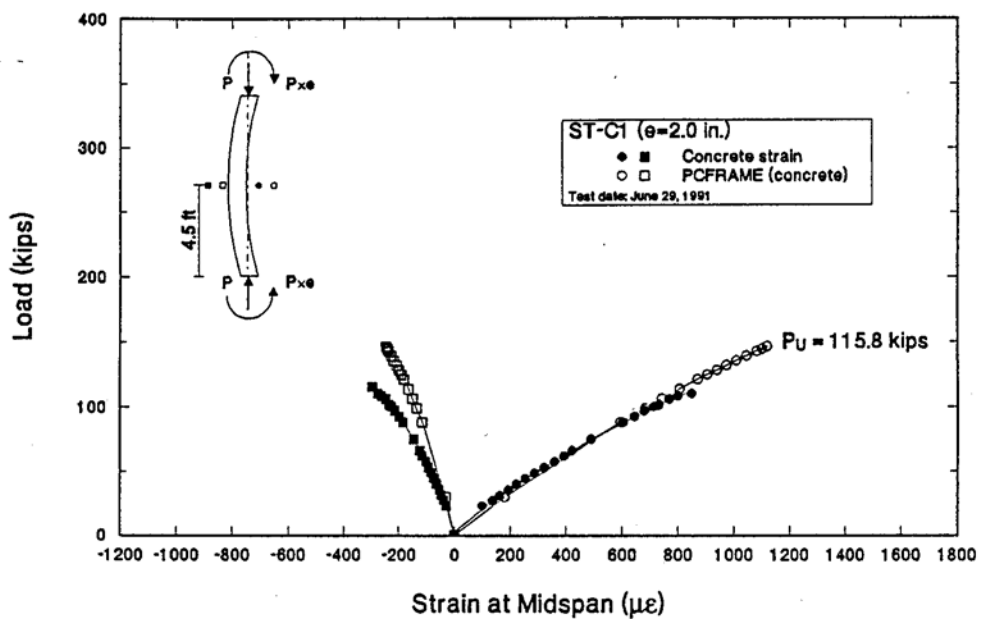


Figure 8.17 Test and Theoretical Load-Strain Response for Column ST-C1

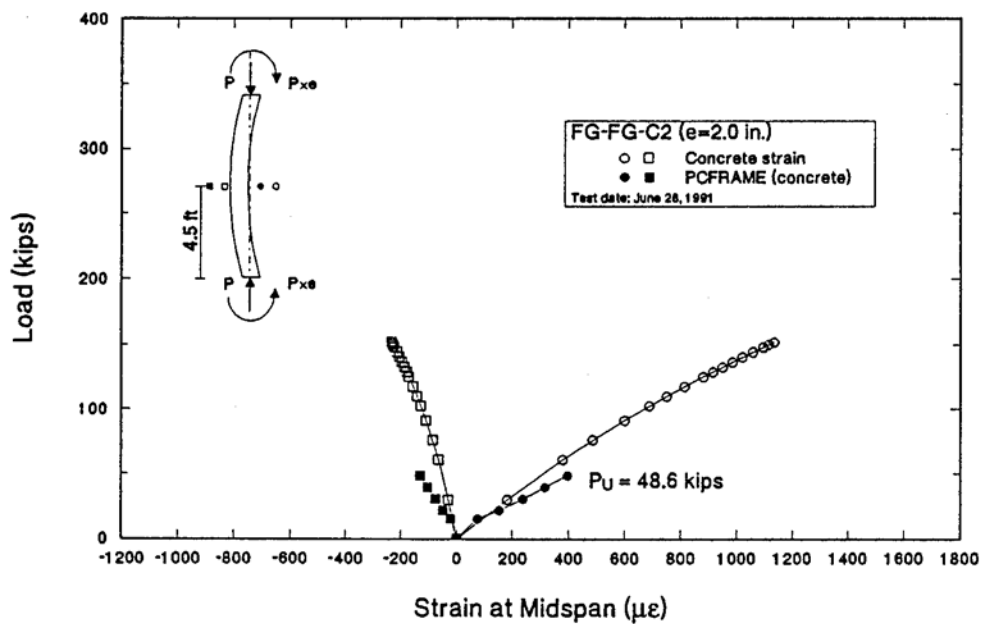


Figure 8.18 Test and Theoretical Load-Strain Response for Column FG-FG-C2

Figures 8.13-8.16 compare the theoretical and experimental strain variation with load for the four axially tested columns. Inspection of these figures show that correlation is better for columns that failed at lower loads, i.e. ST-C2 and FG-C2 (Figures 8.13-8.14) than it is for the columns failing at higher loads, i.e. FG-C1 and FG-FG-C1 (Figures 8.15-8.16). In one case, FG-C1, the test response is more flexible while in the other, FG-FGC1, it is less flexible. In both cases, agreement is better for strand strains.

The results of comparisons for the eccentrically loaded columns appear in Figures 8.17-8.18. Inspection of these figures show that for this case, agreement is better for the steel column. Figure 8.19 compares theoretical and experimental lateral deflections. The correlation is poor possibly due to the uneven distribution of loading in the testing since the ends of the column were not perfectly level.

Overall, the results of all the comparisons indicate that the response of axially and eccentrically loaded fiberglass and steel pre-tensioned column can be adequately predicted by the non-linear analysis. The correlation is improved if actual stress-strain relations for concrete are input. This may be achieved by either using the input format allowed by PCFRAME or by modifying the parameters used for defining the stress-strain curve. The latter approach is considerably simpler and was used in this study.

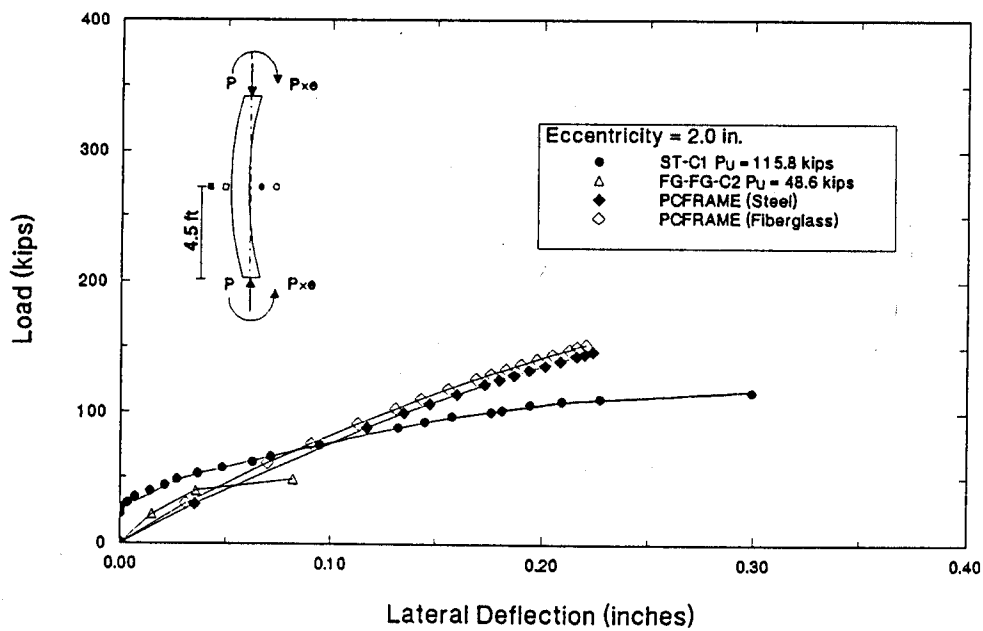


Figure 8.19 Test and Theoretical Load-Deflection Response for Eccentrically Loaded Columns

9. PILE STUDY

9.1 Introduction

To investigate drivability, four fiberglass and two identical steel pretensioned piles were driven at the site of a proposed condominium at Hidden Lagoon, Tierra Verde, FL. As before, the steel piles served as controls to allow the relative performance of the fiberglass piles to be evaluated. The fabrication and instrumentation of these piles is described in Section 4.8.

Tierra Verde is on Cabbage Key, linking St. Petersburg beach to Fort DeSoto Park, on Mullet Key. It is surrounded by the Gulf of Mexico on one side and Tampa Bay on the other (see Plate 9.1). The test piles were driven within 100 ft of Tampa Bay and indeed the ground water at the site was affected by tidal changes (see soil survey in Section 9.4.1).

This chapter describes the scope of the study (Section 9.2) and the drivability study to finalize parameters such as ram weight and drop height that were used for the actual pile driving. For completeness, a brief review of the 'wave analysis' used for the drivability study is presented in Section 9.3. Additional information on this topic may be found in books, e.g. Bowles, 1988 [9.1], reports, e.g. Holloway, 1975 [9.2] and proceedings of specialty conferences, e.g. Fellenius, 1988 [9.3]. Details of the drivability study carried out using the wave analysis computer program WEAP [9.4] are summarized in Section 9.4.

9.2 Scope of Study

As FDOT requires [9.5] piles driven in a marine environment to be very large - at least 24 in. x 24 in. - fabrication and cost considerations ruled out the possibility of testing full sized fiberglass piles. Instead, much smaller 10 in. x 10 in. x 25 ft piles (see Figure 9.1) were driven. In order to allow the feasibility of these smaller piles to be examined, its effective prestress was designed to match those in the larger piles.

Table 9.1 summarizes strand and size information on steel prestressed piles used in FDOT projects. The effective prestress shown in this table has been calculated on the basis of AASHTO [9.6] lump sum losses of 45,000 psi assuming a jacking stress of 70% of the ultimate stress. Inspection of this table shows that the effective prestress varies from a maximum of 1,349 psi for 14 in. x 14 in. piles to a minimum of 614 psi for 30 in. x 30 in. piles.

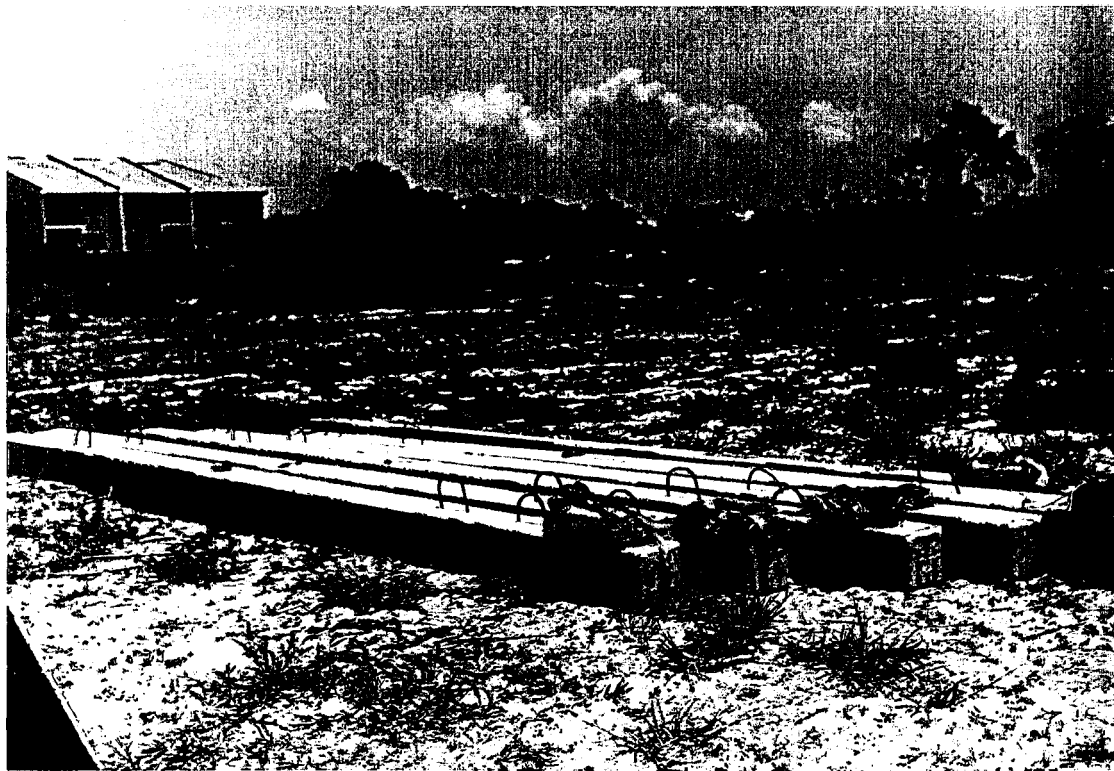


Plate 9.1 (top) Aerial view of Tierra Verde
(btm) Hidden Lagoon site

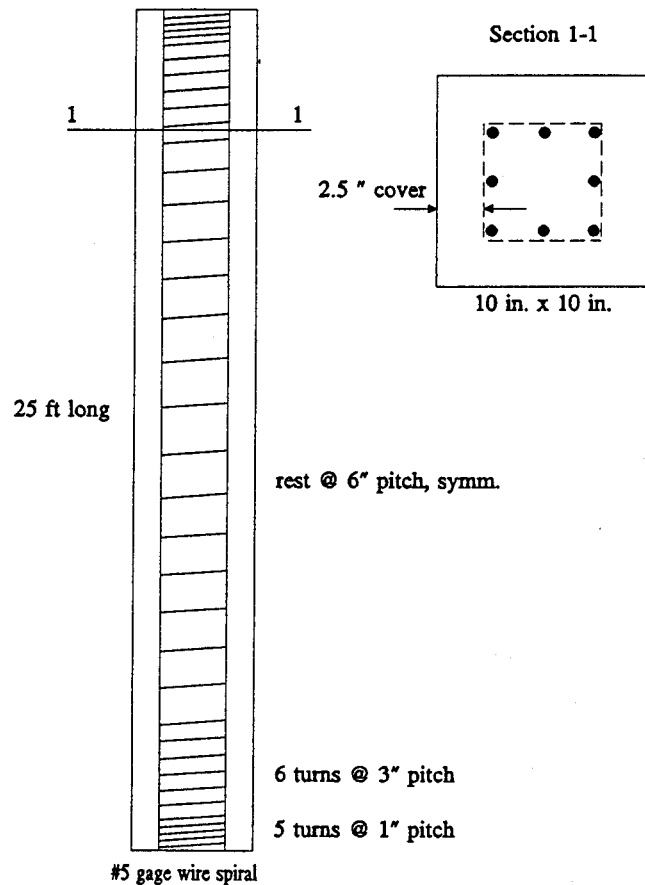


Figure 9.1 Pile Cross-Section and Tie Details

For the larger piles required by FDOT for a marine environment, the effective prestress varies from 614-960 psi. For the 24 in. x 24 in piles, it is between 918-960 psi (average 939 psi) while it is between 614-737 psi (average 679 psi) for the 30 in. x 30 in. piles. The effective prestress of the fiberglass piles tested is estimated to be about 740 psi (see Section 5.5) and is therefore comparable to that in the 30 in. x 30 in. piles. Consequently, to evaluate the feasibility of the fiberglass pretensioned piles, the driving stresses recorded from this study are compared against those in 30 in. square piles used in the construction of the New Edison Bridge over the Caloosahatchee River, Fort Myers, FL. Eighteen of the 435 piles supporting this bridge were instrumented and tested similarly as the fiberglass piles [9.7]. The results of the comparisons are presented in the next chapter.

Table 9.1 Typical Effective Prestress in Piles Used by FDOT

Cross Section	Nº of Strands	A _{ps} (in ²)	f _{pe} (ksi)
12" x 12"	8 - 7/16"	0.920	0.920
	8 - 1/2"	1.224	1.224
	12 - 3/8"	1.020	1.020
	8 - 1/2"	1.020	0.899
14" x 14"	12 - 7/16"	1.380	1.014
	12 - 1/2"	1.836	1.349
	16 - 3/8"	1.360	0.999
	12 - 9/16"	2.304	1.024
18" x 18"	16 - 1/2"	2.448	1.090
	20 - 7/16"	2.300	1.022
	24 - 3/8"	2.040	0.907
	16 - 1/2"	2.448	0.881
20" x 20"	20 - 1/2"	3.060	1.100
	24 - 7/16"	2.760	0.994
24" x 24"	20 - 9/16"	3.840	0.960
	24 - 1/2"	3.672	0.918
	20 - 9/16"	3.840	0.614
30" x 30"	24 - 9/16"	4.608	0.737
	28 - 1/2"	4.284	0.685

Details of the six piles tested are summarized in Table 9.2. Fabrication of these piles and details of material properties is presented in Chapters 2 and 4. As for the column study, the two all fiberglass piles using fiberglass ties are identified by the prefix FG-FG whereas those with conventional steel ties are only designated by the prefix FG. Steel pretensioned piles have the prefix ST. P1 and P2 identify the pile numbers of each type.

Table 9.2 Details of Piles Tested

Pile	Site	Driving Order	Remarks
ST-P2		1	All Steel
FG-P2	SPT 1	2	FG with Steel Ties
FG-FG-P2		3	All Fiberglass
ST-P1		4	All Steel
FG-P1	SPT 2	5	FG with Steel Ties
FG-FG-P1		6	All Fiberglass

9.3 Wave equation analysis

A '*wave equation*' analysis refers to the application of stress wave propagation theory to the solution of the pile driving problem. The use of wave equations was first considered by Isaacs, 1931 [9.8], but it was not until the advent of computers that a numerical solution was possible.

Conventional pile driving formulae, e.g. *Engineering News*, are based on Newtonian energy-momentum principles. The impact of the hammer is assumed to stress the entire pile *instantly* and the driving resistance is equated to the static load capacity of the pile. These assumptions are questionable since impact relationships are only valid for bodies that are free and massive. Piles are neither massive nor free. Nevertheless, a great number of driving formulas are available.

By contrast, a '*wave analysis*' assumes that the impact of the hammer generates elastic strains at the pile head that propagate to the pile tip at the speed of sound, displacing the soil to produce penetration of the pile or a '*pile set*'. The resulting equilibrium equation or equation of motion can be solved for appropriate boundary conditions to yield this displacement. Both *initial* boundary conditions, such as the velocity of impact and physical boundary conditions, such as the end fixity of the pile are considered in the solution.

Since the piles are driven in an infinitely extending soil medium, the '*correct*' wave analysis is one where the soil is considered as a three-dimensional half space. Practical analysis, however, is based on the one dimensional wave equation. This obviously requires many simplifying assumptions but nonetheless it offers a rational procedure for incorporating the numerous parameters that affect pile driving, e.g. drop height, ram weight, soil resistance.

Since the governing differential equations are solved for a known impact velocity, the results from a wave analysis provide information on maximum pile displacements and stresses *corresponding to a single hammer blow*. It also calculates stresses, displacements and velocities at other time intervals following impact. Since parameters affecting pile driving can be varied, the analysis can be used to determine an optimum hammer-pile-soil system that can be used to obtain required pile capacity without damage to the pile. Such an analysis is referred to as a 'drivability' study and is presented in Section 9.4 for the piles tested.

9.3.1 One Dimensional Wave Equation

The one dimensional wave equation or equation of motion (e.g. Holloway, 1975 [9.2]) is given by Equation 9.1 as:

$$c^2 \frac{\partial^2 u}{\partial x^2} - \frac{R}{A\rho} = \frac{\partial^2 u}{\partial t^2} \quad (9.1)$$

where u is the particle displacement, c , the wave propagation velocity, A the pile cross-sectional area, ρ its density and R the resistance of the soil. Equation 9.1 is derived on the basis of linear elasticity neglecting lateral inertial forces. Consequently, it is only applicable if the wave length is at least five times the pile diameter, Kolsky, 1963 [9.9], a condition nearly always met in practical pile driving problems.

The solution of the second order partial differential equation is obtained by integration for prescribed boundary conditions. Exact solutions are only possible for simple cases, e.g. for a freely suspended bar in air, when $R=0$ in Equation 9.1. Although this does not represent practical pile problems, it does provide insight into the general form of its solution. The solution for this case is given by Equation 9.2 (e.g. Richart, 1970 [9.10]), as:

$$u = f(ct + x) + h(ct - x) \quad (9.2)$$

In Equation 9.2, the displacement, u , is a function of two arbitrary functions, f and h . As demonstrated by Richart, it represents two waves traveling at a velocity of wave propagation, c , - a compressive wave in the positive x direction and a tensile wave in the opposite direction.

At the boundaries, i.e. the ends of the pile, appropriate boundary conditions need to be satisfied. For a freely suspended pile, stress free conditions must be met. Consequently, an incident compression wave is reflected as a tension wave. At a fixed end, displacements (and velocities) must be zero. Because of the relationship between velocity and force, this requires an incident compression wave to be reflected back also as a compression wave thereby doubling its magnitude as illustrated in Figure 9.2. Typical piles have boundary conditions that fall between these extremes.

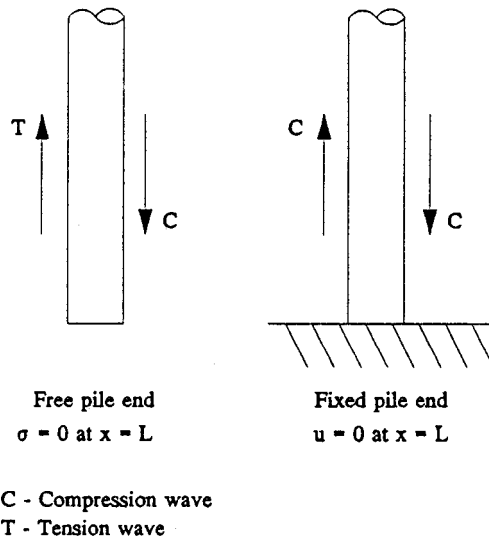


Figure 9.2 Boundary Conditions

The special solution, Equation 9.2, indicates that piles are subjected to tension stresses when they are driven through soft soils, i.e. R is near zero. By contrast, they are subjected to compressive stresses at refusal, i.e. a near fixed end condition. Since both tensile and compressive stresses are determined by superposition of stresses from the incident and the reflected waves, their location along the pile length depends on the boundary conditions and also on the shape and length of the stress wave. The latter depends primarily on the impact velocity. In general, the heavier the ram weight and impact velocity, the higher the maximum pile head stress and longer the wave length, Crapps, 1977 [9.11]

Since a closed form solution for Equation 9.1 is not feasible when hammer and soil characteristics are incorporated, it can only be solved numerically using a finite difference, finite element or boundary element formulation. Nevertheless, the essential characteristics of the closed form solution are retained for this case as well, e.g. reflection of a compression wave into a tension wave at a free end.

The first application of the wave equation for the solution of pile driving problem was described by Smith, 1960 [9.12]. His analysis is based on a finite difference solution of the governing differential equation, Equation 9.1. Subsequently, three dimensional axisymmetric finite element solutions were proposed, e.g. Chow, 1981; Smith & Chow, 1982, Coutinho, Costa, Alves, Landau & Ebecken, 1988 [9.13-9.15]. The high cost and limitations of such analyses led to the development of one dimensional finite element solutions, e.g. Simons & Randolph, 1985 [9.16]. These are briefly described in the sequel.

9.3.1.1 Finite Difference Solution

A finite difference solution of the one dimensional wave equation, Equation 9.1, requires discretization of both time and space. The hammer-pile-soil system must be sub-divided into small segments and solution is achieved by integration of Equation 9.1 for small increments of time.

The discretization used by Smith (1960) is shown in Figure 9.3. Its essential components are 1) the driving system comprising the hammer, pile cap and cushions 2) the pile subdivided into discrete masses interconnected by springs and 3) a simple elastic-plastic soil deformation for the static soil response defined by two parameters - the elastic quake Q and the peak resistance R_U (See Figure 9.4). The dynamic resistance is assumed as the product of the instantaneous static resistance, velocity, V and an appropriate damping constant, J or J' for tip or shaft behavior.

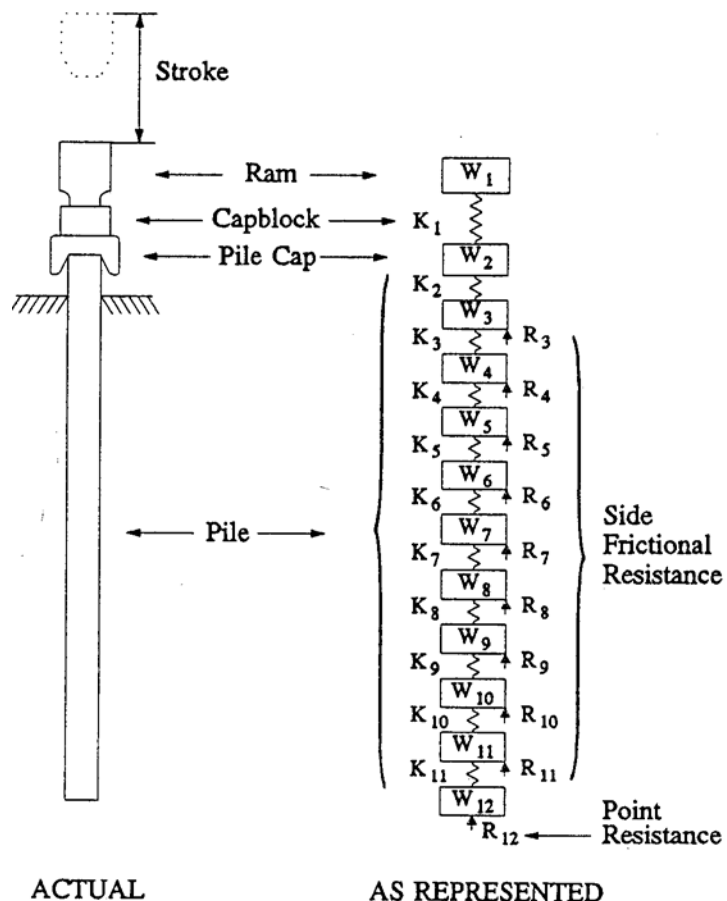


Figure 9.3 Finite Difference Discretization [9.12]

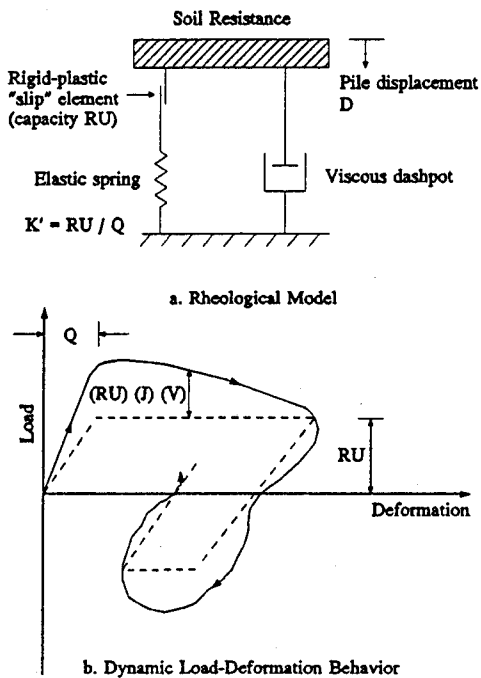


Figure 9.4 Soil Idealization [9.12]

The numerical solution of the one dimensional wave equation was obtained using a computer analysis, Smith, 1960. Subsequently, several other computer programs have been developed, e.g. TTI, WEAP [9.17, 9.4] that have refined the analysis but the classical solution proposed by Smith still forms the basis of these programs.

While the one dimensional analysis is very useful and is indeed routinely used, e.g. by the Florida Department of Transportation, its major weakness is the empirical basis for the soil parameters. Since they are not linked to soil properties, such as undrained shear strength or shear modulus, its application is limited to situations where such information is available.

9.3.2 Finite Element Solution

Unlike a finite difference model, a finite element model takes into account soil continuity and can therefore automatically model inertial and geometric damping effects of the infinitely extending soil medium. Moreover, standard soil mechanics parameters may be used to describe properties of the soil mass.

Since a full three dimensional analysis is prohibitively expensive, its application is limited to the axi-symmetric case. In such analyses, e.g. Smith & Chow, 1982 [9.14] the pile and soil are modeled by axi-symmetric isoparametric elements with special interface

elements for modeling soil-pile interaction and suitable 'infinite' elements to model boundary conditions. Material non-linearity can also be considered.

The finite element modeling of a three dimensional half space does have inherent limitations that have been addressed by Simons & Randolph, 1985 [9.16]. In essence, both spatial and time discretization introduce dispersive effects, i.e. the wave propagation velocities are different especially at high frequencies, characteristic of impact, for the finite element model compared to the actual structure. Moreover, the interface elements cannot rigorously model failure along the shaft interface. Thus, its solution would only be valid for determining short term response where no slip occurred.

In view of the limitations of the three dimensional analysis, Simon & Randolph proposed an alternative one dimensional analysis in which the dynamic soil stiffness along the pile shaft and pile base is obtained from elasticity based solutions proposed by Novak, 1978 [9.18] (to model shaft resistance) and Lysmer & Richart, 1966 [9.19] (to model bearing resistance). Since these 'analogs' are independent of frequency, but are functions of the shear modulus of the soil and the shear wave propagation velocity, this approach allows the definition of a spring and dashpot model for the soil to be directly linked to conventional soil properties such as undrained shear strength.

A one dimensional finite element model using this soil model was successfully used by Simon & Randolph to extend the application of wave analysis to offshore structures where soil parameters proposed by Smith, 1960 could not be used. Subsequently, similar analyses have been reported by other researchers, e.g. Chow, Wong, Karunaratne & Lee, 1988 [9.20].

9.4 Pre-driving Analysis

As noted earlier, a pre-driving analysis refers to the application of wave analysis to determine the optimum driving system for the pile. Since this analysis requires the ultimate capacity of the pile, the soil properties of the test site must be known. These are described in Section 9.4.1. Additionally, maximum allowable driving stresses must be determined so that the stresses obtained from the analysis comply with these limits. The stresses allowed by FDOT are presented in Section 9.4.2. The drivability study that was carried out using a PC Version of the wave analysis computer program GRLWEAP, 1990 [9.21] is described in Section 9.4.3.

9.4.1 Test Site

The test piles were driven at the site of a proposed condominium at 1701 Pinellas Bayway, Tierra Verde, FL. Three Standard Penetration Test borings (SPT 1, 2 and 3), were made by Brown Testing Laboratory, Tampa [9.22] in accordance with ASTM D-1586-67 using a standard split-spoon sampler and a 140 lb hammer with a 30 in. drop

height. Spacing interval between each sample varied from 2-5 ft. The soil samples left in the split spoon indicated dense to very dense sands with only a slight trace of organic matter. Since the site was close to the sea, groundwater was influenced by tidal action and varied between depths of 4-5 ft. The variation in blow count with depth at two of these borings is shown in Figure 9.5.

Since the six test piles formed two identical sets comprising a steel prestressed pile, an all fiberglass pile and a fiberglass pretensioned pile with steel ties, only two of the three SPT locations adjacent to SPT 1 and 2 were used (see Table 9.2). Inspection of Figure 9.5 shows these sites are very similar with a denser layer underlain by a softer layer.

9.4.2 Allowable Stresses

To prevent possible damage, the Florida Department of Transportation Specifications [9.23] sets limits on allowable compressive, s_{apc} , and tensile, s_{apt} , stresses given by Equations 9.3-5:

$$s_{apc} = 0.7f_c - 0.75f_{pe} \quad (9.3)$$

$$s_{apt} = 6.5\sqrt{f_c} + 1.05f_{pe} \quad (\text{for piles less than 50 ft long}) \quad (9.4)$$

$$s_{apt} = 3.25\sqrt{f_c} + 1.05f_{pe} \quad (\text{for piles-50 ft long}) \quad (9.5)$$

It may be seen that the allowable stresses are related to the compressive strength of the concrete, f_c , the effective prestress, f_{pe} , and the length of the pile.

Since 25 ft piles were tested, only Equations 9.3-9.4 apply. The average compressive stress at the time of the pile driving was 7,790 psi (see Table 4.3) and the effective prestress was about 740 psi (see Section 5.5). Substitution of these values in Equations 9.3 and 9.4 yields a *maximum allowable compressive stress of 4.89 ksi and a maximum tensile stress of 1.36 ksi*. In the drivability study, driving stresses were limited to comply with these limits.

9.4.3 GRLWEAP Analysis

The computer program GRLWEAP [9.21], which is based on Smith's finite difference solution, was used to carry out the drivability study. In view of its widespread use in Florida, reliable information on soil parameters to be used in the analysis is available.

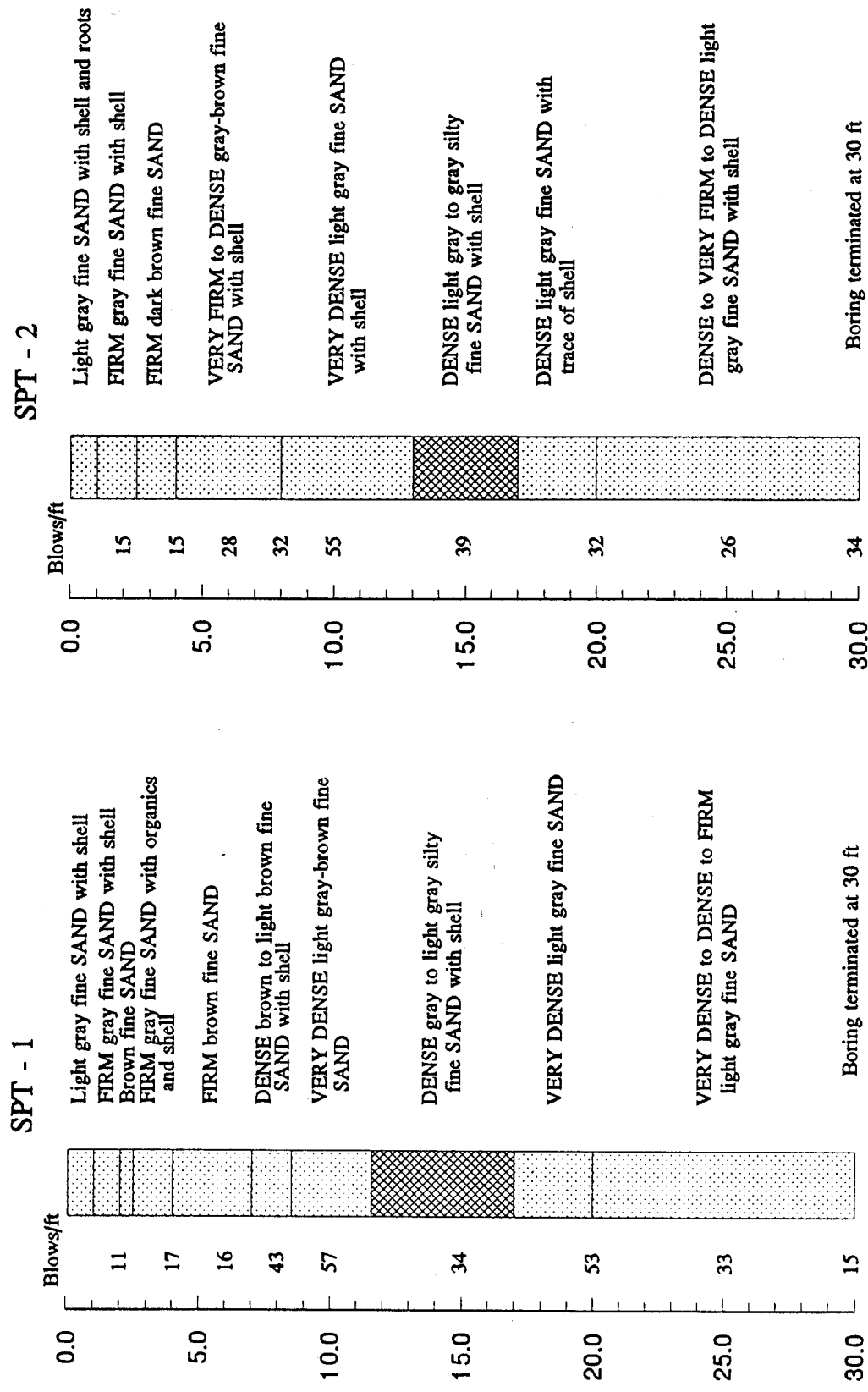


Figure 9.5 Blow Count for Test Site

The feasibility of an alternative fiberglass prestressing system could only be assessed if its driving stresses matched those in prototype steel piles. In view of this, a drop hammer, the simplest impact hammer, was selected since it allowed control over the input energy to the pile by varying the drop height. This contrasts with diesel hammers where the stroke varies automatically with soil resistance. Other factors, such as cost, ease of mobilization and simplicity of operation also influenced this decision. The drop hammer, however, operates at a relatively slow rate and its drop height and efficiency are dependent on the skill of the operator.

Apart from the hammer, the driving system consists of leads, a pile helmet and cushions made of plywood to protect both the hammer and the pile. Plates 9.2-9.3 show the driving rig used.

9.4.3.1 GRLWEAP Input

The basic input required by the computer program GRLWEAP to carry out a wave analysis is summarized below:

Hammer	:	Weight, dimensions, efficiency and drop height
Helmet	:	Weight, dimensions
Cushions	:	Area, thickness, elastic modulus and coefficient of restitution.
Pile	:	Area, modulus, density and length
Soil	:	Static capacity, percent skin friction and its distribution, maximum elastic compression (quake) and damping along the pile shaft and at the pile base

Since only a single blow is analyzed by GRLWEAP, several ultimate capacities ranging from very low to very high capacities were input to determine the range of pile driving stresses that could be anticipated. The smaller values simulate initial driving conditions when the pile is being driven through relatively soft soil (this causes maximum tension stresses). The larger bearing capacities correspond to conditions at refusal (when maximum compressive stresses develop).

With the selection of the pile and driving system, the dimensions of the hammer and helmet were known as were the pile properties. The soil properties, quake and damping factors, were based on recommendations in the GRLWEAP Manual for cohesionless soils. In essence, they comply with Smith's original recommendations, i.e. the quake was 0.1 in. for side friction and 0.083 in. at the pile tip; the viscous damping coefficient, J, was 0.15 s/ft at the base and a third of this value, 0.05 s/ft along the pile sides.

The static capacity was found using four different methods, Wadsack, 1991 [9.24], two theoretical methods and two based on FDOT procedures. The results from these analyses are summarized in Table 9.3. Inspection of this table shows that the capacities

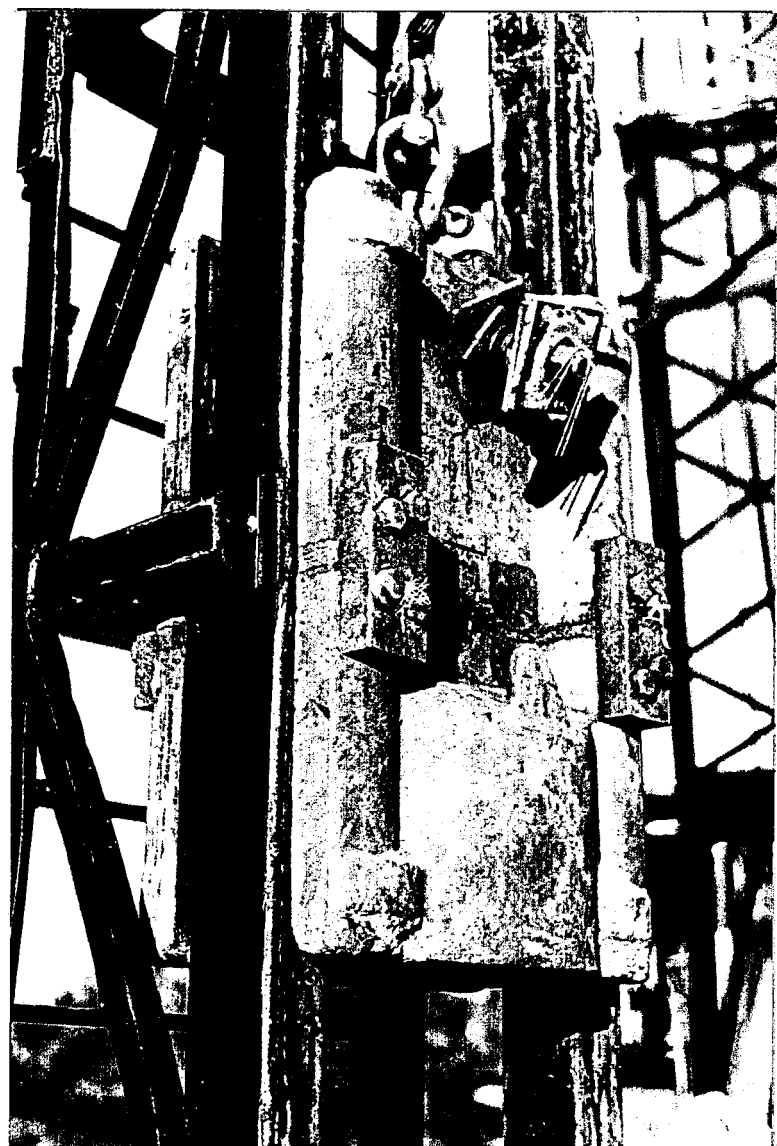


Plate 9.2 Drop hammer used for test piles.

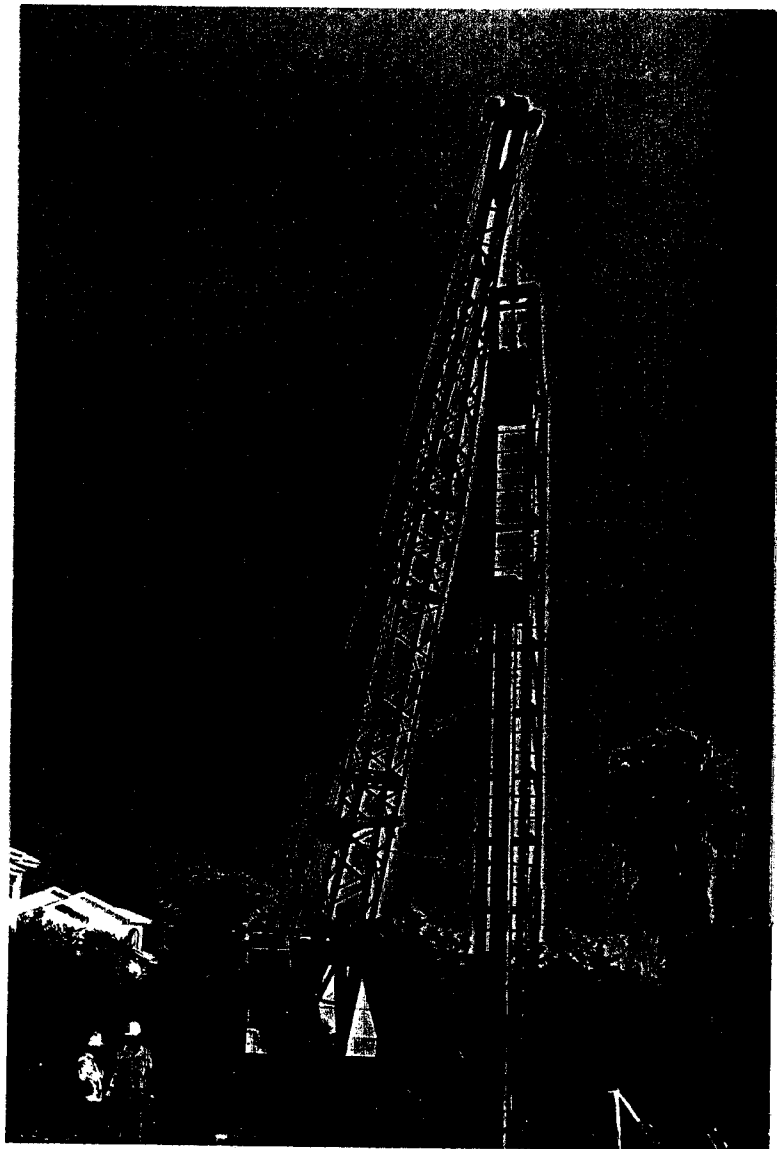


Plate 9.3 Pile driving rig and set up

predicted vary considerably with the FDOT based procedures predicting much higher values. Moreover, the percentage of loads carried by skin friction and end bearing also differ significantly.

Table 9.3. Results of Static Bearing Capacity Calculations

Method Used	SPT Boring Location	Skin Friction (tons)	End Bearing (tons)	Bearing Capacity (tons)	% Skin Friction
Effective Stress & Vesic [9.25]	1	9.3	53.2	62.5	17
	2	9	51.6	60.6	15
Effective Stress & Meyerhof [9.26]	1	9.3	60	69.3	13
	2	9	60	69	13
FDOT 121 [9.27]	1	46	66	112	41
	2	44	66	110	40
SPT 89 [9.28]	1	41.8	78.6	120.4	35
	2	40.7	63.7	104.4	39

In view of this, two separate runs of GRLWEAP were made using the results from both analyses. For the first analysis, based on SPT 89 [9.28], the skin friction was taken as 40%. For the second analysis, based on Vesic's approach [9.25], the skin friction was assumed to be 25 %. For either case, the skin friction was assumed to vary linearly and the soil resistance in the top 20% disregarded, i.e. a distribution corresponding to a 'Type 2' in the GRLWEAP program.

The only variables in the analysis were the drop height, efficiency, and thicknesses of the pile and helmet cushions. The maximum efficiency of the drop hammer was estimated as 67%, somewhat lower than the 75%-85% range generally used, e.g. Holloway, 1975 [9.2]. A GRLWEAP analysis on a PC 386/20 takes less than a minute and several preliminary analyses were carried out primarily to establish cushion thicknesses and drop heights that would ensure that there would be no damage to the pile.

A summary of the input data for a GRLWEAP analysis is presented in Table 9.4. Since some of the parameters assumed in the pre-driving analysis were changed during driving, a second post-driving GRLWEAP analysis was also carried out. For convenience, the input for this analysis is also shown, in brackets, in Table 9.4. The changes related to hammer efficiency (estimated as 57%), helmet weight (0.43 kips - it was changed during

Table 9.4 Summary of Typical Input Data for GRLWEAP Analysis

<i>Drop Hammer</i>	Weight	3.14 kips; 24.8 in. equivalent $\phi \times 40.5$ in.
	Drop height	6 ft (8 ft)
	Efficiency	0.67 (0.57)
<i>Pile Helmet</i>	Helmet	0.32 kips (0.43 kips)
	Cushion Material	Pine plywood
	Modulus	30 ksi
	Coeff. of Restitution	0.5
	Helmet Cushion	2.25 in.
<i>Pile</i>	Pile cushion	3.75 in.
	Pile length	25 ft. (21 ft)
	Pile Area	100 in ²
	Density	150 pcf
	Pile Modulus	6000 ksi
<i>Soil</i>	Coeff. of Restitution	1.0
	Toe Quake	0.10 in.
	Skin Quake (d/120)	0.083 in.
	Toe Damping	0.15 sec/ft
	Skin Damping	0.050 sec/ft
	Side Resistance	(1) 25% of End Bearing - Vesic, 1966 (2) 40% of End Bearing - SPT 89
	Distribution	Triangular with zero resistance in top 20% (Type 2)
	Resistance Analyzed	5, 10, 40, 80, 120, 160, 200 kips.

driving), pile length (21 ft) and drop height (increased from 6 ft to 8 ft during driving).

The results from both pre-driving and post driving GRLWEAP analysis are summarized in Table 9.5. Inspection of this table shows that the results from the wave analysis are not particularly sensitive to the distribution of skin friction assumed. The maximum tensile stresses and the maximum energy transferred are comparable; the maximum compressive stresses are larger for the SPT 89 analysis primarily because it predicts a

larger capacity. These predictions are compared against field measurements made during testing in Section 10.4.1.

Table 9.5 Drivability Study

	Analysis I (SPT89)	Analysis II (Vesic)
Ultimate Capacity (kips)	225	123
Tip Resistance (%)	60	75
Side Resistance (%)	40	25
Efficiency	67 (57)	67 (57)
Maximum Stroke (ft)	6 (8)	6 (8)
Helmet weight (kips)	0.32 (0.43)	0.32 (0.43)
Pile length (ft)	25 (21)	25 (21)
Maximum tension (ksi)	-0.90 (-0.78)	-0.89 (-0.77)
Maximum compression (ksi)	3.33 (2.8)	2.75 (2.41)
Maximum energy (kip-ft)	8.2 (9.0)	8.3 (9.0)

Note: Figures in brackets indicate values used for post-driving analysis

The insensitivity of the GRLWEAP analysis to variation in skin friction parameters has also been noted by others, e.g. Dover, Ping, Locke, 1982 [9.29] who found that a variation of distribution within reasonable bounds only led to a 6% change in drivability. It is evident therefore, that for a drivability study, simpler analyses such as those provided by FDOT 121 or SPT 89 are preferable to complex theoretical analyses such as those proposed by Vesic.

On the basis of the drivability study the following conclusions were drawn:

1. Drop height for the 3 kip hammer was determined as 6 ft. The helmet cushion was selected as 2.25 in., i.e. from three 3/4 in. plywood sections. The pile cushion was selected as 3.75 in., i.e. from five 3/4 in. plywood sections. This gave driving stresses that were within allowable limits specified by FDOT.
2. The static capacity of a pile should be determined from very simple analyses since results from GRLWEAP analyses were insensitive to variations in assumed distribution of skin friction.

10. PILE DRIVING

10.1 Introduction

The drivability study reported in the previous chapter established critical parameters such as ram weight, drop height and cushion thicknesses (see Table 9.5 and Plate 9.2) that were used to drive the test piles. The results obtained from this operation are presented in this chapter. Additionally, driving stresses in the fiberglass pretensioned piles are compared against those in identically tested 30 in. x 30 in. prototype piles used in the construction of the New Edison bridge, Fort Myers, FL.

As noted earlier, pile driving is a wave propagation problem that is characterized by a short duration excitation rich in high frequencies. Consequently, the response of interest is also over a very short time period - multiples of the time taken by stress waves to traverse the length of the pile. Since it only takes 2 ms for a stress wave to reach the end of a 25 ft long pile (assuming an average wave velocity in prestressed concrete of 12,500 ft/sec), the response of interest is between 6-8 ms to allow wave reflection effects to be captured. It is evident, therefore that data collection and analysis must be sophisticated enough to allow the response over such a short time period to be accurately and reliably recorded.

A widely used specialist data acquisition system known as a Pile Dynamic Analyzer" (PDA, manufactured by Pile Dynamics, Inc., Cleveland, Ohio) was used in this study and is described in Section 10.2. The test procedure and instrumentation of the piles is presented in Section 10.3. The results from the PDA are summarized in Section 10.4. Finally, the feasibility of fiberglass pretensioned piles from the standpoint of drivability is examined in Section 10.5.

10.2 Pile Driving Analyzer

An essential requirement for instrumenting and testing piles is mobility, reliability and robustness combined with the sophistication to record high frequency excitation. The Pile Driving Analyzer (PDA) was used to monitor the test piles during installation since it offers such a capability.

The PDA is a computerized data acquisition system developed under the direction of Professor G. G. Goble at the Case Western Reserve University, Cleveland (formerly Case Institute of Technology) for field testing of piles [10.1,10.2]. It is widely used in the United States and elsewhere in both research, e.g. Tucker and Briad, 1988 [10.3] and

routine field testing of piles, e.g. Fellenius, 1988 [10.4]. Several district offices of the Florida Department of Transportation own and operate their own PDA's.

The PDA uses a pair of re-usable bolt-on strain transducers and low impedance piezoelectric accelerometers, both manufactured by Pile Dynamics, that are attached to opposite faces of the pile. Since the strain signal voltage is very low it is conditioned and amplified for display on a oscilloscope. The oscilloscope allows signals to be visually monitored for data quality and possible pile damage. A fast Motorola 68000 micro-processor can analyze up to 120 blows per minute and specified results can be printed for each blow. Field signals are also recorded on a magnetic tape using a tape recorder for subsequent re-analysis by the CAPWAPC [10.5] computer program. It can also accomodate several types of standard peripheral equipment, e.g. Hussein, Likins & Rausche, 1988 [10.6].

As input, the PDA requires the pile length below the gages, its cross-sectional area, elastic modulus, density, calibration information for the gages and an assumed value of J , the damping factor for the soil. Pile forces are calculated from strain measurements assuming the response to be elastic and velocities are determined by integrating acceleration data. Using these values at impact and at a time interval $2L/c$ (to capture the reflected wave), up to 40 dynamic variables may be calculated in real time using the Case Method, e.g. Hussein & Likins, 1991,[10.7].

For each blow, five variables are printed out that can provide information such as the maximum displacement (DMX), the maximum energy (EMX), integrity factor (BTA), the maximum computed tension (CTN), the maximum force (FMX), the static capacity (RS1) and the maximum Case-Goble capacity (RMX). The analysis used to determine these quantities is described in Goble, Rausche, Likins, 1989 [10.8].

10.3 Test procedure and instrumentation

Wooden stakes were driven into the ground to identify the location near the SPT borings where the piles were to be driven (see Plate 10.1). To ensure identical driving conditions, six sets of plywood cushions were prepared, one for each pile (see Table 10.2). Their thicknesses were established on the basis of the drivability study reported in the previous chapter. Helmet cushions were 2.25 in. thick (3 layers of 3/4 in. plywood) and pile cushions, 3.75 in. thick (5 layers of 3/4 in. plywood).

To allow the blow count to be accurately determined, transverse lines were drawn across the piles at 1 ft intervals along its length. Apart from the blow count, the drop height of the hammer was also recorded. Since this is decided by the operator, variations from the stipulated drop height were noted during the driving.

A pair of re-usable piezoelectric accelerometers (sensitivity of 200 g/volt) and strain transducers (sensitivity of 120 micro-strain per volt) were bolted on opposite faces of the



Plate 10.1 Test pile layout

pile 3 feet from the pile head as shown in Plate 10.2. These were hooked up to the PDA system that was placed at the back of a station wagon as shown in Plate 10.2. A total of six channels were recorded: each force and their average and each velocity (obtained from integration of the acceleration) and their average. The measured strain and acceleration were used to determine pile top force and velocity respectively.

Piles ST-P2, FG-P2 and FG-FG-P2 were driven first in the vicinity of SPT 1; the remaining three piles, ST-P1, FG-P1 and FG-FG-P1 were subsequently driven near SPT 2. At each site, the steel pretensioned piles were driven first, i.e. ST-P2, ST-P1 with the all fiberglass piles, i.e. FG-FG-P2, FG-FG-P1, driven last. The drop height of the hammer was initially set at 6 ft but since the hammer efficiency was lower than estimated, it was increased to 8 ft.

Since the driving stresses during the initial driving were generally well within allowable limits stipulated by Eqs. 9.3-5, the drop height of the hammer was increased by 1 foot increments to a maximum drop of 15 ft for the last four piles driven. For each drop height, a complete printout of all 40 variables was obtained. During this operation, maximum compressive stresses approached the allowable limits. These results are also reported in the next section.

Gulf Coast Marine Construction, Inc. (of St. Petersburg, FL) were contractors for the pile driving operation. Mr. Mohamad Hussein, Partner, GRL & Associates, Orlando monitored the pile driving operation using a PDA. The results presented are summarized from GRL & Associate's report [10.9].

The set up for the pile driving operation is shown in Plate 9.3. The six test piles were driven in Tierra Verde, FL on May 9, 1991. The entire operation including instrumentation and driving took almost 12 hours. During driving, the original pile helmet cracked and was replaced by a similar helmet that weighed 0.43 kips.

10.4 Test results

The prime objective of the testing was to determine driving stresses in the pile and to check its structural integrity. Additional objectives were to estimate static capacity of the piles and to evaluate the performance of the hammer.

A printout of the compression force at the pile head (FMX), the computed tension in the pile (CTN), the static capacity calculated using the Case Method (RS1), the maximum displacement (DMX) and the energy transferred to the pile (EMX) was obtained from the PDA for each hammer blow. In addition, a complete printout of all 40 parameters was also obtained at periodic intervals. These results are presented and discussed in Sections 10.4.1-10.4.3.

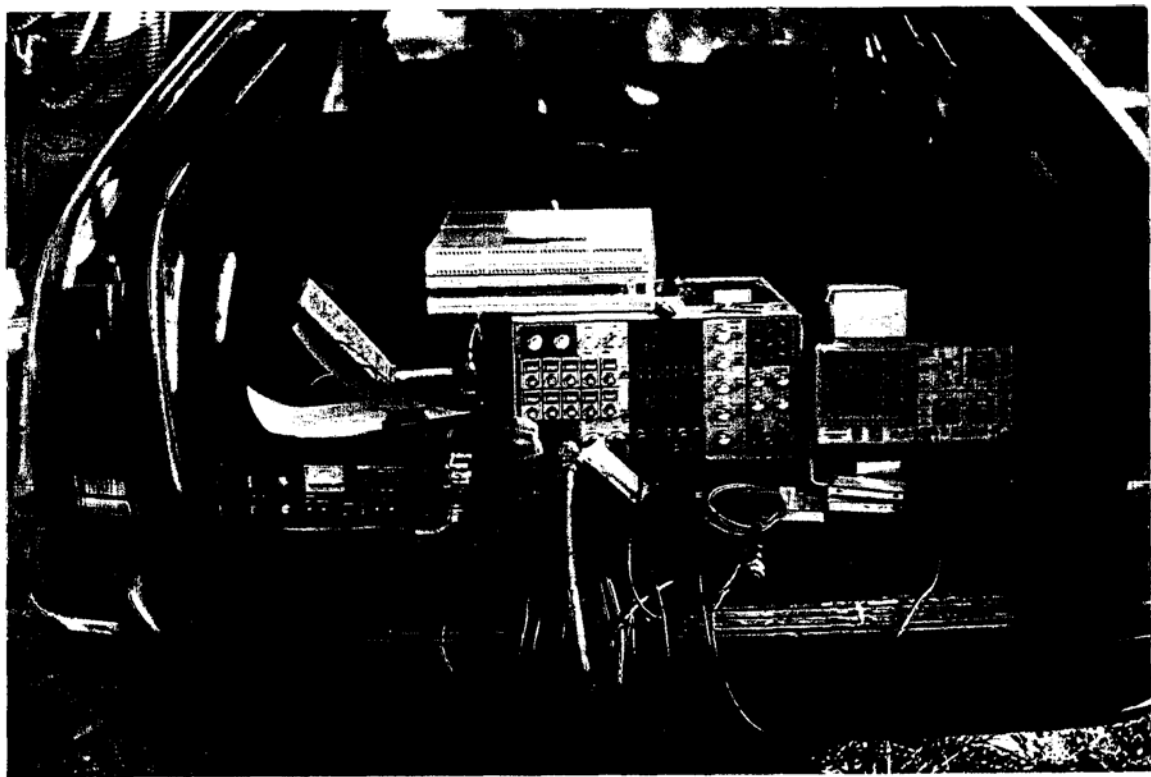
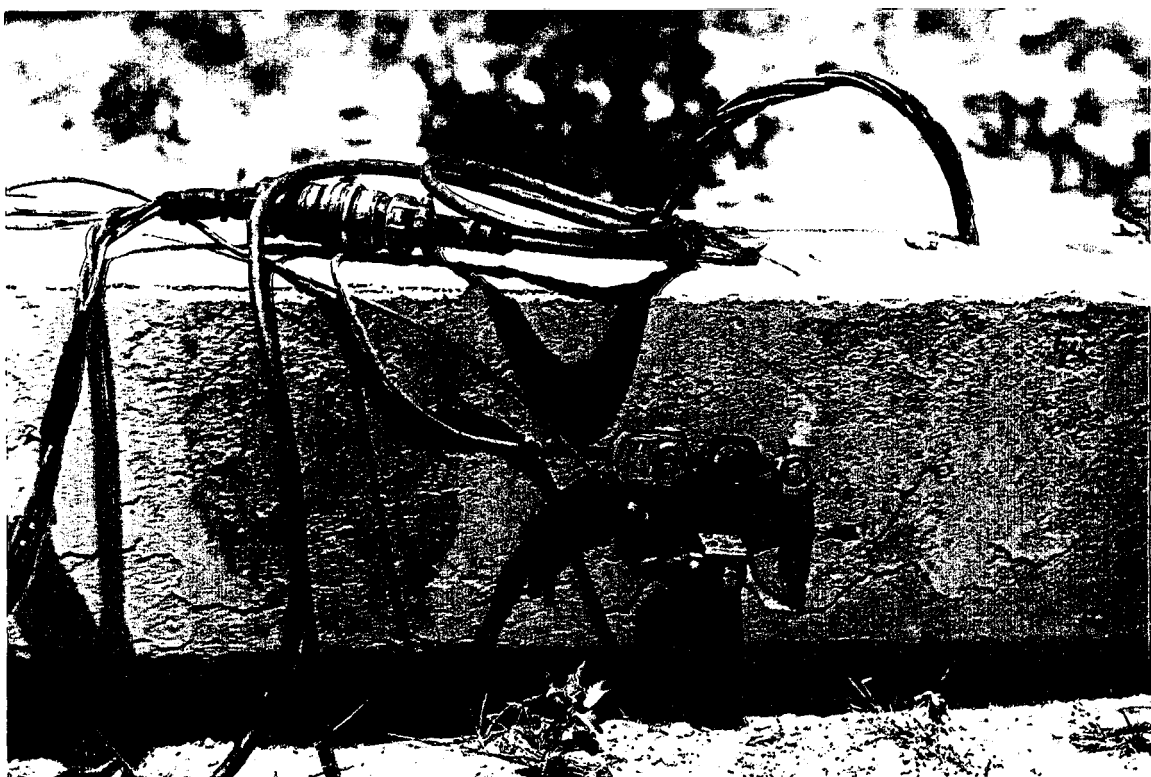


Plate 10.2 (top) Strain transducer, upper ; accelerometer, lower
(btm) PDA set up for testing

10.4.1 Driving Stresses

Plots showing the variation in blow count with depth for the three piles at the two sites are shown in Figures 10.1 and 10.2. Inspection of these plots confirm the correctness of the soil boring data and also indicates that the fiberglass and steel pre-tensioned piles were driven through very similar soils.

A summary of the maximum pile driving stresses is presented in Table 10.1. Compressive stresses were determined from strain transducer measurements located three feet below the pile head. Since tensile stresses depend on the reflected wave and can occur anywhere along the pile length, they are calculated values based on the measured accelerations.

Inspection of Table 10.1 shows that the maximum stresses in the fiberglass piles ranged from 3.58-3.78 ksi in compression and from 0.74-1.15 ksi in tension. The corresponding stresses in the steel piles were 2.5-3.32 ksi and 0.13-0.74 ksi respectively. The maximum values recorded are less than the allowable values of 4.89 ksi (compression) and 1.36 ksi (tension) (see Section 9.4.2). The observed stresses do however, compare favorably with the SPT 89 based pre-driving WEAP predictions of 3.33 ksi (compression) and 0.9 ksi tension summarized in Table 9.5.

Table 10.1 Summary of Pile Driving Stresses

Pile	Depth in Soil (ft)	Tensile Stress (ksi)	Comp. Stress (ksi)	Max. Energy Trans. (kip-ft)	Blow Count (bl/ft)	Dis ¹ (in)
ST-P2	15.4	-0.13	2.50	9.4	36	0.59
FG-P2	16.4	-0.79	3.58	11.0	31	0.66
FG-FG-P2	15.8	-0.74	3.71	11.0	34	0.61
ST-P1	21.3	-0.74	3.32	10.7	27	0.64
FG-P1	21.0	-1.15	3.70	11.5	32	0.58
FG-FG-P1	21.0	-0.46	3.78	12.3	28	0.67

¹ DMX values averaged for last five blows

Although the driving stresses in the steel pretensioned piles are comparable to those in the fiberglass pretensioned piles, the stresses in the latter (fiberglass) piles are consistently higher. This is probably due to the order of the pile driving; since the steel piles were driven first they presented a barrier so that the geometric damping in the piles

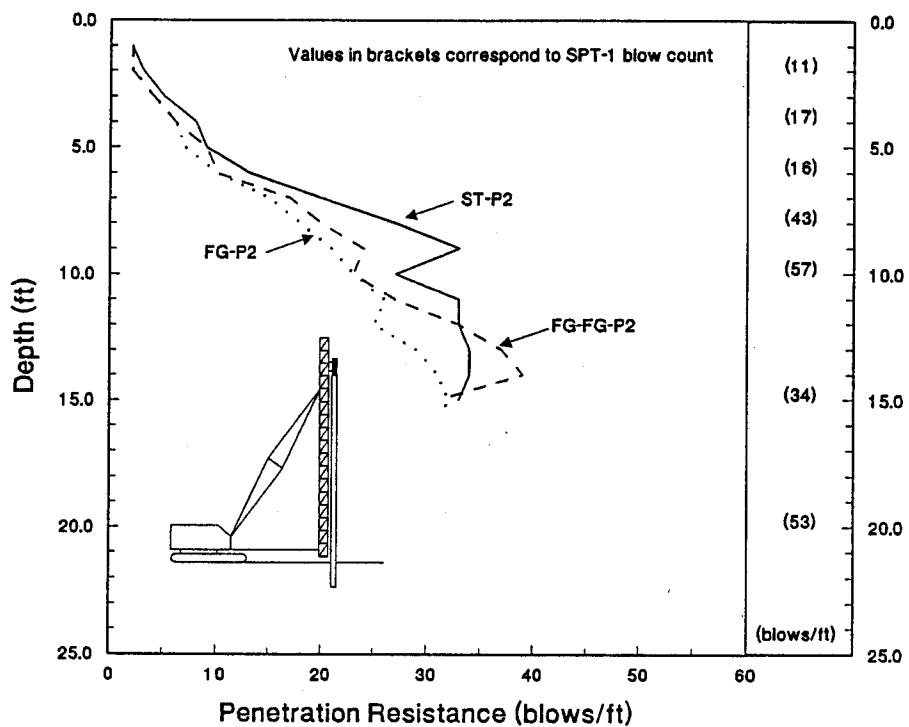


Figure 10.1 Blow Count Variation with Depth (Site 1)

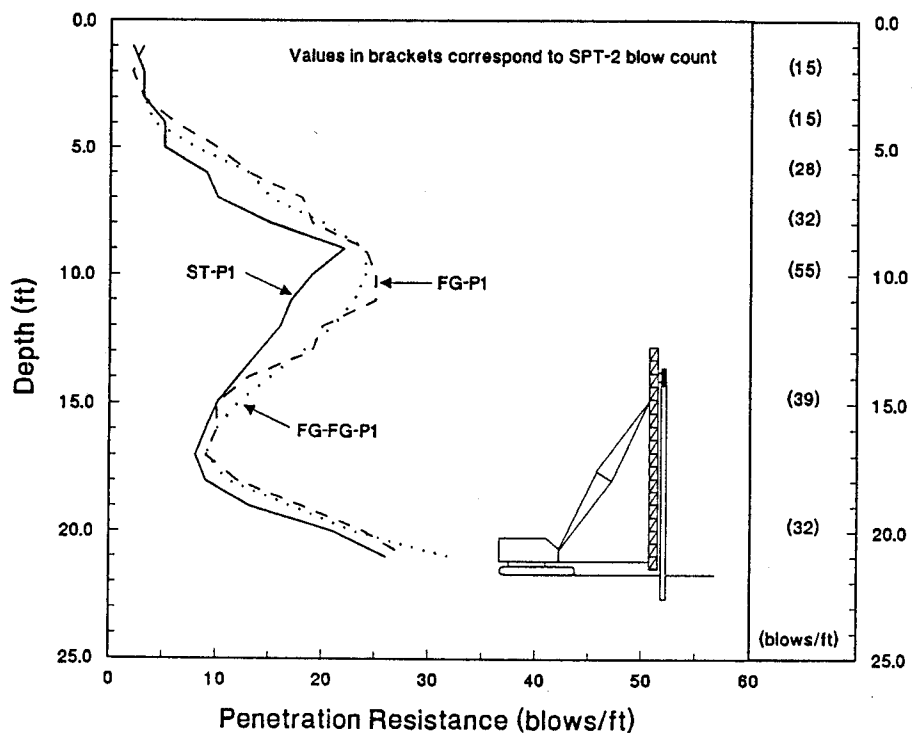


Figure 10.2 Blow Count Variation with Depth (Site 2)

driven subsequently was less. Moreover, the soil at the vicinity was also stiffened as a result of the steel pile thereby increasing its resistance.

Plots showing the variation of tension and compression stresses in the piles as it was being driven at the two sites is shown in Figures 10.3 and 10.4. In each plot, the depth refers to the depth of embedment of the pile, taken at 1 ft increments, for which the PDA printed out the driving stress. As before, the compressive stresses relate to the gage location, i.e. 3 ft below the pile head, whereas tension stresses are calculated values. Inspection of these figures shows that a maximum tensile stress occurred in pile FG-P1 as it was being driven through a softer layer underlying a harder layer (see Figure 12.5 for SPT data). This is in broad agreement with qualitative predictions from wave analysis discussed in Section 12.3.1.

Following the end of initial driving, the four of the six piles were driven with the drop height varying from 1 ft to 15 ft in increments of 1 ft. The driving stresses recorded during this operation are summarized in Table 10.2. It may be seen that in this phase, no tensile stresses were recorded although fairly high compressive stresses were measured. In fact, the maximum allowable compressive stresses in the fiberglass pile FG-FG-P2 equalled the allowable stress given by the FDOT specifications without suffering any damage (see Plate 10.3).

Table 10.2 PDA Result Summary for 15 ft Drop

Pile	Max. Tensile Stress (ksi)	Max. Comp. Stress (ksi)	Max. Energy Transf. (kip-ft)	Max. Displ. (in)	Remarks
FG-FG-P2	0.0	4.89	20.3	1.02	No damage
ST-P1	0.0	4.33	16.8	0.98	Minor Spalling at corner
FG-P1	0.0	4.61	19.8	0.96	No damage
FG-FG-P1	0.0	4.19	20.0	0.90	Extensive spalling

Notes: 1. For FG-FG-P1, maximum values correspond to a 13 ft drop for stresses and a 14 ft drop for energy.

During the initial driving there was some minor spalling of the steel pretensioned but not the fiberglass pretensioned pile. However, pile FG-FG-P1 showed extensive spalling during the post driving operation in which drop height was increased to 15 ft. One of the fiberglass ties in this pile was observed to have ruptured (see Plate 10.4). This suggests that the fiberglass ties did not provide the same degree of confinement as the

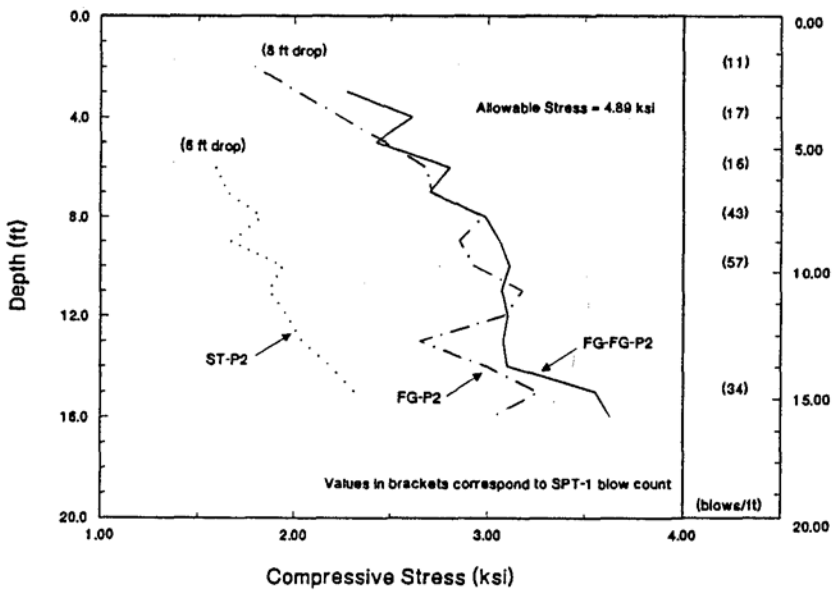
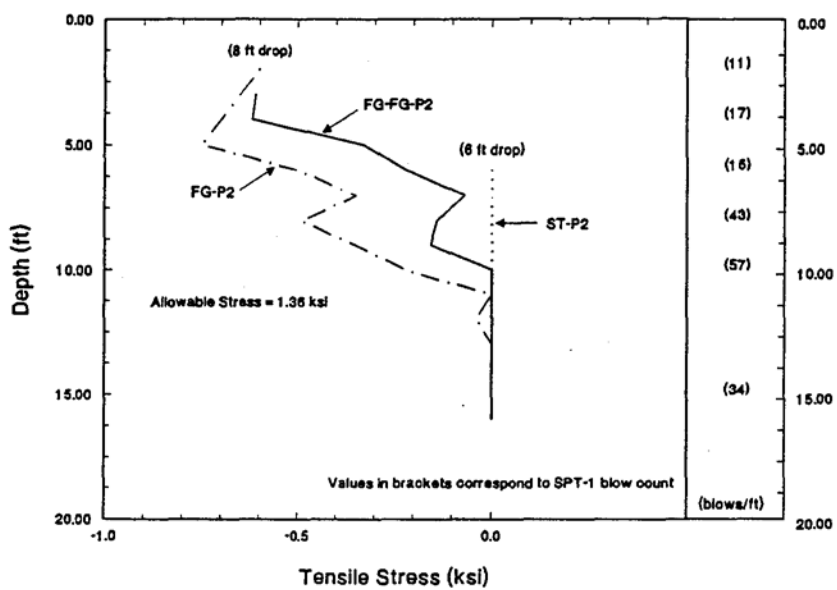


Figure 10.3 Pile Driving Stresses (Site 1)

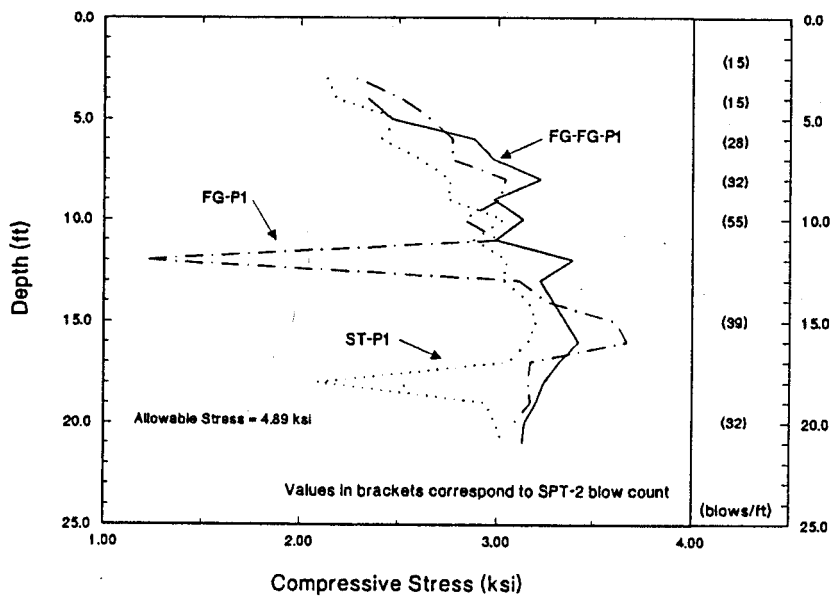
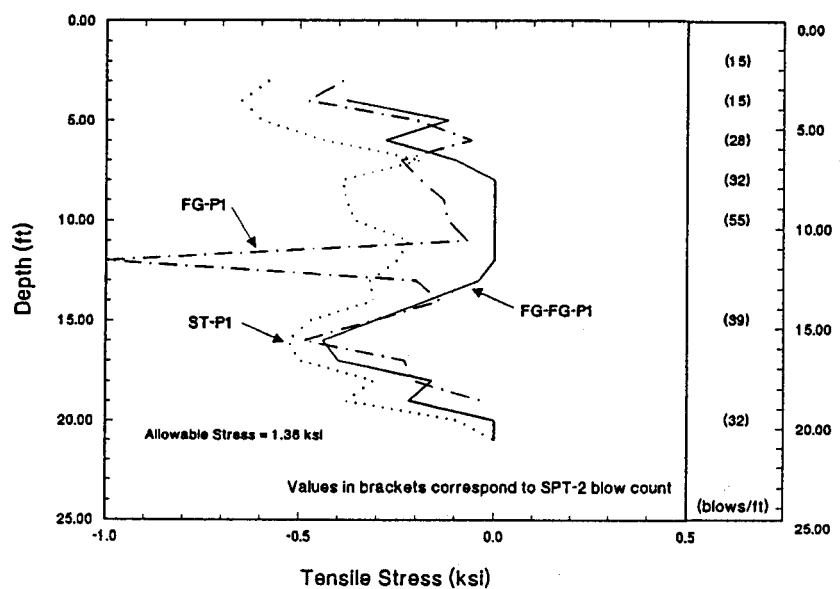


Figure 10.4 Pile Driving Stresses (Site 2)

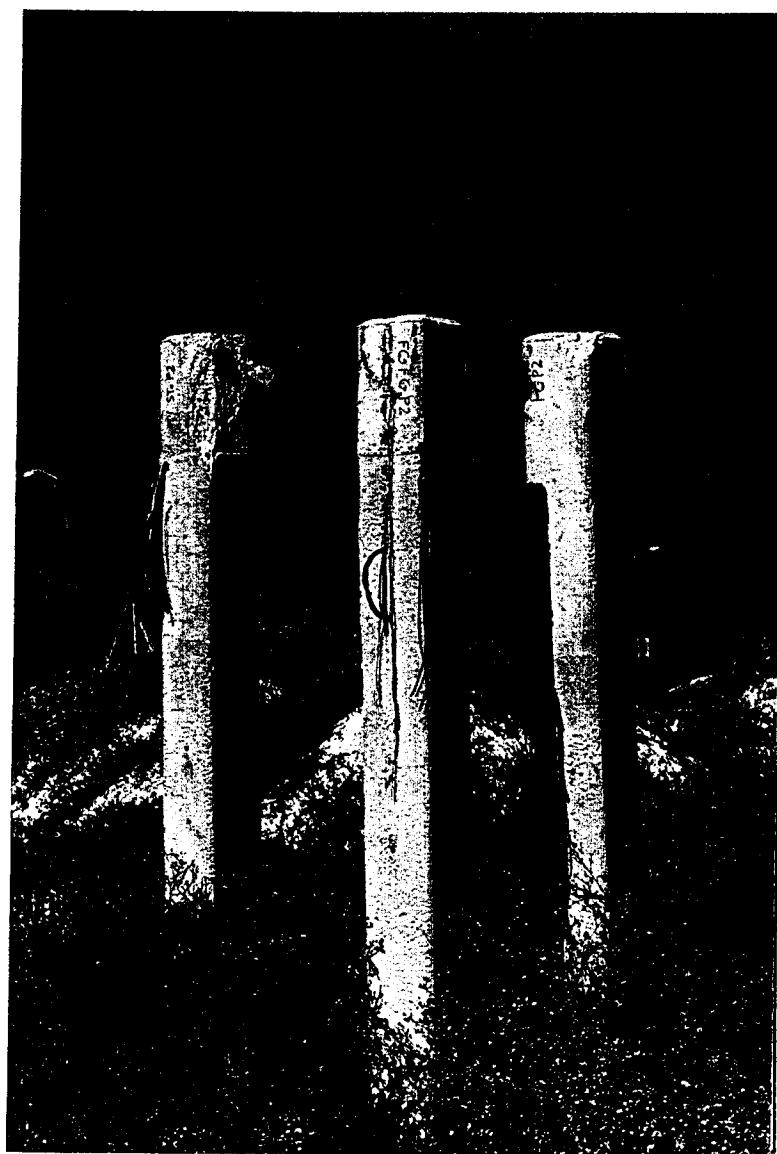


Plate 10.3 View of piles after driving at Site 1

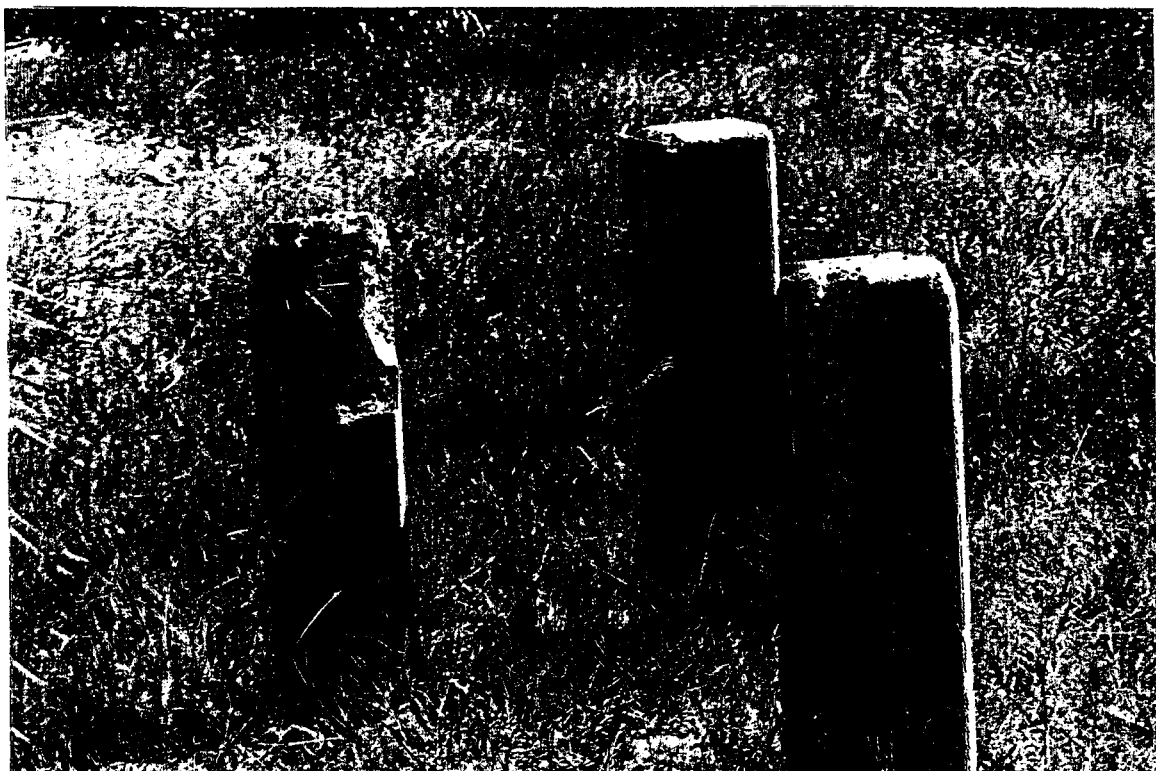


Plate 10.4 (top) Pile damage after 15 ft drop test at Site 2
(btm) Rupture of fiberglass ties in FG-FG-P1

steel ties since no corresponding damage was recorded in the fiberglass pile FG-P1 driven in its vicinity. GRL & Associates noted that "this minor damage is common in pile driving operations and in this case may be attributed to hammer-pile misalignment". Printout of the pile integrity parameter BTA indicated that there was no damage to the structural integrity of the piles.

10.4.2 Hammer & Driving system

The PDA also monitored the energy transferred to the pile (EMX). The maximum energy transferred to each pile during the initial operation is summarized in Table 10.1. As noted earlier, the drop height was initially set as 6 ft based on the WEAP analysis. Since the hammer was found to be less efficient than anticipated, it was increased to 8 ft. The energy readings for the first pile driven, ST-P2, reflect the lower drop height. At the end of driving, the maximum energy transferred averaged 9.6 ft-kips that indicates an efficiency of 38% when compared to the rated hammer energy of 25.12 kip ft for a 8 ft drop.

10.4.3 Bearing capacity

The final blow from the end of the initial driving was used to determine the static capacity of the piles using the CAPWAPC computer program. By varying soil parameters such as side and tip quakes and the load along the pile shaft and at the pile tip, this program allows measured and theoretical force and velocity signals to be matched. The static capacity can then be determined by summing the resulting loads at the pile base and along the pile shaft. Although numerous studies have shown good correlation between this capacity and load bearing tests, e.g. Crapps, 1977; Goble et al, 1980; Hussein and Rausche, 1991 [10.10-10.12], it should be noted that the capacity estimated is the mobilized resistance. If, the full resistance of the soil is not mobilized, then errors may result, e.g. Thompson & Devata, 1980 [10.13].

The bearing capacity predictions from CAPWAPC [10.5] and those based on the soil properties are summarized in Table 10.3. CAPWAPC predicts a variation of the ultimate load capacity ranging from 176 kips-214 kips. These correspond exactly to the driving order, i.e. the piles driven first have lower capacities than those driven later. This confirms the stiffening influence of piles on the soil resistance that was noted earlier (see Section 10.4.1).

A breakdown of the skin friction and end bearing soil resistance of the piles is also summarized in Table 10.3. The average skin friction value predicted by CAPWAPC is 42%. This compares favorably with the analyses obtained from SPT 89 [10.17] that predicted an average value of 37 %. By contrast, Vesic's [10.14] formula predicted a much lower skin friction component of 16%. The ultimate capacities from SPT 89 and

Table 10.3 Comparison of Static Bearing Capacity [10.14-10.17, 10.5, 10.18]

Method	SPT 1				SPT 2			
	Skin Friction (tons)	End Bearing (tons)	Total Capacity (tons)	% Skin Friction	Skin Friction (tons)	End Bearing (tons)	Total Capacity (tons)	% Skin Friction
Vesic	9.3	53.2	62.5	17	9	51.6	60.6	15
Meyerhof	9.3	60	69.3	13	9	60	69	13
FDOT 121	46	66	112	41	44	66	110	40
SPT 89	41.8	78.6	120.4	35	40.7	63.7	104.4	39
CAPWAPC	42.5	55.5	98	43	41.5	58	99.5	42
Engineering News ¹	--	--	111.6	--	--	--	107.7	--
Hiley ²	--	--	88.7	--	--	--	83.1	--

¹ Ultimate load calculated using a safety factor of 6 and an average set of 0.35 (SPT 1) and 0.4 in. (SPT 2)

² For $C_1 = 0.5$, $C_2 = 0.2$ and $C_3 = 0.1$ and hammer efficiency of 67%

FDOT 121 [10.16] are also closer to CAPWAPC values though they are somewhat larger. For completeness, static bearing capacity predictions from two pile driving formulas are also shown in Table 10.3. These are the Engineering News formula and Hiley formula [10.18]. The latter finds favor with consulting engineers in the Tampa Bay area. The capacity is over estimated using the Engineering News Formula (for a safety factor of 6) whereas predictions from Hiley's formula are slightly below the CAPWAPC values.

10.5 Assessment of Fiberglass Piles

As noted earlier, the effective prestress in the fiberglass pretensioned piles matched those in 30 in. x 30 in. square piles. Consequently, it is instructive to compare stresses in the fiberglass piles with those in steel pretensioned 30 in. x 30 in. piles used in on-going FDOT projects [10.19].

The New Edison bridge is a 5,253 ft long bridge in Lee County, FL connecting Fort Myers to North Fort Myers over the Caloosahatchee River. The roadway width is 59 ft 1 in. having three traffic lanes and two hard shoulders. A typical span is 143 ft long. A total of 435 prestressed concrete piles 30 in. x 30 in. in cross-section and between 76 ft to 81 ft long were required to support the superstructure. The minimum required capacity for a typical pile was 300 tons for a minimum blow count of 118 b/ft. The piles were driven in a layer of fine calcareous silty clayey sand overlaying dense to very dense silty sands using a Conmaco 300-E5 single acting air hammer. The ram weight was 30 kips with either a 2 ft or a 4 ft stroke and a rated energy of 60 k-ft or 120 k-ft respectively.

A PDA system was used to monitor 18 of the 435 piles driven in February 1991. The results of the PDA summary for these piles is shown in Table 10.4. Inspection of this table shows that the tensile stresses ranged from a minimum of 0.71 ksi to a maximum of 1.27 ksi. The compressive stresses ranged from a minimum of 1.80 ksi to a maximum of 3.27 ksi. These compare favorably with the stress range in the fiberglass pretensioned piles of 0.74 ksi-1.15 ksi (tension) and 3.58-3.78 ksi in compression (see Table 10.1).

Although, the actual compressive strength of the concrete at the time of pile driving is unavailable, its minimum strength must be 6,000 psi (for Class V concrete used in FDOT piles). An indirect measure of the strength obtained from the measured wave velocity suggests that its concrete strength was similar to that in the fiberglass piles (12,800 ft/sec versus 12,600 ft/sec velocity recorded for the fiberglass piles). Since the fiberglass pretensioned piles were subjected to stresses similar to prototype piles and did not suffer any damage, it is reasonable to conclude that as far as drivability is concerned, fiberglass piles are suitable.

Table 10.4 PDA Results Summary: New Edison Bridge

Pier/ Pile	Depth in Soil (ft)	Tensile Stress (ksi)	Compressive Stress (ksi)
10/7	71	0.83	2.84
11/10	71	1.03	3.14
12/11 ¹	67	1.16	2.80
14/11	61	1.07	2.07
17/10	68	0.82	2.24
18/11	68	0.86	1.80
19/10	71	0.80	2.80
20/11	68	0.89	2.93
21/6	66	0.82	2.86
22/7	67	1.01	2.37
23/6	64	0.91	2.85
24/7	59	0.93	2.62
25/6	60	0.87	2.81
27/7	67	0.86	3.00
30/7	64	0.71	3.21
33/7	68	0.98	2.97
36/4 ¹	64	1.27	3.27
39/7 ¹	64	1.08	3.17

¹ 6.75" plywood cushion; all others, 9" plywood cushion.

11. FATIGUE RESPONSE

11.1 Introduction

Fatigue is the "process of progressive permanent internal structural change in a material subjected to repetitive stresses" ACI 215 Committee, 1974 [11.1]. Fatigue resistance is usually described by an S-N curve (Figure 11.1). In this curve S is the stress range, i.e. the variation between maximum and minimum stress under repetitive loading, and N the number of cycles to failure. It is customary to plot this on semi-logarithmic paper, with the stress range being plotted to the linear scale and the number of cycles to failure to a logarithmic scale. Since the stress range in "fully" prestressed (no tension under service loads) is very small, they are not vulnerable to fatigue failure. By contrast, fatigue is an important consideration for "partially" prestressed members where stress ranges are much larger due to cracking of the concrete under service loads as shown in Figure 11.2.

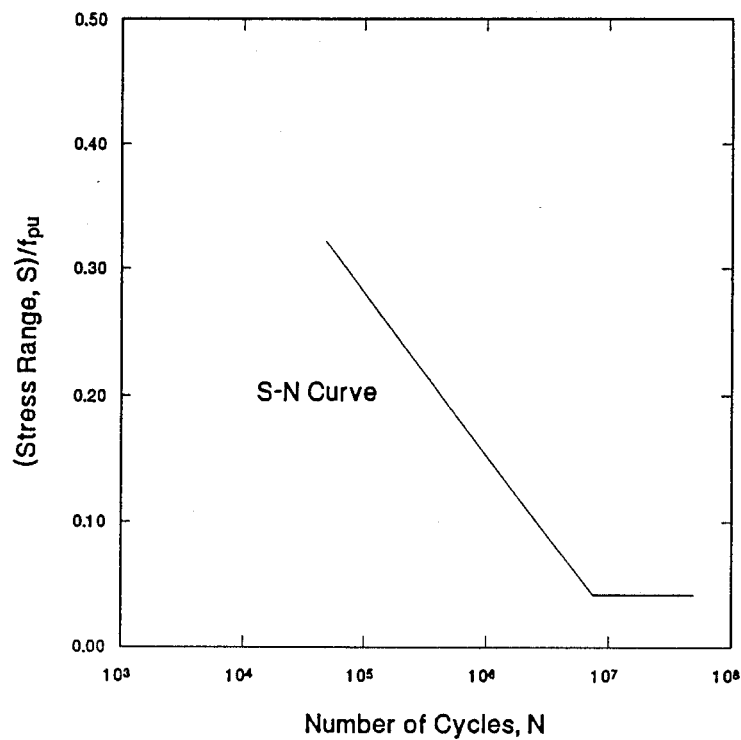


Figure 11.1 Typical S-N Curve

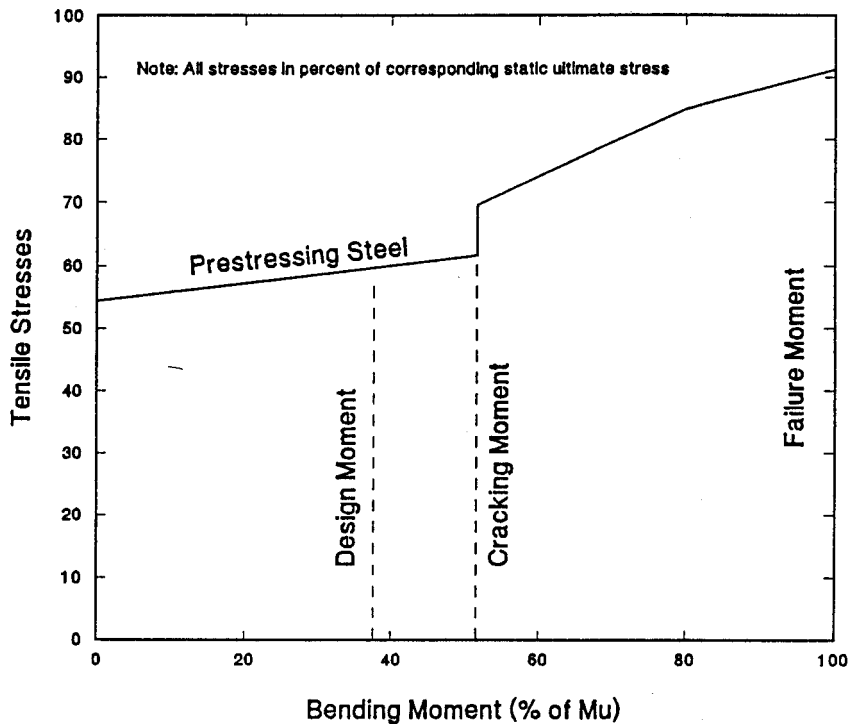


Figure 11.2 Stress-Moment Diagram

In addition to stress range and number of repetitive cycles of applied loading, fatigue of prestressing steel strands is greatly affected by the minimum stress level in the strand. Since S-N curves cannot show this effect, a Goodman-Johnson diagram, e.g. Ekberg, et al., 1957 [11.2] shown in Figure 11.3 is used that shows the allowable stress range for different minimum stress limits. It is evident that from this figure that the lower the minimum stress, the higher the allowable stress range. Typically, the minimum stress in prestressing steels vary between 0.5-0.6 f_{pu} , Namaan, 1982 [11.3] and between 0.30-0.4 f_{fg} for fiberglass strands.

Since fatigue resistance is strongly influenced by the presence of any flaws, test results are inherently variable. Accordingly, predictions of fatigue life must be based on a statistical analysis of fatigue data to provide indication on failure probability. ACI Committee 215 Report [11.1] provides guidelines on the number of tests required for such an analysis. It notes that at least six and preferably twelve tests are necessary for each stress level to establish fatigue strengths for survival probabilities ranging from 90 to 10 percent. In view of time and cost considerations, few tests reported in the literature comply with these recommendations. In most instances, a limited amount of testing is carried out with the intention of contributing to a data base that can subsequently be used for developing reliable design rules.

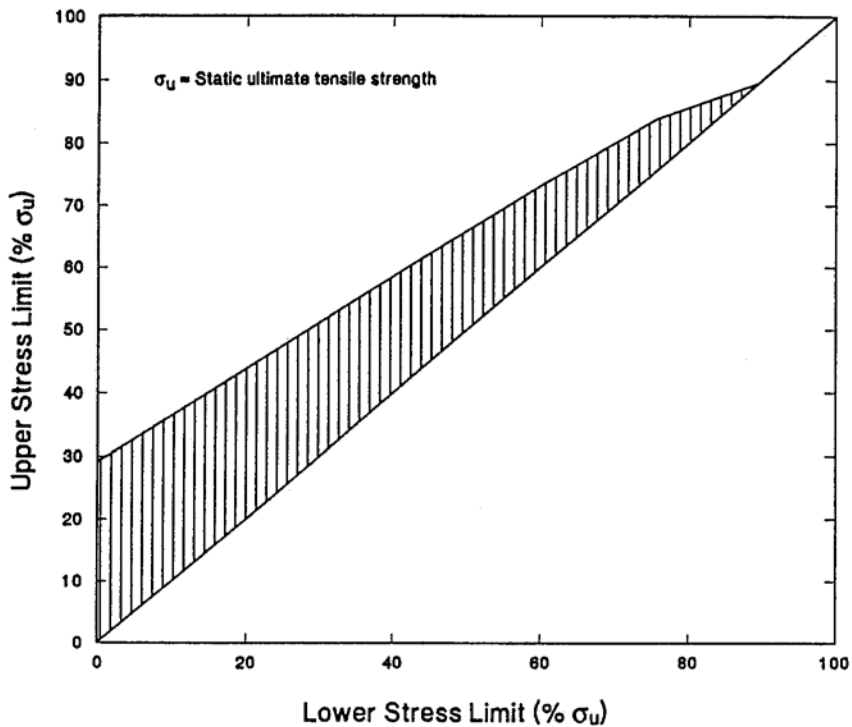


Figure 11.3 Fatigue Failure Envelope for Prestressing Steel [11.2]

A brief review of research on fatigue in partially prestressed members is presented in Section 11.2. The scope of the study and the test parameters are discussed in Sections 11.3 and 11.4 respectively. Details of the experimental set up, instrumentation, test procedure and results obtained are presented in Section 11.5. These are evaluated in comparison with results of similar steel pretensioned beams presented by Harajli & Namaan, 1984 [11.4] in Section 11.6.

11.2 Literature Review

Fatigue of prestressed concrete structures should consider separately fatigue effects of its constituents - concrete, reinforcing bars and prestressing steel. The review is only limited to fatigue of prestressing materials since this is the subject of this chapter. Information on fatigue in concrete and in reinforcing bars may be found in the ACI Committee 215 Report [11.1].

11.2.1 Steel strands

The fatigue resistance of steel prestressing strands have been determined from beam tests, Harajli & Naaman, 1984; Hanson *et al.*, 1970; Rabbat *et al.*, 1978; Ozel & Ardamian, 1956; Abeles *et al.*, 1974; Bennet & Dave, 1969; Dave & Garwood, 1975; Foo & Warner, 1984; Mansur, 1983 [11.4-11.12] and from tests on strands in air, Tide & Van Hore, 1966; Warner & Hulsbos, 1966; Edwards & Picard, 1972; Gylltoft, 1979; Fisher & Viest, 1961 [11.13-11.18]. Experimental results are however, inconclusive at this time [11.1] ; some studies indicate a shorter fatigue life [11.4-11.12] and others longer [11.13-11.18] or comparable fatigue life [11.5,11.6].

An excellent review of the published literature until 1983 is given by Harajli & Naaman [11.4]. They commented that the main drawback was the absence of "technical information related to the experiment... Few investigations give simultaneously information on ..basic material properties, crack widths, deflections ... None give a complete set of data.."

In their study, Harajli & Namaan fatigue tested 12 rectangular beams with reinforcing indices varying between 0.1 to 0.37. Beams tested included those with and without nonprestressed reinforcement in the tension and compression zones. A sinusoidal load was applied at a frequency of 6-7 Hz that varied between 40 % and 60 % of the ultimate static capacity. A two point load configuration was used. Instrumentation provided data on the variation in deflection, crack width and strains with the number of cycles. Beams were subjected to 5 million cycles and then tested statically to failure.

Table 11.1 contains a summary of equations proposed by various investigators. Note that these equations relate to the mean design life, i.e. with a failure probability of 0.5. The FIP Recommendations for a fatigue strength of 2 million cycles and a failure probability of 0.10 are for a stress range of 29 ksi for strands. This is somewhat higher than the 0.1 f_{pu} range recommended by ACI Committee 215.

11.2.2 Fiberglass strands

Based on fatigue tests carried out on Polystal (E glass fibers), it has been proposed that it can be subjected to two million cycles with a 10% probability of failure for a stress range of 8 ksi and a maximum stress of 0.44 f_{fg} , Miesseler & Preir [11.19]. However, it is stated that "failures still have to be expected even with higher stress cycles. A possible consequence thereof is that the stress cycles to be expected for a structure must be forecast and investigated in each individual case to determine whether the tolerable stress ranges are sufficient". The meaning of this is not entirely clear.

Iyer and Kumararaswamy, 1988 [11.20] reported tests on a pretensioned beam using S-2 glass fibers and polyester resin that was subjected to 600,000 cycles with a load range variation of 0.065 to 0.32 of the ultimate load (smaller than the cracking load). No

visible cracking was observed during the test period. In addition, Iyer, 1991 [11.21], cyclic (air) reported tests on S-2 glass tendons at 3 Hz that failed after 558,390 cycles at a mean load of 9,150 and a minimum to maximum load ratio of 0.81. A similar strand, tested at 7 Hz with a minimum to maximum load ratio of 0.91 survived two million cycles and showed little deterioration in its material properties.

Table 11.1 Proposed S-N Equations for Prestressing Steel Strands

Research Study	Fatigue Life
Fisher & Viest [11.18]	$\text{Log}_{10}N = 9.354 - 0.0423f_r$ $- 0.0102f_{s,\min}$ $f_r = f_{s,\max} - f_{s,\min}$
Warner & Hulsbos [11.15]	$\text{Log}_{10}N = 1.4332/R + 5.5212 - 0.0486R$ $R = S_{\max} - (0.83S_{\min} + 23)$ Valid for $40\% < S_{\min} < 60\%$ $0 < R < 15\%$
Hilmes & Ekberg [11.2]	$S_r = (1640 - 11.5S_{\min})N^{-0.320}$ For $40,000 < N < 400,000$ $S_r = (115.5 - 0.78S_{\min})N^{-0.1154}$ For $400,000 < N < 4,000,000$
Van Horn [11.14]	$\text{Log}_{10}N = 6.356 - 0.1373R_s + 0.00303R_s^2$ $R_s = S_{\max} - (1.05S_{\min} + 8.0)$ Valid for $40\% < S_{\min} < 60\%$ $0 < R_s < 20\%$
Naaman [11.4]	$(S/f_{pu}) = -0.123\log N + 0.87$

11.3 Scope of Study

It is evident from the literature review that very little data is available on the fatigue response of S-2 glass pretensioned beams. The available data does not relate to loads in the post-cracking range nor does it provide information on deflection, strain and crack width that can assist in the understanding of the fatigue response. The aim of this study therefore was to conduct fatigue tests with the intention of obtaining a comprehensive set of data that could be used as a data base in the future.

Two fiberglass pretensioned beams were tested under fatigue loading. These were FG-W9 (6 in. x 12 in.) and FG-E9 (6 in. x 1'0 in.). The comparable steel pretensioned beams used in the static test are ST-W8 and ST-E8. As seen in Table 7.1, the reinforcing indices for these beams are 0.11 and 0.14, respectively.

Since fatigue resistance is sensitive to the minimum stress and the minimum stress in the fiberglass strands as a proportion of its ultimate tensile strength is much lower compared to steel (0.3-0.4f_u, vs 0.5-0.6f_u) direct comparisons of the fatigue response of steel and fiberglass pretensioned beams may not be very meaningful. Nevertheless, to evaluate the fatigue response of the fiberglass pretensioned beams, test parameters (see Section 11.4) were kept very similar to those used by Harajli & Naaman [11.4] for steel pretensioned beams for which a comprehensive set of test results is available.

Of the beams tested by Harajli & Naaman, beam PD 1 with a reinforcing index of 0.14 corresponds exactly to that used in beam ST-E8 in this study. Beam PP2D1 with a reinforcing index of 0.10 almost matches the reinforcing index of beam ST-W8 used in this study. It differs, however, in having tensile non prestressed reinforcement. The results for these beams are compared against the response of the fiberglass pretensioned beams to assess their performance under fatigue loading.

11.4 Test Parameters

The test parameters used by Harajli and Naaman [11.4] and also those used in this study are summarized in Table 11.2. The most important parameters are the type, location, range of applied loading, number of cycles and its frequency. It may be seen that excepting for the applied frequency which is, 3 Hz in our study (more representative for applications involving highway loading) and, the number of cycles of load (2 million in our study) the design parameters are very similar.

The amplitude of the applied sinusoidal loading varied between 40% and 60% of the observed ultimate capacity of an identical' sister beam in both studies. This range corresponds to the application of the full design live load on the beam. It may be seen from Table 11.2 that the maximum load exceeded the cracking load of the beams and therefore stress ranges in the prestressing strands were in the range where fatigue aspects need serious consideration.

11.5 Experimental Study

The set up, instrumentation and test procedure are described in Section 11.5.1. The results from the fatigue test are presented in', Section 11.5.2. This includes a discussion on the fatigue life and also the fatigue response that considers deflection, crack width and strain variation in the concrete and the fiberglass strands. Finally, the static ultimate load test following completion of two millions cycles of the applied loading are described.

11.5.1 Test Set Up

The set up used for the fatigue test was very similar to that used in the static test (see Plate 7.2). The only difference is that all supports and instrumentation was secured to

Table 11.2 Fatigue Test Parameters

Parameter	Our Study	Harajli & Naaman
Type of beam	$6 \times 12"$ and $6 \times 10"$	$4.5 \times 9"$
Strand	$3/8" \phi$ Fiberglass	$3/8" \phi$ & $5/16" \phi$ Steel
Range of Loading	$0.4P_u$ to $0.6P_u$	$0.4P_u$ to $0.6P_u$
Frequency	3 Hz	6-7 Hz
Nº of cycles (target)	2 million	5 million
Reinforcing index	(1) 0.11, (2) 0.14 ¹	0.10 (PP2D1), 0.14 (PD1)
Concrete strength	6,840 psi	5,570 - 6,040 psi
Span	8 ft	9 ft
Type of loading	Two point loading	Two point loading
Cracking load	(1) $0.45P_u$, (2) $0.49P_u$	$0.47P_u$, $0.5P_u$

¹ beams ST-W8 and ST-E8 respectively

the supporting beam to prevent any movement during the application of the cyclic loading.

The instrumentation was identical to that used for the static testing with the exception that a strain transducer was attached on each face of the beam at the level of the prestressing strand where the first crack occurred to measure the crack width (see Plate 7.1). A TML transducer, PI-5-150, having a gage factor of 2 was used. This could record a maximum crack width of 5 mm. Other measurement¹ that were recorded were deflections using LVDTs, slip (using digital dial gages accurate to 0.0001 in.) and strains in the concrete and the fiberglass strands.

11.5.5.1 Test Procedure

The fatigue tests were carried out immediately after the completion of the static testing that provided information on the ultimate static capacity of the beams. Since only one beam was tested, the capacity of this beam¹, and that of its calculated value from strain compatibility analysis was used to estimate its ultimate capacity. The minimum and maximum loads were set respectively as 40% and 60% of this value. All readings were initialized before the test commenced. This¹, means that only increments in strains were recorded during the testing.

An initial cycle was applied statically to the beams. Since the maximum applied load exceeded the cracking load, cracks developed. The location where the beam cracked was noted and transducers for measuring crack width were attached to both faces of the beam at the level of the prestressing strand, i.e. two inches from the bottom of the beams. Two more static cycles were then applied and for each cycle, strains, deflections and crack widths were recorded. The cyclic test between the maximum and minimum load was then commenced at a frequency of 3 Hz by means of a hydraulic load actuator under electronic feedback control operating in a load control mode. The fatigue loading was interrupted periodically and a static cycle applied between the minimum and maximum load. During this cycle, 5 or 6 measurements were taken for equally spaced load increments over the loading and unloading cycles.

The fatigue tests took about 8 days to complete. After two million cycles were completed and if the beam did not fail, the beam was unloaded and a static test conducted to determine the effect of cyclic fatigue on the ultimate load capacity and deformation of the beam.

11.5.2 Fatigue Response of Fiberglass Prestressed Beams

The results from the fatigue tests on the two fiberglass prestressed beams are presented in this section. The fatigue life is discussed in 11.5.2.1 and detailed results for deflection, crack width and strains are subsequently described in Sections 11.5.2.2 to 11.5.2.4, respectively.

11.5.2.1 Fatigue Life

Of the two fiberglass pretensioned beams tested, beam FG-W9 failed after the application of almost 1.5 million cycles. Failure appears to have been caused by loss of bond since slips of 7/16 in. were recorded in two strands at one end. There was no corresponding slip at the other end. As with the static test, individual rods making up the strands slipped. The loss of slip led to increased permanent deflection and opening out of the crack width. It is of interest to note that the maximum crack width did not occur where the transducer was located but near the central section of the beam. The strands visible at the opening were somewhat frayed but had not ruptured. Plate 11.1 shows beam FGW9 after failure. The other beam, FG-E8 survived two million cycles and no slip was recorded for this beam. It was subsequently tested to determine its ultimate capacity.

11.5.2.2 Deflection

The load-deflection curves for two beams are shown in Figure 11.4-11.5 along with some relevant data pertaining to the beam tested. These curves show the variation of the load

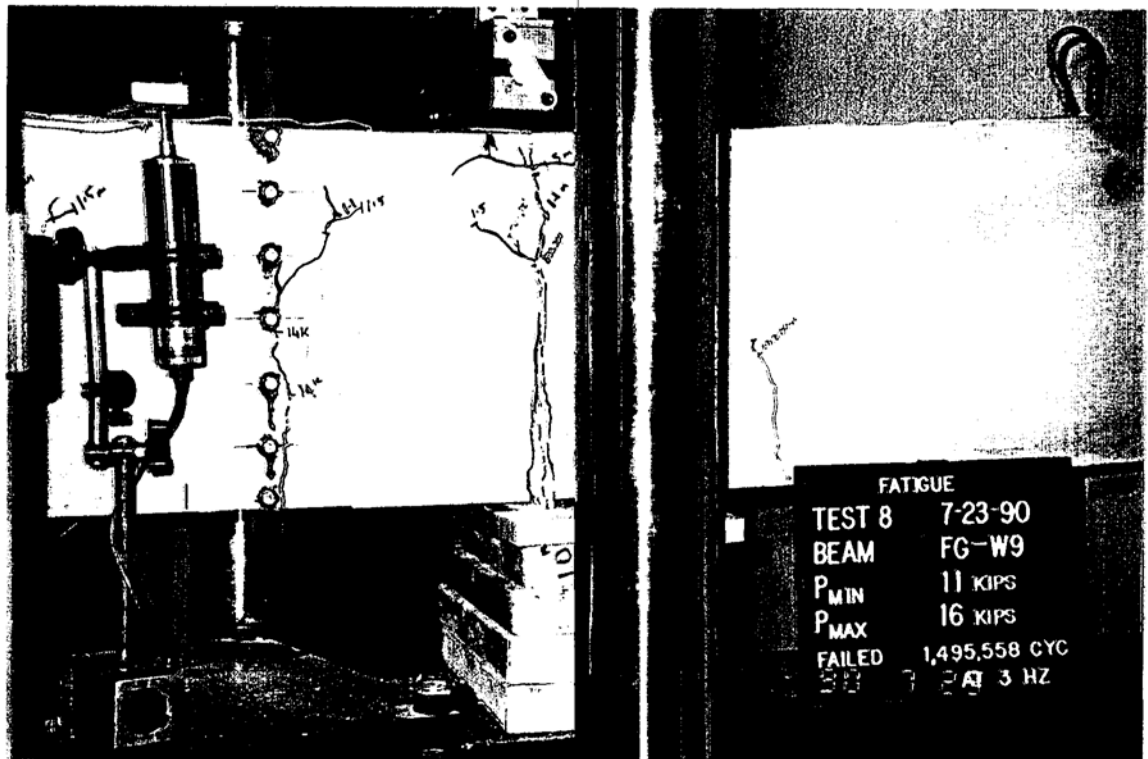
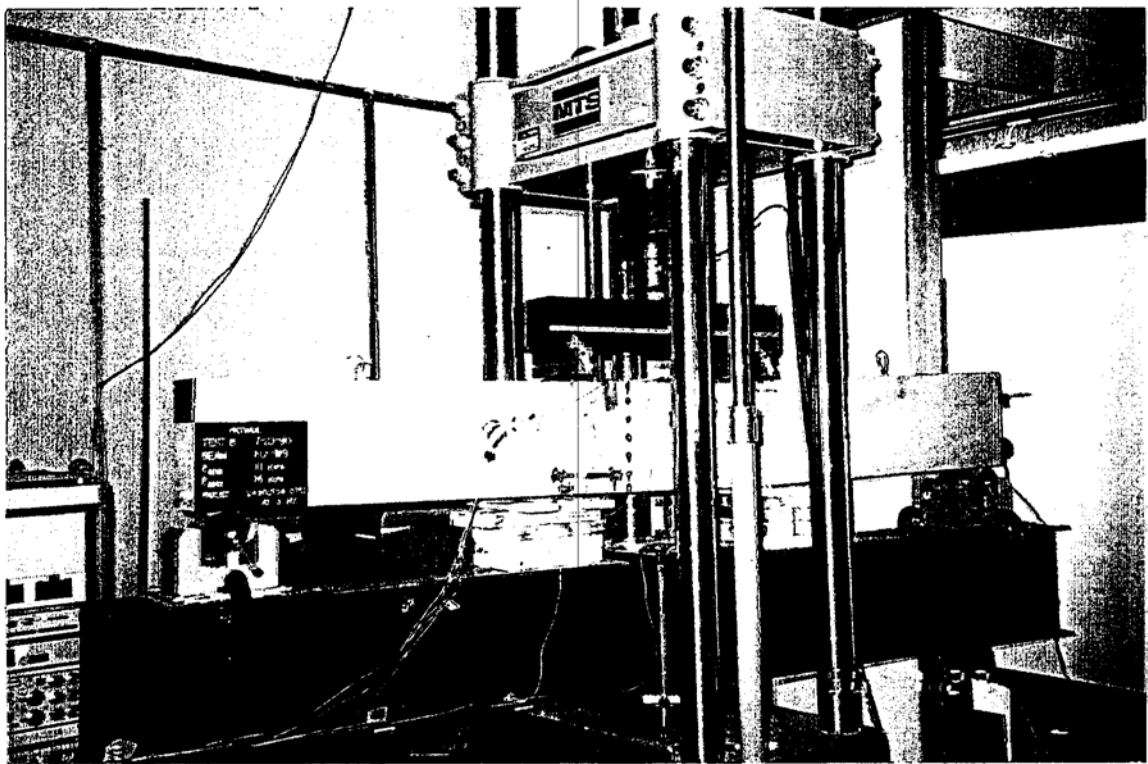


Plate 11.1 (top) View of beam G-W9 after fatigue failure
(btm) Close up of large crack at mid-span

deflection hysteresis loop measured between P_{min} and P_{max} with increasing number of cycles. It can be seen that the residual deflection of FG-W9 and FG-E9 increased progressively with approximately constant load-deflection slope for most of their fatigue life. In FG-W9, however, the residual deflection is observed to increase dramatically, accompanied by a tremendous increase in the area enclosed within the load-deflection loop and a substantial reduction in stiffness. This behavior is a clear indication of the degree of distress and softening suffered by these beams due to fatigue.

The deflection vs number of cycles at $0.6P_{ax}$ and $0.4P_{ax}$ for both beams is plotted in Figure 11.6. The maximum deflection at P_{ax} measured in the last reading before failure (1.25 million cycles) was 0.556" for FG-W9. The corresponding deflection in FG-E9 after 2 million cycles was 0.274". Beam FG-E9 was subsequently statically tested to failure.

11.5.2.3 Crack width

Both beams cracked during the first static cycle to P_{ax} . Beam FG-W9 and FG-E9 cracked at loads corresponding respectively to 45% and 49% of the ultimate load capacity of the identical beams tested under static loading (see Table 7.2). The transducers were attached at this location at the level of the prestressing strand and crack width measurements relate to this location. In the beam that failed however, the maximum crack occurred elsewhere (see Plate 11.1). The crack width at P_{ax} at the first cycle was 0.451 and 0.228 mm for FG-W9 and FG-E9 respectively. The variation of crack width at $0.6P_{ax}$ and $0.4P_{ax}$ with increasing number of cycles (drawn on a semi-log scale) is shown in Figure 11.7. Beam FG-W9 that survived the fatigue loading shows a modest increase in crack width over the loading cycle. Beam FG-W9, however, shows increases in crack width after 10,000 cycles and again after 100,000 and 750,000 cycles. The maximum crack width was 1.168 mm for beam FG-W9 before failure and 0.297 mm for beam FG-E9 at 2 million cycles.

11.5.2.4 Strains

The variation in the concrete and fiberglass strains with increasing number of cycles is shown in Figures 11.8 and 11.9. The trend in these curves is similar to that for crack width. Beam FG-E9 that did not fail shows steady increases whereas Beam FG-W9 shows quantum increases in strain after certain cycles. In the strands this is indicative of the development of cracking that causes strains to be transferred to the steel. The cracking causes an upward migration of the neutral axis that leads to increased strains in the concrete.

The observed stress ranges in the prestressing¹ strands for the two beams were calculated from strain gage readings (strain \times modulus) in the early cycles. These were 21.2 ksi and 13.1 ksi for FG-W9 and FG-E9 respectively. The stress range observed at the last reading before failure of FG-W9 was 21.7 ksi at 1.25 million cycles and 12.0 ksi for

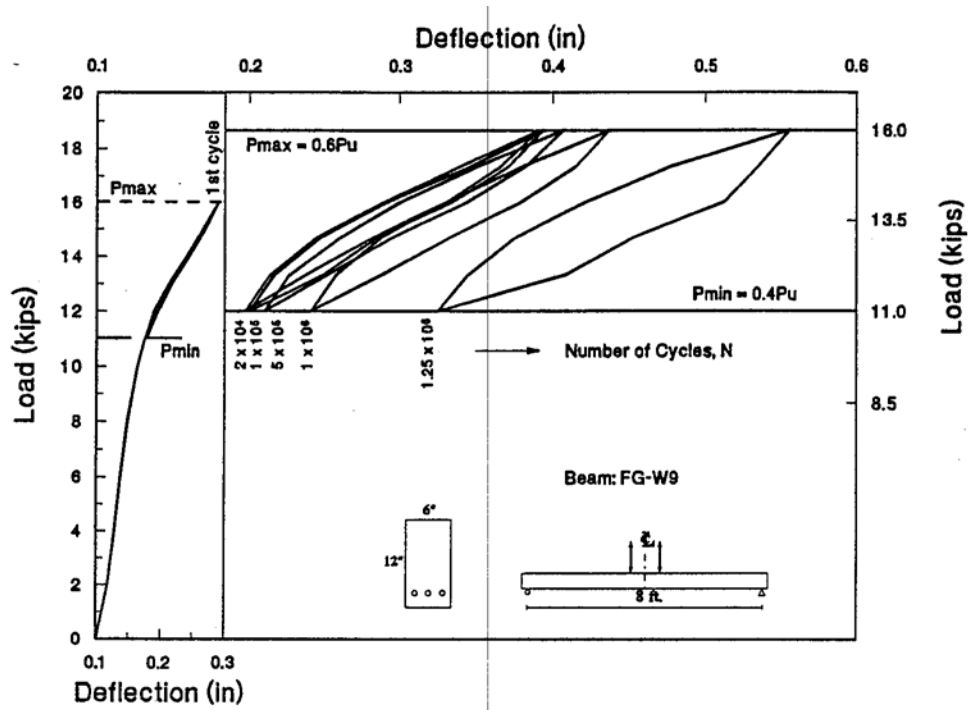


Figure 11.4 Load-Deflection Curves for Beam FG-W9

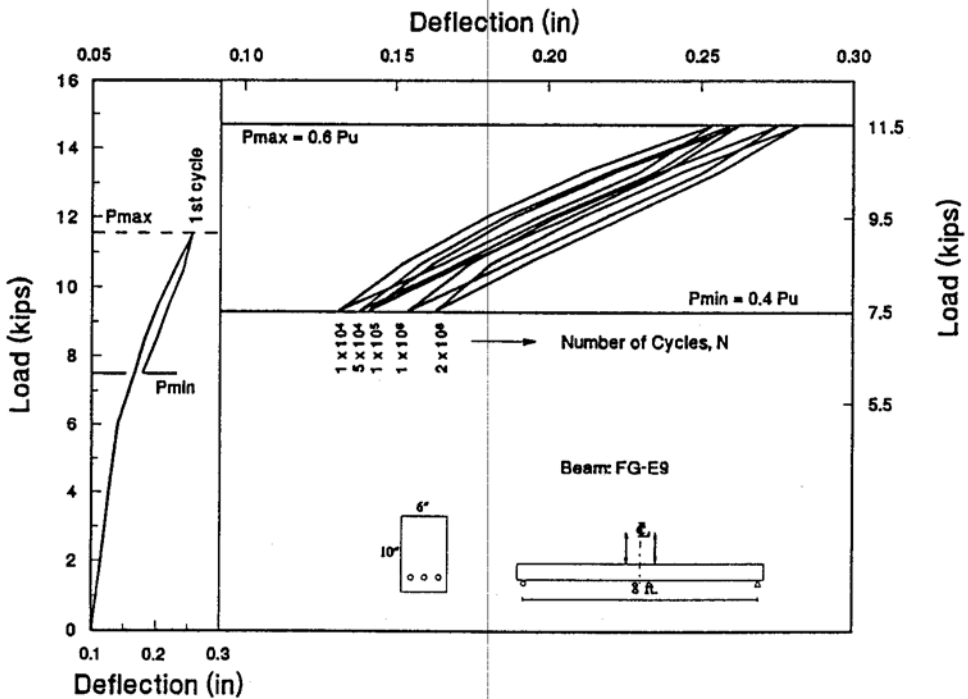


Figure 11.5 Load-Deflection Curves for Beam FG-E9

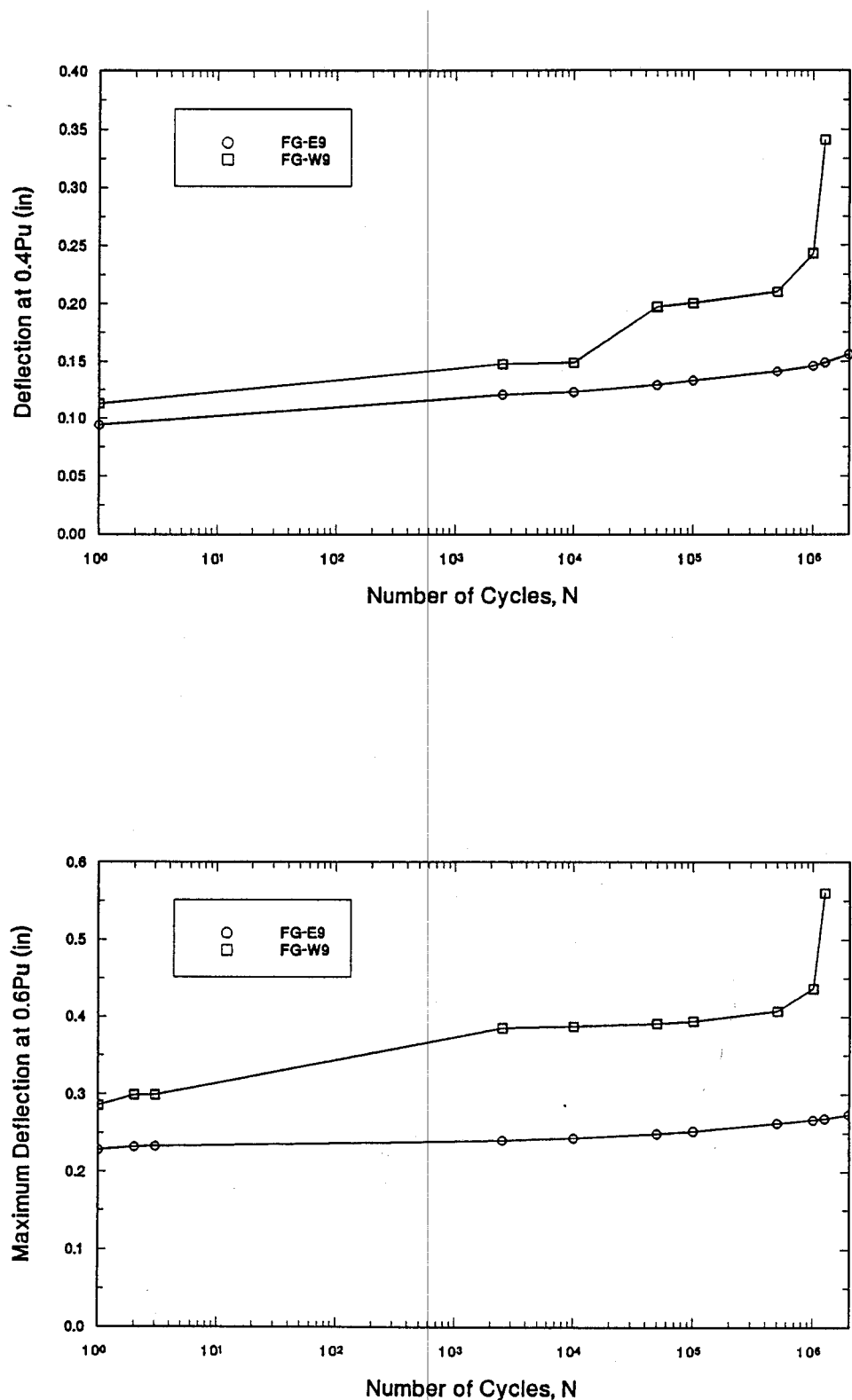


Figure 11.6 Deflection Versus Number of Cycles at 0.6P_u & 0.4P_u

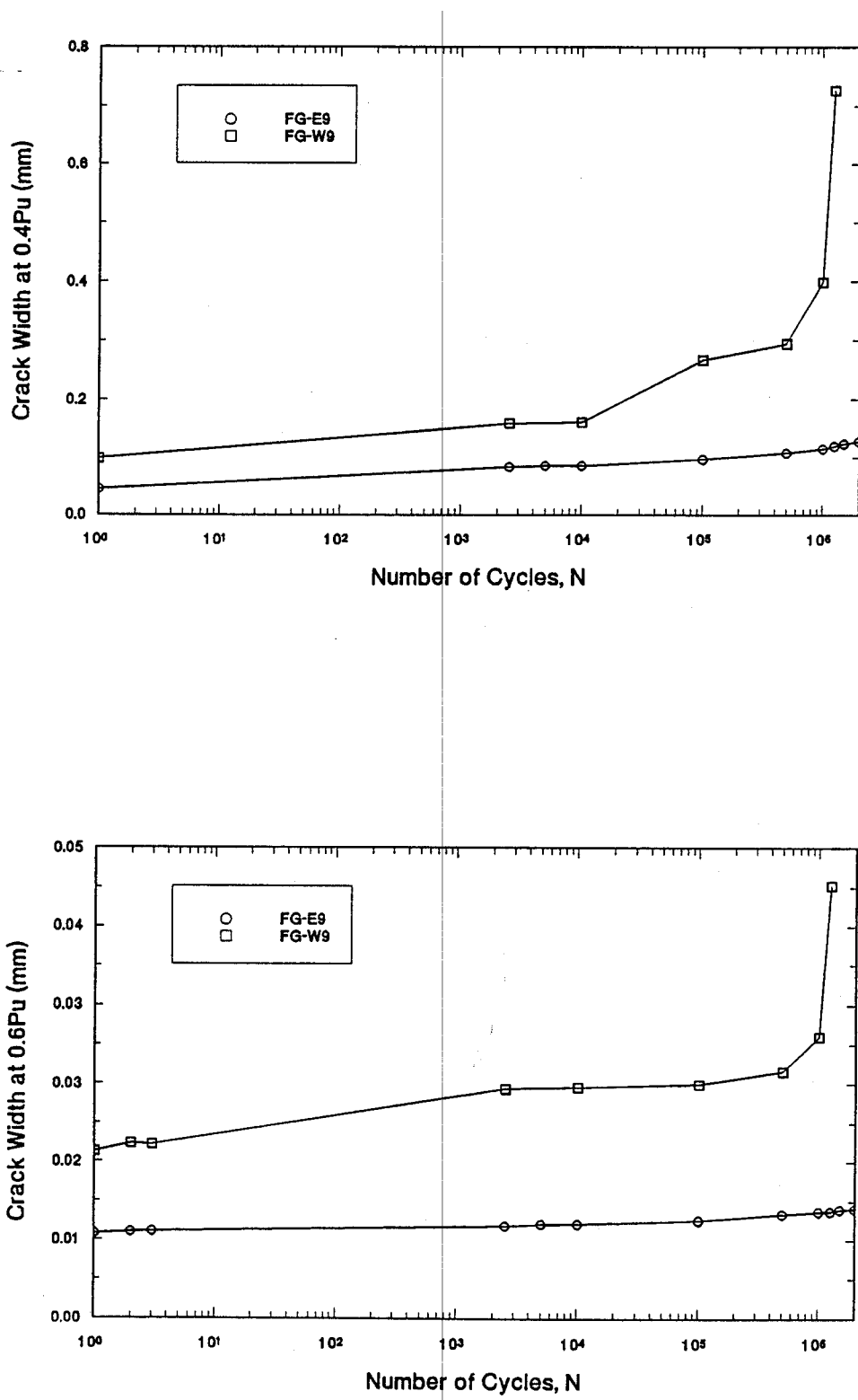


Figure 11.7 Crack Width Versus Number of Cycles at $0.6P_u$ & $0.4P_u$

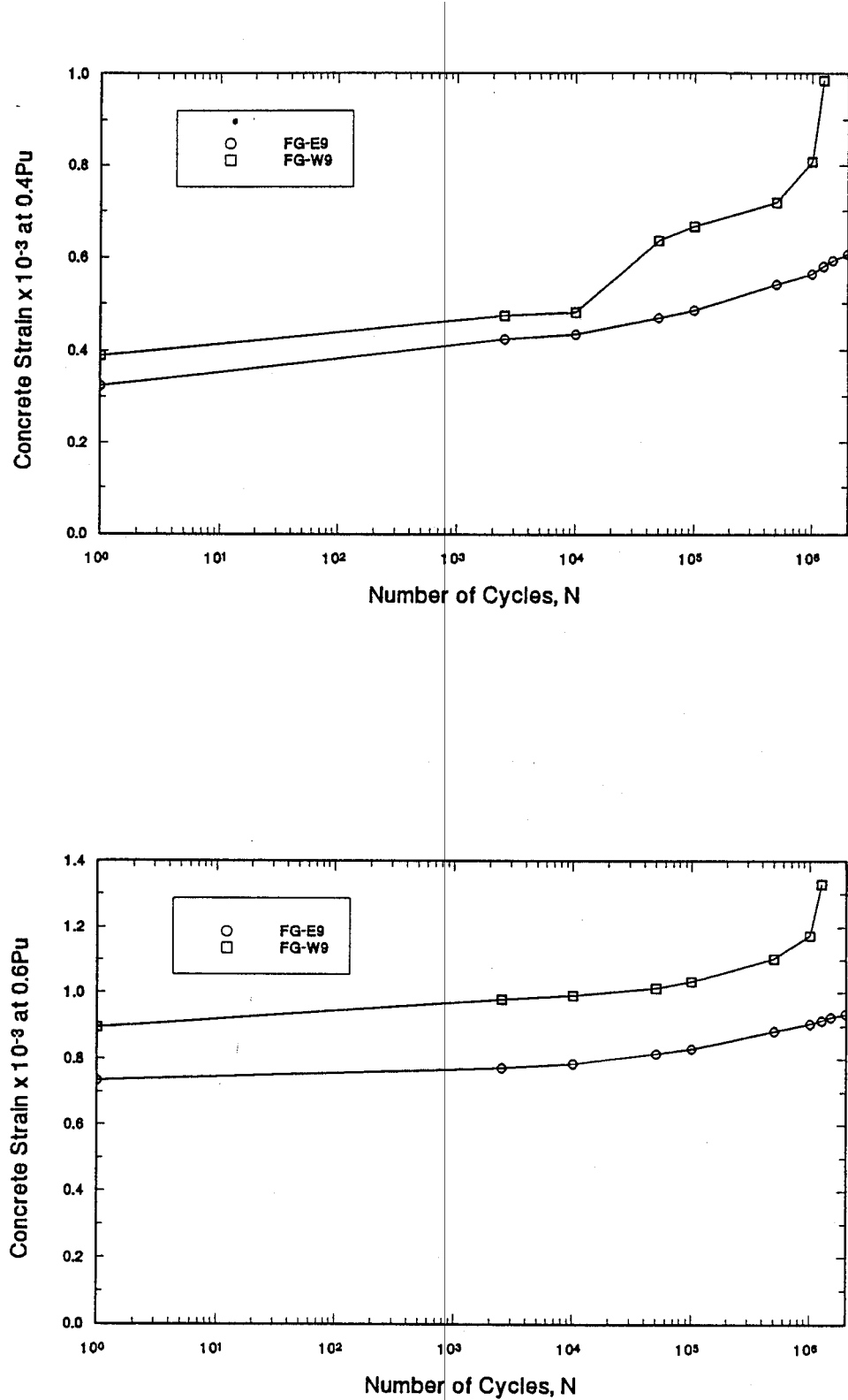


Figure 11.8 Concrete Strain Versus Number of Cycles at 0.6P_u & 0.4P_u

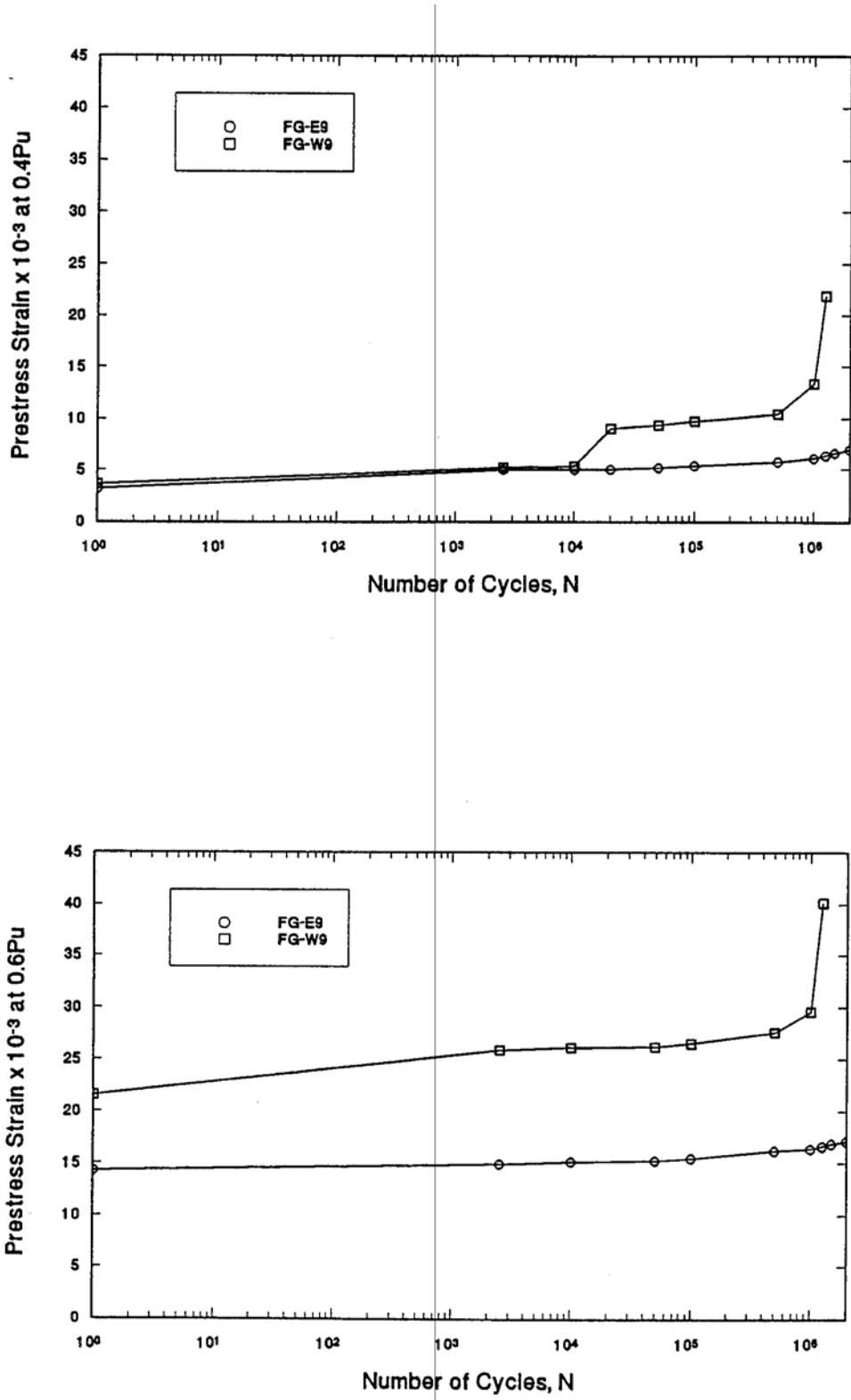


Figure 11.9 Prestressing Strand Strain Versus Number of Cycles at $0.6P_u$ & $0.4P_u$

FG-E9 after 2 million cycles. Beam FG-W9 failed at 1.5 million cycles at a stress range equal to $0.072f_{fg}$ ($21.7/300$) and minimum stress level equal to $0.42f_{fg}$ ($121.5+4.3/300$). After 2 million cycles, beam FG-E9 did not fail and had a stress range $0.040f_{fg}$ ($12/300$) and minimum stress level equal to $0.42f_{fg}$ [$(121.1+3.8)/300$] after 2 million cycles.

11.5.2.5 Ultimate Capacity After Cyclic Load

Beam FG-E9 was tested to static failure following the fatigue test (see Plate 11.2). Its static capacity showed a small reduction compared to beam FG-E8. This is consistent with results from other investigators, e.g. [11.4]. Comparative plots showing the load deflection, concrete and strand strain variation are shown in Figures 11.10 and 11.11. Failure crack patterns for both beams (see Figure 11.12) show great similarity.

11.6 Comparison with Harajli & Namaa [11.4]

Plots showing variation in deflection and crack width for beams PD 1, PD2 and PP2D 1 are shown in Figures 11.13 and 11.14. These indicate generally higher values for the fiberglass beams. This is not surprising since the post-cracking response of fiberglass pretensioned beams is somewhat more flexible. It is interesting to note that both beams without non-prestressed reinforcement (PD and PD2) failed before they reached the targeted 5 million cycles. Beam PD 1 failed after 1.21 million cycles while beam PD2

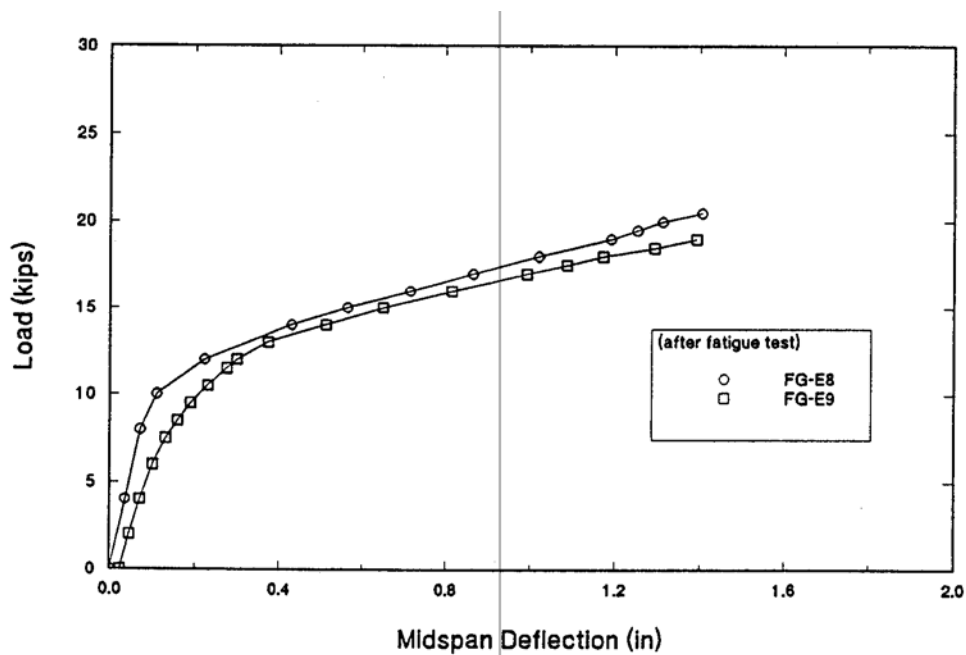


Figure 11.10 Comparison of load deflection for beams FG-E9 and FG-E8

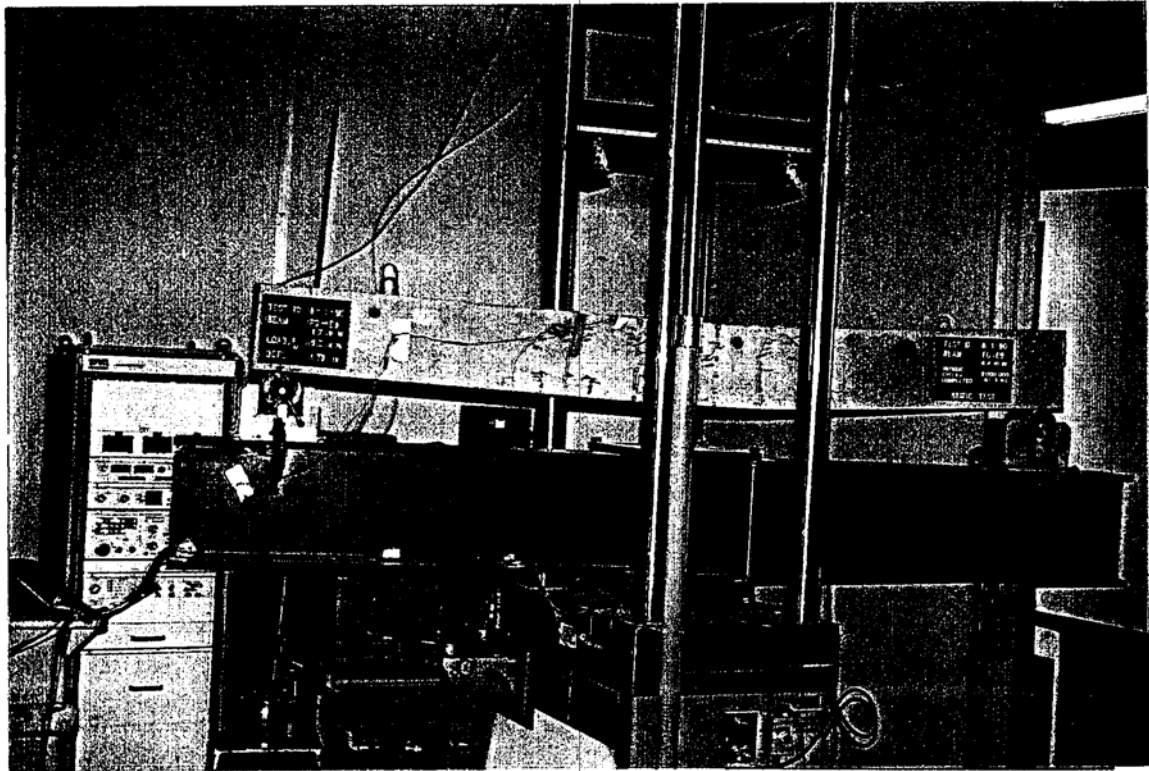
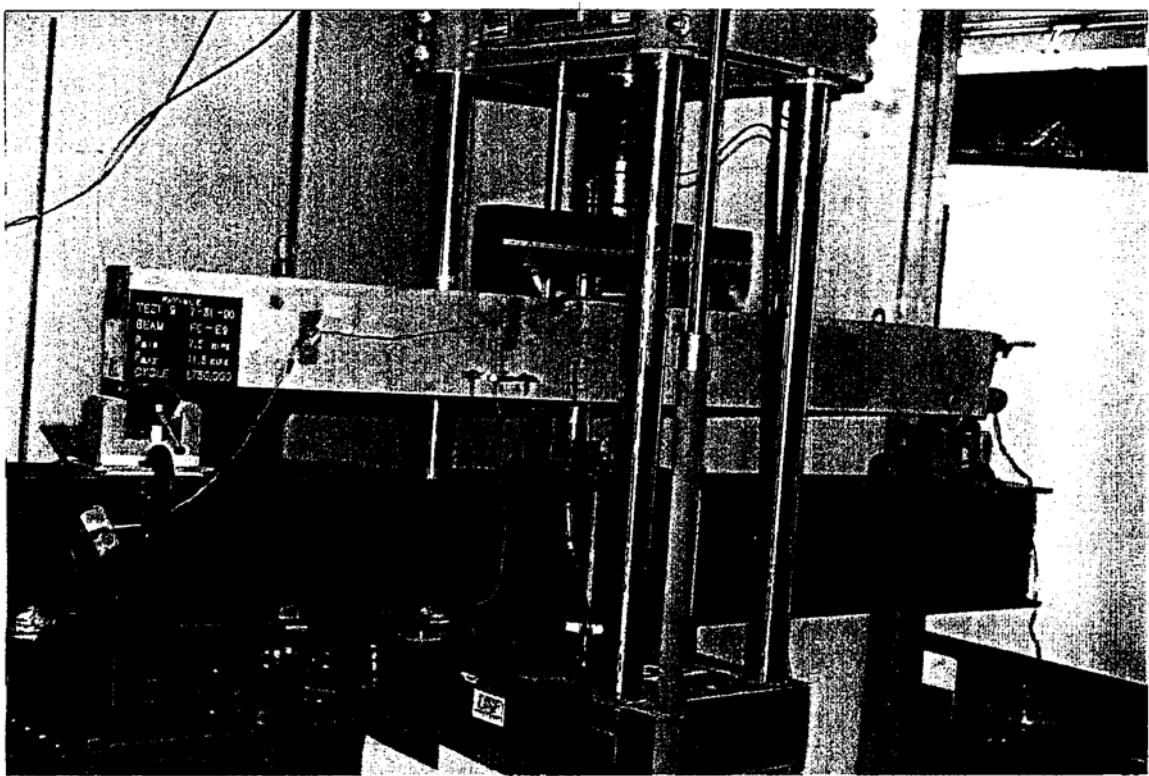


Plate 12.2 (top) View of FG-E9 after 1.75 million cycles
(btm) Ultimate deflected shape of FG-E9 after static test

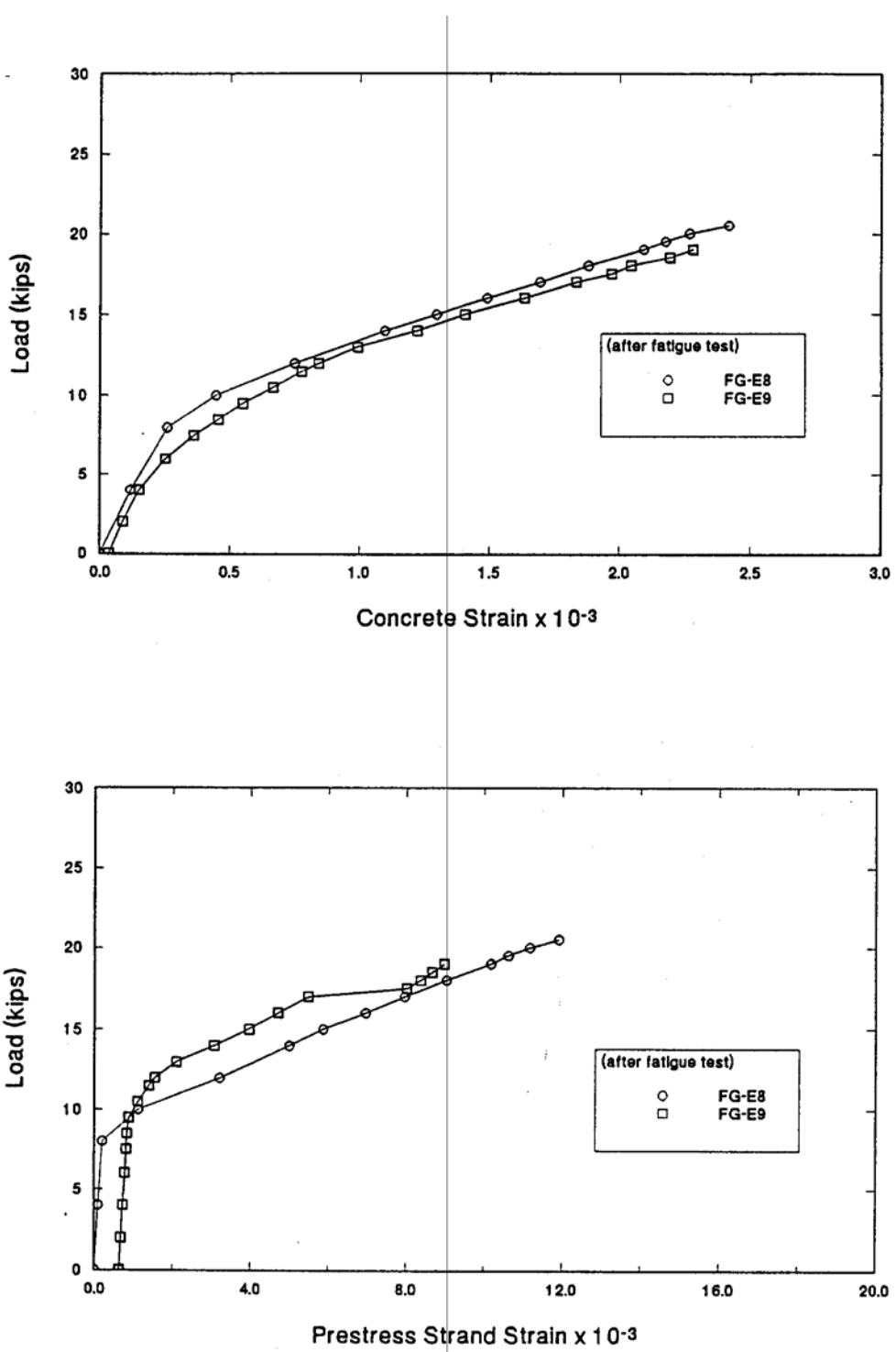


Figure 11.11 Comparison of strains in beams FG-E9 and FG-E8

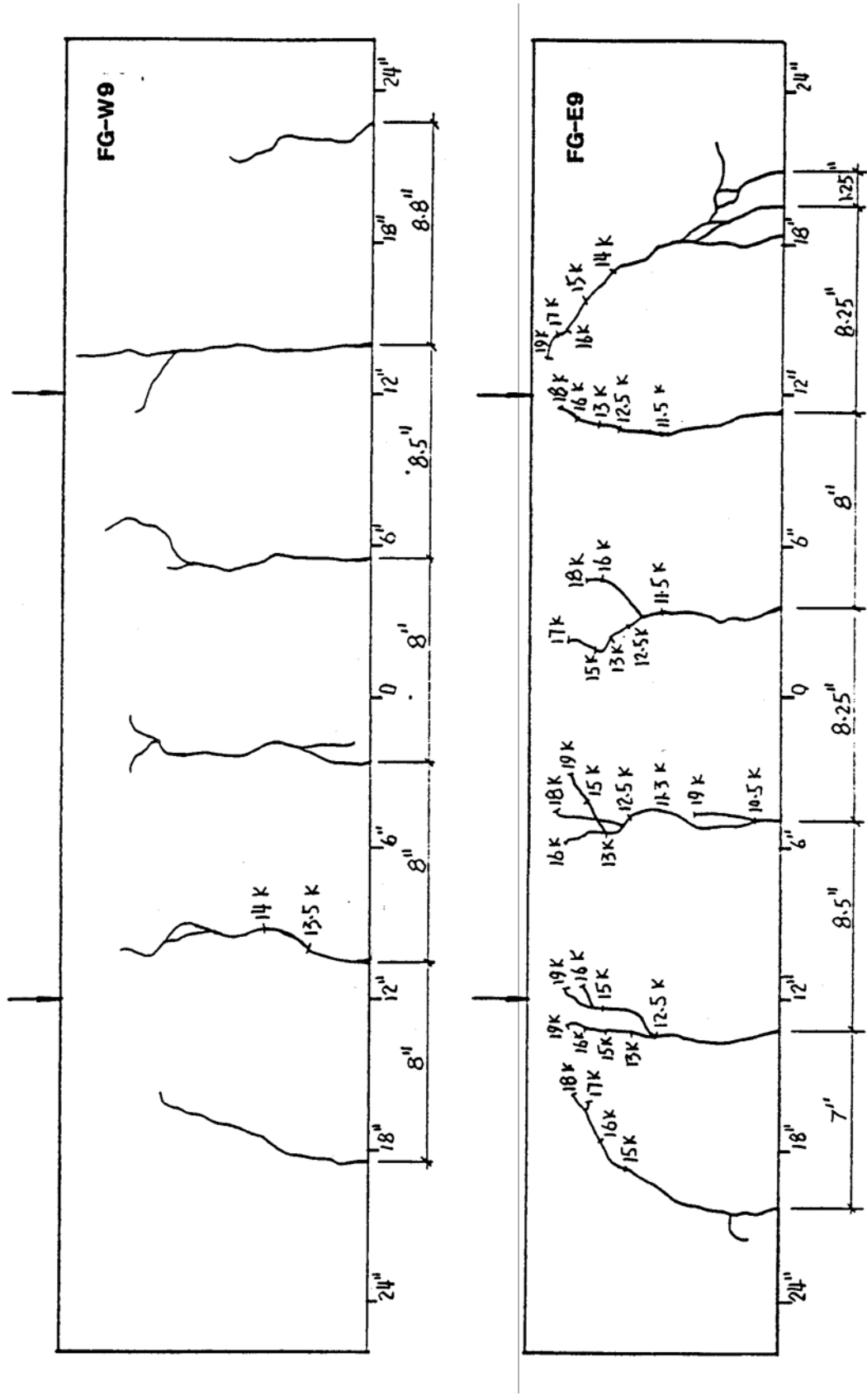


Figure 11.12 Crack Pattern for Beam FG-W9 and FG-E9

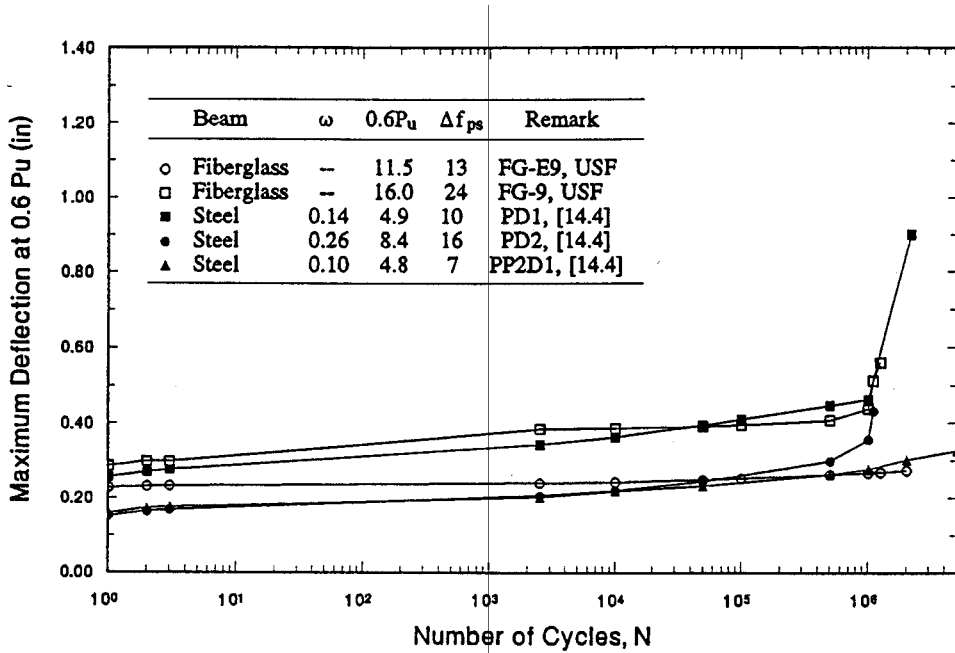


Figure 11.13 Maximum Fatigue Deflection Comparison with Naaman

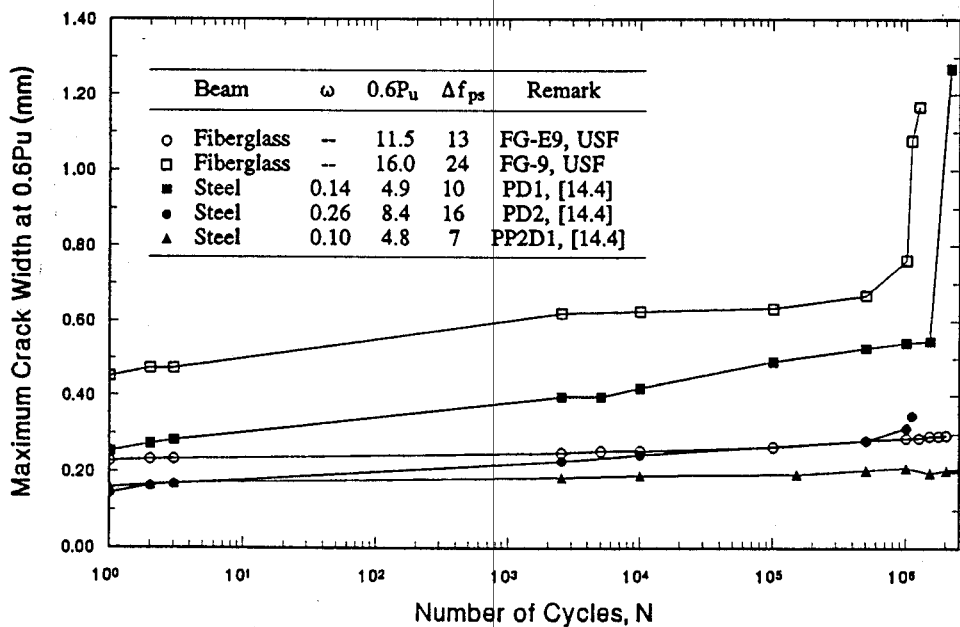


Figure 11.14 Maximum Crack Width Comparison with Naaman

failed after 2.2 million cycles. For the fiberglass beams, beam FG-W9 failed after 1.5 million cycles although FG-E9 survived 2 million cycles.

A summary of comparison of stress ranges and fatigue life for the fiberglass and steel pretensioned beams is presented in Table 11.3. The stress ranges are based on the last reading or at two million cycles for the steel retensioned beams. Inspection of this table indicates that the steel pretensioned beams failed at stress ranges comparable to those for the fiberglass beams. Note also that the minimum stress for the fiberglass pretensioned beam did not show the same fluctuation as comparable steel beam (FG-E9 vs PD1, PD2, PP2D1). This is because the gages for this fiberglass beam were not at crack locations (see Figure 11.9, note absence of any step increases signifying crack propagation).

The fatigue life for the fiberglass beams in comparison to those from those Harajli and Naaman [11.4] and other tests are shown in figure 11.15. This is a plot of test data and an equation to estimate fatigue life that was originally proposed by Naaman. The graphs appear to suggest that the fatigue life of fiberglass is similar to that of steel.

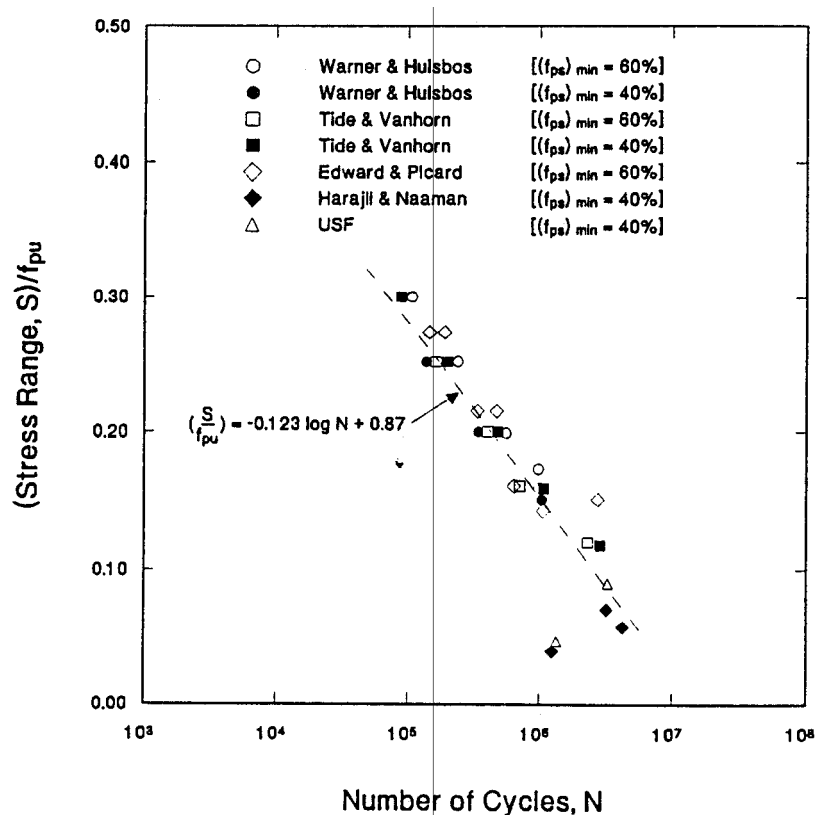


Figure 11.15 Comparison of Fatigue Life

Table 11.3 Comparison of Fatigue Results with Harajli & Naaman [11.4]

Beam	Min. Stress (ksi)	Max. Stress (ksi)	Stress Range (ksi)	Fatigue Life
FG-W9	125.8 (0.42 f_{g}) cycle N°1	169.1 (0.56 f_{g})	21.7 (0.073 f_{g})	Failed after 1.5 million cycles
	147.4 (0.49 f_{g}) ³	at 1.25 × 10 ⁶ cycles ³		
FG-E9	124.9 (0.42 f_{g}) cycle N°1	141.3 (0.47 f_{g})	12.0 (0.040 f_{g})	No failure after 2 million cycles
	129.3 (0.43 f_{g}) at 2.0 × 10 ⁶ cycles ³	at 2 × 10 ⁶ cycles ³		
PD1 ¹ ($\omega = 0.14$)	175.3 (0.65 f_{pu}) cycle N°1	201.0 (0.74 f_{pu})	16.0 (0.059 f_{pu})	Failed after 1.21 million cycles
	185.0 (0.68 f_{pu}) at 1.6 × 10 ⁵ cycles ³	at 1.6 × 10 ⁵ cycles ³		
PD2 ¹ ($\omega = 0.26$)	146.8 (0.54 f_{pu}) cycle N°1	179.6 (0.67 f_{pu})	9.3 (0.072 f_{pu})	No failure after 2 million cycles
	160.3 (0.59 f_{pu}) at 1.0 × 10 ⁵ cycles ³	at 1.0 × 10 ⁵ cycles ³		
PP2D1 ² ($\omega = 0.10$)	169.44 (0.63 f_{pu}) cycle N°1	192.7 (0.71 f_{pu})	8.2 (0.03 f_{pu})	No failure after 2 million cycles
	184.5 (0.68 f_{pu}) at 2.0 × 10 ⁶ cycles	at 2.0 × 10 ⁶ cycles		

¹ Only prestressing steel [11.4].

² Prestressing plus reinforcing steel [11.4].

³ Last gage reading.

12. CREEP CONCRETE

12.1 Introduction

As part of an investigation on the long term performance of fiberglass pretensioned specimens, two creep studies were initiated. In the first study, material creep in concrete was investigated for sustained loading of 0.2f'c and 0.3f'c corresponding to expected service loads in piles. This is described in this chapter. In the second study, long term deformation in identical steel and fiberglass pretensioned specimens subjected to the same loading was investigated. This study, which was carried out at the University of Illinois at Chicago, is described in the next chapter.

The investigation of the material creep in concrete was carried out in accordance with ASTM C512 [12.1]. Observations for seventeen months are presented. The concrete used was made with Florida limerock and high early strength type III cement. The mix design is FDOT approved (see Table 4.2). It was plant mixed at Southern Prestressed, Tampa and delivered to the Structures Laboratory at the University of South Florida. The coarse aggregates were quarried from Brooksville in Hernando County, FL and its maximum size was 3/4 inch. Quality control data for two hundred samples of limestone coarse aggregate for this area indicates that about 40% of the aggregates are smaller than 1/2 inch, FCPA, 1990 [12.2]. Devane sand, a fine silica sand was used as the fine aggregate. This was quarried from Florida Mining's pit in Polk City, Polk County, FL.

The experimental set up for the creep study together with instrumentation details are described in Section 12.2. The creep coefficients determined experimentally are compared against those from ACI equations [12.3] in Section 12.3.

12.2 Test Setup

The test set up is shown in Plate 12.1 and is in accordance with ASTM C512. Two creep rigs were used to investigate the two different load levels. Each used three cylinders in conjunction with 6 in. x 3 in. concrete plugs at the top and bottom as shown. To ensure uniform stress distribution, 1 in. thick steel plates were used and all cylinders and plugs were capped to provide plane surfaces.

The loads were applied by an Enerpac RCS50 hydraulic jack linked to a P84 hand pump by high pressure hoses through a manifold. Glycerine gages indicating the applied pressure were calibrated prior to the application of the loads. The applied load levels in the rigs of 0.2f'c (Rig 1) and 0.3f'c (Rig 2) are relatively low (maximum 0.4f'c by ASTM) but correspond to service load level in piles.

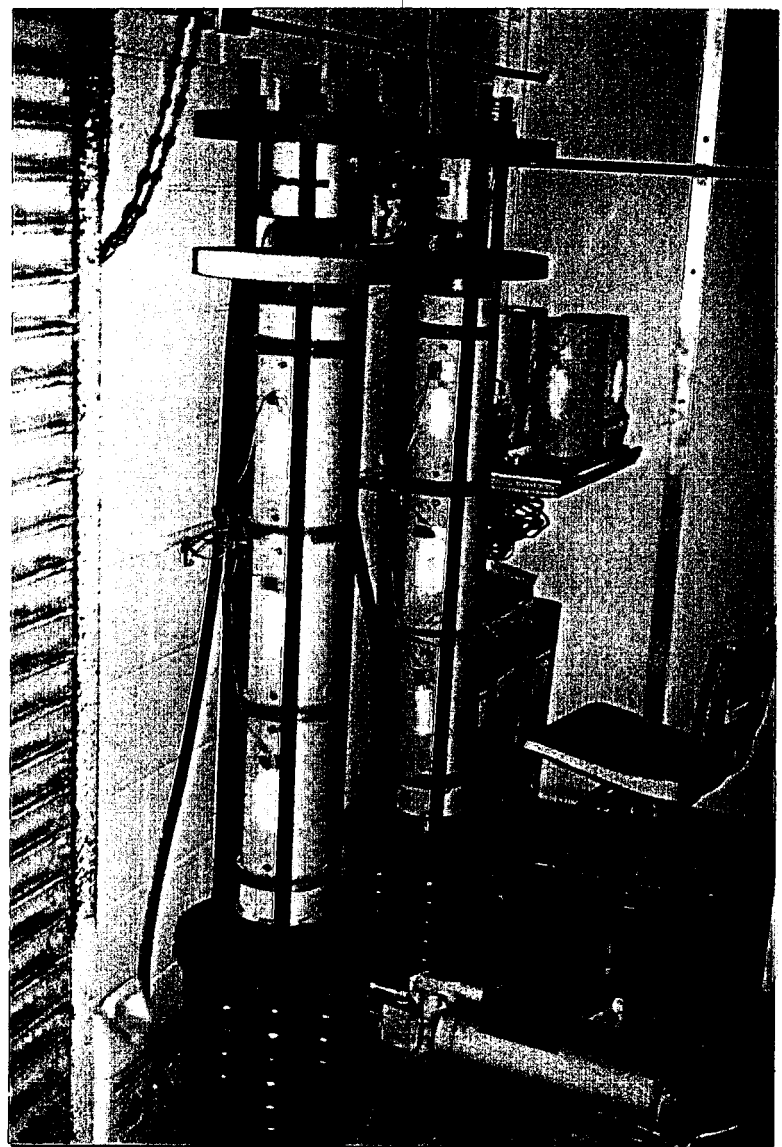


Plate 12.1 Set up and instrumentation for creep study

Each cylinder was instrumented by two TM PL-60 strain gages located on the middle of diametrically opposite faces of the cylinders. Each gage was 2.36 in. long - greater than three times the maximum aggregate size of 0.75 in. required by ASTM. A P3500 digital strain indicator was used in conjunction with two SB-10 switch and balance units to measure strains (see Plate 12.1). In addition, two cylinders were also instrumented similarly to measure shrinkage strains.

12.3 Results

The creep strains were determined by subtracting out the initial strain and the shrinkage strain from the total measured strain. The results are expressed in terms of the *creep coefficient*. This is the ratio of the additional strain under sustained loading, i.e. the creep strain, to the initial strain. From a design standpoint, knowledge of the creep coefficient and the initial (elastic) strain allows the creep strain to be determined.

Plots of the creep coefficient for the two sustained load levels of 0.2f_c and 0.3f_c investigated after 17 months are shown in Figures 12.1 and 12.2. For comparison, minimum, maximum and average creep coefficients suggested by ACI Committee 209 are also shown in the same graphs. These range from 1.3-4.15 with an average value of 2.35. The ACI values in the plots have been corrected for non-standard conditions corresponding to loading age, ambient humidity, member thickness, slump, percentage fines, cement content and air content, Sada t, 1991 [12.4].

Inspection of Figures 12.1-12.2 show that the experimentally determined creep coefficients fall broadly within the average values recommended by ACI. The values are almost the same as the ACI average for Rig 1 (0.2f_c) and are slightly higher for Rig 2 (0.3f_c). The creep coefficients after seventeen months of observation are 1.49 and 1.62 for Rigs 1 and 2 respectively compare to the ACI average value of 1.5.

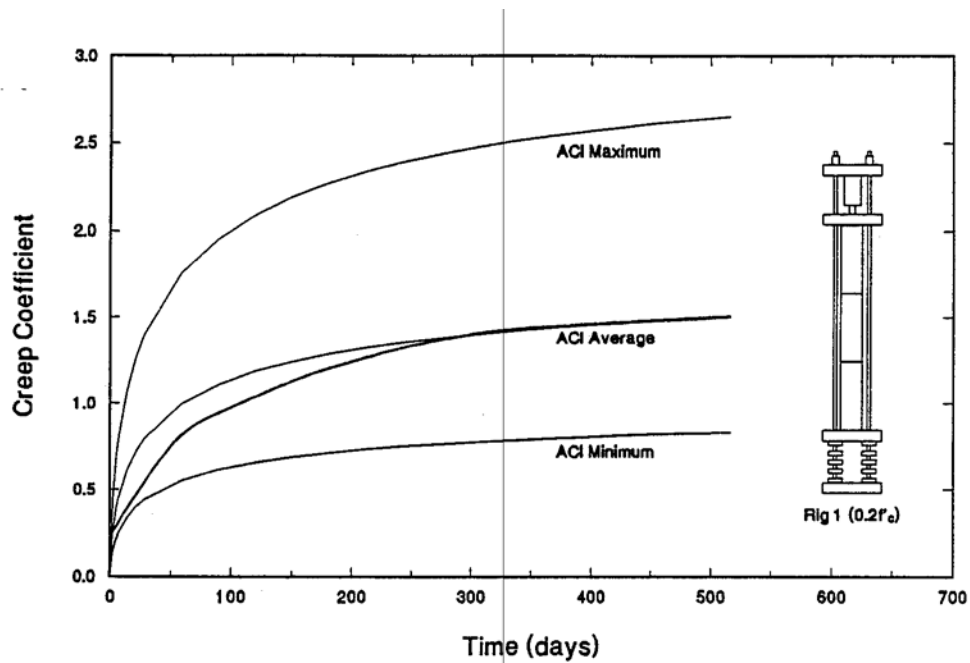


Figure 12.1 Comparison of Creep Coefficient for Rig 1 ($0.2f'c$) with ACI

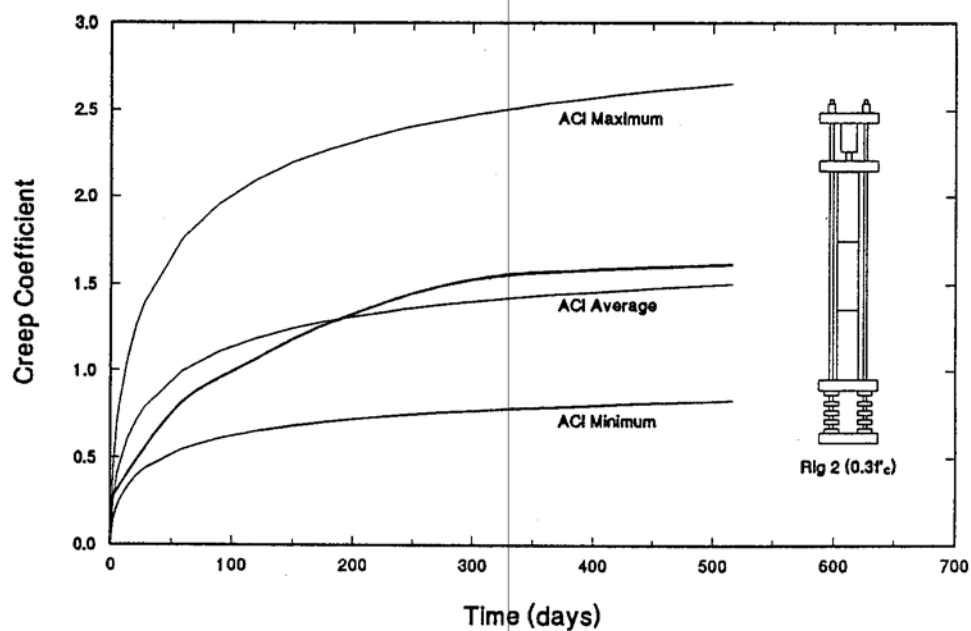


Figure 12.2 Comparison of Creep Coefficient for Rig 2 ($0.3f'c$) with ACI

13. LONG TERM CREEP LOSSES

13.1 Introduction

This chapter presents results of investigation on long term creep losses. The specimens for this study were cast in March and June 1990 and shipped to the University of Illinois at Chicago where this investigation was carried out. In all, twelve specimens, six fiberglass and six steel, were tested. The sustained loading used corresponded to the expected service loads in piles and was $0.2f_c$ and $0.3f_c$, identical to that used in the material creep study reported in the previous chapter.

The scope of the experimental program is described in Section 13.2 and test results are presented in Section 13.3. An analysis and discussion of these results is summarized in Section 13.4. An analytical prediction is presented in Section 13.5.

13.2 Experimental Program

The objective of this study was to evaluate the relative creep and shrinkage losses in identical steel and fiberglass prestressed concrete columns under sustained axial loading. Two identical investigations were conducted in which creep effects were investigated under laboratory conditions and also those corresponding to Florida's environment [13.1]. The first study (Group I) commenced in April 1990 and the second (Group II) commenced in July 1990.

For each of the two groups, six specimens – three sets of identical fiberglass and steel – were investigated. All specimens were stressed to about the same stress level as summarized in Tables 13.1 and 13.2. To determine shrinkage for Group I specimens, two 6 in.x 12 in. concrete cylinders and six standard shrinkage bars (2 in.x 2 in.x 12 in.) were used. Typical shrinkage strains for tie concrete cylinders are shown in Figure 13.2. These specimens were subjected to the same laboratory environment (temperature of 70°F and relative humidity of 70%) as the creep test specimens. For Group II, two standard concrete shrinkage cylinders and one standard shrinkage bar was used.

The specimens were fabricated in the laboratory as shown in Plate 4.2. Electrical and mechanical strain gages were mounted on the concrete surface as shown in Figure 13.1 to measure the change of strains throughout the whole testing period. The material properties of concrete, steel, and fiberglass used are presented in Chapters 4 and 2 respectively. The strength of concrete at release is summarized in Table 4.2.

Table 13.1 Average Prestress Forces Before Loading (Group I)

Specimen Type	Strands per Column	Strand Diameter (in.)	Jacking Force per Strand (kips)	Strand Prestressing Force ¹ (kips)	f_{si} , Stress ¹ (ksi)	f_{se} , Stress ² (ksi)
Fiberglass	2	3/8	9.1	8.92	127	116
Steel	1	1/2	18.7	18.3	109.6	98.8

¹ Stress before release
² Effective stress at 28 days

Table 13.2 Average Prestress Forces Before Loading (Group II)

Specimen Type	Strands per Column	Strand Diameter (in.)	Jacking Force per Strand (kips)	Strand Prestressing Force ¹ (kips)	f_{si} , Stress ¹ (ksi)	f_{se} , Stress ² (ksi)
Fiberglass	2	3/8	9.56	8.7	124	117.9
Steel	1	1/2	20.0	18.03	108	86.7

¹ Stress before release
² Effective stress at 150 days

The columns were assembled in a framework shown in Plate 13.1 for Group I and Plate 13.2 for Group II. Steel end plates and masticord pads were used to ensure an even stress distribution. At 28 days ($f_c = 7300$ psi) Group I specimens were axially loaded. For Group II specimens, loading was applied after 150 days when the environmental chamber was ready. The compressive strength of concrete at that time was 6,600 psi.

In each of the groups, Set I was *unloaded* used as a control specimen. Sets II and III were subjected to concentric axial loading Tables 13.1 and 13.2 present the effective stress, f_{se} at loading after losses due to elastic shortening, relaxation, shrinkage, and creep.

Tables 13.3 and 13.4 summarize pertinent information relating to the prestress force and sustained loading for all specimens in the both tests. It may be seen that the sustained stress to the concrete strength is 0.1, 0.2 an 0.3 in each of the two tests. Following the application of the loading, readings were en after 2 hours, 6 hours and 12 hours. Subsequently, readings were taken twice a day for a week and then daily for the first month. As readings stabilized, the time intervals between readings was increased. The applied sustained loads were checked before each reading was taken.

Table 13.3 Stress/Strength Ratios (Group I)

Set Number	I		II		III	
	Steel	Glass ¹	Steel	Glass ¹	Steel	Glass ¹
Prestress Force at loading (kips)	16.5	16.3	16.5	16.3	16.5	16.3
Applied Load (kips)	0	0	18.6	18.6	36.6	36.6
Sustained Load (kips)	16.5	16.3	35.1	34.9	53.1	52.9
Sustained Stress (psi)	688	679	1462.5	1454.2	2212.5	2204.2
Concrete Strength at Loading (psi)	7300	7300	7300	7300	7300	7300
Stress/Strength Ratios	0.1	0.1	0.2	0.2	0.3	0.3

¹ Fiberglass

13.3 Experimental Results

13.3.1 Laboratory Environment (Group I)

Strains were measured at 3 in., 15 in., 27 in., and 51 in. from one end of each specimen as shown in Figure 13.1. The variation of stains under a sustained stress level of 0.3f', over 20 months is shown in Figures 13.4 an 13.5 for the fiberglass and steel columns respectively. This shows that the strain readings at column midheights are larger than those at the column ends by nearly 30% for fiberglass and 50% for steel.

Figures 13.6 and 13.7 show the strain history at the midheight of the column for the fiberglass and steel specimens under the different stress levels investigated. It may be seen that the strain increases with the increase in stress level. Figure 13.8 compares the strain history of fiberglass and steel columns for the sustained stress level of $0.3f_c$. The strain in fiberglass columns is greater than I steel columns.

Table 13.4 Stress/Strength Ratios (Group II)

Set Number	I		II		III	
	Steel	Glass ¹	Steel	Glass ¹	Steel	Glass ¹
Prestress Force at loading (kips)	14.5	16.6	14.5	16.6	14.5	16.6
External Applied Load (kips)	0	0	16.0	16.0	32.0	32.0
Total Sustained Load (kips)	14.5	16.6	30.5	32.6	46.5	48.6
Total Sustained Stress (psi)	604	692	1271	1358	1938	2025
Concrete Strength at Loading (psi)	6600	6600	6600	6600	6600	6600
Stress/Strength Ratios	0.09	0.1	0.19	0.21	0.29	0.31

¹ Fiberglass

Figure 13.9 shows the variation in total prestress losses at column midheight with time for the fiberglass and steel columns at the stress level of $0.3f_c$. Figure 13.12 shows that the prestress losses increase as the stress level increases. For stress levels between $0.2f_c$ and $0.3f_c$ the loss rate increases faster in steel columns than the fiberglass. Figures 13.10 and 13.11 show the total prestress losses over time for different stress levels in fiberglass and steel columns. The variation in effective prestressing force obtained by subtracting the measured prestress losses from the prestressing force before release are plotted in Figure 13.13 for both the Fiberglass and steel columns under a sustained stress level of $0.3f_c$.

13.3.2 Environmental Chamber (Group II)

Group II results were collected to study the effect of varying the temperature and relative humidity on the prestress losses.

Figures 13.16 and 13.17 show strain history at column midheight for fiberglass and steel columns, respectively, under different stress levels. These figures, also indicate variations in temperature and relative humidity over the duration of testing. Figure 13.22 shows the strain history comparison between fiberglass and steel columns for constant sustained stress of 0.3f'. The strains in the fiberglass and steel columns are nearly equal.

Figures 13.18 and 13.19 show the total pre stress losses at column midheight with time for fiberglass and steel under different stress levels. Figure 13.23 compares the total prestress losses for fiberglass and steel at a stress level 0.3f".

The effective prestress for fiberglass and steel columns under different stress levels are shown in Figures 13.20 and 13.21. The effective prestress comparison for both fiberglass and steel is shown in Figure 13.24.

13.4 Analysis and Results

13.4.1 Laboratory Environment (Group I)

For the prestressed concrete columns studied, the dimensions were 6 in.x 4 in.x 102 in. and the concrete strength was 5,800 psi at the time of release. The prestress level in the columns before applying the external load was 688 psi for the fiberglass columns and 679 psi for the steel columns. The prestress level on the strands before release, f_{sj} , was nearly 127 ksi for the fiberglass strands and 109.6 ksi for steel (see Table 13.1).

After twenty months of investigation, the total prestress loss in the fiberglass strands at column midheight were 9.0 ksi for column I, 17.42 ksi for column II, and 21.0 ksi for column III, corresponding to 7.1 %, 13.7 %, and 16.5 % of the stress before release, respectively. The corresponding loss in the steel strands were 27.0 ksi, 37.7 ksi and 56.0 ksi or 24.6%, 34.4%, and 51.1% of the stress before release for columns I, II, and III, respectively.

In a given prestressed concrete column, the prestress losses for fiberglass columns is less than that of steel columns at midheight, even though the strain change in the fiberglass strands is larger. This is due to the low modulus of elasticity of fiberglass. The percentage variation of prestress losses in steel columns is greater than in fiberglass columns by 17.5 % to 34.6 %. The range of losses depends on the sustained stress level as shown in Figure 13.12.

In general, the prestress losses at column midheight are slightly more than at quarter points for both fiberglass and steel columns. This is similar to the strain-change pattern shown in Figures 13.4 and 13.5. The prestress losses increase with an increase in stress levels as shown in Figure 13.12 for both fiberglass and steel columns. The rate of prestress losses is higher in steel than in fiberglass .

Effective prestress in the fiberglass strands were 118.0 ksi, 109.6 ksi, and 106.0 ksi at column midheight for sets I, II, and III, respectively. For the steel strands the effective prestress was 82.6 ksi, 74.3 ksi, and 56.0 ksi for sets I, II, and III, respectively. Figure 13.12 shows clearly that the permanent effective prestress in fiberglass strands is significantly higher than for steel strands.

For a stress level of $0.3f'_c$, the shortening was 0.229 in. for the fiberglass columns and 0.195 in. for the steel. After twenty month of data collection, the fiberglass columns exhibited an axial deformation of about 17% more than the steel. This is not surprising since the effective sustained force in the fiberglass columns is greater because of lower losses. This increase in deformation must be considered in the design of fiberglass compression members.

The creep coefficients for the columns (Group I) are shown in Figure 13.3. The value of measured creep strain was calculated by subtracting the elastic, shrinkage, and relaxation strains from the total measured stain. Figure 13.3 also shows the best fit curve equation for the measured creep coefficients.

13.4.2 Environmental Chamber (Group II)

For the prestressed concrete columns studied ~n the environmental chamber, the concrete strength was 4,739 psi at the time of release. The prestress level in the columns before applying the external load was 604 psi for fiberglass columns and 692 psi for steel columns. The prestress level on the strands before release was nearly 124 ksi for fiberglass strands and 108 ksi for the steel (see Table 13.2). This means that the two groups were pretensioned almost to the same) prestress level.

After twelve months of investigation, the to prestress losses in the fiberglass strands at column midheight were 6.9 ksi for column I, 13.26 ksi for column II, and 15.13 ksi for column III, corresponding to 5.6%, 10.7%, and 12.2% of the stress before release, respectively. The corresponding losses in tile steel strands at the same location were 23.1 ksi, 42.1 ksi and 46.4 ksi or 21.4 %, 38.9 %, and 42.9 % of the stress before release for columns I, II, and III. The prestress los percentages are nearly equal for the two groups. The small difference is possibly ue to the shorter duration of this study, differing concrete properties and the later application of the loading (after 150 days compared to 28 days for Group I).

Effective prestress at column midheight for he fiberglass strands were 117.1 ksi, 110.7 ksi, and 108.9 ksi for sets I, II, and III, respectively. For the steel strands, the effective prestress was 84.9 ksi, 66.0 ksi, and 61.7 ks for sets I, II, and III, respectively. Figure 13.24 shows clearly that the permanent effective prestress in fiberglass strands is significantly higher than in steel.

13.5 Analytical Prediction

A computer program was written to predict the total strain and the effective prestress of the fiberglass column Group I. ACI equations for creep and shrinkage were used to predict shrinkage and creep strain variations with time [12.3]. The relaxation strain variations with time for fiberglass tendons were derived from Figure 3.2. The elastic strains were calculated using fiberglass modulus of elasticity.

The predicted and measured total strain and effective prestress of fiberglass columns for different stress levels are shown in Figures 13.14 and 13.15. The figures show reasonable agreement between predicted and measured values of total strain and effective prestress.

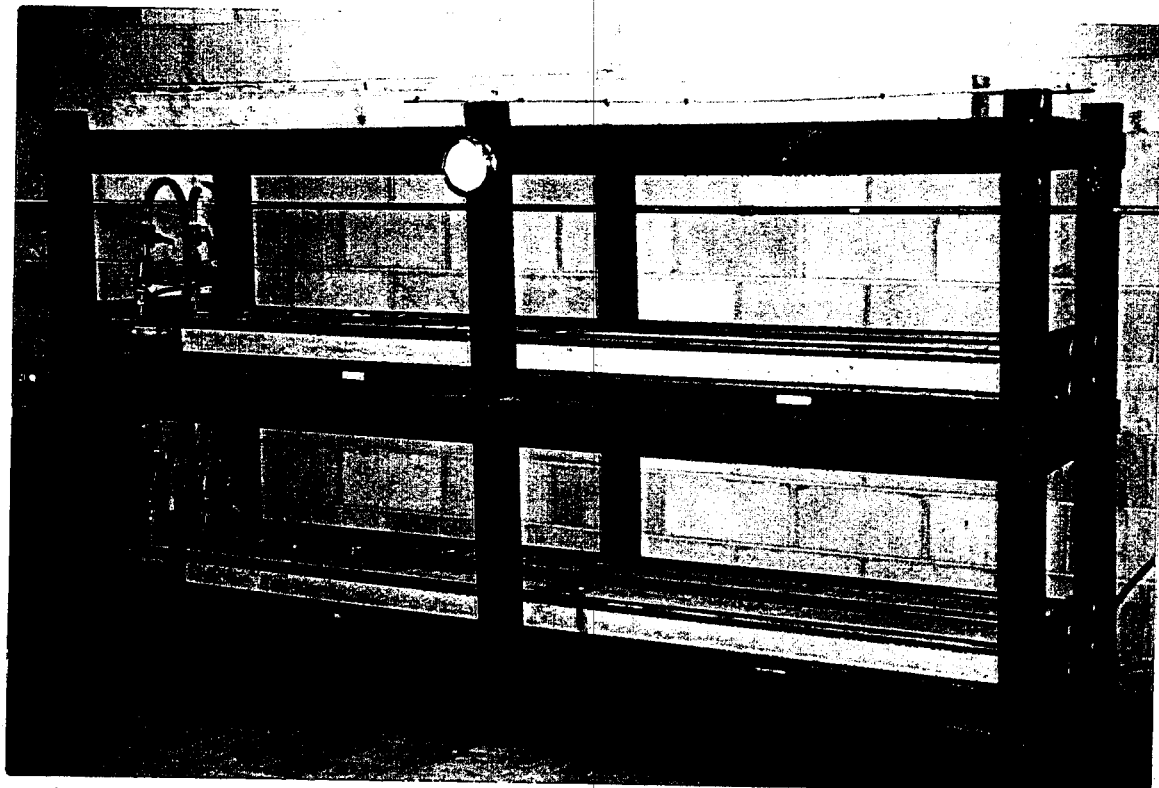


Plate 13.1 The Three Sets of Compression Members in Laboratory Environment



Plate 13.2 The Three Sets of Compression Members Inside Environmental Chamber

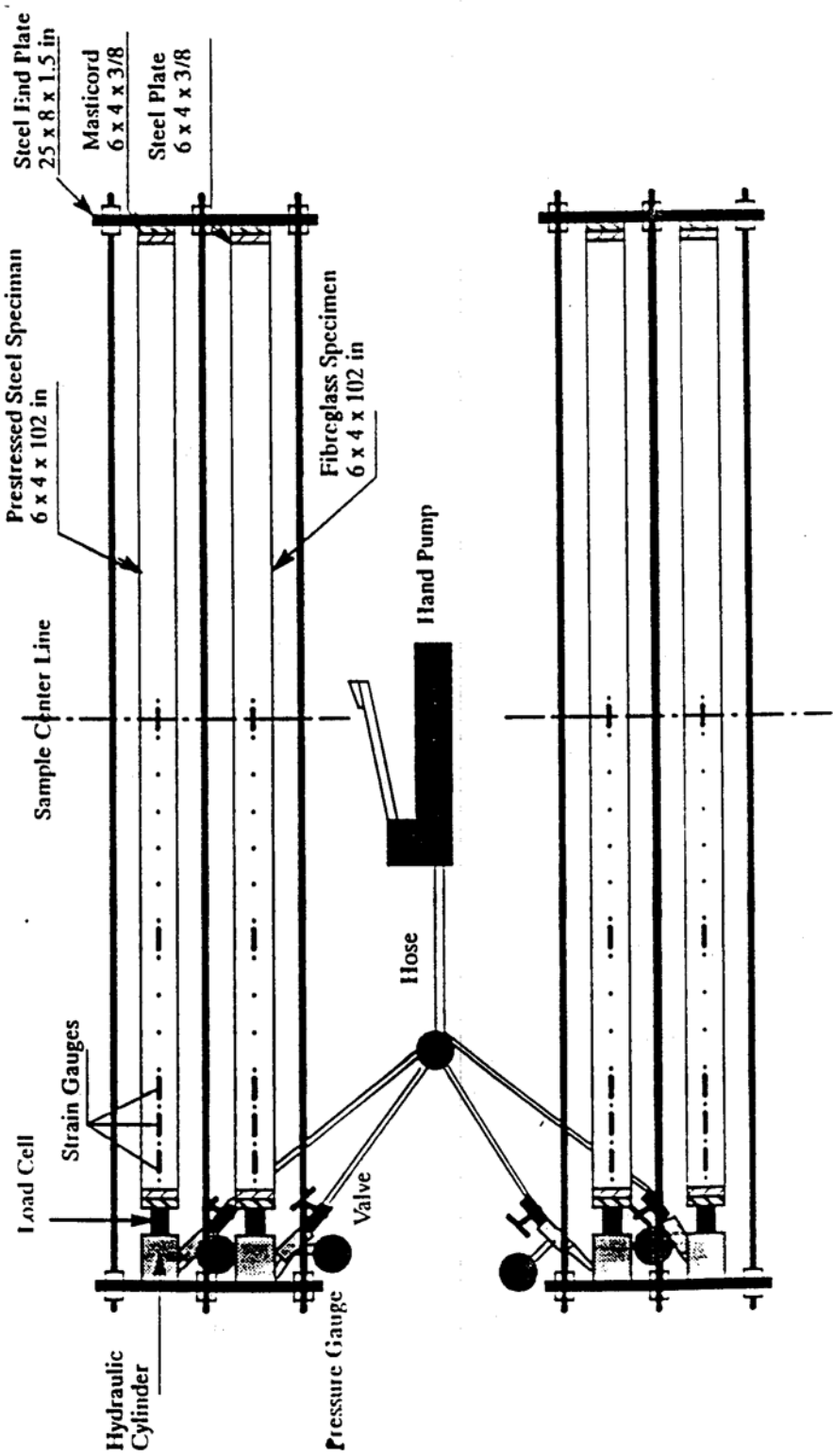


Figure 13.1 Test Setup Details (Plan view)

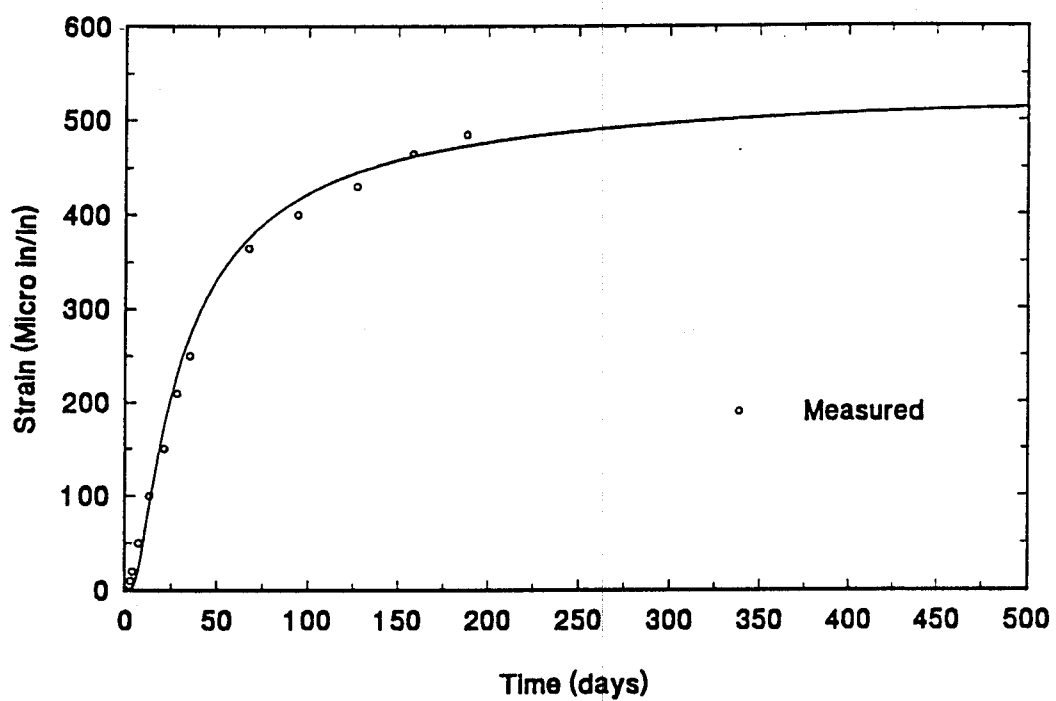


Figure 13.2 Typical Strain History of Shrinkage Specimen

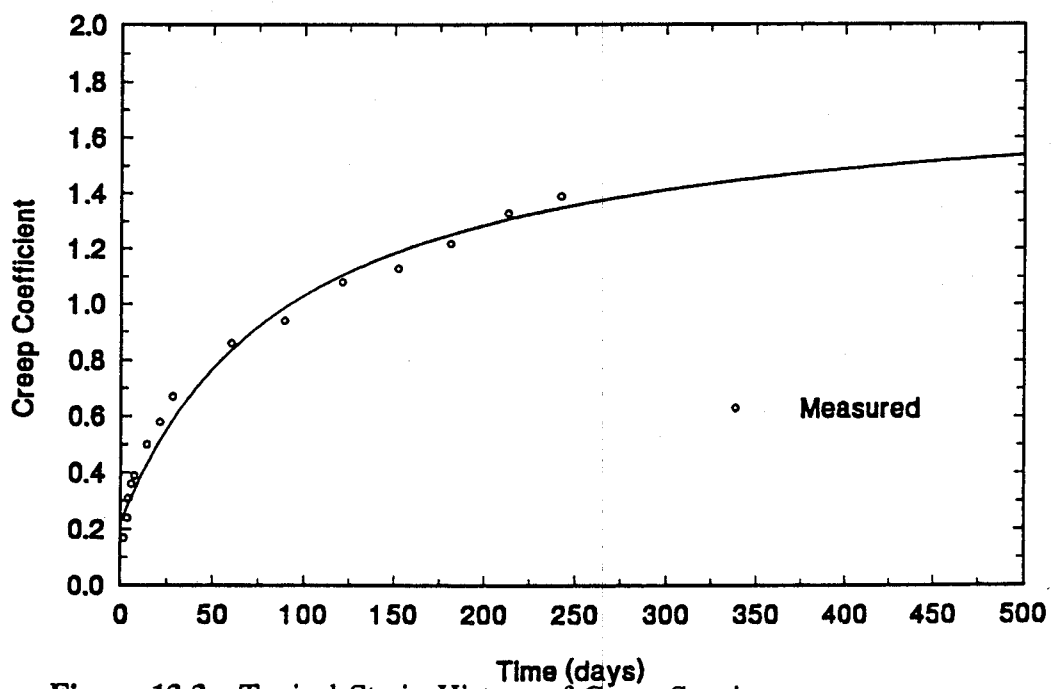


Figure 13.3 Typical Strain History of Creep Specimen

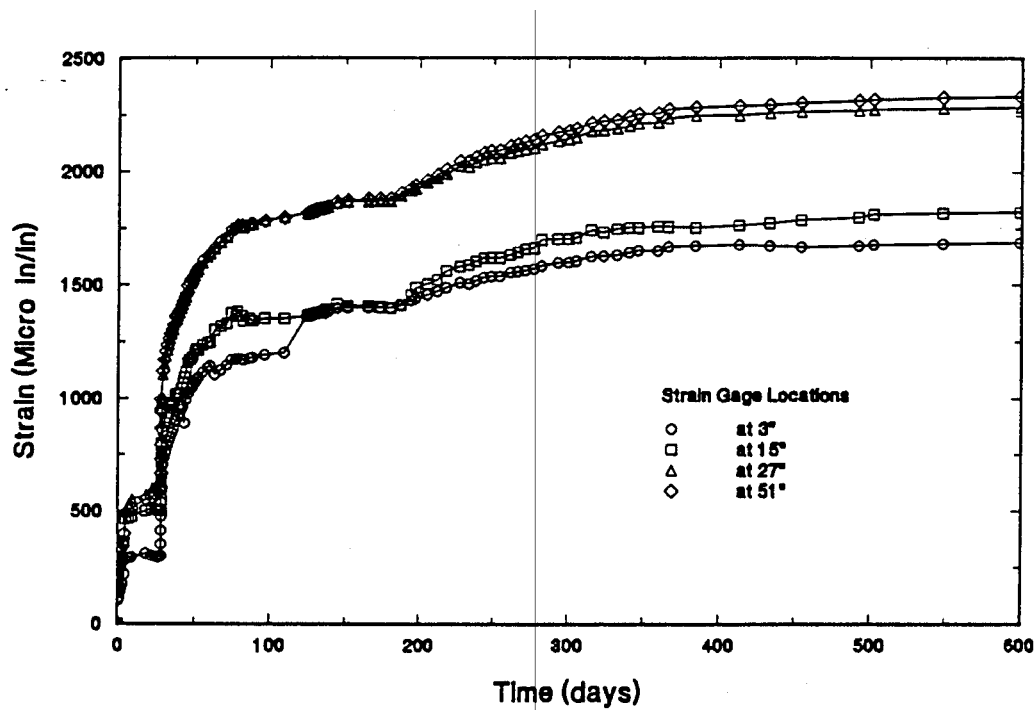


Figure 13.4 Strain History for fiberglass Column at Stress Level 0.3 $f'c$

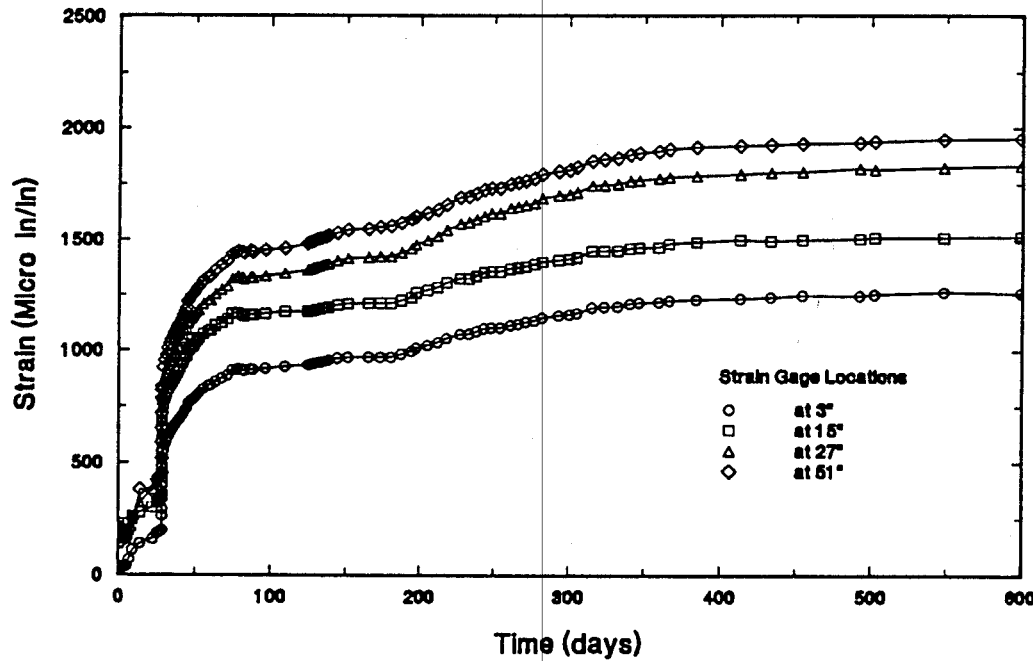


Figure 13.5 Strain History for Steel Column at Stress Level of 0.3 $f'c$

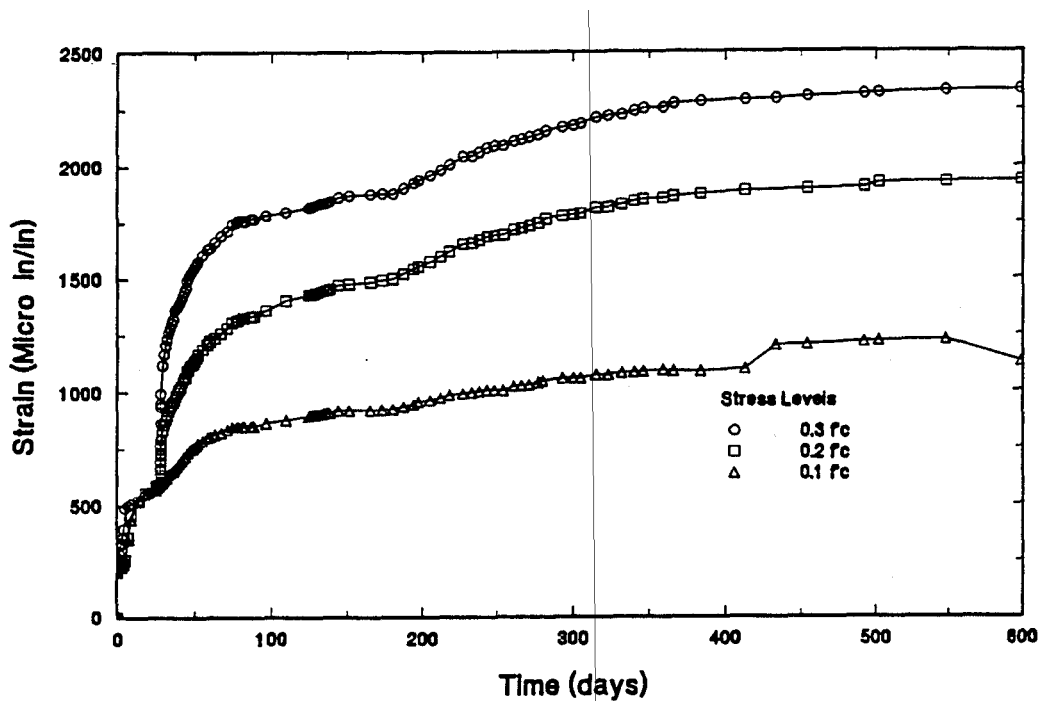


Figure 13.6 Strain History for Fiberglass columns at Different Stress Levels

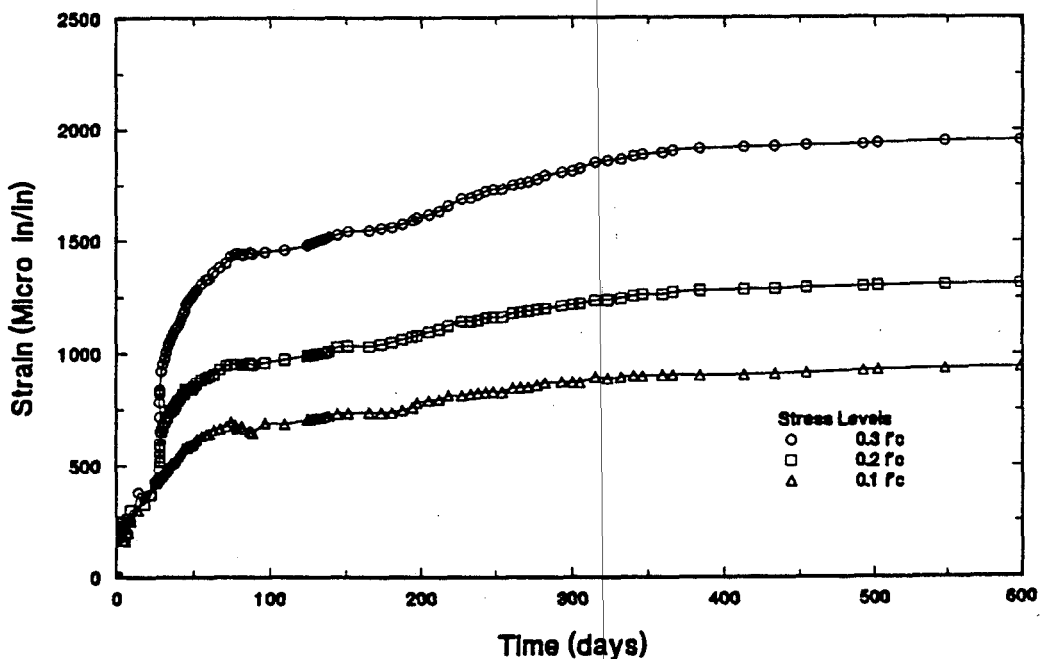


Figure 13.7 Strain History for Steel columns at Different Stress Levels

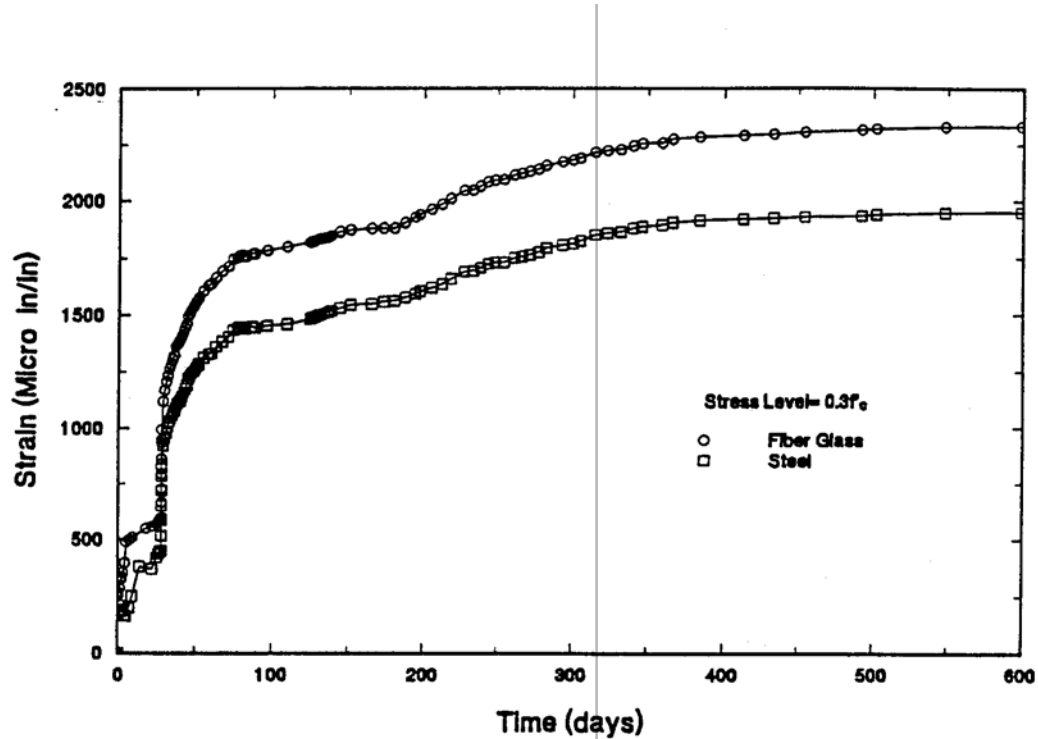


Figure 13.8 Strain History for Fiberglass and Steel Columns at Midheight

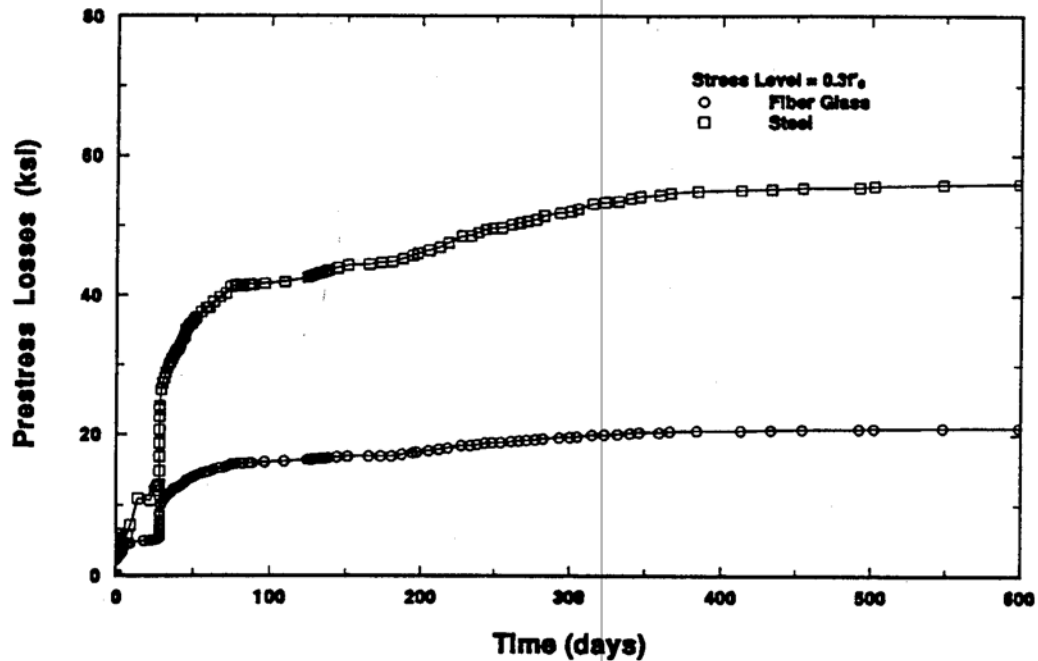


Figure 13.9 Prestress Losses for Fiberglass and Steel Columns at Midheight

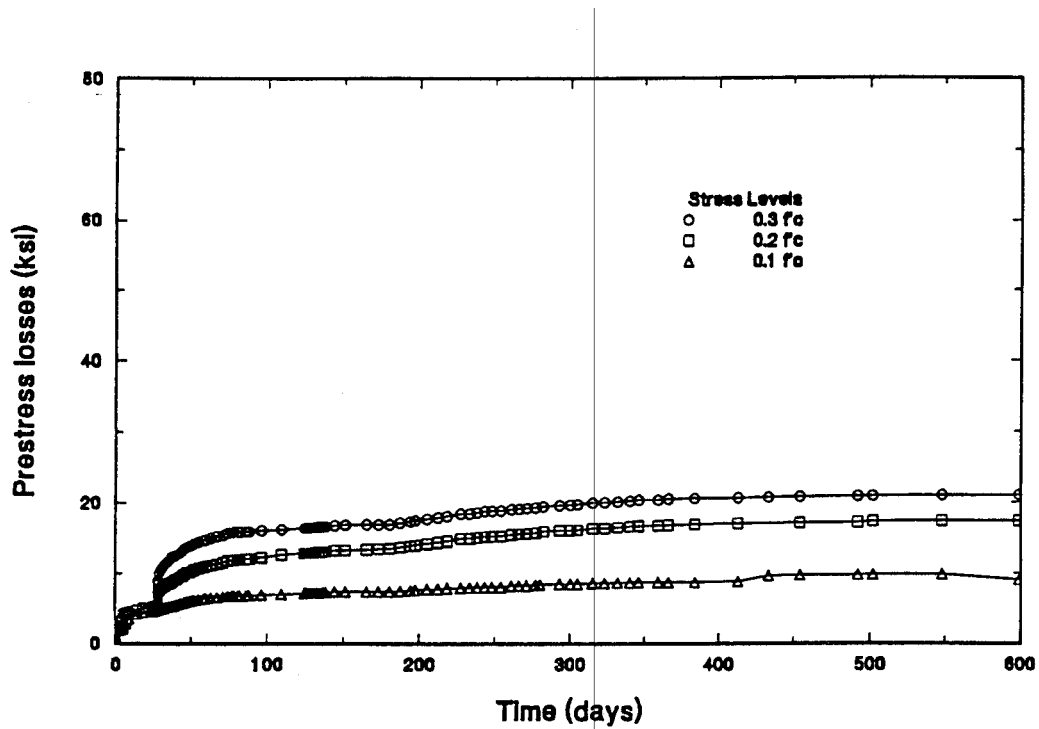


Figure 13.10 Prestress Losses for Fiberglass Columns at Different Stress Levels

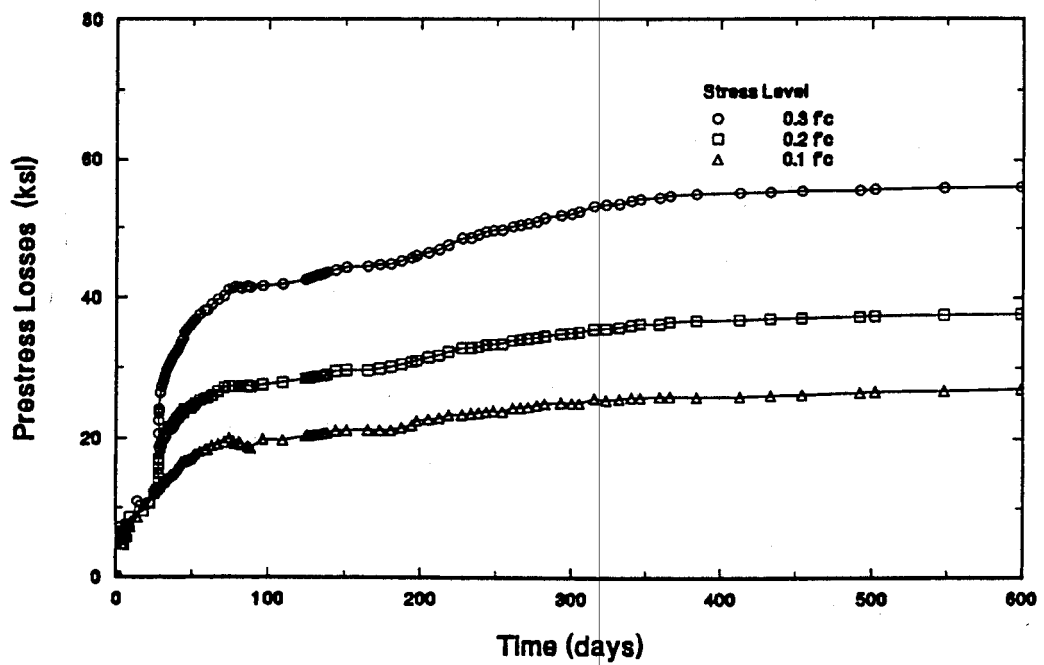


Figure 13.11 Prestress Losses for Steel Columns at Different Stress Levels

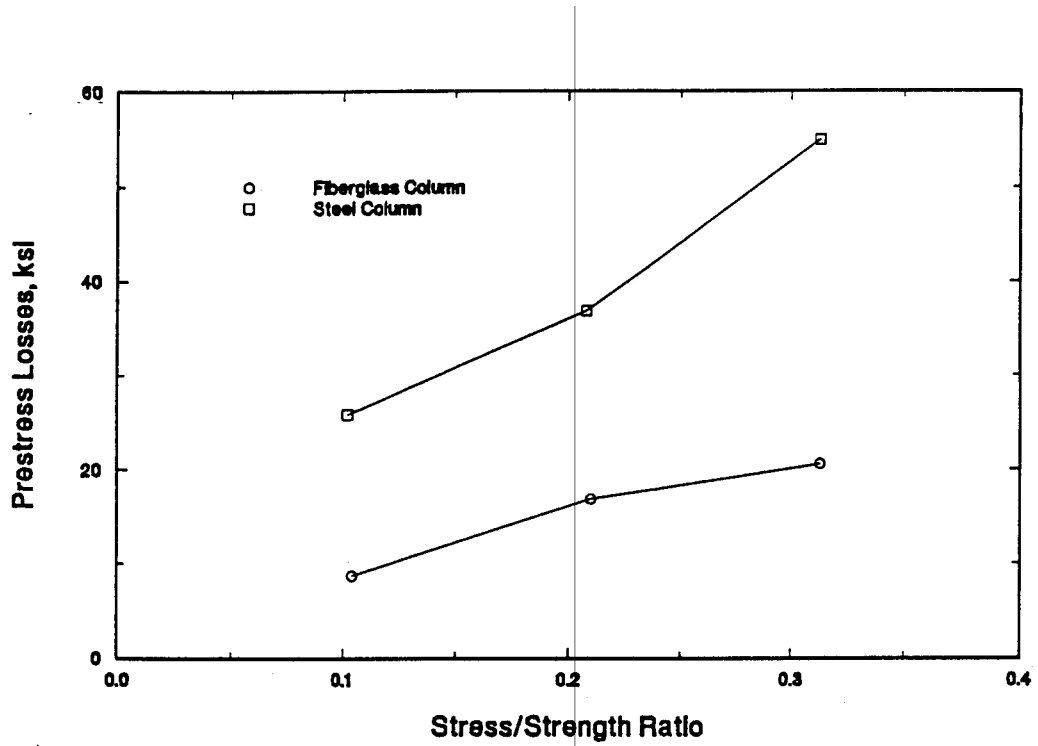


Figure 13.12 Prestress Losses Vs. Stress/Strength Ratios

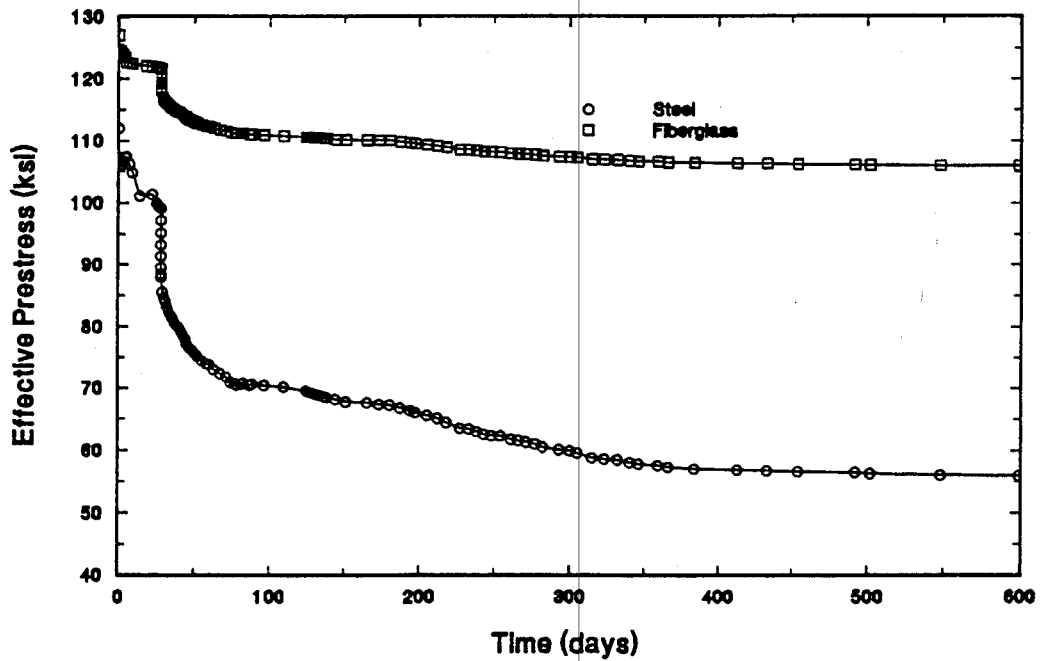


Figure 13.13 Effective Prestress for Stress Level of $0.3 f'_c$

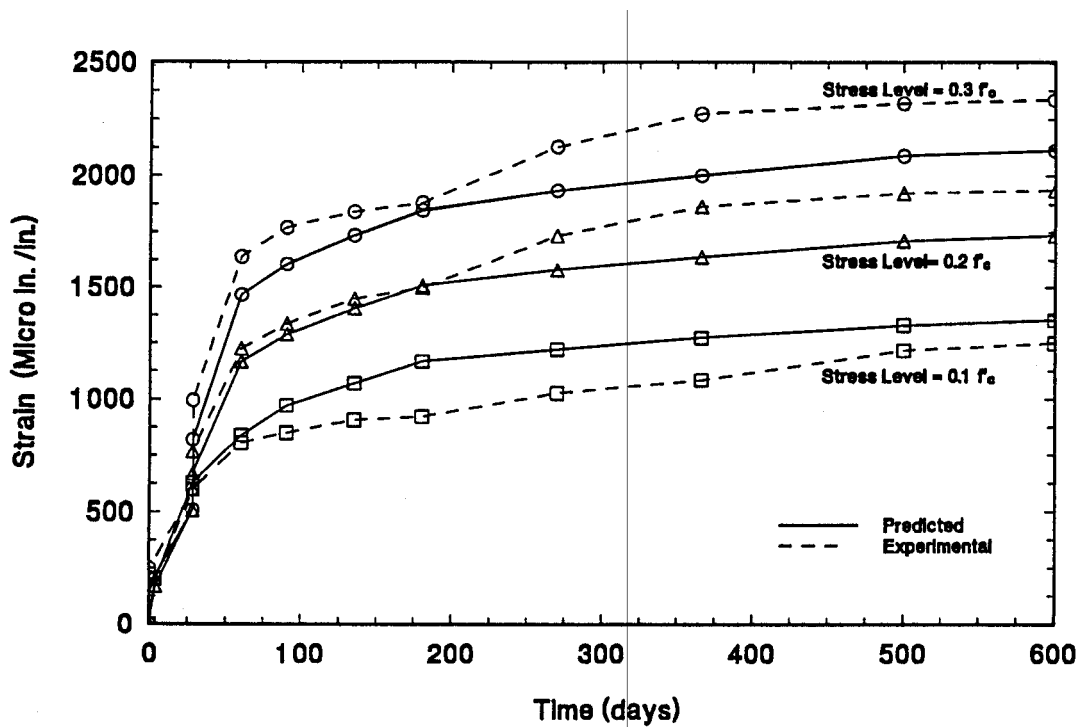


Figure 13.14 Measured and Predicted Strain History for Fiberglass Columns

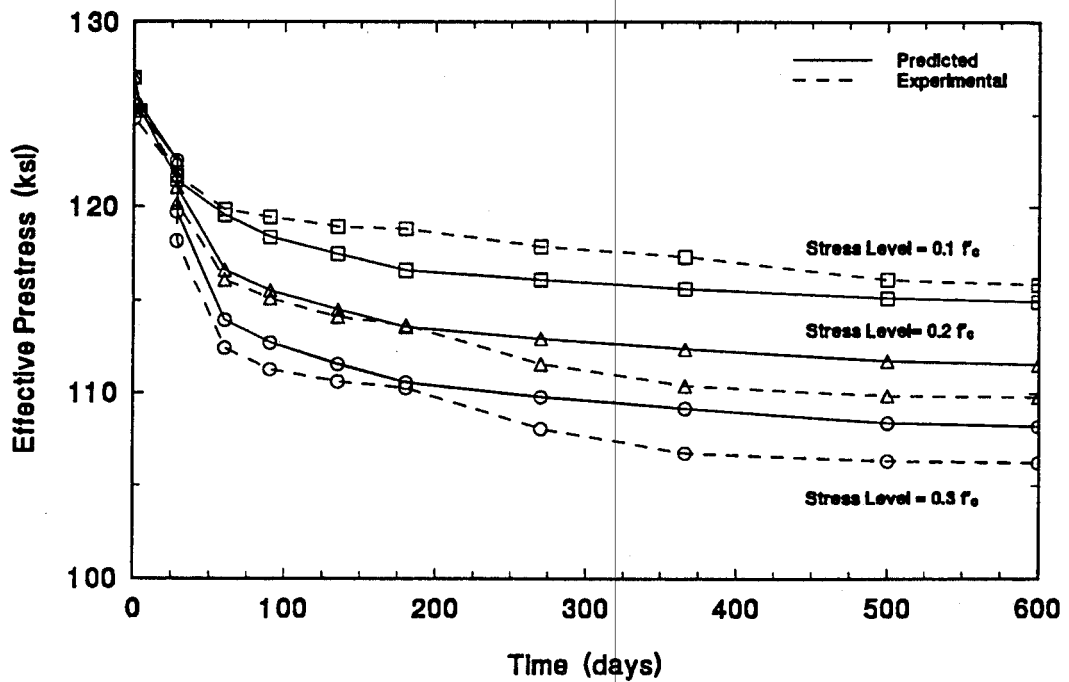


Figure 13.15 Measured and Predicted Effective Prestress for Fiberglass Columns

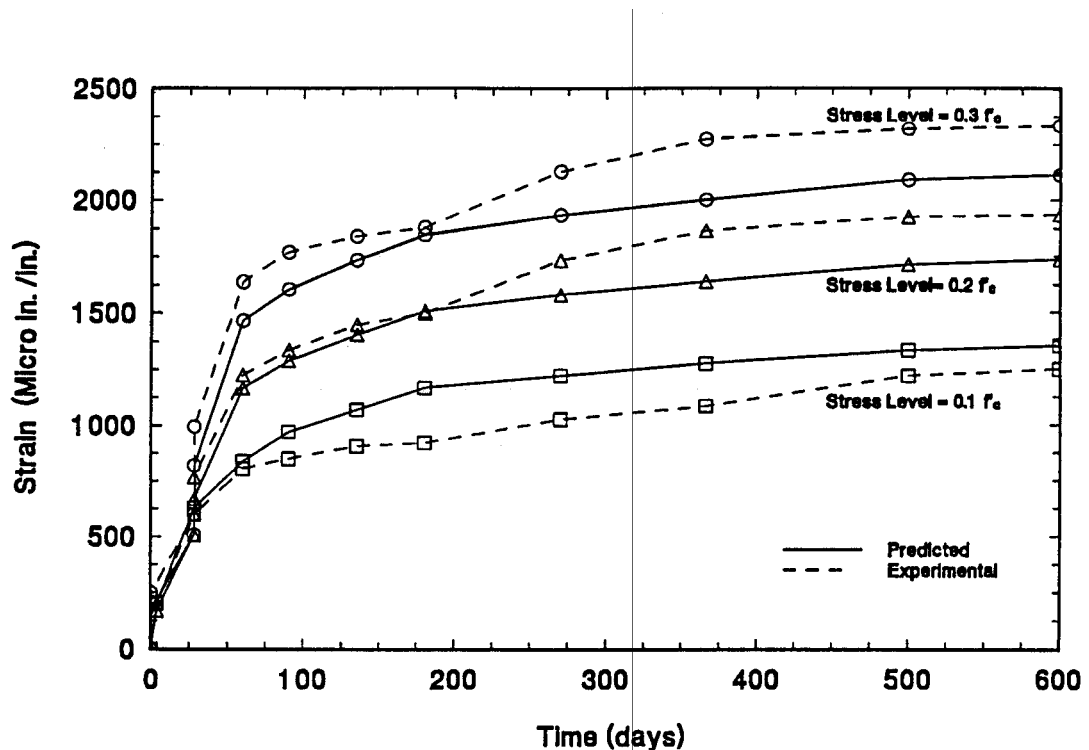


Figure 13.14 Measured and Predicted Strain History for Fiberglass Columns

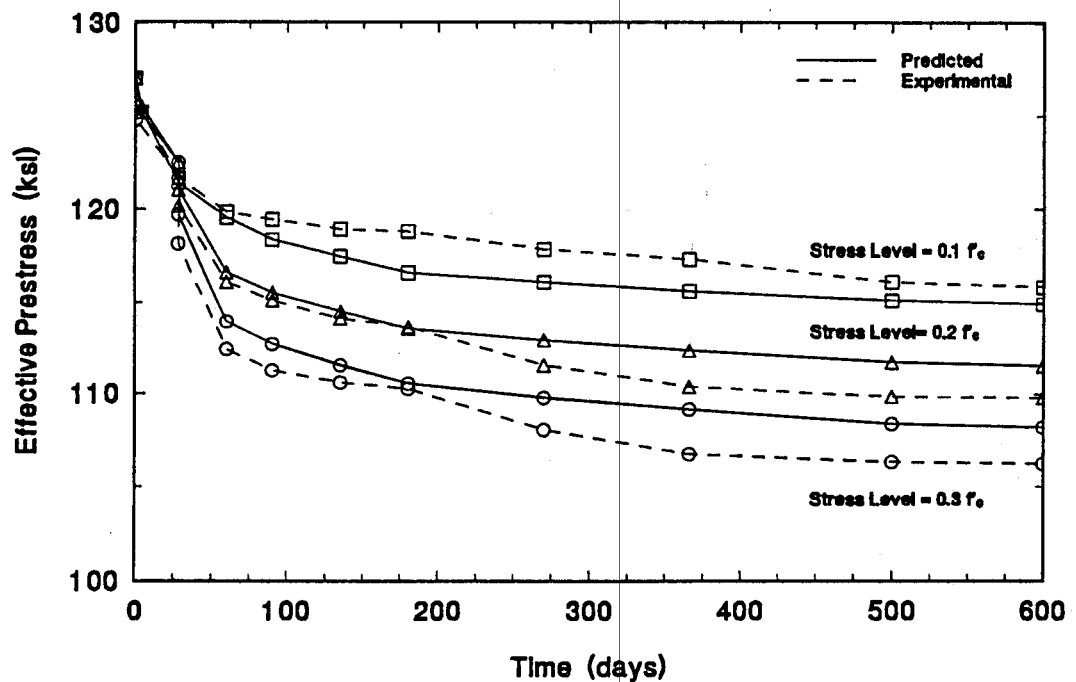


Figure 13.15 Measured and Predicted Effective Prestress for Fiberglass Columns

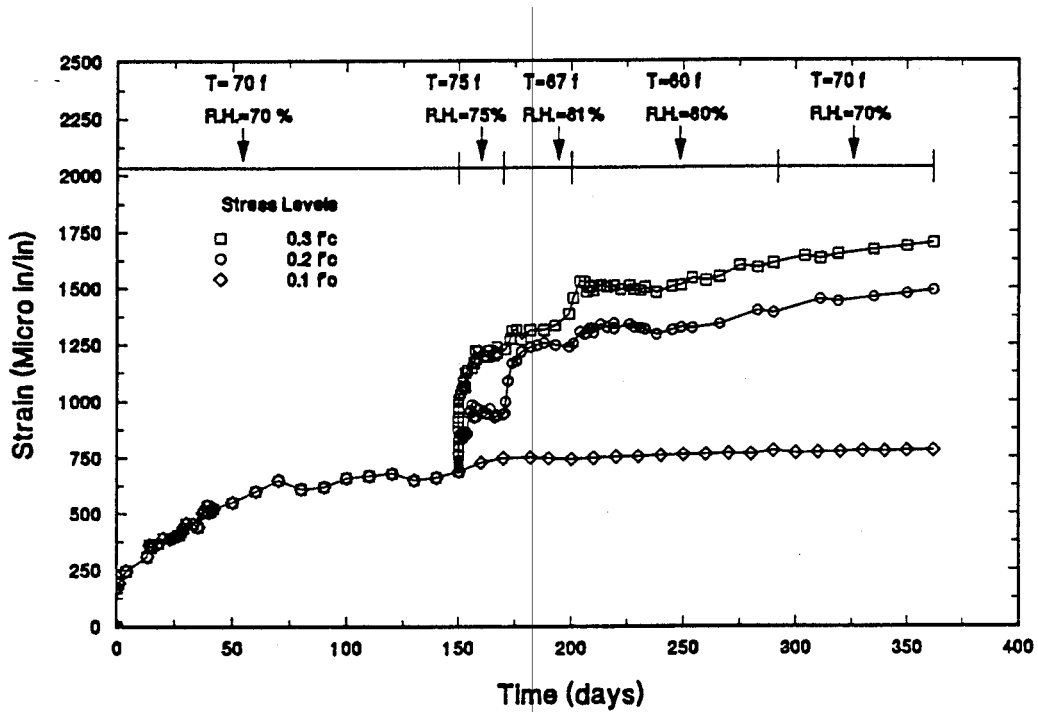


Figure 13.16 Strain History for Fiberglass Columns at Different Stress Levels

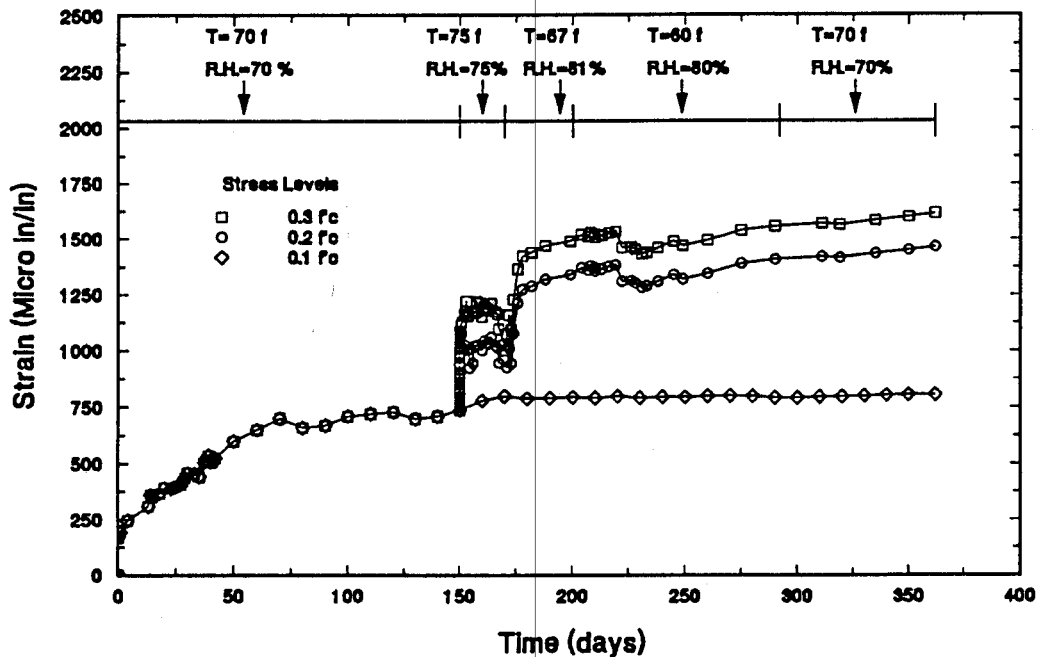


Figure 13.17 Strain History for Steel Columns at Different Stress Levels

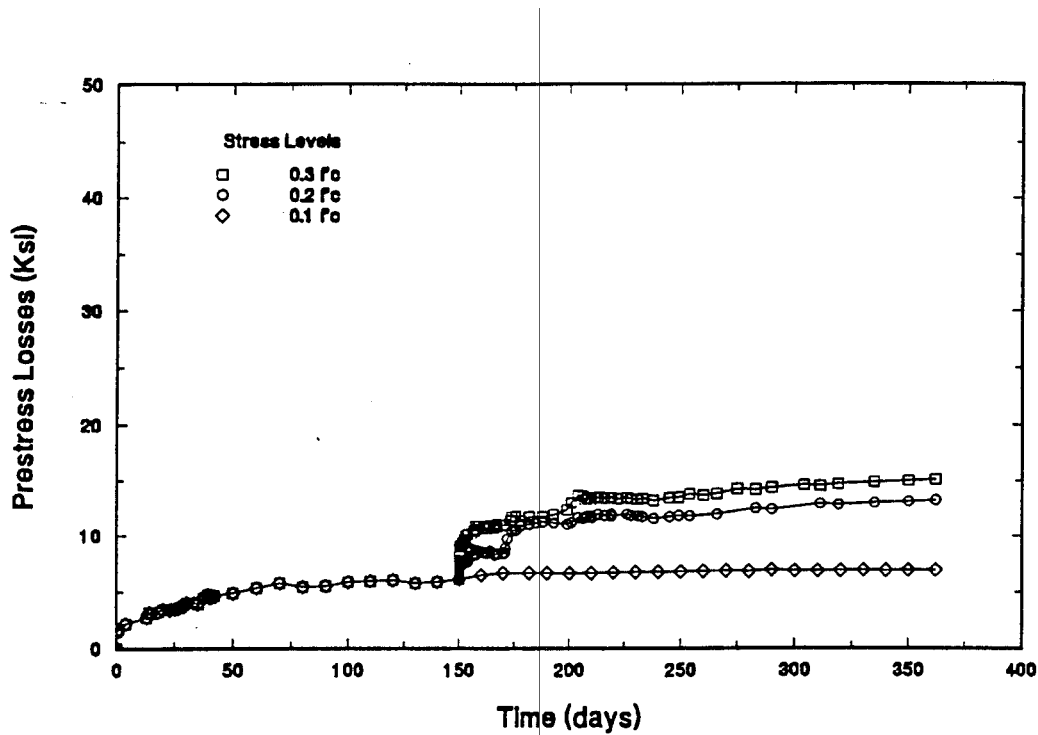


Figure 13.18 Prestress Losses for Fiberglass Columns at Different Stress Levels

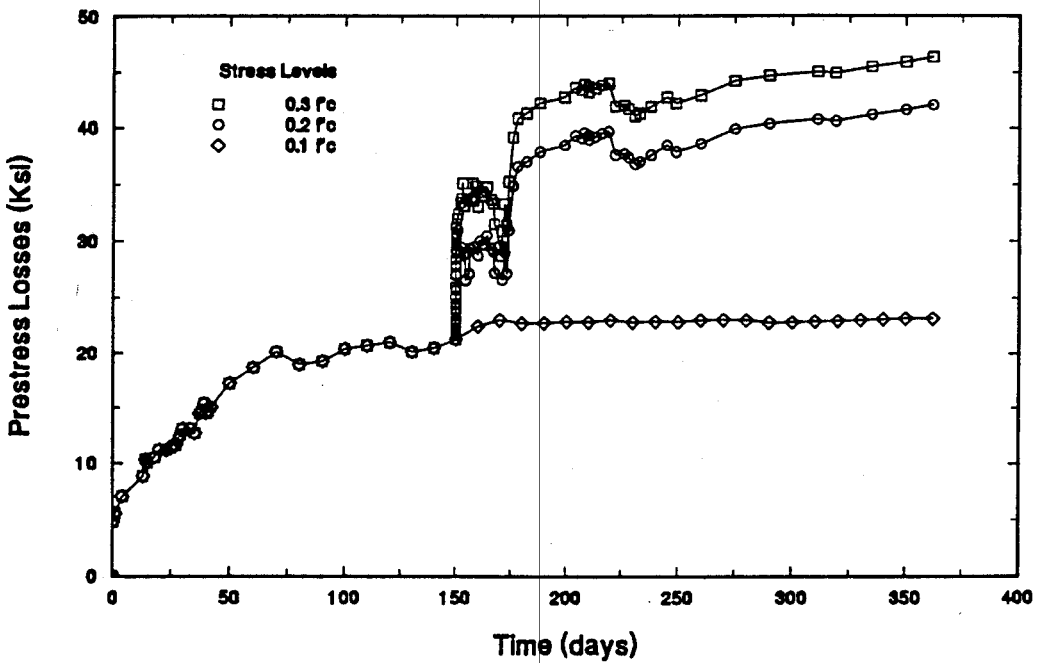


Figure 13.19 Prestress Losses for Steel Columns at Different Stress Levels

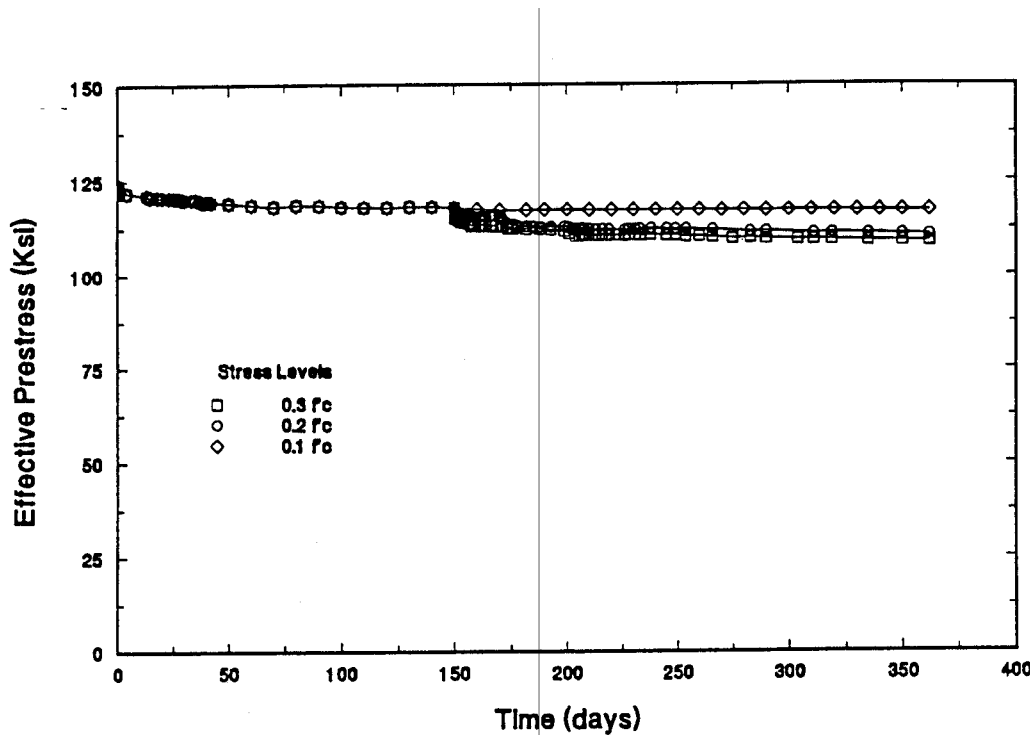


Figure 13.20 Effective Prestress for Fiberglasss Columns at Different Stress Levels

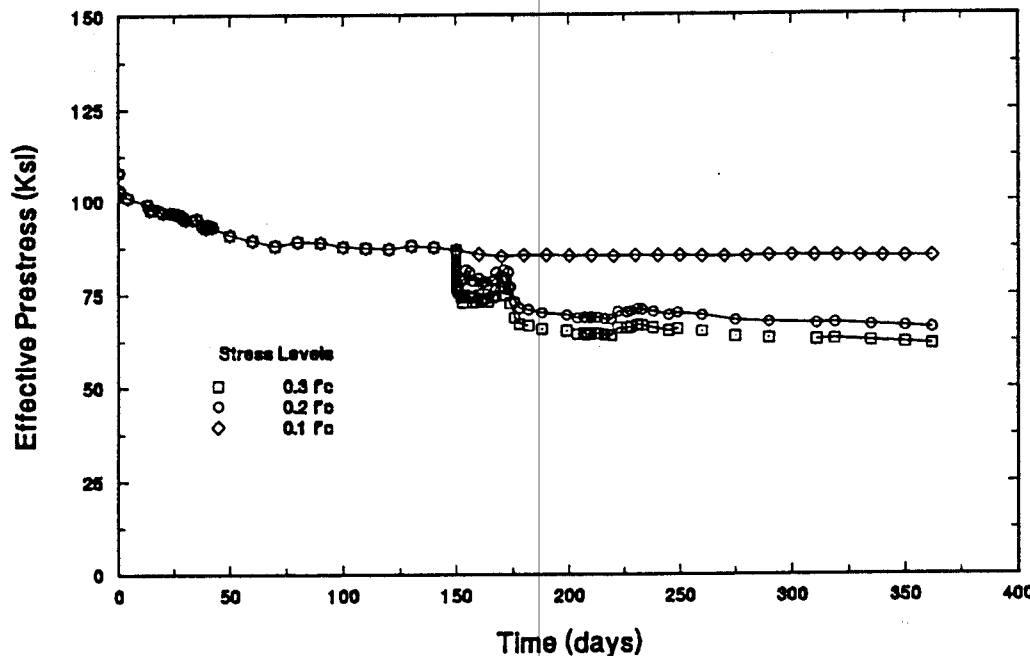


Figure 13.21 Effective Prestress for Steel Columns at Different Stress Levels

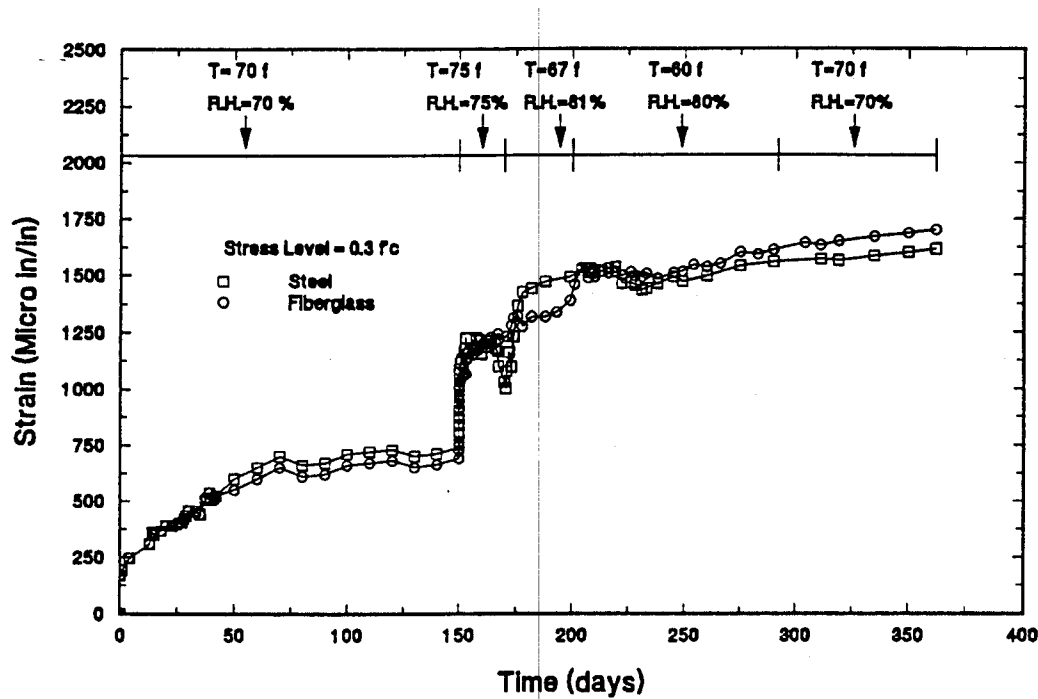


Figure 13.22 Strain History for Fiberglass and Steel Columns at Midheight

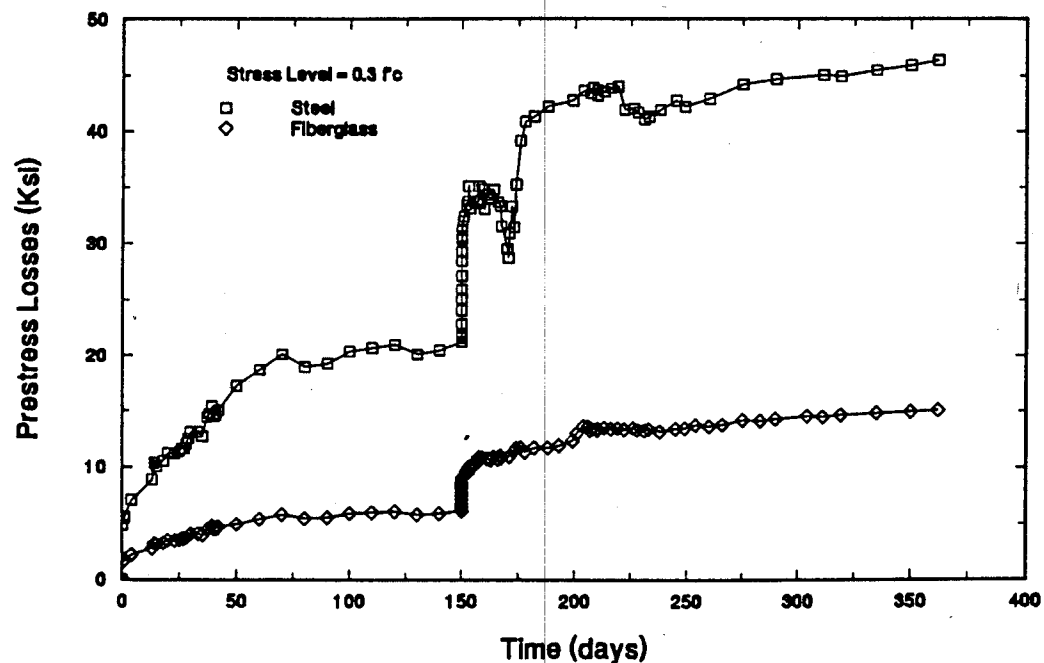


Figure 13.23 Prestress Losses for Fiberglass and Steel Columns at Midheight

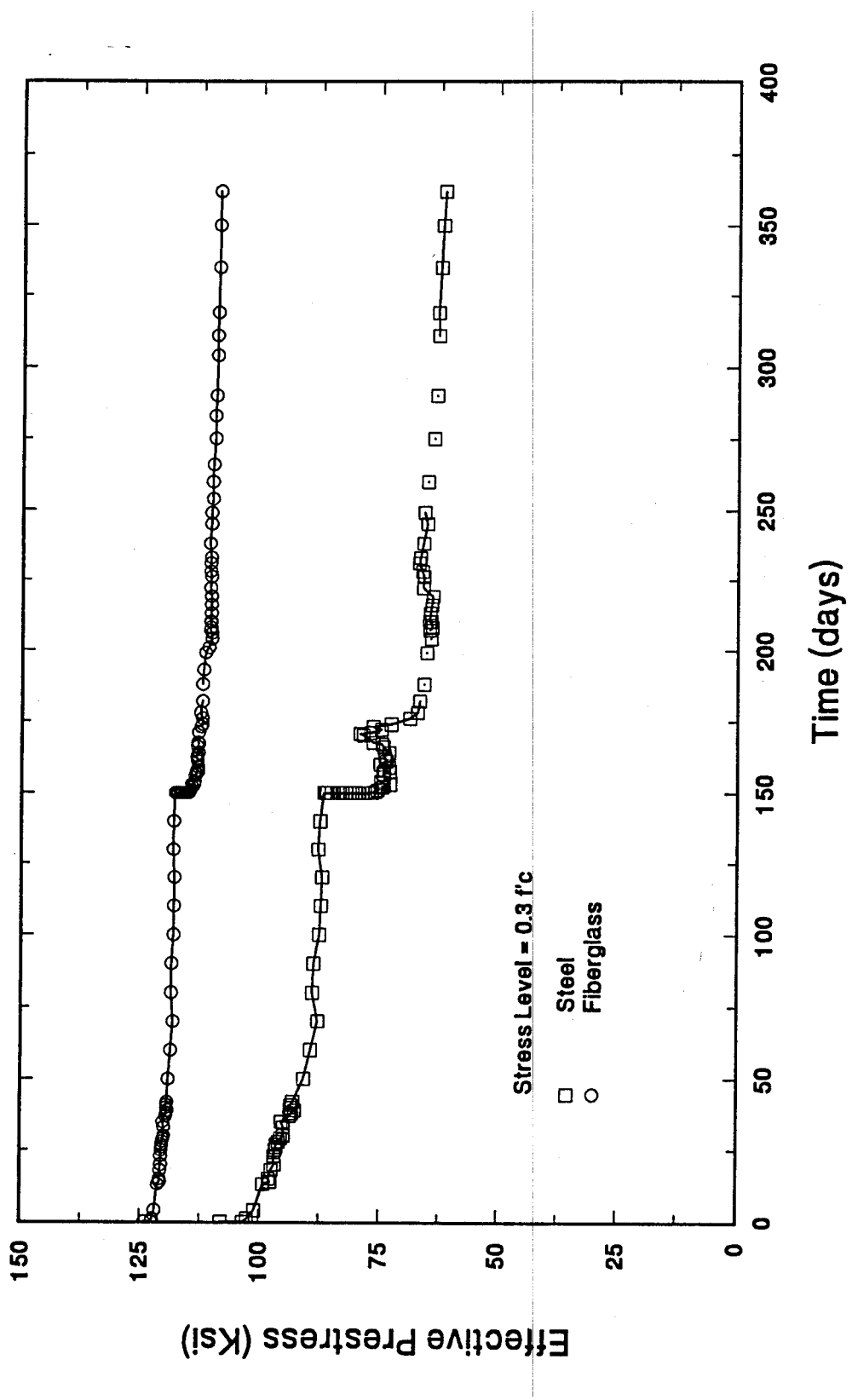


Figure 13.24 Effective Prestress for Fiberglass and Steel columns at Midheight

14. DURABILITY STUDY

14.1 Introduction

Although numerous studies have been undertaken to investigate corrosion of steel, e.g. Stark, 1984; Pfeifer *et al.*, 1986 & 1987 [14.1-14.3], these have primarily considered the extent of corrosion in isolation without reference to its effect on the overall strength and stability of the member. From a structural viewpoint, however, the link between corrosion and strength is more critical because of its obvious implications on safety.

The aim of the present investigation, therefore, was to assess reduction in ultimate strength of identical steel and fiberglass pre-tensioned specimens under conditions that may be anticipated in a marine environment. Since conditions favoring corrosion in steel have been well studied, e.g. Mozer *et al.*, 1965 [14.4], experimental parameters were set to maximize its corrosion rate. The rationale was that if the fiberglass pre-tensioned specimens survived this environment intact they would have adequately demonstrated their corrosion resistance.

The basis of selection of test parameters and the experimental set up to simulate tidal cycles in piles is described in Section 14.2-14.3. Measurements undertaken to monitor corrosion to establish the order of testing are discussed in Chapter 15. The results of the ultimate load tests are presented in Chapter 16. Since a reduction in strength may be attributed to deterioration in bond or changes in concrete strength in salt water, investigations on the effect of these factors is also included in the same chapter. Post ultimate corrosion measurements, visual inspection, carbonation tests and chloride analysis for representative specimens are 'discussed in Chapter 17. The results of scanning electron microscope investigations on fiberglass specimens are presented in Chapter 18.

14.2 Basis of Experimental Program

Since the aim of the study was to determine the feasibility of using fiberglass pretensioned piles in a marine environment, the experimental set up attempted to simulate conditions experienced by piles in this environment. In particular, simulation of the 'splash' zone, i.e. a region 2-6 ft from the water line subjected to wet/dry cycles where corrosion is initiated in steel pre-tensioned piles was the focus of the experimental set up. Since corrosion can be a slow process, a maximum cover of 1 in. was used. Larger covers did not lead to any visible signs of corrosion within eighteen months of exposure to salt water in a previous laboratory study [14.3]. To simulate the effect of pile damage

during driving, half the specimens were pre-cracked top and bottom at mid-span. To allow comparability with Pfeifer et al.'s [14.3] corrosion study on square prestressed piles, a 15 % sodium chloride solution was used and the 'tide' changed every seven days. All steel strands were used as-received since their study showed that prior cleaning did not materially affect the onset of corrosion; Moreover, such a study would be more indicative of corrosion conditions that may actually be anticipated in practice.

14.3 Tidal Simulation

A total of twenty four beams - twelve steel pre-tensioned and twelve fiberglass pre-tensioned - were tested. These were each 6 in. wide x 4 in. deep x 8.5 ft long. The steel prestressing reinforcement consisted of a single strand placed at mid-width, whereas the fiberglass comprised of a set of two strands placed 3.5 in. center as shown in Figure 14.1. To minimize fabrication differences, they were cast at the same time and were identically compacted and cured. The fabrication was originally scheduled for two pours on December 22 and December 28, 1989 but failure of one of the fiberglass lines obligated a third pour on June 6, 1990 (see Section 4.6 for details).

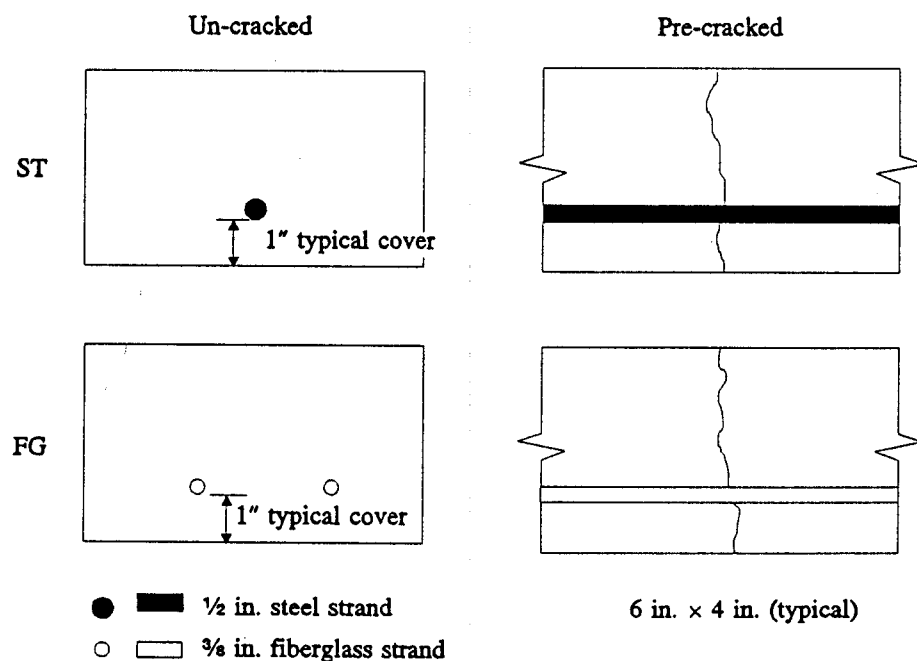


Figure 14.1 Beam Details

The identical fiberglass and steel prestressed specimens were placed in two reinforced fiberglass tanks 4.5 ft wide x 10 ft long x 2 ft high containing 15% sodium chloride solution (see Table 14.1 for details). The saline solution was made by diluting Water Softener Pellets (see Table 14.2 for chemical composition) manufactured by Morton Salt Inc., Chicago, Illinois, with tap water (see Plate 14.1). The set up used to simulate tidal effects is shown in Plate 14.2.

Of the twenty four specimens, only sixteen (eight steel and eight fiberglass) could be accommodated in the tanks. These were subjected to wet/dry cycles and tested every three months, excepting for the first and last beams which were tested after one and a half months and twenty months, respectively. Of the remaining eight beams, six (three steel and three fiberglass) were used as controls. These were tested at the beginning, after one year and at the end of the study. Two specimens were reserved for unexpected contingencies. In the testing, the steel specimen was used as a control while the fiberglass specimen was used as a pre-cracked specimen to repeat the '9 months' exposure test.

The 'splash zone' was focused at midspan of the beams by placing the specimens in an inclined position using 4.5 ft long wooden 'horses'. The beams were placed so that the face with a 1 in. cover was exposed to the air, i.e. their tensioned side was on top. Prior to their placement in the tanks, half the beams were pre-cracked top and bottom at the midspan region. A load of approximately 1,800-2,000 lbs was used to pre-crack the bottom section. A much smaller load, 300-400 lbs, was used to pre-crack the section at top (see Table 14.3).

A protective coating of *Permakote epoxy resin*, manufactured by Pilgrim Permocoat, Inc., Tampa, Florida, was applied to the ends to prevent corrosion from being initiated in the exposed steel (see Plate 14.3). For comparability, the same coating was applied to the fiberglass beams and to the control specimens. Nine locations for half-cell potentials, electrical resistivity and chloride content measurements were marked permanently (see Plate 14.3). Points 1 (closest to the submerged end) and 9 (closest to the permanently dry end) were 6 inches from their respective ends; points 2-8 were located exactly one feet apart between points 1 and 9, as shown in Figure 14.2. Since the steel was expected to corrode, a stainless steel hose clamp was attached to the exposed steel strand, to facilitate electrical 'connection for projected half cell potential measurements.

Low tide was produced by keeping 6 in. of water in the tank and high tide by keeping the water level at 15 in. The tidal cycle was simulated by alternating the water level in the two tanks every seven days by means of a piping system that connected the two tanks. Two 1/200 hp Teel model 1P680A epoxy-magnetic submersible pumps, manufactured for Dayton Electric Mfg. Co., Chicago, Illinois, were used to accomplish the transfer of water.

Table 14.1 Details of Experimental and Control Beams

Steel			Fiberglass			
	Beam	Date Cast	Remark ¹	Beam	Date Cast	Remark ¹
Tank #1	ST-E1		U	FG-E1		P
	ST-E2	12/22/89	P	FG-E2	12/22/89	U
	ST-M1		U	FG-M1		P
	ST-M2		P	FG-W2		U
Tank #2	ST-E3		U	FG-E3	12/28/89	U
	ST-E4	12/28/89	P	FG-M3		P
	ST-M3		U	FG-M6	06/06/90	U
	ST-M4		P	FG-E6		P
Control	ST-W1	12/22/89	U	FG-M2	12/22/89	U
	ST-W2		P	FG-W1		P
	ST-W3	12/28/89	U	FG-W3	12/28/89	U
Extra	ST-W4	12/28/89	P	FG-W6	06/06/90	P

¹ U — Un-cracked beams; P — Pre-cracked beams

Table 14.2 Chemical Composition of Water Softening Pellets

Component (%)	Typical	Range
Sodium Chloride	99.70	99.5 - 99.9
Calcium Sulfate/ Sodium Sulfate	0.17	0.0 - 0.30
Other Salts	0.03	0.0 - 0.10
Additives	--	Less than 0.2
Moisture	--	Less than 0.1
Water Insolubles (ppm)	20	5 - 40

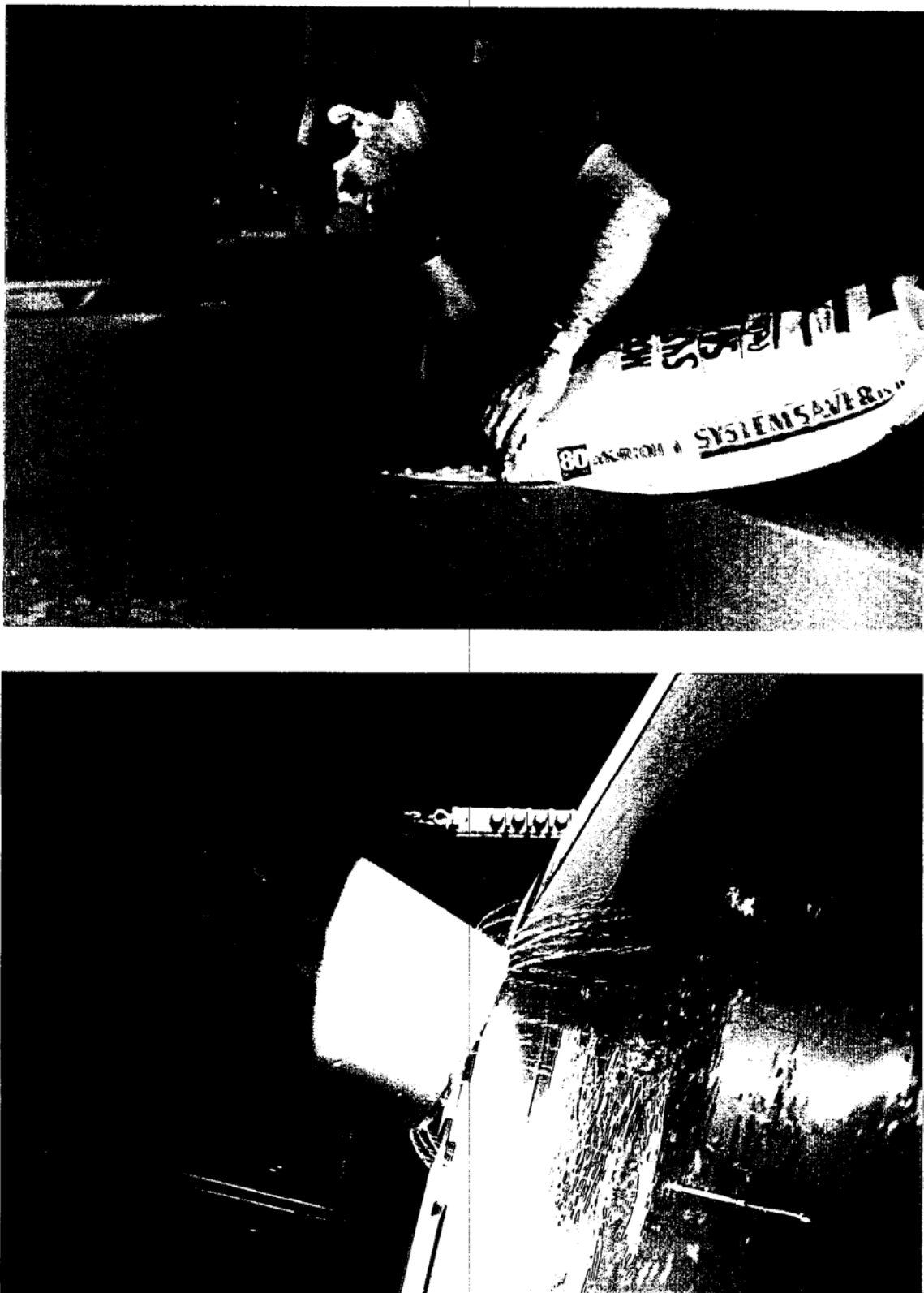


Plate 14.1 (top) Placing salt in mixing container
(btm) 15% salt solution in test tank

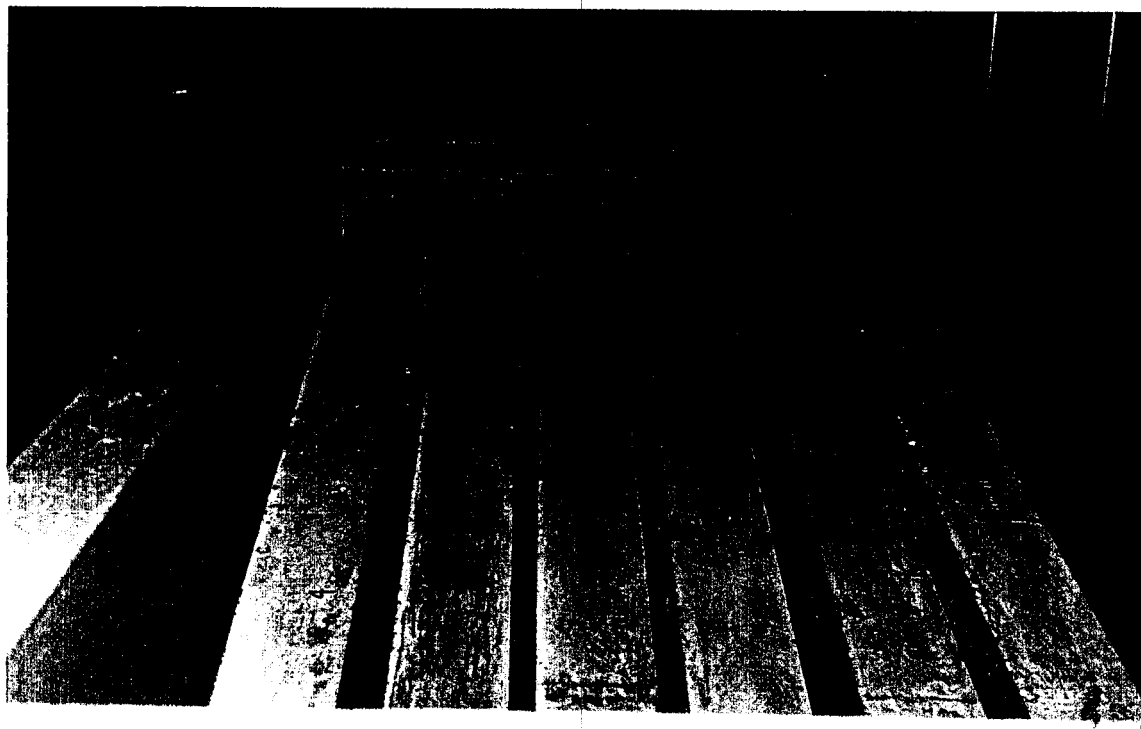
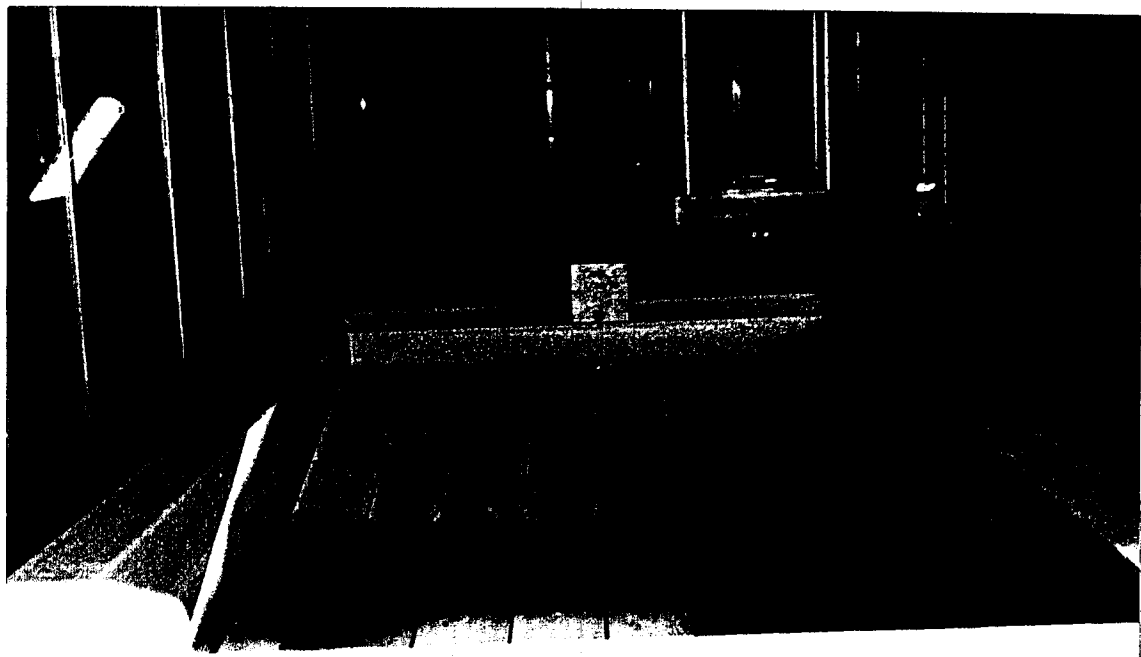


Plate 14.2 (top) High tide - tank N² 1
 (btm) Low tide - tank N⁴ 2

Table 14.3 Applied Load for Pre-cracked Specimens

Beam	Cast Date	Cracking Load (kips)	
		Bottom	Top
ST-E2		2.2	0.4
ST-M2	12/22/89	2.0	0.3
ST-W2 ¹		2.2	0.4
ST-E4		2.0	0.3
ST-M4	12/28/89	2.0	0.3
ST-W4 ¹		2.0	0.3
FG-E1		1.8	0.4
FG-M1	12/22/89	1.8	0.4
FG-W1 ¹		1.8	0.4
FG-M3	12/28/89	2.0	0.4
FG-E6		1.8	0.4
FG-W6 ¹	06/06/90	1.8	0.3

¹ Control Specimens

Since the specimens were kept in an inclined position at a slope of 1:4.25, a large portion of the specimens, approximately 4 to 4.5 ft long, were subjected to alternate wet/dry cycles. Smaller zones at the ends, of between 2 to 3 ft in length, were either permanently submerged or permanently dry. Figure 14.2 shows the characteristics of the test set up and the 'splash zone' generated.

Since reductions in strength can also be attributed to a deterioration in bond between the prestressing material and concrete or to changes in the compressive strength of concrete in salt water, additional tests were conducted in which the tidal simulation set up was also used to investigate these effects. In two series of tests conducted, identical (unstressed) fiberglass and steel pullout specimens were placed in Tank 2 and subjected to weekly wet/dry cycles. Additionally, cylinders were placed in both tanks and were tested to failure at the same time as the exposed specimens. The results from both these studies are summarized in Chapter 16.

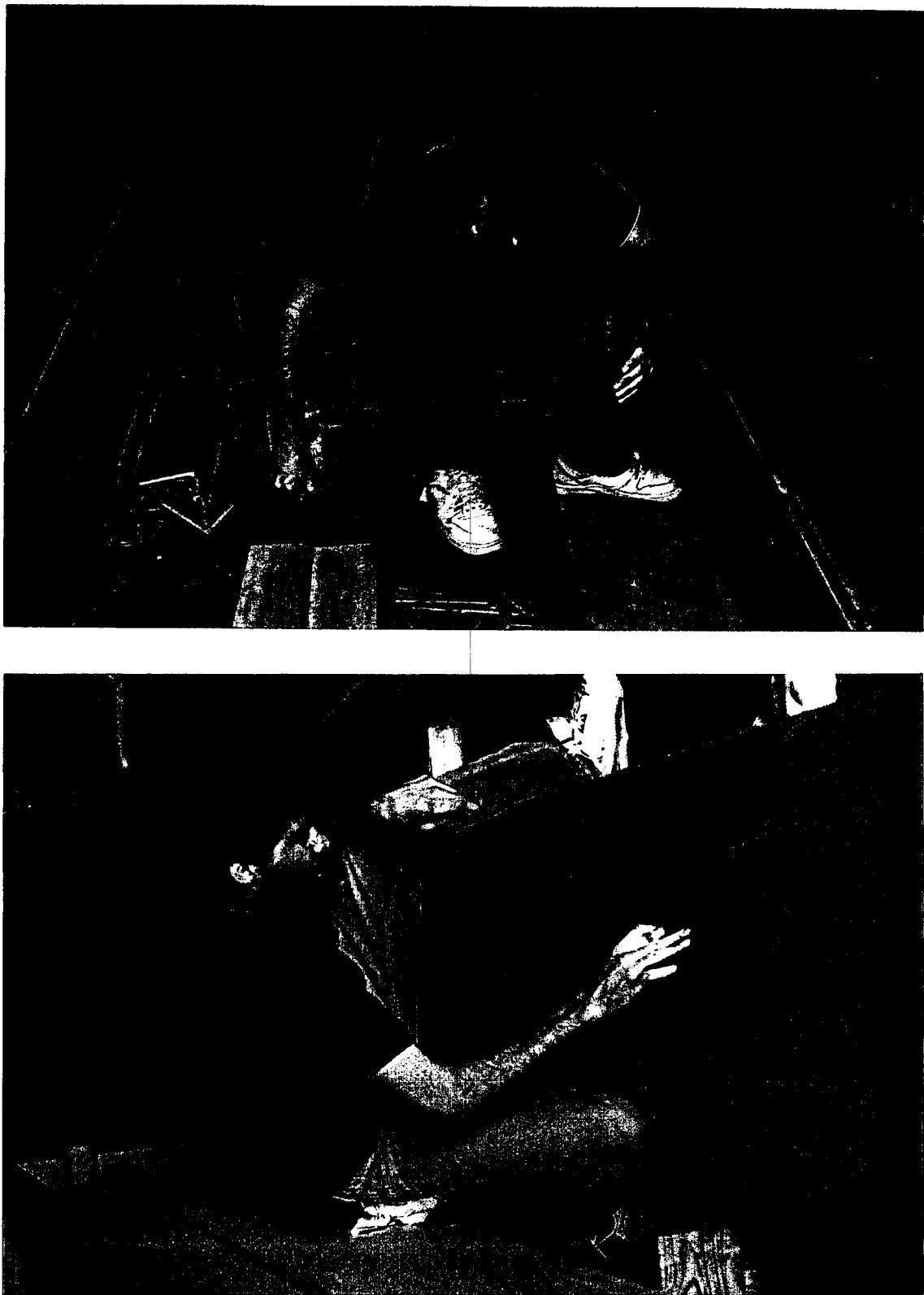


Plate 14.3 (top) Application of epoxy coating at ends
(btm) Marking locations for half-cell readings

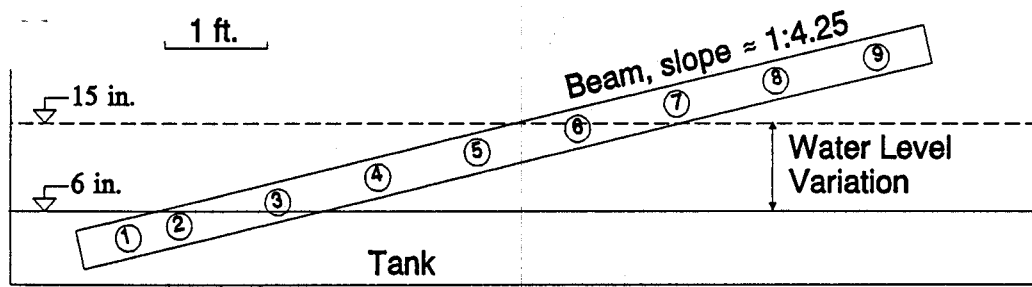


Figure 14.2 Beam Position in Tank

15. DETERMINATION OF SEQUENCE OF TESTING

15.1 Introduction

Since the link between corrosion and ultimate strength was the primary goal of the durability study, it was important to identify the rate of corrosion in order to avoid prematurely testing specimens corroding the most. To this end, electrical measurements, such as half cell potentials, impedance and resistivity were taken over the entire duration of the study so that the order in which specimens were removed from the tanks and tested was rationally based.

Since corrosion of steel is electro-chemical, the half-cell and impedance measurements taken related only to the steel specimens. Concrete resistivity measurements were consequently undertaken to obtain information on the relative state of the concrete in the fiberglass and steel pretensioned specimens kept in the tanks. Thus, it provided an indication as to whether both fiberglass and steel pre-tensioned specimens were subjected to the same conditions.

The task of determining the sequence of testing of specimens was greatly simplified since pre-cracked and un-cracked specimens were alternately tested to allow comparison of their relative performance. Since there were only four un-cracked and pre-cracked specimens (see Table 16.1), the measurements essentially reduced to the determination of the order of testing four specimens of each type. As the electrical measurements related primarily to the steel pre-tensioned specimens, fiberglass specimens were to some extent picked at random although due consideration was given to the cast dates of the steel specimens that appeared to corrode the most.

This chapter presents results and analysis of corrosion measurements that were used to establish the sequence of testing of the specimens. Essential information relating to halfcell potentials, impedance and resistivity measurements together with typical results are summarized respectively in Sections 15.2 to 15.4. Each section provides results for un-cracked and pre-cracked specimens from each of the two tanks. The sequence of testing implied by the measurements is presented in Section 15.5.

15.2 Half-Cell Potentials Measurements

The simplest procedure available to evaluate .corrosion of steel in concrete is the half-cell potential measurement. It involves the measurement of potentials on the concrete surface to outline the presence of galvanic (corroding) cells in the steel.

The potentials are measured against a reference electrode, in this case a copper-copper sulfate (CSE) half-cell, using a voltmeter. To take measurements, the electrode is connected to the negative pole and the reinforcement to the positive pole. Half-cell potentials were measured using a copper-popper sulfate electrode (CSE) model 2A, manufactured by Tinker & Rasor, San Gabriel, California. The results are presented to show its variation with time.

Figures 15.1 and 15.2 show typical potentials recorded for un-cracked and pre-cracked specimens exposed to saltwater. Figures, 15.3 and 15.4 show the corresponding potentials for the control specimens that were kept outside the tanks. Even though the potentials were recorded for all the nine points marked on each steel pretensioned beam (see Figure 14.2), measurements for only three representative points - #1, #5 and #9 - are shown. These correspond to the locations that are permanently submerged (#1), in the 'splash zone' (#5) and in the permanently dry zone (#9). Since potentials measurements corresponding to 'low tide' and 'high tide' were different, they are plotted separately in Figures 15.1- 15.2.

Two horizontal dashed lines are incorporated in the graphs to separate three regions identified by ASTM C 876-87 as relating to different states of corrosion (see Table 15.1). The upper part where the magnitude of the half-cell potential exceeds -350 mV (for CSE) corresponds to the region of "high" probability of active corrosion; the middle (between potentials of 200-350 mV) to the "uncertain" region, i.e. corrosion may or may not have been initiated; and the lower part (potentials below 200 mV) to regions of "low" probability of active corrosion

Table 15.1 Different Half-Cell Potential Thresholds for Corrosion [15.1,15.2]

Potential Level (mV vs CSE)	% Probability of Active Corrosion	
	ASTM	COLEBRAND
0 to -200	10%	5%
-200 to -350	uncertain	50%
-350 >	90%	95%

15.2.1 Discussion of Results

It may be seen from Figures 15.1 and 15.2 that potentials measured in the dry zone (point #9) did not typically exceed threshold', limits for 50% probability of corrosion for either un-cracked or pre-cracked specimens in salt water. On the other hand, potentials measured at the wet/dry ('splash') and permanently wet zones exceeded the high

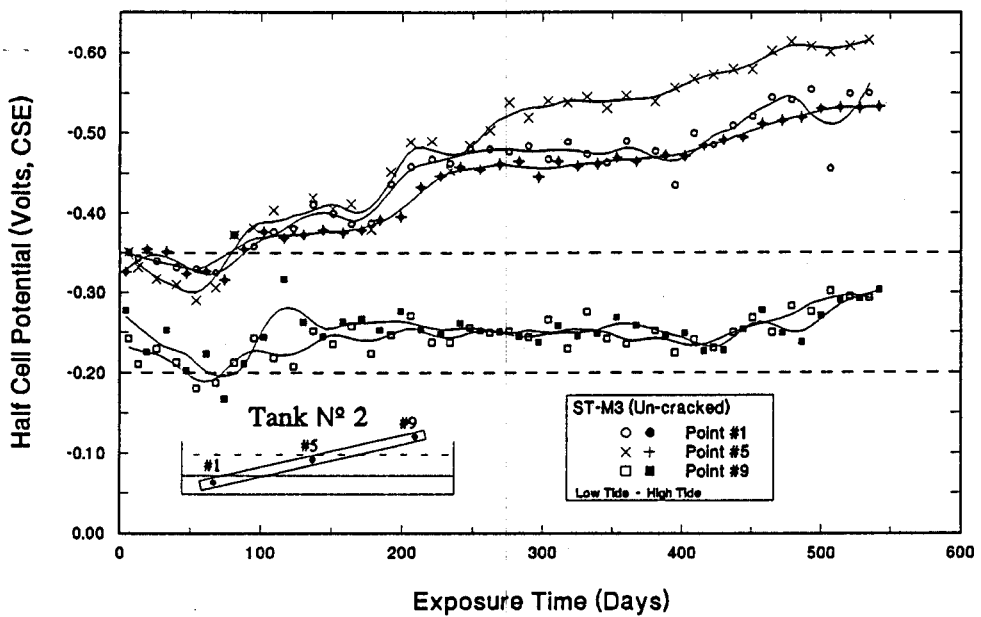


Figure 15.1 Half-Cell Potentials for Un-cracked Beam

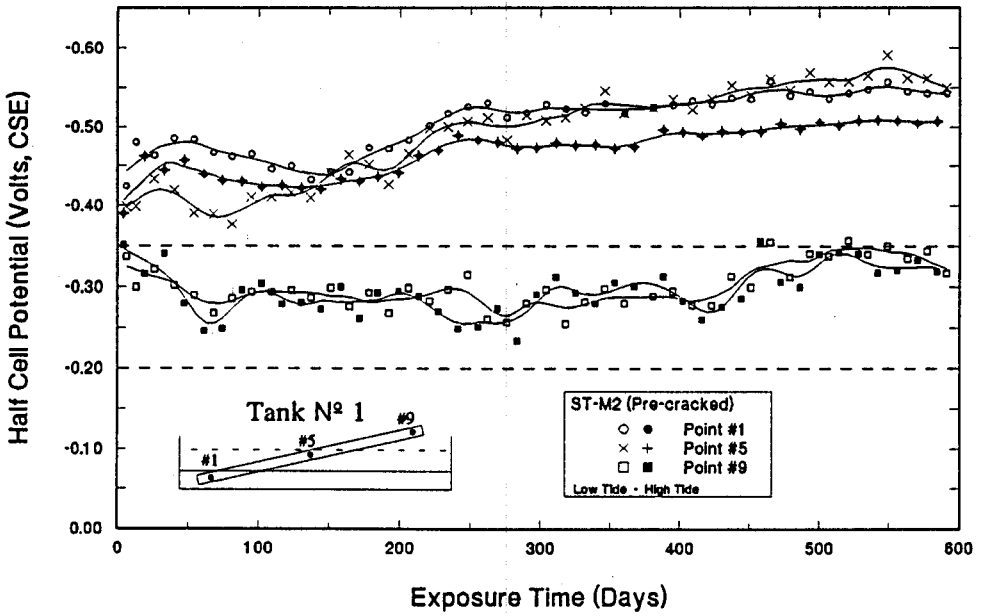


Figure 15.2 Half-Cell Potentials for Pre-cracked Beam

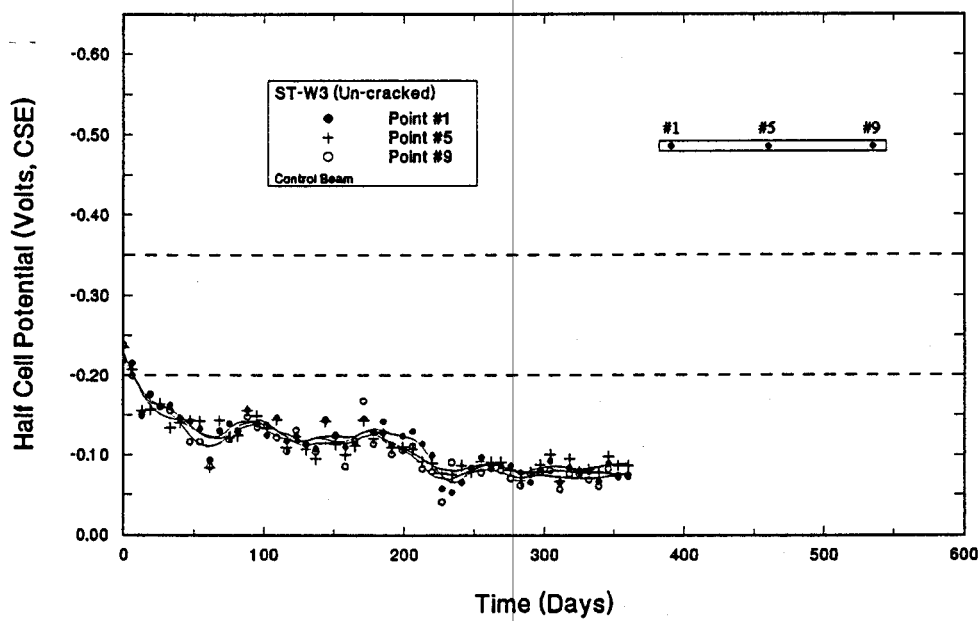


Figure 15.3 Half-Cell Potentials for Un-cracked Control Beam

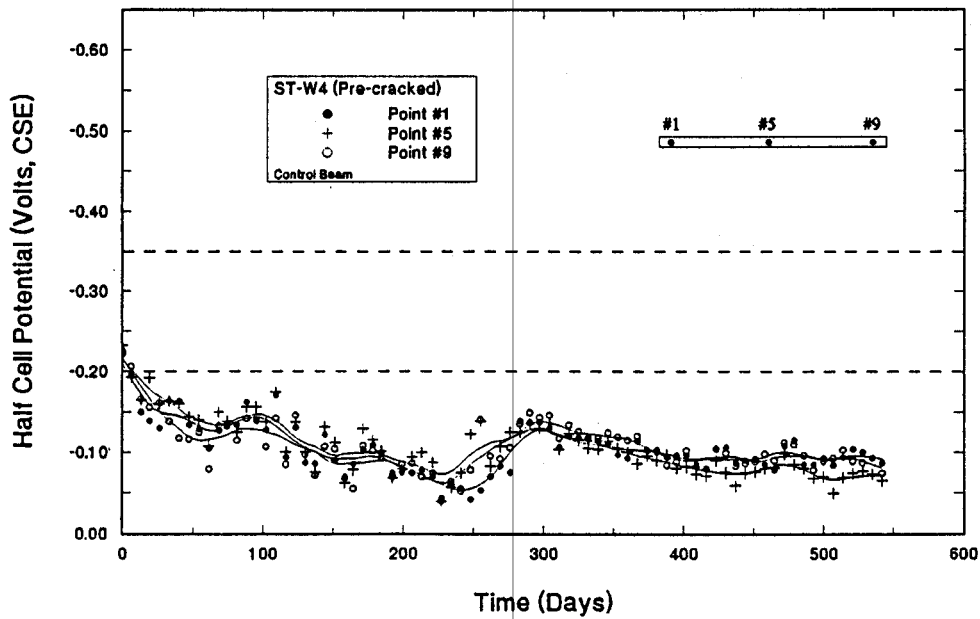


Figure 15.4 Half-Cell Potentials for Pre-cracked Control Beam

probability limit. This threshold was reached in pre-cracked specimens almost immediately (after 7 days). By contrast, un-cracked specimens reached this limit after 35 to 75 days.

The effect of tidal change is also evident in the same graphs. In general, absolute potential values measured at the 'splash' and permanently wet zones were higher, i.e. greater expectancy of corrosion during 'low' tides than during 'high' tides. This suggests that corrosion cells were more active when exposed to air.

In contrast to specimens exposed to saltwater, potentials measured on control beams (Figures 15.3 and 15.4) were always below, the threshold for low or 5 % probability of corrosion. This suggests that no corrosion cells formed in these specimens.

15.3 A.C. Impedance Measurements

A. C. impedance measurements provide quantitative results on the rate of corrosion of steel. The theory of operation is described elsewhere, e.g. Silverman, 1986 [15.3]. In essence, it consists of subjecting the embedded steel to harmonically induced currents and measuring the electrode potential response. This requires a more complicated apparatus which is detailed for example by Sagues, 1988 [15.4].

Since corrosion of steel was not expected to develop significantly within the first year of the study, A. C. impedance measurements were initiated after one year. Therefore, only four beams (two un-cracked and two pre-cracked) were tested. These measurements were used in conjunction with half-cell potentials for determining the sequence of testing of the steel pre-tensioned specimens.

Typical impedance measurements for steel specimens are presented in Figures 15.5 and 15.6 and correspond to the Nyquist's plot for two steel pretensioned specimens (one un-cracked and one pre-cracked) in the top part. Bode's plots of the impedance modulus vs. frequency (center) and phase angle vs. logarithm of frequency (bottom) are also presented in the same figures for completeness.

15.3.1 Discussion of Results

Results for A.C. impedance measurements are presented in a qualitative rather than quantitative manner. These provided additional information for establishing test sequence of the steel pre-tensioned specimens.

For analyzing impedance data, the curves corresponding to the Nyquist's plot (top of Figures 15.5 and 15.6) can be approximated, to a depressed semicircle, i.e. its center is

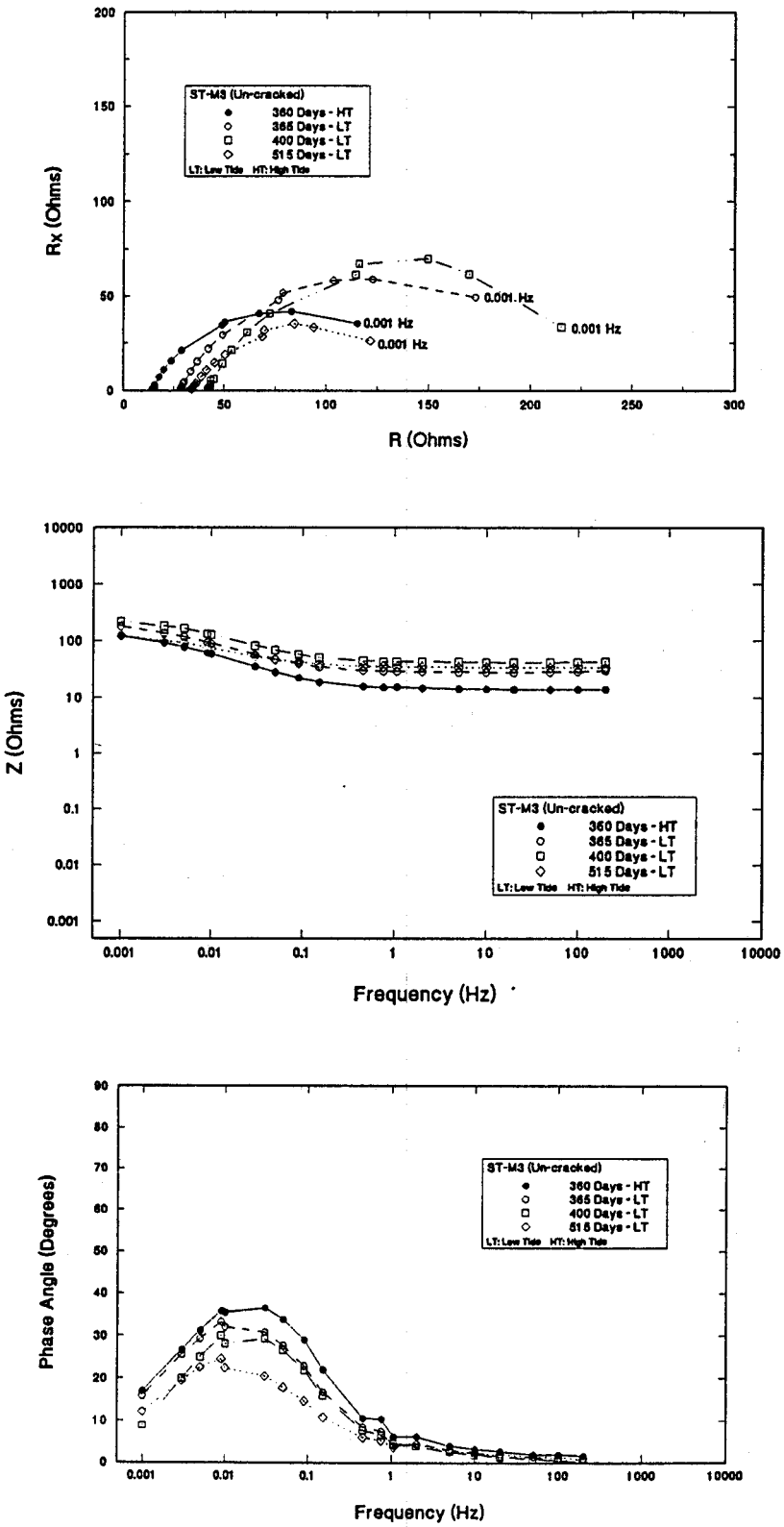


Figure 15.5 EIS Measurements for ST-M3

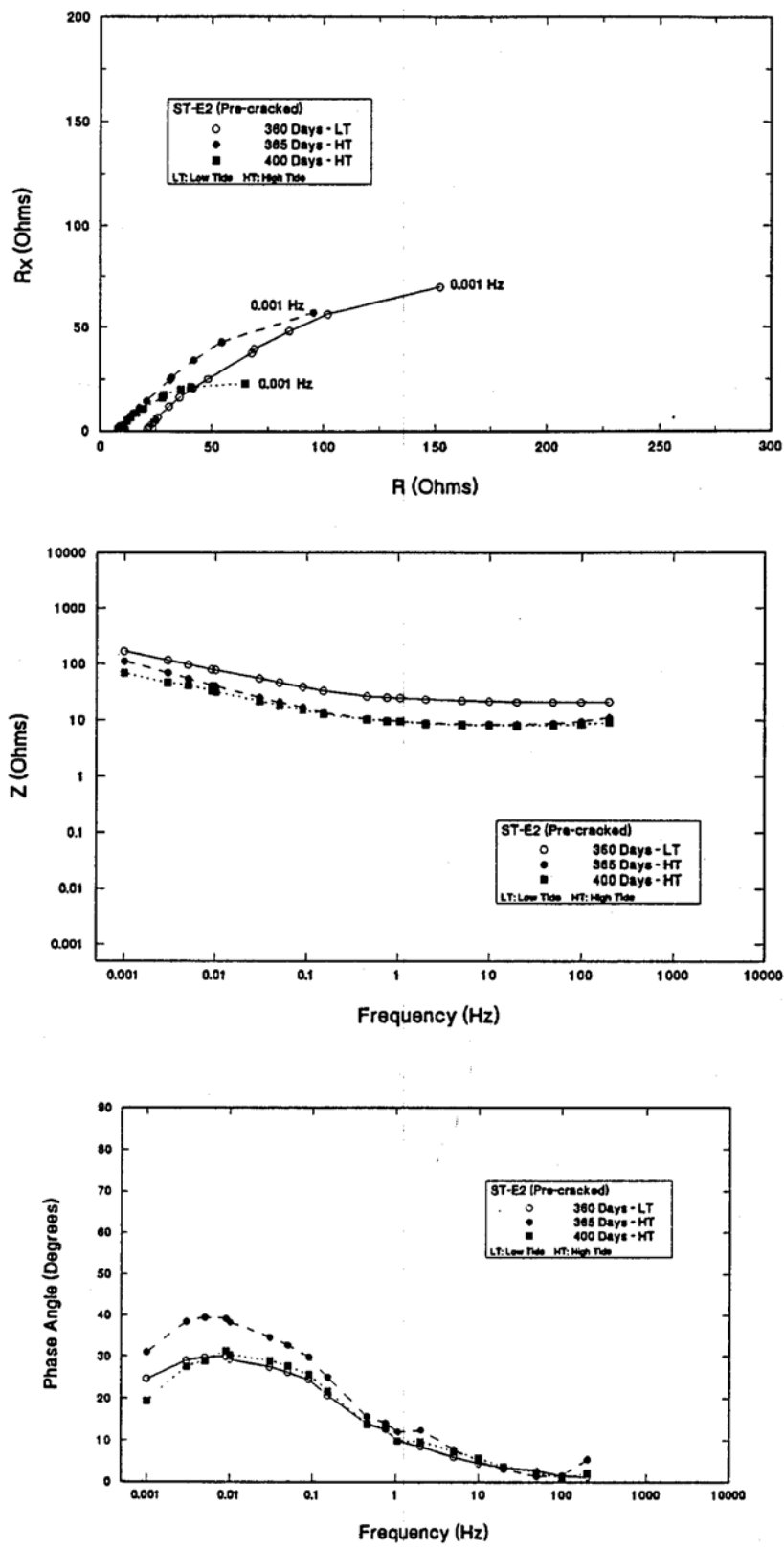


Figure 15.6 EIS Measurements for ST-E2

below the real axis. The corresponding diameter will be equivalent to the polarization resistance, R_p . By applying the Stern-Geary equation (Equation 15.1), this diameter can be related to the corrosion rate Aguilar, Sagues and Powers, 1990 [15.5].

$$I_{corr} = \frac{B}{R_p} \quad (15.1)$$

In Equation 15.1, B is the corrosion constant for iron (usually taken as 26 mV for active iron), hence the rate of dissolution (corrosion) will be inversely proportional to the diameter measured from the Nyquist's Plot. Accordingly, a larger diameter corresponds to a lower corrosion rate and vice-versa.

Inspection of Figures 15.5 and 15.6 show that, typically, diameters calculated for pre-cracked specimens are smaller than for un-cracked specimens, i.e. it displays a faster corrosion rate. Moreover, measurements taken during the same tide level at progressive times of exposure reveal an evident reduction in the Nyquist's plot diameter. However, diameters corresponding to measurements performed during 'low' tides led to larger diameters, i.e. lower corrosion rate, than those measured during 'high' tides. This is in contrast with half-cell potentials that were "more negative", i.e. higher probability of corrosion (see Section 15.2.1).

15.4 Resistivity Measurements

Electrical resistivity provides a measurement of capability of the concrete surrounding the reinforcement to conduct electric currents, and thus to support a corrosion process. In essence, it measures the change in alternating current applied between two pairs of electrodes coupled with the concrete (four-electrode method) using a soil resistance meter.

Resistivity measurements provide information on the probability of the rate of corrosion. However, these measurements are sensitive to the conditions under which they are made. Nonetheless, they can provide additional information to assist the interpretation of potential measurements. Table 15.2 presents resistivity thresholds for corrosion rates proposed by Colebrand [15.2]. Additionally, since underground corrosion is also affected by moisture, salt, and oxygen levels, Table 15.2 presents estimated corrosion rates of steel in soils proposed by Borgard, 1990 [15.6]. In both cases, a level of 10,000 0-cm seems to be a critical value of concrete resistivity to support severe corrosion.

In order to obtain information on the concrete surrounding the reinforcement, resistivity measurements were initiated after about 225 days. Only eleven out of a total of sixteen specimens were tested (five ST and six FG). Figures 15.7 and 15.8 show typical concrete resistivity measurements for steel and fiberglass specimens exposed to saltwater in Tank N⁴ 1.

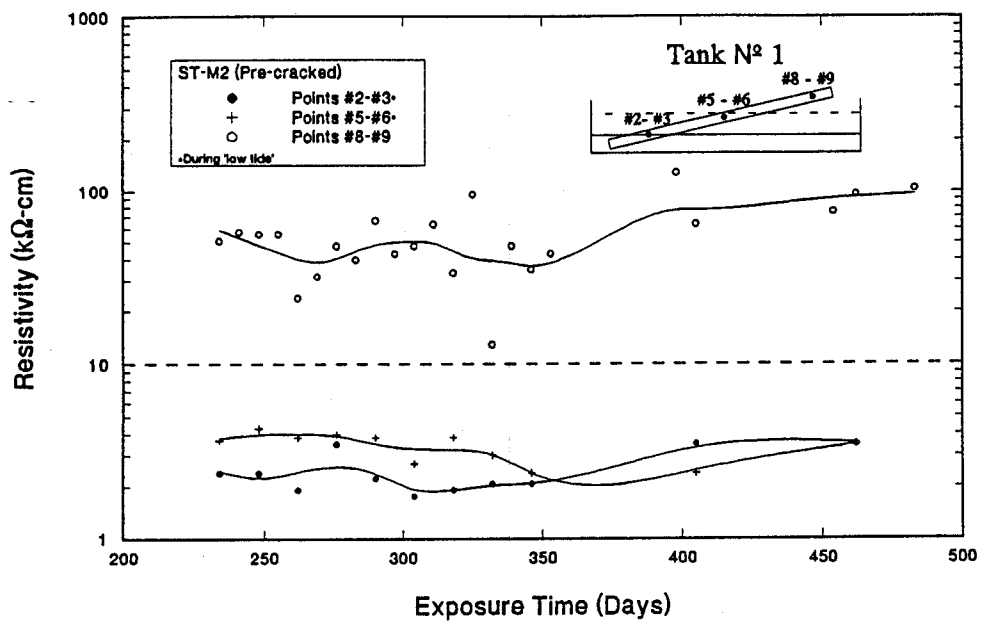


Figure 15.7 Concrete Resistivity for Pre-cracked Beam in Tank N° 1

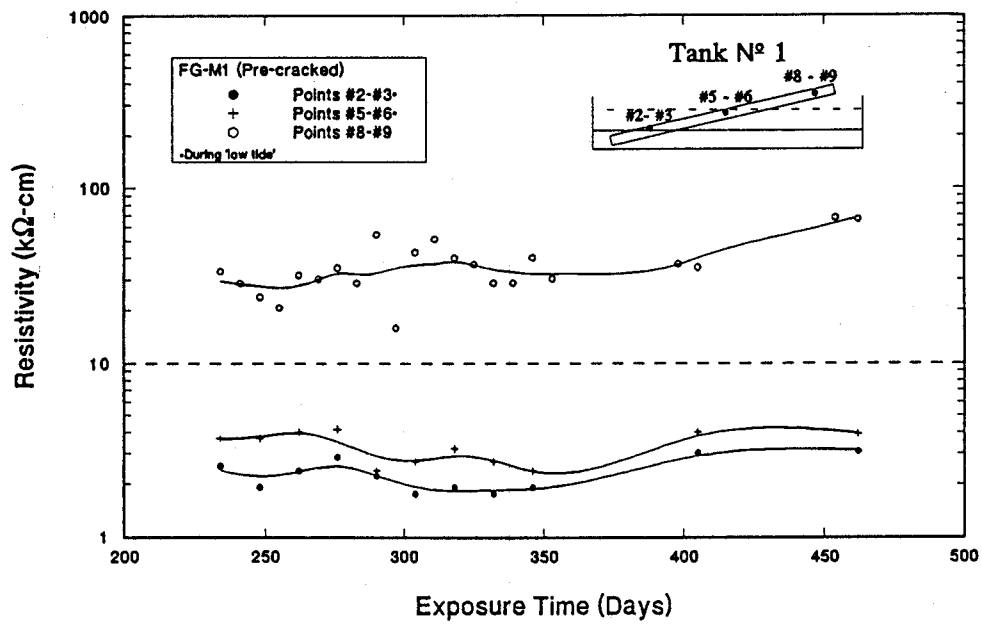


Figure 15.8 Concrete Resistivity for Pre-cracked Beam in Tank N° 1

Resistivity measurements are plotted for only three zones (#2-#3, #5-#6 and #8-#9), as for half-cell potentials. They corresponded also to the permanently submerged, 'splash' and the permanently dry zones, respectively (see Figure 14.2). Readings in the two first zones could be recorded only during low tide. A dashed line indicating a typical threshold value of 10 k Ω -cm (see Table 15.2) for concrete resistivity required for sustaining corrosion of steel, is included in the graphs.

Table 15.2 Different Concrete Resistivity Thresholds for Corrosion [15.2,15.6]

COLEBRAND		BORGARD	
Resistivity (k Ω -cm)	Probable Corrosion Rate (in Concrete)	Resistivity (k Ω -cm)	Anticipated Corrosion Activity (in Soils)
< 5	very high	< 2	severe
5 to 10	high	2 to 10	moderate
10 to 20	low to moderate	10 to 30	mild
> 20	low	> 30	unlikely

15.4.1 Discussion of Results

Since the mechanism of corrosion of glass is different from that of steel, i.e. electrochemical processes are unlikely to be involved, resistivity measurements provided the only information on its surrounding concrete.

The concrete resistivity at dry zones of beams in saltwater (see Figures 15.7 and 15.8) exceeded the corrosion threshold of 10 kg-cm, and therefore probable corrosion was low (see Table 15.2). By contrast, the concrete in the 'splash zone' had a resistivity below 10 k Ω -cm indicating that the probability of corrosion was high. Inspection of Figures 15.7 and 15.8 shows that the concrete for the steel and fiberglass specimens was in a very similar state.

15.5 Selection of Sequence for Testing

15.5.1 Sequence for Steel Pre-tensioned Specimens

The sequence of testing of the steel pretensioned beams was decided by their prevailing state of corrosion, i.e. those corroding the least were tested first. Initially, half-cell potential measurements provided the necessary information. However, since half-cell readings did not provide any indication of the corrosion rate, only probability of its onset, impedance and resistivity measurements were additionally considered.

Apart from electrical measurements, other factors were also considered in determining the basic sequence of testing. Since pre-cracked beams were expected to corrode faster, the last beam tested was pre-cracked. Additionally, un-cracked and pre-cracked beams were tested alternately to allow comparison of their relative response.

Tables 15.3 and 15.4 summarize the relative half-cell potentials for all beams prior to testing. The lowest reading in these tables identify the beams corroding the least. Inspection of these tables indicate that by and large the beam selected for testing had the lowest half-cell reading. The only exceptions relate to un-cracked specimens ST-E1 (the previous weeks' readings were lower) and ST-M1 (its half-cell reading of -0.414 mV was only marginally higher than ST-M3) in Table 15.3.

The selection of the last two un-cracked and pre-cracked beams in Table 15.3 and 15.4, i.e. ST-E3, ST-M3, ST-E2, ST-M2 on the basis of half-cell potentials were also borne out by the impedance measurements. Nyquist's plot diameters for these beams summarized in Tables 15.5 and 15.6 show that ST-M3 and ST-M2 had smaller diameters (195 and 67 Ohms) compared to ST-E3 and ST-E2 (383 and 107 Ohms), respectively. As noted earlier, smaller diameters indicate greater corrosion rates (see Equation 15.1). The sequence of testing of the steel pretensioned beams that was selected is summarized in Table 15.7.

15.5.2 Sequence for Fiberglass Pre-tensioned Specimens

Since the electrical measurements only related to steel, the fiberglass pre-tensioned specimens were selected at random. However, since the concrete cast on December 22, 1989, had a higher slump (see Table 4.2) more specimens corresponding to this cast date were left to be tested later. Tables 15.8 summarizes the sequence of fiberglass pre-tensioned beams tested.

Table 15.3 Half-Cell Potentials (mV) for Un-cracked Specimens

Beam	Months in Tank			
	1.5	6	12	18
ST-E1	-0.376	--	--	--
ST-M1	-0.324	-0.414	--	--
ST-E3 ¹	-0.419	-0.467	-0.423	--
ST-M3 ¹	-0.324	-0.412	-0.472	-0.616

¹ see Tables 15.5 and 15.6 for impedance measurements

Table 15.4 Half-Cell Potentials (mV) for Pre-cracked Specimens

Beam	Months in Tank			
	3	9	15	20
ST-M4	-0.346	--	--	--
ST-E4	-0.566	-0.487	--	--
ST-E2 ¹	-0.577	-0.507	-0.562	--
ST-M2 ¹	-0.430	-0.531	-0.571	-0.577

¹ see Tables 15.5 and 15.6 for impedance measurements

Table 15.5 Nyquist's Plot Diameters (ohms) for Un-Cracked Specimens

Beam	Days in Tank	
	365 ¹	515 ¹
ST-E3	383	--
ST-M3	195	113

¹ Measured during 'low' tide

Table 15.6 Nyquist's Plot Diameters (ohms) for Pre-Cracked Specimens

Beam	Days in Tank	
	400 ¹	515 ¹
ST-E2	107	--
ST-M2	67	58

¹ Measured during 'high' tide

Table 15.7 Sequence of Steel Pre-Tensioned Beams Tested

Beam	Cast Date	Tank	Remark	Test Date	Months in Tank
ST-W1	12/22/89	Control	U	03/14/90	--
ST-E1	12/22/89	Nº 1	U	03/14/90	1.5
ST-M4	12/28/89	Nº 2	P	05/04/90	3
ST-M1	12/22/89	Nº 1	U	08/01/90	6
ST-E4	12/28/89	Nº 2	P	11/01/90	9
ST-W3	12/28/89	Control	U	02/05/91	--
ST-E3	12/28/89	Nº 2	U	02/05/91	12
ST-E2	12/22/89	Nº 1	P	05/02/91	15
ST-M3	12/28/89	Nº 2	U	08/01/91	18
ST-W4	12/28/89	Control	C	08/09/91	--
ST-M2	12/22/89	Nº 1	P	09/23/91	20
ST-W2	12/22/89	Control	P	09/23/91	--

Notes:

- 1 P — Pre-cracked specimen; U — Un-cracked specimen
- 2 Extra beam ST-W4 tested as control

Table 15.8 Sequence of Fiberglass Pre-tensioned Beams Tested

Beam	Cast Date	Tank	Remark	Test Date	Months in Tank
FG-M2	12/22/89	Control	U	03/14/90	--
FG-E2	12/22/89	Nº 1	U	03/14/90	1.5
FG-E6	06/06/90	Nº 2	P	10/04/90	3
FG-M6	06/06/90	Nº 2	U	12/31/90	6
FG-W3	12/28/89	Control	U	02/05/91	--
FG-W6	06/06/90	Nº 2	P	08/09/91	9
FG-E3	12/28/89	Nº 2	U	02/05/91	12
FG-M1	12/22/89	Nº 1	P	05/02/91	15
FG-W2	12/22/89	Nº 1	U	08/01/91	18
FG-M3	06/06/90	Nº 2	P	11/01/90	9
FG-E1	12/22/89	Nº 1	P	09/23/91	20
FG-W1	12/22/89	Control	P	09/23/91	--

Notes:

- 1 P — Pre-cracked specimen; U — Un-cracked specimen
- 2 Extra beam FG-W6 used as a repeat specimen for 9 month pre-crack test

16. ULTIMATE CAPACITY TESTS

16.1 Introduction

This chapter presents results of ultimate load tests on fiberglass and steel pre-tensioned specimens that were part of the durability study. A total of twenty four beams - twelve fiberglass and twelve steel - were tested over a period of almost two years.

The set up, instrumentation and procedure for testing is described in Section 16.2. Since the beams tested were identical in all respects other than exposure, many of the test results were similar. Consequently, individual results are not presented. Instead, results for groups of un-cracked, pre-cracked and control steel and fiberglass beams are presented in Section 16.3 to help identify any underlying trends.

The main objective of the tests was to assess the reduction, if any, in the strength of steel and fiberglass pre-tensioned beams as a result of degradation of strands in salt water. Since concrete's strength is adversely affected in salt water, e.g. Gjorv, 1971; Grahams and Backstrom, 1975; Kato and Ohtsuki, 1984 [16.1-16.3], the effect of wet/dry cycles on the compressive strength of concrete is examined in Section 16.4. Additionally, two series of pull out tests were conducted to examine the effect of wet/dry cycles on bond. The results from these tests are summarized in Section 16.5. The implications of the test results on the relative durability of fiberglass and steel is discussed in Section 16.6.

16.2 Experimental Program

The ultimate bending capacity of eight steel and eight fiberglass pre-tensioned beams exposed to wet/dry cycles in salt water were compared against identical control beams that were unexposed. The sequence of testing of the exposed specimens was based on corrosion measurements as described in Chapter 15. In essence, it attempted to ensure that the beams corroding the most were left to be tested at the end. The difference in capacity between the exposed and unexposed beams provided a measure of the deterioration in strength due to corrosion.

16.2.1 Test Set Up

The ultimate capacity tests were performed at the Structures Laboratory at the University of South Florida, Tampa, Florida. The set up was identical to that used in the flexure tests with the exception that the two point loads were a foot apart. Typical set ups for testing the steel and fiberglass beams are shown in Plate 16.1.

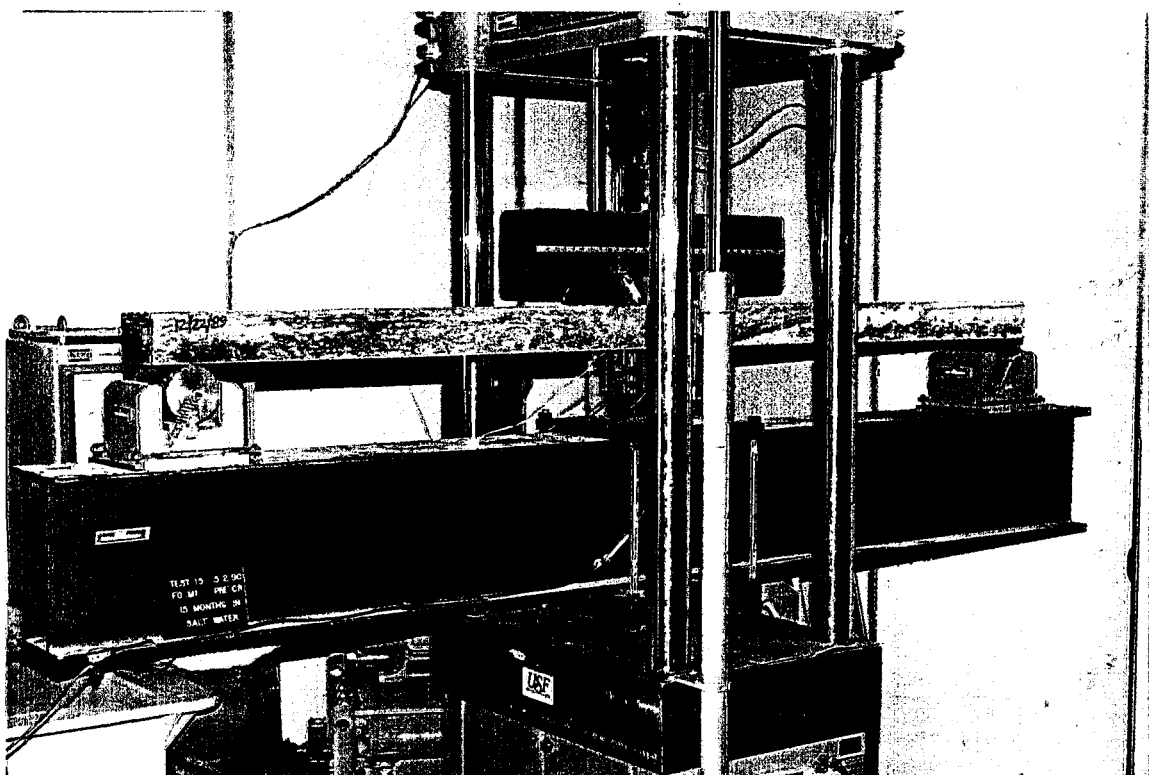
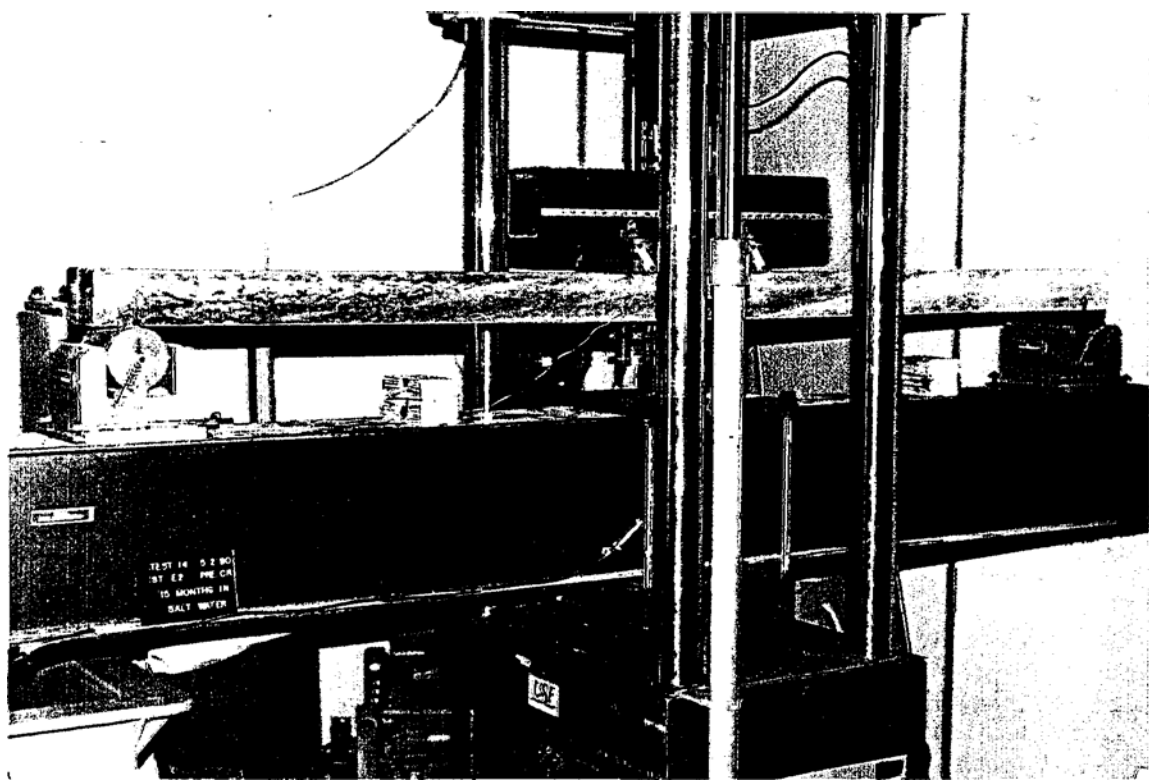


Plate 16.1

(top) Typical set up for steel pretensioned beams
(btm) Typical set up for fiberglass pretensioned beam

The beams were supported 8 ft apart on rollers that were screwed on to its box frame support. The load was applied to the specimens by a 6 in. x 6 in. x 3/8 in. hollow section that was attached to the MTS machine by a swivel head assembly. Lead plates were inserted between the two loading points and the concrete surface to ensure an even load distribution.

The loads were applied using an MTS closed loop electro-hydraulic system under load control mode. The total capacity of the system was 200 kips but in the tests the range was limited to 10% of this load, i.e. 20 kips. The load increments were 1-1.5% of this value.

16.2.2 Instrumentation

Concrete strains and deflections were monitored at midspan using strain gages and LVDTs. Two concrete gages (model PL-60-1L, Gage factor 2.11, from Texas Measurements) were symmetrically attached to the top surface of the beam on either side of the center line. A metal plate was attached to the top surface of the beam at midspan using epoxy. Two LVDTs, model CDP-50 (with a maximum stroke of 2 in.), were placed under the projection of this plate on either side to measure deflection. Average values of concrete strains and deflections were used in all the results presented.

All strain gage and LVDT data was recorded using a P-3500 Strain Indicator Box in conjunction with SB-10 Switch and Balance Unit, both supplied by Micro Measurements Group.

16.2.3 Test Procedure

Prior to the actual test, the beams were pre-loaded to about 5 % of its ultimate load to stabilize them and also to prevent any possible twisting. The strain gages and LVDTs connected to the Switch and Balance Unit were then zeroed. The static load was applied in increment of 1 % of the total load (2001bs) until 15 % of the total load (3,000 lbs) was reached. Above this value increments were made at 0.5%, depending on the response of individual beams. For each load increment, deflection and concrete strain were recorded.

Initially, the beams were loaded to destruction; in subsequent tests, however, they were deemed to have failed when the concrete strain exceeded 2400 micro-strains to facilitate drilling for chloride samples. At such strains, the deflection generally exceeded an inch (see load vs deflection response in Tables 16.2-16.4). Cracking and ultimate load were recorded for each beam and additional information about the failure mode and cracking pattern were taken.

16.3 Test Results

16.3.1 Steel Pre-tensioned Beams

A summary of the measured eccentricities, concrete strength, reinforcing index, code based cracking and failure loads for the twelve beams tested is presented in Table 16.1. The measured eccentricities varied because of the slope in the structural floor (this problem was corrected for specimens cast later as shown in Plate 4.6). Inspection of this table shows that all the beams are over-reinforced having reinforcing indices ranging from 0.268-0.315 that exceed the 0.360, limit also listed in the same table. The cracking load ranges from 1.50 kips to 1.68 kips. This was calculated assuming a prestress loss of 25 % of the jacking force, P_j , that was found from the beam study (Section 5.4). The predicted failure load was calculated using ACI equations for over-reinforced sections. The calculated values ranged from 2.94 kips to 3.43 kips due to differing eccentricities and concrete strengths.

The results from the ultimate load tests for the un-cracked beams, pre-cracked and control beams are summarized in Tables 16.2-16.4, respectively. As noted earlier, these relate to loads corresponding to a strain of 2400 $\mu\epsilon$ at which the test was stopped. Inspection of these tables shows that of the twelve beams tested, all but three failed in compression as can be anticipated in view of the high reinforcing index. Typical compression failure modes are shown in Plate 16.2. Three beams, including a pre-cracked beam (ST-M2) and two control specimens (ST-W4 and ST-W2) failed in shear. This may have been due to honeycombing in the specimens that was detected in a similar failure for a fiberglass beam (see Plate 16.3 and Section 17.2.2.2).

Excepting for the three beams that failed in shear, the magnitude of the failure loads for the seven remaining beams ranged between 3-3.19 kips with one beam failing of 3.4 kips. These values are in broad agreement with the failure loads ranging from 2.94-3.43 kips predicted by the ACI equations (see Table 16.1). For the un-cracked beams (Table 16.2) the maximum deflection varied from 1.11-1.44 in. The corresponding values for the precracked and control beams (see Tables 16.3 and 16.4) were respectively 0.78-1.46 in. and 1.30-1.67 in. Whereas pre-cracked beams subjected to wet/dry cycles deflected more than their un-cracked counterparts, no such pattern is immediately evident for the control beams. For example, larger deflections were recorded for the un-cracked beams ST-W 1 and ST-W3 than for the pre-cracked beams ST-W2 and ST-W4. This is probably the result of greater eccentricities (see Table 16.1) and correspondingly larger creep effects.

Load-deflection curves for the sets of un-cracked, pre-cracked and control beams appear in Figures 16.1-16.3, respectively. These provide a measure of the elastic stiffness of the beams. Beams tested later should show greater deflection because of larger camber due to creep. However, creep effects were variable since the eccentricities and concrete strengths for all the beams differed (see Table 16.1). Since three of the beams failed in shear, their load deflection curves are separately plotted in Figure 16.4.

Table 16.1 Details of Steel Beams Tested

Beam	Cast Date	f (ksi)	01 (in)	W _P	0.360, (kips)	(kips)
Un-cracked						
ST-E1	12/22/89	6.54	0.72	0.72	0.277	0.260
ST-M1	12/22/89	6.05	0.75	0.84	0.299	0.269
ST-E3	12/28/89	6.17	0.74	0.91	0.294	0.267
ST-M3	12/28/89	6.38	0.73	0.91	0.283	0.263
Pre-cracked						
ST-M4	12/28/89	6.26	0.74	0.72	0.289	0.265
ST-E4	12/28/89	6.75	0.71	0.77	0.268	0.257
ST-E2	12/22/89	5.74	0.76	0.88	0.315	0.275
ST-M2	12/22/89	5.62	0.77	0.91	0.322	0.277
Control						
ST-W1	12/22/89	6.54	0.72	0.84	0.277	0.260
ST-W3	12/28/89	6.16	0.74	0.91	0.294	0.267
ST-W4(P)	12/28/89	6.27	0.74	0.72	0.292	0.265
ST-W2(P)	12/22/89	6.08	0.75	0.97	0.297	0.269

Notes:

1 Measured eccentricities used in calculations

2 P_j = 20 kips; P_e = 0.75P_j assumed

3 P_{cr} = 2 M_{cr}/a, using f_r = 7.5√f'_c; a = 3.5 ft.

4 P_u = 2 M_u/a where M_u = f'_c bd² (0.36 β₁ - 0.08 β₁2)

5 cc is clear cover

Table 16.2 Ultimate Results for Steel Beams

Beam	Cast Date	Tested After (mth)	F'_c (ksi)	Ultimate ²		Failure Mode
				Load (kips)	Defl. (in)	
ST-E1	12/22/89	1.5	6.54	3.00	1.11	Compression
ST-M1	12/22/89	6	6.05	3.09	1.44	Compression
ST-E3	12/28/89	12	6.17	3.19	1.41	Compression
ST-M3	12/28/89	18	6.38	3.16	1.26	Compression

Table 16.3 Ultimate Results for Pre-cracked Steel Beams (in salt water)

Beam	Cast Date	Tested After (mth)	F'_c (ksi)	Ultimate ²		Failure Mode
				Load (kips)	Defl. (in)	
ST-M4	12/28/89	3	6.26	3.06	1.37	Compression
ST-E4	12/28/89	9	6.75	3.08	1.41	Compression
ST-E2	12/22/89	15	5.74	3.40	1.46	Compression
ST-M2	12/22/89	20	5.62	2.40	0.78	Shear

Table 16.4 Ultimate Results for Control Steel Beams

Beam	Cast Date	Tested After (mth)	F'_c (ksi)	Ultimate ²		Failure Mode
				Load (kips)	Defl. (in)	
ST-W1	12/22/89	1.5	6.54	3.12	1.67	Compression
ST-W3	12/28/89	12	6.16	3.07	1.47	Compression
ST-W4	12/28/89	18	6.27	2.62	1.34	Shear
ST-W2	12/22/89	20	6.08	2.86	1.30	Shear

¹12/22/89 Tank 1; 12/28/89 Tank 2² For 2400 $\mu\epsilon$ concrete strain or actual failure

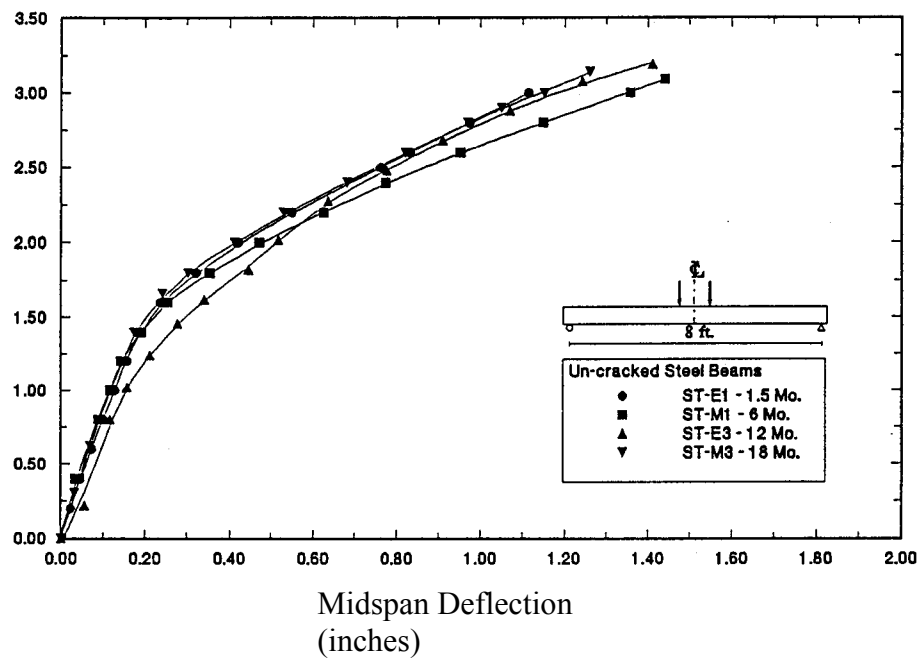


Figure 16.1 Load-Deflection for Un-cracked Steel Beams

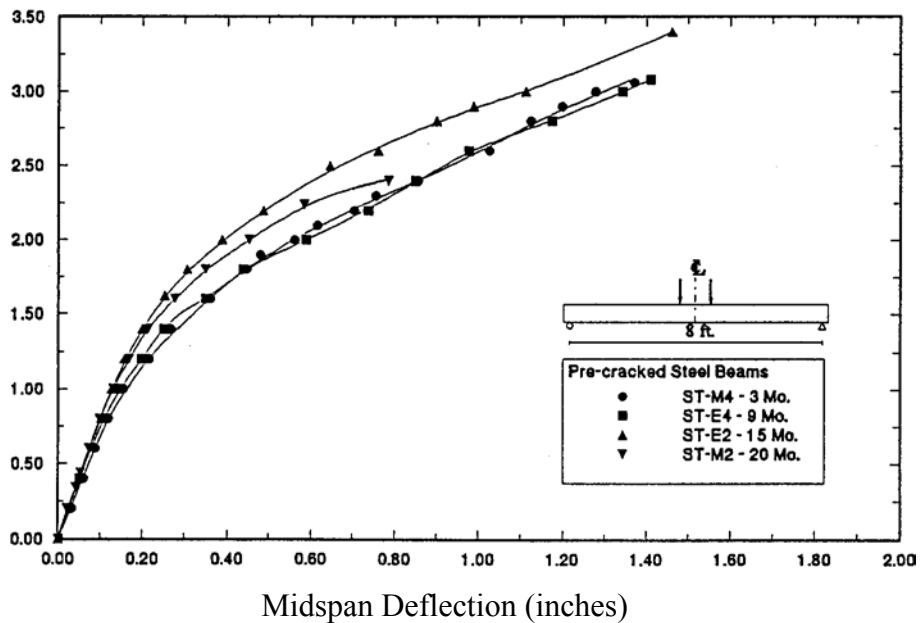


Figure 16.2 Load-Deflection for Pre-cracked Steel Beams

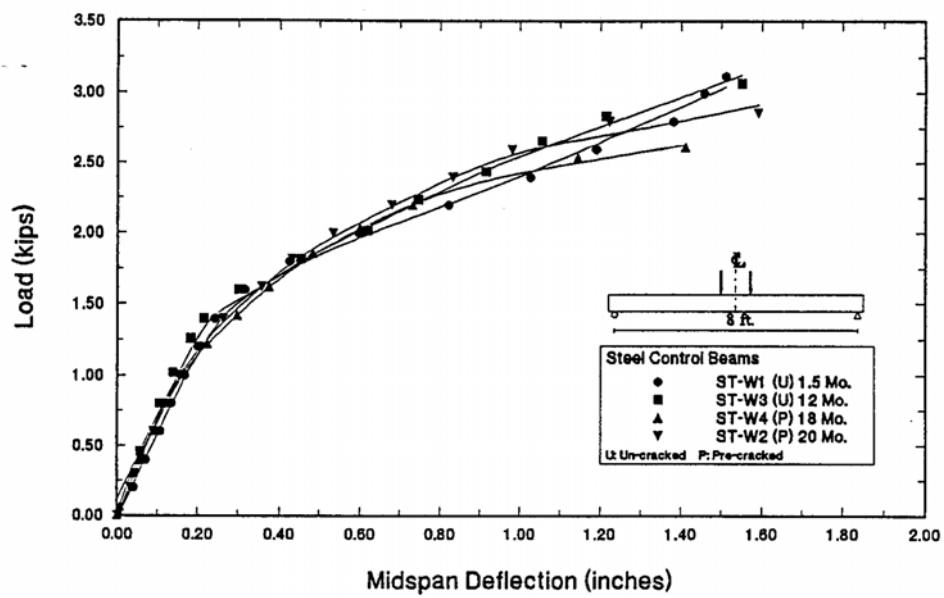


Figure 16.3 Load-Deflection for Control Steel Beams

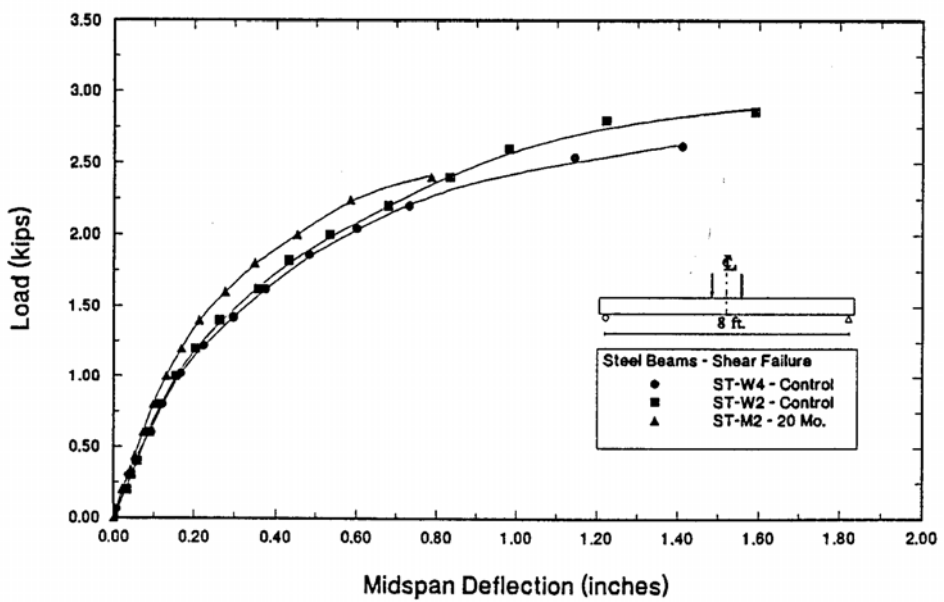


Figure 16.4 Load-Deflection for Steel Beams — Shear Failure

By and large there was little difference in the ultimate loads for un-cracked and pre-cracked beams. This is evident from Figure 16.5 which plots the variation in ultimate load with time for all twelve beams tested. Therefore, it can be concluded that after 20 months, corrosion had relatively little effect on the strength of steel pre-tensioned beams.

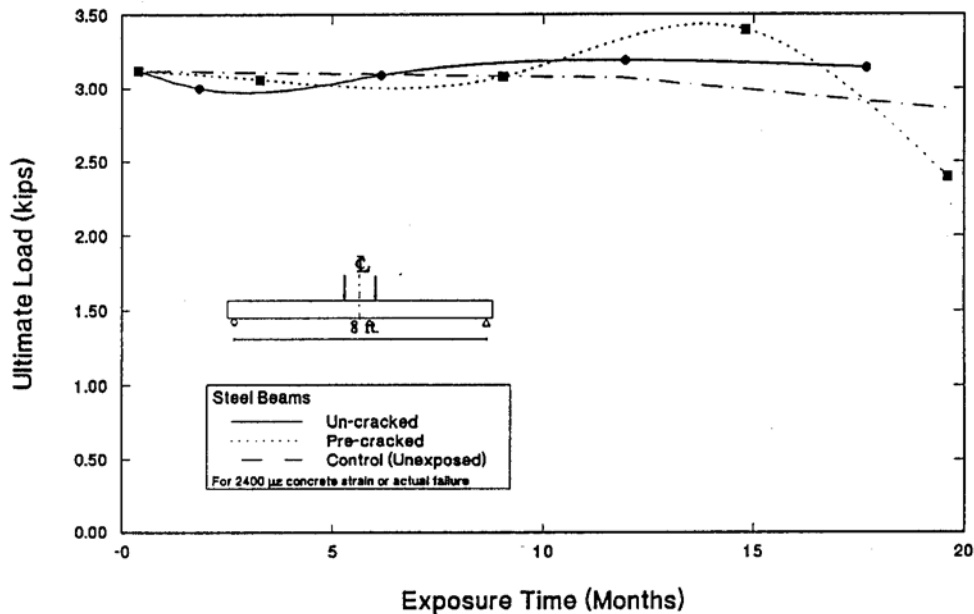


Figure 16.5 Load Variation Relative to Time for Steel Beams

16.3.2 Fiberglass Pre-tensioned Beams

Whereas the failure mode for steel pre-tensioned beams can be predicted on the basis of its reinforcing index, no similar criteria is currently available for fiberglass pre-tensioned beams. On the basis of the tests and comparisons reported in Chapter 7, a criterion for identifying over-reinforced fiberglass was proposed by Sun, 1991 [16.4]. This defines a beam as over-reinforced if the depth of the neutral axis (c) exceeds 35% of the effective depth (d). In essence, this reflects a reinforcing index of $0.3\beta_1$. This criteria is used to identify the failure mode in the fiberglass pre-tensioned beams.

Details of the twelve fiberglass beams tested are summarized in Table 16.5. As for the steel pretensioned beams, the effective prestress was based on losses determined from the beam study. This was taken as 17% of the jacking stress (Section 5.4). Inspection of Table 16.5 indicates that all the beams are over reinforced since c/d values of 0.37-0.40 exceed the 0.35 the maximum limit proposed.

Table 16.5 Details of Fiberglass Beams

Beam	Cast Date	F'_c (ksi)	β_1	P_j (kips)	cc (in)	c/d	$0.3\beta_1$	P_{cr} (kis)	P (kips)
Un-cracked									
FG-E2	12/22/89	6.54	0.72	15.7	0.81	0.38	0.217	1.48	2.77
FG-M6	06/06/90	6.30	0.74	17.7	0.79	0.39	0.221	1.58	2.67
FG-E3	12/28/89	6.17	0.74	16.5	0.69	0.38	0.222	1.43	2.45
FG-W2	12/22/89	6.05	0.75	15.7	0.64	0.38	0.224	1.34	2.33
Pre-cracked									
FG-E6	06/06/90	6.68	0.72	17.7	0.93	0.38	0.215	1.70	3.05
FG-M3	12/28/89	6.75	0.71	16.5	0.67	0.37	0.214	1.44	2.55
FG-W6	06/06/90	6.69	0.72	17.7	0.68	0.37	0.215	1.51	2.56
FG-M1	12/22/89	5.74	0.76	16.3	0.61	0.39	0.229	1.34	2.20
FG-E1	12/22/89	5.62	0.77	16.3	0.81	0.40	0.231	1.48	2.51
Control									
FG-M2	12/22/89	6.54	0.72	15.7	0.63	0.37	0.217	1.35	2.43
FG-W3	12/28/89	6.16	0.74	16.5	0.64	0.38	0.223	1.39	2.36
FG-W1 (P)	12/22/89	6.08	0.75	16.3	0.62	0.38	0.224	1.36	2.30

Notes:

1 Measured eccentricities used in calculations ; cc is clear cover

2 $P_j = 20$ kips; $P_e = 0.83 P_j$

3 $P_{cr} = 2 M_{cr}/a$, using $f_r = 7.5 \sqrt{f'_c}$ and $a = 3.5$ ft.

4 $P_u = 2 M_u/a$ where $M_u = f'_c bd^2 (0.3 \beta, - 0.055 \beta_1^2)$

$$5 \quad f_{fgu} = f'_{fg} \left(1 - \frac{0.65}{\beta_1} \rho_p \frac{f'_{fg}}{f'_c} \right)$$

Thus, a compression mode of failure is predicted. Cracking and failure loads for these beams range from 1.34-1.70 kips and 2.20-3.05 kips respectively. The failure stress in the fiberglass strands was determined using an equation proposed by Sun, 1991 that is based on a parametric study using non-linear finite element analysis. As for the steel pretensioned beams, differences in the failure loads and cracking moments are due to variations in concrete strength and eccentricity in the beams.

A summary of the ultimate load results is presented in Tables 16.6-16.8. Of the twelve beams tested, half failed in the compression mode as expected (see Plate 16.2). Significantly, all three control beams, FG-M2, FG-W3 and FG-W 1 (see Table 16.8) failed in this mode and there was no noticeable reduction in the ultimate capacity. Of the remaining six beams, two failed in shear (un-cracked beam FG-E3 and pre-cracked beam FG-W6), as shown in Plate 16.3, and four others (un-cracked beam FG-W2, pre-cracked beams FG-M3, FG-M1 and FG-E1) in a new mode that is identified here as the corrosion mode. This is shown in Plates 16.3 and 16.4. In this type of failure, a crack propagates at the middle of the beam from the tension zone and moves up to split the beam in two. This was not a violent compression type of failure but one in which the beams failed as if it were un-reinforced, i.e. the fiberglass or its bond with concrete had been totally destroyed. Additional tests conducted on the beams that failed in the corrosion mode are reported in the next section.

The ultimate capacities of the first two un-cracked beams tested after 1.5 months and 6 months were respectively 2.88 kips and 2.79 kips (Table 16.6). The third beam tested after a year failed in shear at a load of 1.32 kips. Some evidence of honeycombing was observed in the section where failure initiated when the beam was cut open for carbonation tests (see Section 17.2.2.2). As noted already, the last un-cracked beam failed in the corrosion mode.

Excepting for the first pre-cracked beam tested after 3 months in salt water, all the remaining beams failed in a corrosion mode. Since this failure was unexpected an additional beam, FG-W6, was also tested after 9 months. This beam did not however fail in a corrosion mode but in a shear mode (see Table 16.7). Since this beam was cast at a different time, this appears to indicate that the concrete used in the latter case offered better protection. Additionally, the fiberglass strands used were not pultruded by Owens-Corning, but by Polygon (see Section 2.4-2.5). It may be recalled that an additional coating of resin was added to provide a smooth finish in these rods. This resin appears to have provided additional protection for the fiberglass strands in the concrete.

The load-deflection curves for the un-cracked, pre-cracked and control beams are plotted in Figures 16.6-16.8. Additionally, separate plots are presented for the beams that failed in the corrosion mode. These are shown in Figure 16.9. As for the beam tests, the fiberglass beams showed greater flexibility than the steel pretensioned beams especially after cracking (see Tables 16.2-16.8 and also compare Figures 16.1-16.3 for the steel pretensioned beams with Figures 16.6-16.8 for the fiberglass beams).

Table 16.6 Ultimate Results for Un-cracked Fiberglass Beams (in salt water)

Beam	Cast ¹ Date	Tested After (mth)	F'_c (ksi)	P_{cr} (kips)	Ultimate ²		Failure Mode
					Load (kips)	Defl. (in)	
FG-E2	12/22/89	1.5	6.54	1.61	2.88	1.98	Compression
FG-M6	06/06/90	6	6.30	1.74	2.79	1.57	Compression
FG-E3	12/28/89	12	6.17	1.66	1.32	0.84	Shear
FG-W2	12/22/89	18	6.05	1.59	--	--	Corrosion

Table 16.7 Ultimate Results for Pre-cracked Fiberglass Beams (in salt water)

Beam	Cast ¹ Date	Tested After (mth)	F'_c (ksi)	P_{cr} (kips)	Ultimate ²		Failure Mode
					Load (kips)	Defl. (in)	
FG-E6	06/06/90	3	6.68	1.75	3.03	1.82	Compression
FG-M3	12/28/89	9	6.75	1.67	0.40	0.06 ³	Corrosion
FG-W6	06/06/90		6.69	1.75	2.02	1.64	Shear
FG-M1	12/22/89	15	5.74	1.62	0.42	0.06 ³	Corrosion
FG-E1	12/22/89	20	5.62	1.62	0.88	0.29	Corrosion

Table 16.8 Ultimate Results for Control Fiberglass Beams

Beam	Cast ¹ Date	Tested After (mth)	F'_c (ksi)	P_{cr} (kips)	Ultimate ²		Failure Mode
					Load (kips)	Defl. (in)	
FG-M2	12/22/89	1.5	6.54	1.61	2.45	2.02	Compression
FG-W3	12/28/89	12	6.16	1.65	2.34	1.45	Compression
FG-W1	12/22/89	20	6.08	1.63	2.22	1.70	Compression

¹ 12/22/89 Tank 1; 12/28/89 and 06/06/90 Tank 2

² For 2400 [,e concrete strain or actual failure

³ Estimated

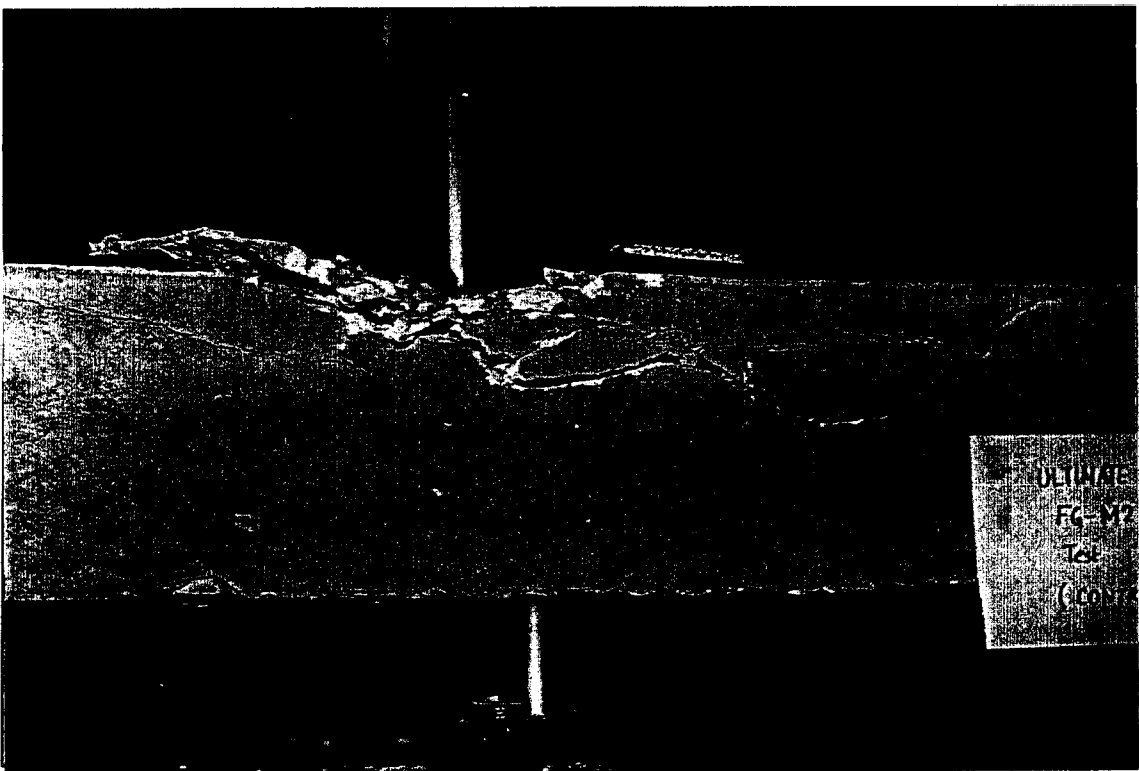
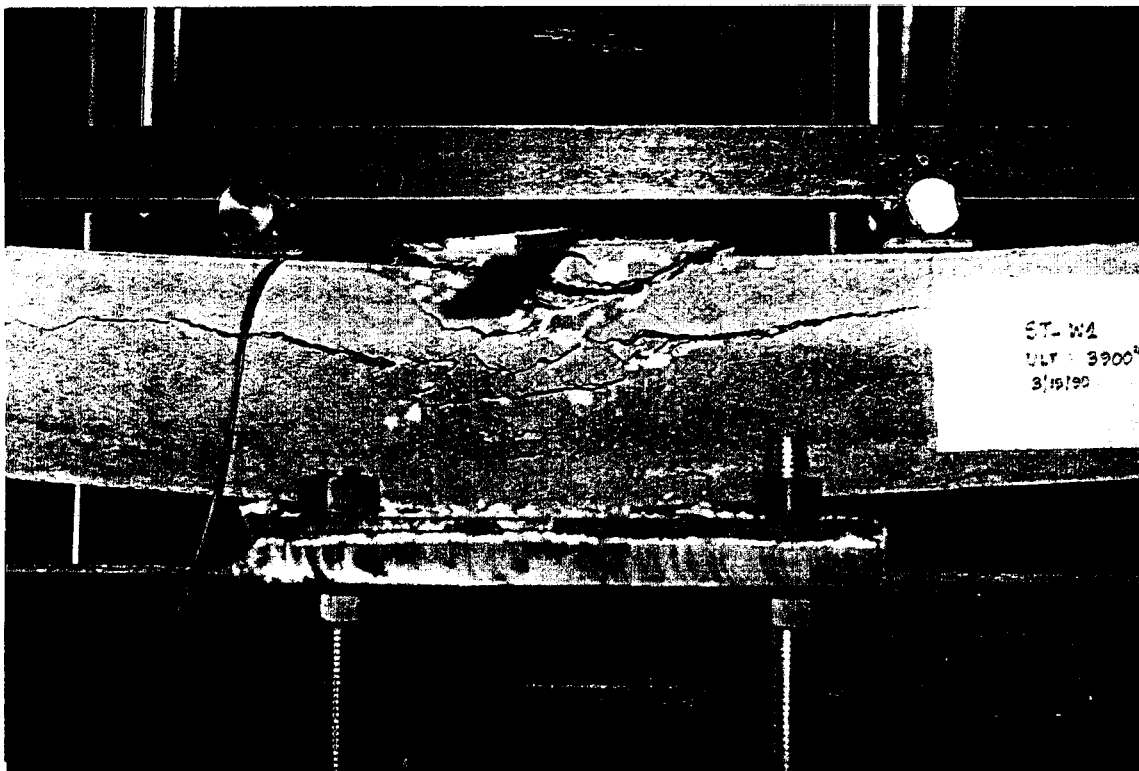


Plate 16.2 (top) Compression failure mode in steel beam
(btm) Compression failure mode in fiberglass beam

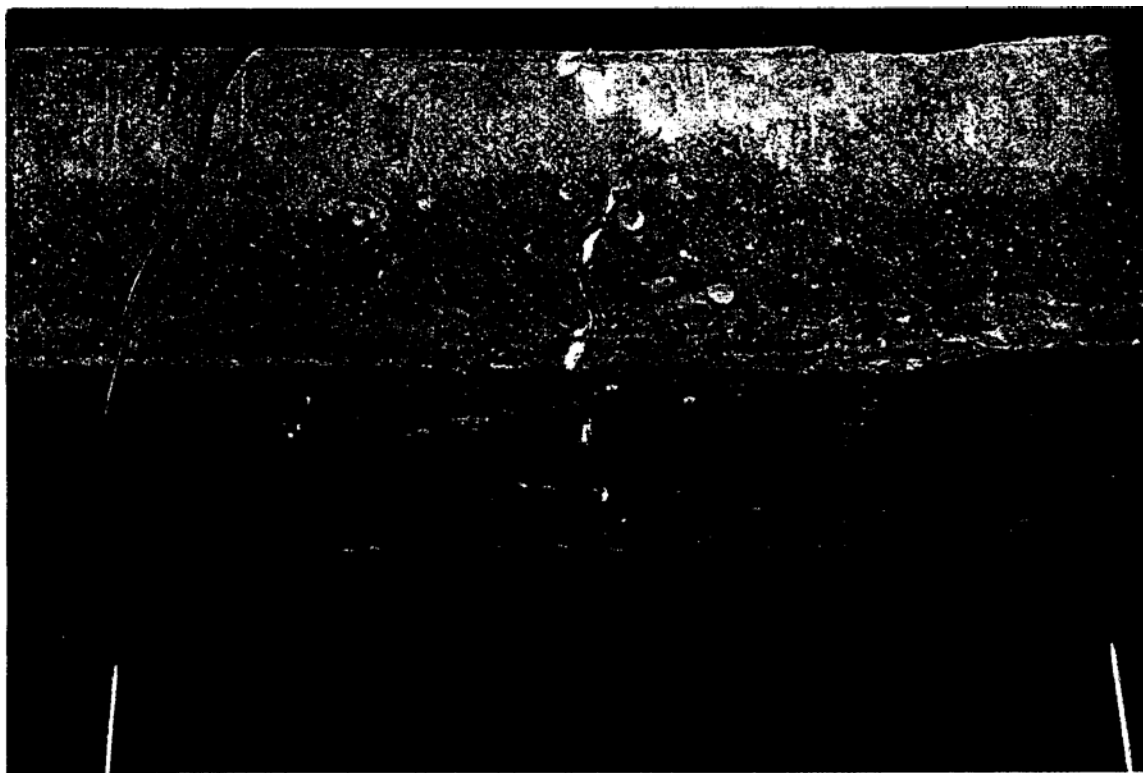


Plate 16.3 (top) Shear failure mode in fiberglass beam
(btm) Corrosion failure mode in fiberglass beam

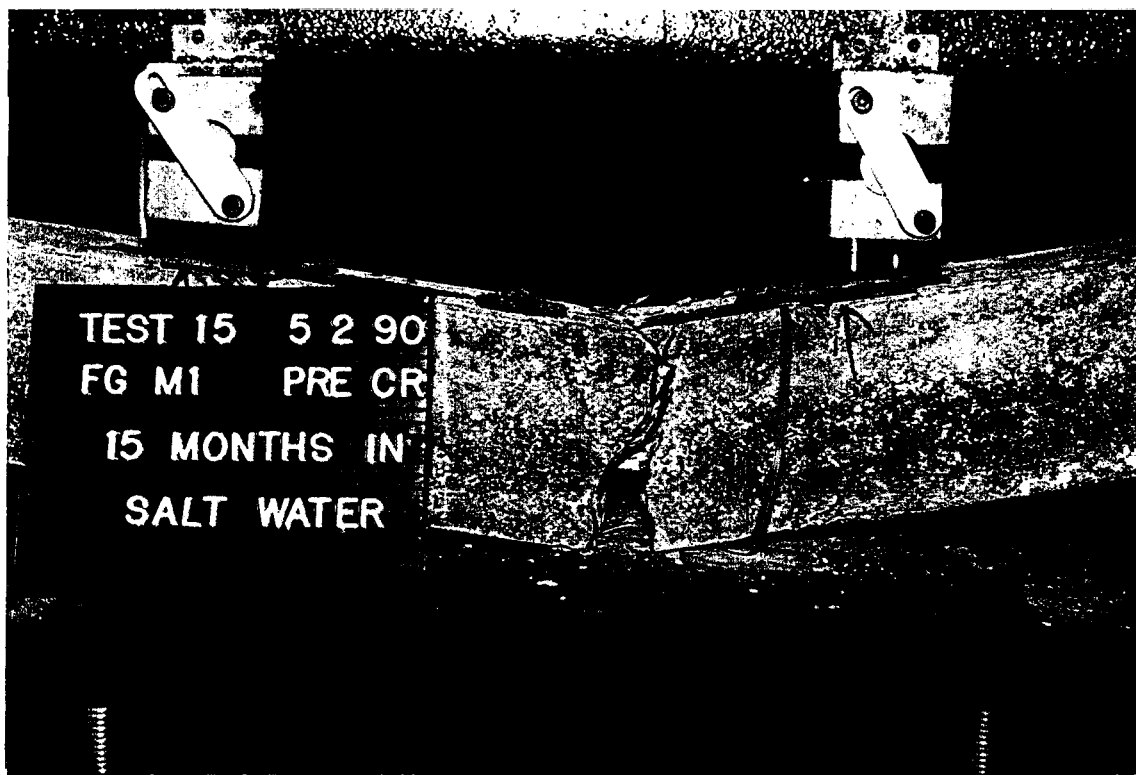


Plate 16.4 (top) Corrosion failure in pre-cracked fiberglass beam
(btm) Close up of failure

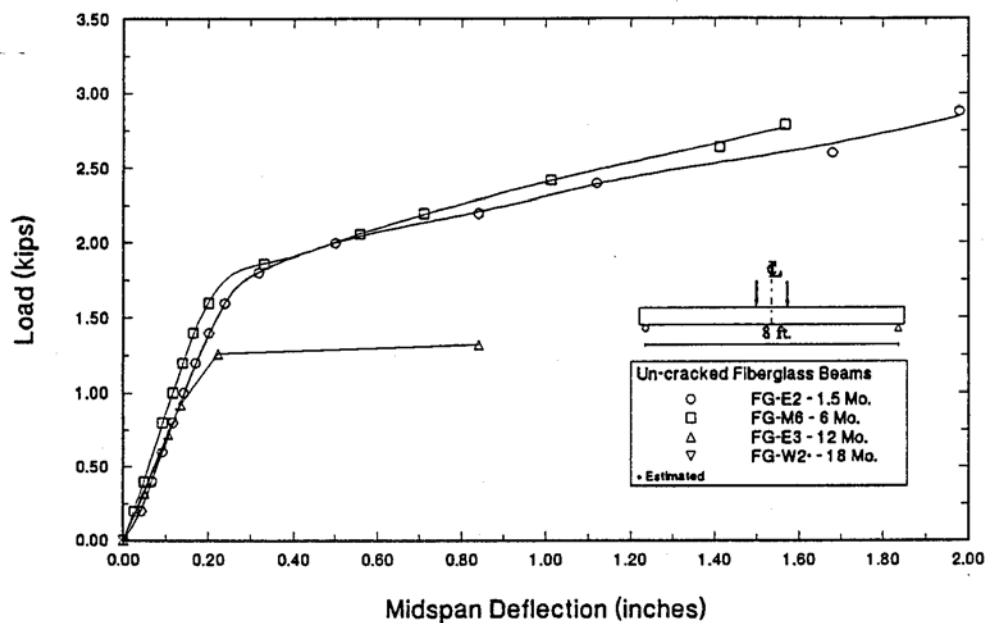


Figure 16.6 Load-Deflection for Un-cracked Fiberglass Beams

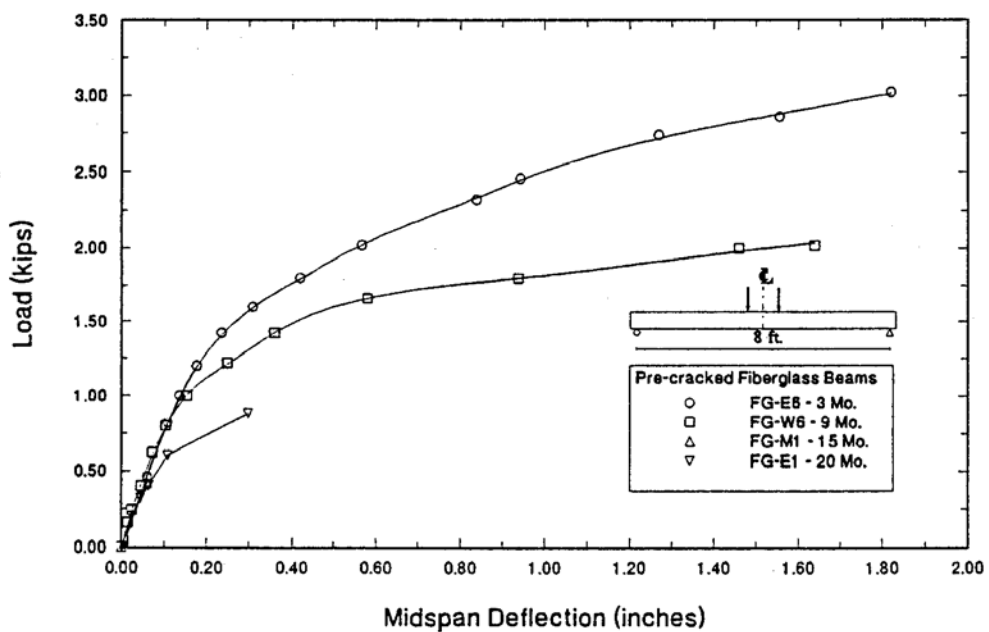


Figure 16.7 Load-Deflection for Pre-cracked Fiberglass Beams

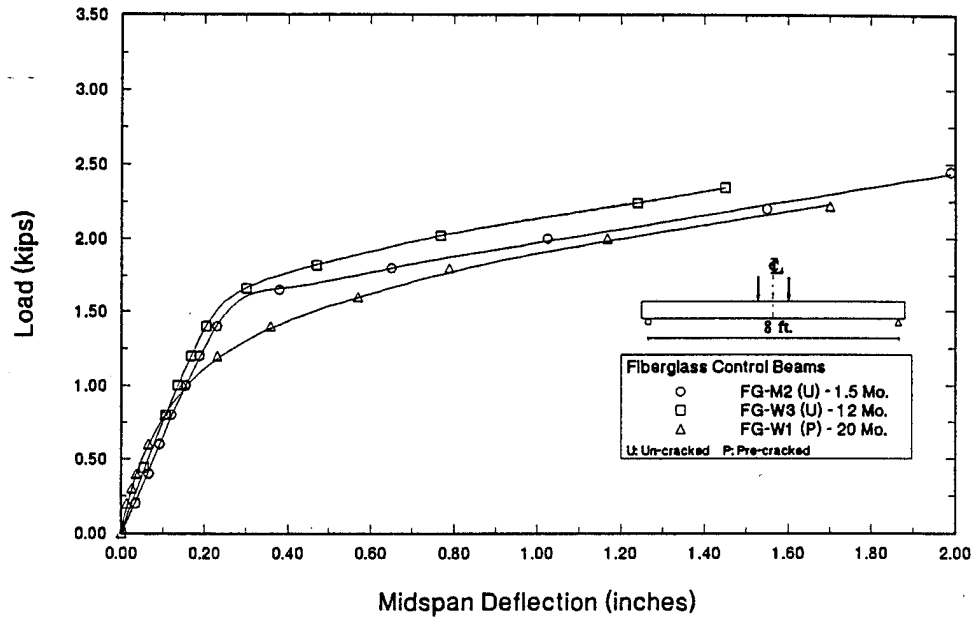


Figure 16.8 Load-Deflection for Fiberglass Control Beams

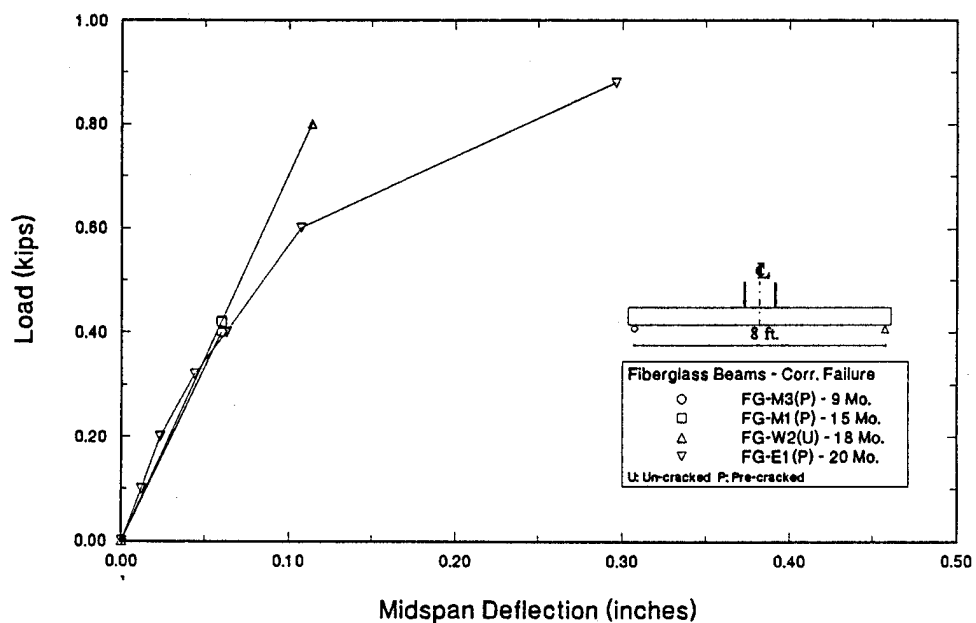


Figure 16.9 Load-Deflection for Fiberglass Beams — Corrosion Failure

An overview of the strength reduction with exposure time for all the beams is shown in Figure 1_6.10. For completeness, the variation in strength with time for the three control beams is also shown in the same plot. It may be seen that whereas there is little reduction in strength in the control specimens, both un-cracked and pre-cracked experienced a significant loss in strength. It should be noted, however, that some of the beams shown in this graph failed in shear so that the strength reduction picture is somewhat misleading specially for the un-cracked beams. Nevertheless, Figure 16.14 graphically illustrates the dramatic reduction in strength of the fiberglass beams exposed to salt water.

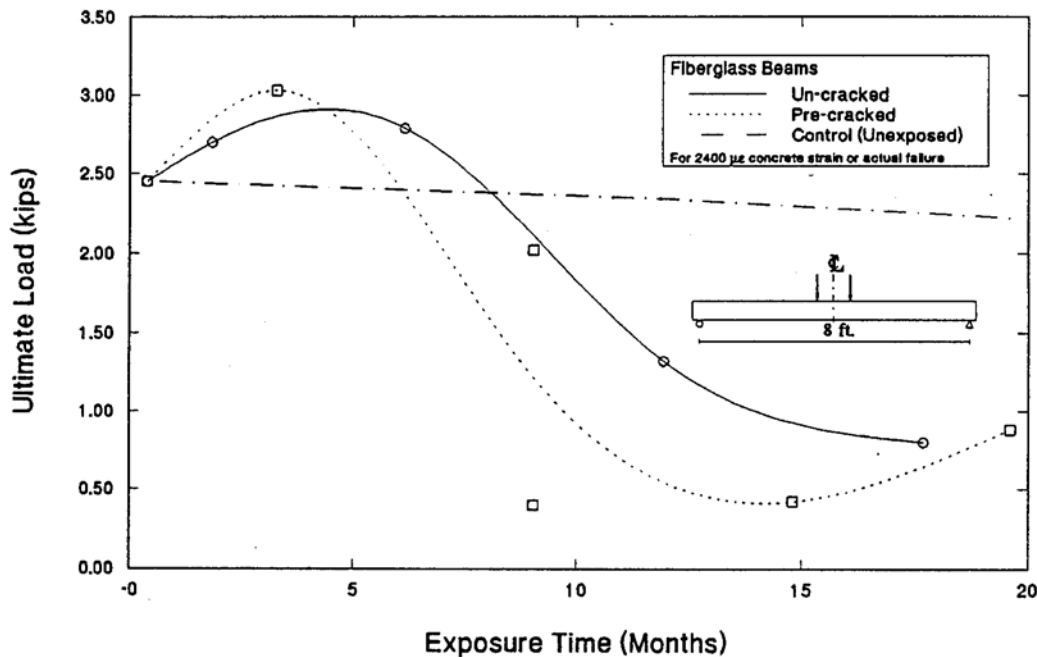


Figure 16.10 Load Variation Relative to Time for Fiberglass Beams

16.3.2.1 Corrosion Failure Mode

Since the fiberglass strands in the beams that failed in the corrosion mode (see Plates 16.3-16.4) could not be directly tested, additional tests were carried out in which 'half' sections were separately tested to determine whether the damage or loss of bond was only confined to the 'splash' zone or whether it extended over the entire beam. Of the four beams that failed in the corrosion mode only three (FG-M3, FG-W2 and FG-E1) were tested in this manner. In each case a concentrated point load was applied at mid-span and cracking and failure loads determined (see Plate 16.5).

The results from these tests are summarized in Table 16.9. Details of the beam segments tested, ACI based cracking loads for un-reinforced and prestressed sections together with

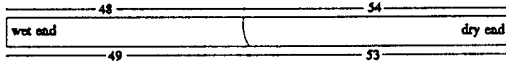
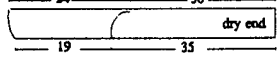
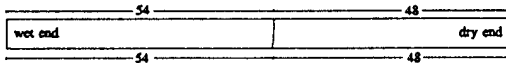
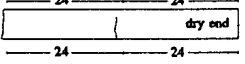
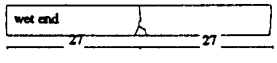
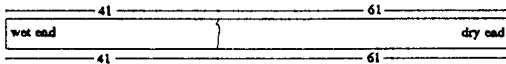
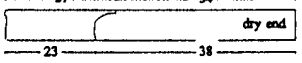
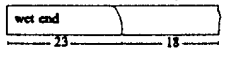


Plate 16.5

(top) Corrosion failure in wet half after 9 months
(btm) Corrosion failure in wet half after 18 months

the measured cracking and ultimate load obtained from the tests are summarized in Table 16.10. Since the sections were also over reinforced, a compression mode of failure could be expected.

Table 16.9 Corrosion Failure Mode for Fiberglass Pre-tensioned Beams

Beam	Tested After (mth)	Ult. Load (kips)	Failure Mode
FG-M3	9	0.40	
		2.18	
		1.66	
FG-W2	18	--	
		2.98	
		1.98	
FG-E1	20	0.88	
		2.24	
		2.32	

Inspection of Table 16.9 shows that the failure load was generally larger for the dry segment compared to the wet segment. In all cases failure was initiated by a tension crack that propagated along the weakest line of resistance. It may be seen that the failure crack patterns for the dry and wet segments are somewhat different.

A summary of all test results together with calculated values of cracking load for both the plain and prestressed sections is presented in Table 16.10. It may be seen that for the last beam tested, FG-E1, the dry and wet segments failed almost immediately after cracking. For the wet segments, the cracking and failure loads are relatively close and therefore their failure mode has been classified as 'corrosion'. This is not the case for the dry segments of beams FG-M3 and FG-W2.

Table 16.10 Summary of Beam Segment Test Results

Beam	Exposure Time (mths)	Segment Tested	Span	ACI Code		Test Results	
				Per (kips) Plain	Per (kips) Prestressed	P _{cr} (kips)	P _u (kips)
FG-M3	9	Beam ^a	96.0	0.47	1.44	0.40	0.40
		Dry	48.0	0.82	2.52	1.12	2.18
		Wet"	48.0	0.82	2.52	1.14	1.66
FG-W2 ¹	18	Beam ^a	96.0	0.44	1.34	---	--
		Dry	48.0	0.78	2.35	1.98	2.98
		Wet'	48.0	0.78	2.35	1.70	1.98
FG-E1	20	Beam ^a	96.0	0.43	1.36	0.62	0.88
		Dry'	55.6	0.64	2.02	2.20	2.24
		Wet'	37.0	0.97	3.09	2.20	2.32

¹ Corrosion failure mode

² Un-cracked

None of the failures were, however, accompanied by slip at the ends. This indicates that failure was the result of destruction of the fiberglass.

Although the tests ruled out bond failure, a limited pull out study was conducted to investigate deterioration, if any, of the bond between concrete and fiberglass subjected to wet/dry cycles. Since these relate to un-stressed specimens they are not directly applicable for fiberglass beams. Nevertheless they do provide a measure of bond changes experienced by the beams.

16.4 Effect of Salt Water on Concrete

Concrete cylinders (with the same cast dates as the beam specimens) were placed in the respective tanks so that changes in compressive strength under the same wet/dry cycles could be monitored. Figure 16.11 shows the variation in compressive strength that was obtained. Inspection of this figure shows that, whereas the strength of concrete cast on 12/28/89 and 06/06/90 is somewhat constant, that of concrete cast on 12/22/89 decreased to about 86 % of its initial value. This reduction may be attributed to the higher permeability of this concrete indicated by its higher slump and its lower temperature (see Table 4.2). In any event, since the same concrete was also used for the steel specimens, it can be ruled out as cause of the reduction in ultimate capacity for the fiberglass pretensioned beams.

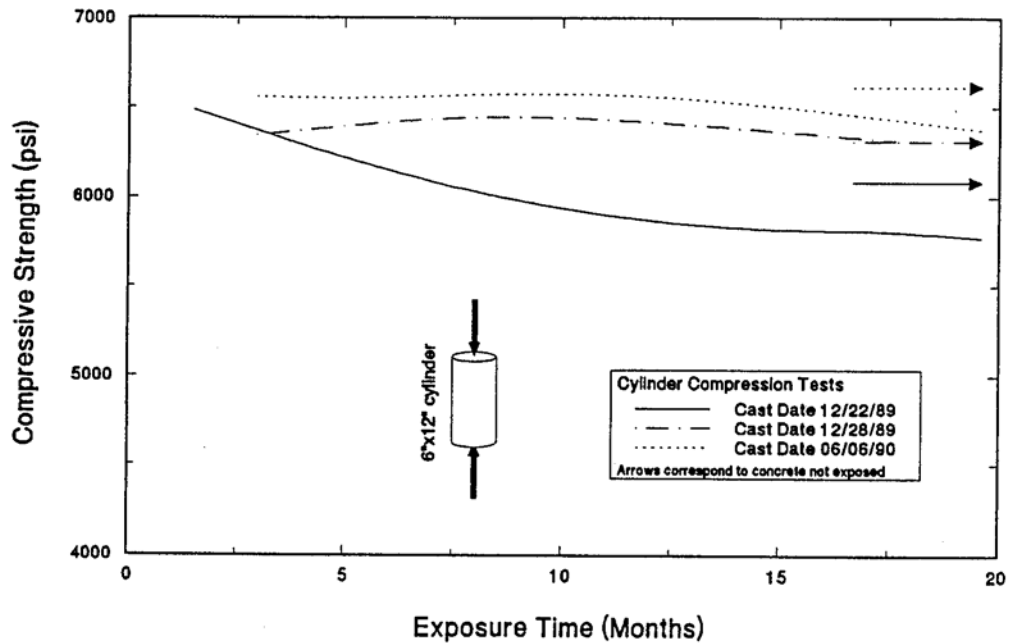


Figure 16.11 Variation of Concrete Strength with Time

16.5 Effect of Salt Water on Bond

To determine the possible deterioration in the bond between fiberglass and concrete, supplementary pull-out tests (see Plate 16.6) were carried out on eighteen 3 in. x 3 in. x 12 in. prisms containing a single (unstressed) steel or fiberglass strand. Two series of tests were conducted. In the first series, six specimens -three steel and three fiberglass- cast on December 28, 1989 were tested in January 1990. In the second series, twelve specimens -six steel and six fiberglass- cast on March 13, 1990 were placed in Tank N⁰ 2 used in the

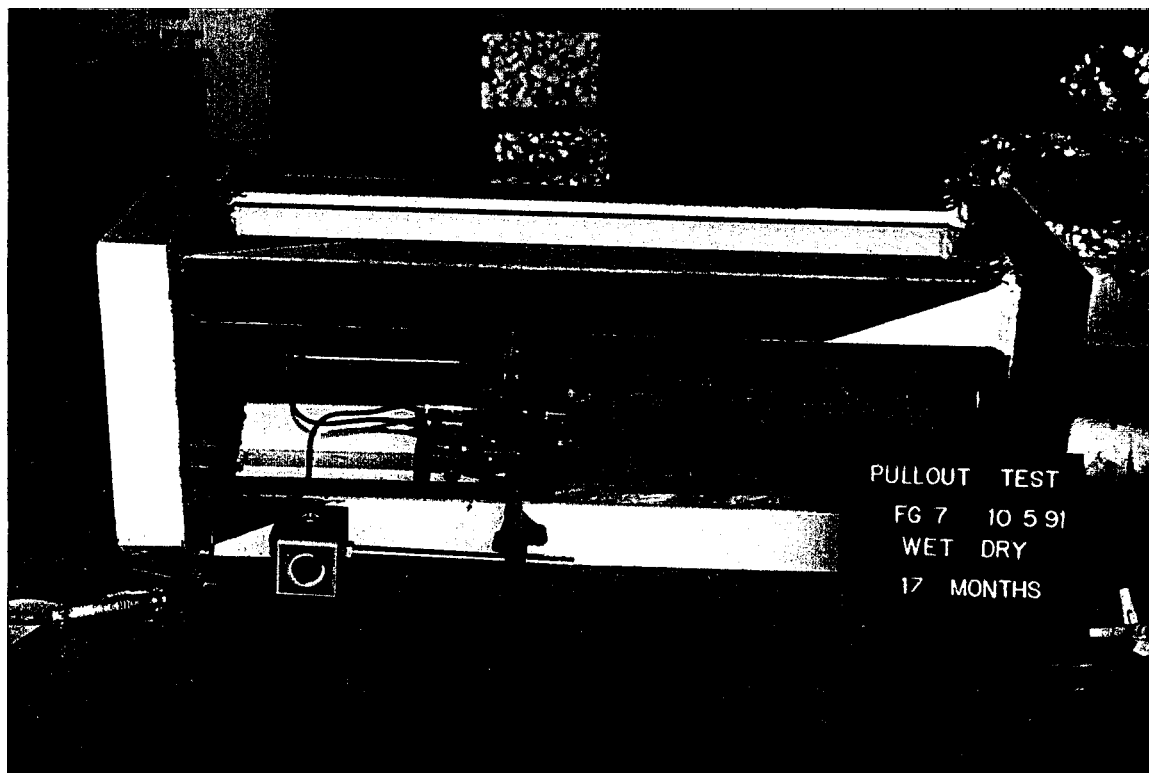
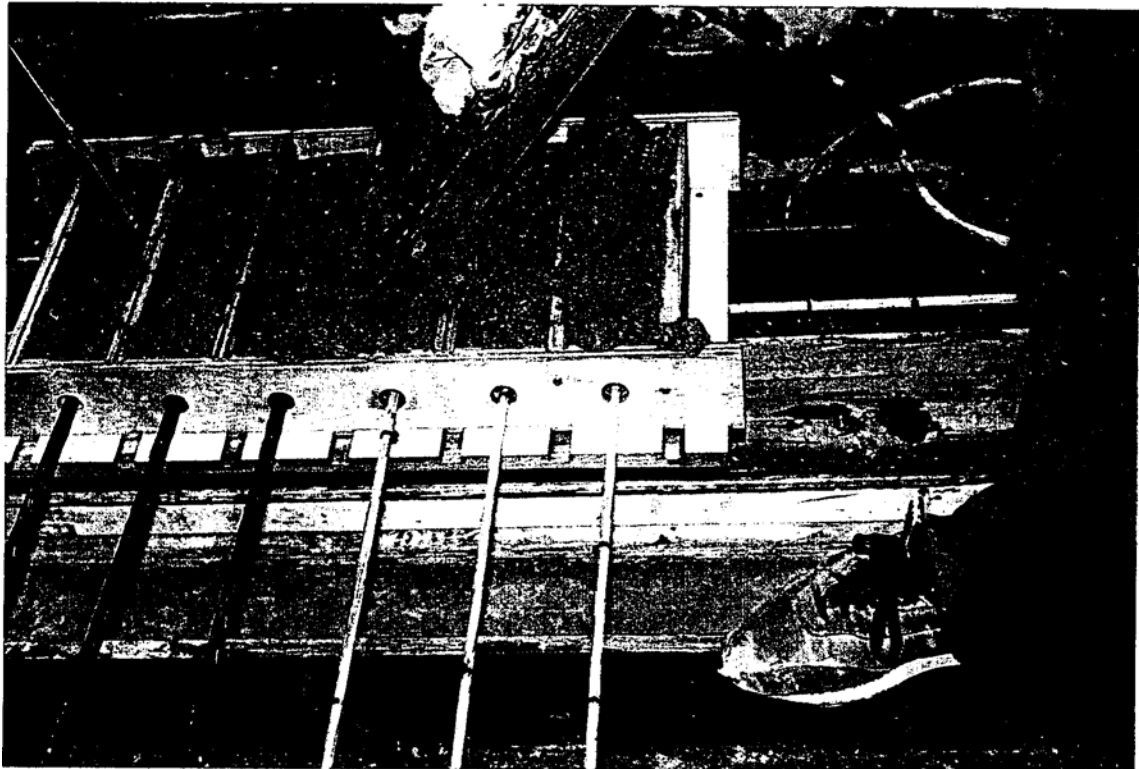


Plate 16.6 (top) Fabrication of pull out specimens
(btm) Set up for pull out test

durability study (in May 1990) and were subjected to identical wet/dry cycles experienced by the beams for 17 months.

Since the pull-out study was linked to the long-term durability tests, the embedded steel and fiberglass strands sizes were identical to those in beams, i.e. $\frac{1}{2}$ in. for steel and $\frac{3}{8}$ in. for fiberglass. Thus, the object was to determine the relative changes in bond with time as a result of exposure, rather than to compare the relative performance of fiberglass and steel. Since the specimens tested were un-stressed, the results from this study provide a lower bound on bond resistance. Obviously much higher resistance would be recorded for prestressed samples. Nevertheless, the study provides a measure of changes in bond resistance that can be anticipated as a result of a combination of moisture, salt and wet/dry cycles.

The basic scheme in testing pull-out specimens is to subject the concrete to compression while the steel acts in tension. The test set up is shown in Plate 16.6. Two LVDTs, one at tip of the strand and the other against the concrete, were used to record the slip. Unfortunately, results of slip measurements were inconclusive.

16.5.1 Test Results

Since the distribution of stresses along the embedded length during pull-out tests is not uniform, only the average bond stress could be calculated. Tables 16.11 and 16.12 summarize the test results for all specimens, including ultimate load and bond stress. The failure stress was calculated by dividing the ultimate load by the product of the perimeter of the strand times the embedded length. Since the strands are made of seven rods, an equivalent diameter was determined that was used in all calculations. For the normal and special steel strands, the equivalent perimeters were 1.39 in. and 1.45 in., respectively. For the fiberglass strands it was 0.939 in.

The variation of bond stress with exposure is plotted in Figure 16.17. Due to the variability of the results from the first series of tests (see Table 16.11), and since only a limited number of durability specimens were tested, error bounds are incorporated. These were based on the variation observed in the first set of tests.

16.5.2 Discussion of Results

The variation of bond' stress with exposure appears to suggest that there is an initial reduction followed by an increase which is more pronounced for the steel specimens. This is probably the result of rust formation.

Table 16.11 Pull-Out Test Results (cast 12/28/89)

Specimen ¹	Test Date	Failure Load (lbs)	Ultimate Bond (psi)	Average Bond (psi)
Steel				
ST-1	01/03/90	15,000	902	
ST-2	01/03/90	11,600	697	729
ST-3	01/04/90	9,800	589	
Fiberglass				
FG-1	01/03/90	8,000	710	
FG-2	01/03/90	9,000	799	707
FG-3	01/04/90	6,880	611	

¹ f_c for all specimens was 5,978 psi

While no definite conclusion can be drawn on the magnitude of the bond resistance, it is evident from Figure 16.12 that there is no dramatic change in bond as a result of exposure to salt solution. This indicates that the premature failures recorded for the fiberglass pretensioned beams was due to other causes, e.g. alkali attack on glass fibers.

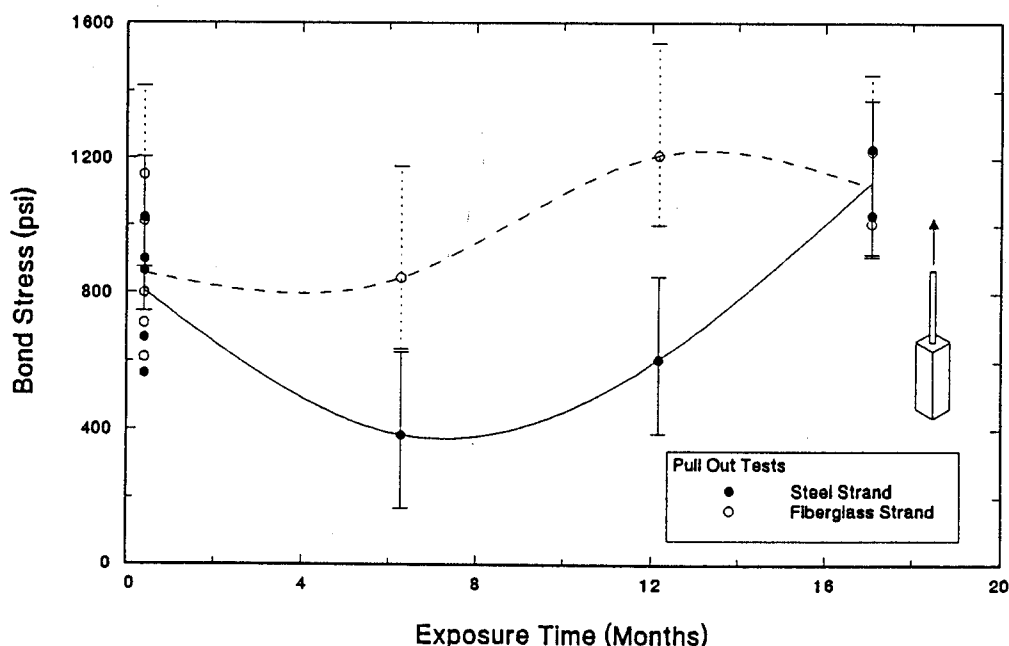


Figure 16.12 Variation of bond stress with time of exposure

Table 16.12 Durability Study (cast 03/13/90)

Months in Tank	Specimen	Test Date	F' _c (psi)	Failure Load (ibs)	Ultimate Bond (psi)
Steel					
Control	ST-4	11/09/90	8,477	15,600	898
6	ST-9	11/09/90	7,665	6,640	382
12	ST-6	05/16/91	6,840	10,500	604
Control	ST-7	10/05/91	7,906	17,760	1,022
17	ST-5 ST-8	10/05/91	7,464	17,920 21,360	1,032 1,229
Fiberglass					
Control	FG-9	11/09/90	8,477	11,400	1,012
6	FG-4	11/09/90	7,665	9,500	843
12	FG-6	05/16/91	6,840	13,614	1,208
Control	FG-8	10/05/91	7,906	12,960	1,150
17	FG-5 FG-7	10/05/91	7,464	11,360 13,780	1,008 1,223

16.6 Implications of results

The steel specimens showed very little reduction in strength (see Figure 16.5). By contrast, the fiberglass exposed specimens, especially the pre-cracked ones, showed a dramatic reduction in strength (see Figure 16.10). Since none of the control specimens showed any marked reduction in strength, it is evident that the epoxy resin used can provide a degree of protection to the S-2 glass strands in the alkaline concrete environment. The failure of the exposed specimens suggests, however, that this protection breaks down when fiberglass strands in direct contact with concrete are additionally exposed to moisture and salt.

As has been explained elsewhere (see Section 3.4.3), fiberglass is unaffected by salt water. Consequently, the cause of failure is the result of water soluble hydroxyl ions coming into direct contact with the glass fibers. In essence, the epoxy resin allowed passage of these deleterious compounds to the fiberglass.

17. POST-ULTIMATE TEST EXAMINATION

17.1 Introduction

Post-ultimate examinations of beams were conducted after one year, eighteen months and twenty months exposure to salt water. In the tests, both uncracked and pre-cracked beams were sawed open longitudinally for visual signs of deterioration in the fiberglass and steel strands and carbonation tests conducted.

In the first test, conducted after twelve months' exposure to salt water, both steel and fiberglass beams were examined. However, the bond between fiberglass and concrete was so strong that it could not be separated from the concrete without damage. Consequently, only the steel specimens were examined in the remaining tests. The deterioration in the fiberglass strands was assessed by examining representative specimens under a scanning electron microscope. The results from this investigation are summarized in the next chapter.

In addition to the visual inspection and carbonation tests, concrete samples were removed from all twenty four beams in this study and chemically analyzed to determine its chloride content at the level of the strand. For each beam exposed to salt water, fourteen samples were extracted from locations # 1, 3-7 and 9 in Figure 14.2. At each of these seven locations, two samples were drilled with the strand depth approached from the top, i.e. 2.5 in. cover, and from the bottom, i.e. 1 in. cover. For the eight control beams, six samples were similarly tested but these were taken from three locations corresponding to points # 1, 6 and 9 in Figure 14.2. In all, 560 samples were analyzed, Mariscal, 1991 [17.1]. A summary of these results is presented in Section 17.3.

17.2 Visual Inspection

Following the completion of the ultimate load tests and the collection of chloride samples, three steel pre-tensioned and one fiberglass pre-tensioned beam were cut open and carbonation tests carried out. In addition, steel strands were examined for signs of corrosion.

Although carbonation is not a problem in North America, tests were nevertheless conducted for its detection. These results are presented in Section 17.2.1. Results of the visual inspection of the fiberglass and steel specimens examined are summarized in Section 17.2.2.

17.2.1 Test Procedure for Carbonation

Since carbonation results in a reduction in alkalinity, testing for carbonation is a simple procedure that is actually a test for alkalinity. A solution of alcoholic phenolphthalein reactant is commonly used in the testing. The colorless reactant is sprayed over a freshly cracked portion of concrete from the surface inward. A change of color to a strong pink denotes the absence of carbonation, i.e. an increase in pH from 8.2 to 10. An absence of color change indicates a reduction in alkalinity due to carbonation, thus denoting that the environment is not alkaline enough to protect the steel from corrosion. The extent of this transparent portion is called the *depth of carbonation*.

17.2.2 Visual Inspection and Carbonation Results

Three steel and one fiberglass beams were cut open to test for carbonation and visual inspection. These were ST-E3 and FG-E3 (uncracked after 12 months), ST-M3 (uncracked after 18 months) and ST-M2 (pre-cracked after 20 months).

A one inch deep longitudinal cut was made along the center line of the beam using a circular concrete saw (see Plate 17.1). A sledge hammer was subsequently used to split the beam along the cut and the strand removed. Phenolphthalein was then promptly squirted over the freshly cracked section to test for carbonation.

17.2.2.1 Inspection of ST-E3

Negligible depths of carbonation (a maximum of about $\frac{1}{8}$ in.) was detected over the first two feet from the dry end of the beam. No carbonation was found elsewhere. The steel strand was thoroughly inspected for evidence of corrosion. Two types of corrosion products were found: a thin reddish layer (commonly known as rust) and a pasty dark greenish layer somewhat thicker than the first. Both were dispersed at several locations along the steel surface. No metal loss was related to the first layer, but, some loss was associate with the second deposit at four locations. Measured form the wet end these were located at 6 in. ($\frac{1}{8}$ in. long oval cavity), 45 in. ($\frac{3}{8}$ in. & $\frac{1}{8}$ in. long fissures) and 51.5 in. and 54.5 in. (some pitting). In general there was no generalized corrosion, the metal loss and corrosion products found were insignificant.

17.2.2.2 Inspection of FG-E3

Since this beam failed at a lower load than expected, it was cut open to visually inspected the strands (see Plate 17.1). Since it was impossible to separate the strand from the concrete without damage, only a small portion of the beam was inspected. The examination revealed a $\frac{7}{8}$ in. long honeycomb contiguous to the strand at the location where the beam failed during testing. Several small air pocket were also detected.

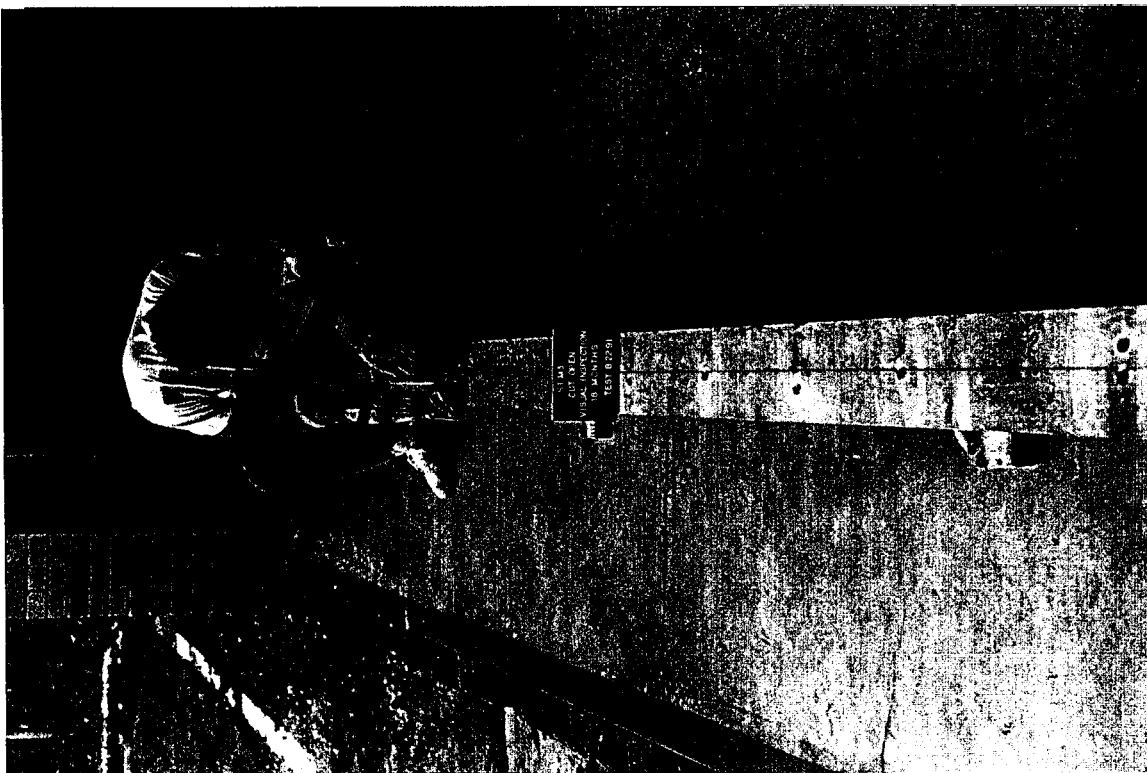


Plate 17.1

(top) Sawing beam

(btm) Fiberglass beam after 12 months in tank

17.2.2.3 Inspection of ST-M3

Some evidence of carbonation was detected near the dry end of this beam. Its maximum depth was about $\frac{1}{8}$ in. However, no carbonation was detected over the 'splash' zone or at the submerged end.

Signs of corrosion were evident in the steel strand that was thoroughly inspected. A rust layer was found to have spread along the strand but no metal loss was associated with it. However, considerable metal loss was associated with the dark greenish paste that was also found in beam ST-M3. Twelve oval cavities were observed, seven of which could be measured, indicating a substantial metal loss. This loss after only 18 months exposure, contrasts with the results of a similar study on prestressed piles reported by Pfeifer et al, 1987 [17.2] in which the effects were found to be negligible.

Three of the largest cavities were measured at 47 in. from the wet end (ranging from $\frac{3}{8}$ in. to $\frac{1}{4}$ in. long), and involved three of the seven rods that constituted the strand. The localized corrosion was developed adjacent to a honeycomb, as shown in Plate 17.2. Two more of the cavities were 44 in. from the submerged end (about $\frac{1}{8}$ in. long). The peculiarity about these cavities is that they developed underneath electrical tape and epoxy that was used to attach and protect strain gages. As noted earlier, a greenish paste coated the corroded areas.

In order to estimate the metal loss, the dimension of the cavities were measured using a micrometer (see Plate 17.2). The weight of metal lost was calculated by multiplying the volume lost by the density of iron, i.e. 7.87 gr/cm³. The volume was approximated as 75 % of the volume of half an ellipsoid. This yielded a metal weight loss of 0.427 gr. after 18 months of exposure.

17.2.2.4 Inspection of ST-M2

As for the other beams tested, the carbonation depth was insignificant. Only a $\frac{1}{16}$ in. depth was measured in the dry end.

Surprisingly, even though this beam was pre-cracked and had been cast on December 22, 1989 when conditions were unfavorable (low concrete temperature and high slump as shown in Table 4.2) there was little corrosion in comparison to the uncracked beam STM3 that was tested after 18 months. Only three corrosion cells were measured 9 in., 49.5 in. and 64 in. from the wet end. These cells were characterized by the formation of black corrosion products which had to be scraped off to reveal negligible metal loss. The lack of deterioration in ST-M2 emphasizes the importance of proper concreting and also suggests the inadvisability of using coverings (electrical tape and epoxy in the case of ST-M3) that trap moisture and assist the corrosion process.



Plate 17.2 (top) Carbonation tests on ST-M2
(btm) Metal loss in steel strand in ST-M3

17.3 Chloride Content

Since corrosion effects due to chloride were assessed in this study, an exhaustive investigation was carried out to determine *total* chloride content at the level of the prestressing strand. The Florida Method, Kessler *et al*, 1978 [17.3] was used to determine the *total* chloride content at seven locations along the beam where corrosion measurements were previously undertaken. In essence, it involves digestion of 3 grams of powdered samples in nitric acid and subsequent titration against a 0.1N silver nitrate reagent. The end point is obtained from a Berman potentiometric titration procedure using sensing electrodes, rather than color indicators (see Plate 17.3).

17.3.1 Test Results and Discussion

Figures 17.1-17.4 plot the variation in chloride content along the length in exposed uncracked and pre-cracked specimens. Inspection of these plots shows that the chloride content is maximum over the splash zone but is very low in the dry zone. Moreover, pre-cracked beams have higher chloride levels than uncracked beams and their magnitudes are dependent on the concrete cover; chloride levels are proportionately lower as the cover is increased. The chloride content in the fiberglass and steel pretensioned beams were found to be very similar after comparable periods of exposure, Mariscal, 1991 [17.1].

Figures 17.5 and 17.6 show the variation in chloride content for the control specimens that is also indicative of the initial chloride content in the cement and aggregates used. This ranged from 0.003% to 0.012% with an averaged of 0.057% and is between 3.75%-15% of the ACI Committee 222 limit of 0.08% total chloride ion content for prestressed concrete construction [17.4].

The maximum measured chloride content was 1 % in the pre-cracked beam ST-M2 after 20 months exposure (see Figure 17.2). Even though this value greatly exceeded proposed minimum chloride level thresholds for corrosion of steel, e.g. 0.11%-0.17% by Stark, 1984 [17.5] and 0.17%-0.21 % by Pfeifer *et al*, 1987 [17.2], the corrosion in this beam was less than in beam ST-M3, exposed to salt water for 18 months. This may be because higher chloride concentrationse can reduce the solubility of oxygen resulting in a decrease in corrosion activity, Mozer *et al*, 1965 [17.6].



Plate 17.3 (top) Filtration of digested sample
 (btm) Potentiometric titration of sample

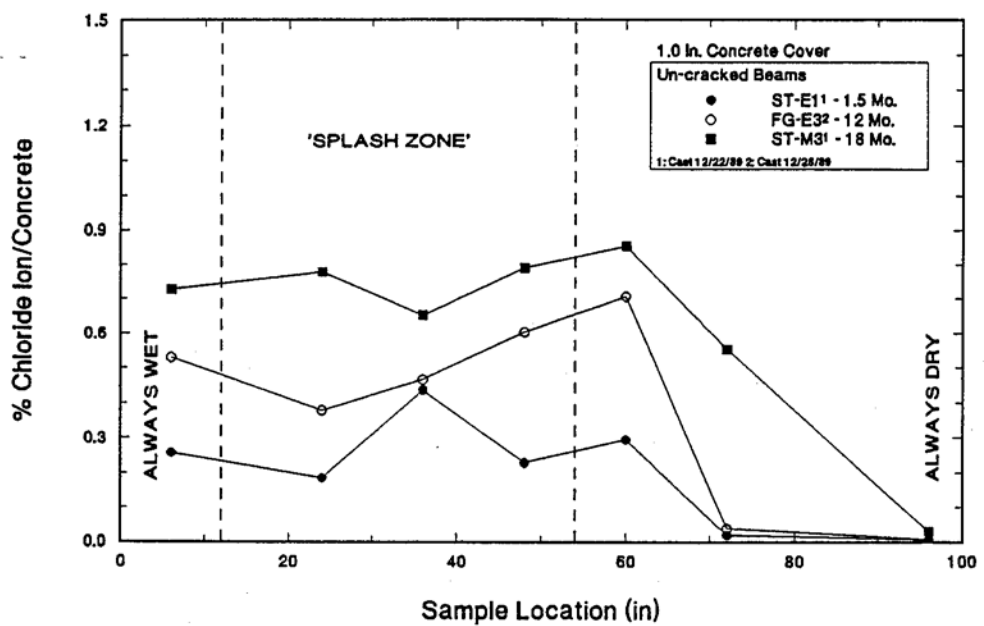


Figure 17.1 Typical Chloride Content for Un-cracked Beams — 1.0 in. Cover

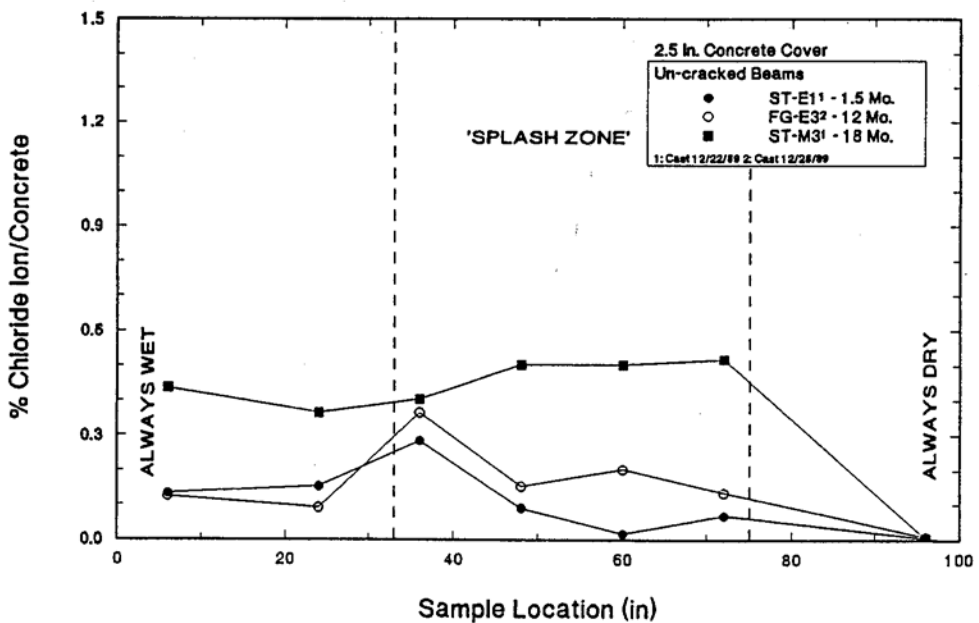


Figure 17.2 Typical Chloride Content for Un-cracked Beams — 2.5 in. Cover

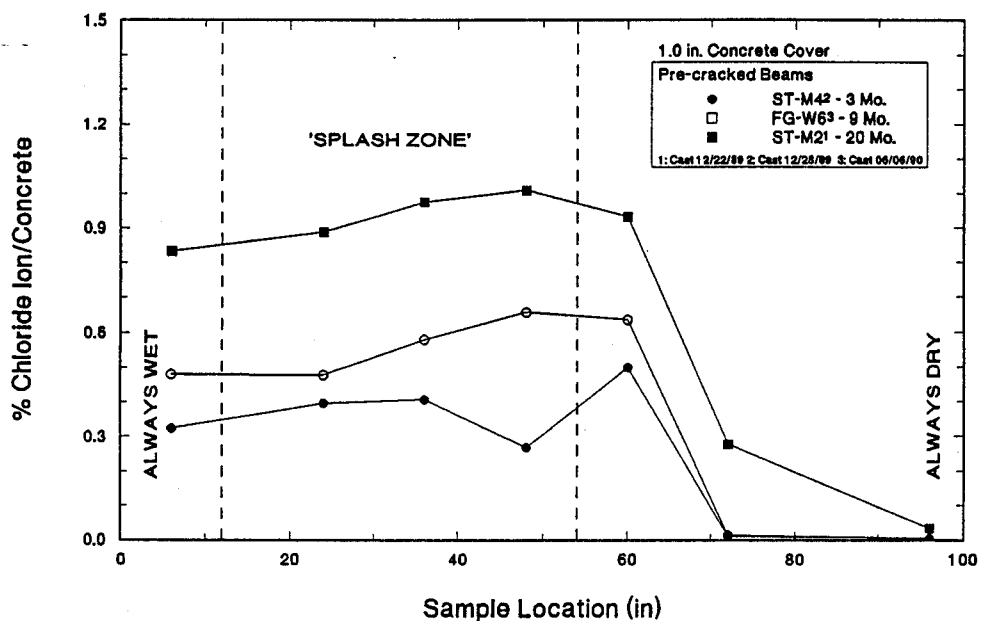


Figure 17.3 Typical Chloride Content for Pre-cracked Beams — 1.0 in. Cover

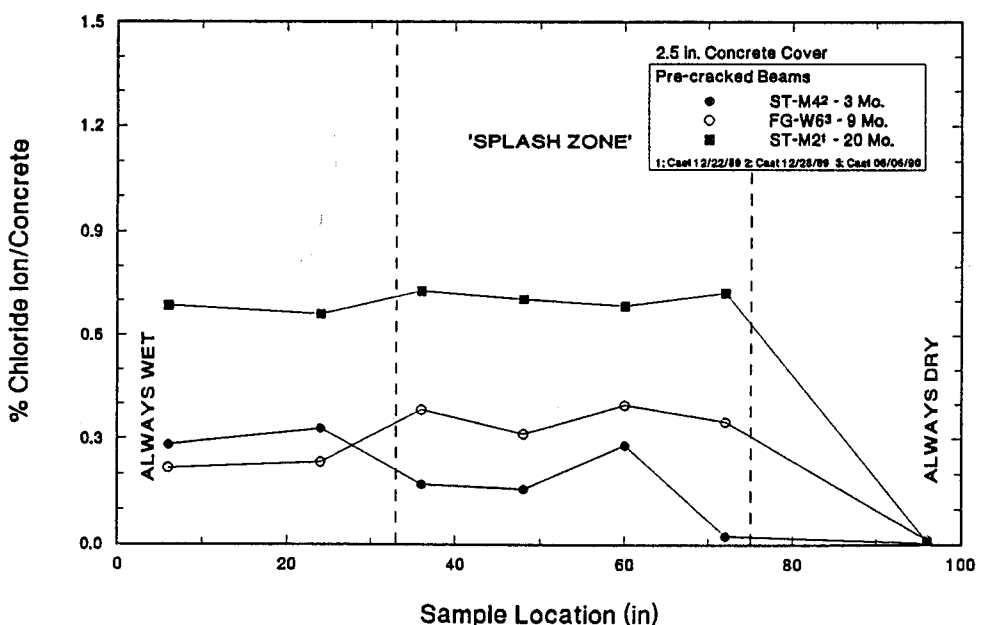


Figure 17.4 Typical Chloride Content for Pre-cracked Beams — 2.5 in. Cover

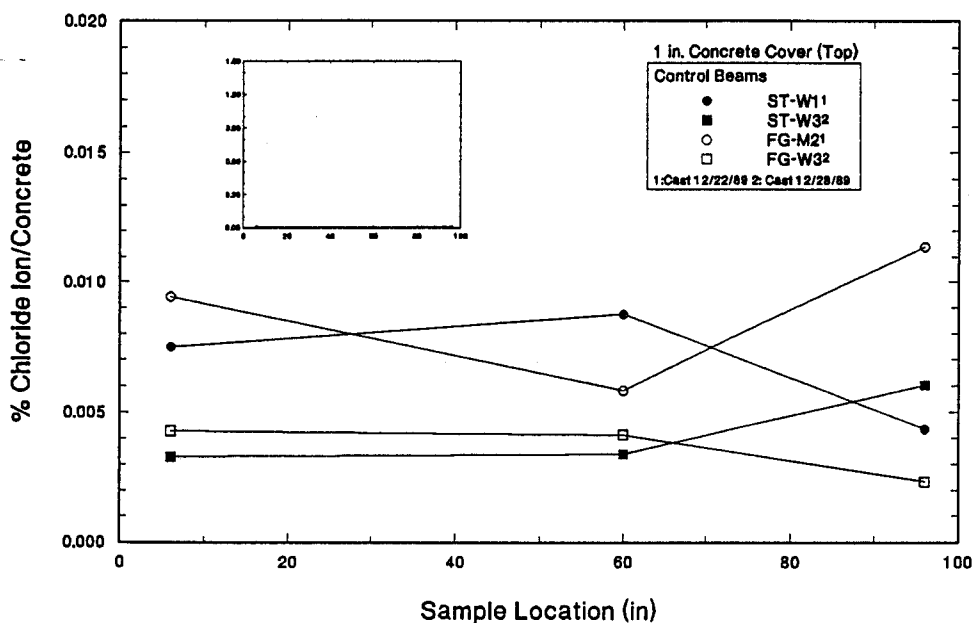


Figure 17.5 Typical Chloride Content for Control Beams — 1.0 in. Cover

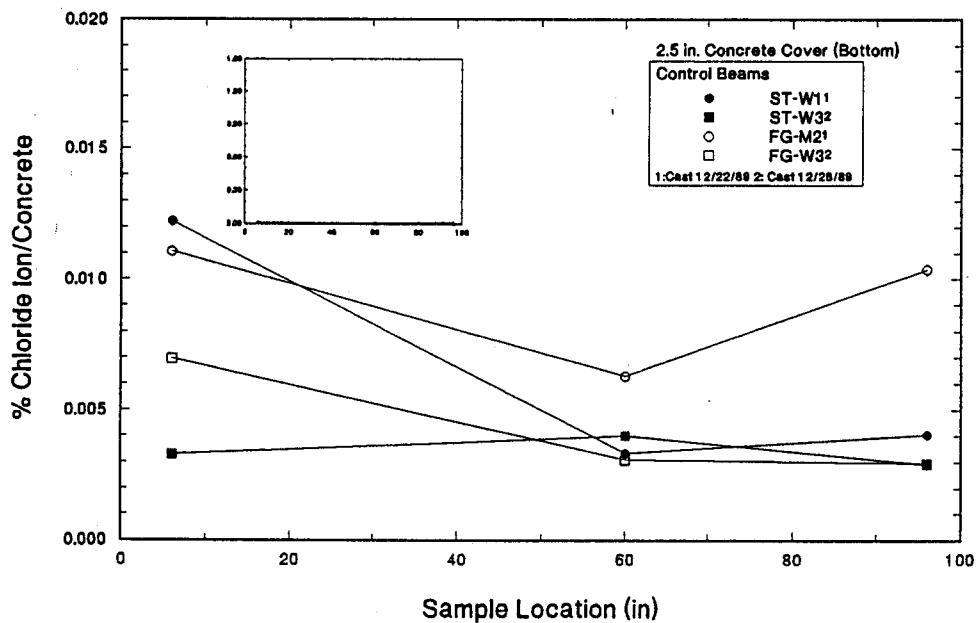


Figure 17.6 Typical Chloride Content for Control Beams — 2.5 in. Cover

18. SCANNING ELECTRON MICROSCOPY EXAMINATION

18.1 Introduction

The results of the ultimate load tests and the pull-out study presented in Chapter 16 provide confirmation that the loss of strength of the exposed fiberglass pre-tensioned beams was the result of deterioration of S-2 glass/epoxy composites in a wet alkaline environment rather than due to a loss of bond or a reduction in concrete strength. To determine the extent of the degradation in the glass fibers, scanning electron microscopy (SEM) examinations were carried out on selected samples. In view of limitations on time and cost only one fiberglass beam (FG-W2) was examined. This had displayed the classic corrosion mode of failure after 18 months exposure as described earlier (see Table 16.9).

Representative samples were taken from FG-W2 at locations #1, #5 and #9 (see Figure 14.2) corresponding to the permanently wet, 'splash' and permanently dry zones, respectively. To obtain a measure of the damage, if any, a stressed fiberglass strand exposed only to laboratory conditions was used as control. This strand had been tensioned during the fabrication of the durability specimens on December 28, 1989 but not used since the other strand failed.

All samples were professionally prepared for the SEM examination to a half micron final polish (see Plates 18.1). They were subsequently sputter coated with gold palladium and stored in a dust free vacuum chamber prior to their examination at the Surface Analysis Laboratory of the University of South Florida, Tampa. The electron microscope used was a JEOL JSM 840 which allows a magnification of up to 300,000.

It should be stressed that in view of the limited number of samples examined, the findings presented are necessarily *preliminary* observations that require detailed follow up examinations of much larger samples. Nevertheless, they do provide information on the relative state of identically prepared samples taken from exposed and un-exposed parts of failed beams.

18.2 Scope of Investigation

The aim of the SEM examination was to investigate two possible mechanisms of hydroxyl ion ingress -matrix cracking due to prestressing or the permeability of the epoxy resin.



FGW2 #1
Always Wet
11/1191

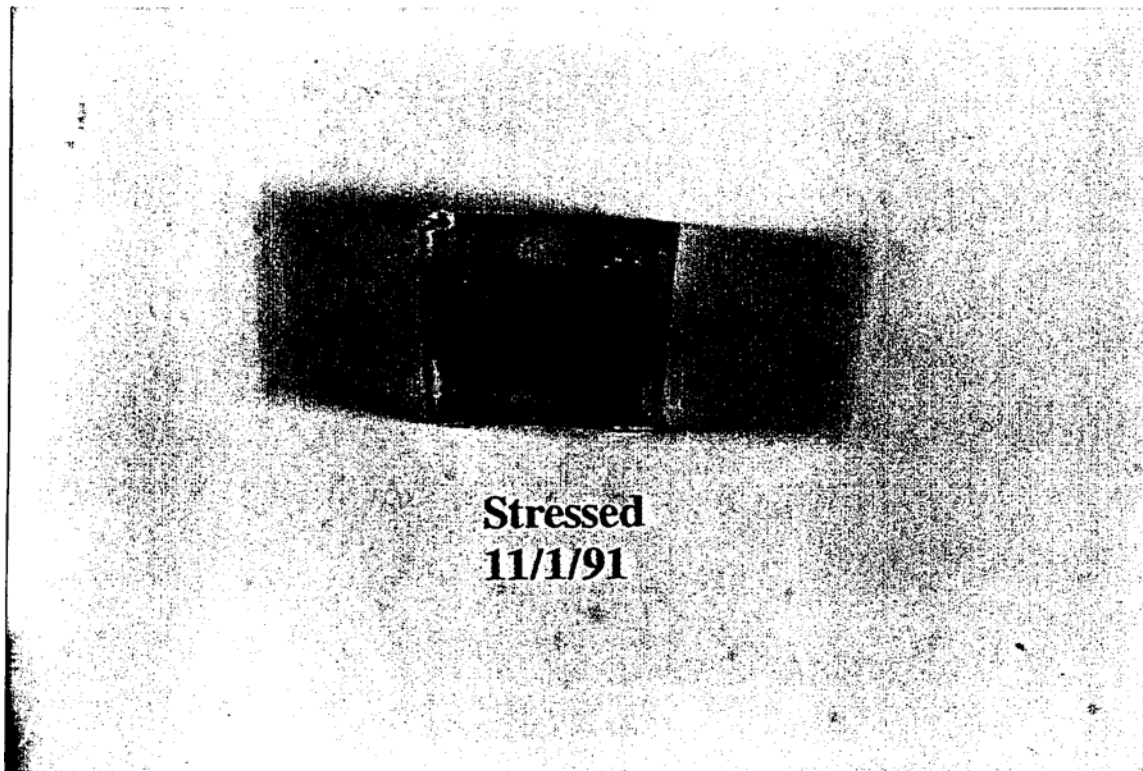


Plate 18.1

- (top) Permanently wet sample in concrete for 18 months
(btm) Unexposed fiberglass sample used as control

Under prestressing loads of 10,000 lbs the strain in the fibers and resin would be $10,000/(0.0702 \times 9.04 \times 10^6) = 1.6\%$ (see Table 2.5), which is considerably lower than the 5.6% (see Figure 2.1) ultimate strain of the resin. Thus, cracking of the resin during prestressing is unlikely.

On the other hand, since Epon resin has a moisture absorption of 1.5 % by weight at 200°F over 14 days (see Table 2.3), it should also have some moisture absorption capacity at room temperature. This absorption should manifest itself by a modest increase in resin volume which can induce transverse compressive and shear stresses in the fibers due to non-uniformity. Since fiberglass composites are relatively weak in directions other than longitudinal (see Table 2.4), their cracking may be anticipated.

18.3 Results of SEM Examination

Since four related samples were examined, the micrographs are presented in sets of two that compare samples taken from the permanently dry location (point #9 and the control (both un-exposed), and samples that were permanently wet (point #1) or located in the splash zone (point #5). For the samples subjected to exposure, fibers from two locations were examined - near the middle of the fiber and at the concrete interface. Only a few of the micrographs taken are presented here. Additional micrographs may be found in Mariscal, 1991 [18.1].

18.3.1 Permanently dry location

Plate 18.2 presents micrographs taken for the control specimen and for the sample taken from the dry end of the beam (point #9). Inspection of this plate shows that the relative state of the glass fibers is comparable with little evidence of degradation of the fibers though there is some cracking. This corroborates the test results where no reduction in strength was observed for the control beams.

18.3.2 Splash zone

Plate 18.3 presents two micrographs for the sample at the splash zone (point #5). The first is taken from a rod away from the concrete interface and the second, from one located at the interface. Inspection of this plate shows that there are signs of deterioration and degradation of the glass fibers near the concrete interface. By contrast, there is far less damage in the fibers located farther away. However, there is substantially more cracking in comparison to the glass fibers located in the dry end (see Plate 18.2).

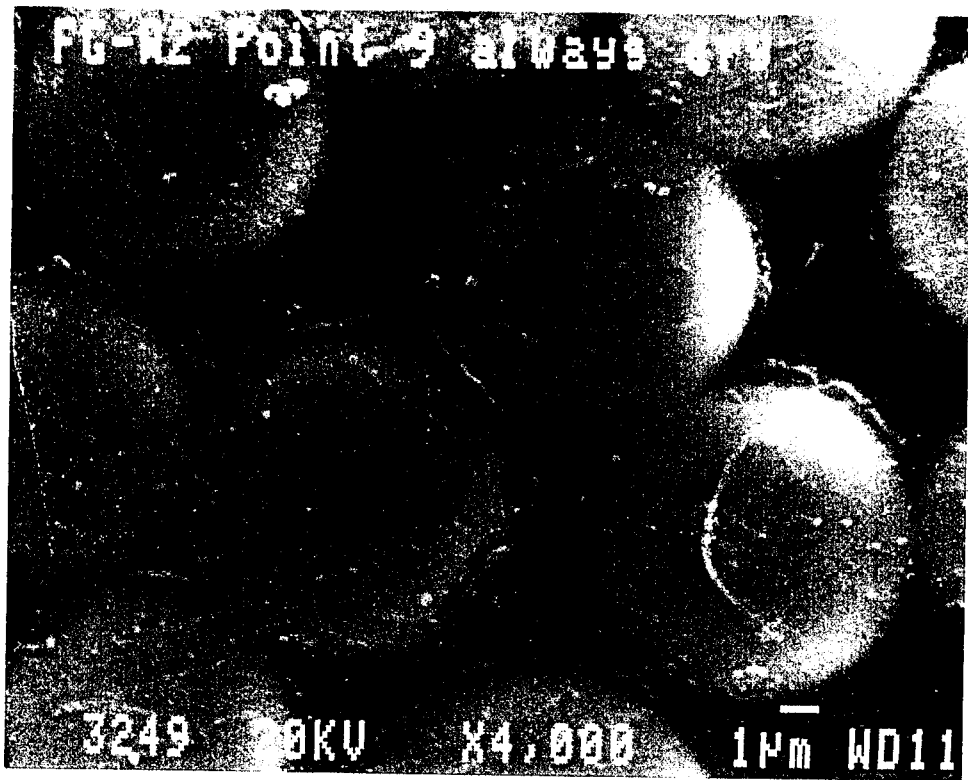


Plate 18.2 (top) Unexposed control specimen at x4,500
(btm) Always dry specimen at x4,000

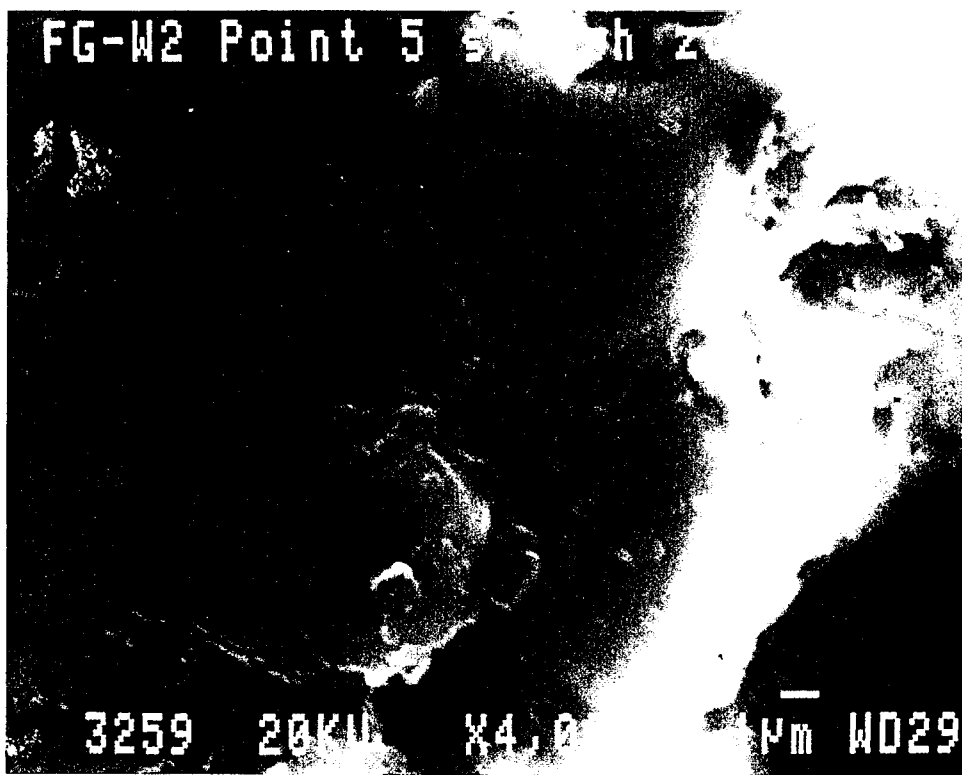
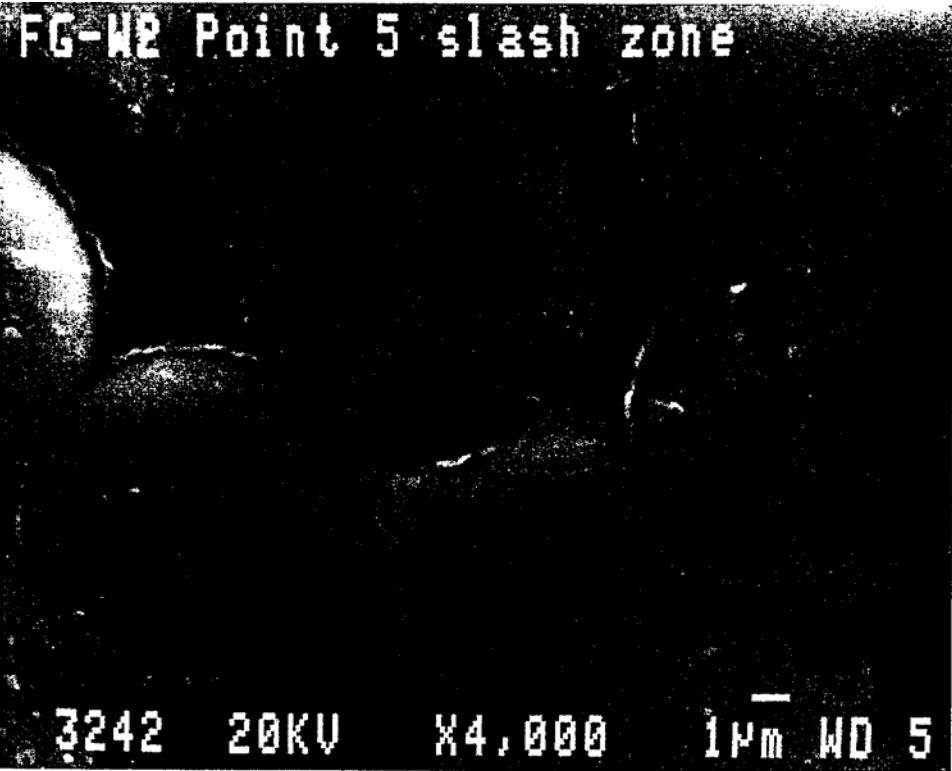


Plate 1.8.3 (top) Splash zone specimen away from concrete interface
(btm) Splash zone specimen near concrete interface
(at x295,000)

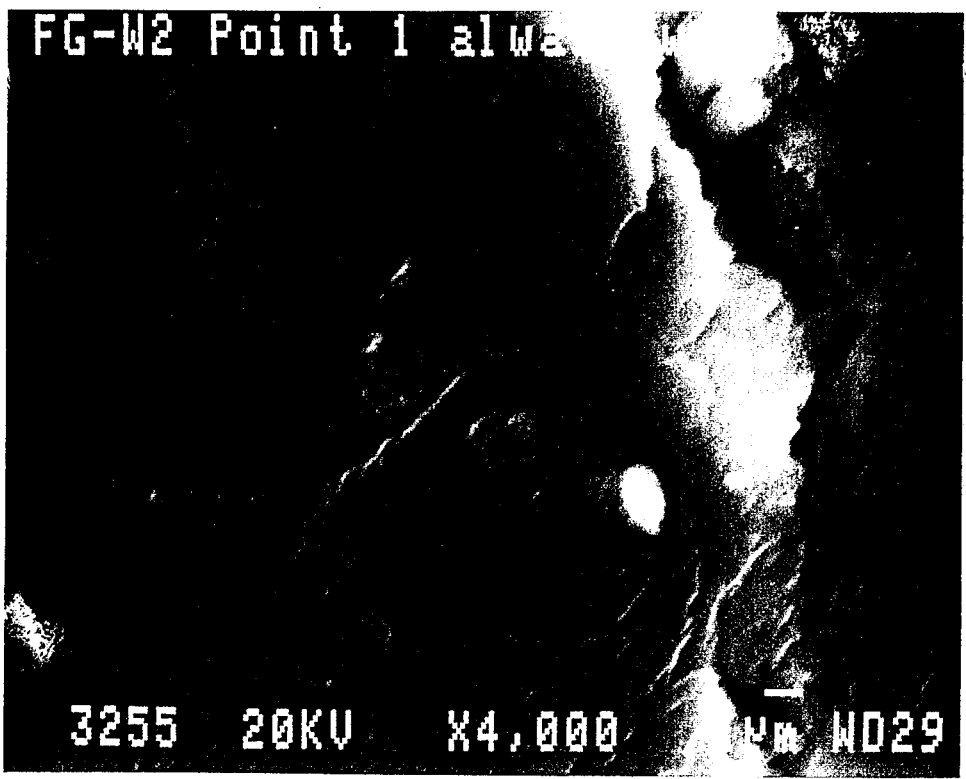
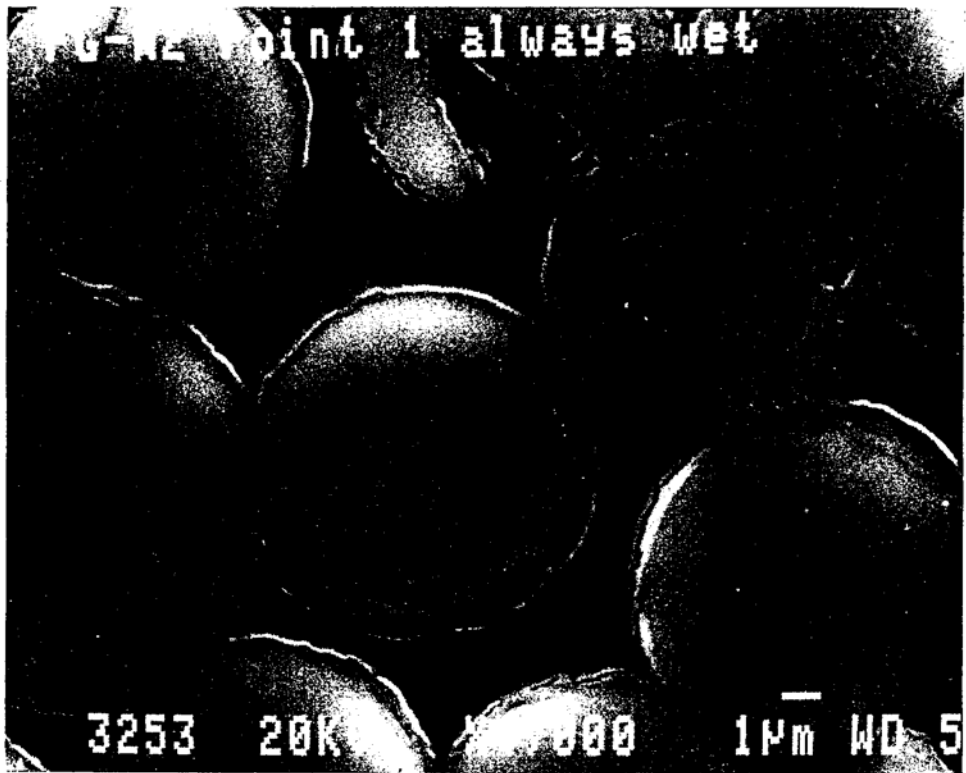


Plate 18.4 (top) Submerged specimen away from concrete interface
(btm) Submerged specimen near concrete interface
(at x4,000)

18.3.3 Permanently wet location

Plate 18.4 presents two micrographs for the sample that was permanently submerged (point # 1) taken from a rod away from the concrete interface and one at the interface. As for the sample taken from the splash zone, there is considerable evidence of deterioration and degradation in the fibers located near the concrete interface. In comparison to the sample at the splash zone (Plate 18.3), there appears to be even greater degradation of the glass fibers.

18.4 Discussion of results

The micrographs show little evidence of cracking of the resin. The only visible crack is in the control sample (Plate 18.2) and may have occurred during sample preparation. Since there are definite signs of deterioration of the glass fibers in samples that were submerged or subjected to wet/dry cycles, the likely cause of this degradation is absorption of aqueous hydroxyl ion solution by the resin itself. The greater deterioration observed at the concrete interface suggests that the alkaline concentration was greater at this location. Furthermore, a larger surface area of fibers was also exposed to the hydroxyl ion. The greater cracking of fibers in Plates 18.3-18.4 may be the result of transverse stresses induced as a result of moisture absorption by the resin. As noted earlier, the transverse strength of glass fibers is much smaller compared to its strength in the longitudinal direction.

19. CONCLUSIONS

19.1 Introduction

The object of this study was to investigate the feasibility of fiberglass pretensioned piles in a marine environment. As part of the study, several short term and long term tests were undertaken in which the response of identical fiberglass and steel pretensioned specimens was compared. The short term investigations included determination of transfer length (Chapter 6), flexural response (Chapter 7), axial response (Chapter 8) and pile driving response (Chapter 10). The long term investigations included fatigue (Chapter 11), creep (Chapters 12 and 13) and durability (Chapters 14-18). This chapter summarizes the principal conclusions from each of these studies. Conclusions relating to the short term tests are summarized in Section 19.2 whereas those from the long term tests are presented in Section 19.3. The overall implications of these conclusions are addressed in Chapter 20.

19.2 Short Term Response

19.2.1 Transfer Length

1. The transfer length for 3/8 in. S-2 glass/epoxy strands was about 10 in. This is 23 % lower than the ACI value for a 3/8 in. steel strand stressed to the same level.
2. Bond between fiberglass and concrete appears to be superior to that between steel and concrete because of better adhesion between fiberglass and concrete.
3. The measured transfer strains were within 5-10% of theoretical strains based on ACI elastic modulus equation. Better correlation was obtained using modulus values based on Nilson's equation.
4. The transfer length of fiberglass strands can be determined from values for steel using Eq. 6.5 provided data on the relative coefficient of friction between fiberglass, steel and concrete is available.
5. Transfer length increases with time for both fiberglass and steel tendons, but the rate of increase is almost double for fiberglass compared to steel.

19.2.2 Beam Study

1. Measured prestress losses from jacking to release in the fiberglass strands (averaging 15.6%) was 70% of that in comparable steel pretensioned specimens that averaged 22% (see Table 5.4). The total lump sum loss in the fiberglass beams of 24.8 ksi was slightly under half the 50.7 ksi loss recorded for the steel pretensioned beams (see Table 5.6).
2. The pre-cracking response of steel and fiberglass pretensioned beams under the same effective prestress is identical. The post-cracking response of fiberglass pretensioned beams is more flexible than steel pretensioned beams (see Figures 7.2-7.5).
3. Cracks in fiberglass pretensioned beams are slightly more widely spaced over the constant moment zone than in the comparable steel pretensioned beams at failure (see Table 7.3 and Figures 7.12-7.14).
4. The fiberglass pretensioned beams displayed considerable ductility. The ultimate deflection as a fraction of the cracking deflection is larger than for comparable steel pretensioned beams. Maximum recorded strains were 2.8 %. This suggests that failure will be accompanied by adequate warning (see Plate 7.2 and Table 7.2).
5. No slip accompanied failure of the steel pretensioned beams. Failure in the fiberglass pretensioned beams was accompanied by slip (see Table 7.3). This indicates that the development length of fiberglass strands providing the same effective prestress in a section, is greater.
7. All steel pretensioned beams failed by secondary compression, i.e. tension mode of failure. Fiberglass pretensioned beams also failed the same way excepting that tension failure was generally initiated by slip of one of the strands.
8. The correlation between predictions from the non-linear finite element analysis and test results for fiberglass pretensioned beams is generally close for ultimate load, deflection and concrete strain, but is poorer for fiberglass strand strains. Finite element analysis under estimated the strains compared to test results. It is believed that this is because the stress-strain relation for fiberglass is non-linear under bending strains (see Figure 7.21).

19.2.3 Column Study

1. Theoretically, steel pre-tensioned columns should have a higher capacity than fiberglass columns jacked to the same stress since its effective prestress is lower (see Section 5.5) and its post-cracking response less flexible because of a higher

elastic modulus. However, test results were inconclusive since failure was initiated at the ends (see Plate 8.1) and not by compression or instability. There was, however, sufficient evidence to indicate that the response of fiberglass and steel pretensioned columns was essentially similar (see Figures 8.10-8.11).

2. Fiberglass ties used in two of the tests did not provide the same degree of confinement as the steel ties and ruptured during testing. Steel ties, on the other hand, only deformed. However, the overall response and ultimate capacity of the columns was largely unaffected by the type of lateral reinforcement, e.g. capacities of FG-FG-C1 (with fiberglass ties) and FG-C1 (with steel ties) were comparable. Perhaps of greater importance was the absence of the full pre-compression at the ends (due to insufficient transfer length) in the eccentrically loaded columns that failed at relatively low loads as a consequence (see Table 8.2).
3. The response of fiberglass pre-tensioned columns can be predicted with reasonable accuracy by non-linear finite element analysis (see Figures 8.13-8.19).

19.2.4 Pile Study

1. The driving system selected on the basis of wave analysis was satisfactory. The maximum driving stresses recorded were within the allowable values specified by MOT and agreed reasonably with predictions from the pre-driving analysis (see Table 9.5 and Table 10.1).
2. The stresses in fiberglass and steel pretensioned piles driven through very similar soils (see Figures 10.1-10.2) were comparable although stresses in the fiberglass piles were somewhat larger. There was very little damage to the piles (see Plate 10.3) indicating that the pretensioned fiberglass piles can withstand impact loading resulting in tensile stresses as high as 1.15 ksi.
3. The effective pre-stress in the fiberglass piles was comparable to those in 30 in. x 30 in. piles used by FDOT in a marine environment. Stresses in the fiberglass piles compared very favorably with those in eighteen similarly instrumented 30 in. x 30 in. piles used for supporting the New Edison Bridge (compare Tables 10.1 and 10.4)
4. The allowable driving stresses stipulated by FDOT (Eqs. 9.3-9.5) appear to be reasonable. No damage was recorded for piles even though allowable stresses based on measured cylinder strengths at the time of testing were approached (see Table 10.2) in tests where the drop height was increased to 15 ft. In practice, nominal values, i.e. based on a concrete strength of 5,000 psi, would be used and these were exceeded during driving.

5. Under very severe driving conditions, the E glass/epoxy spirals used in pile FG-FG-P1 ruptured even though it had been designed to withstand a greater ultimate force than the steel ties. No comparable damage was observed in pile FG-FG-P2 (provided with 33 % more fiber area in its E glass/ epoxy ties) nor in the steel ties. This suggests that if fiber reinforced plastic ties are to be used for confining concrete, they must be made substantially stronger to compensate for its low ductility.
6. Pile capacities from CAPWAPC were comparable- to those obtained from SPT 89. Hiley's formula gave better agreement than Engineering News formula using a safety factor of 6 (see Table 10.3).
7. Values of skin friction predicted by CAPWAPC were in close agreement with predictions from SPT 89. The correlation was much poorer with predictions from Vesic's analysis.
8. The Pile Driving Analyzer used to monitor driving stresses proved reliable and effective.

19.3 Long Term Response

19.3.1 Fatigue Response

1. The overall fatigue characteristics of the two fiberglass pretensioned beams tested were comparable to those of similarly loaded steel pretensioned beams (see Table 11.3).
2. Fatigue failure (see Plate 11.1) was not due to rupture of the strands but due to slip. This suggests that fatigue tests for fiberglass strands in air may not provide reliable data.
3. The stress range in the failed beam, FG-W9, was 21.7 ksi ($0.073f_{fg}$) at a maximum stress level of 169.1 ksi ($0.56f_{fg}$). The stress range for the beam that survived the application of 2 million cycles, FG-E9, was 12 ksi ($0.04f_{fg}$) at a maximum stress level of 141.3 ksi ($0.47f_{fg}$).
4. There is very little reduction in the ultimate static capacity as a result of the application of 2 million cycles of fatigue loading.
5. Fatigue loading of fiberglass pretensioned beams in the post-cracking range should be avoided since deflections and crack width are proportionately much greater than in steel because of its low elastic modulus.

19.3.2 Material creep in concrete

1. The creep coefficient for plant mixed concrete using Type III cement (see Table 4.2 for mix design) was comparable to the average creep coefficient predicted by the ACI Equations (see Figures 12.1-12.2).

19.3.3 Long term creep losses

1. Prestress losses in fiberglass columns are considerably lower than in steel columns due to its low modulus of elasticity. Depending on the stress level, prestress losses in steel columns were between 16% to 33.9% greater than that in comparable fiberglass columns.
2. Prestress creep losses increase with the increase in axial compression force for both fiberglass and steel columns. The prestress loss rate is higher in steel columns than in fiberglass columns.
3. For average field temperature and relative humidity in Florida, the percentage prestress loss is about the same as that in a laboratory environment.
4. The permanent effective prestress in fiberglass columns is significantly higher than in steel columns.
5. The shortening in fiberglass columns was about 17% higher than the comparable shortening in the steel column.
6. ACI creep and shrinkage equations, modified to account for different material properties of fiberglass, can be used to approximately predict the total strain and effective prestress in the fiberglass columns.

19.3.4 Durability study

1. Significant strength reductions were recorded for pre-cracked fiberglass pretensioned beams subjected to dry/wet cycles. This was initiated after 3-9 months exposure. Strength reduction for un-cracked fiberglass pre-tensioned beams was also recorded but after a greater period of exposure of 12-18 months (see Tables 16.6-16.7 and Figure 16.10). No commensurate decrease in strength was recorded for control specimens tested after 20 months (see Table 16.8).
2. There was no physical manifestation of deterioration of the fiberglass pretensioned beams exposed to wet/dry cycles. This is in marked contrast to steel pretensioned specimens where evidence of rust stains and spalling of concrete provides an

index of corrosion damage. The absence of any such warning makes the use of fiberglass strands potentially more dangerous in structural applications.

3. Failure of fiberglass beams showing substantial reductions in strength was characterized by a new mode of failure termed "corrosion mode" in which the beams failed without warning immediately after the initial tension crack. In essence, the beams responded as if they were un-reinforced (see Plate 16.4). Tests on 'half segments of failed beams showed that the extent of the damage was more severe in the wet end compared to that for the dry end (see Tables 16.9-16.10).
4. The results of the scanning electron microscope investigation corroborated the findings from the durability testing. There was little damage to glass fibers in the dry segment but much greater damage in the wet or wet/dry segments. Damage was also greater near the concrete interface than away from it.
5. The repeat test of a pre-cracked fiberglass beam exposed to nine months of wet/dry cycles did not fail in the corrosion mode. This may be because the fiberglass strands for this beam were provided with extra resin coating to provide a smooth surface (see Table 16.7).
6. The primary cause of deterioration of S-2 glass/epoxy strands was diffusion of alkaline pore solution through the Shell Epon 9310 resin (see Table 2.3). The low stress level and the relatively short duration of the study (20 months) tend to rule out stress rupture. Other possible causes such as surface damage or resin cracking can only be contributory since it cannot explain why pre-cracked beams failed earlier than the un-cracked ones.
7. It is highly improbable that the Shell Epon 9310 resin used in the study is the only resin that absorbs hydroxyl ions by diffusion. Less expensive polyesters and vinylesters can be expected to show comparable diffusion characteristics. In view of this, the durability of all glass fiber composites in concrete must be carefully investigated.
8. Considerable loss of section was noted in the un-cracked steel pre-tensioned beam ST-M3 after 18 months exposure (see Section 17.2.2.3). The greatest loss of section occurred adjacent to a honeycomb and also where epoxy had been used to attach strain gages to the steel surface. The approximate loss of material was 0.427 g. No commensurate reduction in section was observed in any of the other beams cut open, i.e. un-cracked beam ST-E3 after 12 months and pre-cracked beam ST-M2 at the end of the study. However, no capacity reductions were recorded since failure was initiated by crushing of concrete.
9. No evidence of carbonation was detected in beams cut open at the end of the study (see Section 17.2.1).

10. Electrical measurements such as half cell potentials, concrete resistivity and AC impedance can be collectively used to establish the state of active corrosion in steel. However, proposed thresholds (Tables 15.1-15.2) should be refined to reflect additional conditions such as type of exposure, type of structure, type of concrete, etc. Resistivity measurements do not appear to provide a clear measure of the state of corrosion (see Section 15.4).
11. The chloride levels in the concrete for control specimens were between 3.75 %15 % of the maximum ACI Committee 222 limit of 0.08 % by weight of cement. After 20 months exposure, pre-cracked specimens ST-M2 and FG-E1 reached chloride levels of 1.01 % and 0.93 % respectively. Un-cracked steel specimen ST-M3 which lost the most metal had a chloride level of 0. 85 % after 18 months exposure.
12. The chloride variation along the beams and with exposure were consistent (see Figures 17.1-17.6) and indicated that the equipment used for sample extraction did not lead to its contamination and additionally that the Florida Method used for its determination had been correctly implemented.

20. RECOMMENDATIONS

20.1 Introduction

Although this study demonstrated conclusively the inadequacy of the Shell Epon 9310 resin in protecting stressed glass fibers from alkali attack, the potential of fiberglass as a pre-tensioning material should not be discounted as a result. Of the alternative materials available, carbon fiber is vastly more expensive and its very low failure strain makes it unsuitable for prestressing applications (see Table 3.1). Aramid fibers are less expensive than carbon but have much higher creep rates. They are also somewhat vulnerable to alkali attack (see Figure 3.4), though their durability is far superior compared to fiberglass.

It may be recalled that the choice of S-2 glass for this study was primarily based on its superior impact resistance and mechanical properties. The results of this study indicate however, that in future applications much more attention must be paid to durability. This chapter recommends measures for enhancing the durability of fiberglass in concrete. This is discussed in Section 20.2. Additionally, stressing related measures that can help eliminate potential damage to fiberglass strands are briefly considered in Section 20.3.

20.2 Enhancing alkali resistance

Since diffusion of the alkaline pore solution through the epoxy resin was identified as the primary cause of the deterioration of the fiberglass, it might be argued that the use of an epoxy with zero diffusion to hydroxyl ions would be the ideal solution. From a practical standpoint however, such a resin is likely to be prohibitively expensive and may be impossible to use in a pultrusion process. Alternatively, the use of non-alkaline cement could be a potential solution. Unfortunately, this may not be feasible at the present time. In view of this, a strategy for protecting fiberglass must be devised that is both feasible and economic. At its core, the alkali resistance of the glass should be increased while simultaneously reducing alkalinity and porosity of the concrete. Some suggestions are listed below:

1. Research should be directed towards the development of concrete with low alkalinity, e.g. using silica fume aggregates. Such a concrete is likely to offer the best protection at the lowest cost.
2. The use of alkali resistant (AR) glass should be given serious consideration in applications involving direct contact with concrete.

3. The resin system used in the composite should have the lowest hydroxyl ion diffusion rate compatible with the highest ultimate strain. The use of polymer concrete may provide an additional barrier against ingress of hydroxyl ions.
4. The use of a protective polymeric coating on the fiberglass strands, such as used in carbon fiber cables should be considered. This will prevent damage and additionally provide a barrier against alkali attack.
5. The long term durability of new fiberglass composites should be determined on the basis of tests in concrete rather than in aqueous hydroxyl solutions. The latter tests cannot simulate possible damage to fiberglass during concreting nor other unexpected effects, e.g. honeycombing that traps moisture. Additionally, stress rupture tests should be conducted to establish the safe jacking stress.

20.3. Prestressing requirements

Although the specimens for this study were successfully pretensioned, the procedures used were intended for laboratory work. Serious shortcomings were evident during the prestressing of the larger pile and column specimens that was carried out in one of Florida's largest prestressing yards (see Section 4.8). If fiberglass is to be a serious contender for replacing steel, a simple yet reliable prestressing system must be developed that can be used in commercial applications. A thorough review of current commercial prestressing operations should be undertaken with a view to changes needed to adapt it for fiberglass. Some areas of improvement and concern are listed below:

1. Strict quality control procedures must be instituted so that the mechanical properties of fiberglass are reliable and do not vary from supplier to supplier. A careful study should be made of actual construction practice so that the properties of fiberglass under these conditions are known.
2. Since the jacking force for fiberglass is very low compared to steel (to offset its lower long term tensile strength under sustained loads) a proportionately greater strand area is required to provide the same prestressing force. This larger area may be more conveniently provided by using other shapes, e.g. rectangular strips, successfully used with Arapree. Moreover, the greater surface area for such shapes will simplify anchorage requirements.
3. Header plates, chucks and spacers should be lined with plastic to minimize damage to strands. Fiberglass stirrups and ties should be developed together with a simple system for tying the strands to the stirrups.
4. A system for monitoring corrosion in fiberglass due to alkali attack should be developed. Additionally, methods of correcting damage should be investigated.

21. REFERENCES

- 1.1 Powers, R. (1988), Florida Department of Transportation, Private Communication.
- 1.2 Structures Design Guidelines (1987), Florida Department of Transportation, Tallahassee, FL, Section 7.6F.
- 1.3 Gerritse, A. and Schurhoff, H.J. (1986) Prestressing with Aramid Tendons, FIP 10th Congress, New Delhi.
- 1.4 Rostásy, F.S., (1988) "New Prestressing Materials", Congress Report, FIP'88-IXth Congress, Jerusalem, Israel, September, pp. 148-159.
- 1.5 Dolan, C.W., (1990) "Developments in Non-Metallic Prestressing Tendons", PCI Journal, Vol. 35, Nº 5, September-October, pp. 80-88.
- 1.6 Mallick, P.K. (1988) *Fiber-Reinforced Composites: Materials Manufacturing, and Design*, Marcel Dekker, Inc., New York.
- 1.7 Rostásy, F.S. (1990) "Working Group on High Strength Fibrous Tensile Elements", Congress Report, FIP'90-XIth Congress, Hamburg, Germany, June, pp. 30-34.
- 1.8 S-2 Glass® Fiber (1990) Enhanced Properties for Demanding Applications, Publication Nº 15-PL-16154, Owens-Corning Fiberglas Corporation, Ohio, March.
- 1.9 CFCC Technical Data (1989), Tokyo Rope Manufacturing Company, Limited, October.
- 1.10 Richmond, B. and Head, P.R. (1988) "Alternative Materials in Long-Span Bridge Structures", 1st Oleg Kerensky Memorial Conference, London, England, June.
- 1.11 Babaei, K. and Gloyd, C.S. (1989), "Fiber Reinforced Plastic Rods for Prestressing Concrete Structures", Pre-print, Paper 880197, Transportation Research Board 68th Annual Meeting, January 22-26.
- 1.12 Rubinsky, I. and Rubinsky, E. (1951) Report on Preliminary Investigation on the Feasibility of using Fiberglass for Prestressing Concrete, Princeton University, Princeton, New Jersey, August, 32 pp.

- 1.13 Miesseler, H.J. and Preis, L., High Performance Glass Fiber Composite Bars as Reinforcement in Concrete and Foundation Structures, Strabag Bau-AG, Cologne, Germany, and Bayer AG, Leverkusen, Germany, (no date).
- 1.14 Iyer, S. (1992) Construction of an Advanced Composite Prestressed Concrete Bridge. Presentation for TRB Committee A2C07, 71st Transportation Research Board Meeting, Washington, DC, January.
- 1.15 Burgoyne, C.J. and Chambers, J.J. (1985) "Prestressing with Parafil Tendons, Concrete, October, pp. 12-15
- 1.16 Dolan, C.W. (1989) "Prestressed Concrete Using Kevlar Reinforced Tendons", Ph.D. Dissertation, Cornell University, New York, August.
- 1.17 Gerritse, A. and Werner, J. (1991) "ARAPREE, a Non-Metallic Tendon", Proceedings of the Specialty Conference, Advanced Composite Materials in Civil Engineering Structures, Edited by S.L. Iyer and R. Sen, American Society of Civil Engineers, New York, 1991
- 1.18 Chawla, K.K. (1987) *Composite Materials*, Springer-Verlag, New York.
- 1.19 Somes, N.F. (1963) "Resin Bonded Glass Fiber Tendons for Prestressed Concrete". Magazine of Concrete Research, Vol 15, No 45, November, pp.151-158.
- 1.20 Wines, J.C. and Hoff, G.C. (1966) Laboratory Investigation of Plastic Glass Fiber reinforcement for Reinforced and Prestressed Concrete, Report 2, July, US Army Engineering Waterways Experiment Station, Corp of Engineers, Vicksburg, MS.
- 1.21 Iyer, S. and Kumaraswamy, C. (1988) "Performance Evaluation of Glass Fiber Composite Cable for Prestressing Concrete Units". 33rd International SAMPE Symposium 33, Anaheim, CA.
- 2.1 Iyer, S.L. (1991) Final Report on Fiberglass Cable Testing for Feasibility of Using Fiberglass Prestressed Piles in Marine Environment, December.
- 2.2 Nawy, E.G. and Neuwerth, A.M. (1977) "Fiberglass Reinforced Concrete Slabs and Beams", Journal of the Structural Division, Proceedings of the ASCE, Vol. 103, № ST2, February.
- 2.3 Textile Fibers for Industry (1985) Publication № 5-TOD-8285, Owens-Corning Fiberglas Corporation, Ohio, September.
- 2.4 Greenwood, M.E. (1991). Personal Communication, Owens-Corning Fiberglas

Corporation, Ohio, November.

- 2.5 S-2 Glass® Fiber (1990) Enhanced Properties for Demanding Applications, Publication Nº 15-PL-16154, Owens-Corning Fiberglas Corporation, Ohio, March.
- 2.6 Shell Chemical Company (1990), Technical Bulletin SC:712:90, Epon Resin 9310, Houston, Texas.
- 2.7 SPI Composites Institute (1990) Introduction to Composites, Washington, D.C.
- 2.8 Greenwood, M.E. (1990) Personal Communication, Owens-Corning Fiberglas Corporation, Ohio, August.
- 2.9 Babaei, K. and Gloyd, C.S. (1989), "Fiber Reinforced Plastic Rods for Prestressing Concrete Structures", Pre-print, Paper 880197, Transportation Research Board 68th Annual Meeting, January 22-26.
- 2.10 Rostásy, F.S. (1988) "New Prestressing Materials", Congress Report, FIP'88-IXth Congress, Jerusalem, Israel, September, pp. 148-159.
- 2.11 Iyer, S.L. (1991) Progress Report on Fiberglass Cable Testing for Feasibility of Using Fiberglass Prestressed Piles in Marine Environment, January.
- 3.1 Miesseler, H.J. and Preis, L., High Performance Glass Fiber Composite Bars as Reinforcement in Concrete and Foundation Structures, Strabag Bau-AG, Cologne, Germany, and Bayer AG, Leverkusen, Germany, (no date).
- 3.2 Gerritse, A. and Werner, J. (1991) "ARAPREE, a Non-Metallic Tendon", Proceedings of the Specialty Conference, Advanced Composite Materials in Civil Engineering Structures, Edited by S.L. Iyer and R. Sen, American Society of Civil Engineers, New York.
- 3.3 CFCC Technical Data (1989) Tokyo Rope Manufacturing Company, Limited, October.
- 3.4 Dolan, C.W. (1990) "Developments in Non-Metallic Prestressing Tendons", PCI Journal, Vol. 35, Nº 5, September-October, pp. 80-88.
- 3.5 High Strength Tension Members Made of Carbon Fiber Composites, BASF, Ludwigshafen, Germany, (no date).
- 3.6 Zoch, P., Kimura, H. and Heym, M. (1990) Carbon Fiber Composite Cables - A New Class of Prestressing Members. Presented at the 69th Transportation Research Board Meeting, Washington, DC.

- 3.7 Burgoyne, C.J. and Chambers, J.J. (1985) "Prestressing with Parafil Tendons", Concrete, October, pp. 12-15
- 3.8 Glaser, R.E., Moore, R., L. and Chiao, T.T. (1983) "Life Estimation of an S-Glass/Epoxy Composite Under Sustained Tensile Loading", Composites Technology Review, Vol. 5, Nº 1, pp. 21-26.
- 3.9 Rostásy, F.S. (1988) "New Prestressing Materials", FIP'88-IXth Congress, Jerusalem, Israel, September, pp. 148-159.
- 3.10 Collins, M.P. and Mitchell, D. (1991) *Prestressed Concrete Structures*, Prentice Hall, New Jersey.
- 3.11 ACI 215 Committee (1974), "Consideration For Design of Concrete Structures Subjected to Fatigue Loading", ACI Journal, Vol. 71, Nº 3, March, pp. 97-121.
- 3.12 Walton, J.M. and Yeung, Y.C.T. (1986) "The Fatigue Performance of Structural Strands of Pultruded Composite Rods", Conference Publication, Vol. II, International Conference on Fatigue of Engineering Materials and Structures, University of Sheffield, September, pp. 315-320.
- 3.13 S-2 Glass® Fiber (1990) Enhanced Properties for Demanding Applications, Publication Nº 15-PL-16154, Owens-Corning Fiberglas Corporation, Ohio, March.
- 3.14 Bentur, A. and Mindess, S. (1990) *Fibre Reinforced Cementitious Composites*, Elsevier Science Publishers, New York.
- 3.15 Greenwood, M.E. (1991) Personal Communication, Owens-Corning Fiberglas Corporation, Ohio, June.
- 3.16 Gerritse, A. (1988) "Prestressing With Arapree; The Artificial Tendon", Contribution to the Symposium on: New Materials for Prestressing and Reinforcement of Heavy Structures, Paris, October.
- 3.17 Hahn, H.T. (1987) "Hydrothermal Damage in Graphite/Epoxy Laminates", Journal of Engineering Materials and Technology, Vol. 109, January.
- 3.18 Springer, G.S. (1982) "Moisture Absorption in Fiber-Resin Composites", Development in Reinforced Plastics, Vol. 2.
- 3.19 Ishai, O. and Arnon, U. (1978) "'Instantaneous' Effect of Internal Moisture Conditions on Strength of Glass-Fiber-Reinforced Plastics", Advanced Composite Materials-Environmental Effects, ASTM STP 658.
- 3.20 DeIasi, R. and Whiteside, J.B. (1978) "Effect of Moisture on Epoxy Resins and

- Composites", Advanced Composites Materials-Environmental Effects, ASTM STP 658, Philadelphia, pp. 2-20.
- 3.21 Kasturiarachchi, K.A. and Pritchard, G. (1983) "Water Absorption of Glass/Epoxy Laminates Under Bending Stresses", Composites, Vol. 14, № 3, July, pp. 244-250.
- 3.22 Lou, A.Y. and Murtha, T.P. (1987) "Environmental Effects on Glass Fiber Reinforcement PPS Stampable Composites", Journal of Composite Materials, Vol. 21, October.
- 3.23 Ashbee, K.H.G. and Wyatt, R.C. (1969) "Water Damage in Glass Fibre/Resin Composites", Pros. Roy. Soc. London, Series A, Vol. 312, p. 553.
- 3.24 Kaelble, D.H., Dynes, P.J., Crane, L.W. and Maus, L. (1975) "Interfacial Mechanisms of Moisture Degradation in Graphite/Epoxy Composites", J. Adhesion, Vol. 7, p. 25.
- 3.25 Fried, N. (1968) "Structures of Reinforced Plastics", Machine Design, Vol. 40, January, pp. 178-183.
- 3.26 Fried, N. and Graner, W.R. (1966) "Durability of Reinforced-Plastic Structural Materials in Marine Service", Marine Technology Society Journal, Vol. 1, July, pp. 321-327.
- 5.1 Harajli, M.H. and Namaan, A. (1984) "Deformation and Cracking of Partially Prestressed Concrete Beams under Static and Cyclic Fatigue Loading", Report No. UMEE 84R1, Department of Civil Engineering, The University of Michigan, Ann Arbor, MI.
- 5.2 Somes, N.F. (1963) "Resin-Bonded Glass-Fiber Tendons for Prestressed Concrete", Magazine of Concrete Research, Vol. 15, № 45, November, pp. 151-158.
- 5.3 American Association of State Highway and Transportation Officials (1989), Standard Specifications for Highway Bridges, Washington, DC.
- 6.1 Somes, N. F. (1963) Resin bonded glass fiber tendons for prestressed concrete. Magazine of Concrete Research, Vol. 15, No. 45, November.
- 6.2 Iyer, S. and Kumaraswamy, C. (1988) Performance Evaluation of Glass and Fiber Composite Cable or Prestressed Concrete Units, 33rd International SAMPE Symposium, March, Anaheim, CA.
- 6.3 Iyer, S., Khubchandani, A. and Feng, J. (1991) Fiberglass and Graphite Cables

- for Bridge Decks. Advanced Composite Materials in Civil Engineering Structures (Ed. S. Iyer and R. Sen), ASCE, NY. NY.
- 6.4 Zia, P. and Mostafa, T. (1977) Development Length of Prestressed Strands. PCI Journal, Vol. 22, No. 5, September-October.
 - 6.5 Nilson, A. (1987) Design of Prestressed Concrete, Second Edition, John Wiley & Sons., NY, NY.
 - 6.6 Carrasquillo, R., Nilson, A. and Slate, F. (1981) Properties of High Strength Concrete Subject to Short Term Loads, J. ACI, Vol. 78, No. 3.
 - 6.7 Kaar, P. H., Lafraugh, R. W., and Mass, M. A. Influence of concrete strength on strand transfer length, PCI Journal, October 1963.
 - 6.8 Hoyer, E. and Friedrich, "Beitrag Zur Frage der Hafspannung in Eisenbetonbauteilen," Beton und Eisen, Berlin, 1939 (Vol. 38, No. 6), pp. 107-110. Also, T. Y. Lin and N. H. Burns, Design of Prestressed Concrete Structures, John Wiley & Sons Inc., New York, 1981.
 - 7.1 Kang, Y. (1977) "Non-Linear Geometric, Material and Time Dependent Analysis of Reinforced and Prestressed Concrete Frames", Ph.D Dissertation, university of California, Berkeley.
 - 7.2 Sun, Z.L (1991) "Static and Fatigue Response of Fiberglass Pretensioned Beams", MSCE Thesis submitted to the Department of Civil Engineering and Mechanics, University of South Florida, Tampa, Florida, June.
 - 8.1 Yuan, R.L. (1989) "Prestressed Concrete Column Behavior", Prestressed Concrete Institute, Research Project № 3, Department of Civil Engineering, University of Texas, Arlington, Texas.
 - 8.2 Aroni, S. (1968) Slender Prestressed Concrete Columns, Journal of the Structural Division, ASCE, Vol 94, No. ST 4, pp. 875-904.
 - 8.3 Kang, Y. (1977) "Non-Linear Geometric, Material and Time Dependent Analysis of Reinforced and Prestressed Concrete Frames", Ph.D Dissertation, University of California, Berkeley.
 - 8.4 Mariscal, D. (1991) "Strength and Durability of Fiberglass Pretensioned Elements". MSCE Thesis submitted to Department of Civil Engineering & Mechanics, University of South Florida, Tampa, FL, December.
 - 9.1 Bowles, J.E.(1988) *Foundation Analysis and Design*, Fourth Edition, McGraw-Hill, NY, NY.

- 9.2 Holloway, D.M. (1975) Wave equation Analyses of Pile Driving, Technical Report S-75-5, US Army Engineer Waterways Experimental Station Soils & Pavement Laboratory, Vicksburg, MS.
- 9.3 Fellenius, B. (1988) Editor, Third International Conference, Application of Stress Wave Theory to Piles, Ottawa, Canada.
- 9.4 Goble, G.G. and Rausche, F. (1976) Wave Equation Analysis of Pile Driving - WEAP Program. Prepared for the US Department of Transportation, Federal Highway Administration, Implementation Division, Office of Research and Development.
- 9.5 Structures Design Guidelines (1990), Florida Department of Transportation, Bureau of Structures Design, Tallahassee, Section 7.6.
- 9.6 American Association of State Highway and Transportation Officials (1989), Standard Specifications for Highway Bridges, Washington, DC.
- 9.7 GRL & Associates, Orlando (1991) Report on Dynamic Pile Tests for New Edison Bridge, Lee County, FL, March.
- 9.8 Isaacs, D.V. (1931) Reinforced concrete pile formulae. Paper No. 370, Transactions Australian Institute of Civil Engineers, Vol 12, pp. 321-323.
- 9.9 Kolsky, H. (1963) *Stress Waves in Solids*, Dover Publications, NY.
- 9.10 Richart, F.E., Hall, J.R. and Woods, R.D. (1970) *Vibrations of Soils and Foundations*, Prentice-Hall, Englewood Cliffs, NJ.
- 9.11 Crapps, D. (1977) Wave equation study and recommended specifications for the impact driving of prestressed concrete piles. Ph.D Thesis. University of Florida, Gainesville, FL.
- 9.12 Smith, E.A.L (1960) Pile driving analysis by wave equation. ASCE, Journal of Soil Mechanics and Foundation Engineering, Volume 86, SM2, pp. 1145-1171.
- 9.13 Chow, Y.K. (1981) Dynamic behaviour of piles. Ph.D Thesis. University of Manchester, Manchester, UK
- 9.14 Smith, I.M. and Chow, Y.K. (1982) Three dimensional analysis of pile drivability. Second International Conference on Numerical Methods in Offshore Piling, University of Texas, Austin, TX, pp. 1-18.
- 9.15 Coutinho, A., Costa, A., Landau, L. and Ebecken, N. (1988) Pile Driving Simulation and Analysis by the Finite Element Method. Third International

- Conference on Application of Stress Wave Theory to Piles, Edited by B. Fellenius, Ottawa, Canada, pp. 197-207.
- 9.16 Simons, H.A. and Randolph, M.F. (1985) A new approach to one dimensional pile driving analysis. Proceedings of the Fifth International Conference on Numerical Methods in Geomechanics, Edited by T. Kawamoto & Y. Ichikawa, A.A. Balkema, Rotterdam, pp. 1457-1464.
- 9.17 Lowery, L.L. (1976) Wave equation utilization manual, draft user's guide for TIDYWAVE, Texas A & M University.
- 9.18 Novak, M., Nogami, T. and Aboul-Ella, F. (1978) Dynamic soil reactions for plane strain case. Journal of Engineering Mechanics Division, ASCE, Vol 104, No EM4, pp. 953-959.
- 9.19 Lysmer, J. and Richart, F.E. (1966) Dynamic response of footing to vertical loading. Journal of Soil Mechanics and Foundations Division, ASCE, Vol. 92, Vol. 104, No. EM4, pp. 953-959.
- 9.20 Chow, Y.K., Wong, K.Y., Karunaratne, G.P. and Lee, S.L. (1988) Wave equation analysis of piles - a rational theoretical approach. Application of Stress Wave Theory to Piles, Third International Conference (Edited by B. Fellenius), Ottawa, Canada, pp. 208-217.
- 9.21 GRLWEAP (1990) Wave Equation Analysis of Pile Driving, GRL & Associates, Cleveland, OH.
- 9.22 Brown Testing Laboratory (1991) Report on Hidden Lagoon at Arrowhead Point, Tierra Verde, FL.
- 9.23 Standard Specifications for Road and Bridge Construction (1990), Florida Department of Transportation, Tallahassee, FL, Section 455.
- 9.24 Wadsack, P. (1991) Feasibility of fiberglass as a prestressing material for piles. MSCE Thesis submitted to the department of Civil Engineering & Mechanics, University of South Florida, June.
- 9.25 Vesic, A.S. (1977) Design of Pile Foundations, National Cooperative Highway research Program Synthesis of Highway Practice # 42, Design of Pile Foundations, Transportation Research Board, National research Council, Washington, D.C.
- 9.26 Meyerhoff, G.G. (1956) Penetration tests and bearing capacity of cohesionless soils. Journal of Soil Mechanics and Foundation Division, ASCE, Vol 82, SM1, pp. 1-9.

- 9.27 FDOT Bulletin 121 A SPT Drilling Data Correlations, Pile Foundations, Florida Department of Transportation, Tallahassee, FL.
- 9.28 SPT 89 Design of Pile Foundations, PC Version of RB 121, Florida Department of Transportation, Tallahassee, FL.
- 9.29 Dover, A.R., Ping, W.C.V. and Locke, G.E. (1982) Parametric Study on Driveability of Large Piles". Second International Conference on Numerical Methods in Offshore Piling, University of Texas, Austin, TX.
- 10.1 Goble, G.G. (1975) Bearing Capacity of Piles from Dynamic Measurements. Final Report, Department of Civil Engineering, Case Western University, Cleveland, Ohio.
- 10.2 Likins, G. (1984) Field Measurements and the Pile Driving Analyzer. proceedings of the Second International Conference Seminar on the Application of Stress Wave Theory to Piles, Stockholm, pp. 298-305.
- 10.3 Tucker, L.M. and Briad, J.L. (1988) Analysis of the pile load test program at the lock and dam 26 replacement project. Final report prepared for US Army Engineer District, St. Louis, Missouri.
- 10.4 Fellenius, B. (1988) Editor, Third International Conference, Application of Stress Wave Theory to Piles, Ottawa, Canada.
- 10.5 Rausche, F., Goble, G. and Likins, G. (1985) Dynamic Determination of Pile Capacity, Journal of Geotechnical Division, ASCE, Vol 111, March, pp. 367-383.
- 10.6 Hussein, M., Likins, G. and Rausche, F. (1988) Testing Methods of Driven Piles, Pile Buck Manual, Jupiter, FL.
- 10.7 Hussein, M. and Likins, G. (1991) Static pile capacity by dynamic methods. First Geotechnical Engineering Conference, Cairo University, October.
- 10.8 Goble, Rausche, Likins & Associates, Inc. (1989) An introduction into dynamic pile testing methods, Cleveland, OH.
- 10.9 GRL & Associates, Orlando (1991) Report on Dynamic Pile tests on Fiberglass Prestressed Piles, Tierra Verde, July.
- 10.10 Crapps, D. (1977) Wave equation study and recommended specifications for the impact driving of prestressed concrete piles. Ph.D Thesis. University of Florida, Gainesville, FL.

- 10.11 Goble, G., Rausche, F. and Likins, G. (1980) The analysis of pile driving - A state of the art. International Seminar on the Application of Stress Wave Theory of Piles, Stockholm, pp. 131-161.
- 10.12 Hussein, M. and Rausche, F. (1991) Bearing capacity of deep foundations from dynamic measurements and static tests - ten correlation cases. Piletalk International, Kuala Lumpur, Malaysia, August.
- 10.13 Thompson, C.D. and Devata, M. (1980) Evaluation of ultimate bearing capacity of different piles. International Seminar on the Application of Stress Wave Theory of Piles, Stockholm, pp. 163-195.
- 10.14 Vesic, A.S. (1977) Design of Pile Foundations, National Cooperative Highway research Program Synthesis of Highway Practice # 42, Design of Pile Foundations, Transportation Research Board, National research Council, Washington, D.C.
- 10.15 Meyerhoff, G.G. (1956) Penetration tests and bearing capacity of cohesionless soils. Journal of Soil Mechanics and Foundation Division, ASCE, Vol 82, SM1, pp. 1-9.
- 10.16 FDOT Bulletin 121 A SPT Drilling Data Correlations, Pile Foundations, Florida Department of Transportation, Tallahassee, FL.
- 10.17 SPT 89 Design of Pile Foundations, PC Version of RB 121, Florida Department of Transportation, Tallahassee, FL.
- 10.18 Poulos, H. and Davis, E. (1980) *Pile Foundation Analysis & Design*, John-Wiley & Sons, NY, NY.
- 10.19 GRL & Associates, Orlando (1991) Report on Dynamic Pile Tests, New Edison Bridge, Lee County, FL.
- 11.1 ACI Committee 215 (1974) "Consideration For Design of Concrete Structures Subjected to Fatigue Loading," ACI Journal, Vol. 71, No.3, March, pp. 97-121.
- 11.2 Ekberg, C.E., Walther, R.E., Slutter, R.G. (1957) "Fatigue Resistance of Prestressed Concrete Beams in Bending," Journal of Structural Division, July, pp. 4-17.
- 11.3 Naaman, Antoine E. (1982) *Prestressed Concrete Analysis and Design*, McGraw-Hill Company.
- 11.4 Harajli, Muhamed H. and Naaman, Antoine E. (1984) "Deformation and cracking of Partially Prestressed Concrete Beams under Static and Cyclic Fatigue

Loading," Report No. UMEE 84R1, Department of Civil Engineering, The University of Michigan.

- 11.5 Hanson, J.M., Hulsbos, C.L. and Van Horn, D.A. (1970) "Fatigue Tests of Prestressed Concrete I-Beams," Proceedings, ASCE, Vol. 96, No. ST11, November, pp. 2443-2463.
- 11.6 Rabbat, B.G., Kaar, P.H., Russell, H.G., and Bruce, R.N. (1978) "Fatigue Tests of Full-Size Prestressed Girders," Technical Report No. 113, Portland Cement Association, Research and Development Laboratories, June.
- 11.7 Ozel, A.M., and Ardaman, E. (1956) "Fatigue Tests of Pretensioned Prestressed Beams," ACI Journal, Proceedings, Vol. 53, No. 4, October, pp. 413-424.
- 11.8 Abeles, P.W., Brown, E.I., and Hu, C.H. (1974) "Fatigue Resistance of Under-Reinforced Prestressed Beams Subjected to Different Stress Ranges; Miner's Hypothesis," ACI Journal, SP-41, Paper 11, pp. 237-277.
- 11.9 Bennet, E.W., and Dave, N.J. (1969) "Test Performance and Design of Concrete Beams With Limited Prestress," The Structural Engineer (London), Vol. 47, No. 12, December, pp. 487-496.
- 11.10 Dave, N.H., and Garwood, J.J. (1975) "The Limit State Behavior of "Class-3" Post-Tensioned Beams Under Short-Term, Sustained and Fatigue Loading," In Behavior in Service of Concrete Structures, Colloquium Interassociation I.A.B.S.E., F.I.P., C.E.B., R.I.L.E.M., I.A.S.S., Liege, June, pp. 319-330.
- 11.11 Foo, M.H., and Warner, R.F. (1984) "Fatigue Test on Partially Prestressed Concrete Beams," In Partial Prestressing From Theory To Practice, NATO Advanced Research Workshop, Paris, France, June 18-22.
- 11.12 Mansur, M.A. (1983) "Partially Prestressed Concrete Beams Under Repeated Loading," International Symposium - Nonlinearity and Continuity in Prestressed Concrete, University of Waterloo, Waterloo, Ontario, Canada, July 4-6.
- 11.13 Conrad Paulson, Jr., Frank, Karl H. and Breen E. John (1983) "A Fatigue Study of Prestressed Strand," Research Report No. 300-1, Center for Transportation Research Bureau of Engineering Research, The University of Texas at Austin, April.
- 11.14 Tide, H.R. and Van Horn D.A. (1966) "A Statistical Study of the Static and Fatigue Properties of High Strength Prestressing Strands," Report No. 309.2, Fritz Engineering Laboratory, Lehigh University, June, pp. 86.
- 11.15 Warner, R.F. and Hulsbos, C.L. (1966) "Probable Fatigue Life of Prestressed

- Concrete Beams," Prestressed Concrete Institute Journal, Vol.11, No.2, April, pp. 16-39.
- 11.16 Edwards, A.D. and Picard, A. (1972) "Fatigue Characteristics of Prestressing Strands," Proceedings, ICE (London), Vol. 53, September, pp. 323-336.
- 11.17 Gylltoft, K. (1979) "Bond Properties of Strands in Fatigue Loading," Division of Structural Engineering, University of Lulea, Research Report No. TULEA 1979:22.
- 11.18 Fisher, J.W. and Viest, I.M. (1961) "Fatigue Tests of Bridge Materials of the AASHTO Road Test," Special Report No. 66, Highway Research Board, pp. 132-147.
- 11.19 Miesseler, H.J. and Preis, L., "High Performance Glass Fiber Composite Bars as Reinforcement in Concrete and Foundation Structures," STRABAG BAU-AG, Germany (no date).
- 11.20 Iyer, S. and Kumaraswamy, C. (1988) "Performance Evaluation of Glass Fiber Composite Cable for Prestressing Concrete Units," 33rd International SAMPE Symposium 33, Anaheim, CA.
- 11.21 Iyer, S.L. (1991) Final Report on Fiberglass Cable Testing for Feasibility of Using Fiberglass Prestressed Piles in Marine Environment, December.
- 11.22 Ontario Highway Bridge Design Code, 1991 (under review).
- 12.1 ASTM C 512 -76 Standard Test Method for Creep of Concrete in Compression, pp. 326-329.
- 12.2 MacCaulley, D., Mittelacher, Martin, Mross, J., Roebuck, J. and Winemberg, R. (1990), Florida Aggregates in Construction, Florida Concrete and Products Association and the Concrete Materials Engineering Council.
- 12.3 ACI Committee 209 (1982) "Prediction of Creep, Shrinkage and Temperature Effects in Concrete Structures,. Report ACI 209R-82, Designing for Creep and Shrinkage in Concrete Structures, Special Publication 76, American Concrete Institute, Detroit, MI.
- 12.4 Saadat, A. (1991) "Studies in Prestressed Concrete". MSCE Thesis submitted to the Department of Civil Engineering and Mechanics, University of South Florida, Tampa, FL.
- 13.1 United States National Oceanic and Atmospheric Administration (1985) "Climate of the States", 3rd Edition.

- 14.1 Stark, D., (1984) "Determination of Permissible Chloride Levels in Prestressed Concrete", PCI Journal, Vol. 29, № 4, July-August, pp. 106-119.
- 14.2 Pfeifer, D.W., Landgren, J.R, and Perenchio, W., (1986) "Concrete, Chlorides, Cover and Corrosion", PCI Journal, July-August, pp.42-53.
- 14.3 Pfeifer, D.W. Landgren J.R. and Zoob A., (1987) "Protective Systems for New Prestressed and Substructure Concrete", U.S. Department of Transportation, Final Research Report, Virginia, April.
- 14.4 Mozer, J. D., Bianchini, A. C. and Kesler, C. E., (1965) "Corrosion of Reinforcing Bars in Concrete", ACI Journal, Proceedings Vol. 62, № 9, August, pp. 909-931.
- 15.1 ASTM Test Method for Half-Cell Potentials of Uncoated Reinforcing Steel in Concrete (C 876-87).
- 15.2 Colebrand Limited, Resistivity Logger Pamphlet, London, (no date).
- 15.3 Silverman, D. C. (1986) "Primer on the A.C. Impedance Technique", Electrochemical Techniques for Corrosion Engineering, NACE, Houston, pp. 73-79.
- 15.4 Sagüés, A. A. (1988) "A System for Electrochemical Impedance Corrosion Testing Using a PC with ISAAC-CYBORG Interface", Paper № 104, Corrosion 88, St. Louis, March 21-25.
- 15.5 Aguilar, A., Sagüés, A. A. and Powers, R. G. (1990) "Corrosion Measurements of Reinforcing Steel in Partially Submerged Concrete Slabs", Corrosion Rates of Steel in Concrete, ASTM STP 1065, ASTM, Philadelphia, pp. 66-85.
- 15.6 Borgard, B., Wareen, C., Somayai, S. and Heidersbach R. (1990) "Mechanisms of Corrosion of Steel in Concrete", Corrosion Rates of Steel in Concrete, ASTM STP 1065, ASTM, Philadelphia, pp. 174-188.
- 16.1 Gjorv, O.E (1971) "Long-Time Durability of Concrete in Seawater", ACI Journal, January, pp. 60-67.
- 16.2 Graham, J. R. and Backstrom, J. E. (1975) "Influence of Hot Saline and Distilled Waters on Concrete", Durability of Concrete, ACI Publication SP-47, pp. 325-341.
- 16.3 Kato, O. and Ohtsuki N. (1985) "Research on Resistance of Concrete to Seawater", Ocean Space Utilization '85, Proceedings of the International Symposium Nihon University, Tokyo, Japan, June, pp. 413-419.

- 16.4 Sun, Z.L (1991) "Static and Fatigue Response of Fiberglass Pretensioned Beams", MSCE Thesis submitted to the Department of Civil Engineering and Mechanics, University of South Florida, Tampa, Florida, June.
- 17.1 Mariscal, D. (1991) "Strength and Durability of Fiberglass Pretensioned Elements". MSCE Thesis submitted to Department of Civil Engineering & Mechanics, University of South Florida, Tampa, FL, December.
- 17.2 Pfeifer, D.W. Landgren J.R. and Zoob A. (1987) "Protective Systems for New Prestressed and Substructure Concrete", U.S. Department of Transportation, Final Research Report, Virginia, April.
- 17.3 Kessler, J., Arrebola, V. E., Lingerfelt, R. S. and Brown, R. P (1978) "Determination of Low-Levels of Chloride in Concrete and Raw Materials", Florida Department of Transportation, Research Report 203, Tallahassee, July.
- 17.4 ACI 318-89 (1989) Building Code Requirements for Reinforced Concrete and Commentary, ACI, Detroit, MI.
- 17.5 Stark, D. (1984) "Determination of Permissible Chloride Levels in Prestressed Concrete", PCI Journal, Vol. 29, № 4, Jul-Aug 1984, pp. 106-119.
- 17.6 Mozer, J. D., Bianchini, A. C. and Kesler, C. E. (1962) "Corrosion of Reinforcing Bars in Concrete", ACI Journal, Proceedings Vol. 62, № 9, Aug., pp. 909-931.